THE EFFECT OF PARTICLE SIZE ON

ELECTROSTATIC POWDER COATINGS

by

RICHARD A. SIBBETT

A Doctoral Thesis

Submitted in partial fulfilment of the requirements

for the award of

Doctor of Philosophy

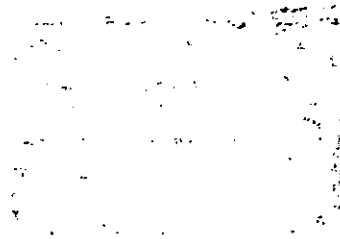of the Loughborough University of Technology

September 1982

Supervisor : P.J. Lloyd

Chemical Engineering Department

To MUM and DAD

———— II ————

for their unceasing support

ACKNOWLEDGEMENTS

Synopsis

In the electrostatic powder coating industry an increase in deposition efficiency and a controlled decrease in film thickness are constantly strived for. If adjustments to the size distribution of powders are made in order to improve the process in any way it is important that the excellent physical properties of the coating are not sacrificed.

The aim of this study is to gain an understanding of the effects of particle size on the packing and final film properties of electrostatically sprayed coatings so that recommendations can be made to increase the effectiveness of the process.

Experimental studies involved the production of stoved sample coatings of various thicknesses obtained by spraying narrow size ranges of a commercial powder using a reproducible coating method. A testing programme was developed to assess the effect of particle size on the physical properties of the films produced. A three way comparison of physical property, size of sprayed powder and coating thickness has been compiled and results are discussed. It was observed that particle size had no significant physical effect on film properties.

A method for determining a spreading factor, representative of the flow characteristics of a given powder, was developed. Observations from these stoving experiments suggested that the excellent flow properties of the powder used in earlier experiments accounted for the small variations in those results. However, photomicrographs of typical coatings showed that large particles were dominant in the

upper layers of packings. A loss of fines was identified from size analysis of various powders on coated plates compared to the original feed materials.

Computer plots simulating the packing of particles on a substrate showed similar trends. Integration of the trajectory equation for individual particles, represented by means of a force balance, was carried out with consideration of all interparticulate electrostatic forces of the packed layer together with field and aerodynamic forces. Simulations of packings of monosized and size distributed powders sprayed at various transport air velocities show that, as a packing increases in thickness, various sizes behave differently. The results from these theoretical experiments give indications for the explanation of previous results.

CONTENTS

INTRODUCTION

Consideration of conserving energy, resources, money and controlling pollution has never been more important (A.D. Moore, 1973). The electrostatic powder coating industry is one which has developed because of its many advantages in saving materials, energy, being non-polluting and generally producing a very good protective coating (R. Lever, 1978; J.D. Toff, 1979). In the last 10-15 years its growth has accounted for approximately 10% of the world protective finishing market (Anon, 1979).

However, in spite of the long list of advantages to its credit, as shown in Table I1, electrostatic powder coating has some major disadvantages which have curtailed its growth in the large commercial industries (W. Crisp, 1973; E. Miller, 1974; D. Payne, 1973; K.C. O'Neill, 1977). One of the largest users of protective coatings is the automobile industry and as yet electrostatic powder coating has not had a large impact on this market (S.L. Mason, 1974; E.W. Drew, 1977; M. Cowley, 1974).

The car industry first used a spray gun in 1912 for applying primer coats to car bodies, but although this method is used for applying both primer and finishing coats the application is in liquid form. This has many drawbacks.

Thick films have to be built up in layers and the process is very wasteful. Sludge systems to remove and dispose of the waste are therefore required. Even after many advances in controlling the system it is still apt to air and water pollution. The final coat is susceptible to corrosion. In these respects powder coating is highly advantageous.

Table I1

Advantages of Electrostatic Powder Spraying Process

System Advantages

No solvents used hence no pollution or fire risks.

Overspray can be reused by incorporating recycling system.

Highly skilled labour is not necessary.

Cleaning of booth is more easily carried out.

Builds up thick films in one coat.

Lower capital outlay and energy costs.

Less preparation required for surface.

Film Quality Advantages

Very good adhesion.

High abrasion, scratch and impact resistance.

Extremely high chemical resistance.

Very good electrical Insulation.

Orange peel and wrap around effects.

However, the electrostatic powder coating system has its own disadvantages. Problems are encountered in the production of thin films and also when colour changes are required. Unlike liquid paint systems, powder systems must be totally cleaned out when a colour change is required, and in practice this can be quite frequent. This is necessary to avoid any contamination of the next colour by airborne particles. In the paint industry colour change is effected by a simple change of paint supply, since oversprayed paint will not become airbourne again.

In powder coating the colour change is both labour intensive and time consuming. Although the usage of powder can be up to 99% efficient by use of a recycling system, the actual deposition efficiency is only about 40-60%. An increase in this efficiency to 95%, by the manipulation of powder characteristics and operating conditions would remove the necessity for colour change.

The second problem is the production of thin films. Although powder coating can very efficiently give final films of 50-150µm thick in one coat, a more economic thickness of 25-50µm is required. The associated high quality finishes must also be maintained. This would lead to a considerable saving on raw material costs.

Investigations into the mechanisms involved in powder coating show that a spraying system has a self limiting coating thickness (J.A. Bassett et al, 1975; J.A. Cross et al, 1980). This is due to the repulsion of charged particles away from the charged packed layer of particles, and due to the onset of back ionisation. However, this limiting effect only occurs at thicknesses above 100µm and after long coating times.

It is with these problems in mind that the work described here is directed. The effects of particle size and size distribution on the properties of electrostatically sprayed powder coatings have been investigated. It is important that any change in the feed powder that is made to give rise to an improved coating process in terms of economy does not lead to a decrease in the standard of finish. The effects of particle size on the physical properties of various thicknesses of commercially applied coatings have been investigated using a range of test methods. A review of the generally accepted test procedures for testing organic coatings is given following a brief outline of the electrostatic powder coating process (Chapters 1 and 2).

Size fractions (10μm wide) of a commercial powder were sprayed under similar operating conditions and at various coating thicknesses. These were then stoved and tested for differences in physical properties. Results are expressed in terms of sprayed particle size, film thickness and physical property as a three way comparison. The powder used in the experiments was a standard epoxy resin type as often used in the coating industry and supplied by powder manufacturers. No significant differences were found in the results for changes in particle size sprayed or film thickness.

Exploratory experiments were carried out to investigate the reasons behind these results. Fundamental stoving experiments and microscopic observations of coatings (unfused) showed interesting results. Studies of the flow properties of powders suggested that a powder that has good flow characteristics would not be subject to effects due to particle size. Packing experiments have shown that

when a powder with a wide size distribution (e.g. commercial) is sprayed a loss of fines takes place and large particles preferentially deposit on the top of thick coatings.

Theoretical investigations based on these results were directed towards the understanding of how powders with different size distributions pack on a substrate. In particular a comparison of mono sized and size distributed powders was made. A computer program has been developed using the force balance given in Chapter 5 and is described in Chapter 6. The program simulates the landing of particles on a substrate taking into account field and aerodynamic forces acting on them, and also all interparticulate electrostatic forces due to the charged powder layer. Results are presented in the form of computer plots.

It has not been an intention of this study to observe changes in deposition efficiency with different sized particles that have been sprayed. This work has studied any effects that particle size has had on the properties of the stoved films and also any changes in the way in which particles are deposited on a substrate or powder layers. In doing so a better understanding of the importance of particle size on the electrostatic powder process has been obtained.

CHAPTER 1

ELECTROSTATIC POWDER COATING - THE BASICS

1.1   Introduction

1.2   Electrostatic Powder Coating Process

    1.2.1   Powder Supply

    1.2.2   Spray Gun

    1.2.3   Spray Booth

    1.2.4   Powder Recovery System

    1.2.5   Stoving Ovens

    1.2.6   Powder

    1.2.7   Colour Change

    1.2.8   Substrate Preparation

1.3   Previous Research

1.4   Levelling in Powder Coating

1.5   Practical Problems

1.6   Summary

1.1 Introduction.

It was only in 1953 that the first commercial powder coating was made by an American factory dipping heated metal parts into powder (S.T. Harris, 1976). Since then, and especially in the past 15 years, powder coating, and in particular electrostatic powder spraying, has grown to take over about 10% of the world market in the finishing industry (P.G. Delange, 1978).

The reasons for the increase in powder coating in various coating industries can easily be seen. When raw material prices are escalating it is not surprising that new techniques, such as powder coating, which improve the overall efficiency are considered as replacements. The industry has further been enhanced by the need to reduce air pollution and sustained by the possibility of better or equal finishes at lower costs. However, the increase in popularity also raises the interest in more control over finishes, namely producing 1-2 mil. smooth coatings.

The obvious advantages of using dry powder coating have already been shown in Table I1. In the early stages of the industry manufacturers were conscious of the great deal of work and research that was necessary in order to break into various markets. Apart from the obvious disadvantage of colour change, which gives difficulty due to the easy contamination of materials and equipment, many other problems had to be dealt with.

Development of recovery facilities, equipment design and powder specifications was required. Since the beginning of the seventies the range of powders available to coating companies has become extensive (J.D. Tierney, 1975). An understanding of formulation on final film properties has been obtained. Powders now come in

many colours and hence can be used in a vast amount of applications.

However, the effects of the particle characteristics and electrical properties (excluding formulation) on the packing and properties of the dry and fused films is far from clear. It is with respect to the understanding of the process and the effects due to particle characteristics that this work is aimed. Firstly it is necessary to know something about the process itself and the problems encountered.

There are two main types of electrostatic powder coating equipment:-

(1) Electrostatic fluidised bed

High voltage wires are introduced into a fluidised bed to give electrostatic charge to particles. The article to be coated is positioned in a high voltage space and is earthed. The article does not have to be preheated as in non-electrostatic fluidised bed coating and it is not actually dipped into the bed. The particles are attracted to the object as it approaches and a uniform layer of coating is obtained. However, with larger particles this gives varying coating thicknesses between the top and bottom. Particle size and voltage have significant effects on the coating deposition and thickness. Electrostatic effects will be preferential to a certain size range (between 20 and 80 μm) and so fresh powder is required otherwise coating thickness will decrease.

(2) Electrostatic powder spraying.

In electrostatic powder spraying charged powder in an air stream is directed at the earthed object so as to bring the powder adjacent to the surface. In order to accomplish a successful coating the method comprises of a combination of elements.

   (i)   Delivery of powder

  (ii)   Charging of powder

 (iii)   Transfer of powder from charging region to object

  (iv)   Adhesion of powder to object

   (v)   Stoving of coating

  (vi)   Recovery of powder

This is shown diagrammatically in Figure 1.1.

The fluidised bed method is limited by being a fixed position applicator. Spraying of powder overcomes this. Spraying plants vary immensely depending on the type of articles that are to be coated (S. Kut, 1971a, 1972, 1974; M. Drury, 1974). They can either be large scale; fully automated robot systems spraying large articles which are transported by conveyors, or small scale; articles are coated by a hand gun and carried to an oven. However the basis of the equipment in each case is very similar. One such arrangement is shown in Figure 1.2.

The powder is transported by compressed air from a hopper or reservoir to a spray gun. The powder then passes one or more high potential electrodes in the gun whence the particles are charged. The mechanism of charging particles will be discussed in detail later. The particles are propelled forwards by means of electrostatic forces and the transport air towards the object, which is earthed and enclosed in a booth. The charge on the particle attracts it to the substrate where it is held by various adhesion forces. The powder layer is then stoved in an oven to form a continuous coating. Oversprayed powder is recovered by a recycling system.

Finished Product

```
+-------------+                          +-------------+
|   H.T.      |                          |   Stoving   |
|   Supply    |                          |   Oven      |
+-------------+                          +-------------+
       |                                        ^
       |                                        |
```

Spray Booth

```
   - - - - - - - - - - - - - - - - - - - - - - - - - - -
   |   |                                        |        |
   |   v                                        |        |
   |  +-------------+          +-------------+   |        |
-->|  |    Gun      |--------->|   Target    |   |        |
|  |  |             |          |             |   |        |
|  |  +-------------+          +-------------+   |        |
|  |         ^                                   |        |
|  - - - - - |- - - - - - - - - - - - - - - - - -|- - - -
|            |                                   |
|            |                                   v
|     +-------------+          +-------------+
|     |   Powder    |<---------| Recycling of|
|     | Feed Hopper |          |   Powder    |
|     +-------------+          +-------------+
|            ^
|            |
|     +-------------+
|     |             |
+-----|  Air Supply |
      |             |
      +-------------+
```
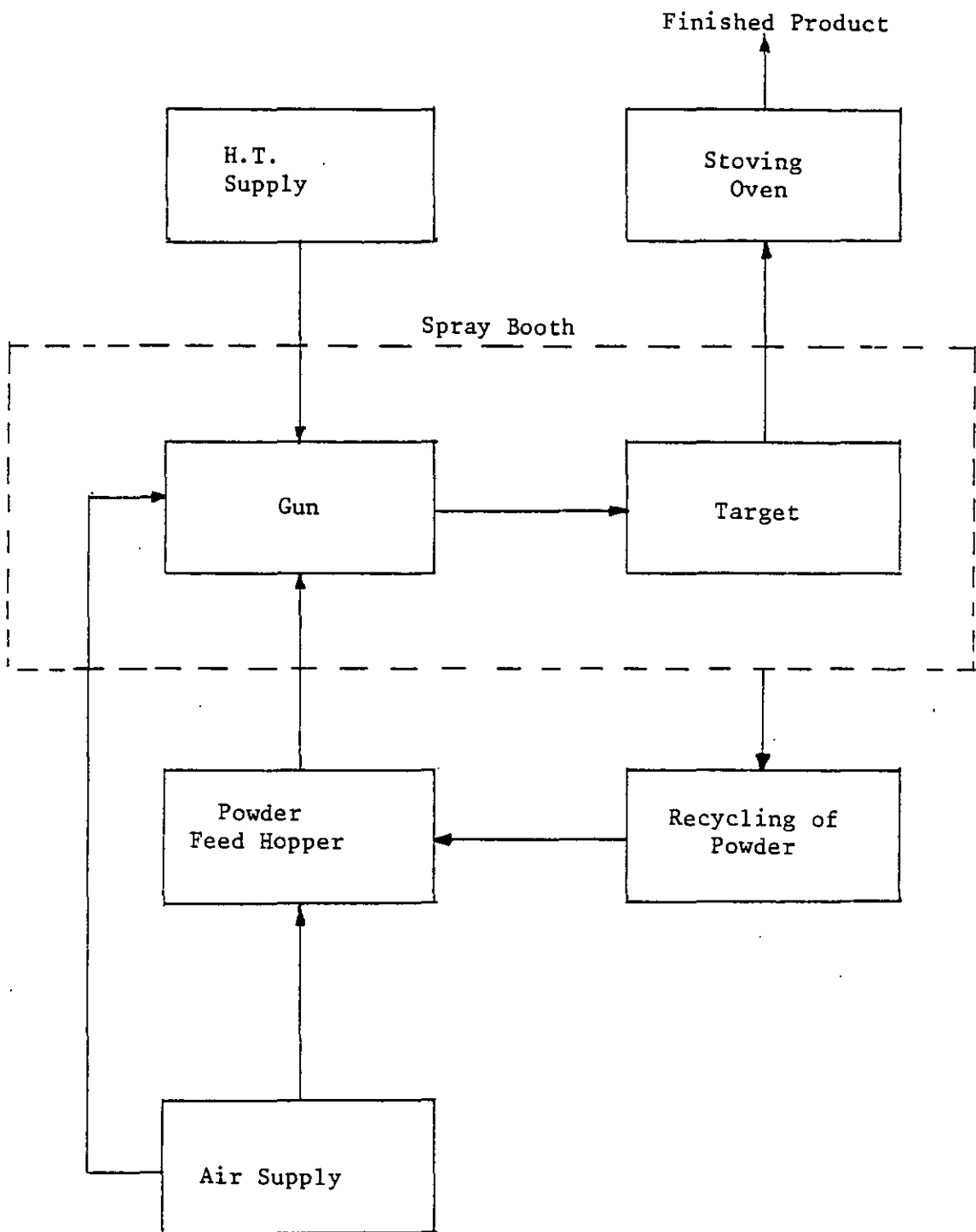
Figure 1.1. Diagram of Typical EPC Process
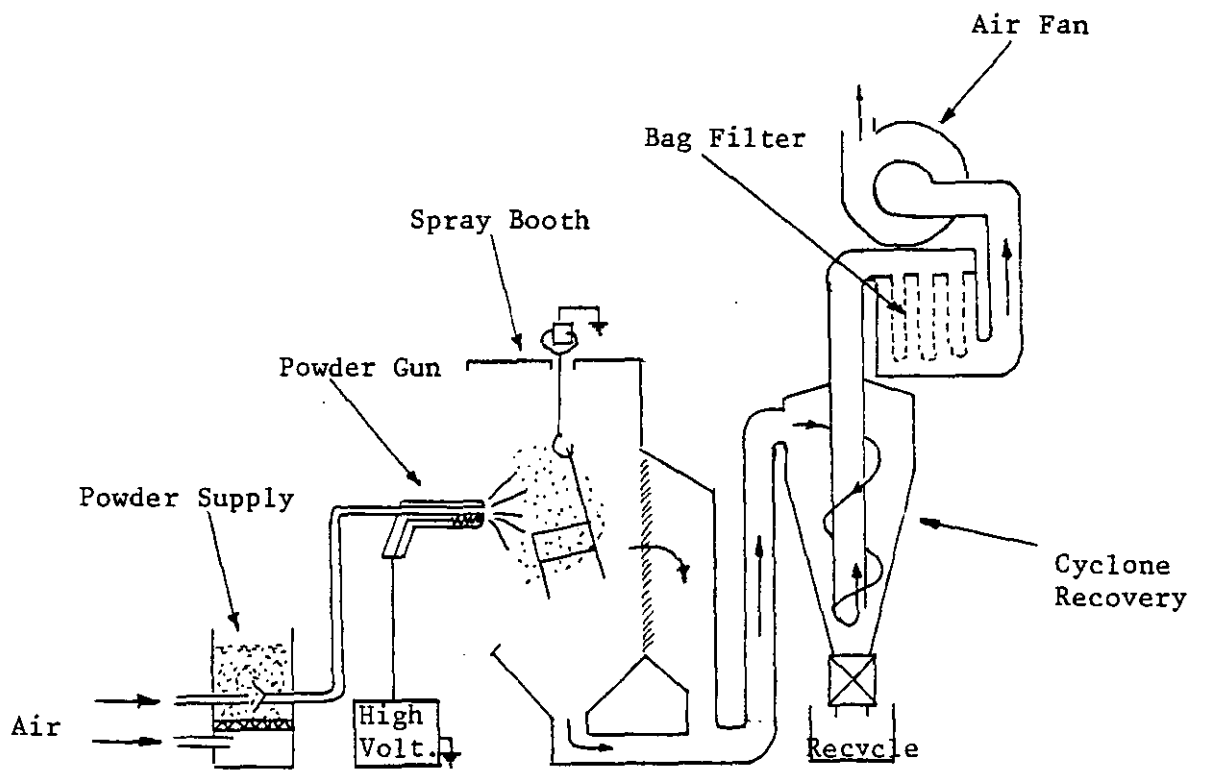
Figure 1.2. Electrostatic Powder Coating Equipment

Each section of the process will now be described.

1.2   Electrostatic Powder Coating Process

1.2.1   Powder Supply

It is very important that the amount of powder supplied to the powder gun and hence onto the object is carefully controlled. Starting and stopping of the powder supply system must be possible without surging or blocking.

The most popular system incorporates a venturi feeder. Possible types are shown in Figure 1.3 (a),(b) and (c). Air is supplied to the injection part of the venturi and this causes powder to be drawn from the hopper which is then suspended in the air. To aid powder being drawn out of the hopper the bed can be agitated by an external vibrator (1.3(a)). A further modification is to incorporate a motor driven blade and a screw feeder within the powder (3(b)). The delivery of the powder is then more easily controlled.

Another way of aiding the exit of powder is by fluidising the bed structure, 1.3(c). Air is passed through the powder via a gauze at the bottom of the bed and the venturi pump is then immersed in the hopper. Each air supply can be controlled by a solenoid valve which is connected to the main generating system or to the trigger of the spray gun.

Where multiple guns are in operation a venturi pump valve combination is used for each gun. This gives interdependence of each gun. For multiple arrays of guns a single supply cylinder can be used.

The output of the feeder system is obviously a function of the number of guns in use and connected to it. In general the output from a single spray gun is about 2-5 gms/second of powder, the lower
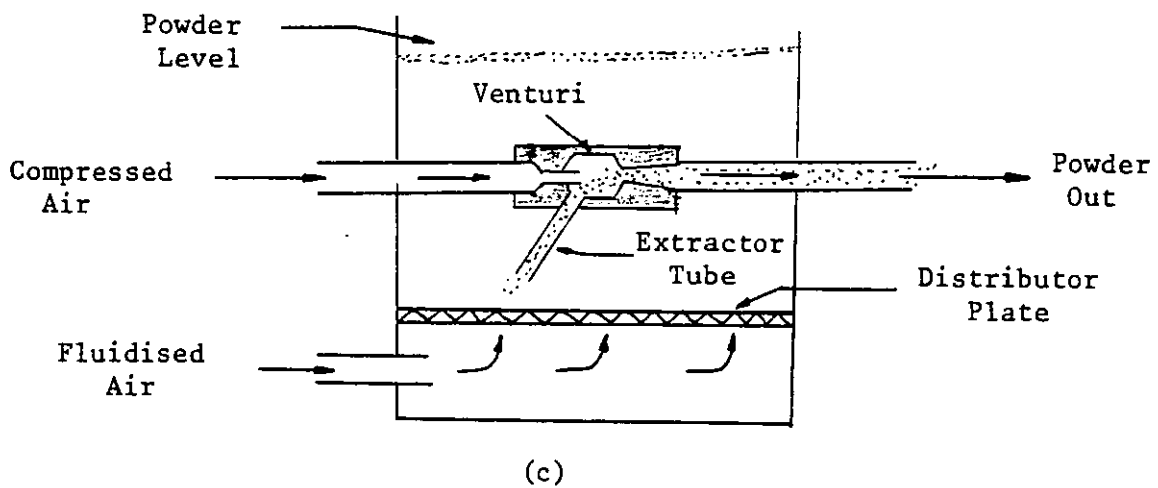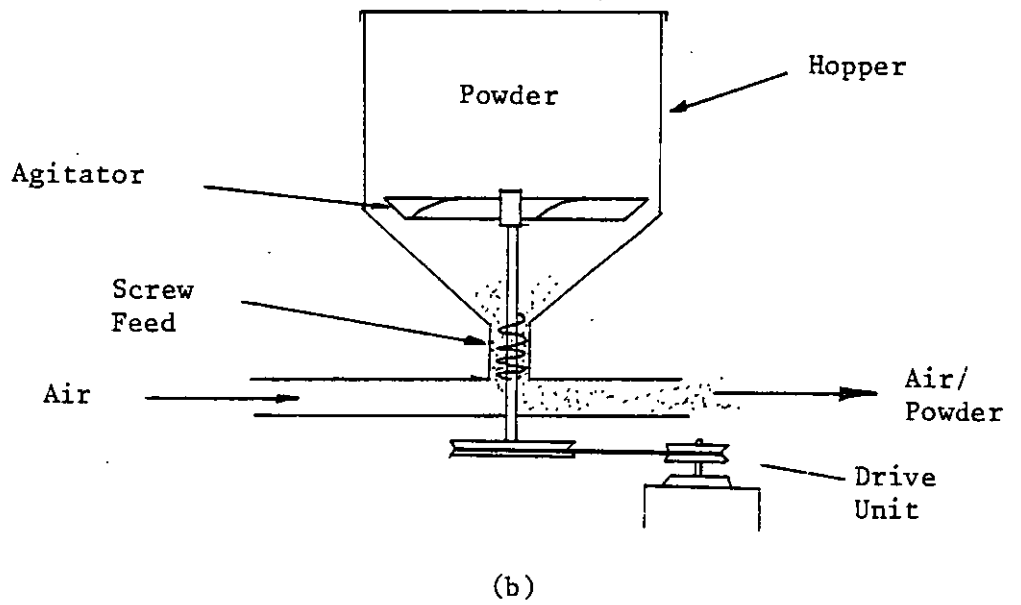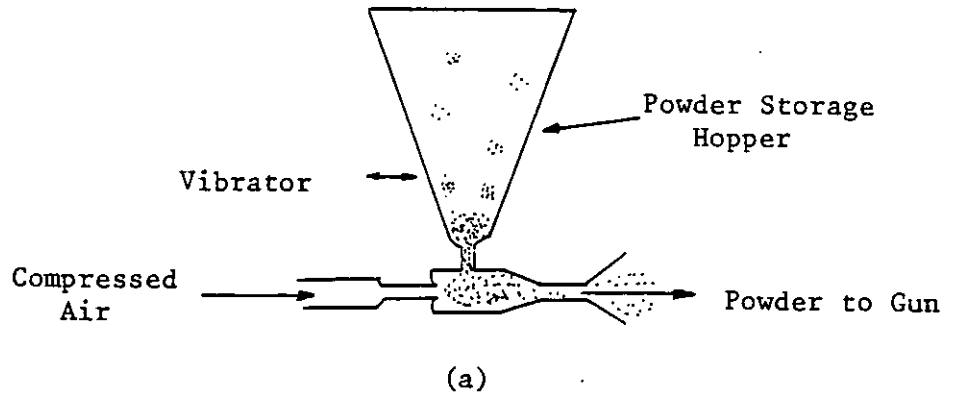
Figure 1.3. Typical Powder Feed Systems

the output the harder it is to obtain a consistent flow.

1.2.2 Spray Gun

The nature of the gun is very important since it is responsible for charging and spraying the particles.

The shape of the spray pattern is controlled by means of a deflector (stationary or rotating) at the nozzle of the gun (Plates 1.1 & 1.2). In addition to the powder supply air, there is a separate air supply to the gun which controls the pattern of the spray. This air passes through the gun and is emitted at the nozzle or just before the deflector. Manipulation of this air supply enables control of the amount to which the powder is 'splayed out'. The higher the air input then the higher the turbulence and the larger the spray pattern.

A pointed electrode is positioned near the nozzle or at the front of the deflector. A resistor of 10^8 Ω is incorporated in the body of the gun, or comprises the voltage supply cable to the gun, to act as a safety device. The corona electrode may consist of pointed wires, whiskers or edges of a disc. The electrical field around the sharp point must reach the breakdown strength of the air to produce a stable corona. In general the potential applied is 40-80 kV.

Resistive guns are those in which resistors have been added (as opposed to stiff guns) so that discharges and sparking to grounded objects is prevented. As the gun is brought near a grounded substrate the voltage will decrease and current increase so that energy output is constant. A stiff gun would give a constant voltage but the current would increase rapidly so as to cause sparking at a close distance. The normal output of a gun is about 10 Kg/hr of powder, with an exit air velocity of between 2-7 m/s.

Plate 1.1. Spray Gun Nozzle

Plate 1.2. Spray Gun in Operation (hand-held)
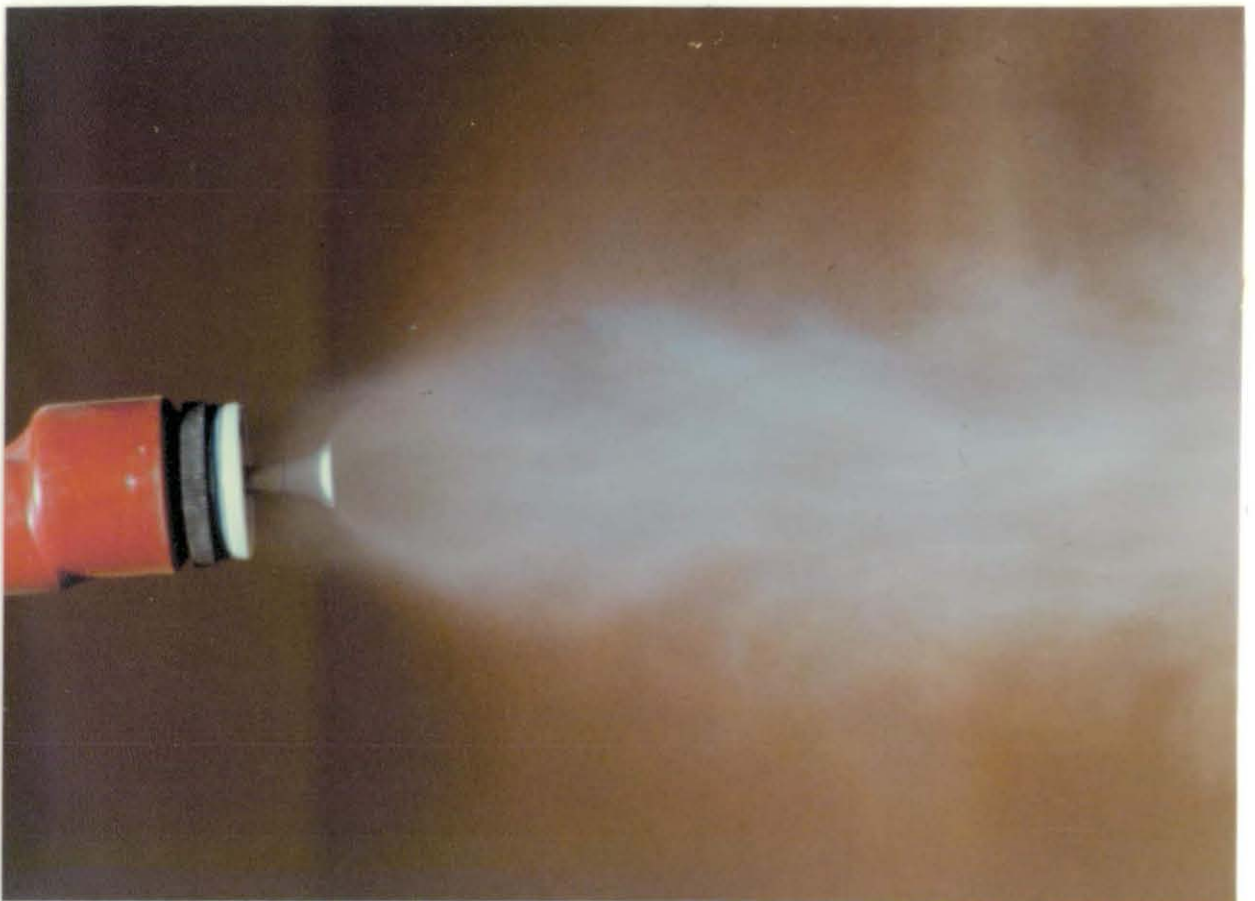
1.2.3 Spray Booth

The spray booth in powder coating is designed so as to aid the deposition of powder onto an article and to collect the overspray for recycling. This is unlike the wet paint system which traps overspray for disposal. Ideally the air in a spray booth would be perfectly still so that the electrostatic forces and powder velocity from the gun would control the coating process. In practice a stream of air across the workpiece is required for several reasons:-

(i)   Keeping powder concentration low in the booth (below safety explosive limits of 10 gms/cm^3)

(ii) Minimises effects of extraneous draughts from other areas of plant

(iii) Prevents backdraught of overspray towards operator

(iv) Acts as first stage of the recovery system

(v)   Confines any possible fire

The booths can be made of either steel or plastic. Steel is least expensive and provides protection in case of fire but becomes coated with the charged particles, hence problems are increased during colour changing. Plastic booths are more expensive.

A spray booth is designed so that there is little tendency for powder to accumulate. Therefore sloping floors are used to give a funnel shape to the opening of the air withdrawal. The size of the booth is determined by the parts to be coated, the speed of the conveyors (if used) and the number of guns. The air movement in the booth is dependent on the size of the booth and should be about 0.3-0.4 m/s. The air flow should be sufficient to stop powder forming high concentrations but not enough to blow the powder cloud away from the workpiece.

The inside of the booth should be free from ledges, where powder can collect, and generally be designed so that it is easy to clean. Access to the booth should be quick and simple, but it should be ensured that automated booths cannot be entered whilst in operation.

1.2.4 Powder Recovery System

For both economic and environmental reasons the over sprayed powder must be recovered with equipment that will separate powder from the air exhausted from the booth. By removing overspray an electrostatic powder system removes complaints of air pollution and eliminates the need for dispersal equipment. It can also make the system as a whole up to 99% efficient on powder usage.

Any recovery system consists of several elements that separate the powder from air, collect it, and return it for use in the system. In general, two types of equipment are used, namely the cyclone separator and bag filters. These are either used separately or in a combination. Combinations of cyclones and filter cloth systems help in cases where rapid colour changes are needed.

Bag filters have a very large filtering area for a small volume and can easily be cleaned by using reverse air flow. The cyclone is a very simple device in which a spiral air stream is generated to give the particles a centrifugal force. The large particles are thrown out to the walls and drop to the bottom of the cyclone where they are collected. Very small particles escape collection. If colour changes are required frequently then a cyclone followed by a bag filter can be used. The powder recovered from the cyclone (about 85%) is recycled and the powder from the bag filter is not reused. Hence colour changeover is effected by cleaning only the spray booth and cyclone. However, the loading on the bag filter must be carefully monitored as high loading will cause a drop in air

velocity through the system, which in turn will lead to a loss in efficiency of the cyclone separator.

Other systems include a counter current cyclone and a powder centrifuge. The recycled powder must be sifted at about 120 µm to remove any agglomerates, fibrous contaminants and dirt etc. The collected powder is either directly fed back to the feed hopper or accumulated for later addition in bulk. A typical system has been shown in Figure 1.2.

1.2.5 Stoving Ovens

The type of stoving that is required to produce a good powder coating film is dependent on the type of powder being used. The curing time of any powder is determined by the temperature of the oven but is a function of the formulation of the powder and its cure and gel characteristics. It is essential that the stoving cycle for a particular powder is closely followed for each and every particle. Problems can be encountered with large heavy objects where the base metal takes a long time to heat up. With heat applied from the powder surface to the substrate it is possible to fuse the upper layers into a continuous film and leave the lower layers unfused. This results in very poor film qualities and in severe cases leads to flaking off of large sheets of the coating i.e. no adhesion.

When considering the type of oven to be used it is necessary to consider the size and type of articles to be stoved; whether a conveyor line or batch process; amount of air supply required; and the temperature requirements of the powders to be used.

There are two main types of oven - Chamber or box ovens and continuous ovens, which are open at both ends. The heat for stoving can be supplied in a number of ways.

Convection ovens are one of the commonest types. Gas or oil fired burners are used to heat air which is then transferred to the enclosure of the oven. The length of the oven depends on the production rate required, curing time etc. The higher the air flow rate through the oven the shorter the stoving time, but the air velocity is generally kept to 1.5 m/s to avoid powder being blown off.

Articles can be stoved by infrared radiation which affords very fast heating with low air velocity. The hot source is created by electric elements or gas burners.

Induction heat is when the part to be stoved is exposed to an alternating electromagnetic field causing eddy currents to be induced and, therefore, the production of heat within the article. This is very useful for thin plate and large quantities of small parts, but it has the disadvantage of being extremely expensive when stoving large items, due to the necessity to heat all of the object. However, this method does eliminate the possibility of bad adhesion due to incomplete fusing near the substrate since stoving occurs from inside to out.

1.2.6 Powder

The powder formulation and characteristics are of great importance in coating any particular article. The powder will be chosen for a particular purpose according to its formulation and the properties it exhibits in the fusing cycle. There are many types of powder used in the industry but they can be classified into two main categories.

(i)   Thermoplastic powders

When fused, these powders form a smooth continuous film. They have very high molecular weights due to long straight chain hydrocarbons. They have very few chemical groups attached to the chains and hence have a fairly high resistance to chemical attack.

(ii)   Thermosetting powders

These are usually low molecular weight powders which melt and flow during fusion and undergo chemical conversion at the same time. Hence, once a thermoset has been cured it cannot be remelted to a plastic material. These powders are more easily used in industry giving high quality thin films from the small particle size range powder, which is difficult to produce for high molecular weight thermoplastics.

Thermosetting powders crosslink across the polymer backbone and hence the formulation, curing, flowing and viscosity charac-teristics can be carefully adjusted to produce a powder for a specific purpose. Thermosets have several advantages over thermoplastic powders. They need no primer; have excellent chemical and solvent resistance; and are capable of higher pigmentation levels. However, a powder is generally chosen for its individual properties with regard to a particular system (J. Smarsh, 1972; C. Korf, 1976).

The choice of the resin and hardner is made with respect to the final coating properties. Apart from the colour contribution made by the pigment, consideration must be given to the properties of:-

    (i)   thermal stability

   (ii)   chemical stability

  (iii)   hiding power

   (iv)   particle size

    (v)   electrical properties

The formulator must, therefore, take into consideration the following essentials:-

(i)   Method of production: Pigment loadings and addition of hardener is dependent on the type of equipment used, be it batch or continuous.

(ii)   Resin/hardener choice: Toxicity and particle size must be considered with regards to the homogeneity of compounding operations

(iii)   Correct level of gloss and colour

(iv)   Choice of grinding process to give correct size distribution

(v)   Storage stability and flowability

(vi)   Capability of recycled powder to be used again without reprocessing.

A typical manufacturing sequence of a powder is given in Figure 1.4. The final product that is achieved should be a homogeneous compounding of all the ingredients with a uniform particle size distribution and each particle having the same composition.

The first stage of the manufacture can be done in one of two ways. Both have the same objective to mix the ingredients to ensure homogeneity. Premixing, using tumble, horizontal, conical or high speed mixers and blenders, is followed by hot melt compounding of the powder by means of Z-blade mixers, heated rolls or continuous extrusion methods. The Z-blade mixer has the advantage of not needing any premixing. The mixture is first melted in the blender and when molten the other ingredients are added slowly, whilst using the blade. This mixer gives good dispersion and is relatively cheap but it is difficult to clean and cannot be used for fast curing systems. The flow agents and hardener are finally added and the mixture is then

```
                    ┌─────────────────────┐
                    │  Granulate Resins   │
                    └─────────────────────┘
                               │
                               ▼
              ┌──────────────────────────────────┐
              │        Weighing Station          │
              │  Resins          Pigments        │
              │  Additives       Hardness        │
              └──────────────────────────────────┘
                 │                           │
                 ▼                           ▼
                                      ┌─────────────────┐
                                      │   Premixing     │
                                      └─────────────────┘
                                               │
                                               ▼
        ┌─────────────────┐           ┌─────────────────┐
        │  Z blade mixer  │           │    Extruder     │
        └─────────────────┘           └─────────────────┘
                 │                           │
                 └────────────┬──────────────┘
                              ▼
                    ┌─────────────────────┐
                    │    Cooling Band     │
                    └─────────────────────┘
                               │
                               ▼
                    ┌─────────────────────┐
                    │    Granulation      │
                    └─────────────────────┘
                               │
                               ▼
                    ┌─────────────────────┐◄──────────────┐
                    │      Grinding       │               │
                    └─────────────────────┘               │
                     │                   │                 │
                     ▼                   ▼                 │
        ┌─────────────────┐           ┌─────────────────┐ │
        │     Sieving     │           │   Classifying   │─┘
        └─────────────────┘           └─────────────────┘
                     │                   │
                     └─────────┬─────────┘
                               ▼
                    ┌─────────────────────┐
                    │      Packing        │
                    └─────────────────────┘
                               │
                               ▼
                    ┌─────────────────────┐
                    │     EPC Process     │
                    └─────────────────────┘
```
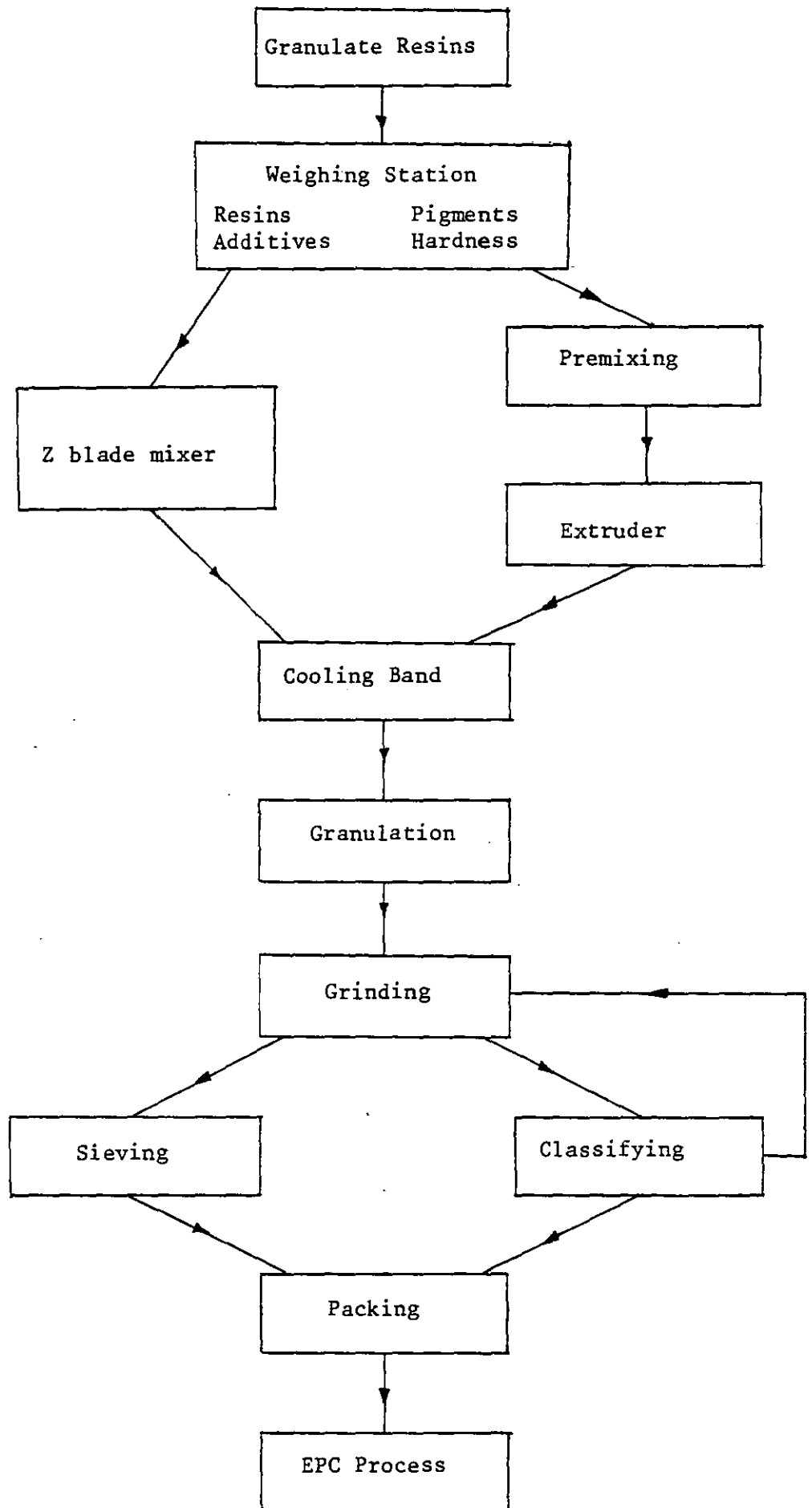
Figure 1.4.   Powder Manufacture Sequence

cooled rapidly on a roller cooling band.

The semicontinuous method of using rollers is not widely used for powder coatings but can be used for thermoplastic powders.

Extrusion is the most common method of producing powders. The mixture is passed through a heated screw extruder in which the resin melts and leaves as a homogeneous mixture. The extruder has the advantages of being very easy to clean and that it is easy to operate and control the temperature. The extrudate is quickly cooled and grinded roughly before passing into the pulverising and classification section.

The ease of particle size reduction mainly depends on the molecular weight of the base resin. Hence thermoplastics are extremely tough and resilient and these types of powders are reduced in size at low temperatures by freeze grinding or similar methods. The grinding of the particles is otherwise effected by ball, rod and tube, or hammer mills. Once the material is processed through this equipment it has a wide particle size range and so a classifier is used to recycle the large particles back to the grinder. The classification of the particles is mainly carried out by cyclones or sieves.

There are many types of powders available. Table 1.2 gives an outline of the usage of the various commercial powders in use. Each one is greatly influenced by its formulation and method of manufacture (S. Kut, 1971c).

Epoxy powders still account for the largest proportion of market. However development of powders for the automobile market is in progress and it is thought that the successful powder will more likely be a polyester or acrylic.

Table 1.2

Properties and Usages of Various Types of Commercial Powders

Powder	Properties	Uses
Epoxy	A. Excellent electrical insulation outstanding adhesion, impact, abrasion and scratch resistance High temp resistance No primer required Thin films D. Chalking and UV weathering	Functional items Rotors, Stators. Pipe coatings Wire goods Light fittings
Polyesters	A. Very versatile High light and heat stability High exterior resistance Good gloss & levelling D. Can hydrolyse - lower chemical resistance Primer required	Transformers, control boxes Guard rails, highway posts Wire shelving Hardware
Acrylic	A. Light and heat stability Excellent weathering resistance. High gloss. Good adhesion D. Primer required	Automotive and exterior applications Window frames Gas heaters switch gear.
Nylon	A. Average environmental prop. V. good mechanical & wear props. Good electrical prop. D. Weak to strong acids	Aircraft batteries furniture, safety devices, handles, door hinges, springs, valve stems and seats
Cellulose	A. Thick films Solvent & weather resistance D. Needs primer	Food racks - trays Screwdriver handles Outdoor signs
Vinyl	A. Good water immersion and corrosion resist. Outdoor resistance. Good chemical resistance D. Primer required	Dishwashers, wire goods Chain-link fencing Posts and rails

1.2.7 Colour Change

In powder spraying it is absolutely vital to remove the last powder sprayed from the whole plant before another powder is used. The time it takes to do this is dependent on the equipment in use. The design of spray booths is important in that difficult cleaning places must be minimised. The type of recovery unit is also important with regards to cleaning. As previously mentioned, bag filters are not suitable for frequent colour changes.

Therefore the engineering approach to the design of the coating system has included the combination of one or more of the following components

> (i)   Spray equipment
>
> (ii) Spray booth
>
> (iii) Cyclone
>
> (iv) Fabric filter

The arrangement and multiplication of each of these components is dependent on a series of factors governing the type of use of the system:-

> (i)   Number of colours to be used
>
> (ii) Usage time for each colour
>
> (iii) Required change-over time
>
> (iv) Type of system in use
>
> (v)   Allowable colour contamination/colours in use.

The ideal approach would be to disregard the oversprayed powder but this is not economically viable. The problem is to find a relatively simple and economic system using a high percentage of the powder, which is easy to operate and not space consuming. Hence there is a need to understand the basic fundamentals of the system, and to

investigate the effects of powder and operational characteristics

on the efficiency of the process so as to minimise this problem.

1.2.8   Substrate Preparation

However much time is spent in determining the best

formulation of a powder it should always be remembered that the

substrate surface must be in proper condition to make a coating

effective. In powder coating, just as in any other coating process,

operations must be carried out to remove imperfections from the

substrate; create a surface susceptible to bonding; and prevent

corrosion, through a break in the coating, by a chemical protective

coating (S. Kut, 1971b; H. Stein, 1972; R.A. Ashdown, 1974; W.G. Willows,

1968).

Methods for cleaning the substrate include:-

(i)   Solvent wipe

(ii)   Emulsion cleaning

(iii) Alkali cleaning

(iv)   Acid cleaning

(v)   Abrasive blasting

The choice of method of pretreatment depends on whether the coating

is for internal or external use; the type of coating; and the type

of substrate to be coated. The most popular methods of pretreatment

are:

(i)   Spraying iron or zinc phosphate

(ii)   Zinc phosphate Dip

(iii) Chromating process

(iv)   Anodising

It has been shown that each type of pretreatment can give
different results to adhesion and salt spray tests. These results,
however, are also a function of substrate material. For steel,
chromate coating was found to be very resistant to corrosion and for
both aluminium and steel iron phosphate gave balanced results.

Results have been observed to vary for the flow of the powder
layer during melting on different pretreated. substrates. The surface
condition was found to be responsible for this, grit blasting giving
lower areas of flow (B. Whiting, 1977).

Hence to ensure a coating that has good corrosion resistance
it is necessary to combine powder coating with pretreatment, the
method of which is dependent on the demands on mechanical properties
and use of the coating.

1.3   Previous Research

In the previous sections of this chapter the electrostatic
powder process and the powders used therein have been briefly
described. In order to clarify the reasons for this work there are
certain phenomena and practical problems that should be mentioned.
These are important when considering the effectiveness of the process.

The limitations of the industry at present have been mentioned
in the introduction. Problems of colour change and film control
must be eliminated or simplified so that markets are increased.
This means that production of 25-50μm films, with minimal overspray,
must be achieved and yet the excellent film properties that the EPC
process presently possesses must still be maintained. The effect of
particle size and film thickness on the properties of the final film
are therefore investigated and described in detail later. Following
these experiments, research into the way in which different sized

particles pack is reported to try and understand the fundamental effects already observed. Recommendations can then be made to solving the above problems when the mechanisms involved are more fully understood.

There have been several workers that have already made fundamental investigations into the effect of operational variables on the coating (A. Gólovoy, 1973abc; G.F. Hardy, 1974; G.D. Cheever, 1975; A. Golovoy, 1975). These effects have been reported with reference to the film thickness and to the deposition efficiency. This is the ratio of powder deposited on a substrate to the amount of powder sprayed from the gun. Some of the results that have been obtained are shown in Figures 1.5-1.12.

Figure 1.5 shows a basic effect in that the deposition efficiency of the system, as the packing builds up, decreases. This effect is also shown in Figures 1.6, 1.7, 1.8 and 1.10 in a similar way. Deposition efficiency decreases as charging voltage applied to the electrodes of the spray gun is decreased (Figure 1.8) and is lower for thicker films.

The charge on the particle is a very important factor in these cases. The theoretical considerations of charging particles and the forces acting on the particles will be fully discussed in a later chapter. However it is worth stating here that the size of the particle, its charge, and the forces acting on the particle are all inter-related. A change in any one of these factors can give rise to one or more of many different effects.

In brief, the charge on a particle is dependent on the particle size, its electrical properties, the gun potential and the strength of

V = 60 kV
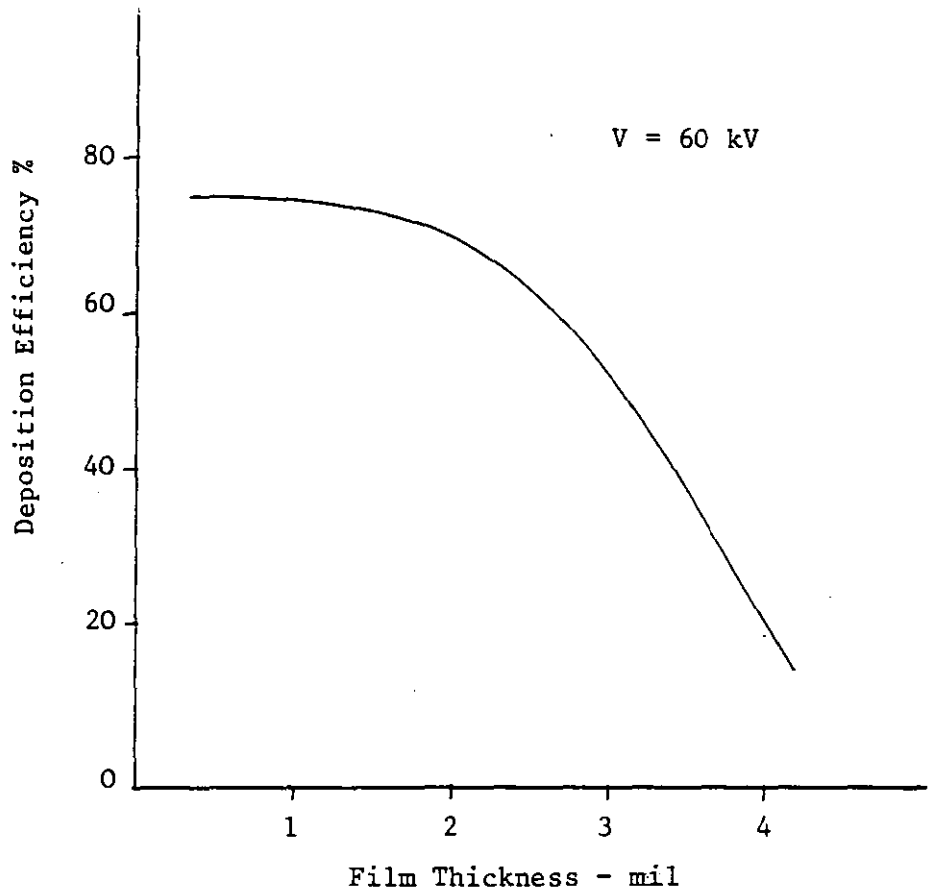
Figure 1.5. Deposition Efficiency vs Film Thickness at 60 kV
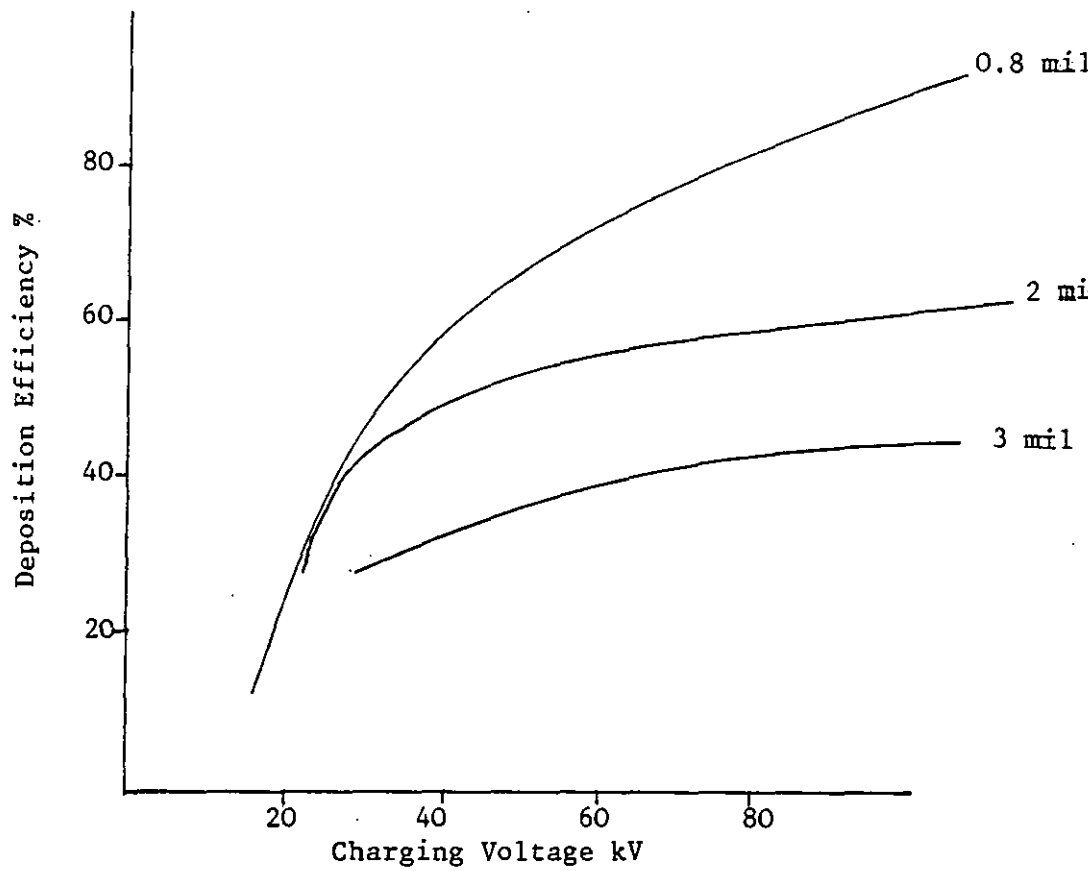
Figure 1.6. Deposition Efficiency vs Charging Voltage for Various Film Thicknesses
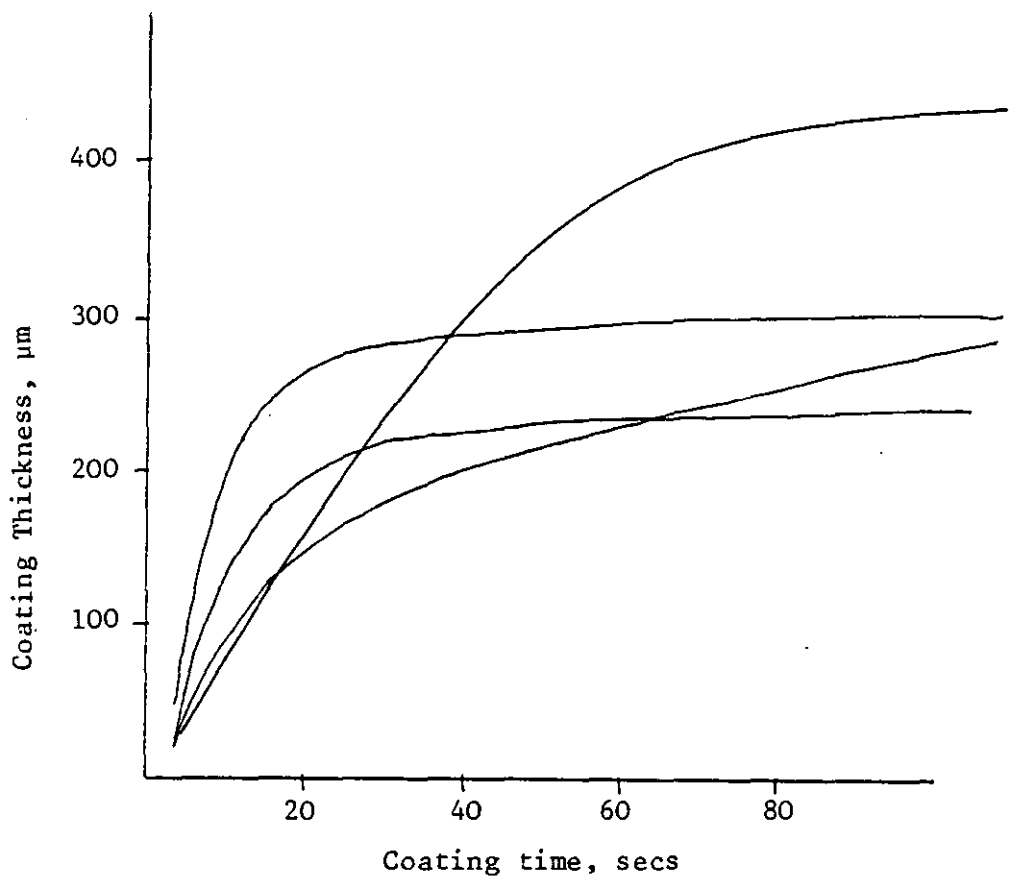
Figure 1.7.   Coating Thickness vs Coating Time
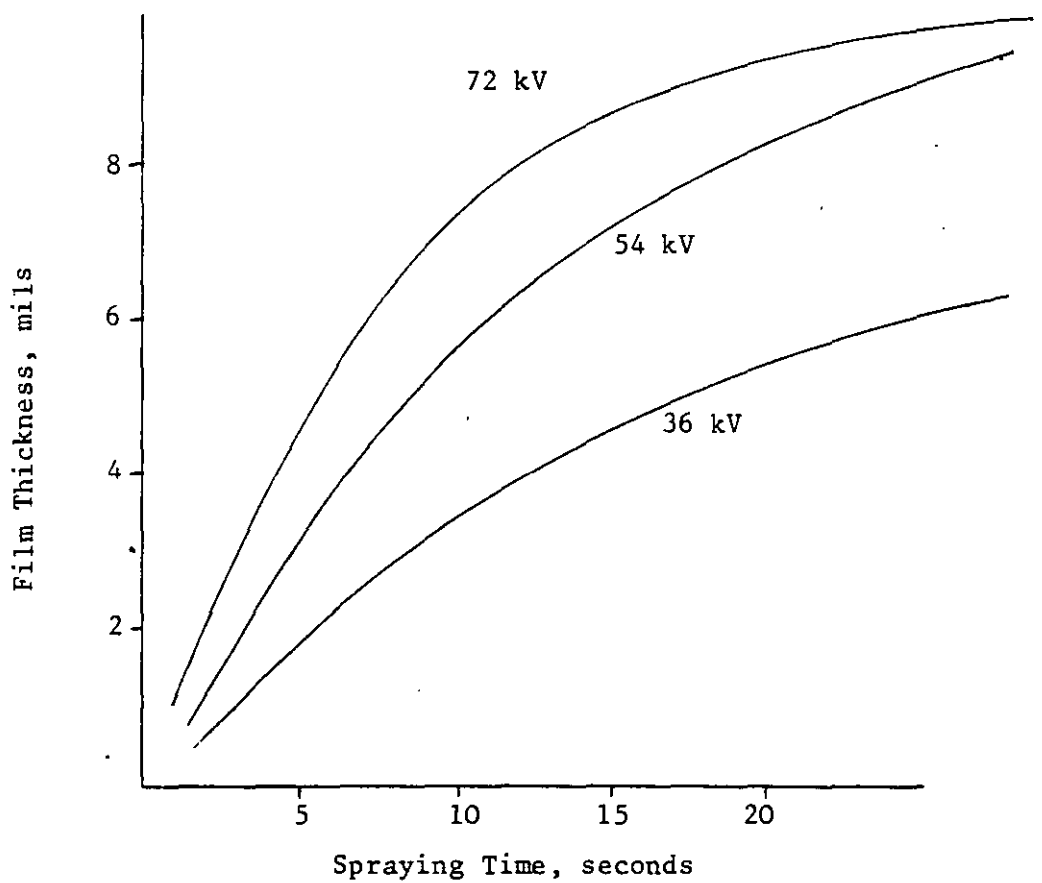
Figure 1.8.   Film Thickness vs Spraying Time for Various Voltages

the field near the gun. A particle is normally charged by passing through a corona region that is produced by application of an H.T. voltage to electrodes near the end of the gun. The particles are designed to have a resistivity of the order 10^{14} Ω cm so that they hold their charge for the time they are being sprayed and stoved. In practice the particles will remain on the workpiece for several hours.

The higher the gun potential the larger the charge on the particle and hence the greater the initial attraction of the charged particle to the substrate. However as coating continues the deposition decreases and the thickness of the film increases only very slowly. In Figure 1.6 it can be seen that a 2 mil thick film has a much lower deposition efficiency. Basset et al (J.D. Basset et al, 1975; Y.V. Ting, 1978) found that the coating was thickness limiting between 0.25 and 0.45 mm after coating times in excess of 20 secs, depending on the operating voltage (Figure 1.7). Golovoy however found that film thickness decreased towards a limit of approx 9 mils in the best case (Figure 1.8). The ability of the system to be limiting can be very useful but occurs at fairly high thicknesses.

The mechanisms involved can be of two types:-

a) Repulsion of particles due to the packed layer of charges, of the same polarity to the oncoming particle. The particle is repelled and will then be attracted to less packed areas or leave as overspray. The 'wrap-around' effect is achieved when these repelled particles are attracted to the 'blind' side of the target, purely by electrostatic forces.

b)   Back Ionisation. This is due to electrical discharges in the

powder layer. Ions of opposite sign leave the surface and

discharge powder being sprayed, such that it is not deposited

(A.W. Bright, 1977).

Observations of back ionisation, shown by an increase in current

to the earthed substrate, take place after a long coating time (above

20 secs), (Y.C. Ting, 1978).

The experiments conducted in this work involve spraying times

much less than 20 secs. In the case of a positive applied voltage

back ionsation is greater. This is due to the fact that electrons

are being emitted from the layer and are able to cause further

ionisation. This is by secondary electron emission from the powder

particles before forming negative ions. The discharge of ions from

the layer is due to dielectric breakdown caused by the increase in

potential within the layer as it builds up.

The 'critical thickness' means the thickness of the unstoved

coating when the potential difference across the powder layer is equal

to the dielectric strength of the powder. Hence when the critical

thickness is exceeded the deposition efficiency is drastically reduced

and the uppermost particles are held on very loosely. Hardy has

shown this with experiments involving the vibrating of sprayed panels

bearing thick powder layers. In the first few seconds of vibration

the majority of weakly charged powder was removed. (G.F. Hardy, 1974).

Similar experiments concerning the adhesion of the powder to

the substrate have been carried out by Ong and Cross (P.H. Ong et al,

1975; J. Cross, 1975).

Golovoy has shown that the average particle size of the powder sprayed affects the limiting thickness achieved. Small particles, with associated high charge to mass ratios, produce thinner films (Figure 1.9).

Operational variables, such as powder output, velocity, spraying distance and substrate size, also effect deposition efficiency (K. Venlet, 1973). The greater the spraying distance the thinner the films produced (Figure 1.10). This is related to the velocity gradient of the air (ratio of air velocity at gun exit and spraying distance). Larger gradients give thinner films (Figure 1.11).

The substrate width compared to the spray diameter has also been investigated by Golovoy and results are shown in Figure 1.12. The larger the substrate width compared to the spray diameter, the better is the deposition efficiency.

The critical thickness of a coating rises with increasing particle diameter and density, increasing dielectric constant and decreasing particle charge. However the inverse is true for the adhesive forces but adhesion is usually adequate under most conditions. The rate of charge decay of a deposited layer is influenced by the powder's chemical composition, temperature and relative humidity. Increase in humidity and temperature cause an increase in rate of charge decay, but providing the resistivity of the powder is kept above 10^{10} Ω cm the residual charge should be ample.
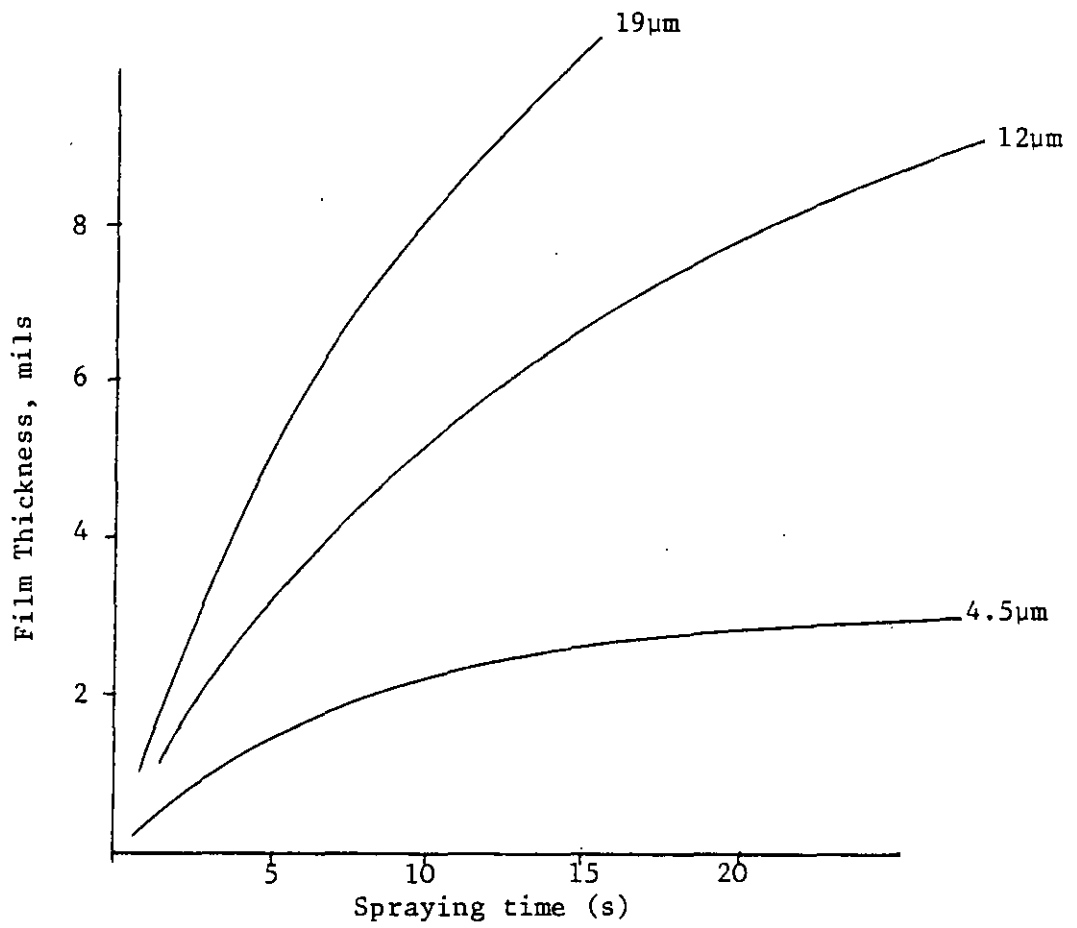
Figure 1.9.   Film Thickness vs Spraying Time for Various Sized Powders
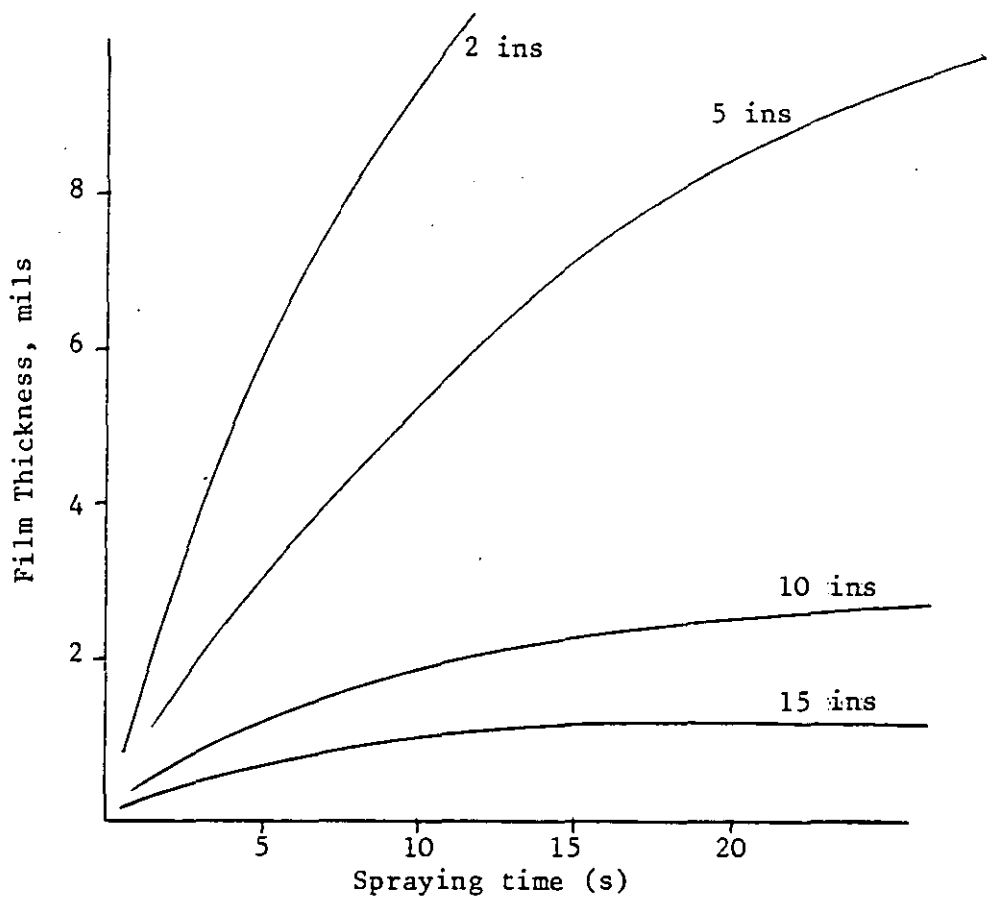
Figure 1.10.   Film Thickness vs Spraying Time for Various gun-target Distances
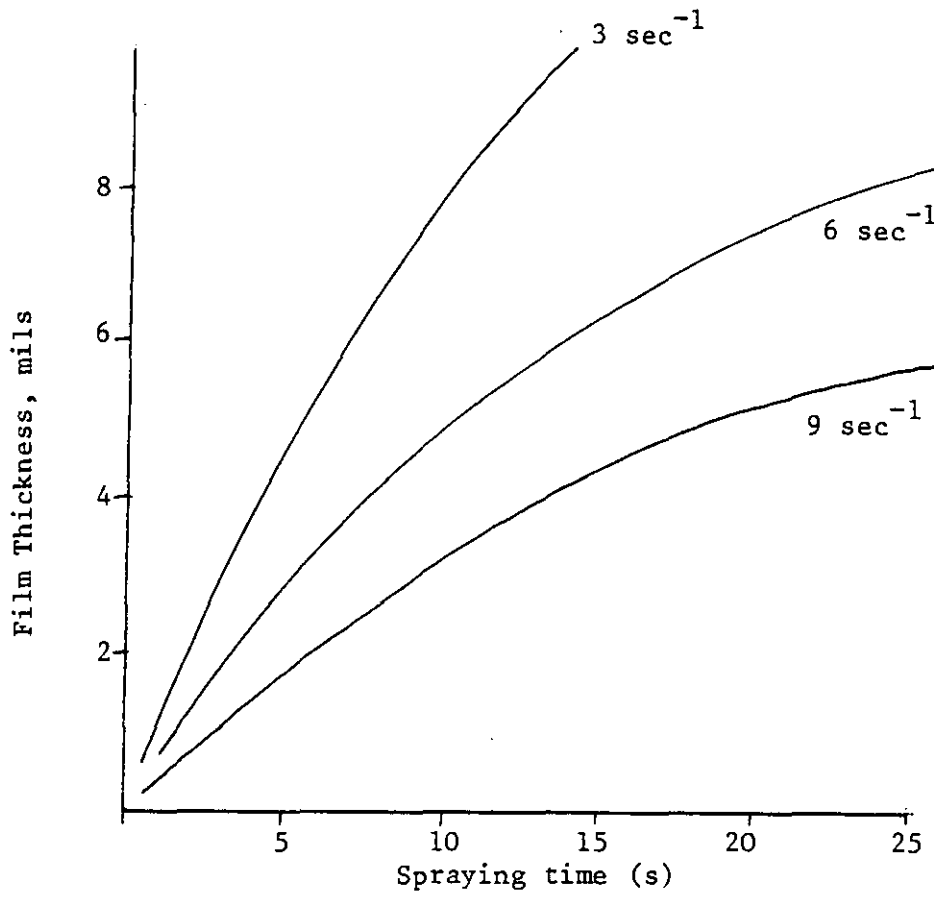
Figure 1.11. Film Thickness vs Spraying Time at Various Air Velocity Gradients
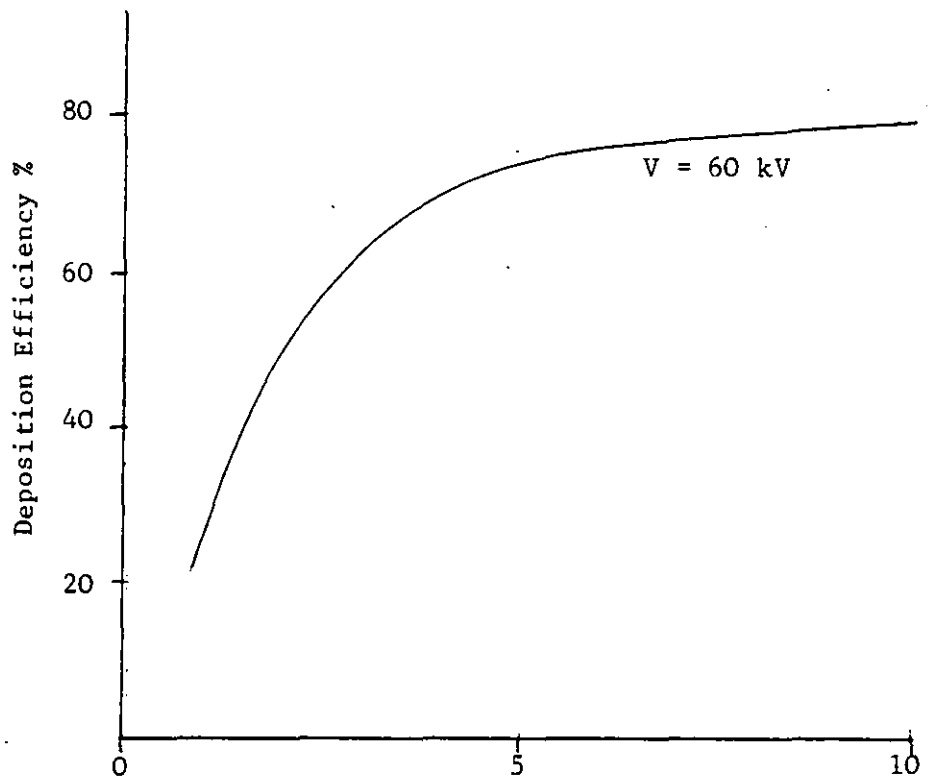
Figure 1.12. Plot of Deposition Efficiency vs Ratio of Substrate Width and Spray Diameter

1.4   Levelling in Powder Coating

After a powder coating is stoved it tends to exhibit a waviness,
or 'orange-peel', which is due to incomplete levelling during the
bake. The extent of this is dependent on the irregulatiries in the
powder layer i.e. the way in which the particles have packed, and
therefore the thickness of the coating (G.T. Spitz, 1973; S.E. Orchard,
1962; S.M. Wolpert, 1973; S. Gabriel, 1975).

As a powder coating is stoved the roughness of the surface
will decrease and will eventually stay at a given amplitude. The
wavelength of the waviness does similarly, but increases with time.

The levelling in powder coatings has been discussed by Spitz,
Nix et al and Wolpert (V.G. Nix et al, 1973). From their experiments
it has been concluded that the ripple in coatings comes from an
uneven deposition of powder, and that those differences due to
particle size have less effect than those associated with the flow
out of particle clusters (Figure 1.13) (S. Wolpert et al, 1972;
C.H.J. Klaren, 1976).

In the process of stoving the particles first melt and then
flow out to cover the substrate surface. The cross-linking reactions
then begin and the polymer starts to gel, preventing any further flow
(M.J. Hannon et al, 1976; A. Quach, 1973). The flow of the particles
is shown in Figure 1.14 with respect to temperature. The time to
gelation is a function of temperature and the type of epoxy powder
being used (shown in Figure 1.15).

Gabriel found that the behaviour of any system during stoving is
determined mainly by the chemical nature of the resin/hardener
combination. For any particular powder the way it cures can be

A : Deflection typical of cratering

B : Deflection typical of dust particles included in film

1 cm = 2µm

1 cm = 500µm
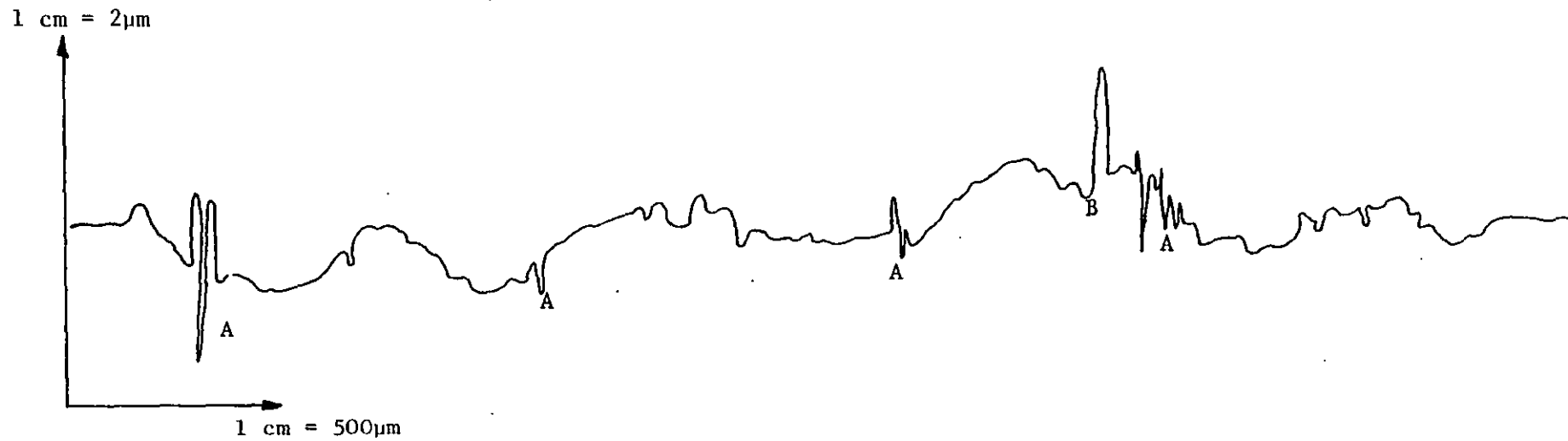
Figure 1.13. A Typical Powder Coating Profile
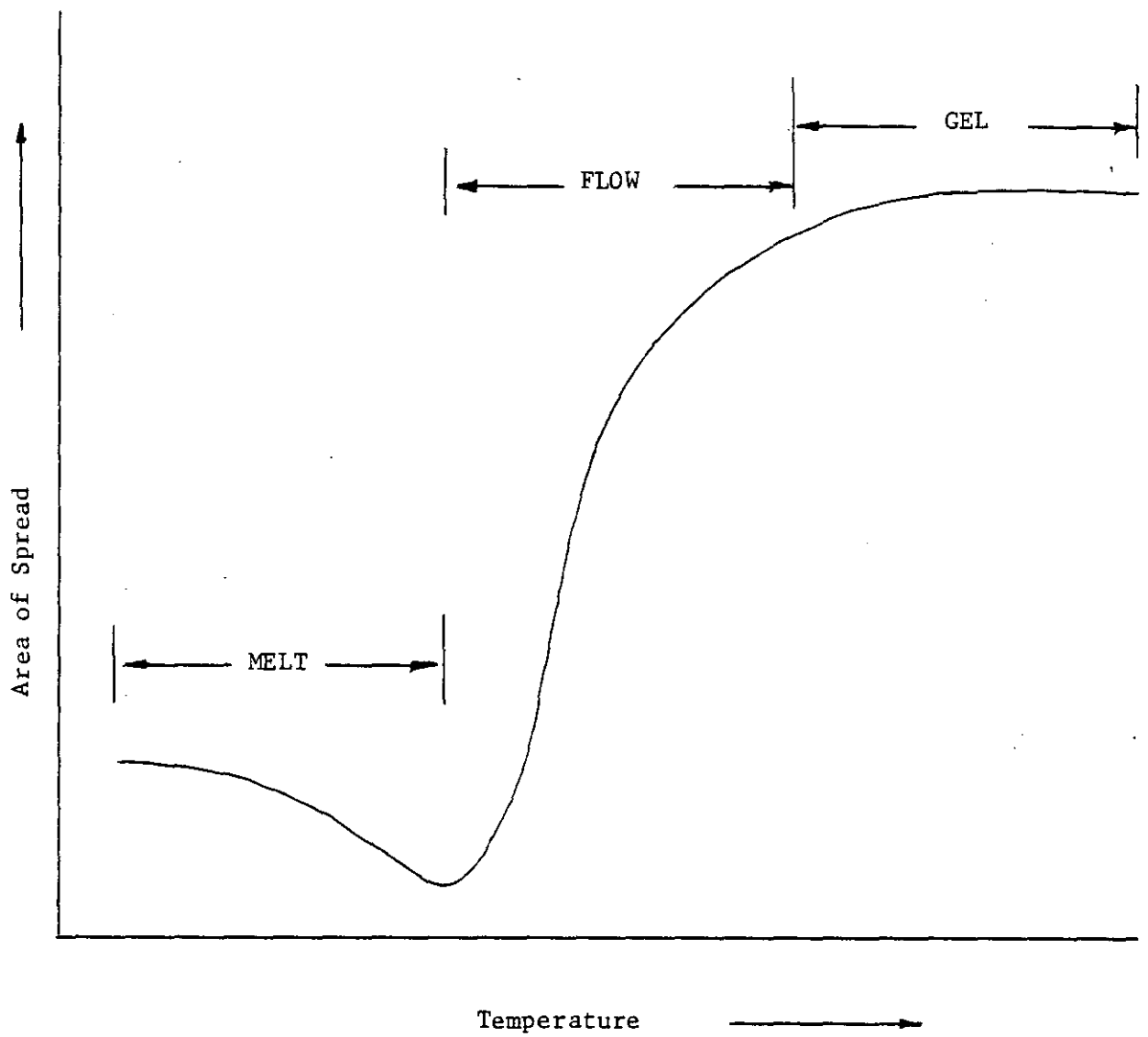
Figure 1.14. Plot Showing Stages in the Melt and Spread of an Epoxy
            Resin with Increasing Temperature
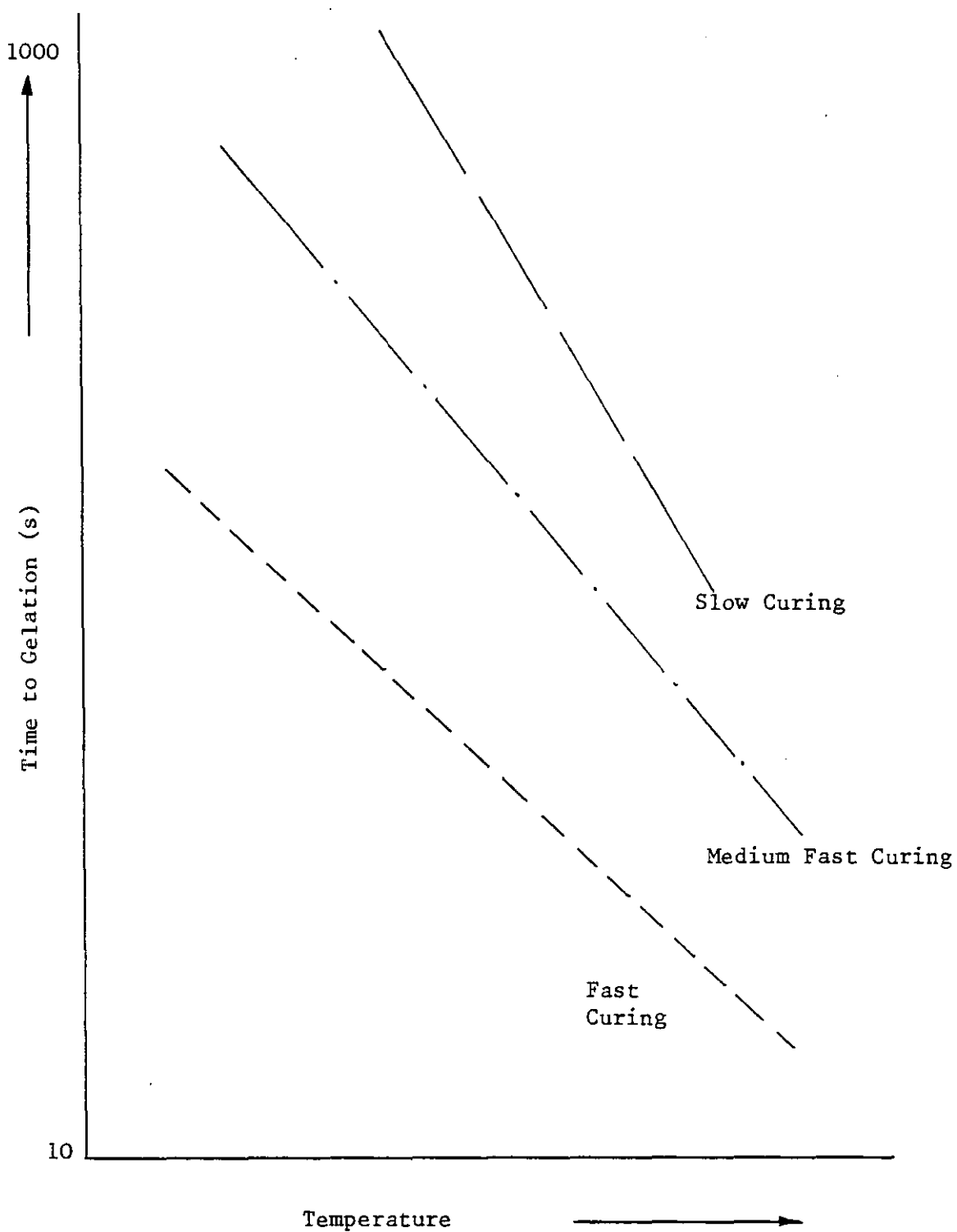
Figure 1.15. Time to Gelation of Various Epoxy Powders vs Temperature

expressed with a DSC (differential scanning calorimeter) thermogram.
Using this method the amount of energy absorbed or evolved by the
sample is recorded as a function of the sample temperature. The
differential of the amount of power required to keep the sample at
the same temperature as a reference, as expressed as energy per
unit time, is plotted against temperature. These thermograms clearly
show the glass transition point and melting and curing times of the
powder, since temperature is proportional to time via the heating
rate applied to the reference (Figure 1.16).

From the combination of all these results it can be seen that
the stoving cycle plays a considerable part with reference to the
final properties of the film, as does also the structure of the
particle packing. In the described experiments, the stoving cycle
for all samples is kept constant so as to eliminate any changes in
properties due to this.

1.5 Practical Problems

As previously mentioned, when the film thickness reaches that
of the critical thickness there is an onset of electric breakdown
within the layer. When discharges take place the surface of the layer
becomes rough and cratered. Positive ions will stream out towards the
gun corona and neutralise oncoming particles. This causes loosely
bound particles near the surface of the coating. The same effect
occurs when the particle charge is continually low. The driving force
for deposition is small and therefore the packing tends to become
loose and rough.
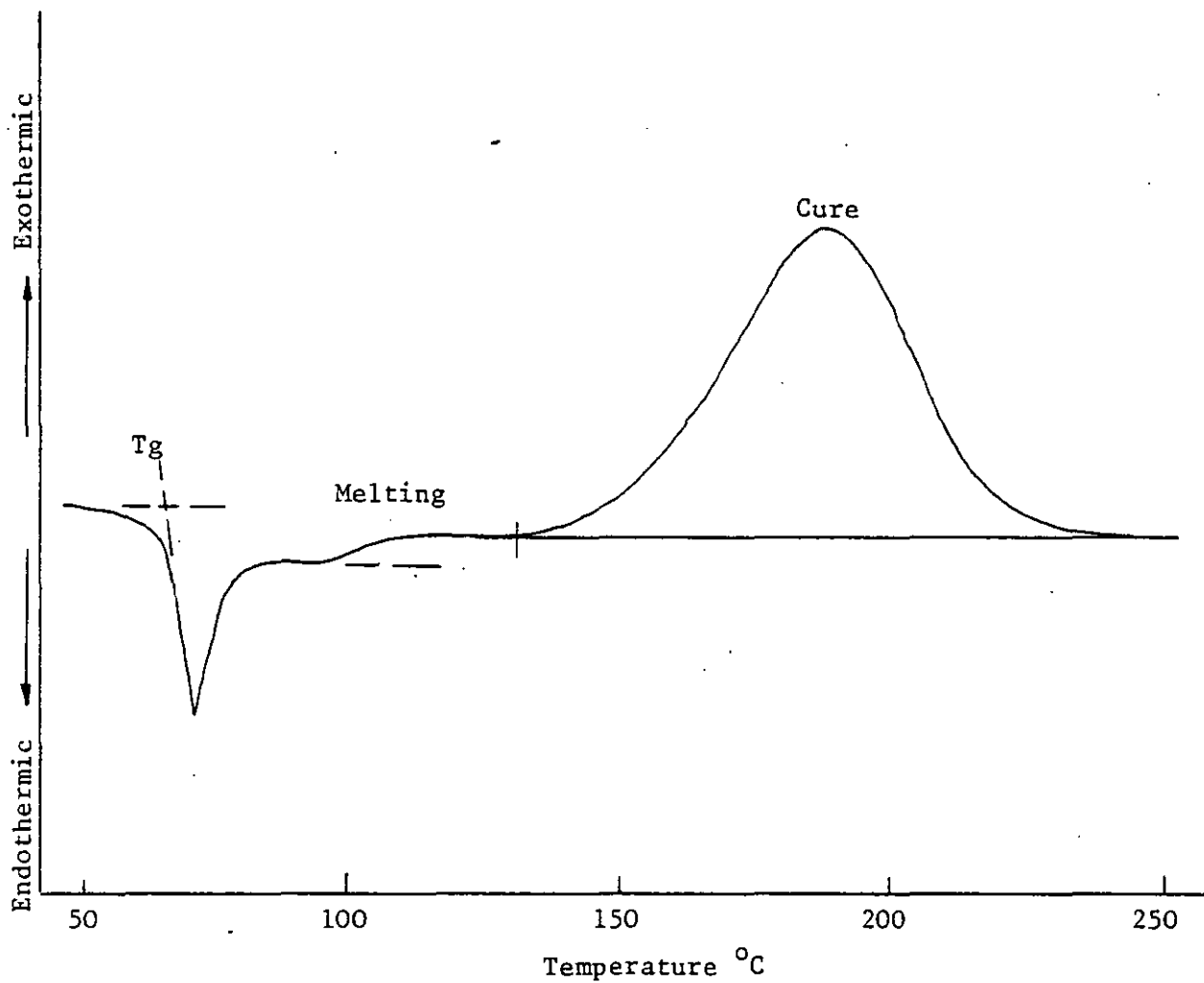
Figure 1.16.   Typical DSC Thermogram for an Epoxy Resin Powder

The sprayed particles tend to follow the lines of the electric field and hence when the voltage on the surface increases due to packing, oncoming charged particles will deposit onto regions of lower thickness. Hence the layers tend to grow fairly uniformly on flat substrates.

However for the case of a can or similar object the shielding effect of the surrounding conductors gives rise to poor penetration. This is known as the Faraday Cage effect, which states that any empty space enclosed within a conductor is free from any field.

Better penetration into a Faraday cage can be obtained by a number of methods:-

i)   reducing turbulence of the transporting air (giving particles higher momentum)

ii)   increasing the particle charge (lowering powder feed rate)

iii)   increasing charging voltage (increases field at opening but also increases particle charge which is more important)

iv)   increase particle size (higher momentum).

All these methods effectively mean that the particle is entering the cage by having higher momentum.

At the edges of a substrate the field lines will tend to be more concentrated and so particles will preferentially deposit here. Therefore better coverage is obtained with powders rather than liquids where the surface tension effects pull liquids away from the edges.

Other problems that arise are the space charge effect and electrode blockage which will effectively quench the corona at the gun. This causes a drop in charging and can even give zero deposition. High humidity can cause electrode blockage, powder particles sticking to the electrode, and also increases the charge decay rate.

1.6 Summary

A brief description of the electrostatic powder coating process has been made. The process, its equipment, powders and operational problems have been discussed. It is evident that there are many factors that contribute to the way in which both dry and fused coatings are formed.

At the electrostatic powder coating conference in London 1968 Prof. D.C. Freshwater said:-

"There is a need for research both applied and fundamental into particle packing and its qualitative effect on the factors outlined.

Until we understand more about relationships involved we shall not be able to make sensible predictions about the desirable properties of powders for powder coatings".

It is the intention of this work to study the effects that particle characteristics and film thickness have on the qualities of the stoved film and also to investigate the way in which single particles pack onto a substrate. In doing this it is hoped that a better understanding of the way in which the EPC process can be controlled will be gained.

CHAPTER 2

A REVIEW OF TEST METHODS

2.1 Introduction

The function of the particle characteristics on the final film produced in powder coating is very complex. There are many properties that can be affected by one or a combination of characteristics in the dry film, formed when spraying, or the conversion of the dry film to the continuous cured film (V.K. Croutch, 1976). Particle size can affect packing porosity, thickness, strength and hence give rise to changes in adhesion, roughness, gloss, corrosion resistance etc. The spraying process and the stoving conditions employed are also very important parameters when considering the effects of any one particular property. The types of effects produced will be briefly discussed later.

With regards to the actual testing of a coating, the tester himself has to decide what standards are required and what the meaning of the results of each test represent (A.E. Claxton, 1975). In practice it is quite possible that experience and knowledge of the coatings themselves with respect to how they should be applied is enough to decide upon a particular coating system, or conditions for a given problem. However, when optimisation and comparison of slight differences is being observed it is often difficult to assess the situation without having some quantitative results for a given set of parameters of the individual coatings. Even then it is necessary to distinguish the relative merits and importance of these differences between the results.

For the problem at hand, one of the greatest difficulties is that a standard commercial powder is being used which is known to give good finishes under normal spraying conditions. To use any chosen size distribution of this formulation of powder and to measure the

properties of the final film means that sensitive tests must be
employed to detect any differences in the measured properties. Hence
a review of the standard test methods is in order and their applic-
ability to the given situation is to be considered. (ASTM D3451,
1975).

Test methods are constantly being devised year by year and
there are many organisations which review and develop tests and
observe their applications to various sections of industry. Two of
these such organisations are the American Society for Testing of
Materials (ASTM) and the British Standards Institution. The main aim
of these organisations is to advise (ASTM Standards, Part 27) on the
possible standard methods for particular purposes which will give
reproducible results within prescribed limits. However, the exact
meaning of these results must also be determined.

The tests on a powder coating can comprise of testing the dry
powder layer and/or the fused film. The following is a brief summary
of the various test methods employed for measuring properties of the
fused film.

2.2   Gloss

It is widely accepted that gloss, besides colour, is one of
the most important features of a coating. There are many methods and
apparatuses for measuring gloss, but one of the most difficult tasks
is to relate from one set of results to another (N.I. Gaynes, 1977).
Gloss in itself is a very complicated property in that changes in
gloss are considered as possible indications of other insufficient
qualities of the film (S. Huey, 1964; H.K. Hammond III, 1974). Indeed
gloss is largely a function of smoothness of surface and hence changes
can mean deterioration of other factors in the film. One of the

simplest tests is to compare the image formed when using the film

surface as a mirror. Here it is very easy to compare one film with

another but proper assessment of the film is very difficult

(B. Svoboda et al, 1962).

Hence the measuring industries have produced many types of

gloss measuring instruments (U. Zorll, 1972; R. Goudie, 1974;

J.A. Fraunhofer(8), 1972c). First of all it is necessary to state

exactly what type of gloss is to be measured since there are several

types of gloss such as specular gloss, sheen, uniform, contrast gloss

etc.

The basic principle of a gloss meter is to shine a beam or

pencil of light onto the surface of the film at a specified angle

(20, 45, 60 or 85°) and the light reflected at this mirror angle is

registered by a photocell.

The light that is received by the photocell will be made up of

the mirror reflected beam and the diffusely reflected light. Hence

two panels might have the same 60° gloss reading but the eye will

notice the haze of the image compared to the distinctness of a

reflected image. Panels with a relatively high degree of haze will

hence have a high gloss rating although the distinctness of image is

low. The 60° gloss meter constantly needs standardising and checking

so that accuracy is maintained.

The correlation between visual impression of gloss and results

obtained with specular gloss meters is not always satisfactory because

of the aforementioned reasons. ASTM D523 and British Standard BS3900

Part D2 (1967) describe how to measure specular gloss. The main

difference between the two methods is that in the UK and Europe the

standard angle of incidence is 45° and in the USA and other parts of

the world it is 60°.

Sheen is the brightness or gloss of a surface observed at very low (grazing) angles of incidence and reflection, normally made at 70° or greater. There are many devices on the market that are available for measuring gloss and sheen, each one of them measuring at a given angle of incidence and so are used for a particular type of finish. For example, Sheen's 85° Specular gloss meter is used for checking gloss within the eggshell to flat classification (or any panel measuring below 30% on the 60° glossmeter). Hence the higher the gloss the smaller the angle of incidence that is used.

A more precise gloss measurement, which takes account of the fine differences between the various types of gloss, must depend on the determination of the distribution of light scattered from the coating surface (J.H. Colling et al., 1968). The goniophotometer is such a device that can show quickly these qualitative differences between samples (M. Tehan et al., 1974; P.S. Quinney et al., 1971).

In this device the sample is illuminated with a parallel beam of light under a fixed angle of incidence and the distribution of the scattered light is measured for a wide range of angles of observation using a photocell. The quantity of scattered light measured can then be plotted against the observed angle (angle of reflection) so giving a gloss curve. It can generally be said that narrow curves indicate high gloss and broad curves indicate low gloss. This curve, also known as the goniophotometric curve, in general yields sufficient detail about the type of gloss and permits the derivation of quantities characterising the latter. It has become common practice to note the maximum and half width of the peak of the goniophotometric curve (T. Kosbahn, 1964; K. Koffman et al., 1966; U. Zorll, 1963).

The comparison of reflectance methods and related methods has been carried out for the study of film surface deterioration due to

weathering (M. Tehan, 1974). Comparisons were made using measurements of the goniophotometric curve, surface average roughness and attenuated total reflection. In comparing these methods it was found that although determining the goniophotometric curve is slow the method is very precise and the results can be represented by various parameters in many different ways.

Since the types of finish produced in the following experiments cannot be known beforehand it is necessary to use such a type of technique, as the goniophotometer, that enables a broad range of gloss measurements to be made. This technique, therefore, gives a broad but precise method of measuring gloss and is therefore well suited to the experiments to be undertaken.

2.3   Film Thickness

Film thickness is now one of the most regarded properties of a powder coating film. The coating industry continually attempts to produce thinner films, with a target of about 25μm, but which still retain all the other film properties, and most important of which is continuity. The shortage of materials and the escalating costs of the same make it increasingly important to maintain all the other properties (corrosion resistance, hiding power etc.) but to decrease film thickness. However, it can be seen that there must be an optimum point when the replacement of protective coatings due to corrosion through thin films outweighs the cost of producing thicker films.

Hence the instrumentation industry has produced a wide range of devices for measuring coating thickness whether the films are on metallic or non-metallic substrates and whether the coatings are

organic or metallic (J. Boxall et al., 1974; J.A. Fraunhofer ,Pt I, 1971).

The types of thickness measuring methods fall into two categories:-

2.3.1 Destructive Methods

Microscopy is one of the most simple and absolute techniques of measuring thickness. A specimen can be mounted in a perspex or resin block and then ground and polished to expose a section of the substrate and coating. Any materials can be used for this technique but problems are encountered with soft or very thin layers.

Another simple method is that of weight change. This is a very quick method but not so accurate. Usually the coating is stripped off the substrate and the surface area of a piece must be accurately found as well as the density of the coating.

A jet of corrosive solution can be directed at the component and the time it takes to penetrate to the substrate is recorded. The coating thickness is then read off calibration charts but again it is difficult to predict accurately because different coatings react at different rates.

The Gardner needle gauge however is simple and relatively accurate for non-conductive coatings on metal substrates. A needle penetrates through the coating until a lamp lights when electrical contact is made with the substrate. A dial gauge is read to obtain the thickness of the film. The Gardner depth gauge is a similar apparatus but uses a scratch to penetrate instead of the needle.

The Elcometer thickness gauge measures film thickness by using a simple dial indicator, such as used in the machinery industry, on a

hole cut in the substrate.

ASTM D1005 uses a similar simple gauge as this but suggests the removal of the film. If the thickness of the substrate is obtained before coating then this device can be used non-destructively.

2.3.2 Non-Destructive Methods

Modern quality control in industry calls for quick, easy to implement, and easily interpretable methods on large, small or odd-shaped items. In general it is required to have fast and reproducible non-destructive methods which can also be automated if desired.

A number of tests rely on the effect on the strength of a magnetic field or eddy current between a probe and substrate caused by the separation due to the coating (T.D. Latter, 1976).

One of the simplest forms of the change in the magnetic field is given in ASTM D1186 where the force that is required to pull off a bar magnet suspended onto a coating and substrate is determined. The force is applied by turning a graduated dial which coils a beryllium copper spiral spring. The thickness is calculated from calibration curves obtained by using reference thickness standards. The more sophisticated forms of this come as the Elcometer Minitector, Mikrotest, Magnetic Gauge, Magne Gauge and Permascope ES8 (Anon, 1976; D.R. Birchenough et al., 1972). These work on the principle that a reduction of flux occurs when the coating is introduced into the magnetic field. It is necessary of course to have the coatings on a magnetic material substrate.

However, in the eddy current method the thickness of electrically non-conducting coatings can be measured on electrically conductive

(usually non-magnetic) substrates. The probe in this case applies a high frequency field which produces eddy currents in the metallic substrate and measurement of the reaction of these currents is made by a test head placed on the surface coating (D. Jarvis, 1974). The strength of the reaction is dependent on the conductivities of the coating and base metal and on the thickness of the coating. Hence test panels must be used for calibration of these instruments. Typical examples are the Permascope EC8 and Eddytector instruments.

Combinations of these two methods are employed in the Twintector and Dualscope so that most coatings and substrates can be catered for (Anon, 1976). Each instrument can operate at a variety of ranges and are simple to use.

The C-Scope can measure very thin coatings on a conducting substrate by using the capacitance method. Here the capacitance formed by a non-conducting coating between a conducting substrate and probe is a measure of the thickness.

In the precious metals industry the Beta-backscatter method is widely used and is dependent on the adsorption of radiation. Beta particles are emitted from an isotope onto the coating and are scattered back in proportion to the coating thickness and atomic number of the coating material and substrate (R. Allen, 1973).

2.4 Roughness

The main method for measuring surface roughness is by the traversing of a stylus across the surface coating. This method has been used since the early 1940's. Vertical movements of the stylus relative to a skid which is used to guide the pick up over the work-piece are converted by a transducer into corresponding changes in an electric current. These changes are then amplified in an electronic

unit and are used to drive a profile recorder and an averaging meter.
The stylus tip is nominally in the order of about 2μm diameter and so
it will enter very fine grooves, and the large taper angle (90°)
enables troughs of up to 100μm to be measured (R.C. Spragg,
D.J. Whitehouse, 1972).

It is generally accepted that the irregularities in the surface
caused by the machine tool used to produce the surface constitute
the roughness whilst the irregularities generated by vibration between
the tool and workpiece are classed as waviness. In the case of powder
coating this can be described as the contribution due to the method of
spraying and the way in which the particles fuse and flow out. The
surfaces are characterised by the mean roughness height which is
expressed as either the Centre-line Average (CLA) in the UK or the
root-mean-square (RMS) in the USA.

A reference length of the surface is taken and a centre line is
drawn through the profile. The sum of all the absolute values of the
height of peaks and depth of troughs from the centre line is
calculated. The sum is then divided by the total number of measurements
within the reference length and the result is expressed in μm or μin.

The simplest method of measuring roughness, however, is to use
a modified dial gauge mounted on a flat base which when placed on the
surface coating will rest on all the peaks. The probe of the device
then projects through into the troughs and grooves in the surface,
hence measuring the surface roughness.

Measurement of surface smoothness is generally performed by
interference microscopy. Variations in the surface smoothness will
cause disturbance of interference fringes (width λ/2) which are
formed on the surface by means of a monochromatic light source
(wavelength λ). The degree of deviation is a measure of roughness.

Very small variations (0.03 - 0.8μm) can be measured by this technique. However, this test is not used as a routine test in industry.

2.5 Environmental and Accelerated Weathering

Since many coatings are on exposed exterior surfaces accelerated testing of coatings is required. This is particularly required in the paint industry where the number of paints that are being developed is considerable. Therefore there is a need for rapid test methods to replace the time-consuming atmospheric exposure methods (M.B. Kilcullen, 1975). For many years coatings were rated in terms of "number of years of Florida exposure" (B. Lindberg, 1975). This type of outdoor weathering test is performed by using racks which face south and which hold the coating materials at angles of 30° or 45° to the horizontal. The racks are situated in industrial atmospheres or close to sea shores etc. so that they are exposed to different climates and atmospheres. These are the simplest form of tests but are very long (in the order of months and years).

The most common indoor accelerated test is the salt spray test (ASTM B117-73). Here the test panels are placed in a fog chamber into which a salt solution (5 parts by weight) is sprayed at a temperature of 35°C. In this case the exposures are made in multiples of 24 hrs. Other forms of this test are a combination of salt and acetic acid which raises the pH from 6.5 - 7.2 to 3.2 - 3.5.

In this test a 'cross' made by a scalpel through the coating to the substrate can be used to examine the corrosion and blistering through undercutting of the coating layer. This is also indicative of the adhesion between the coating and substrate.

ASTM D870 describes the test method of immersion of the panels by 2/3rds into deionised water at 38°C. In each test the sample plate is observed after testing and the amount of surface degradation and corrosion is recorded (I.D. Aitken, 1968).

Humidity cabinets are also used in which water is heated to give the relative humidity in the cabinet above the critical 70% rH level (C.A. Mitton, 1968). The temperature is also altered depending on the cycle of the test that is desired. However, this test is a relatively mild-accelerated test compared to the salt spray test (J.A. Von Fraunhofer, 1972a).

The accelerated weathering apparatus consists of exposing the coated panels to an intermittent distilled water-spray and continual exposure to a high power arc lamp. The plates are sprayed once every 20 mins. The Atlas 'weather-o-meter' model is an example of such an apparatus in which the power of the arc, with or without filters, the dew cycle and humidity can all be independently varied.

In conjunction with weathering tests, whether using simple outdoor environmental or accelerated weathering methods, the optical and surface properties can be observed as the exposure time of the tests is changed. Here the gloss, roughness and adhesion parameters can be monitored with reference to the weathering time.

2.6   Adhesion

One of the most simple adhesion tests is that made by using a fingernail. This tests the strength of all the adhesive forces such as cohesion, Van der Waals, molecular forces etc. but is little use when a quantitative assessment is required (Myers & Long, 1969).

Perhaps the most common adhesion test used today is the cross cut test (BS 3900:E6). This consists of cutting a succession of grooves in the coating through to the substrate, 1 mm apart, and then another set perpendicular to the first ones. The loss of the small squares of the film during the experiment is compared to a classifi-cation test chart which will give a classification of 0-5. This

test can be extended in the form of the tape test which is carried out

by placing masking tape over the cross hatching and then slowly

removing it. (ASTM D3359 (tape test)). This is also compared to

a classification chart. In each case the load applied to the film

(especially in making the grooves) and the cutting edge itself, must

be carefully controlled to ensure reproducibility.

ASTM method D2197 is very similar but uses just parallel

grooves as opposed to cross hatching. In each cut the load applied

must be kept constant. The grooves are made closer and closer

together until the coating between the grooves is torn or lifted

from the substrate.

Cathodic reaction is the basis of the PASS method of determining

adhesion whereby electrolyte is held above a scribed line on the

coating. The amount of coating removed by the reaction in a certain

time is recorded. Adhesion measured in fundamental units of shear or

tensile strength is the feature of the Hesiometer. It is based on

the fact that coating removal is by four mechanisms:- cutting, chipping,

cracking and peeling, and that each of these mechanisms is indicative

of the ratio of the cohesive to interfacial forces (W.J. McGill, 1976).

The coating is removed by use of a fixed cutting tool which assesses

the cutting force in relation to film thickness and can accurately

determine the critical thrust force when the removal mechanism switches

from cohesive to interfacial bond failure. The force required to

remove the coating is recorded against distance and results interpreted.

Another adhesion tester, in the form of an aluminium 'dolly' which is

cemented to the coating, is used to measure the poundage at which the

coating pulls off from the substrate. This is also used for measuring

the strength of adhesives (M.J. Marshall, D.R. Birchenough, 1972).

The adherence of the film depends on many fundamental forces and especially on the ability of the coating fluid to thoroughly wet the surface. Hence the thermodynamics and the kinetics of wetting come into consideration. Therefore, it becomes extremely difficult to devise methods to assess adhesion which accurately determine the influence of these forces and mechanisms without encompassing any other properties.

2.7 Hardness

Hardness indicates a condition which can be described as the ability to resist indentation. This is covered by ASTM D1474 which provides methods for the measuring of the Knupp Hardness No. and the Pfund Hardness No. (S. Spindel, 1973). The test is basically performed by applying a load to the surface of the coating by means of a pyramidal shaped diamond having specified facet angles (R. Allen, 1973). The measurements of the resulting permanent impression are converted to a hardness number. The load is applied slowly (so as not to be an impact) and held for 18 seconds. The length of the impression is then measured with a microscope. The Pfund No. differs in that a quartz or sapphire indentor which has a hemispherical tip of specified diameter is used.

Other types of this apparatus are the Rockwell, Vickers and Brunell hardness tests.

A simpler approach to hardness testing involves scratching the surface with pencils tipped with diamonds where the width of the scratch produced is a measure of the surface hardness (R.R. Blakey, 1977).

Rocking pendulum hardness testers (such as the Sward Hardness

Rocker) give a measure of hardness after a number of oscillations from a fixed initial amplitude.

Pendulum hardness testers are of similar principle in that the hardness is measured by the damping effect due to hysteresis losses of a pendulum fixed to a beam with one or two steel balls placed on the film. The pendulum rests on the surface to be tested and pivots on the two steel balls. The time for the pendulum to decay from some initial amplitude to some final one is a measure of hardness (J.A. Von Fraunhofer(7), 1972b).

A variation of this is the dynamic hardness tester. An indentor tipped with a tungsten carbide hemisphere strikes the test piece with a predetermined kinetic energy. The indentor hence loses energy and the deceleration is detected by a signal to a piezoelectric crystal. The deceleration force (proportional to output voltage) is related to a Vickers hardness value.

2.8 Abrasion and Flexibility

Any coating is subject to wear and hence must function as a protective coating. Mechanical action includes sanding, rubbing, scraping whilst other forms of wear, such as that of the wind, must also be taken into account. There are several wear/abrasion tests available but very few give quantitative and reproducible results. Many use wheels, nylon brushes or rubber cups that impinge on the film and are rotated by a reciprocating motor. The Taber Abraser uses weighted abrasive wheels and the abrasion is measured by either

(a) the number of milligrams of weight lost per 1000 cycles or

(b) the number of cycles to wear down a film to the substrate

(S. Spindel, 1973; D. Jarvis, 1974).

In ASTM method D-968 the resistance to abrasion is measured by the amount of sand required to wear through a thickness of film when the sand falls from a given height onto the panel. A similar device is one in which grit is blown from a tube to the test surface in an enclosed cabinet. Wear is measured in terms of microns of surface thickness removed per 150g of grit.

Flexibility has been defined as the degree to which a dry paint film is able to conform to movement or deformation of its supporting surfaces without cracking or peeling. This, of course, involves adhesion.

Again, as in many tests, thickness of the film plays a very important part in the final results. ASTM D-522 refers to a flexibility test using a mandrel. The panel is bent over a cylindrical mandrel of a specified size (or a conical mandrel) with the coated side up. The panel is then examined for cracks. If no cracks are observed the same procedure is repeated for successively smaller diameters of mandrel (R. Goudie, 1974).

Other methods include the Erickson cupping test where the panel is deformed using a ball or round-head plunger and the maximum deformation before tearing is measured (N.I. Gaynes, 1977).

2.9 Chip or Impact Resistance

There is some interdependence between types of optical properties but in general it is possible to separate the effects and make measurements that can be described as colour, opacity or gloss. Mechanical properties however are almost impossible to isolate, and measurements of hardness, flexibility and adhesion are also highly dependent on the thickness and age of the film, and so can indicate a degree of curing of the film.

Commonly, impact experiments concern the falling of a weight
onto the coating, the type of weight being peculiar to various test
methods. BS 3900:E7 uses a 50 mm diameter steel ball of mass 900g
that falls from an electromagnet held at a height of 3m from the
coating. The procedure is repeated so that the ball falls on the same
spot each time and signs of cracking, flaking and detachment are
recorded.

Other methods vary in the form of the notching of the specimen
due to a weighted pendulum and the way in which the specimen is
clamped. Such tests are the Charpy (both ends clamped) and the IZOD
(only one end clamped) (N.I. Gaynes, 1977).

The chip resistance test is described in ASTM D-3170. Stan-
dardised road gravel is projected at the specimens by compressed air
at a pressure of 70 psi. The effect of temperature on the tests is
very marked and so the panels are kept in a refrigerator at $10^{\circ}F$ until
required for the test. The lower the temperature the more severe the
test. At the end of the run masking tape is pressed over the panel
and then pulled off slowly to remove any loose chips. The panel is
then referred to a set of pictorial standards.

It is worth noting the similarity in the test methods here to
those of abrasion and adhesion, emphasising the fact that isolation
of mechanical properties is extremely difficult.

2.10 Porosity

Porosity can be a major factor where resistance to corrosion is
the main requirement in that pores may provide a site for corrosion
of the substrate.

Large pores may be readily detected by visual inspection or
under low power magnification, but in general micropores tend to be

present which are more difficult to detect.

Porosity tests are designed to detect discontinuities in the coating, such as pores and cracks, after corrosion tests, which try to reproduce in a short time the type of corrosion that might occur over several months, have been carried out. Many tests are based on the corrosion of the substrate that occurs when the coated metal is exposed to an aggressive environment. A test atmosphere of 10% sulphur dioxide and 86% relative humidity can be used in this way and after 24 hours pores are revealed as brown-black spots of corrosion product.

A quicker test for steel substrates is that using a 3% sodium chloride and 0.1% potassium ferricyanide solution. Pores are revealed by blue spots on a solution soaked filter paper. Distilled water at 90-95°C will also produce rust spots in 2-10h and these can be evaluated using ASTM method D-610, using photographic reference standards.

A widely used technique for porosity is the electrographic test. The coating is pressed onto a semi-permeable printing medium (such as absorbant paper) impregnated with electrolyte and made anodic so that the metal substrate dissolves. Metal cations are transferred through the coating discontinuities to the printing medium where they react with a reagent marking the sites of the pores. Complex shapes can often be tested by means of gelatine films impregnated with the detector reagent (N.I. Gaynes, 1977).

Instruments working on the wet sponge principle are simple and inexpensive as low voltage is supplied (M.J. Marshall et al., 1972). A voltage is supplied between the substrate and a wet sponge. The

current is used to activate an audible alarm. An alternative method to this is the Holiday detector which will deal with thicker systems and applies a voltage between 0-20 kV, again giving an alarm when a pore is found (V.K. Croutch, 1976).

The electron microscope can also be used to give an indication of porosity, depending on the type of coating being observed. When used in the transmission mode (i.e. using X-rays as opposed to electrons) absorption will take place within the coating due to the high atomic number elements in the pigments. Pores all the way through to substrate and also air pockets will be shown by a lack of adsorption of the X-rays. A copper target produces the X-rays.

ASTM Method D 1653 describes the measurement of the rate of evaporation of moisture through the coating using a permeability cup. The coating is removed from the substrate and the cup exposes 25 cm^2 of film to high humidity on one side and low humidity on the other. The loss of water is recorded at intervals and used to calculate the rate of movement through the film.

Summary

Brief descriptions have been given on the types of test methods available for assessing the quality of a film. There are very many commercially available pieces of apparatus for carrying out these methods, all differing slightly, and are too numerous to mention. However, the basic principles are described and in most cases the standard method is referenced to either British or American Standards. A list of the tests and related numbers applicable to powder coatings is given in Table 2.1.

One of the most important requirements to consider is the

understanding and significance of the test and its results. It is

obvious that the testing and analysis of data obtained for coating

films is very complex. Each individual must determine which tests to

use and how to interpret the results in order to optimise the

performance of the particular properties of the product. In this

case changes in powder size distribution giving possible increases

in powder deposition must not be employed if physical properties

of the coating are subsequently forfeited. Therefore, a set of

applicable tests have been chosen for the needs of the experimental

investigations being undertaken.

The next chapter fully describes the tests employed and the

results obtained are presented and discussed. The equipment used for

the production of the test coatings is also described.

Table 2.1. Summary of Related British and American Standard Test Methods

British Standards	B.S. 3900
Parts	**Test**
D2	Specular Gloss
E1	Bend Test
E2	Scratch Test
E4	Cupping Test
E5	Pendulum Damping Test
E6	Cross Cut Test
E7	Resistance to Impact (Falling Ball)
E8	" " " (Pendulum Impact)
E9	Bucholz Indentation
E10	Pull off Test for Adhesion
F2	Resistance to Humidity

American Standard Test Methods	
ASTM No's	**Test**
D523	Test for Specular Gloss
D610	Degree of Rusting Evaluation
B117	Salt Spray (Fog) Test
D870	Water Immersion Test
D968	Test for Abrasion Resistance
D1005	Measurement of Film Thickness
D1186	Dry Film Thickness (Magnetic Type Gauge)
D1474	Test for Indentation Hardness
D2197	Test for Adhesion
D3170	Test for Chip Resistance
D3359	Measuring Adhesion by Tape Test
D1653	Permeability Cup Method

EXPERIMENTAL EQUIPMENT AND RESULTS

Contents contd

3.1   Introduction

It is proposed that particle size and particle size distribution might be an important factor in the quality of the final stoved films of an electrostatically sprayed powder coating. In order to investigate this proposition it is necessary to observe the effects of these parameters on various qualities of the final stoved film. This has been achieved by studying the change in film properties of a set of coatings produced using different sized fractions of an epoxy resin powder. By observing the product quality it was hoped that more information on film formation might identify a better size distribution for commercial use.

Although the deposition efficiency of powder of different particle sizes has been investigated in various ways (A. Golovoy, 1973abc) the effect of particle size sprayed on final film coating properties has not been studied. Any advantage gained in deposition efficiency, or in producing thin films, by manipulation of particle size or distribution must not be outweighed by a deterioration in film properties.

Development of a testing program was necessary to quantify any changes in film properties. In the preceeding chapter an outline of the types of test methods available for testing organic type coatings was given. Using this information, a set of test methods were chosen for assessment of films produced for this work. The test methods employed were chosen to encompass a range of physical properties.

It was not the intention of these experiments to measure deposition efficiency of the various classifications of powders used but rather to assess their effects on the final film properties.

To accomplish this, apart from a test procedure, a reproducible method of coating sample plates was required. Using this method the effect of the spraying system was eliminated since coatings were produced and stoved under identical conditions. The equipment and method employed for coating will now be described.

3.2 Spray Equipment

In dealing with powders it is difficult to maintain reproducibility. Slight variations in the way in which a system is operated can produce a variety of different effects. It was therefore necessary to ensure that the experimental methods employed in these experiments, whether in the production of samples or actual testing, were reproducible. Two approaches for the production of sample plates were employed.

3.2.1 Static Gun

Initially a static gun was used for the coating of sample panels. This consisted of a ¾" diameter perspex tube which had six needle electrodes inserted through its walls at the end of the tube. The electrodes were connected to a Bradenburg High Tension supply unit. Powder to the tube was fed by means of a vibratory feeder which poured powder into a funnel. The powder was then drawn into the tube by compressed air passing through a venturi. This compressed air acted as the transport medium for the powder from the gun to the target (see Figure 3.1). A 2" square sample plate was positioned into the back of a supported 10" square aluminium plate and held by an electromagnet. The edges of the small plate were covered by an overlapping brass shim which covered the outside ¼" of each side of the smaller plate. The brass shim was used so as to minimise edge effects (build up of powder near the edges) which give variations in thickness of film. The target plates were earthed and

Figure 3.1. Static Spray Gun and Booth Design
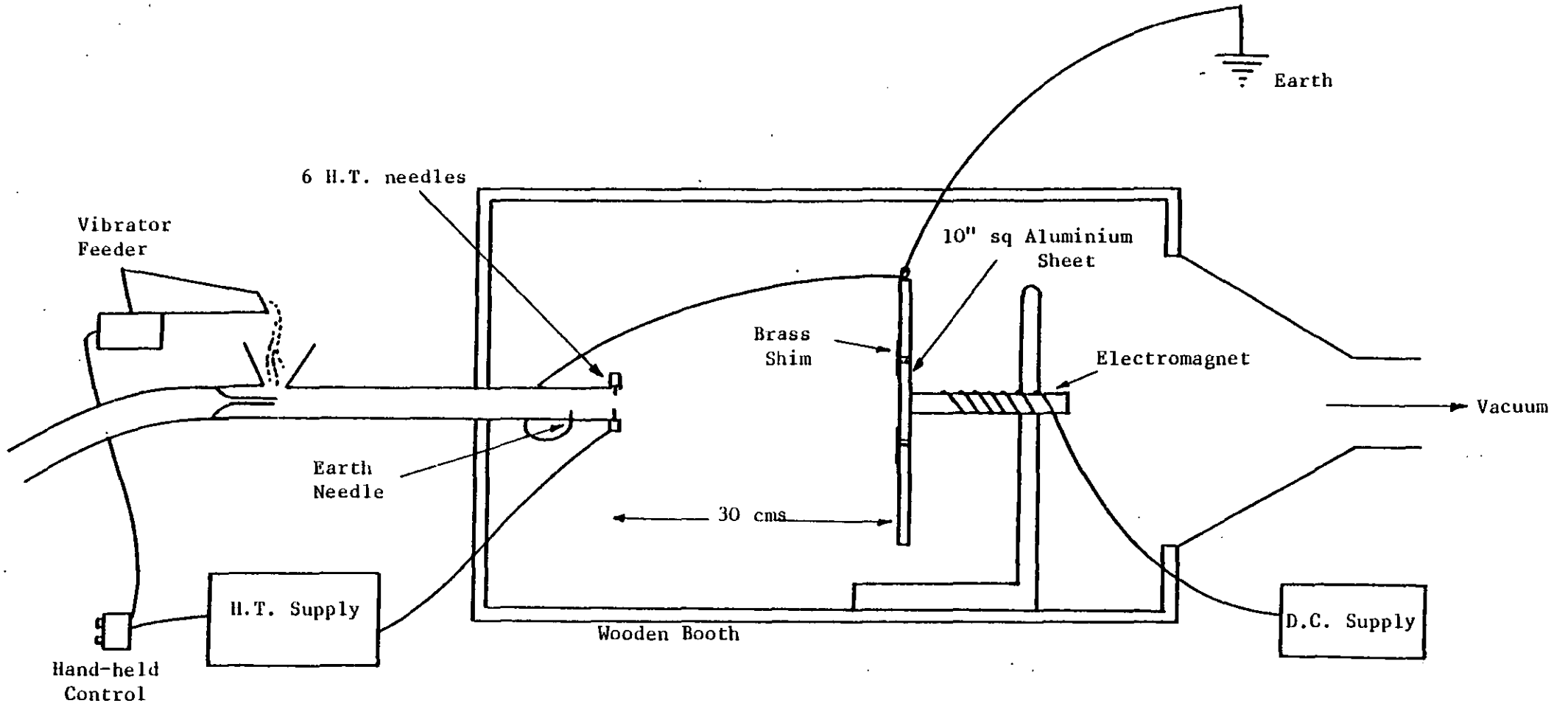
held approximately 30 cms away from the end of the spray gun. The whole assembly was contained in a wooden booth (2' x 3' x 2') of which the door operated a safety microswitch for the HT power supply.

To avoid time between switching on the HT voltage and supply of powder to the gun, and hence the presence of excess ions, the vibratory feeder and voltage were switched by two buttons on a hand held controller. A weighed amount of sample powder was distributed over the vibratory feeder and then the compressed air was supplied to the gun. The feeder and HT voltage were operated by the hand held controller and the sample coated.

The sample plate was carefully removed using the electromagnet which was held by a retort stand. The current supplied to the electro-magnet was switched off and the plate taken by hand to the stoving oven. The coating was cured in a fan assisted electric oven at a typical temperature of $180^{\circ}C$ for 15 mins.

A set of coatings were produced by this method using size fractions of a commercially used powder. These size fractions were <10μm, 10-20μm, 20-30μm, 30-40μm, 40-50μm and +50μm. The commercial powder itself was also used. Each set of samples were produced in the same manner and stoved under identical conditions.

3.2.2 Problems Encountered

The apparatus described was that achieved after problems of powder feed, sample handling, HT control etc had been overcome. It was found that this arrangement gave very reproducible coatings for a given powder when operated under similar conditions. However, problems persisted with this static gun when trying to control film thickness.

When spraying different sized powders at identical air flowrates it was observed that the area covered by the spray gun varied to a very large extent i.e. 'splaying-out'. Therefore, different amounts of powder for each size fractionated powder were required to produce films of the same thickness. By spraying a powder with a wide size distribution it was evident that size distribution effects took place across the 10" sample plate. Indeed, in an experiment where three different coloured powders were used to represent three size ranges (<20, 20-40 & >40μm), rings of different colours were produced. The largest sizes being in the centre and the fines at the outside.

These effects gave concern regarding the comparison of coated samples of the different sized fractions. It also meant that the production of a set of coatings of similar thickness was both very labourious and difficult. A new method was required in which a large number of samples could be produced using a non-static gun for a range of film thicknesses.

3.2.3 Commercial Spray Equipment

To combat the aforementioned problems a commercial type spray booth was kindly donated by Aerostyle Ltd. This consisted of a metal booth with both side and front opening hinged doors and a powder extract section at the floor of the booth. A bag filter unit was connected at the base of the booth to remove overspray. A spray gun powder supply unit and HT unit was supplied by Tam-Sames et Cie. The powder supply unit consisted of a fluidised bed hopper with an air jet ejection system used to supply an air-powder mixture to the spray gun. A third air control was available to control a supply of air to the gun nozzle which varied the spray cloud pattern.

Diagrams of the powder feed hopper and spray gun nozzle are shown in Figures 3.2 and 3.3. Plate 3.1 shows the spray booth and spraying equipment. Plate 3.2 gives a close up view of the spray gun, powder supply unit and high tension voltage supply unit used.

3.2.4 Experimental Method

In order to produce a set of coatings for testing, the following method was employed. A 10" x 8" steel plate was covered with twenty 2" x 2" thin steel plates (1/16" thick) and then placed on a U shaped electromagnet. After switching on the DC supply to the electromagnet the assembly was suspended from a metal bar inside the spray booth, with the plates facing towards the opened door on the long side (see plate 3.1). The HT unit was set to supply 60 kV when the spray gun trigger was depressed. The air flow rate to the fluidised bed was increased to fluidise the 2/3 rds full hopper of epoxy resin powder (commercial type or size fractioned). The air to the jet for powder supply and to the gun nozzle were preset to suitable positions. The spray gun trigger being depressed, powder was sprayed towards the target for a suitable length of time to produce a relatively uniform coating on the plates. The spray system was immobilised and the coated plates, still held by the electro-magnet, carefully removed and placed in a horizontal position. The electromagnet was then switched off and the base plate together with the coated sample plates were placed in a stoving oven. The coatings were stoved for 15 minutes at 180°C, as per the powder manufacturers recommendations.

Figure 3.2. Spray Gun Powder Feed Hopper

Powder +
Air Mixture

Secondary Air
to Spray Gun

Air for Venturi

Air Control
Valves

Fluidised
Bed

Distributor
Plate

Fluidising
Air

Figure 3.3. Spray Gun Head

H.T. Electrode

Secondary
Air

H.T. Cable

to
Trigger

Powder + Air Mixture

Secondary
Air

Deflector
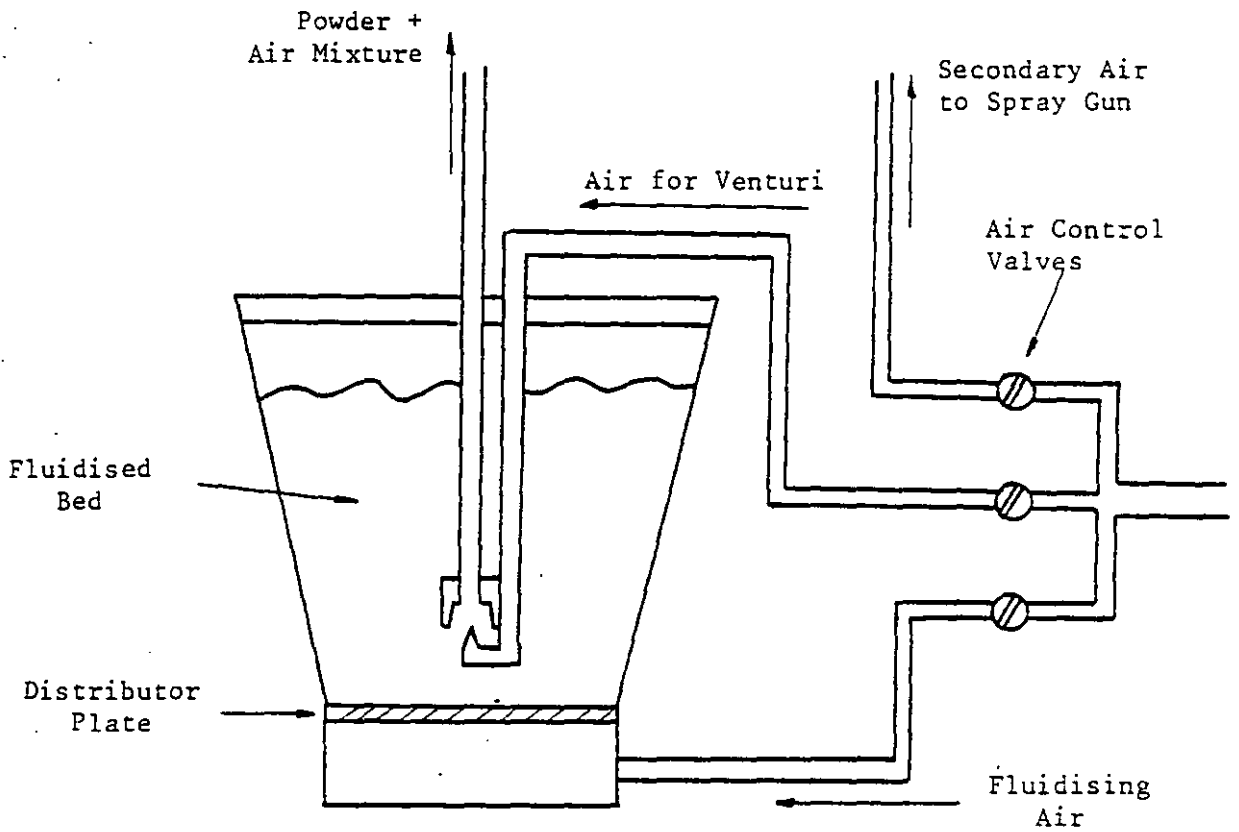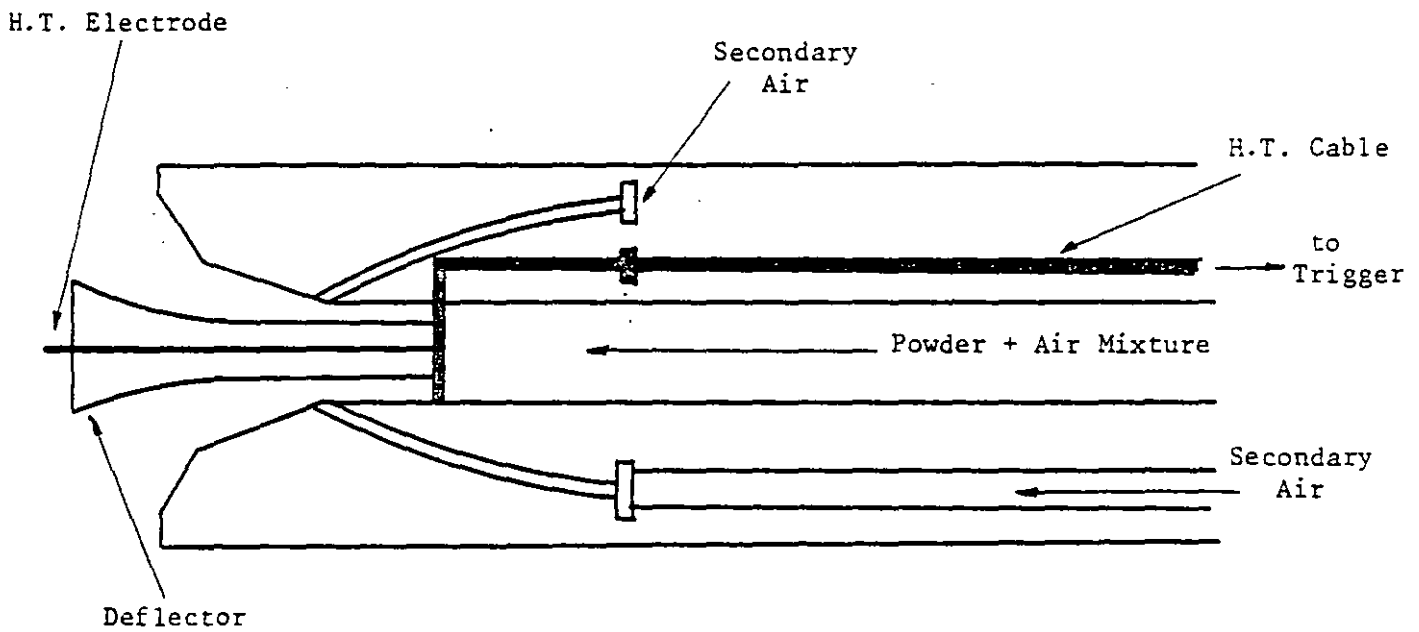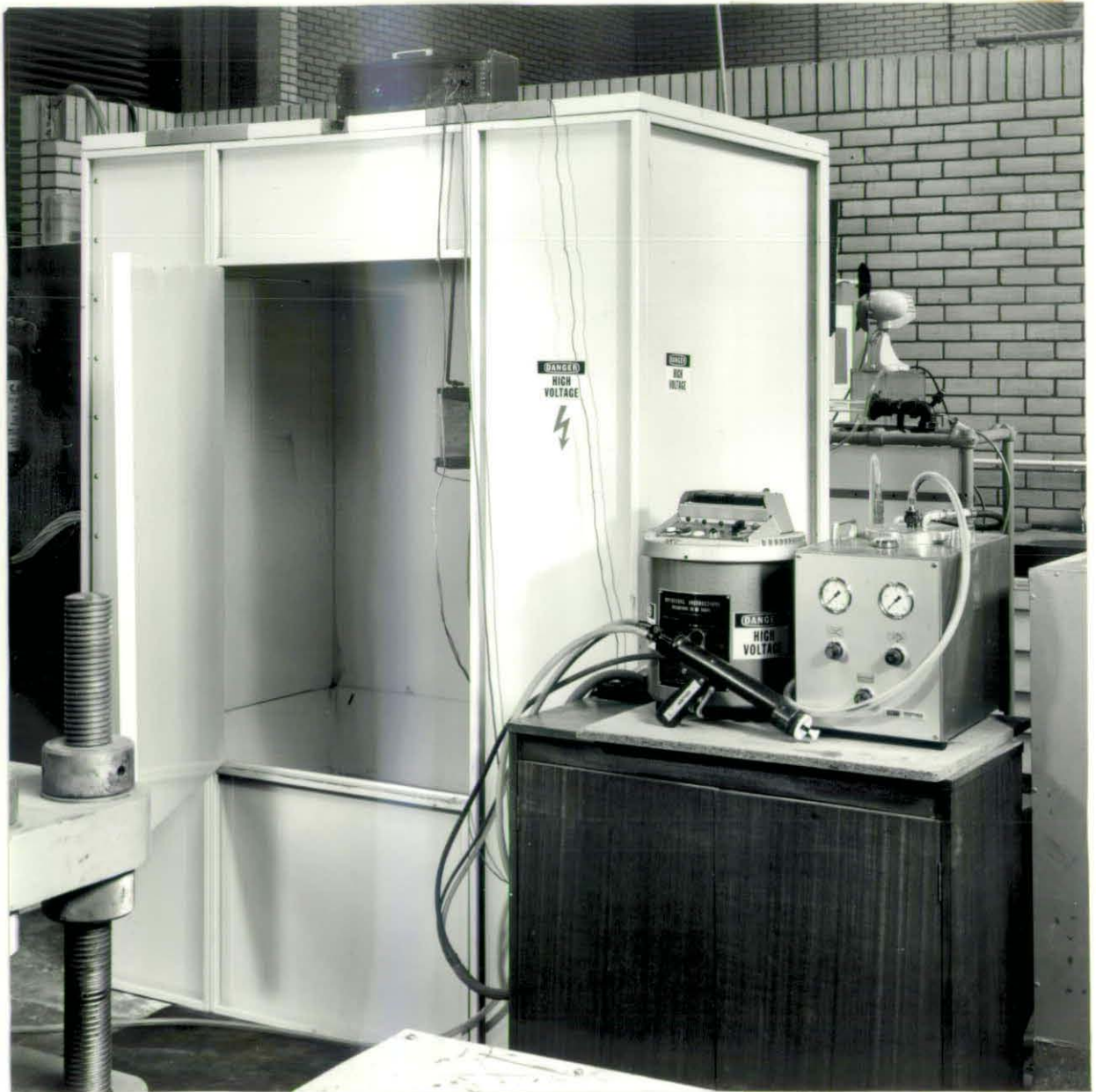
Plate 3.1. Electrostatic Spray Booth and Equipment

Plate 3.2.   Spray gun, H.T. Supply Unit and Powder Feed Unit

This process was repeated for a given sample of powder until a sufficient number of coatings were obtained for further experiments and tests. The only change that was made was in the type of powder used.

A standard commercial epoxy resin powder as supplied by ICI Paints Division, Slough was used as the basis for the experiments. The powder manufacturers confirmed that this powder was representative of the type of epoxy powders currently used in the coating industry. The pigmentation was white and the powder had a size distribution as shown in Figure 3.4. Electron micrographs of this powder are shown in Plates 3.3 and 3.4. It can be seen that the particles are very irregular in shape. The powder was classified into 6 size ranges using an Alpine Zig-Zag air classifier. The ranges were <10μm, 10-20μm, 20-30μm, 30-40μm, 40-50μm and >50μm. The unclassified commercial powder together with the 6 classified fractions were used to produce sample coatings.

Since it was not possible to control the thickness of the final coatings a procedure was adopted in which the thickness sprayed was controlled by eye. The plates were subsequently measured after stoving by the method described later. With experience a required thickness range could be obtained but final classification was made only after measurement.

On completion of the production of coatings a collection of over 2500 sample plates were obtained for the seven different powder grades and these were then selected into groups of film thickness ranges. Poor quality coatings (i.e. those that had been disturbed in some manner) were not included and eventually approximately 10 of each thickness range were kept for further testing.

Figure 3.4. Size Distribution of White Epoxy Powder

Coulter Counter Analysis
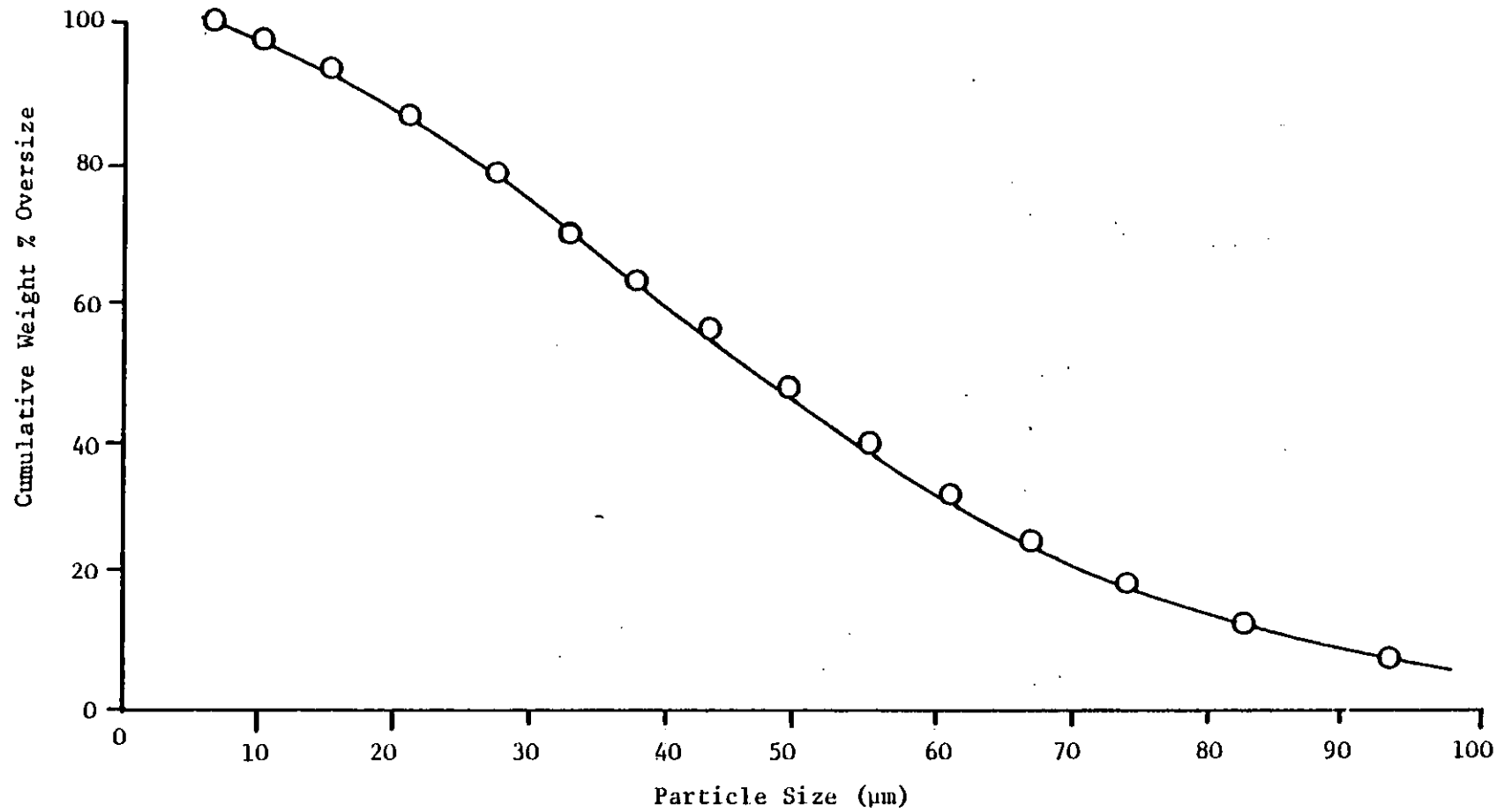
Plate 3.3.   SEM Photograph of Epoxy Resin Powder (x 1000)

Plate 3.4.   SEM Photograph of Epoxy Resin Powder (x 3000)

This spray gun allowed more control of the production of coatings. It was not static and therefore problems of size segregation across the plate were not encountered. This system allowed for faster production of samples and by coating and stoving twenty at one time the risk of disturbing the powder layers by movement was minimised. Edge effects were also reduced since each plate was placed flush against at least two others.

Although movement of the gun and time of spraying was arbitrary, each plate was individually measured for thickness and hence classified into groups.

3.2.5 Pretreatment of Sample Plates

Strips of greased mild steel plate, 2 feet long by 2" wide and 1/16" thick were employed. These strips were guillotined into the 2" square sample plate sizes. It was checked that this method of cutting did not cause any appreciable distortion of the edges of the plates to ensure that they would lie flat on the large sample holding plate. A quantity of plates were cut prior to coating. The plates were degreased using carbon tetrachloride and dried using tissues. Each plate was dedusted, to remove any debris from the tissues, using a compressed air supply. The plates were then stored in a desiccator ready for coating.

Although general pretreatment methods have been described earlier, it was decided that in this case pretreatment was not required. This decision was based on a number of reasons. Firstly, the mild steel plating was particularly chosen for its quality and that it had been greased to protect it from any possibility of corrosion. In these coating trials the samples were not left for any

significant time in either an ungreased state or in a corrosive atmosphere. Secondly, various methods of pretreatment including phosphating and zinc coating were tried and compared using the salt spray test (described later) but very little difference was found using these materials.

3.3 Testing Methods and Equipment

As previously described, the range of tests available to test a particular coating on a substrate is very wide and can be applied to all types of materials and substrates. It is important to find a series of tests that give quantitative results for the properties of a coating.

After careful consideration of the properties that should be investigated, to indicate the effects of particle size on the final film properties of the coating, the following tests have been employed:-

1) Film Thickness

2) Gloss Test including (a) Specular Gloss

(b) Gloss Factor

(c) Scatter

3) Roughness including (a) Average Roughness

(b) Roughness Wavelength

4) Adhesion

5) Corrosion Resistance

6) Porosity

The problems encountered in determining the significance of the results from these types of tests are enhanced by the fact that commercially used powders are being tested, and as such are known to give generally satisfactory results.

Therefore it was decided to consider the adhesion and corrosion tests in preference to all the other mechanical tests that could be employed (i.e. impact, scratch, chipping etc). These tests were used as 'pass/fail' tests and supplied valuable information as to whether the stoving cycle had been effectively carried out.

The test method and equipment used in each case will now be described and results will be presented and discussed with each test in turn.

3.4   Thickness Measurement

The measurement of thickness is an important factor in this work as it enables any effect on a physical property to be observed for both changes in type of powder sprayed and film thickness. This will give guidelines for the optimal film thickness with regards economy and retaining advantages of physical characteristics.

The 'Elcometer Minitector' was employed for the measurement of film thickness (see Plate 3.5).

A probe is placed on the coated plates and the thickness of the organic coating measured directly from the scale on the meter. This device can measure coatings on either non-ferric or ferric substrates by the use of eddy currents. A varying magnetic field induces eddy currents in the conducting substrate material. The change in the apparent impedance of the probe coil that induces the eddy currents is monitored. Changes in the current flow in the coil, produced by various spacings of it from the metal substrate, are an indication of the thickness of the coating.

3.4.1   Experimental Method

The correct setting on the gauge is selected for the thickness of film expected and the type of metal base being used. The probe is placed on a piece of the uncoated substrate and the

Plate 3.5. Elcometer Thickness Measuring Instrument

device zeroed. The device was calibrated by placing a set of film

standards between the probe and the metal plate. The standards

covered the thickness range of interest and the calibration knob

was used to obtain the correct setting.

After every plate had been measured the various size fractions

were sorted onto plates in different thickness ranges, primarily

in 5μm ranges. The best ten sample plates in each film thickness

range were used for further experiments. This assessment was based

on visual observation for evenness of film etc. For the seven

different types of powder samples sprayed a collection of approximately

1000 plates out of the originally measured 2500 were kept.

3.4.2 Experimental Results

The five measurements for each film were taken

approximately ¼" in from each corner and also in the centre of the

coating. The average thickness for the coating was calculated and

recorded against the designated sample number. Table 3.1 shows a

summary of all the thickness ranges that have been used, the

number of plates that were retained in each range, and the average

thickness of the plates in each group. This is done for all seven

powders used in the experiments. This provides a comprehensive

set of samples for the testing of other physical properties.

3.5   Gloss Test

3.5.1   Specular Gloss

Initially the gloss of the coatings was to be assessed

by measurement of the specular gloss only. A Brice Phoenix Light-

scattering photometer would be used to shine a parallel beam of

light at a fixed angle of incidence onto the substrate. The reflected

light, at an angle of reflection equal to the angle of incidence, is

Table 3.1. Distribution of Sample Plates in Film Thickness Groups

Range No.	Commercial			<10µm			10–20µm			20–30µm			30–40µm			40–50µm			+50µm		
	Range µm	No. in Range	Ave.	Range µm	No. in Range	Ave.	Range µm	No. in Range	Ave.	Range µm	No. in Range	Ave.	Range µm	No. in Range	Ave.	Range µm	No. in Range	Ave.	Range µm	No. in Range	Ave.
1	20–24	10	22	10–19	10	16	10–19	10	18	20–29	10	27	20–29	3	29	30–34	9	33	30–39	5	38
2	25–29	10	27	20–24	10	22	20–24	10	22	30–34	10	32	30–34	10	33	35–39	10	37	40–44	10	43
3	30–34	10	33	25–29	10	28	25–29	10	27	35–39	10	37	34–39	10	37	40–44	10	42	45–49	10	47
4	35–39	10	37	30–34	10	32	30–34	10	32	40–44	10	42	40–44	10	42	45–49	10	47	50–54	8	52
5	40–44	10	42	34–39	10	37	35–39	10	37	45–49	10	48	45–49	10	48	50–54	10	52	55–5↓	10	57
6	45–49	10	47	40–49	9	44	40–44	10	42	50–54	10	52	50–54	10	52	55–59	10	57	60–64	10	62
7	50–54	10	52	50–59	4	56	45–49	6	46	55–59	10	57	55–59	10	57	60–69	10	63	65–69	10	67
8	55–59	7	56	60–64	5	62	50–59	6	56	60–64	9	62	60–64	6	62	70–79	3	75	70–74	9	71
9	60–64	10	62	65–69	7	67	60–69	10	62	65–69	10	62	65–69	10	67	80–89	7	84	75–79	7	76
10	65–69	10	67	70–79	7	74				70–74	10	71	70–74	7	72	90–94	5	92	80–84	6	81
11	70–79	7	74	80–89	8	84				75–79	8	77	75–79	5	77	95–99	9	97	85–89	7	87
12	80–89	6	85	90+	9	95				80–90	10	84	80–84	7	82	100–110	5	106	90–94	10	92
13	90+	6	100							90+	5	100	85–90	9	87	111+	10	135	95–99	5	97
14													90–99	8	93				100–110	9	104
15													100+	4	102				+110	6	122

then measured by means of a photocell and measured as millivolts.

This method proved to be very inaccurate because alignment of collimator, photocell and sample plate on the staging proved to be of great importance and difficult. A slight deviation in the comparison of angles of incidence and reflection gave very large errors in the specular gloss measurement.

3.5.2 Goniophotometric Curve

If the angle of reflection (position of photocell) is changed and the reflected light measured for various positions, a graph can be plotted of intensity of reflected light (mV) against angle of reflection, for a given angle of incidence. This is called a goniophotometric curve. From this curve (shown in Figure 3.5) a value of the specular gloss can be calculated as the height of the peak at angle of reflection equal to angle of incidence. In this case a small offset in the setting up of the sample plate can be seen as a movement of the peak from this angle and can hence be compensated for. However, this curve also describes the way in which the incident light is scattered at various angles and from the measurements of specular gloss and scatter a quantity called the 'gloss-factor' can be obtained (as defined in the figure).

The plotting of these curves for each sample (measuring reflectance at various angles) is very laborious and so the photocell mounting stage was motorised and by use of other electrical equipment the goniophotometric curve was plotted directly onto a chart recorder.
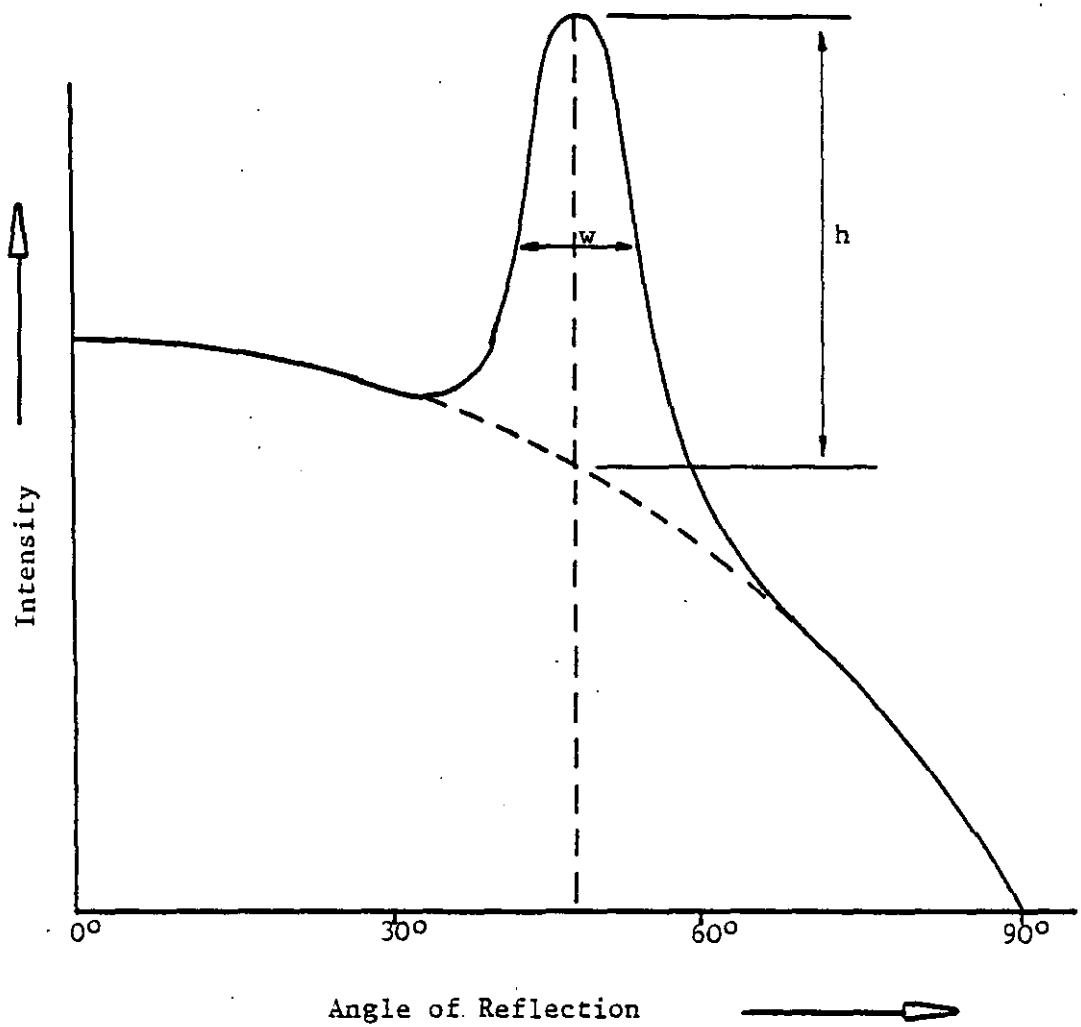
Gloss factor,   GF $= \dfrac{h}{w}$

where

    h = peak height
    w = width of peak at half peak height

Figure 3.5. Goniophotometric Curve Showing Gloss Factor Calculation

3.5.3 Instrumentation

The Brice Phoenix light scattering photometer is generally used for determining particle size distributions, optical properties of liquids etc by measuring turbidity and scatter of light through a light scattering cell. For the goniophotometric studies the photometer was modified in several ways.

The optical features of the system are shown in Figure 3.6. (P.P.I., 1963). The light beam from the lamp (L) passes through a monochromatic filter (F1) and into the shutter collimating tube (C1). The lamp is a high pressure mercury lamp, 85 watts. The intensity of the light beam is controlled by the shutter (S) and a set of neutral filters (F2). After passing through an achromatic lens (L1) and a plano-cylindrical lens (L2) light is emitted from the primary collimating tube (C2) out of the diaphragm (D2). The light impinges on the sample plate which is held on a modified mounting table (G). The light is then transmitted, reflected or scattered, and is measured by the photocell (PT). The specimen table is calibrated (Figure 3.7) so that the mounted plate can be rotated through 360°. It is secured by allen screws at the position required. The holder ensures that the front surface of the coating is in the same relative position to the beam and photocell each time, regardless of the coating thickness.

The photocell can be rotated by 270° by the electric motor which is connected to the graduated disc assembly (D) by means of a rubber wheel. This motor turns the photocell at a constant angular speed so that the time of traverse is proportional to the

Figure 3.6. Optical Features of the Brice Phoenix Light Scattering Photometer
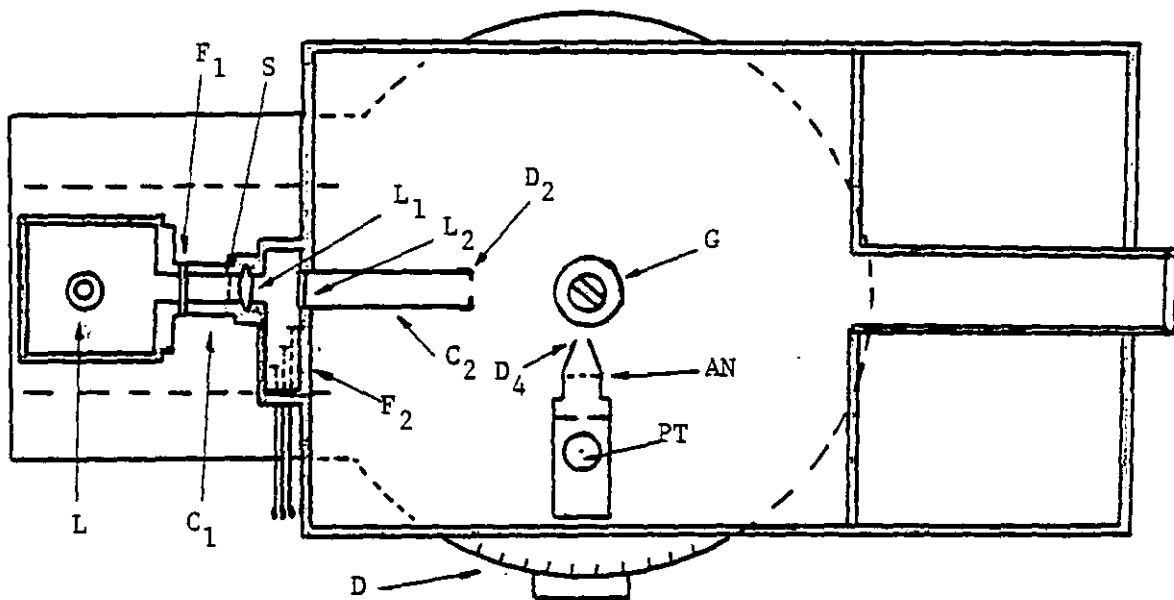
Figure 3.7. Modified Mounting Table
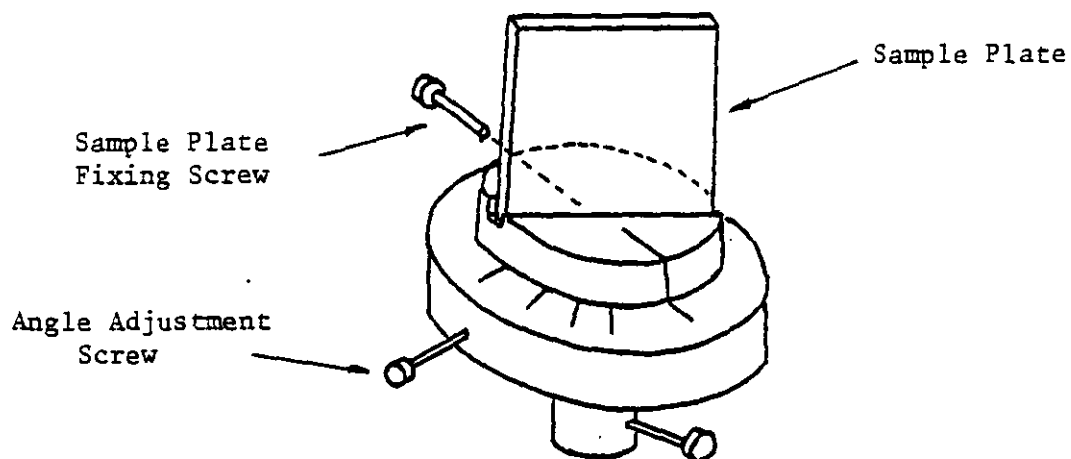
angle of reflection. The photocell can be traversed in either direction and has a removable analyser and variable slit aperture (AN and D4 respectively). All parts inside the scattering compartment were painted matt black, including the mounting table, so that no stray light reflection was considered.

The output from the photocell is fed to a chart recorder so that the goniophotometric curve, for a given angle of incidence, can be directly plotted. The format of this curve has been previously shown. It can be seen that the curve occurs after a threshold level. In order to increase the accuracy of this method a low power supply unit (PSU), used to provide a back e.m.f., and voltmeter are incorporated; the reasons for this are discussed in the experimental method. The complete circuit diagram is given in Figure 3.8. Plate 3.6 shows all the equipment used.

By comparing samples of different finishes i.e. high, medium and low (matt) gloss, the changes in the shape of the goniophotometric curves can be clearly seen (Figure 3.9). For samples of high gloss the curve is tall and narrow and for low gloss it is short and wide. From these curves the gloss factor, which takes into account both these properties of the curve, can be obtained. The gloss factor has been defined in Figure 3.5.

3.5.4 Experimental Method

The mercury lamp was given at least half an hour to warm up so that the emitted light intensity remained constant. The photocell is traversed so that it is directly opposite the beam of light (exact position is when the output from the photocell is a maximum). The output is registered on a D.V.M. and the intensity of light is

Motor Driven
Goniophotometer

Digital
Voltmeter

Power
Supply Unit

Back E.M.F.

Chart
Recorder

Digital
Voltmeter

Recorded Output
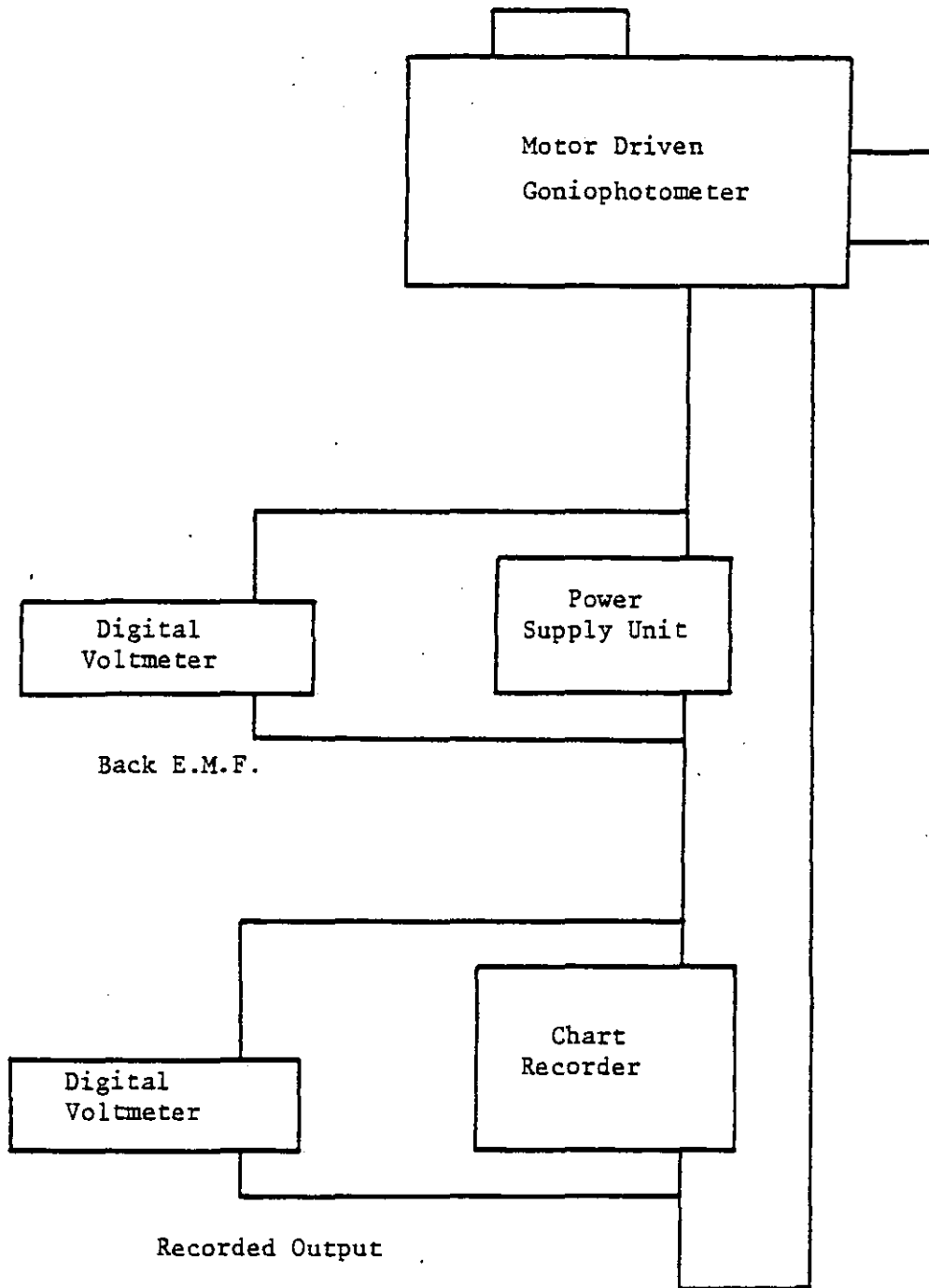
Figure 3.8. Gloss Test Electrical Equipment Arrangement
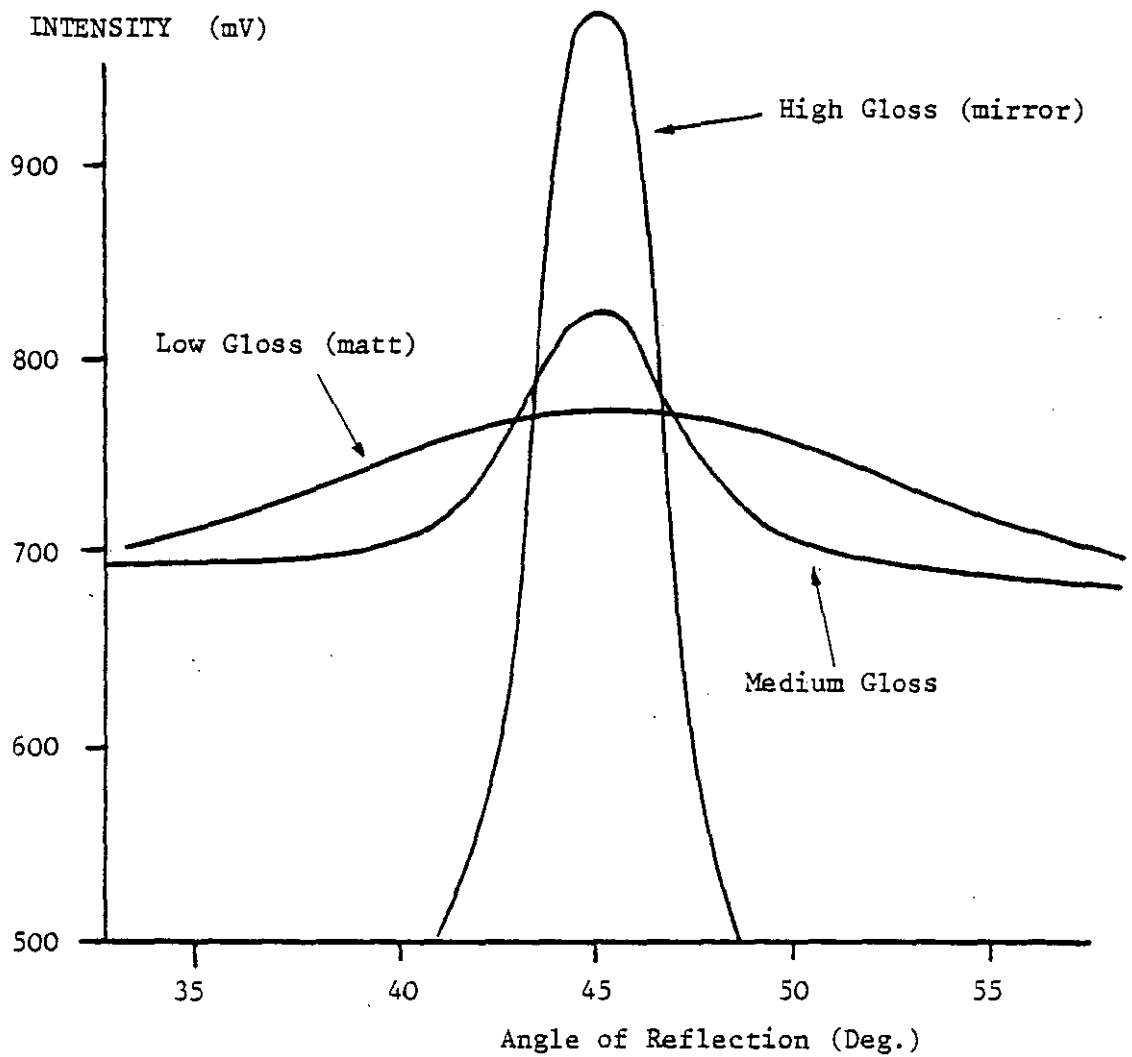
Figure 3.9. Goniophotometric Curves for High, Medium
and Low Gloss Specimens
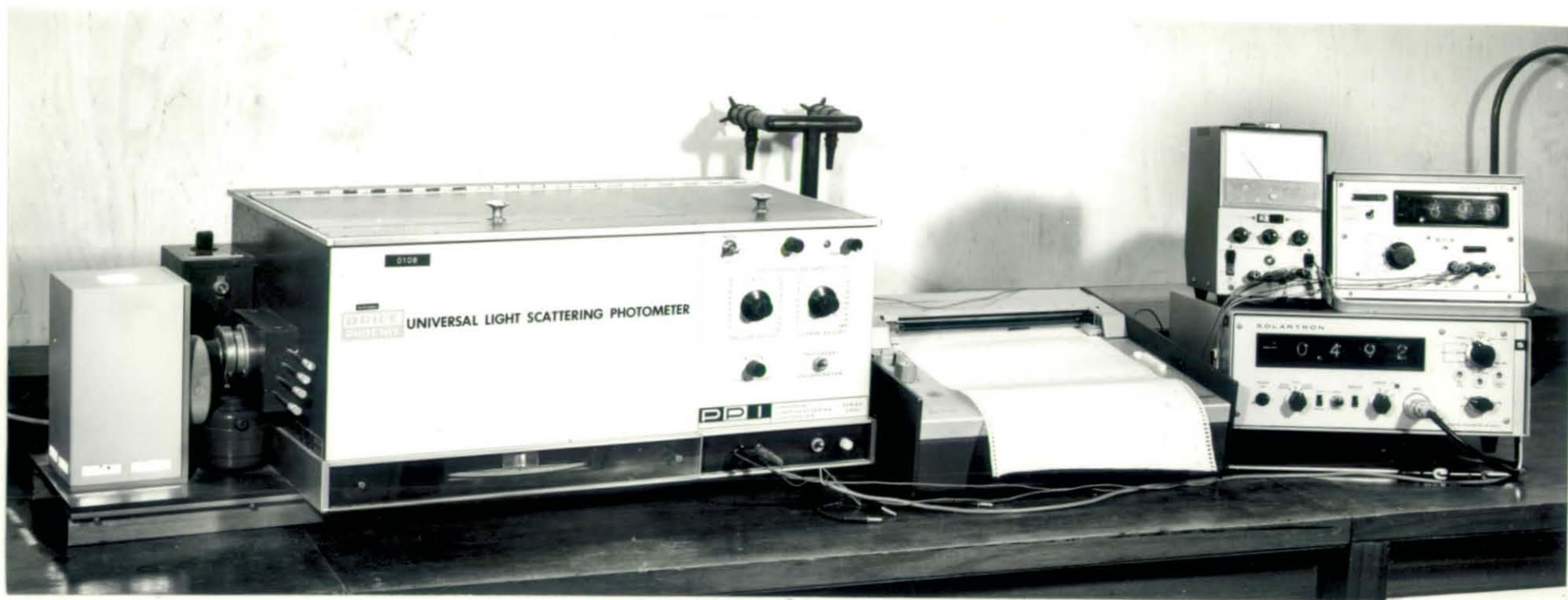
Plate 3.6. Brice Phoenix Light Scattering Photometer and Related Equipment used for Gloss Measurement

adjusted by means of the coarse, medium or fine adjustment knobs until the output is 1.000 Volts.

The sample is then placed in the mounting table at the required angle of incidence to the light beam and the photocell is traversed from 0-90°. The time taken for the photocell to do this was measured ten times and compared to the paper feed rate on the chart recorder. The x axis was calibrated in terms of angle of reflection, degrees/cm. The y axis was calibrated in mV/cm by comparison with the D.V.M.

Figure 3.10(a) shows a recorder output. By using a back e.m.f. a curve of the type shown in Figure 3.10(b) is obtained and hence gives more accurate results. A back e.m.f. of 0.650V was typically used.

Five sample plates from each thickness range of each powder type were tested using this technique. The plates were positioned in the mounting table and placed in the machine. The photocell was traversed through the appropriate angles of reflection from the plate and the goniophotometric curve obtained on the chart recorder. Each curve was analysed and the height of the peak (above the threshold value) and the peak width at half peak height were recorded in terms of centimetres from the recorder paper. These figures were then converted to mV and degrees and the gloss factor was calculated for each curve by ratioing the two measured parameters as described earlier. By initially setting the response of the photocell (to the incident light on the plate) as an output of 1.00V the measured peak height represents the percentage change in intensity of light reflected from the plate.
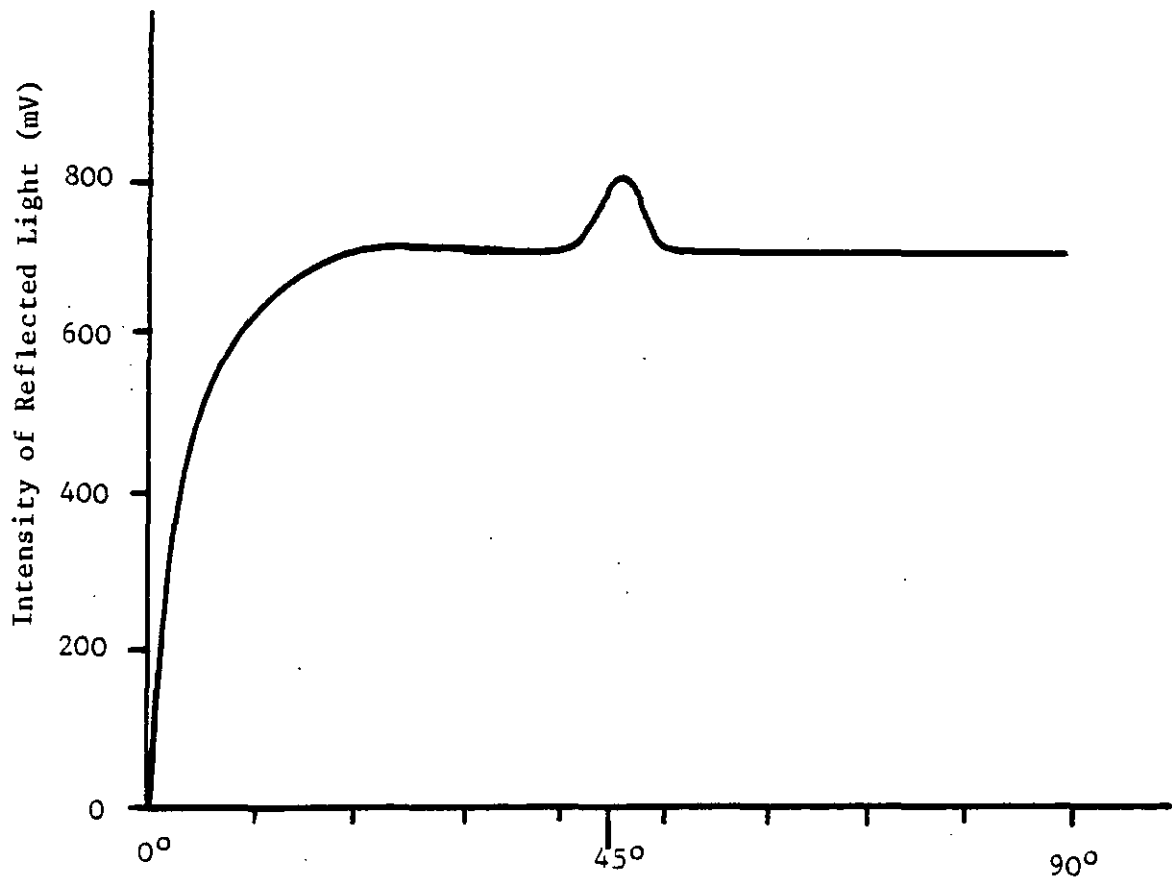
Figure 3.10(a) and (b). Typical chart recorder outputs from goniophotometer with (a) no back e.m.f. (above) and (b) with back e.m.f. of 650 mV
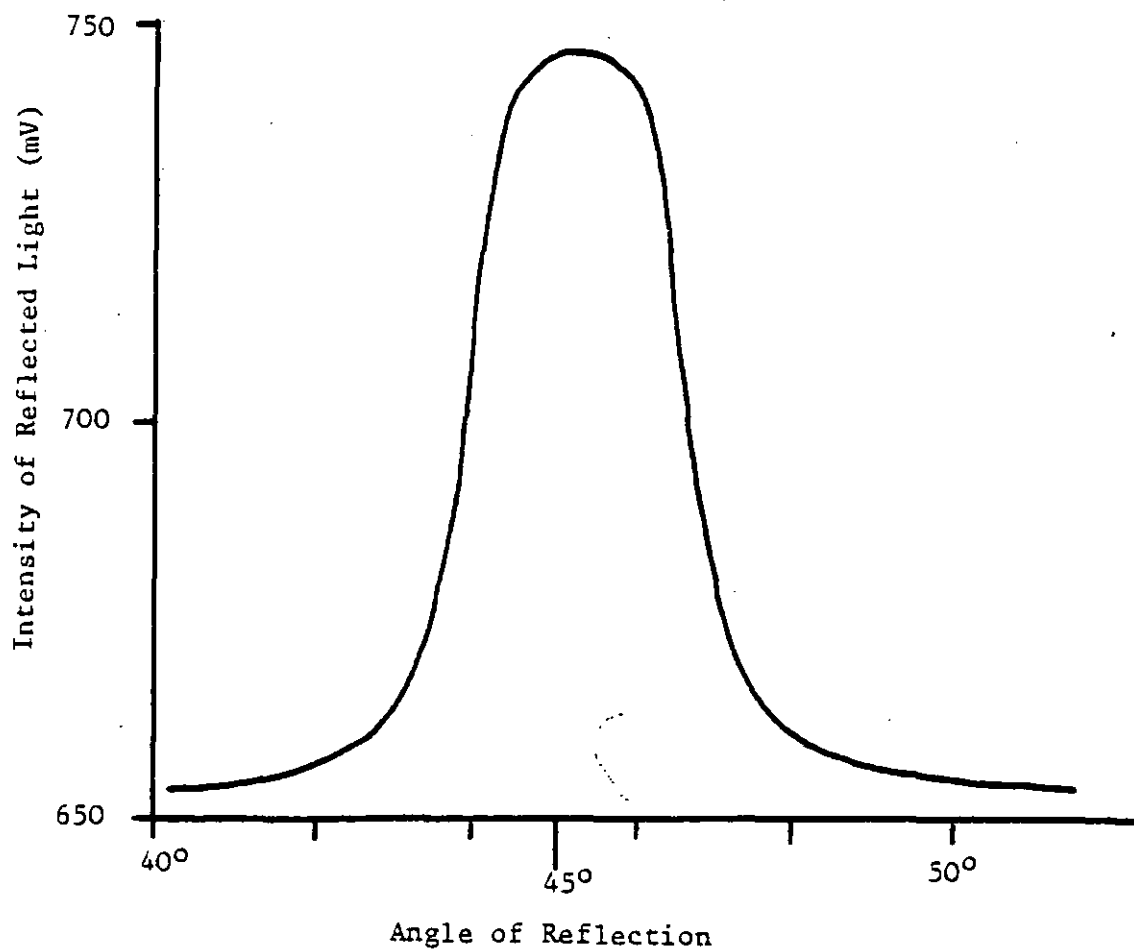
3.5.5. Results and Discussion

The five measurements for each thickness range were averaged and the standard deviations and probable errors calculated. These results are presented in Tables A1 to A7 of appendix A. Each table represents results of the three measured and calculated parameters for each different powder type used. The film thicknesses quoted are the averages for the film thickness range that the samples used come from. The results are plotted in terms of film thickness versus gloss measurement quantity in Figures A1 to A21.

In general it can be seen from the results tables that the standard deviations of each batch of five measurements are less than 10% and this gives an indication of the reproducibility of both the test and the coating method.

The graphs indicate trends in terms of the gloss measurement with increasing film thickness for either the commercial powder or one of its size fractions. There is generally a large spread of results from any possible trend in most of the graphs and so for comparison purposes a linear regression fit has been calculated for each set of data. This is used to approximately represent the trends in the results but is not meant as a correlation. The data used for these fits are given in Table A8 for each of the powder types and measured parameters.

The results of this analysis have been plotted for each of the powder types in Figures 3.11, 3.12 and 3.13 for changes in thickness with gloss factor, peak height and peak width respectively. From these graphs it is possible to compare results of the various powders

Figure 3.11. Gloss Factor vs. Film Thickness for Different Powders Sprayed

Linear Regression Fits
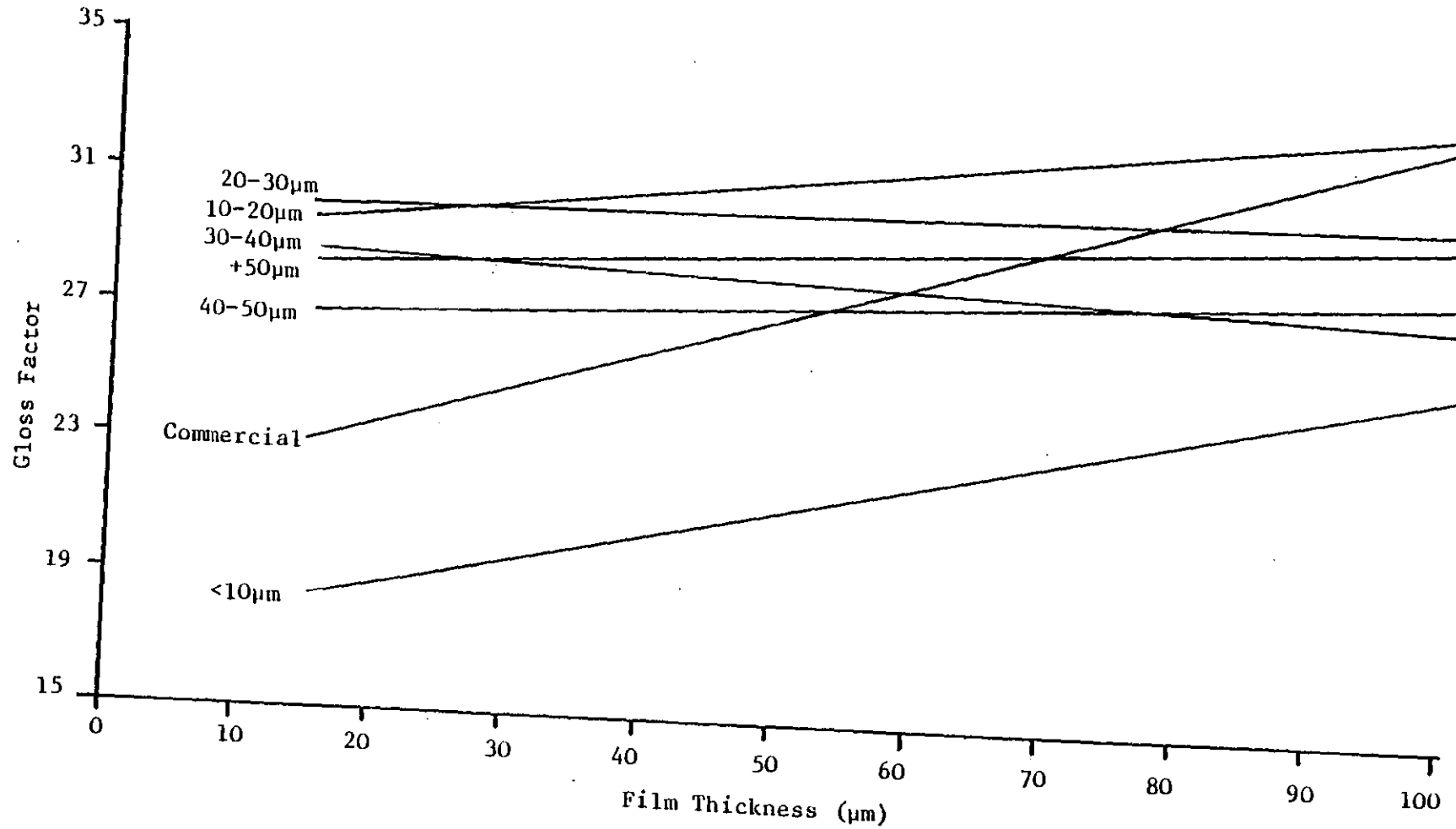
Figure 3.12. Peak Height vs. Film Thickness for Different Powders Sprayed

Linear Regression Fits
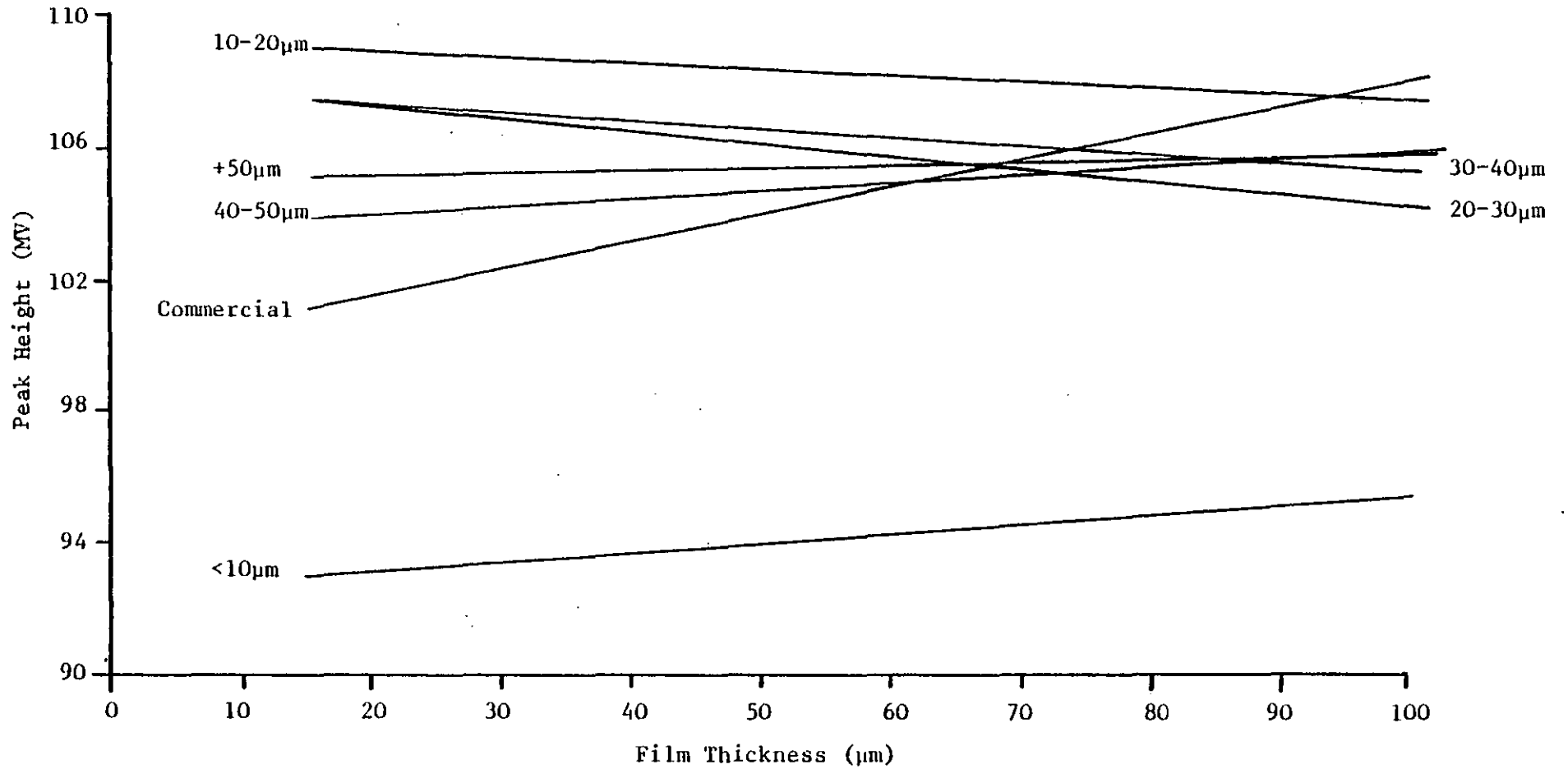
Figure 3.13. Peak Width vs. Film Thickness for Different Powders Sprayed

Linear Regression Fits
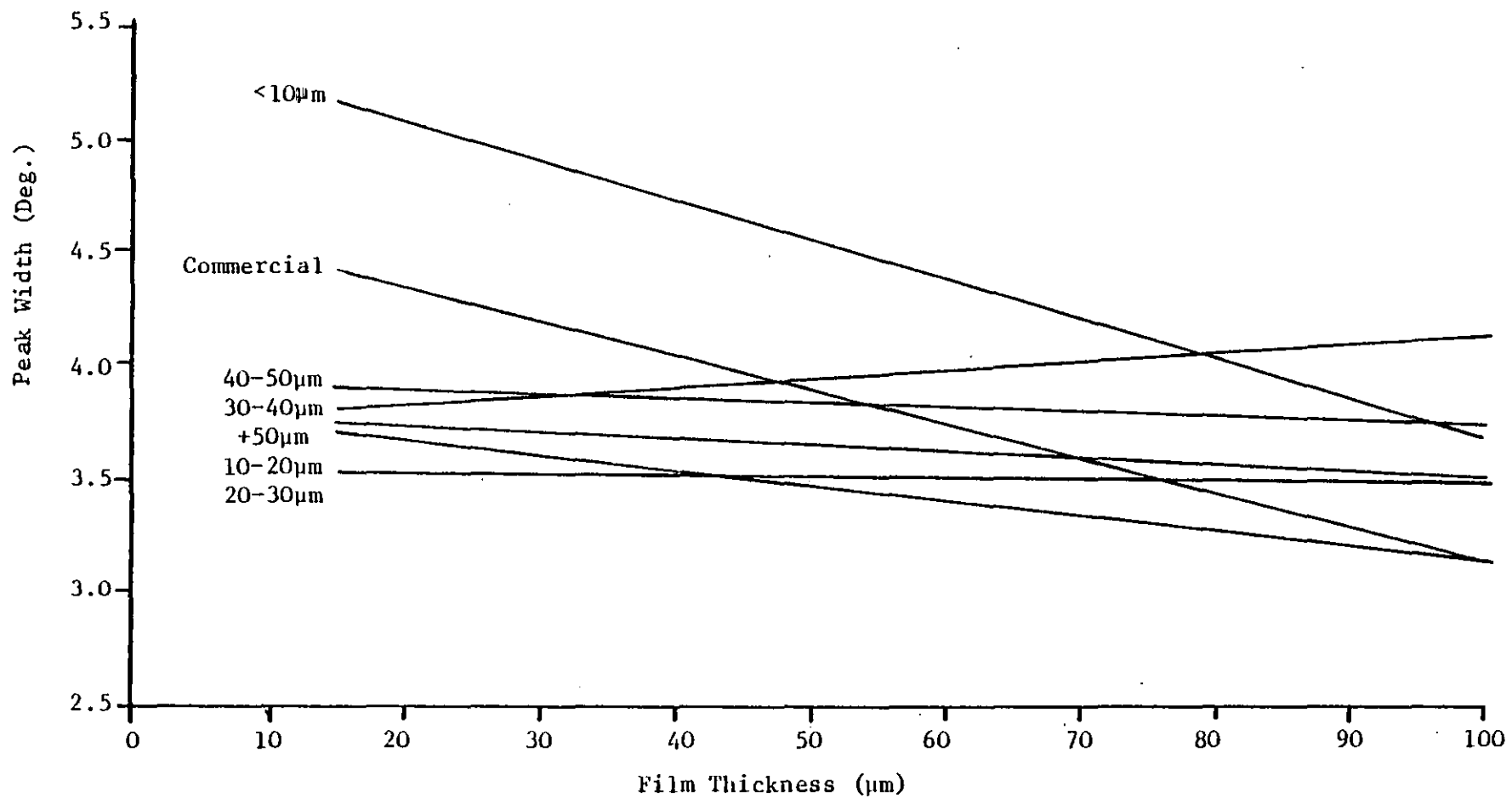
for different thicknesses of film. By doing so the effect of particle size sprayed as a function of the gloss parameters for any given thickness can be observed. Figures 3.14 to 3.16 show these effects for film thicknesses of 30, 50, 70 and 100μm and the data used for these plots is given in Table 3.2. From these graphs it is very obvious that the results for the <10μm range powder are substantially poorer than the other powders. The reason for this is probably due to the fact that particles <10μm in size tend to be very cohesive in nature and as such form larger lumps when placed together in the fluidised bed powder hopper. The particles remain clumped together when the powder is sprayed, so that after stoving an uneven finish is obtained.

Figures 3.17 to 3.19 show the best fit lines to the data of Figures 3.14 to 3.16, ignoring the <10μm range results for the linear regression calculations. Table A9 contains the data used for these fits.

The raw data obtained for each powder type for varying film thicknesses show no marked trends in the figures given in Appendix A. In general the height of peak results, which give indications of the specular gloss of the surface, tend to increase as film thicknesses increase. As might be expected the width of the peaks at half peak height decrease. This measurement gives a measure of the amount of scatter of light from the surface. The wider the scatter the more hazy an image would look if the coating was used as a mirror. When an actual mirror is used in this test the goniophotometric curve is very tall and narrow depicting that a clear, sharp image would be seen.

Table 3.2. **Gloss Test Results for Different Sized**
Powders at Various Film Thicknesses

Powder Type	Test Parameter	Thickness of Coating (µm)			
		30	50	70	100
Commercial	Gloss Factor	24.7	27.0	29.4	32.9
	Peak Height	102.4	104.0	105.7	108.2
	Width	4.20	3.90	3.62	3.18
10µm	Gloss Factor	19.6	21.3	22.7	25.5
	Peak Height	93.5	94.1	94.4	95.5
	Width	4.90	4.56	4.12	3.72
10-20µm	Gloss Factor	30.2	31.0	31.9	33.2
	Peak Height	108.7	108.5	108.0	107.4
	Width	3.61	3.49	3.37	3.29
20-30µm	Gloss Factor	30.1	30.2	30.3	30.4
	Peak Height	106.9	106.0	105.3	104.1
	Width	3.54	3.54	3.54	3.54
30-40µm	Gloss Factor	28.4	28.1	27.8	27.4
	Peak Height	107.0	106.5	106.0	105.2
	Width	3.78	3.80	3.82	3.86
40-50µm	Gloss Factor	27.1	27.5	27.8	28.4
	Peak Height	104.2	104.7	105.2	105.9
	Width	3.88	3.85	3.81	3.75
+50µm	Gloss Factor	28.4	28.9	29.3	29.9
	Peak Height	105.2	105.3	105.4	105.9
	Width	3.70	3.66	3.63	3.55

Figure 3.14. Gloss Factor vs. Size of Powder Sprayed

With Various Thicknesses of Coatings

Key

■ – 30μm Film

□ – 50μm Film

● – 70μm Film

○ – 100μm Film
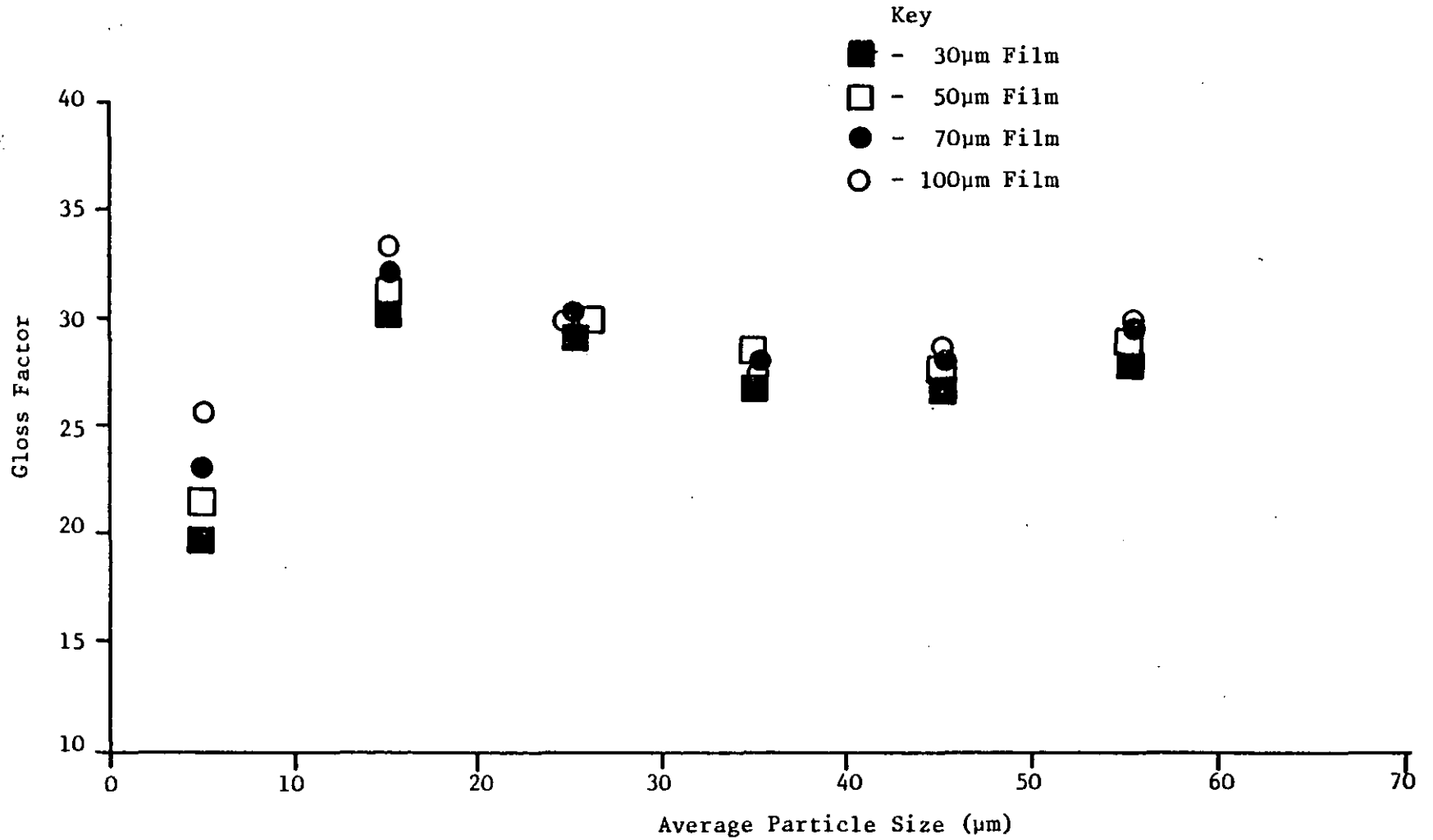
Figure 3.15. Peak Height vs. Size of Powder Sprayed

at Various Film Thicknesses
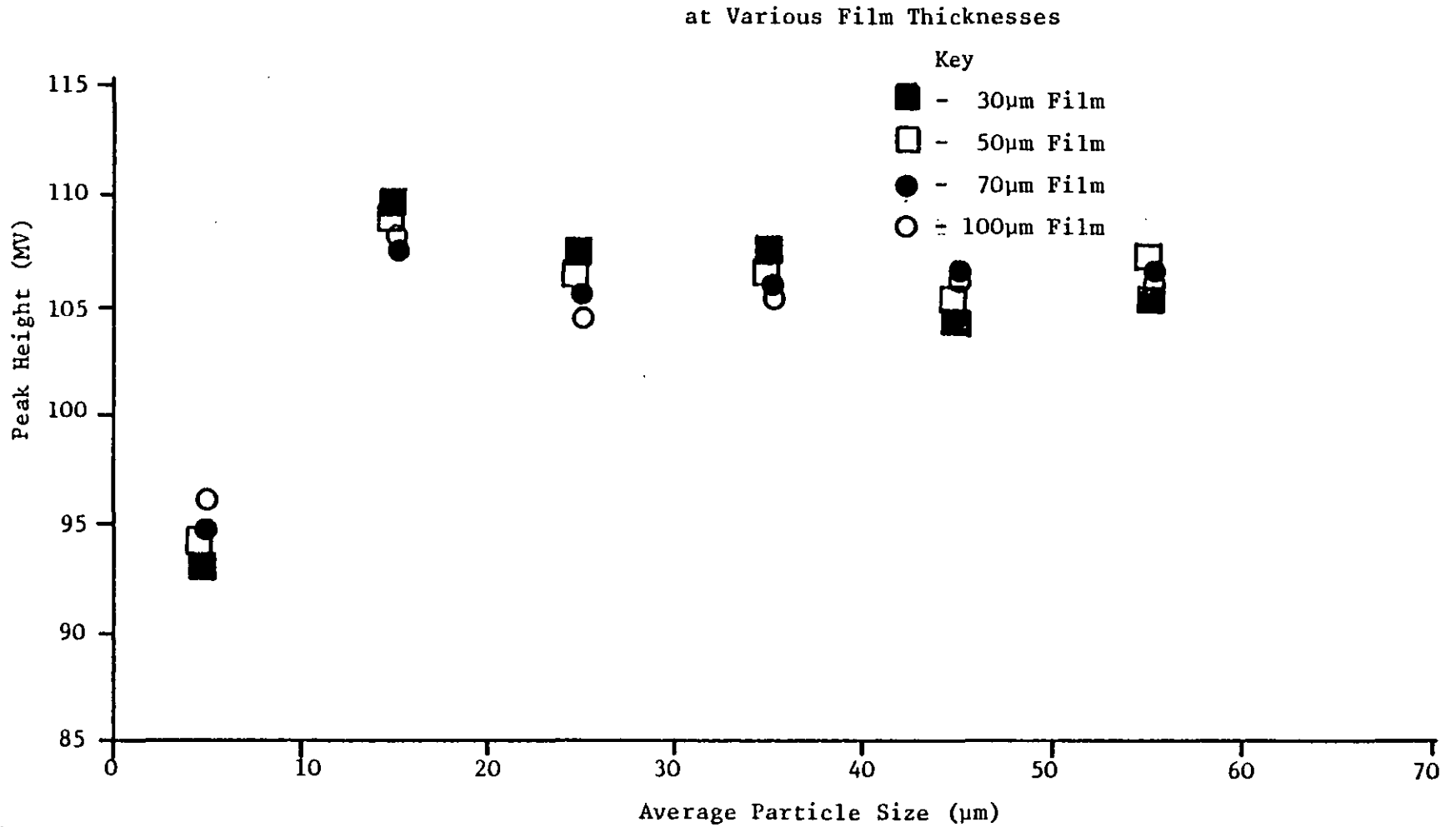
Figure 3.16. Width at Half Peak Height vs. Size of Powder at Various Coating Thicknesses
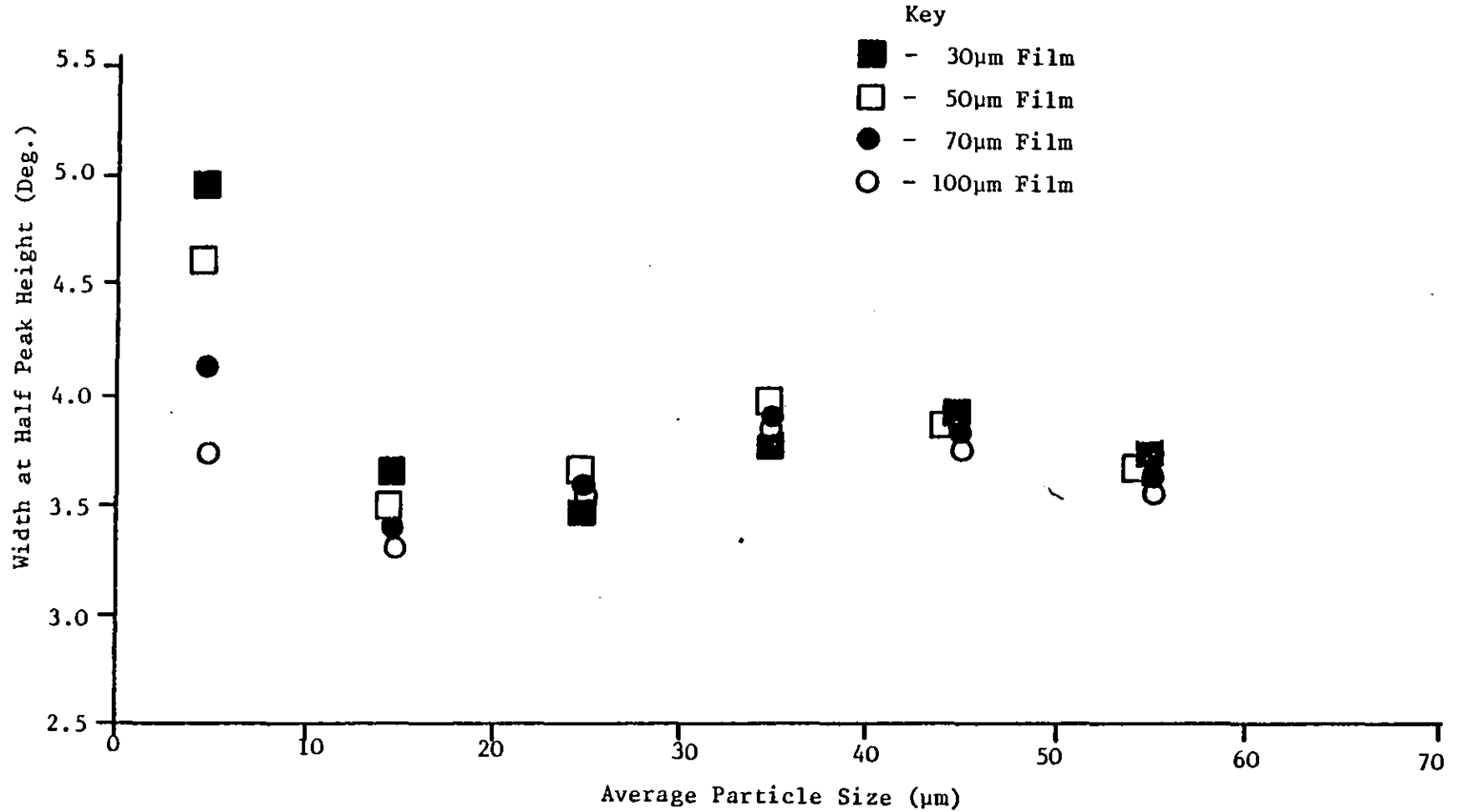
Figure 3.17. Gloss Factor vs. Particle Size Sprayed

Various Film Thicknesses
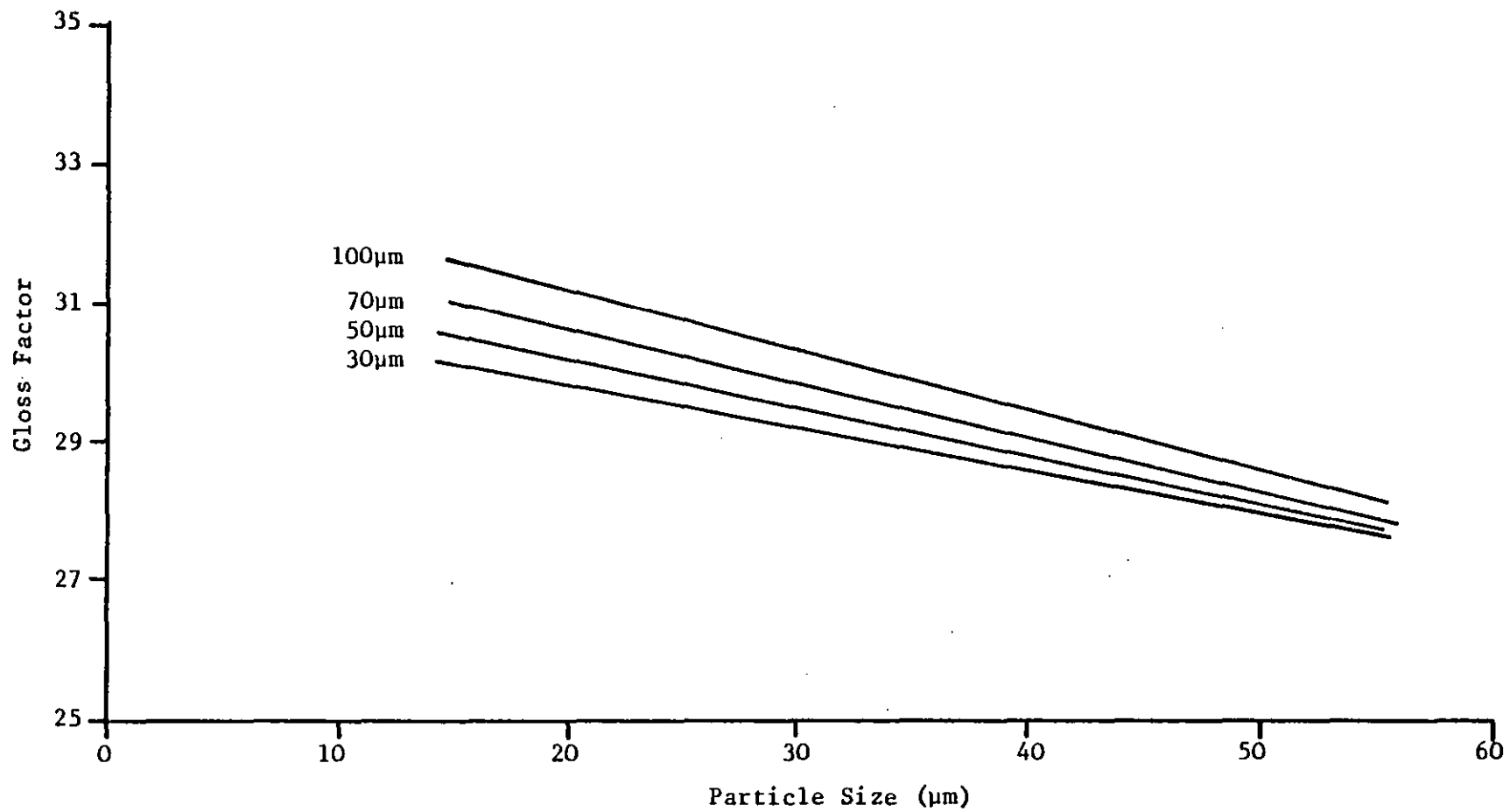
Figure 3.18. Gloss Test Peak Height vs. Particle Size Sprayed

Various Film Thicknesses
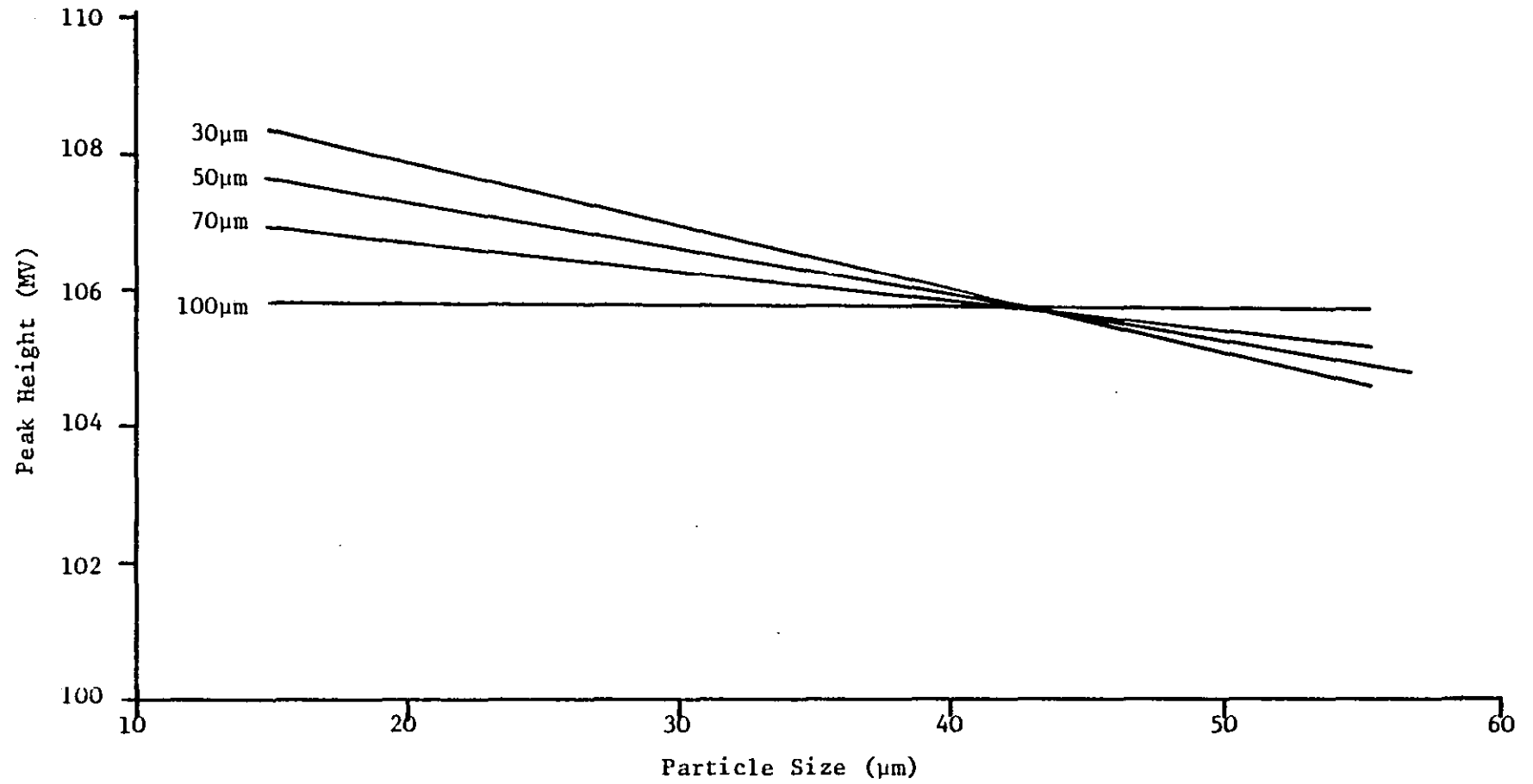
Figure 3.19. Gloss Test Peak Width vs. Particle Size Sprayed

Various Film Thickness
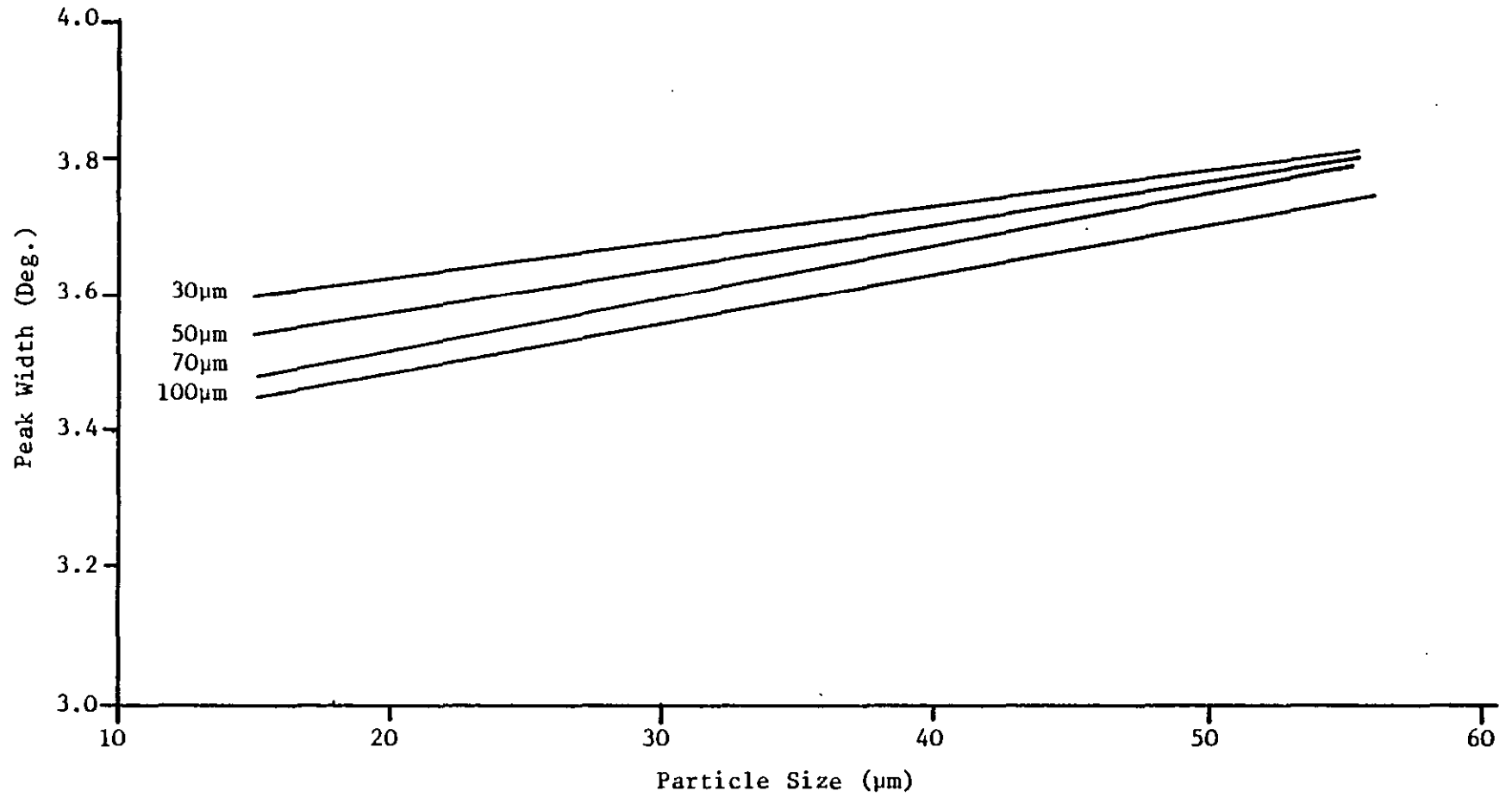
On comparing the results for each powder type it can be seen that there is little difference between the powders. When it is considered that a poor, matt finish (poor with respect to gloss) would have a gloss factor of approximately 3-4 and a mirror finish would be between 30 and 40, these results represent fairly good finishes with little difference between them.

The <10µm size range powder, however, has generally poorer gloss than the others for the reasons previously mentioned. This powder would not be recommended for use in commercial systems as problems of powder flow and dispersion would be encountered.

In Figures 3.14 to 3.16 the change in gloss parameters are shown for changes in particle size of the sprayed powder. Ignoring the <10µm range, the results are not significantly different, although there does appear a slight decrease in gloss with increase in size. Overall the best powder range, based on this data, for the highest gloss would be the 10-20µm range.

However, when the significance of these results are taken into consideration it can be concluded that these size ranges do not have any adverse effects on the gloss characteristics of the coating compared to the commercial powder. Also, the gloss parameters are not unduly effected by changes in thickness of film.

The visual appearance of a coating is extremely important since the eye can be very precise in comparing qualitatively a set of coatings. The visual appearance of the films agreed with the gloss measurements in that they were all of high quality and none were significantly different.

3.6 Surface Roughness

The Talysurf 10 is one of the most widely used devices for the measurement of surface roughness parameters. The assessment of surface roughness by stylus methods has been in use since the early 1940's and they are used in many national standards. This particular method has the advantages of being non-destructive, sensitive and gives quickly readable results (R.C. Spragg and D.J. Whitehouse, 1972).

A surface which is nominally smooth and flat will always exhibit some roughness and it may also exhibit some waviness or a combination of both. This is shown in Figure 3.20.

Roughness and waviness are measured by traversing a pick-up which carries a sharply pointed stylus across the surface. Vertical movements of the stylus with reference to a datum are measured. The quantitative assessment of the surface profile is very difficult since no single number can adequately describe the complex patterns and irregularities of the surface. The Talysurf 10 gives two values that relate to roughness and waviness in order to try and describe the surface profile under observation.

The Roughness Average (Ra) has been internationally accepted for many years now. It is defined as the arithmetical average of the departures of the profile above and below the reference line (centre mean line) throughout the sampling length. Definitions of the centre line and Roughness Average are given in Figures 3.21 and 3.22. The roughness average quoted is usually an average of a number of consecutive measurements taken along the surface.

The roughness average gives no information about the openness or closeness of the profile. The Average Wavelength parameter (λa), however, is a more recent measurement that is based on the spacing of irregularities along the surface.
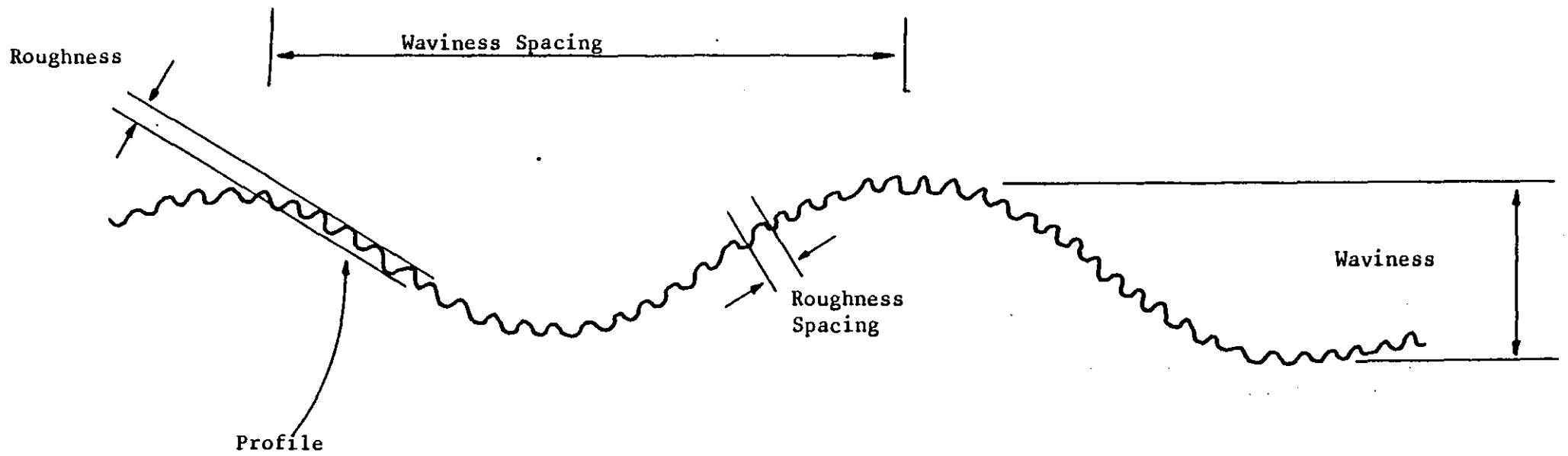
Figure 3.20.   Surface Characteristics of a Coating

Areas B + D + F + H + J = Areas A + C + E + G + I + K
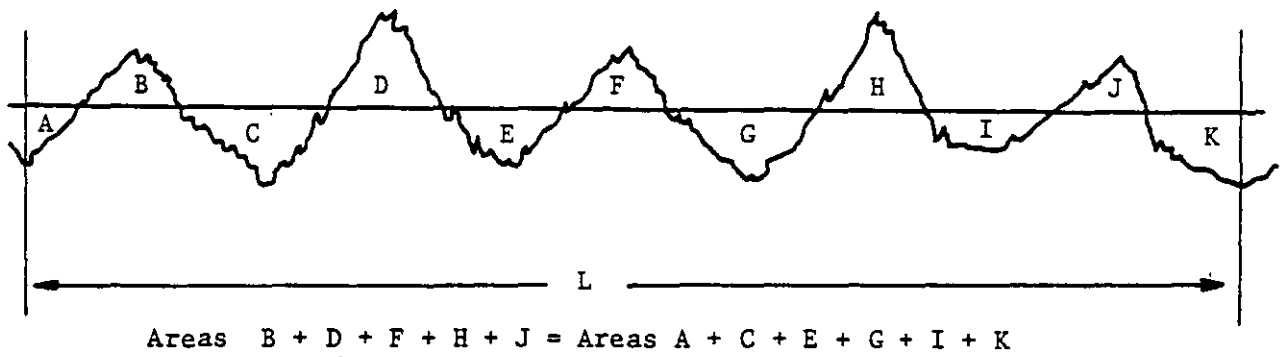
Figure 3.21.   Centre Line Definition

$$Ra = \frac{h_1 + h_2 \ldots\ldots h_n}{L} = \frac{1}{L} \int_o^L |h| \, dL$$
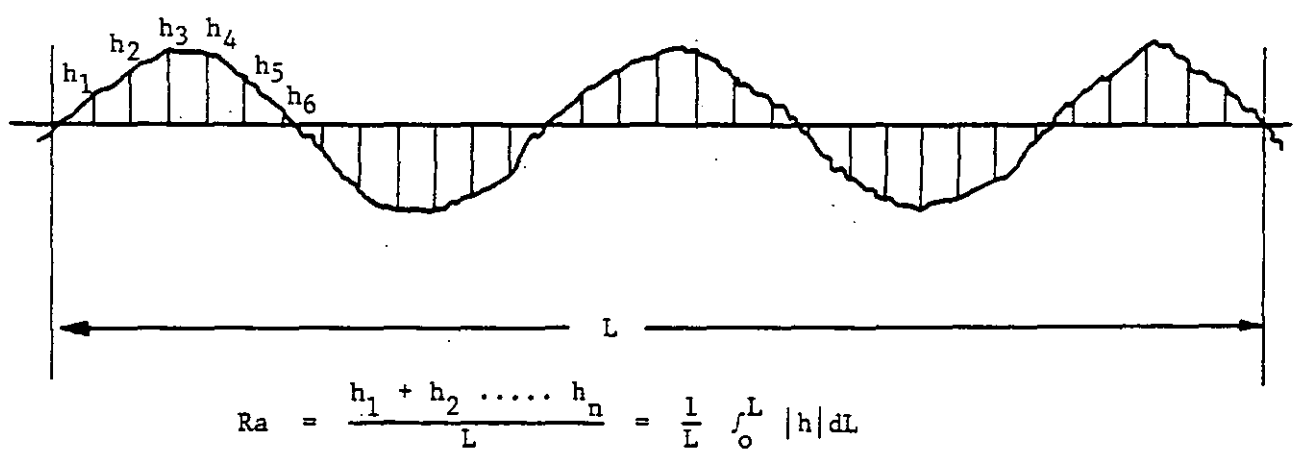
Figure 3.22.   Definition of Ra

By Fourier analysis a series of sine waves can be produced to represent the complex profile waveform. If the power spectrum is plotted (individual intensities for each component in the series), the average wavelength is approximately equal to the weighted mean. This measurement is not an actual measure of the spacing of the peaks or of a theoretical waveform because it is derived from the power spectrum. A comparison of waveforms and their average wavelengths are shown in Figure 3.23, together with their power spectrums.

By quoting both the roughness average and wavelength parameters it is possible to obtain a much clearer impression of the type of surface that is being tested. Figure 3.24 shows a typical range of results as obtained for the surfaces of rolled pieces of sheet for the motor car industry. It can be seen that quoting roughness wavelength is very important when roughness average results are similar. (R.C. Spragg, D.J. Whitehouse, 1972).

3.6.1 Instrumentation

Vertical movements of the stylus that is traversed across the workpiece are converted by a transducer into corresponding changes in an electric current.

These are then amplified electronically to give a surface profile which is obtained as an average reading, or readings, on a meter. A schematic representation of the apparatus is shown in Figure 3.25 and the equipment is shown in Plate 3.7.

3.6.2 Experimental Method

The Talysurf 10 was set up in the skidless mode since the type of irregularities to be encountered were not known. The traverse shaft thus acts as the datum and the pick-up assembly is monitored for movement.

Figure 3.23. Comparison of Roughness Wavelengths
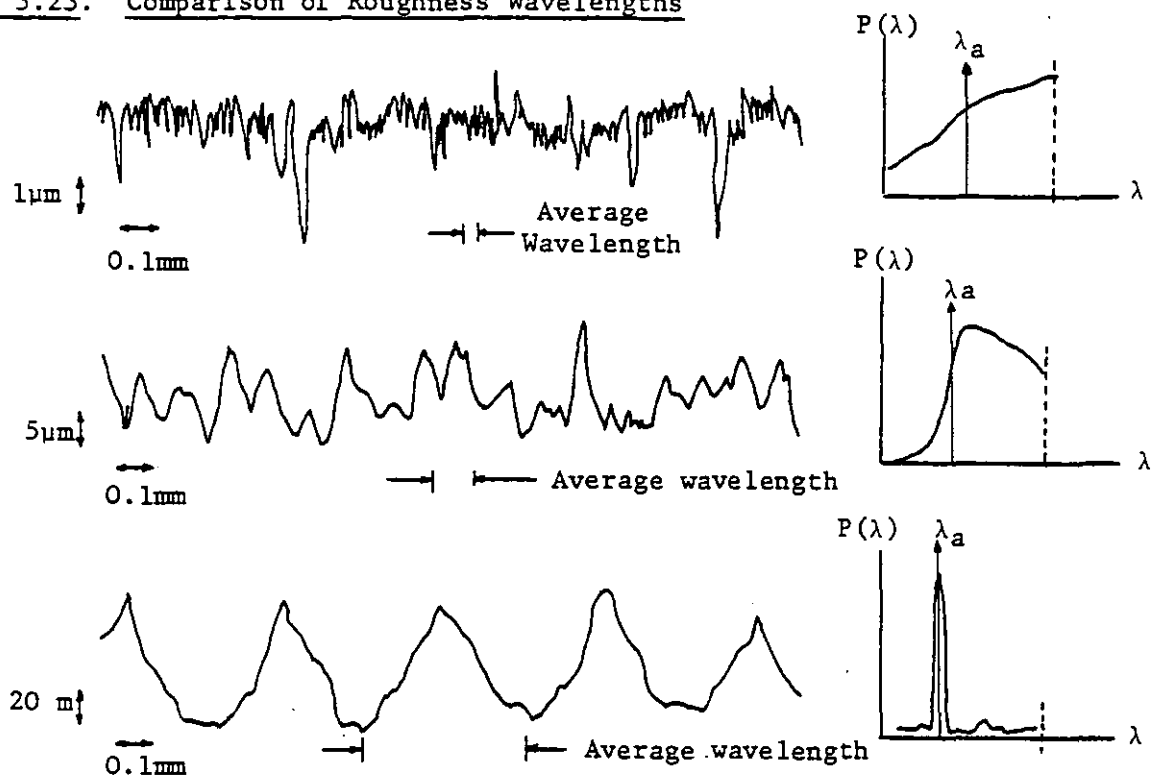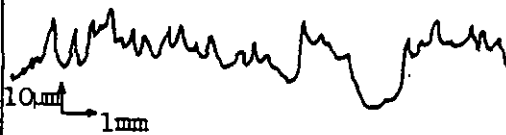
Figure 3.24. Typical Values of R_a and λ_a

No	R_a μm	λ_a μm	Classification
1	2.2	211	Open Irregular
2	6.9	320	Open Smooth
3	0.64	75	Sharp Peak – Sharp Valley
4	2.1	361	Open Smooth
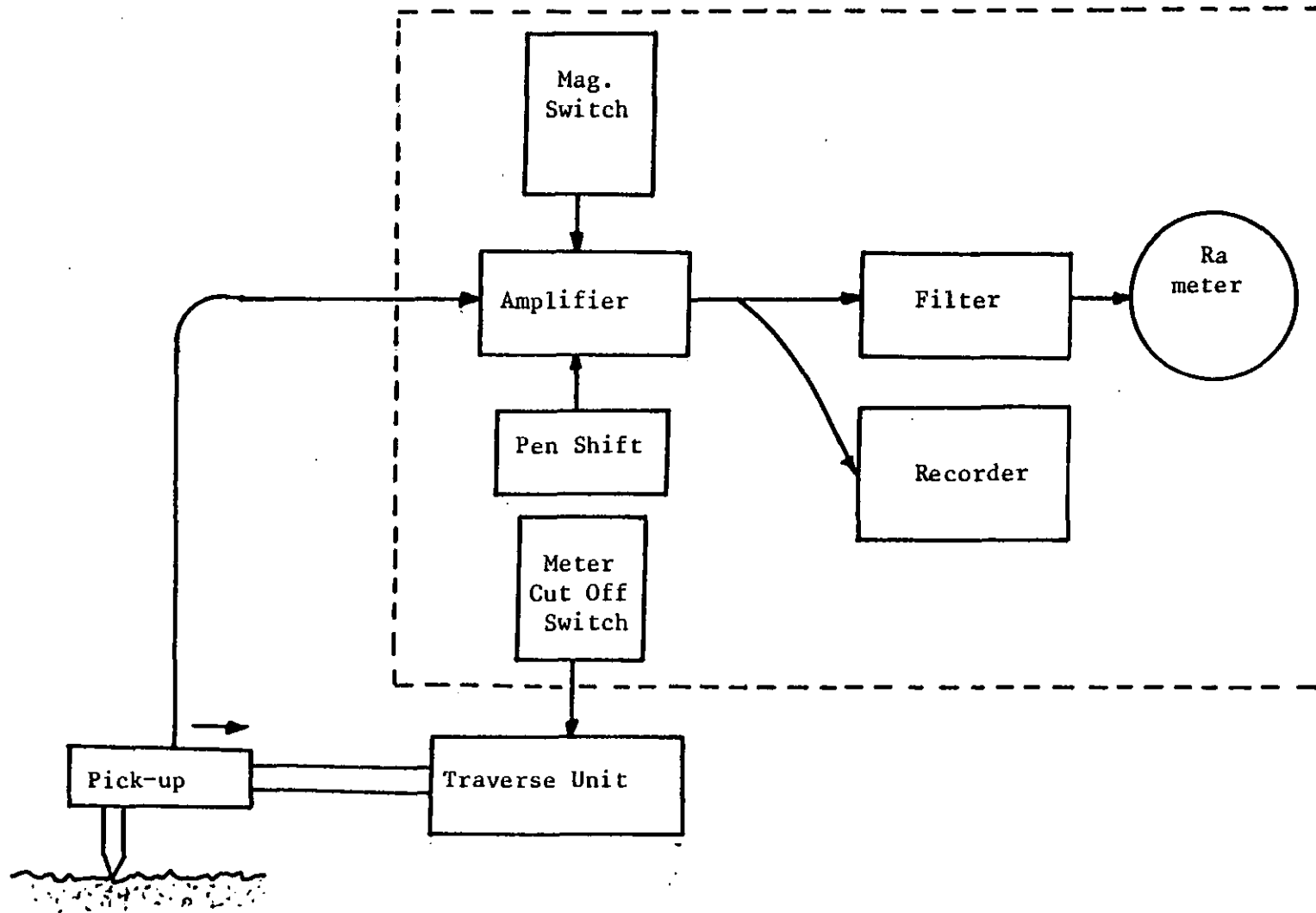
Figure 3.25. Schematic Arrangement of Talysurf 10

Plate 3.7. Taylor-Hobson Talysurf 10 Roughness Measurement Device

A supplied test piece was used to check the calibration of the instrument before each new set of readings. The system is carefully levelled by using the levelling knob in conjunction with the chart recorder as described in the manufacturers instructions. Four test lengths were taken for each sample plate, each time the sample being rotated by 90° to measure the roughness in different directions. The appropriate magnification/sensitivity was used to cover variations in roughness.

3.6.3 Results and Discussion

The averages and standard deviations were calculated for each thickness range from the measurements carried out. In total approximately 3800 measurements were recorded. The overall results for each powder type are given in Appendix B, Tables B1 to B7.

Plots of these results against film thickness are given in Figures B1 to B7 for roughness average and in Figures B8 to B14 for roughness wavelength. Similarly to the results for gloss tests, the data in these plots have been fitted to straight lines using linear regression. These fits have been compounded together for each powder type for roughness average and roughness wavelength onto Figures 3.26 and 3.27 and the data for the linear regression fits is given in Table B8.

Data was extracted from these results to observe the change in roughness with particle size of powder sprayed and the general trend observed was that roughness increased with increase in particle size (see Table 3.3 and Figures 3.28 to 3.31). The <10μm size range was not used in the linear regression fits of the last two graphs due to the poor qualities of film. (See Figures 3.30 and 3.31 and the data given in Table B9).

Figure 3.26. Roughness Wavelength vs. Film Thickness for Various Powders

Linear Regression Fits
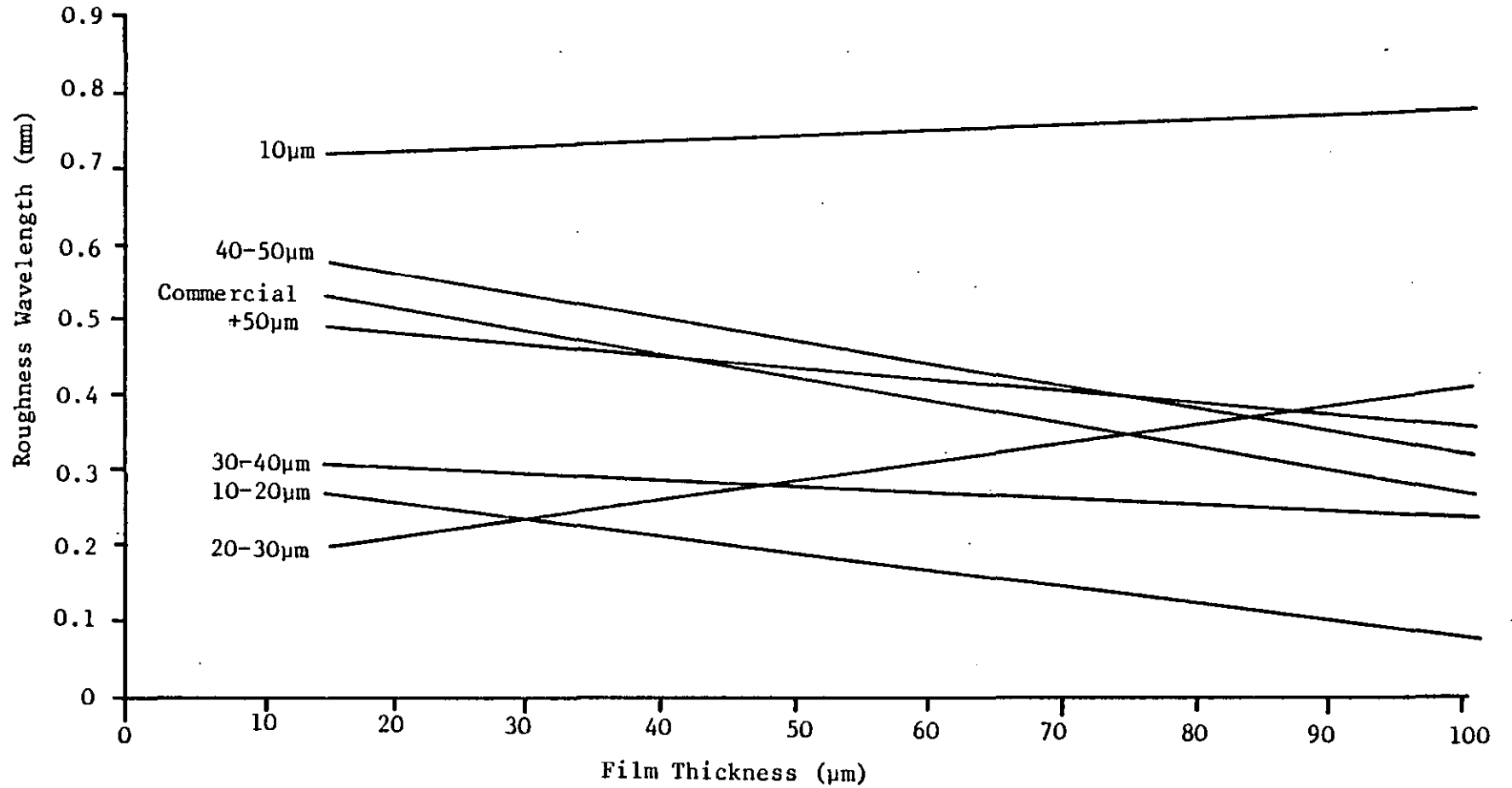
Figure 3.27. Roughness Average vs. Film Thickness for Various Powders
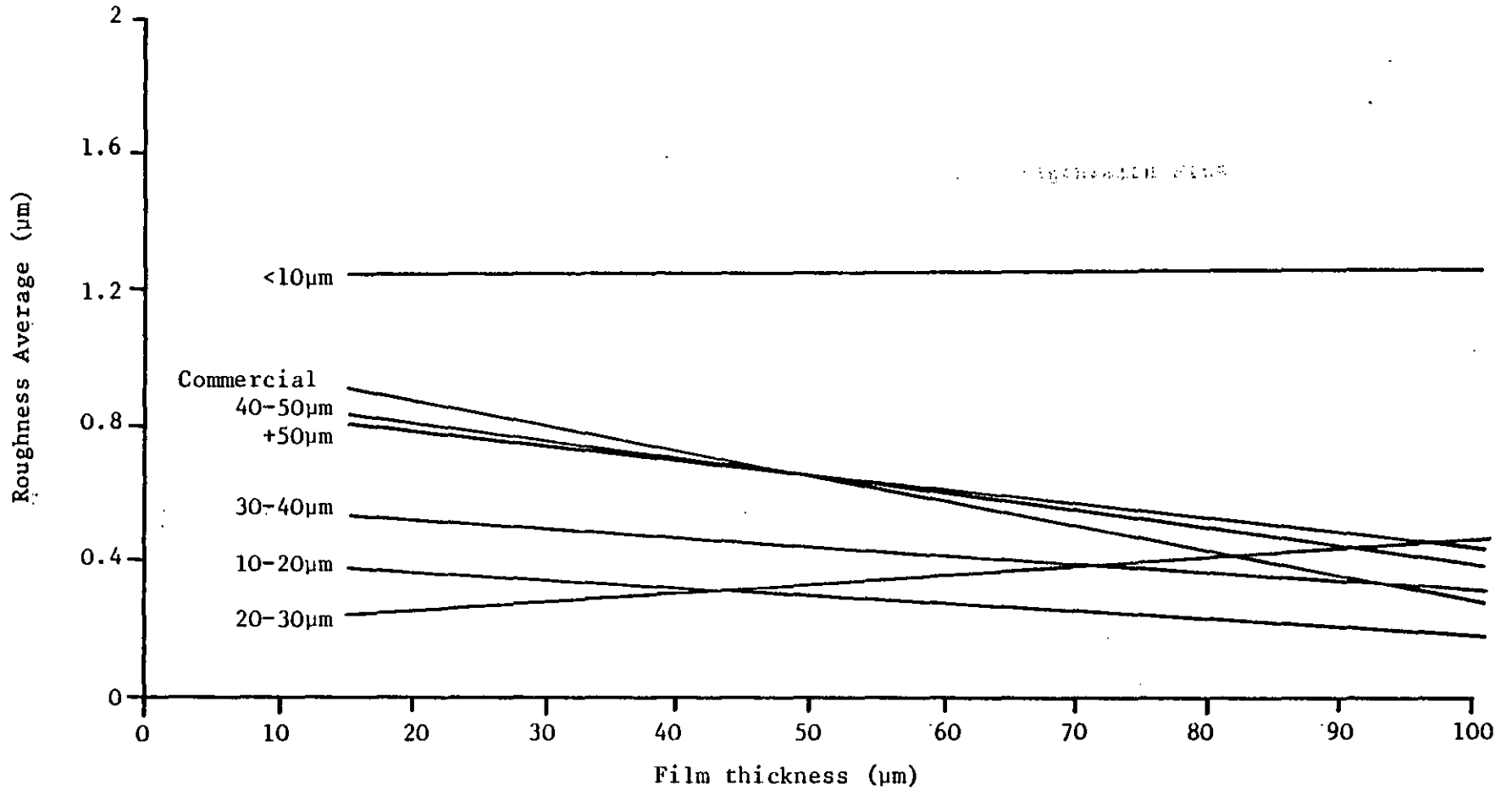
Figure 3.28.   Roughness Average vs. Size of Powder Sprayed

at Various Coating Thicknesses

Key

■ — 30μm Film
□ — 50μm Film
● — 70μm Film
○ — 100μm Film

Roughness Average (μm)

Average Particle Size (μm)
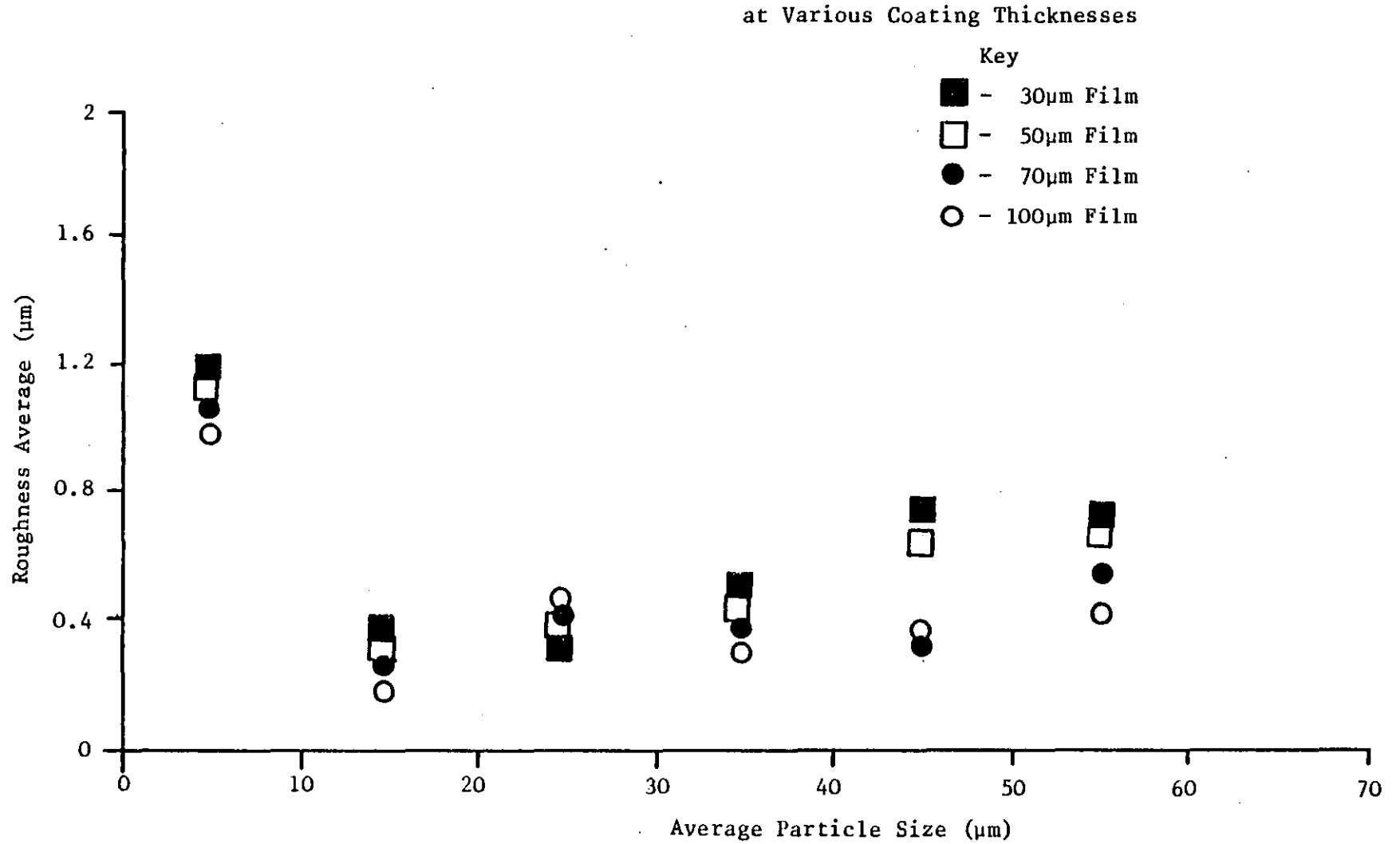
Figure 3.29. Roughness Wavelength vs. Size of Powder Sprayed

at Various Coating Thicknesses
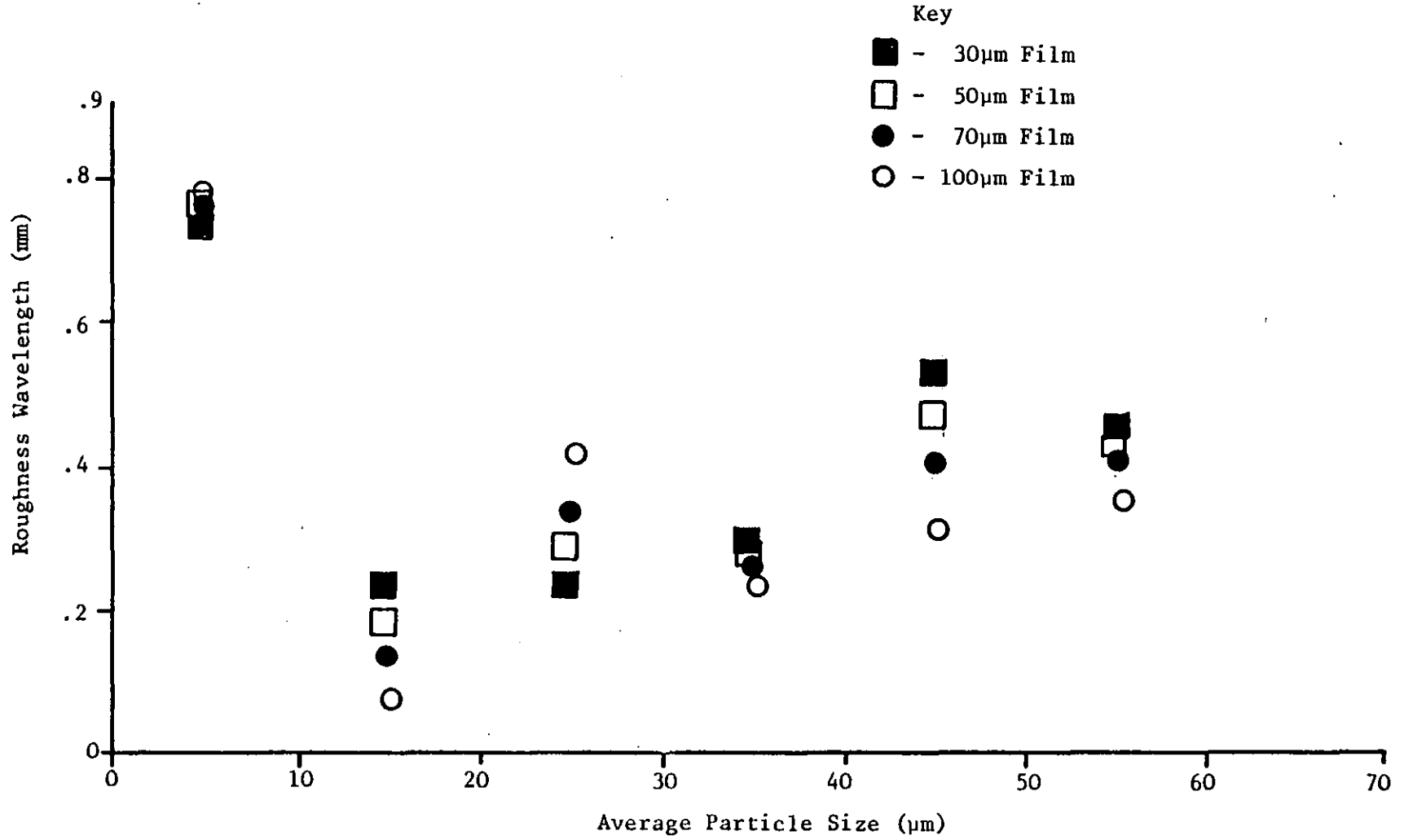
Figure 3.30.   Roughness Average vs. Particle Size Sprayed

Various Film Thicknesses
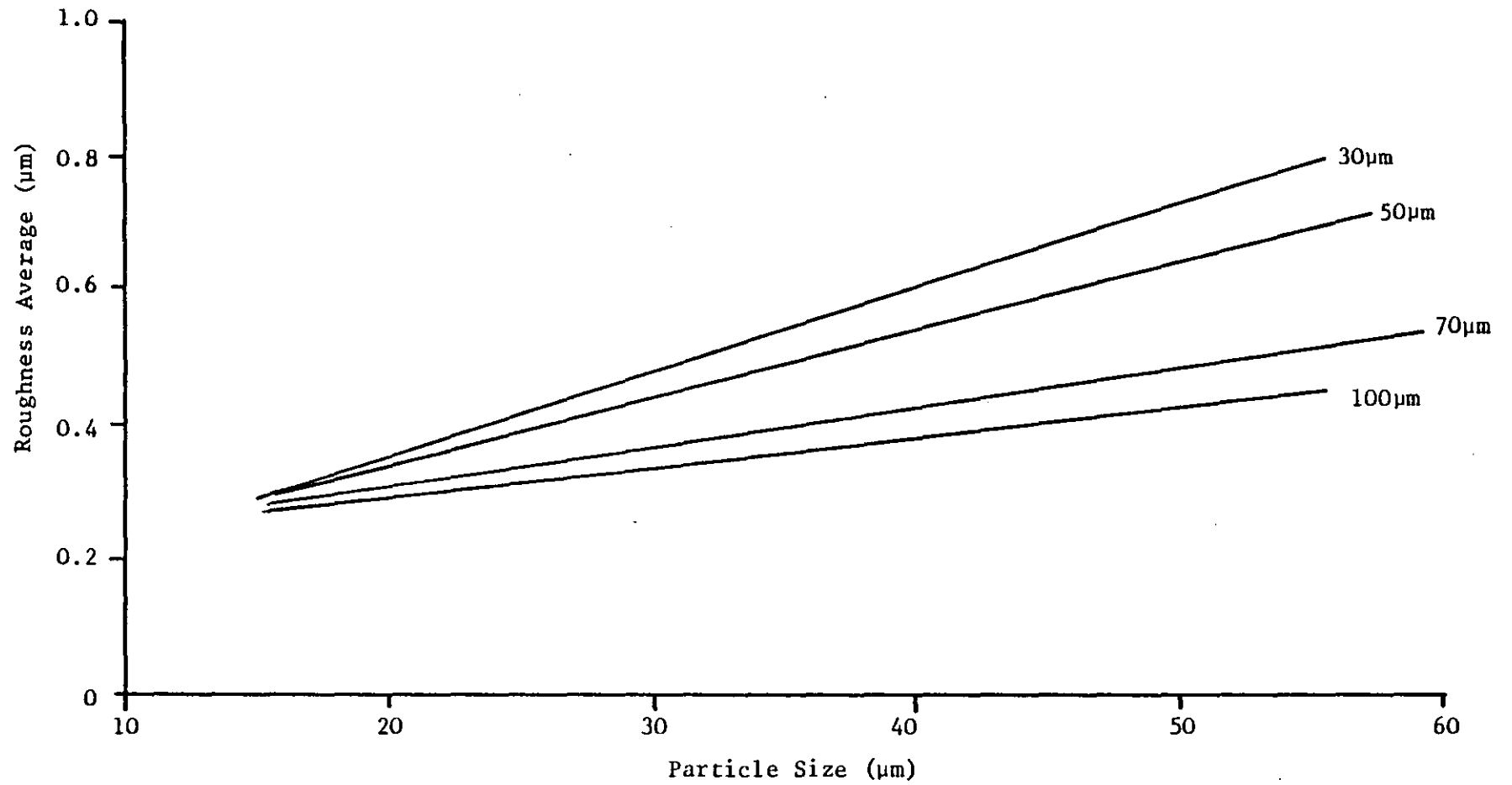
Figure 3.31. Roughness Wavelength vs. Particle Size Sprayed

Various Film Thicknesses
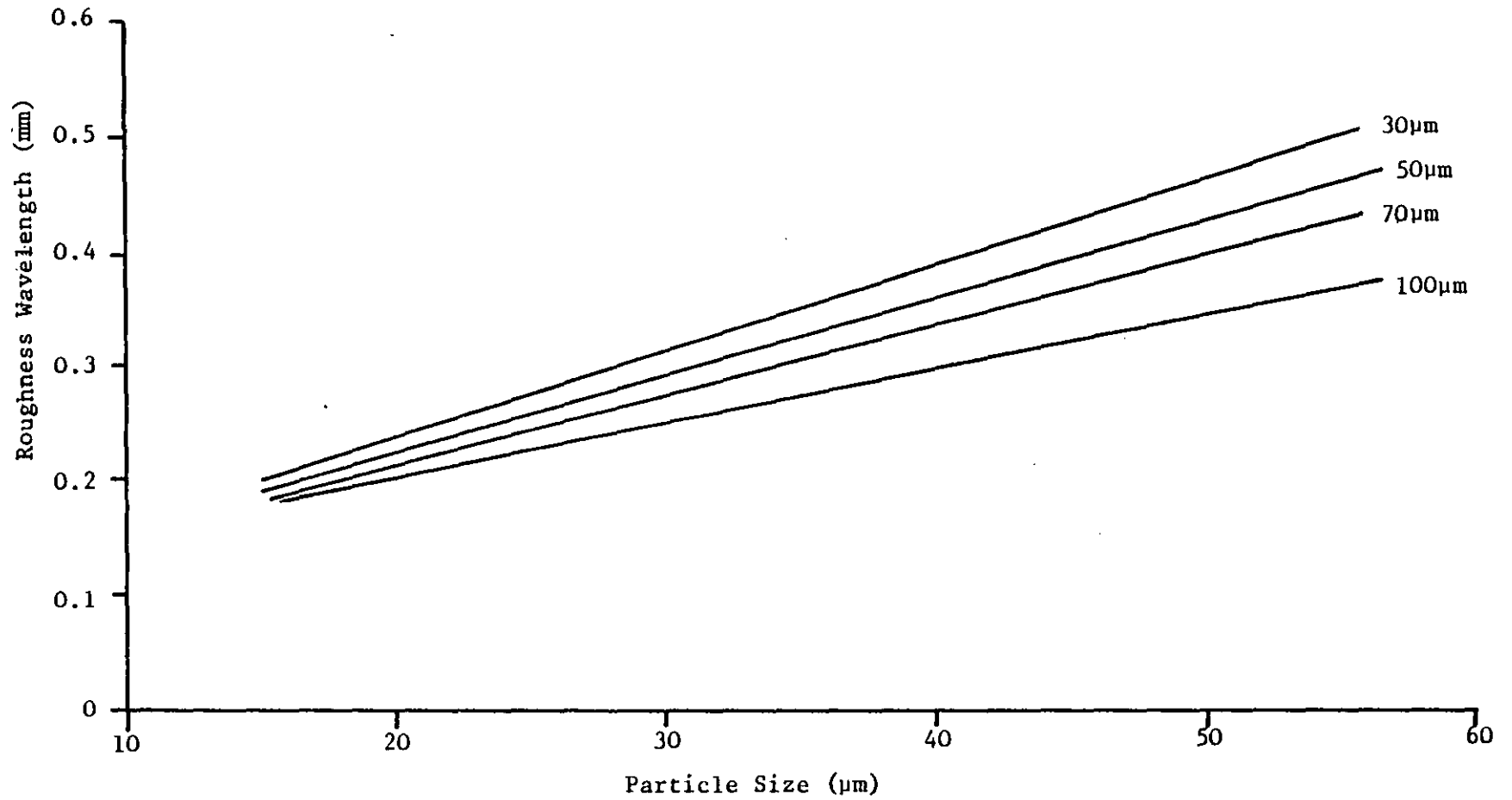
Table 3.3. Surface Roughness Results for Different Sized Powders at Various Film Thicknesses

Powder Type	Test Parameter	Film Thickness (μm)			
		30	50	70	100
Commercial	Roughness Average	0.81	0.66	0.52	0.30
	Roughness Wavelength	0.48	0.42	0.35	0.26
<10μm	Roughness Average	1.18	1.12	1.06	0.97
	Roughness Wavelength	0.73	0.74	0.75	0.77
10-20μm	Roughness Average	0.36	0.31	0.26	0.18
	Roughness Wavelength	0.23	0.18	0.13	0.07
20-30μm	Roughness Average	0.32	0.36	0.41	0.48
	Roughness Wavelength	0.23	0.28	0.33	0.41
30-40μm	Roughness Average	0.51	0.45	0.39	0.31
	Roughness Wavelength	0.29	0.27	0.26	0.23
40-50μm	Roughness Average	0.77	0.66	0.35	0.39
	Roughness Wavelength	0.53	0.46	0.40	0.31
+50μm	Roughness Average	0.76	0.67	0.57	0.44
	Roughness Wavelength	0.46	0.43	0.40	0.35

The Talysurf 10 has enabled the measurement of the surface roughness of coatings in a simple manner. Both the values that have been measured, Ra and λa, complement each other and should be used together to describe a surface profile.

The results in the figures and tables have shown that in general the average roughness decreases with thicker films but increases with larger particle sizes used in the spraying. Comparison of these results with figures for other surfaces reveal that there is little change in these qualities with the parameters being observed here.

As for the gloss tests, the commercial powder shows more definite trends for the change in roughness average and wavelength with film thickness. The linear regression fits, although only shown for comparison, appear quite good correlations in these cases. This could be due to having a less random and loose packing than the narrow size fraction packings.

3.7 Adhesion

The cross hatch test, as described in BS 3900 : Part E6, was employed as it was a test that is commonly used and is simple in nature.

A series of spacing edges were made as described in the British Standard. A block of wood, with a rubber base, of suitable size to be held on the workpiece by hand, was used to hold the eleven spacing edges (See Figure 3.32). Due to the small size of the sample plates difficulty was encountered in keeping the block and spacers steady on the plate whilst the grooves were cut. Therefore a large plate with a 2 in square recess was used to house the plate whilst cutting proceeded. In this way the spacers were held flush against the sample and housing plate.

10 Spacers
1mm thick

Wooden
Block

Rubber Base
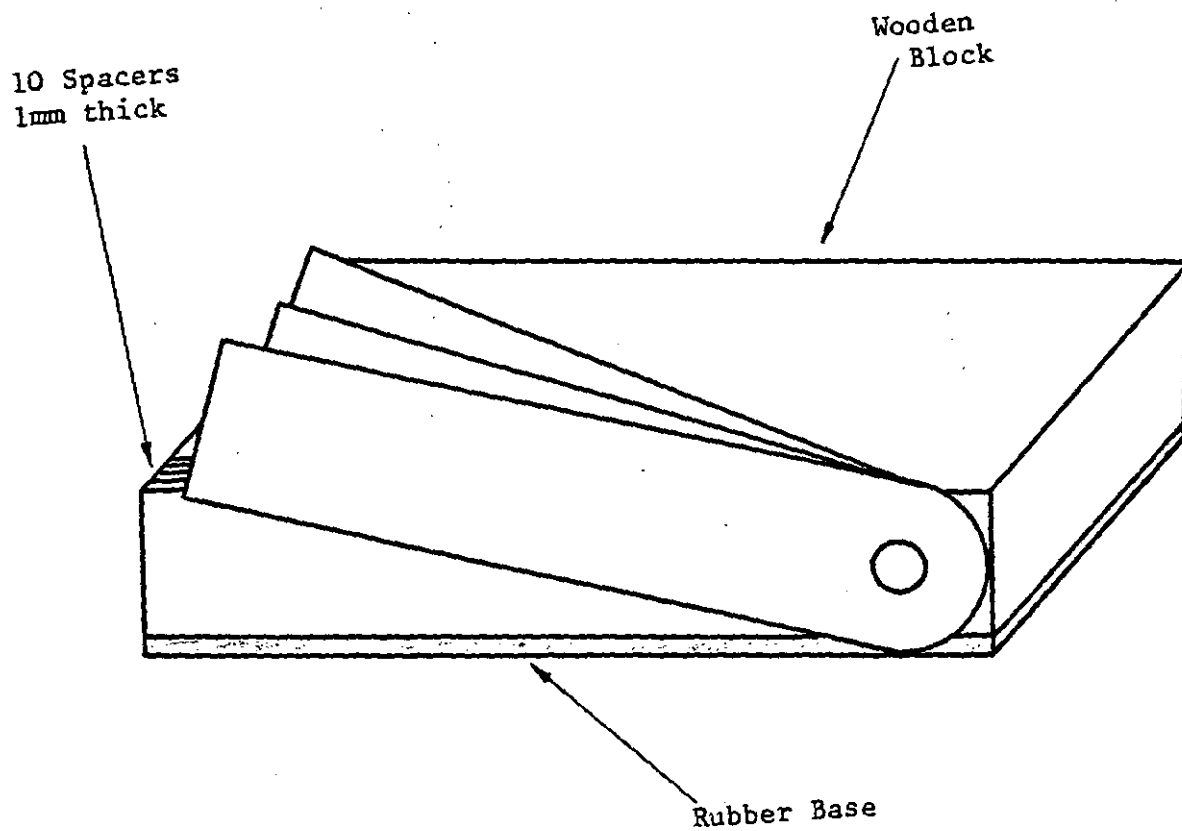
Figure 3.32. Series of Spacing Edges for Cross-Cut Test

3.7.1 Experimental Method

A sample plate was placed in the housing plate and the block of spacers suitably positioned over the plate. Using a new bladed scalpel, 11 grooves were cut through the film to the metal substrate. The cuts were made at a uniform and slow speed across the surface of the coating. The spacers were then rotated by 90° and a similar set of cuts were made to produce a cross hatch on the coating.

The number of small 1 mm squares of coating removed by this action were then compared to the classification chart in the British Standard. (See Figure 3.33).

A further test was carried out, similar to that described in ASTM Standard D3359-74, in which a piece of adhesive tape was placed over the cross hatching. The tape was then removed and the remaining coating was again compared to the classification chart.

Due to the destructive nature of this test (and the corrosion test) only one plate was used to test the adhesion of the coatings for any particular thickness and powder type.

3.7.2 Results and Discussion

Five different thickness ranges were tested for each of the powder types. Table 3.4 shows the results from both these tests in terms of the characterisation number for each of the powder types and film thicknesses. Difficulty was found in cutting completely through the coating to the metal for films that were thicker than 80μm.

Figure 3.33. **British Standard Classification Chart (BS3900)**

Classifi- cation	Description	Appearance of surface or cross-cut area from which flaking has occurred (example for six parallel cuts)
0	The edges of the cuts are completely smooth; none of the squares of the lattice is detached.	
1	Detachment of small flakes of the coating at the intersections of the cuts. A cross-cut area not distinctly greater than 5 % is affected.	
2	The coating has flaked along the edges and/or at the inter- sections of the cuts. A cross-cut area distinctly greater than 5 %, but not distinctly greater than 15 % is affected.	
3	The coating has flaked along the edges of the cuts partly or wholly in large ribbons, and/or it has flaked partly or wholly on different parts of the squares. A cross-cut area distinctly greater than 15 %, but not distinctly greater than 35 % is affected.	
4	The coating has flaked along the edges of the cuts in large ribbons and/or some squares have detached partly or wholly. A cross-cut area distinctly greater than 35 %, but not dis- tinctly greater than 65 % is affected.	
5	Any degree of flaking that cannot even be classified by classification 4.	

Table 3.4.   Results of Adhesion Tests – Cross hatch and Tape Test

<10μm			10-20μm			20-30μm			30-40μm			40-50μm			+50μm			Commercial		
t (μm)	C	T	t (μm)	C	T	t (μm)	C	T	t (μm)	C	T	t (μm)	C	T	t (μm)	C	T	t (μm)	C	T
15	0	0	18	0	0	29	0	0	28	0	0	33	0	0	37	0	0	21	0	0
25	0	0	27	0	0	38	0	1	36	0	0	39	2	3	49	0	0	33	0	0
38	1	2	39	0	0	41	1	3	49	0	0	40	1	2	58	0	0	43	0	0
60	1	2	46	0	0	48	0	0	55	0	0	54	0	0	65	0	0	52	0	0
84	1	3	55	0	0	59	0	0	66	0	0	65	1	2	72	0	0	60	0	0

t   –   film thickness (average of 5 measurements)

C   –   Cross hatch adhesion test

T   –   Cross hatch test followed by tape test

As expected, these coatings typically gave very good adhesion results. Even the <10μm range powder type coatings gave good results. These results reflect the fact that the coatings had been stoved correctly and that the substrate surface was in good condition. Some brittleness was observed in a few of the coatings but this could be due to slight variations in the oven temperature. However, over 75% of all the coatings tested showed no signs of loss of adhesion due to the cutting of the crosshatch or pulling on the film during the removal of the tape.

These results are expected since a commercially formulated powder has been used for the experiments and it should exhibit good flow and adhesion properties after a correct stoving cycle. This test also shows that the powder film has been completely fused. If this was not so and a dry, unfused powder monolayer was left close to the substrate then large areas would be lifted when the upper fused film had been corrupted.

Following the tape test, only 3 samples had a classification greater than 2. In these cases the results show that less than 35% of the film was removed, with no squares being wholly removed.

3.8 Corrosion

ASTM Standard B117 was followed for the assessment of corrosion resistance of coatings using the salt spray test. The apparatus (See Plate 3.8) consisted of a fog chamber, a salt solution reservoir compressed air supply and atomising nozzles. The sample plates were held on larger tin plates inclined at 30° to the vertical and parallel to the principal direction of the flow of the salt spray through the chamber. The coated plates were held by double sided sellotape and

Plate 3.8.   Salt-Spray Test Chamber

the edges of the samples were painted using a zinc based paint to stop the steel edges from corroding and hence keep the main sample area clean from corrosion stains.

3.8.1 Experimental Method

Salt solution of 5 parts by weight sodium chloride in 95 parts distilled water was used. The salt spray chamber was kept at approximately 37°C throughout the period of the test. The condensed fog was collected so that drops of solution did not continually fall onto the specimens.

The samples were split into two halves. One half were scribed with an 'X' using a scalpel blade. It was ensured that the cuts were made right through the coating to the metal substrate. The other half were left untouched. The plates were left in the spray chamber for 48 hours and then removed. Their conditions after testing were recorded.

3.8.2 Results and Discussion

Two plates were taken from the same thickness ranges as used for the adhesion tests. In all cases there was no detachment of coating from the plates scribed with an 'X'. Corrosion had taken place on the metal and was seen by the red/brown stains on the cuts.

There was no evidence of pin holes in any of the surfaces of the coating; no brown spots were apparent.

This test shows the resistance of the film to a corrosive atmosphere but also gives an indication of the adhesion of the coating, especially in the case of the X-cut coating. All powder size fractions of this commercial powder gave excellent results, as expected with epoxy resin powder coatings. No detachment of the coatings again confirmed that the stoving cycle had been correctly

carried out and that adhesion was representative of normal industrially produced coatings.

3.9 Porosity

The measurement of porosity has been carried out in two ways. The first test involved the removal of coatings from the substrate. This was achieved by first coating the substrate with a very thin film of aluminium produced by a vacuum coater. This aluminium coating was then dissolved in nitric acid after the powder coating had been stoved. The coating could then be removed from the plate.

A sample of the coating was then placed in an electron microscope. The coating was subjected to X-rays and a photograph taken of those X-rays permeating through the coating. Where absorbance of X-rays took place due to the high atomic weight pigment atoms the picture was darker. Any holes through the coating or air pockets would be shown as light grey areas as some absorbance took place. Thus the porosity of the film could be seen over a sample area.

The corrosion test previously described also acts as a porosity test. Any pores through to the substrate act for sites of corrosion and red/brown rust spots would appear in the surface of the coating where this has occurred.

3.9.1 Results and Discussion

Analysis of the plates from the corrosion experiments have already shown that no pin holes could be seen in the coating. Electron microscope photography also showed that there were no air pockets in the coatings. These tests were done over a random sample of coatings throughout the various powder types.

The effectiveness of the stoving cycle is again confirmed and suggests that change in particle size does not unduly effect the nature of the coating in this respect.

3.10 Conclusions

A series of tests have been developed such that the physical qualities, and in particular surface properties, of a set of coatings have been examined. A commercial standard epoxy resin powder was fractionated into 6 size ranges. Each fraction was used as a separate powder for coating a set of sample plates. A reproducible method of coating was employed using a commercial type spray gun system and over 2500 plates were produced using this method.

The results from these tests have given a comprehensive study of the effect of particle size range on the final film properties of stoved powder coatings. It has been clearly observed that although different particle sized powders have been used to form a coating, the films still retain excellent properties of corrosion resistance and adhesion. This is true for any thickness of film between 20 and 100 μms.

However, it has been observed that larger sized particles do produce rougher coatings which have a surface profile which has a close structure with very fine superimposed roughness.

Associated with this increase in roughness, larger particle sizes also gave slightly lower gloss results than finer particles. Thicker films on the whole gave films with better gloss characteristics and smoother surfaces than thinner films.

The <10μm range showed poorer surface characteristics than any of the other powders used. This is due to the very poor flow properties of the powder. The powder tended to be very cohesive and

hence gave rise to the spraying of 'clumps' which consequently gave poorer finishes. It would not be recommended that a powder of this type be used for the production of powder coatings. This powder type was not included in the linear regression analysis of results for different powder size ranges.

In general the results of the gloss tests can be considered to show no significant differences when the results are compared to those obtained from other finishes, such as a mirror or matt surface. The coatings appear to be very similar to each other. Visual inspection confirms this and all coatings have very good appearances. The roughness results are very similar in this respect but perhaps show marginally more significant changes in roughness with particle size.

The adhesion, corrosion and porosity tests confirm the excellent qualities of the coatings and that the stoving cycle has been correctly carried out.

These results appear to agree with the findings of Nix and Wolpert, as described in Chapter 1, in that the effects due to particle size on the levelling of coatings are small. In these experiments all the powders came from the same powder batch and therefore no effects due to formulation need be considered. The type of clusters of particles mentioned by Wolpert (S. Wolpert et al, 1972) have given noticeable results for the <10μm range powder.

It can therefore be concluded, on the basis of the results for this powder and its size ranges, that particle size has negligible effect on film properties. Therefore any increase in deposition efficiency gained by changing particle size of the powder can be made

without fear of losing physical qualities of the final film. This conclusion also appears true for coatings of any thicknesses between 20 and 100μm.

3.11 Summary

The apparatus and experimental methods used in the assessment of the physical qualities of electrostatic powder coatings have been described.

Particular emphasis has been placed on the measurement of film thickness, gloss and related properties, and surface roughness. Experimental results, presented as a three way comparison, have been discussed. It has been found that there is no significant difference in the properties of films with size of powder sprayed or thickness of film produced.

The following chapter describes investigations performed in order to discover and understand some of the reasons for these results.

CHAPTER 4

PARTICLE STOVING AND PACKING OBSERVATIONS

4.1   Introduction

The examination of the coatings produced from different sized

particles has shown that there is very little difference in the

physical properties of the coatings for any of the sizes used. The

differences in surface roughness and gloss were greater than in other

properties but the physical significance was negligible. However, it

has been observed that in all the gloss and surface roughness

measurements the coatings of commercial powder exhibit more definite

trends than any other powder. This is the only powder with a wide

size distribution encompassing all the sizes used in the other

powders.

To try and gain some understanding of the reasons why this lack

of any apparent effect is observed further investigations into the

way in which particles pack and stove have been carried out.

Investigations were on a very exploratory basis but some of the

findings gave rise to more formal types of investigations which in

turn produced very interesting results.

4.2   Stoving Observations

Experiments of a very simple nature were conducted to observe

the way in which powders flow out. This was accomplished by observing

particles melting on a microscope hot stage. Some of these experiments

were recorded by using a cine camera placed above the microscope

eyepiece (having removed the objective lens). A diagram of a similar

apparatus employed is shown in Figure 4.1.

A diagram showing the way in which particles flow has been already

given in Chapter 1.

Various stoving experiments, involving sprayed plates and single

particles,were carried out. A few 2" square plates were coated

using the commercial equipment and then placed on the hot stage.
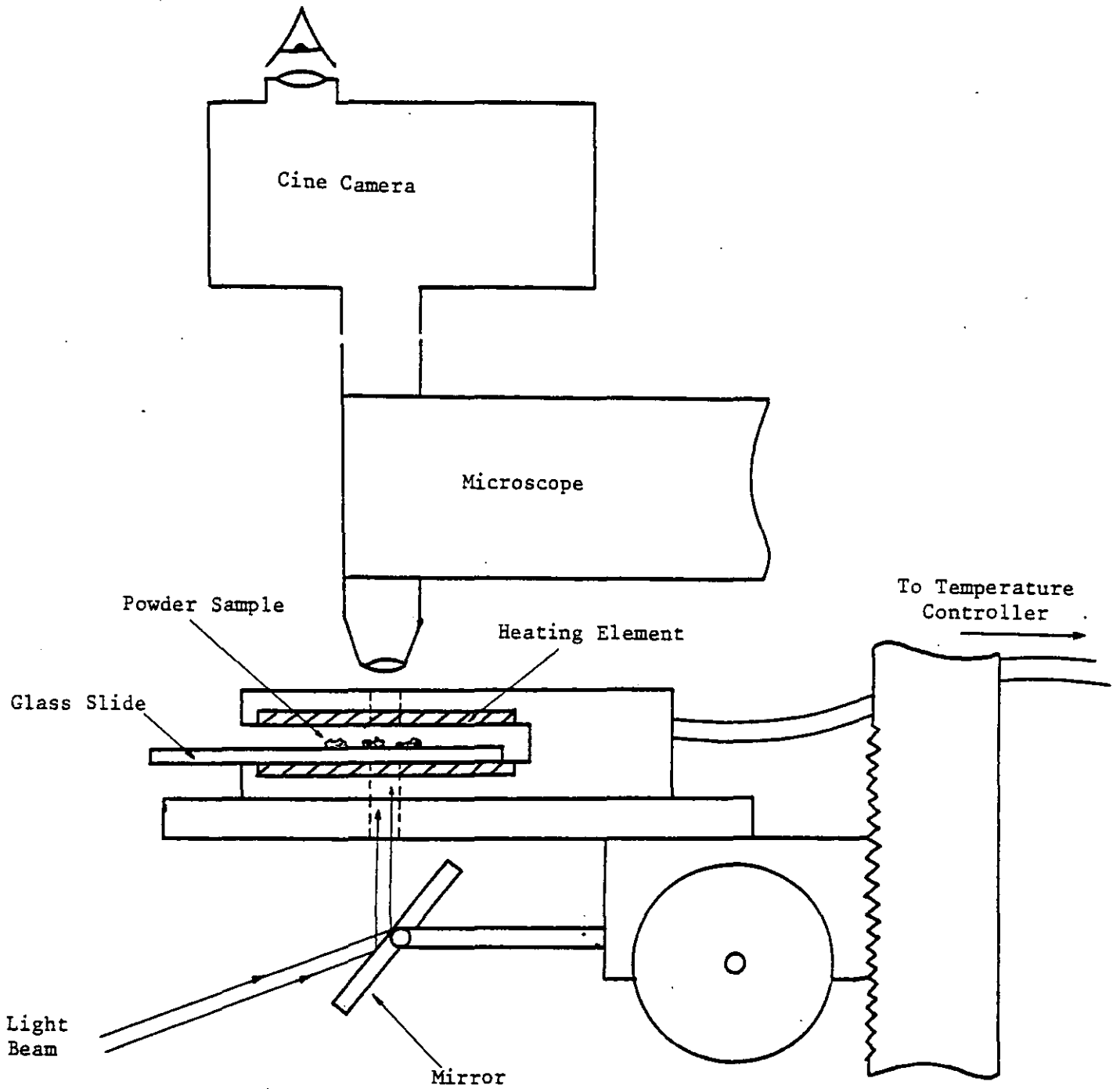
Figure 4.1. Microscope Hot-stage Apparatus

For this case it was found that the thicker layer of particles gave focussing problems. When the packed particles started to melt the level of the coating dropped substantially. Due to the small depth of field of view the coating then moved out of focus and therefore manual adjustment was required whilst filming took place. Also, as the coating levelled out to its characteristic smoothness, the surface could not be clearly seen due to the lack of detail making focussing increasingly difficult.

It should be noted that this method of heating is different to that encountered by a coating in the stoving oven. Heat is only being applied from the base through the metal, and hence, up through the coating.

In a stoving oven the heat, for thin plates, will come from both sides. For large bulky objects that have a large amount of base metal the heat for melting will mainly come through the surface and hence the powder layer. It is more likely in these cases that unstoved powder could be left near the substrate giving poor adhesion qualities. As expected, in the case of the thin sample plates used in the previous experiments, this was not observed and both adhesion and corrosion characteristics were to a high standard.

4.2.1 Experimental Observations

From the cine films that were taken of single and groups of particles melting, it was found surprising the extent to which the powder spread during the flow out stage. When an irregularly shaped particle was melted it initially tended to form a ball. This is shown in Plate 4.1. The particle lost all of its irregular shape characteristics. After this stage the powder then flowed out and covered

Plate 4.1.   Melting of an Irregular Shaped Particle

nearly three times of its initial substrate area.

When a few particles placed together on the same plate were stoved it could be clearly seen how the whole of the surface can be coated with a relatively small amount of powder. This is shown in Plate 4.2. In the first picture the irregular particles are seen to cover a small area of the plate. As the time of heating progresses some of the particles contract into balls and then begin to spread. They then flow into other particles and the flow out continues.

This is also shown on the next plate (Plate 4.3) in which the latter stages of powder flow is shown in silhouette form. These photographs were taken using transmission microscopy. A few separate particles fuse together to form a coating.

However, although this tends to show that the powder from individual particles mixes in with others, the actual mixing between particles is limited. This was confirmed by spraying a sample plate with a mixture of coloured particles. Three different colours were used, equal amounts being mixed together, and these were sprayed onto a glass slide so that the underneath could also be seen. Spraying of glass was effected by first spraying the plate with an anti-static spray agent which allowed the plate to be grounded to a better extent than with a normal glass plate.

The results from this experiment, after stoving of the coating, are shown in Plates 4.4(a) and 4.4(b). It was found very difficult to focus since there was no surface detail. The boundaries between different coloured particles are very hazy and do not help in this matter.
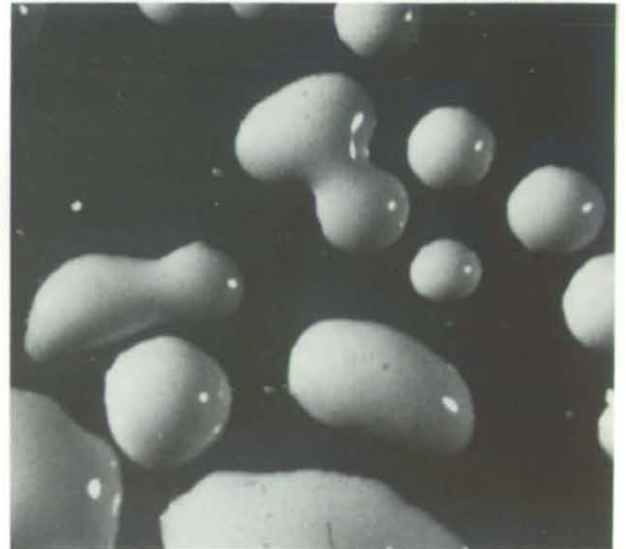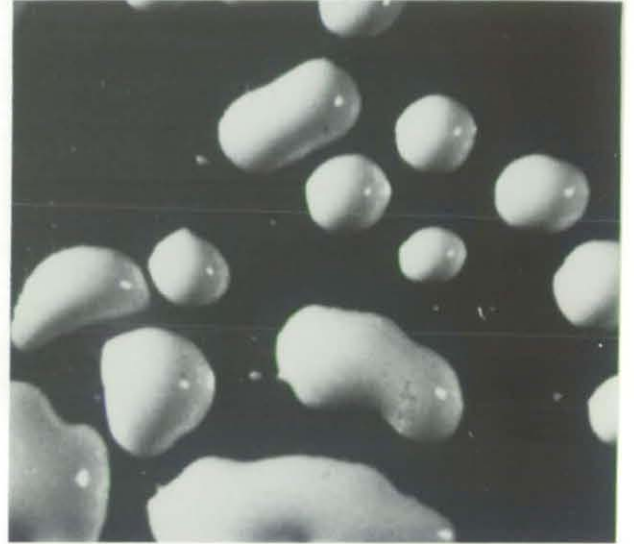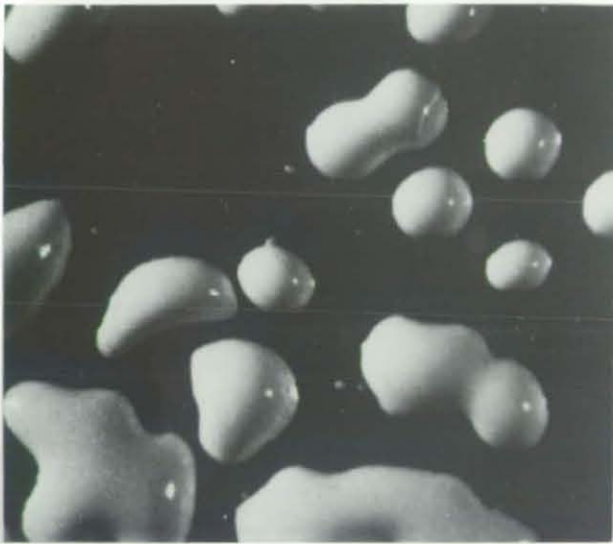
Plate 4.2. Melting and Fusing of Powder Particles
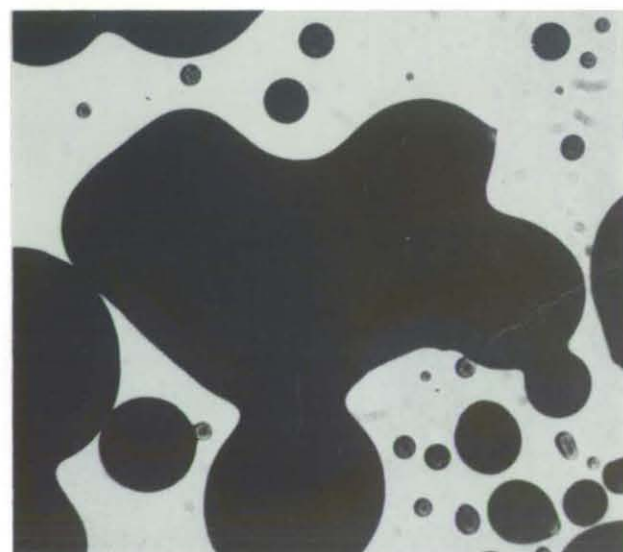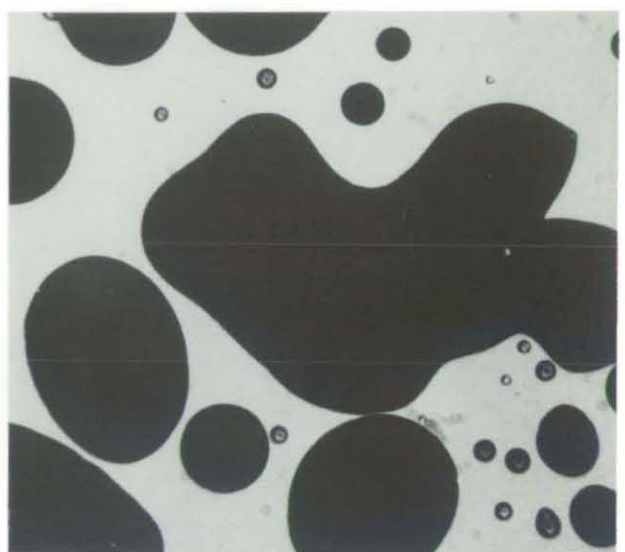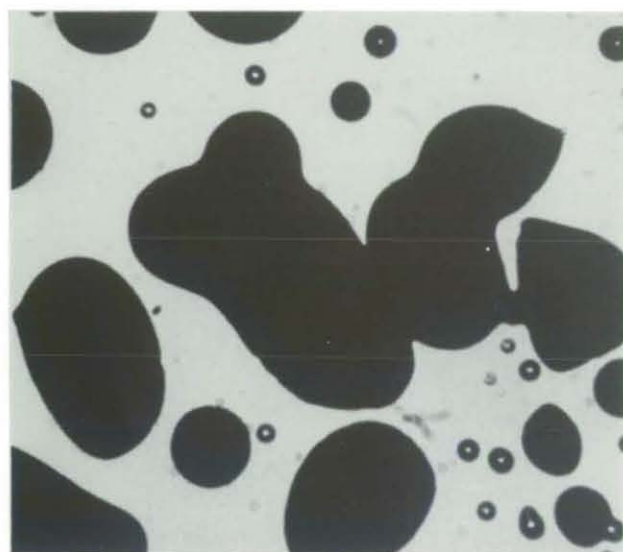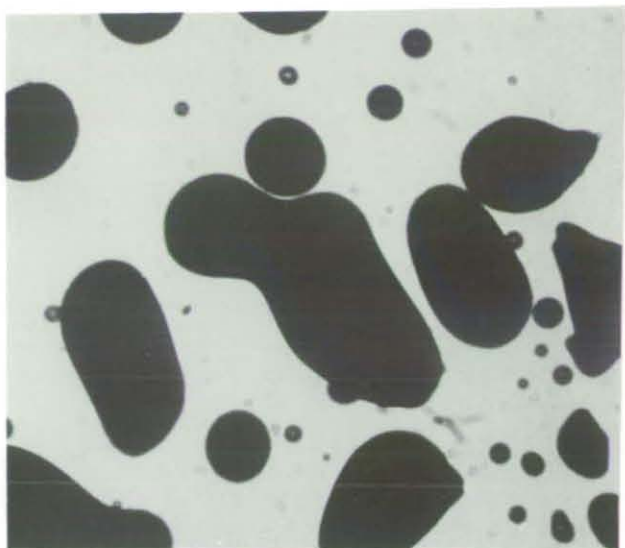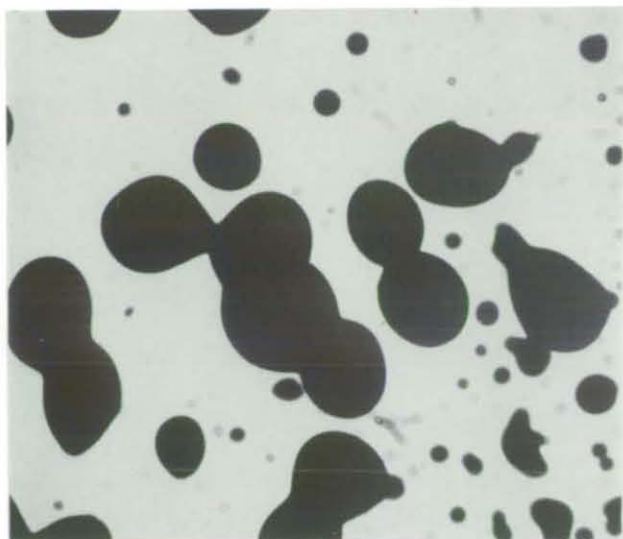
Plate 4.3. Silhouettes of Melting and Fusing of Powder Particles
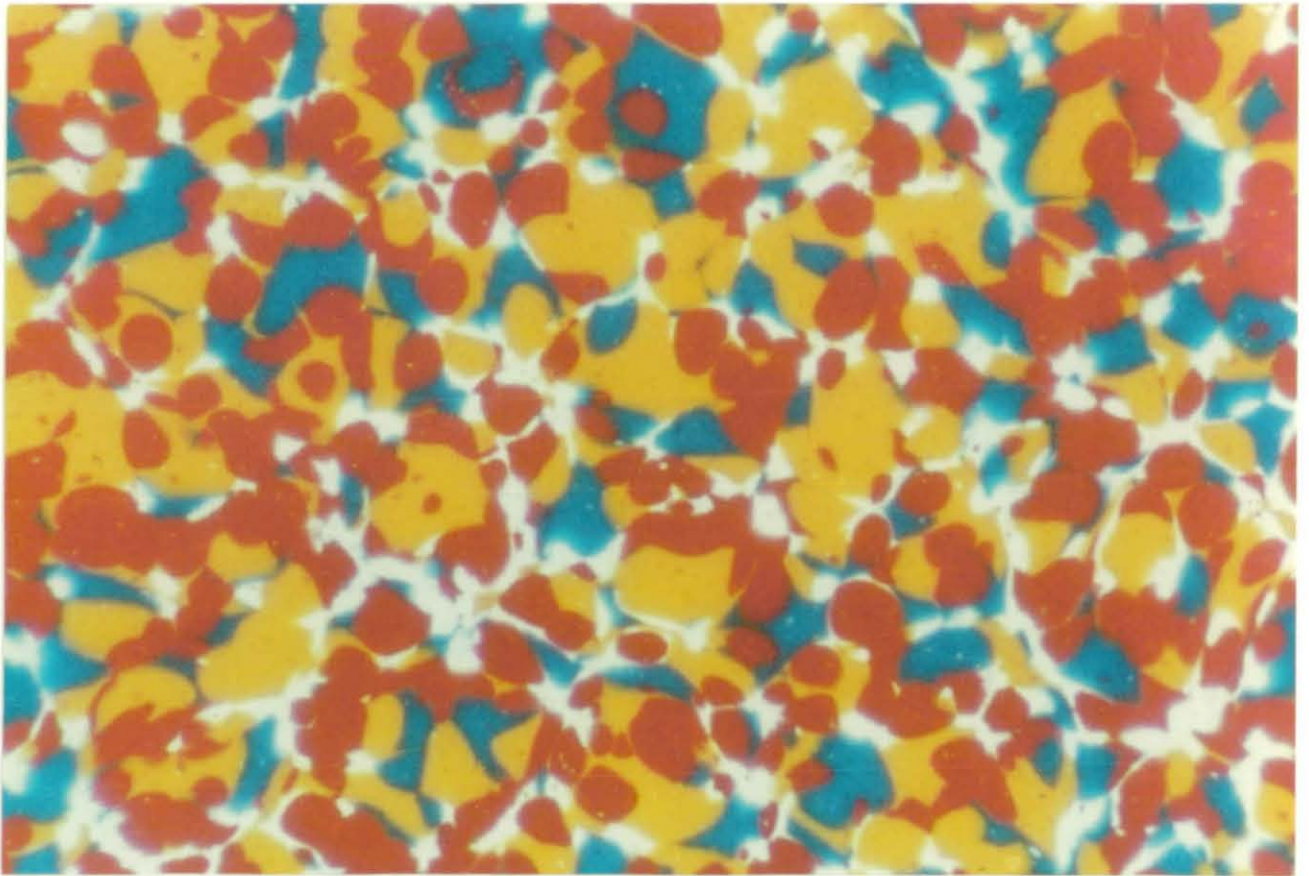
Plate 4.4.   Stoved plate coated with coloured particles viewed from (a) above and (b) underneath (lower picture)
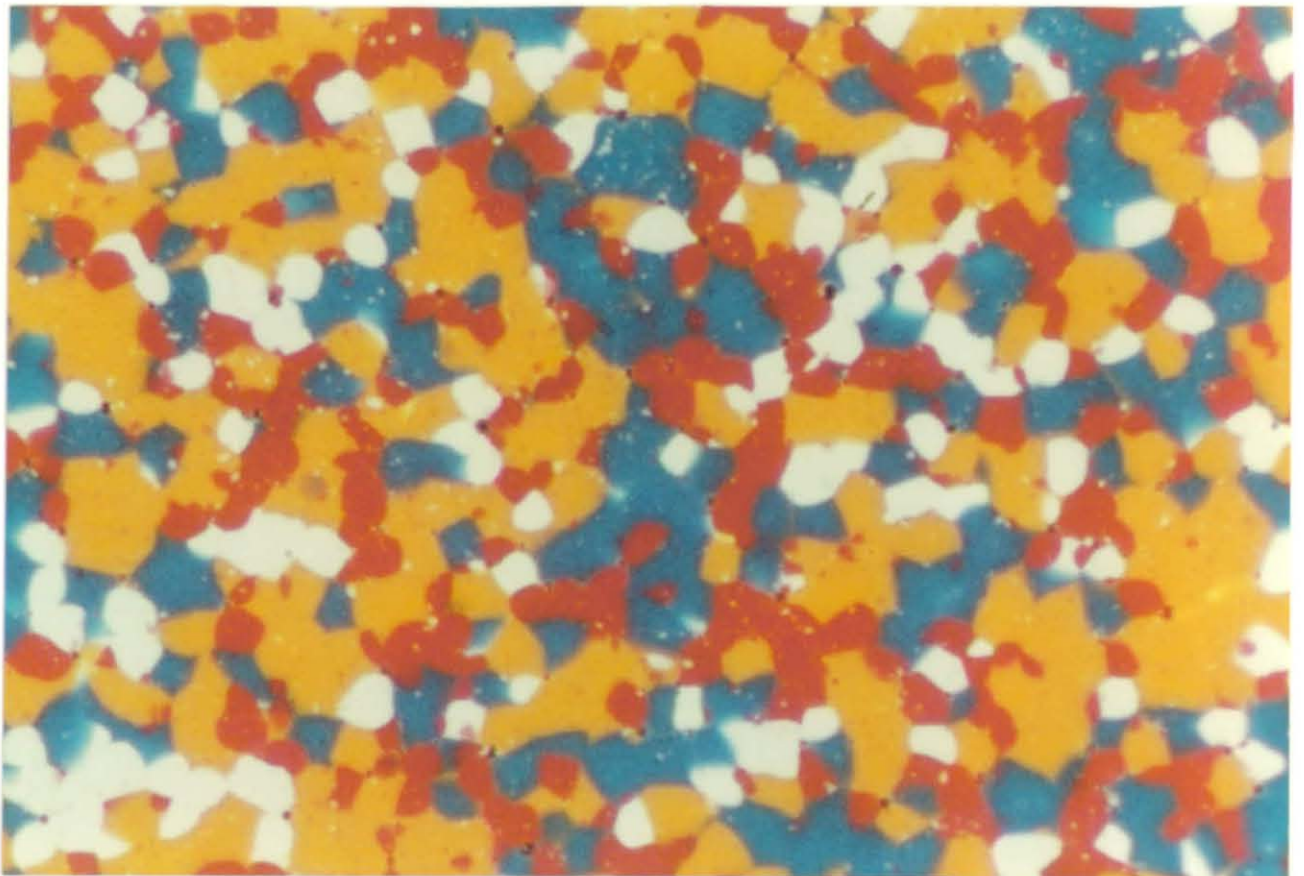
It can be seen that there is a small amount of mixing at the boundaries but the bulk of the particle, although having flowed, keeps its basic colour.

4.2.2   Comparison of Different Types of Powder - Spreading vs Finish

The previous simple experiments have shown that, on melting, this powder flows to a great extent and this could be the overriding factor when comparing coating properties with particle size sprayed.   Due to the excellent flow out characteristics of this powder any effect of particle size could be nullified thus giving only small changes in physical properties observed.

The effect of flow out characteristics was investigated to see if there was any correlation between the flow out properties of powder and the final finish that is produced.   A spreading factor, in terms of the increase in diameter of a particle being heated on a hot plate, was used to represent the flow out of the powder.   The final surface finish was assessed by visual observation of gloss and surface smoothness.

4.2.3   Determination of Spreading Factor

Five different types of powder, which were known to produce different final film finishes, were used.   The apparatus employed is shown in Figure 4.1.   Several particles were placed on a glass slide and placed between the heating elements.   The temperature was rapidly raised to $180^{o}C$ and the melting of particles recorded by a cine camera at 12 frames/sec.

Spray coatings of the powders were produced using the standard technique and then stoved in the oven at the manufacturers recommended conditions.   The coatings were visually assessed and placed in order of merit.

The films of particles melting were analysed using a Vanguard image analyser. This device allows a frame of film to be enlarged onto a screen (0.5 x 0.3m) where, using an electronic cursor, positions on the screen can be logged by computer. The initial diameters of the particles were recorded by logging the leftmost, rightmost, upper and lower points of the particle when it had contracted to its smallest size. This was repeated when the particle had spread on melting to its fullest extent. The change in size of a typical particle as it flows can be seen in Plate 4.5. From this data the vertical and horizontal diameters were averaged for 10 particles of each powder. The data was analysed by a computer program which gave a spreading factor based on the ratio of the initial and final particle diameters.

4.2.4 Experimental Results

A summary of all the results obtained from the determination of spreading factor and visual assessments for the five different powders is shown in Table 4.1.

The recommended time and temperature of stoving for each powder is also given. The spreading factor is given as the ratio of the final and initial melted particle diameters. The ratio of areas is also given.

The best three coatings were difficult to visually assess in that they were all very similar. The polyester powder which was the worst gave a mottled type finish which was very uneven and obviously had not flowed out very well. In this case levelling had not taken place to the same extent as the others.
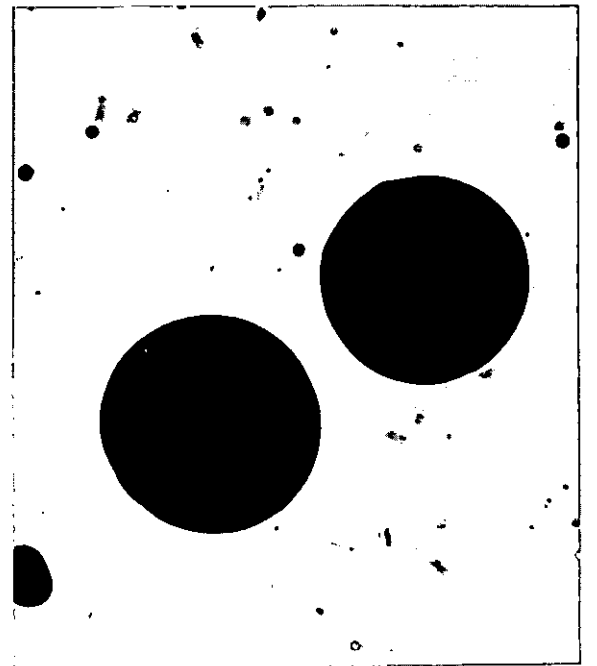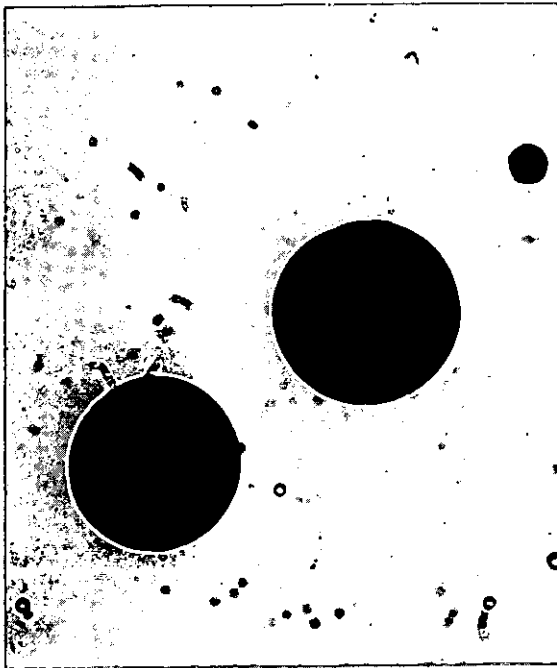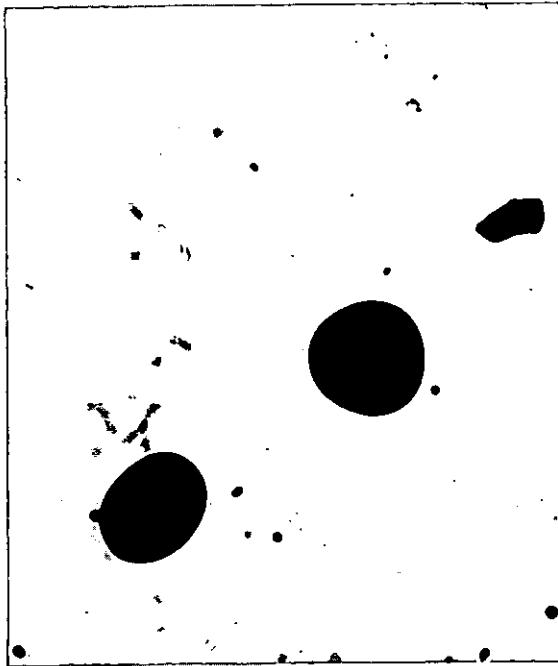
Platéc4᷍5.   Change in Spreaded Area of Particle during Coating

Table 5.1. Stoving of Five Different Powders - Comparison of Spreading Factors

Powder Type	Cure Temp (°C)	Time (mins)	Visual Inspection[†]		Measured Diameter		Diameter Ratio A/B	Area Ratio	Grading[†]
			Gloss	Smoothness	Before	After			
Slow Cure Amine Epoxy	180	20	2	1	1.03	1.82	1.77	3.13	1
Polyester	180	15	5	5	0.97	1.27	1.31	1.72	5
Epoxy Polyester	180	10	1	2	0.99	1.61	1.62	2.62	3
Fast Cure Anhydride Epoxy	180	10	3	3	1.01	1.76	1.74	3.03	2
Fast Cure Amine Epoxy	180	10	4	4	1.09	1.67	1.52	2.31	4

[†]Gradings   1 = best, 5 = worst.

4.2.5 Discussion of Results

The determination of a spreading factor using this method can be seen to show a good indication of the type of finish that might be expected from a powder. The higher the spreading factor, the better the flow characteristics of the powder and hence the higher the quality of the coating produced by electrostatic spraying.

The standard powder used in the earlier experimental tests obviously had excellent flow characteristics which resulted in very good films being produced with respect to adhesion, corrosion resistance and porosity. The effects seen in these stoving experiments agree with the work carried out by Wolpert et al and Nix et al. (S.M.Wolpert et al, 1972; V.G.Nix et al, 1973). Wolpert stated that the levelling of a coating is very dependent on the gel time which occurs when there is a drastic change in viscosity. Viscosity is critical to the levelling but below a certain amplitude surface tension effects are important. Nix agreed with this but found that other factors also have a bearing. Particle clusters were observed to be one source of orange peel. After individual particles had melted and flowed the radius of curvature of imperfections will be due to either the clusters or to orange peel 'hills and valleys'. Trapped air in the dry powder layer also appeared to have an effect on the flow of powder coatings. Spitz concluded that the ripple in powder coatings originates from the uneven deposition of powder due to particle size and particle clusters. Again the clusters were observed to have more effect than particle size. The ripple wavelength increased with levelling according to Orchards theory (G.T. Spitz, 1973; S.E. Orchard, 1962).

In this study the powder sizes investigated originate from the same powder formulation. Therefore any changes in surface property will be due to particle size, packing orientation, porosity (trapped air), and particle clusters; as opposed to different melt viscosities, gel times or surface tensions. For this powder, however, little difference has been observed with particle size or film thickness. This is probably due to the excellent flow properties given by the formulation. Slight increases in roughness with particle size were observed which seem to agree with the findings of the previously mentioned workers.

The commercial powder showed more definite trends than any other powder sprayed and so the observations of packing of this distribution on a substrate is now described.

4.3 Particle Packing Considerations

In line with general observations of particles stoving on a substrate, experiments were carried out to investigate the packing of different sized particles. To achieve this different coloured powders were used to represent size fractions of the powder distribution.

Various colour combinations could then be used to observe where certain sizes had landed on the substrate or in the packed layer.

4.3.1 Effect of Formulation on Powder Characteristics

Since it is possible that different powders have different characteristics with regards charging, stoving etc., it was necessary to look at the characteristics of the powders being used.

It was understood that apart from the obvious difference of pigmentation, the four different coloured powders were basically

chosen for their similar formulation. However to confirm that they

did not behave substantially different they were subjected to two

tests; namely determination of spreading factor and measurement of

charging characteristics.

Films taken of the red, orange, white and blue powders melting

were analysed in the manner previously described. The results are

given in Table 4.2. It can be seen that the standard deviations about

the average of the results is very small. There is very little

difference in the spreading factors of the powders although it was

observed that the red powder was found to be much slower in the time

it took to start melting.

Since the ratio of the diameters on spreading will be dependent

on the size of particles used, particles of similar size were chosen

for analysis. This can also be seen from the table of results. The

orange, white and blue powders were chosen for further experiments

since they provided a contrasting mixture of colours and the red

powder was different in that it had a longer time to melt start.

The charging characteristics measurements were carried out at

the Electrical Engineering Department of Southampton University by

Dr. S. Singh. An airless gun was used to charge the powder and a

Faraday cup used to collect the charged powder. A grid was placed

in front of the Faraday cup to remove excess ions. The weight of

powder collected and the charge leaked away is recorded hence giving

a charge to mass ratio measurement. (S. Singh, 1979).

The results of these measurements are given for the three powders

in Table 4.3. It was not possible to make measurements for the <20μm

range as the powder would not flow well. Slightly higher values of

Q/M were obtained for the orange and blue powders but it was considered

Table 4.2.   Spreading Factor Results of Four Coloured Powders

White			Orange			Red			Blue		
Before	After	A/B	Before	After	A/B	Before	After	A/B	Before	After	A/B
1217	2050	1.684	1270	2188	1.723	1225	1986	1.621	1076	1811	1.683
1337	2287	1.711	1110	1846	1.663	1207	1942	1.609	1489	2360	1.585
1310	2177	1.662	1219	2137	1.753	1011	1721	1.702	1184	2180	1.841
1057	1763	1.668	1512	2601	1.720	1289	2211	1.715	1072	1838	1.714
1205	1770	1.469	1145	1973	1.723	1553	2440	1.571	1384	1969	1.422
1480	2488	1.681	1275	2345	1.839	1772	1988	1.696	1349	2293	1.699
1146	2264	1.975	1169	1883	1.610	988	1748	1.769	1118	1842	1.647
977	1713	1.753	1061	1895	1.786	1136	1813	1.595	1007	1634	1.622
1179	1977	1.676	1076	1897	1.763	1146	1821	1.589	1007	1945	1.931
1209	2084	1.723	1188	2027	1.706	1155	1940	1.679	1241	2020	1.628
1350	2190	1.622	1217	2180	1.791	1168	1903	1.629	1442	2443	1.694
1250	1868	1.494	1421	2035	1.432				994	1596	1.606
Average		1.677			1.709			1.652			1.673
Standard Dev.		0.122			0.101			0.060			0.122

All measurements are in terms of diameter of melting particles

that these were insignificant differences. (S. Singh, 1980a).

None of the powders reached the predicted saturation charge, as shown in the table, and it was noticeable that the small particles had effectively the same charge as large ones.

4.3.2 Experimental Observations

The average size distribution of the coloured powders was found by determining the distribution of each of the powders using a Coulter Counter. Dispersion of the powder in the electrolyte was found difficult, but was aided by addition of 'Tergitol'. The average distribution is shown in Figure 4.2. Each of the powders were classified using the Alpine zig-zag classifier into three fractions, namely <20µm, 20-40µm and >40µm. These fractions were then mixed together in appropriate quantities as given in the table below to form the three different mixtures.

Size Range	<20µm	20-40	>40µm
Wt % in Range	16.0	35.0	49.0
Mixture 1	Orange	White	Blue
Mixture 2	Blue	Orange	White
Mixture 3	White	Blue	Orange

Each of the mixtures were sprayed onto the large 10" x 8" plate which was covered with twenty 2" square sample plates. After spraying, the plates were compared to the original powder fed to the spray gun, and this is shown for the three mixtures in plates 4.6, 4.7 and 4.8.

A leitz microscope and associated equipment was used to photograph the powder coating in closer detail. The apparatus is shown in Plate 4.10.

Figure 4.2.   Average Size Distribution of Coloured Powders
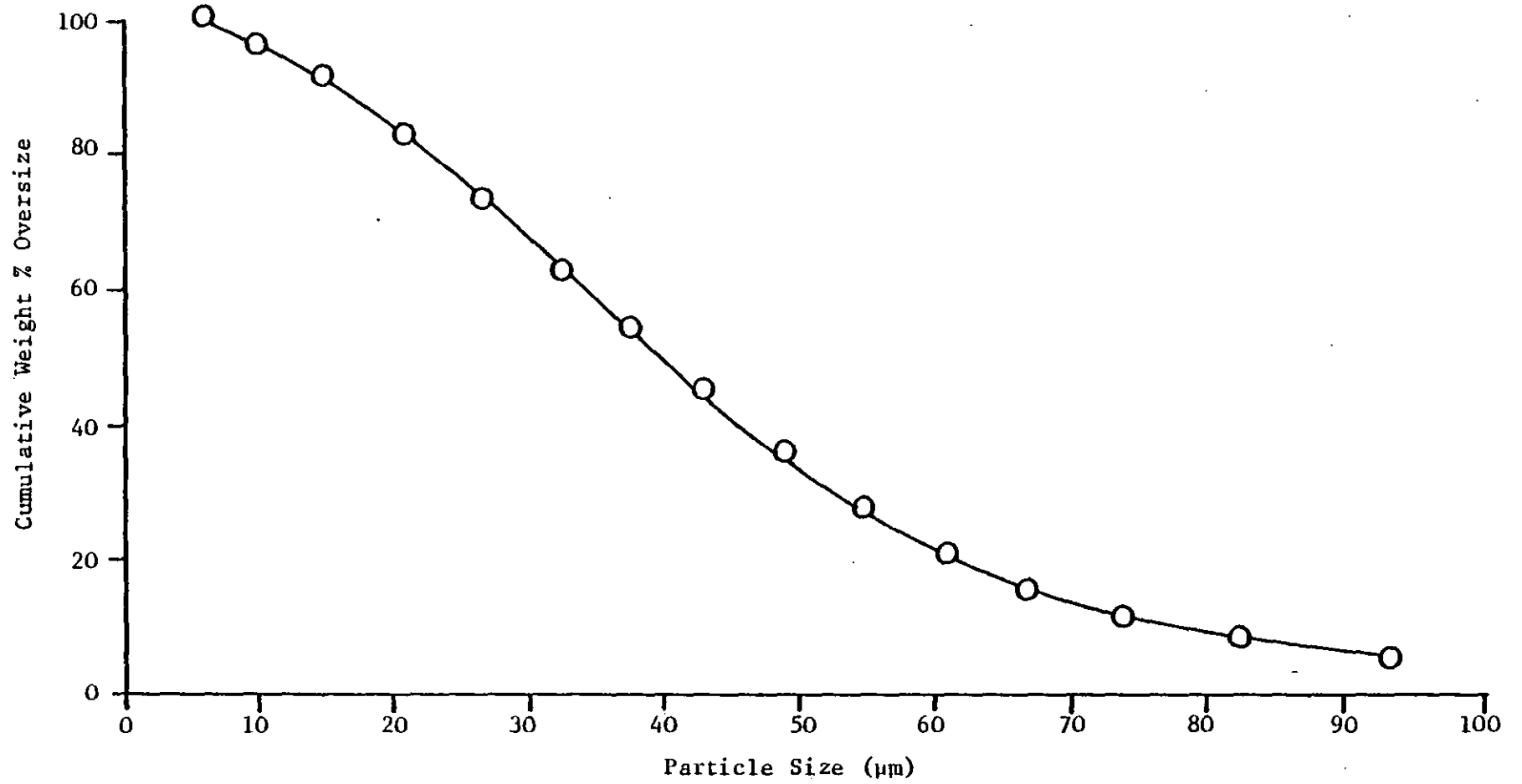
Table 4.3. Charge to Mass Ratio Measurements of Coloured Powders

Powder	Size Fraction	Measured Q/M	Predicted Q/M[†]	Fraction of Predicted
Orange	20-40	5.25×10^{-4}	1.17×10^{-3}	44%
Orange	+40	5.30×10^{-4}	7.07×10^{-4}	75%
Blue	20-40	5.65×10^{-4}	1.17×10^{-3}	48%
Blue	+40	5.05×10^{-4}	7.07×10^{-4}	71%
White	20-40	4.50×10^{-4}	1.17×10^{-3}	38%
White	+40	4.47×10^{-4}	7.07×10^{-4}	63%

[†]assuming saturation charge, where $q_s = 3\pi \left(\frac{K}{K+2}\right)\varepsilon_o d_p^2 E_o$

$$\text{and where} \quad K = 4$$
$$\varepsilon_o = 8.85 \times 10^{-12}$$
$$E_o = 4 \times 10^5 \text{ V}$$

Plate 4.6.   Comparison of coating and feed material for mixture 1
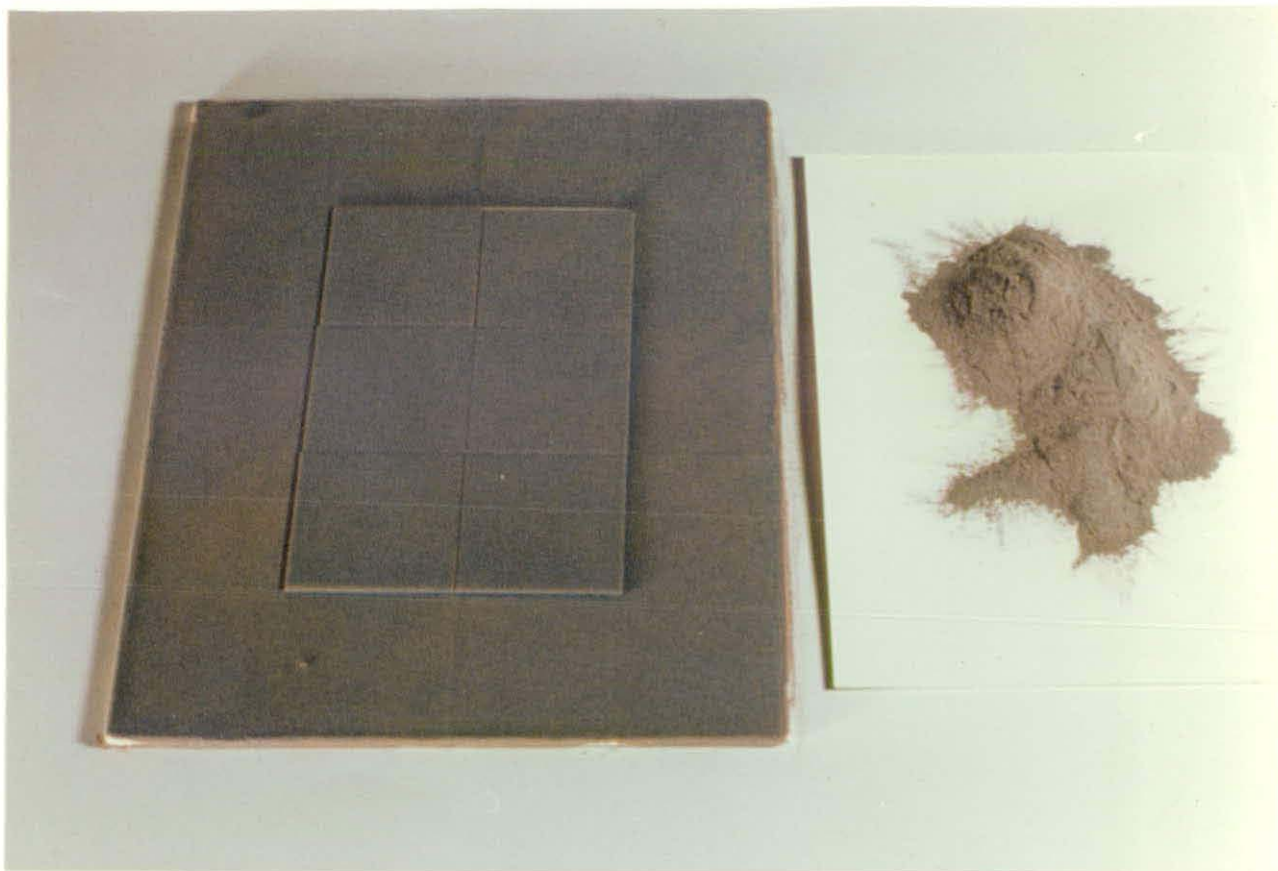
Plate 4.7.' Comparison of coating and feed material for mixture 2
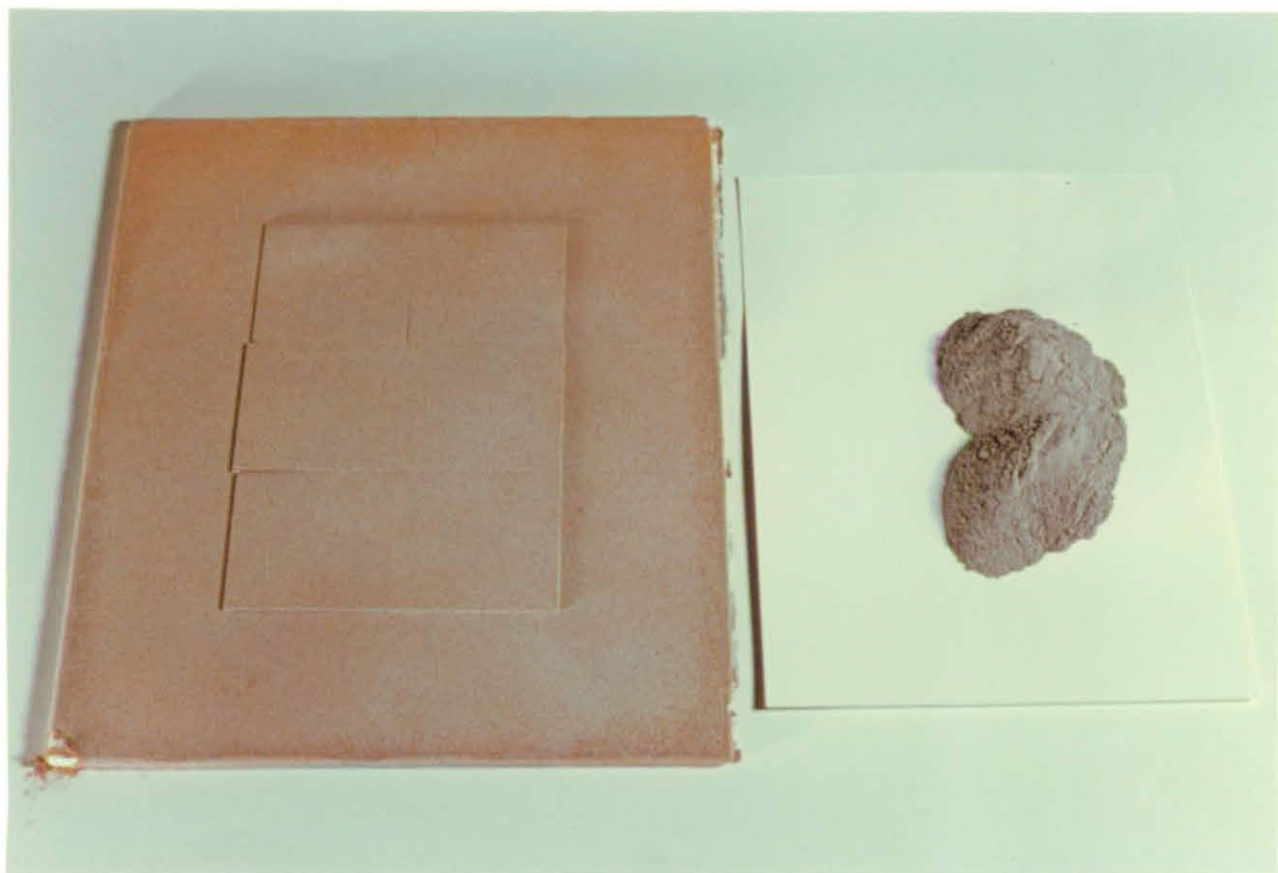
Plate 4.8. Comparison of coating and feed material for mixture 3
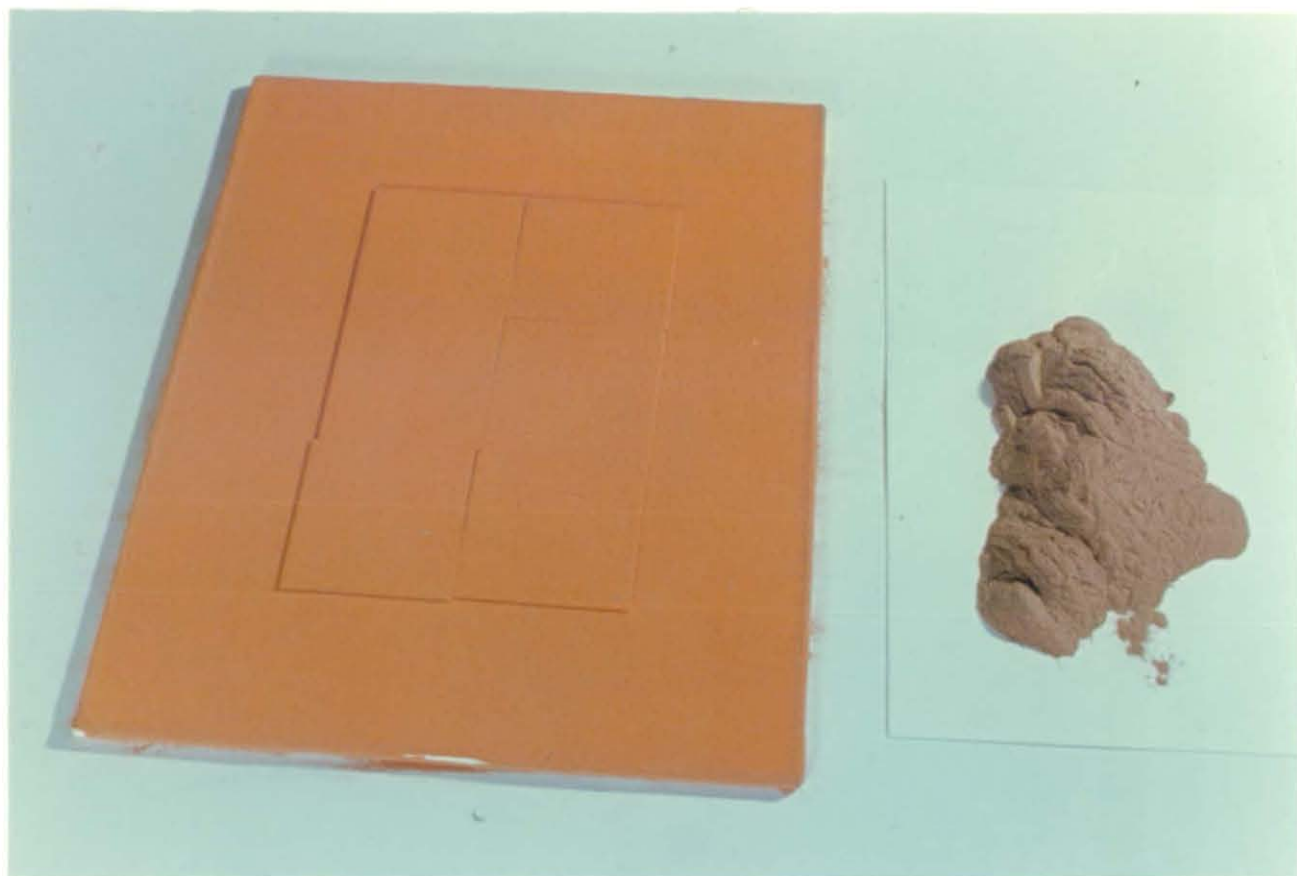
Plate 4.9. Microphotograph of upper layers of coating of mixture 1
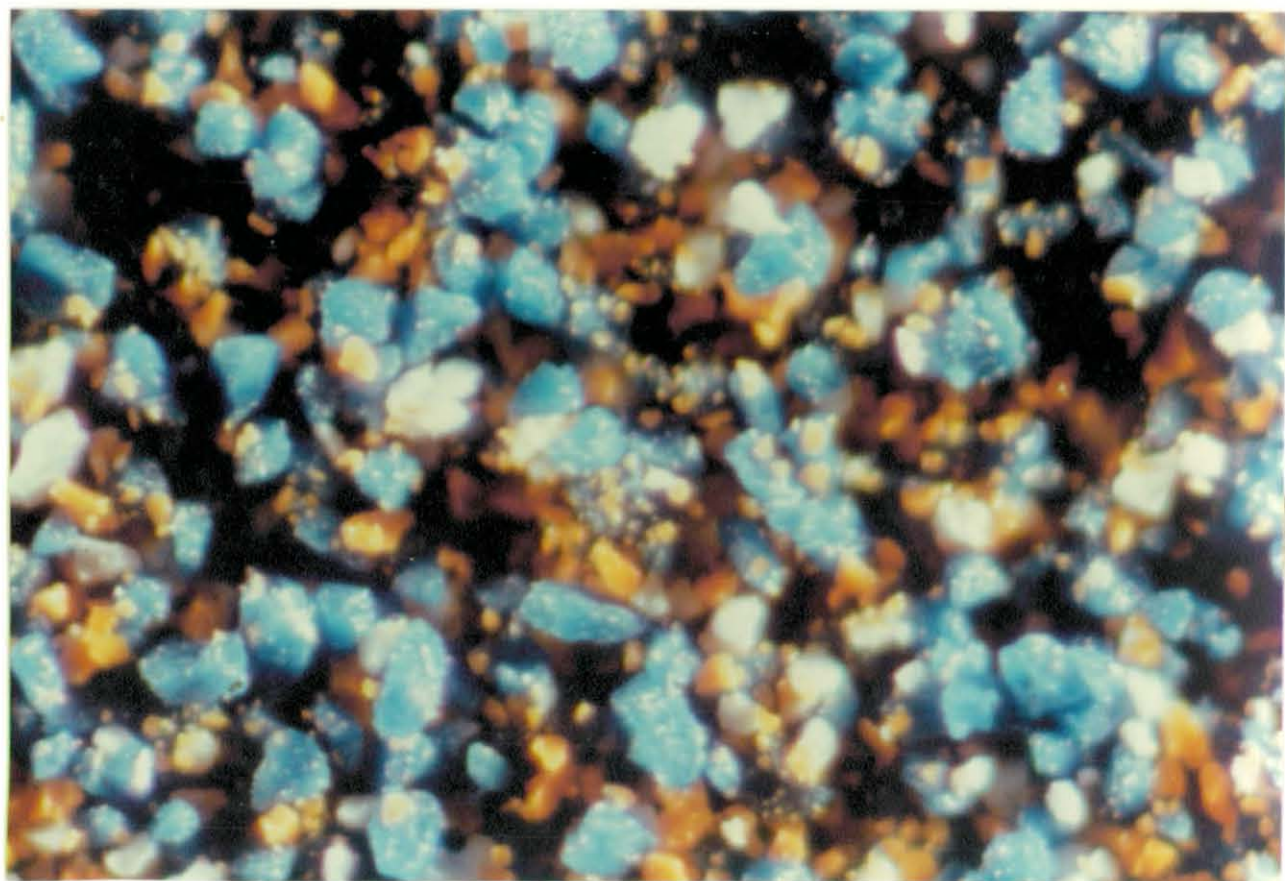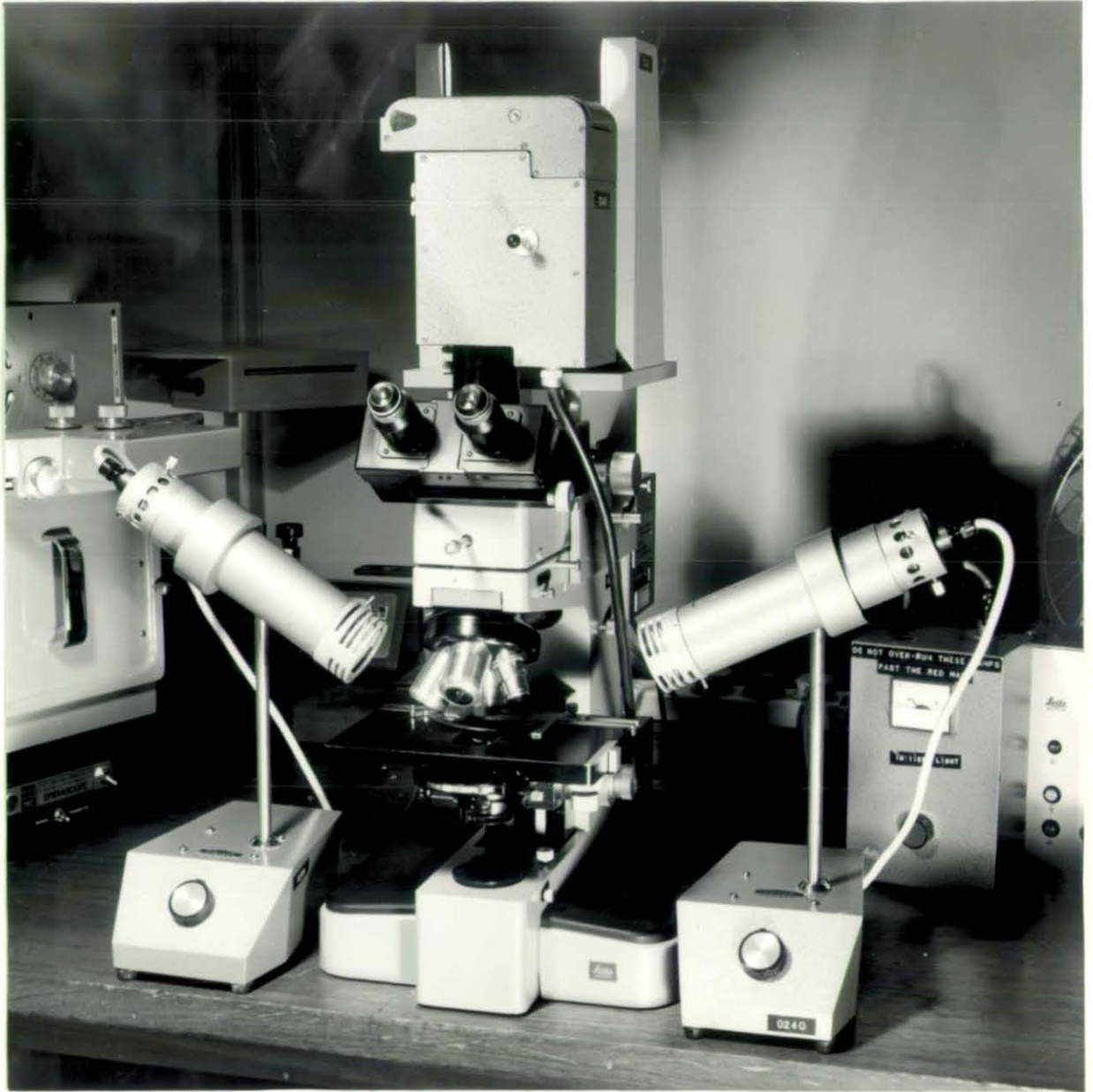
Plate 4.10. Leitz microscope and apparatus

Interesting effects were observed in each case. The uppermost layers predominantly consisted of particles of the largest size fraction. The comparison with the feed material clearly shows the difference in colours. Further microscopic observations of the individual 2" plates confirmed this and an example is shown in Plate 4.9. Here the largest fraction, blue, is seen to be predominant in the upper layers. The smallest fraction, orange, appears to be closest to the substrate. Two other points from this photograph should be noted. Firstly the packing can be seen to be very open; large crevasses are present between particles and the layers are fairly tall compared to the particle size. Secondly, it is observed that very fine particles, typically <10μm, stick to larger ones and in this case very fine orange particles are seen around the large blue particles.

In Plates 4.11 and 4.12 the surface layers are viewed at slightly different angles. Depth of field is very small but similar observations are made and tree-type structures can be seen.

Hence, it appears that a size segregation effect takes place through the packing in that large particles are preferentially deposited in the upper layers.

4.3.3 Quantification of Observed Effect

In order to quantify the effects that have been observed, to obtain data rather than consider only pictures, the size distributions of powders deposited on the plate were measured and compared to that in the feed hopper.

Plate 4.11. Microphotograph of a powder coating viewed at an angle
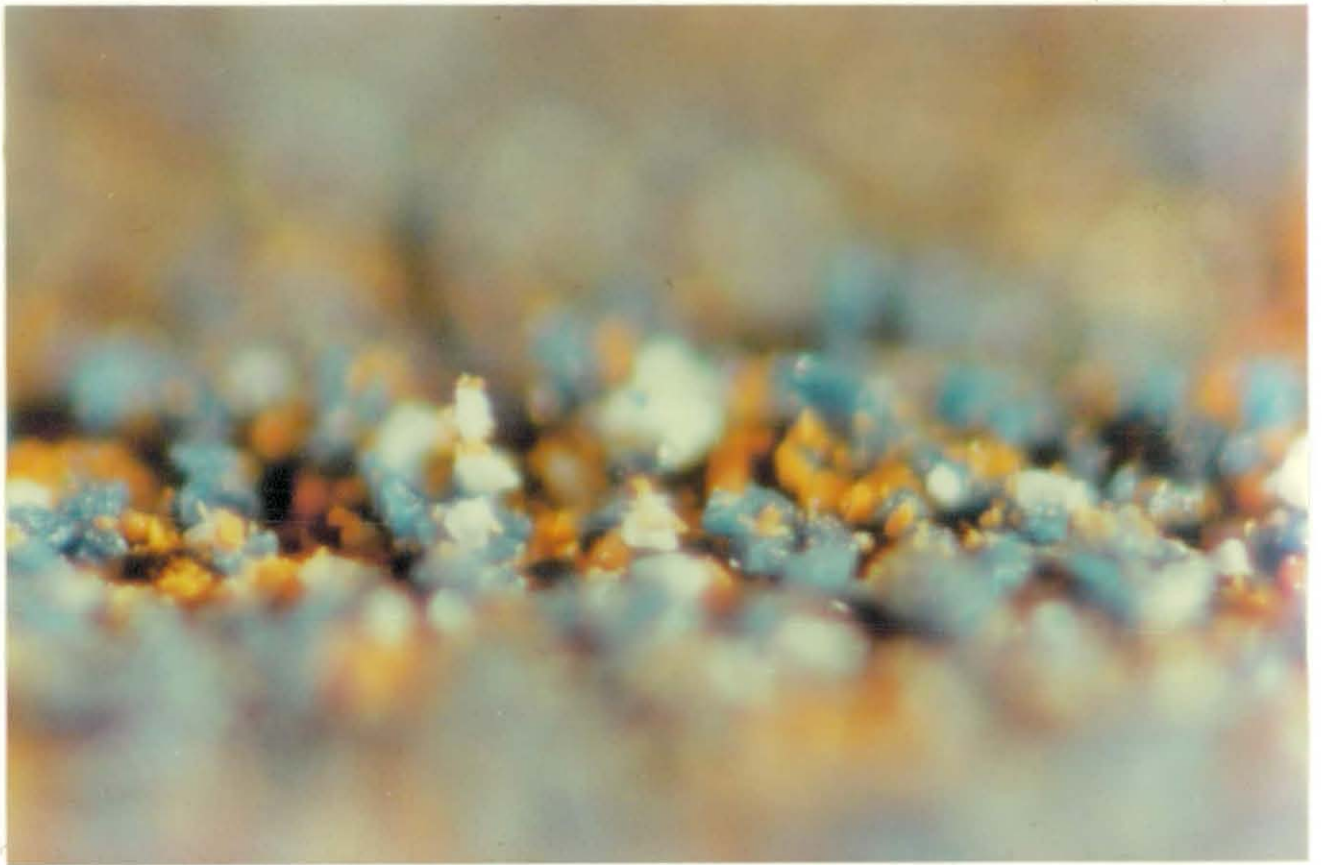
Plate 4.12. Microphotograph of a powder coating
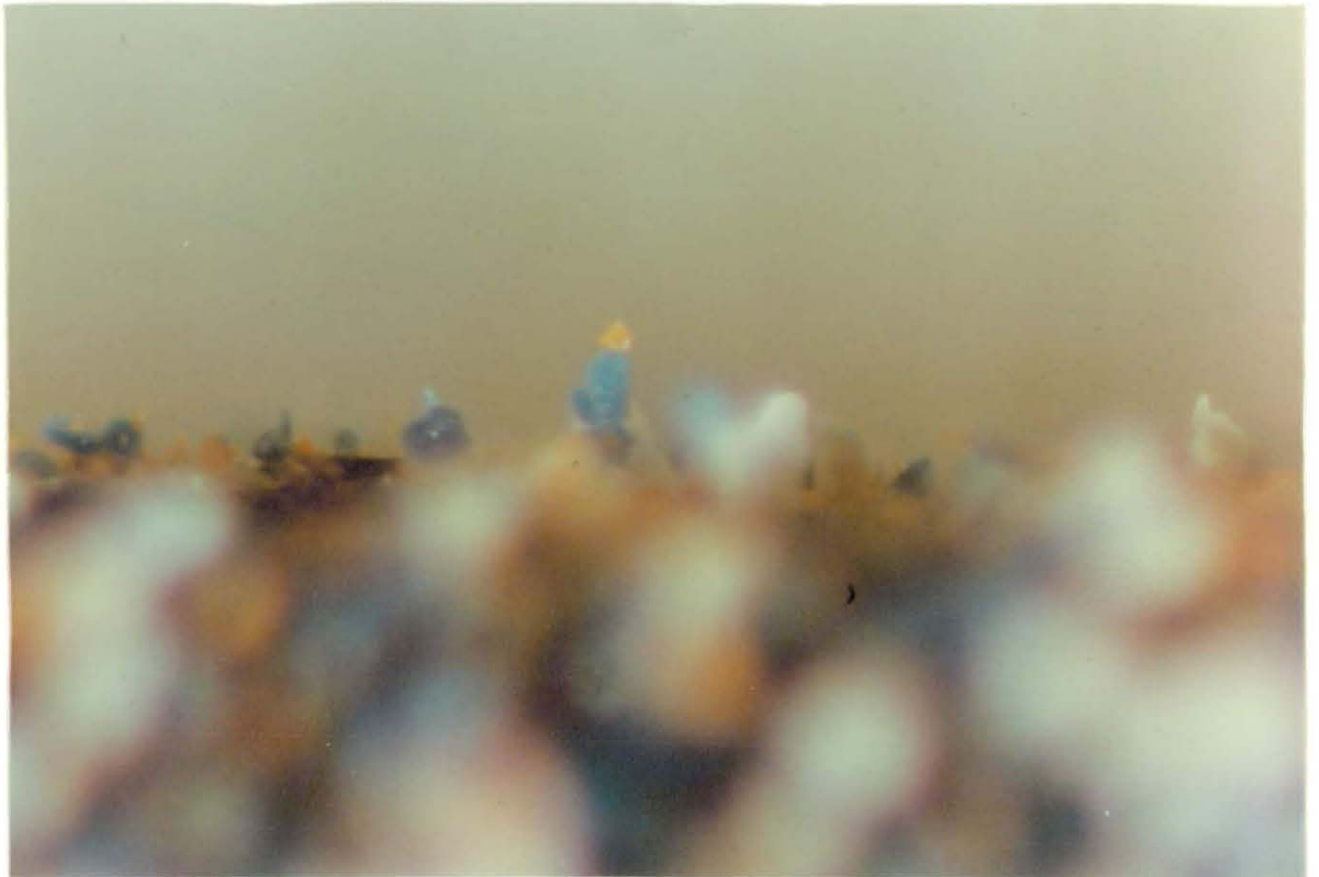
Two of the coloured powder mixtures were initially used for this

with size distributions being measured by the coulter counter.

However, problems of dispersion and sampling made the use of this

instrument unacceptable. Only a very small sample from the plates

can be placed in the coulter beaker and hence difficulty is encountered

in obtaining representative results. Dispersion of large particles

was difficult without using high stirrer speeds which then gave

problems with air bubbles.

The Microscal photosedimentometer was chosen as a device that

would measure size distributions in the range required and which gave

reproducible results because of the amount of sample used.

The experiments previously described were therefore repeated

using four different powders, two black and two white. These were:-

Powder 1 : Drynamels White Epoxy Anhydride (2A-022-C)

Powder 2 : Ault and Wiborg White Epoxy/Polyester (966-651-015)

Powder 3 : Drynamels Black Epoxy Anhydride (LFA 6319)

Powder 4 : Teodur Black Epoxy Polyester (SP 926/18/1)

Each of these powders had Q/M measurements taken at Southampton

University. Their charging characteristics are shown in Table 4.4.

(S. Singh, 1980b). Again there appeared to be very little difference

in the results.

The powders were sprayed onto twenty 2" square sample plates

held onto the larger 10" x 8" plate. One of the samples was then

washed into 500 ccs of distilled water. The Microscal wide angle

scanning photosedimentometer sensitivity control was adjusted so that

an intensity of 100% was obtained, when the light beam through the

Table 4.4. Charge to Mass Ratio Measurements for Four
            Different Powders

Powder Type	Colour	Size Fraction	Q/M x 10^{-4}
Epoxy Anhydride	White	20-40	4.1
		>40	3.6
	Black	20-40	5.3
		>40	4.8
Epoxy Polyester	White	20-40	4.9
		>40	3.8
	Black	20-40	5.0
		>40	3.8

cell of clean liquid was at its maximum. A photograph of the apparatus is shown in Plate 4.13.

The sample was then placed in the glass cell and the suspension was well stirred. At this time the chart recorder was switched on. The scan is started after a suitable length of time, this usually being when the chart recorder falls to below 30% of full scale. The cell is then automatically lowered so that the light beam 'scans' the sedimentation tank and reduces the height of fall of particles in the sampling zone. The chart recording is analysed and the optical density of the suspension (as a ratio) is measured at various times and recorded. A typical chart is shown in Figure 4.3.

The data is then used in a computer program to obtain the size distribution of the sample. This is based on the settling rates of different sized particles as given by Stokes Law:-

$$d_s^2 = \frac{18 \, \mu \, U}{(\rho_s - \rho)g}$$

where U is obtained by knowing the height dropped in time t (U = h/t).

Three samples were used for each powder sprayed, and each feed material. This method has the advantage of analysing all the powder on a sprayed plate and hence reduces sampling errors.

Plate 4.13. Microscal wide angle scanning photosedimentometer

OPTICAL DENSITY (D)

OPTICAL DENSITY (D)

OPTICAL DENSITY (D)

OPTICAL DENSITY (D)

Start of Scan

Start of Experiment
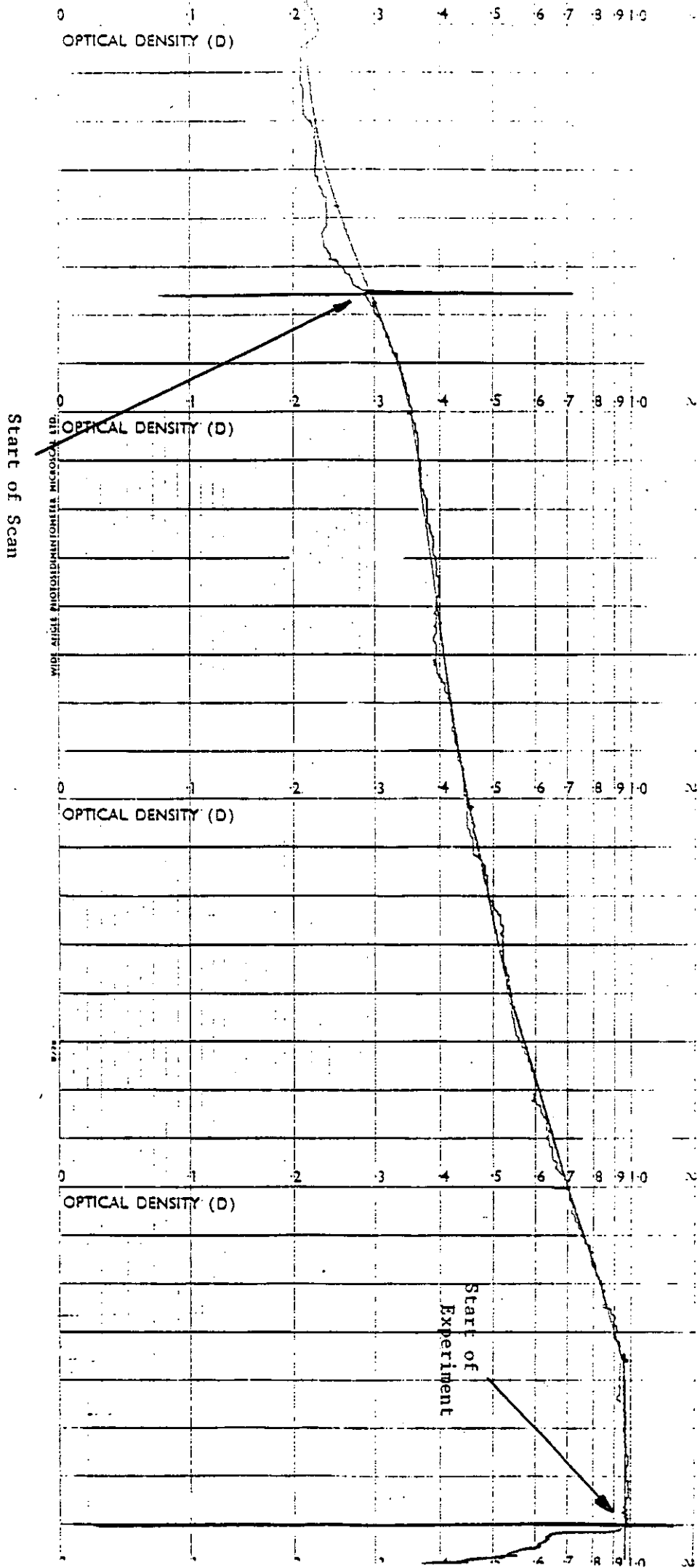
Figure 4.3. Typical Chart from Photosedimentometer

4.3.4 Experimental Results

The results from each of the scans are given, for all of the samples and for each powder, in the tables in Appendix C (Tables C1 to C8). Each of the distributions were drawn and the cumulative weight percentages under given sizes were collected and averaged to form the distributions shown at the right hand side of these tables. These have been determined for each powder, before and after spraying.

The size distributions are summarised in Table 4.5 for the four different powders. The comparison of size distributions are shown in Figures 4.4 to 4.7. Only distributions representing the smallest 50% of the powders have been shown in each case since it is the fines that are of particular interest. In each case the amount of fines is considerably lower in the powder after spraying. On average there is between 7 and 15% by weight less material smaller than 30µm in the powder on the sprayed plates. Therefore there is a definite change in size distribution of the powder on spraying, and involves a loss of small particles. It appears from the graphs that there is equal amounts of particles <10µm. Less particles of this size are lost probably because many of them stick to large particles and hence still land on the plate.

4.3.5 Discussion of Results

The analysis of size distributions of several powders and mixtures before and after spraying have agreed with photographed observations shown in earlier plates. When powders are electrostatically sprayed for a reasonable length of time a general loss of fines takes place. This is quantitatively confirmed by the changes

Table 4.5. **Comparison of Size Distributions of Four Different Powders Before and After Spraying**

Size μm	Cumulative Weight % < Size							
	Powder 1		Powder 2		Powder 3		Powder 4	
	Before	After	Before	After	Before	After	Before	After
10	5.7	4.9	5.8	6.8	5.4	3.5	6.5	3.8
15	7.3	5.6	7.5	6.9	6.5	4.0	9.1	5.1
20	10.9	7.3	10.0	7.6	9.3	6.7	14.1	6.6
25	19.1	10.9	15.5	10.5	14.9	11.0	20.9	9.7
30	29.5	16.8	24.5	18.0	23.0	16.5	29.0	14.5
35	42.0	24.5	35.5	28.3	32.8	22.5	37.9	21.3
40	57.1	34.7	45.8	39.3	43.4	29.5	46.7	29.2
45	70.2	47.3	55.5	50.0	54.2	36.5	56.5	37.2
50	82.1	62.3	–	60.0	–	44.0	–	47.4

Figure 4.4. Size Distribution of Powder 1 Before and After Spraying
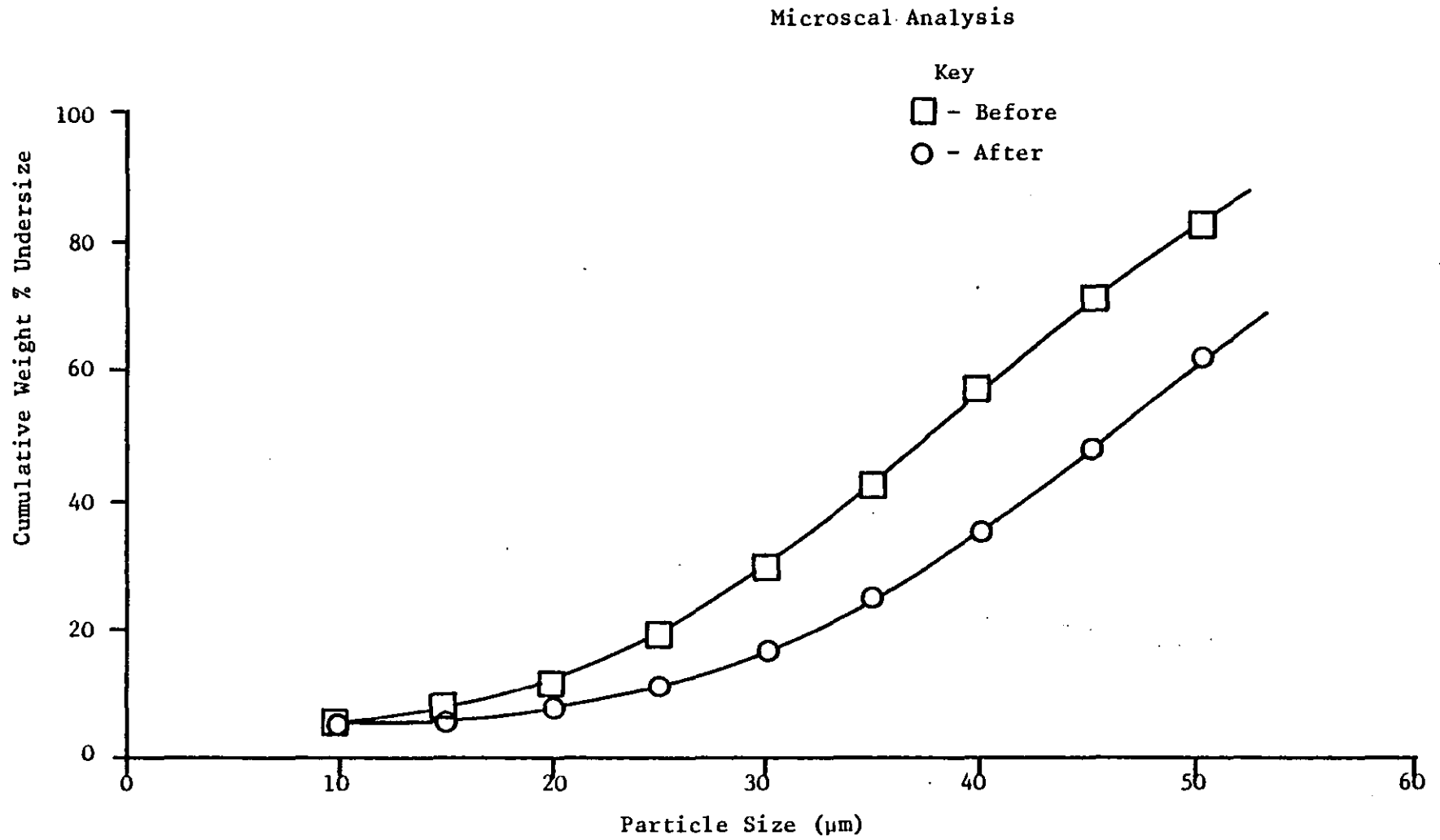
Figure 4.5.   Size Distribution of Powder 2 Before and After Spraying
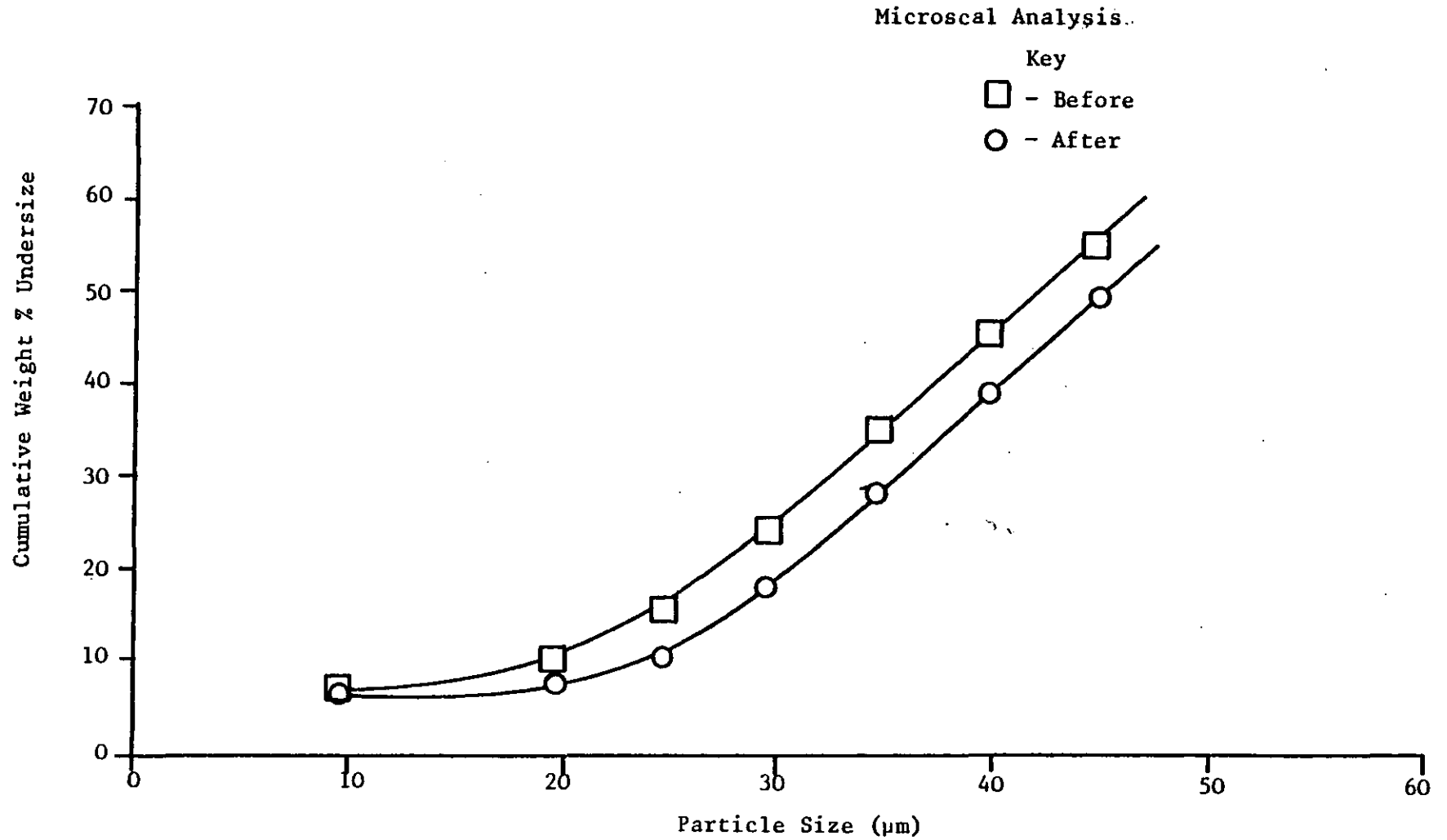
Figure 4.6. Size Distribution of Powder 3 Before and After Spraying
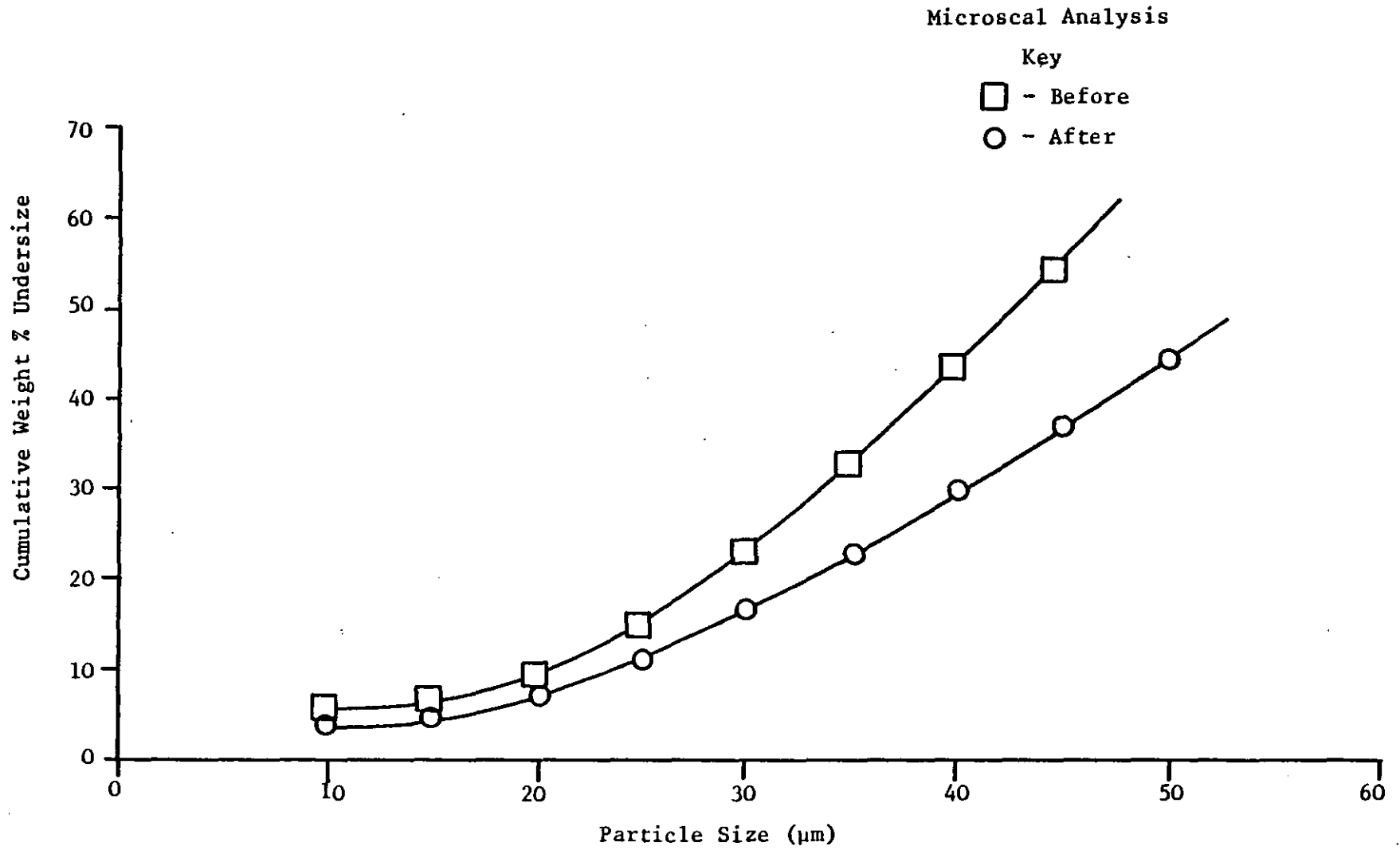
Figure 4.7. Size Distribution of Powder 4 Before and After Spraying
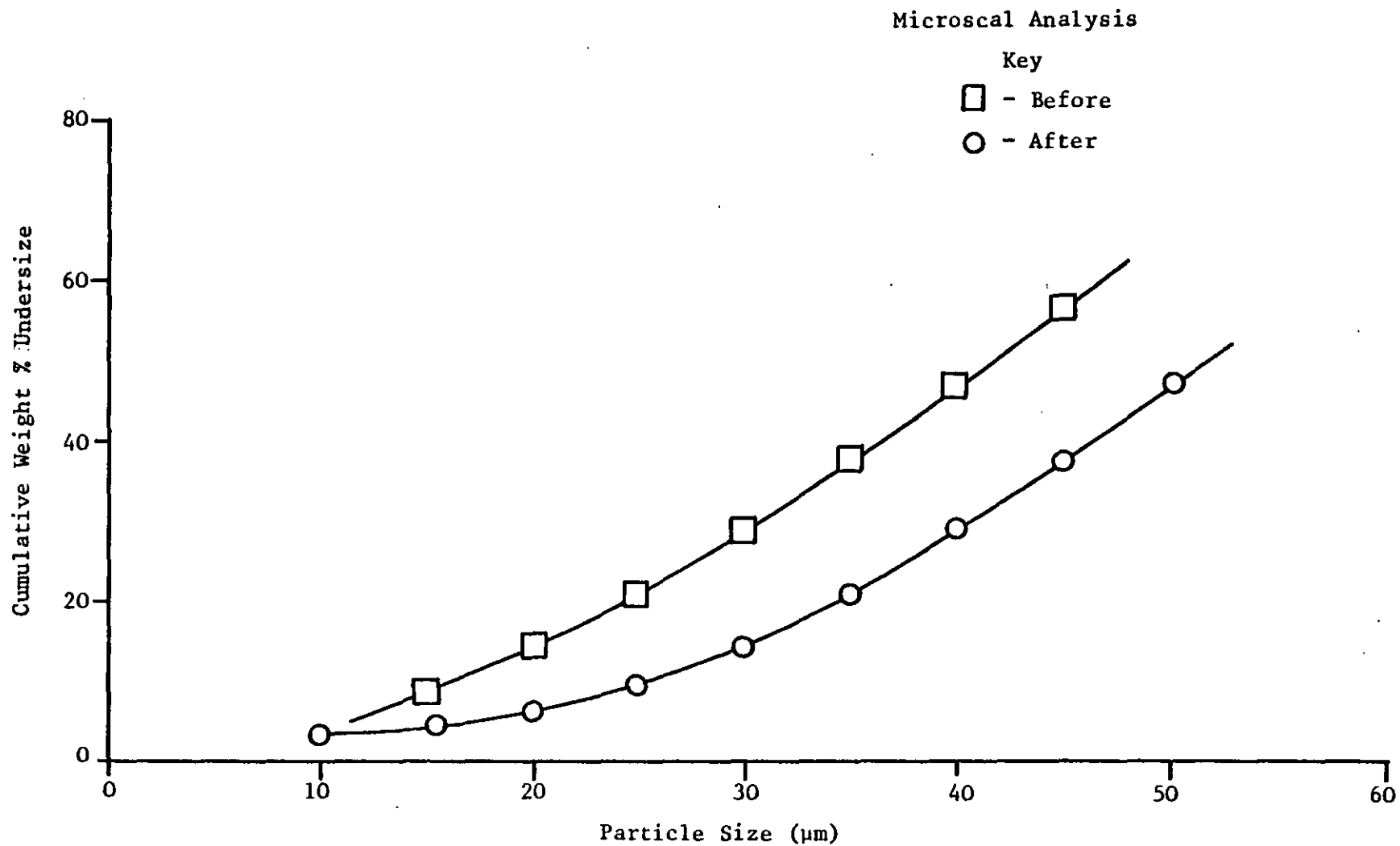
of size distribution shown in the last four figures. For each of four powders there is a definite loss of fines,and some medium sized particles, from the powder. The photographs suggest that this increasingly occurs as spraying progresses such that on the upper layers of the powder packing large particles predominate. It has been observed that near the substrate small particles are present in the powder layer.

However, at this time, it is not clearly understood why these observations take place. These effects could be due to the balance of forces on different sized particles changing with size, velocity etc. Charge on the particles, the depth of the coating could also be controlling factors. It is also possible that there is an optimum size distribution where, for a given thickness of film or spray rate etc, a loss of fines does not occur during spraying.

In the next two chapters the forces acting on the particles will be considered in a theoretical manner with the aid of a computer simulation program. The effects of particle size, air velocity and film thickness will be considered. The effect of monosized distributions on the packing of particles will also be investigated to try to gain a better understanding of the way in which a powder packing is formed. By so doing it is hoped that suggestions can be made for the optimisation of the process.

4.4 Summary

The determination of a spreading factor by measuring the change in size of a melting powder particle has been shown to give an indication of the type of quality of finish to be expected of a powder coating. The results suggest that, for the powder used in the experiments of Chapter 3, its excellent flow characteristics outweigh any effects

caused by the size of powder sprayed on the physical properties of the coating. Plate 4.14 shows how the powder coating can level out.

From macro and micro observations of mixtures of coloured particles, representing different size ranges, a size segregation effect through the powder coating is noticed. A predominance of large particles is observed in the upper layers of the coatings. This effect has been quantitatively investigated by the determination of size distributions of powders before and after spraying. For four different powders a loss of fines was determined in each case.

Although this effect has been observed for powders with a wide distribution it is not clear what occurs for monosized powders. The structure of the packings obtained has been seen to be of a very open nature although comparisons of packings have not been made with those obtained from the narrow size range powders.

It is possible that the observed effects are due to the balance of forces acting on the particles close to the substrate which changes as coating progresses. Therefore a study of the forces acting on particles under different operating conditions has been carried out by computer simulation. The setting up of a force balance equation is described in the following chapter.
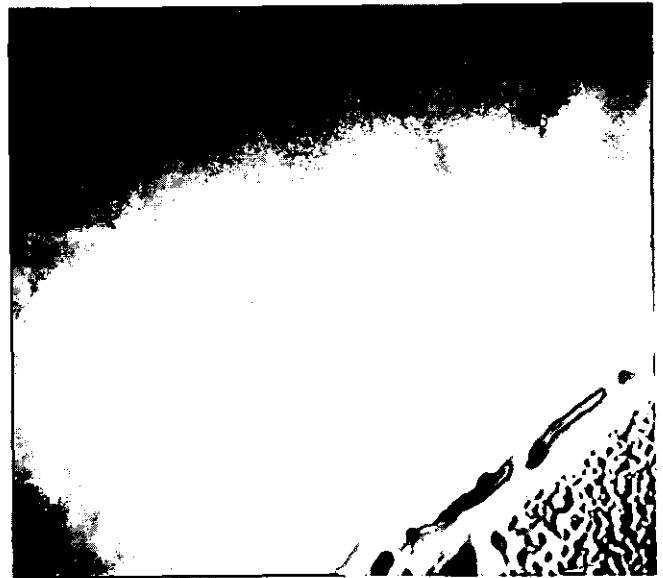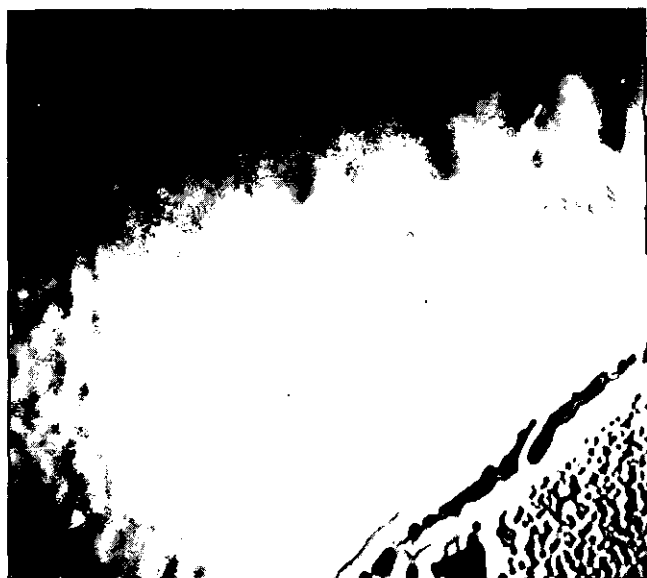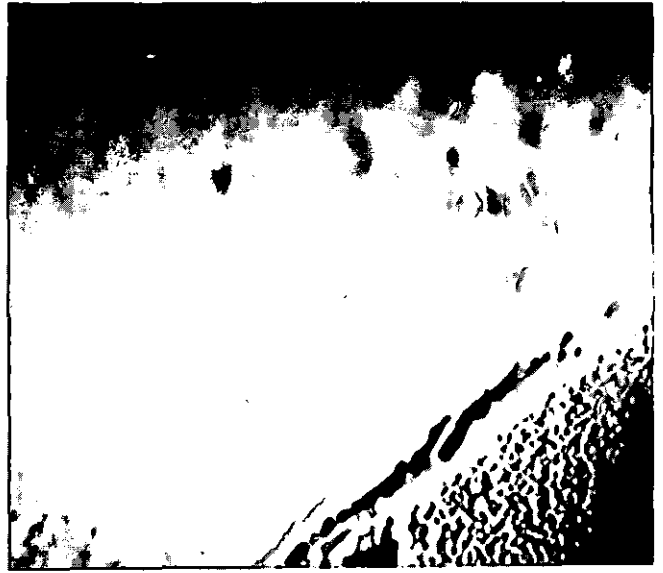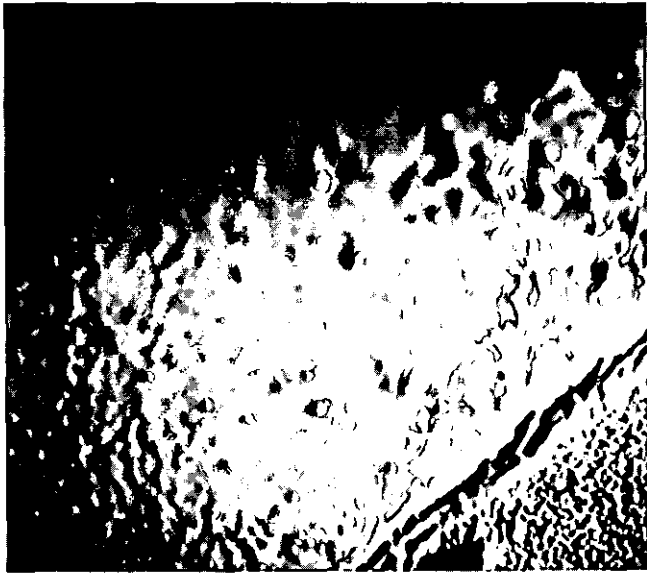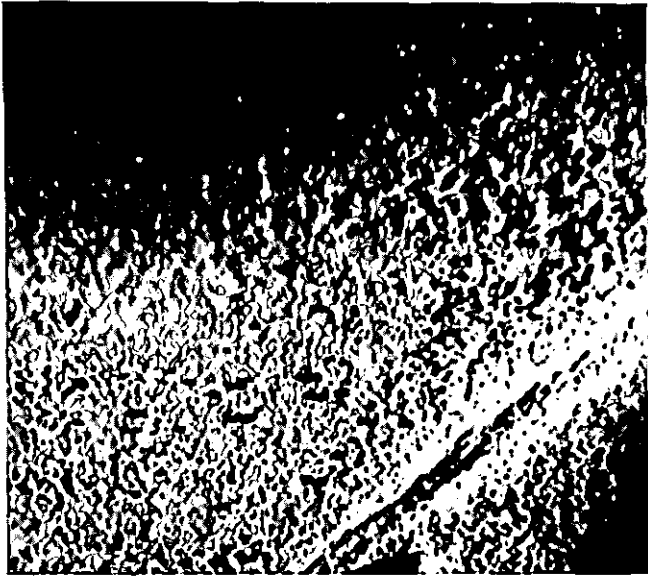
Plate 4.14.   The Surface of a Powder Coating during Stoving

CHAPTER 5

TRAJECTORY EQUATIONS

5.1 Introduction

In the previous chapter investigations into the way particles of a size distribution pack onto a substrate were described. It was found that there was a size segregation effect taking place. Large particles were preferentially deposited on the upper layers of a packing and there was an overall loss of fines. It was suggested that these effects were possibly due to the balance of forces (electrostatic and aerodynamic) acting in the close proximity of the substrate. With an increase in film thickness it could be put forward that these effects accounted for some of the small changes in surface properties for the commercial powder.

Although trends and effects have been observed for this wide size distribution powder it is not clear what differences occur between packings of various monosized powders. In order to gain an insight into the type of packings and variations therein, produced by the spraying of monosized distributions, a computer simulation technique has been employed. The intention of this method was to investigate the variations in orientation and structure of packings obtained for powders of different distributions for various operating conditions. The formation of a computer program to do this would allow many conditions to be examined with relative ease compared to an extensive experimental program. This method also allows comparison of the forces on each particle within a packing. It then might be possible to predict what type of powder size distribution would be most effective for a given situation.

In order to simulate any process mathematically it is first necessary to look at the problem and suggest a model that describes

the system. To enable a study of the spraying of particles onto a
substrate the flight of the particles from the gun to the substrate
must be described and this can be achieved by using a set of trajectory
equations.

By considering a force balance on any particular particle in
flight, taking into consideration all the forces acting on that
particle, differential equations are obtained. These describe the
variation of the position, velocity and acceleration of the particle
in terms of the system variables. Integration of these equations then
enables the movement of a particle to be followed until such time
that it lands onto the substrate, hits another particle or is over-
sprayed.

When dealing with any theoretical simulation technique one of
the biggest problems is to establish and recognise all the assumptions
that are required to enable a solution to be obtained. At the same
time analogy to the real system must be kept where possible in order
for the results to be meaningful. The initial stages of formation of
the simulation concept are kept as simple as possible but as investi-
gations proceed the basic model is continually developed to reflect the
real situation.

This chapter describes the trajectory equations used to represent
the flight of particles onto a substrate and the assumptions employed.

5.2   Force Balance

To obtain the trajectory equation a force balance is applied to
a particle in flight.

Consider a particle heading towards the substrate as shown in
Figure 5.1. It can be seen that the forces acting on the particle
are:-

Figure 5.1. Forces Acting on a Particle in Flight
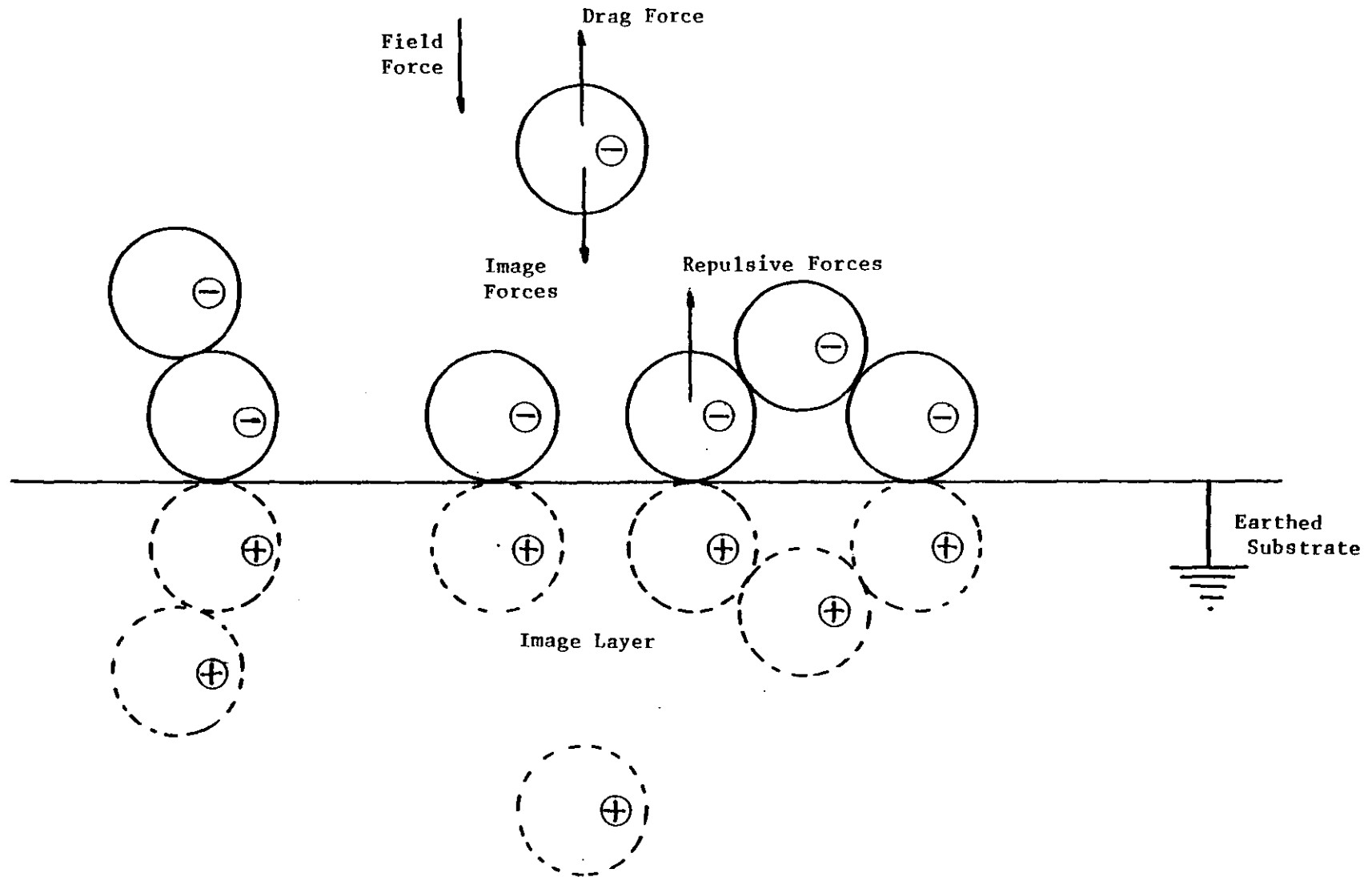
(i)   Drag force due to relative motion with air

(ii)   Field force due to a charged particle being in an electric

       field between the gun and target

(iii) Inertial force due to momentum of the particle

(iv)   Gravity force (dependent on direction of spray and position of

       substrate)

(v)   Image force (attractive) due to induced image of the charged

       particle itself in the substrate

(vi)   Interparticulate electrostatic forces (repulsive and attractive)

       due to charges in packing and their induced images.

       These are all the forces that act on the particle and these must

be adequately described so that the mathematical model will represent

the system.

       Initially the following assumptions will be made for the

construction of the force balance:-

(i)   The spraying of particles is such that they fall onto the

       substrate with no effect due to gravity. Only a small area of

       packing can be considered due to the number of particles

       involved. Gravity effects have been initially ignored because

       the significance of this force on the packing is dependent on

       the direction of the plane of the substrate.

(ii)   The simulation is carried out in 2 dimensions only. This enables

       a pictorial representation of the packing to be obtained. Apart

       from the fact that 3-dimensional analysis is more complex, there

       is no easy method for representing the packing pictorially.

       Reading a set of coordinates and figures does not readily give

       an indication of the type of packing obtained and it is even

more difficult to detect minor differences and especially errors.
Calculation of porosity and analysis of size distribution through
the thickness of packing would be one of the ways an impression
could be gained.

(iii) The particles are spherical. Predicting the drag forces on a
particle taking into account the velocity profile of the air
stream is difficult in itself. Trying to account for the
various shapes of the particles gives an extra degree of
difficulty. It would also create problems when deciding
which surface or edge first touched another particle or the
substrate. Considering spherical particles makes this much
simpler.

Other assumptions will be described as the individual components
of the force balance are considered. In the x and y directions,
therefore, a force balance can be applied to a particle in flight:-

Inertial force = Drag force + Image force + Field force + Attractive + Repulsive
                              of particle   Force due   force due
                              (zero in y)   to images   to packed
                                                                of packing charged
                                                                particles

5.3   Charge on a Particle

As previously mentioned, the charge on a particle, with regards
to this process, plays a very important role with regards to the
packing of particles. Therefore, it is worth considering how the
particles are charged and the value of that charge. For the purpose
of this work only corona charging will be considered since this type
has been used in the experiments and is more common than tribocharging.
Tribocharging does not normally interfere with corona charging unless

the tribocharges produced are very high or are of opposite sign to

the corona electrode, whence they will quench the corona.

The field strength at which a corona begins to form is subject

to various parameters:-

(i)   radius of wire of electrode, a

(ii)   roughness factor for electrode, m

(iii) relative air density, ρ

This field strength is given by Peek to be

$$E = 3 \times 10^6 \, m \, (\rho + 3.0\sqrt{\rho/a}) \quad volts/m$$

Hence, the sharper the point of the electrode the less voltage is

required (F.W. Peek, 1929).

Particle charging takes place between the corona glow boundary

and the earthed substrate. The particles are charged by the electrons

and negative ions in that region. There are two types of charging

mechanism that take place, field and diffusion charging, each being

significant for a particular size range. For particles greater than

a radius of 0.5µm field charging is the dominant mechanism, hence

only this mechanism will be discussed. (S. Oglesby, 1978).

Ions will tend to move along the electric field lines and hence

collide with particles in the air stream. The charges are maintained

on the surface by the image force of the induced dipoles within the

particle. A particle will continue to be charged until the electro-

static field produced by these charges repel further ions. This is

known as the saturation charge. The electric field lines are shown

in figures 5.2 and 5.3 and show how the field lines intersect the

dielectric particles and hence will attract the ions.

If a conducting sphere of radius a, with a charge q, is

suspended in a uniform field E_o the field near the particle will be
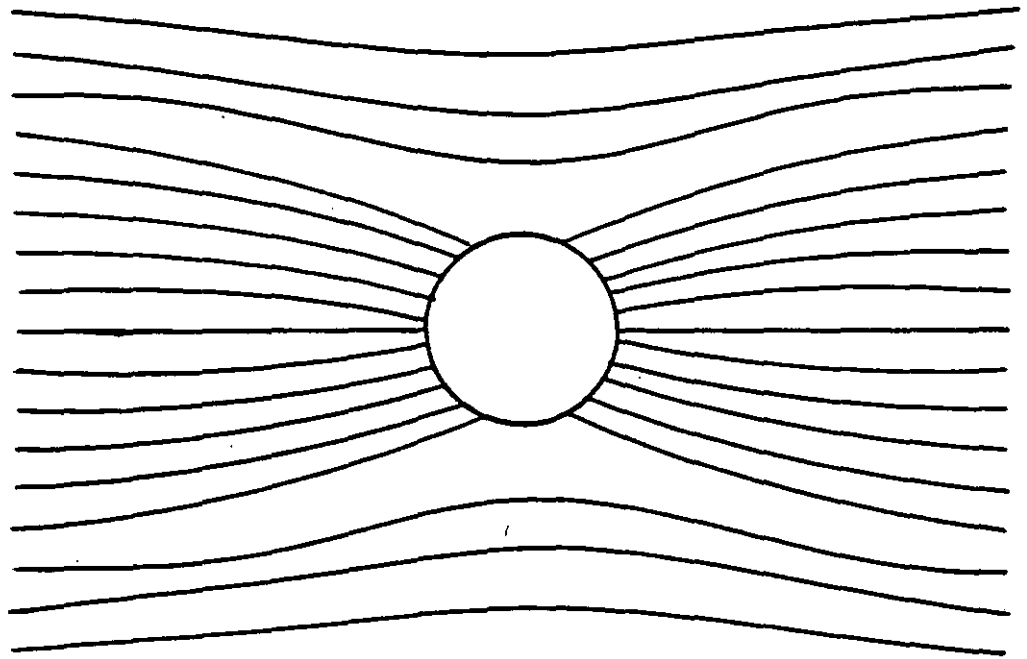
Figure 5.2. Electric Field in the Vicinity of an Uncharged Particle
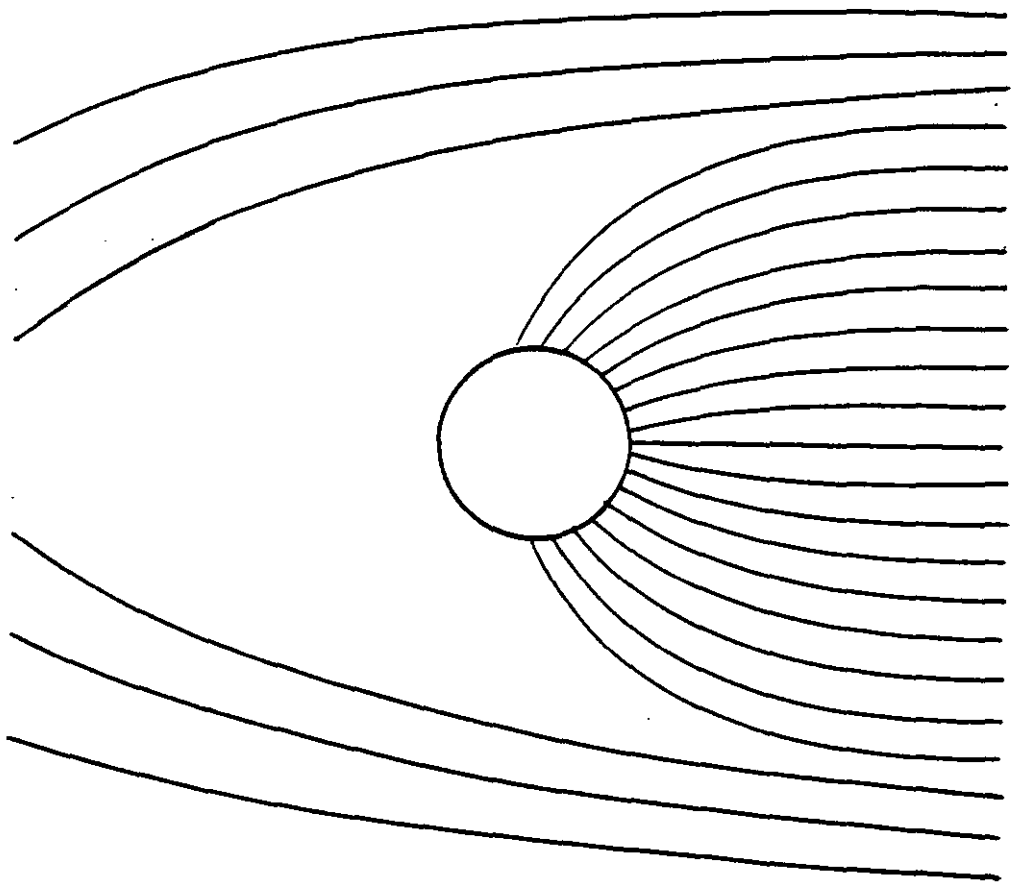
Figure 5.3. Electric Field in the Vicinity of a Charged Particle

due to two components:-

    (i)   Self field caused by the charge on the particle

    (ii)   Applied field, modified by the conducting particle

and is described as

$$E = 3E_o \cos \theta - q/4\pi\epsilon_o a^2$$

where E = resultant field

    θ = angle between point on particle and field

    ϵ_o = permittivity of free space

Since the electric field in the vicinity of the particle (E) is zero
when the saturation charge, q_s, is reached (external field = field
due to charge) then

$$q_s = 12\pi a^2 \epsilon_o E_o$$

θ equals zero as the particle charge increases, hence $\cos \theta = 1$
(M.M. Pauthenier, 1932).

For a non conducting particle the equation is

$$q_s = 12 \left[\frac{\epsilon}{\epsilon+2} \right] \pi\epsilon_o a^2 E_o$$

where ϵ = dielectric constant of particle.

The charge on the particle can be related as a function of time
by the expression

$$q(t) = \left[\frac{1}{1 + \frac{\tau}{t}} \right] q_s$$

where τ = time constant described by $\tau = \dfrac{4\epsilon_o}{\rho_i b}$

    where ρ_i = ionic charge density

    and   b = ionic mobility

The time constant is usually of the order of 10^{-3} or 10^{-4} second and so saturation charge is normally reached within this time. The velocity of the powder from the gun is approximately 2-5 m/sec and the spray distance is normally about 20-30 cms. Hence the time of flight is about 0.1 sec and thus there is ample time available to reach saturation charge.

The dielectric constant of epoxy powder is normally about 4 and the electric field is usually 600 kV/m. (Handbook of Chemistry and Physics, 1980). From the equation it can be seen that a large change in dielectric constant will only cause a small difference in the overall charge. Other physical variables though can effect the charge on a particle.

Climatic conditions, such as humidity and heat can cause clustering of particles and hence effectively give lower charging due to the increase in particle size. This could be responsible for the small changes in measured Q/M with particle size. The charging voltage, gun to target distance and powder feed rate can all affect the acquisition of charge. The charging voltage and gun target distance obviously alter the strength of the charging field thus large spraying distances give lower charge. An increase in powder feed rate can also have the same effect as the powder cloud can shield the electric field or possibly quench the corona by space charge. These effects are shown in Figure 5.4 (S. Wu, 1976).

5.4   Electric Field

The electric field plays a very important part in the electrostatic coating process. It is the mechanism that enables the particles to be charged and aids transport of the particles to the substrate.

Figure 5.4. Effects of Operational Variables on Particle Charge

Thermosetting Acrylic Powder (S. Wu)
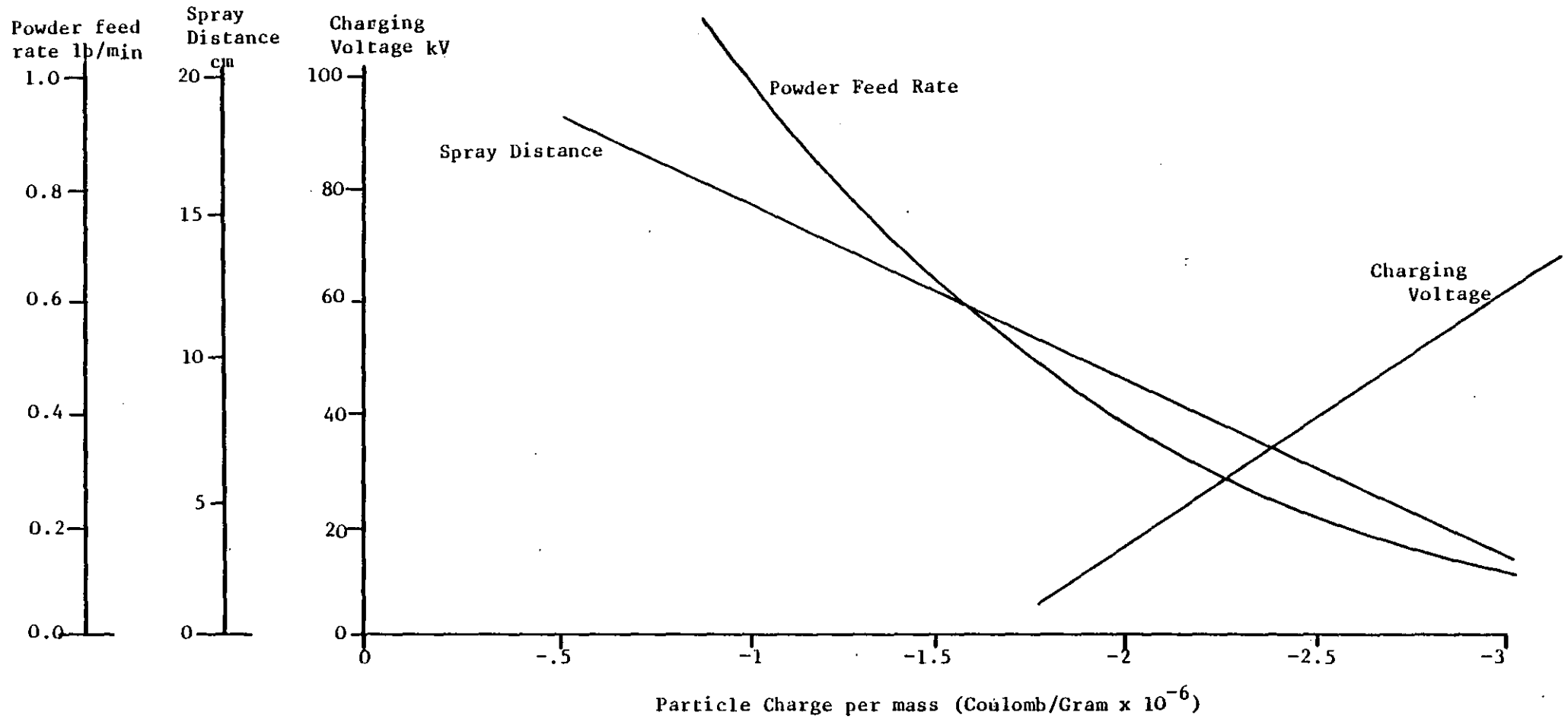
The magnitude of this latter effect is not certain at this time, compared to the drag and other electrostatic forces acting on the particle. However it is obvious that if the particle is not charged it will not be retained if it reaches the target.

To obtain an equation which describes the electric field between the gun and target it is necessary to consider the two main components:-

(i)   Applied voltage at the gun electrode

(ii)   Space charge effect due to the charged powder cloud.

The effect of the space charge is to suppress the effect of the field near the corona but enhance it near the substrate. The magnitude of this effect is dependent on the charge on the particles and the powder output rate.

The system is considered to be a spherical coordinate system with the origin at the electrode of the gun, as shown in Figure 5.5.

If we consider a substrate of radius R at a distance L from the gun and that the substrate is effectively a spherical cap of radius L then all quantities will be symmetrical about the axis in the conical space bounded by the cap and electrode.

Hence the electric field is dependent on the space charge density, ρ_s, and may be found by solving Poisson's equation which is given by

$$\frac{\partial^2 V}{\partial r^2} + \frac{1}{r} \frac{\partial V}{\partial r} = -\frac{\rho_s}{\varepsilon_o}$$

where ε_o is the permittivity of free space

V is the voltage at r

and   r is the radial distance from the electrode

Wu has described a solution to this equation. The effect of ions that go to make up the space charge can be neglected since the charged particles contribute 75% to 95% of the total.
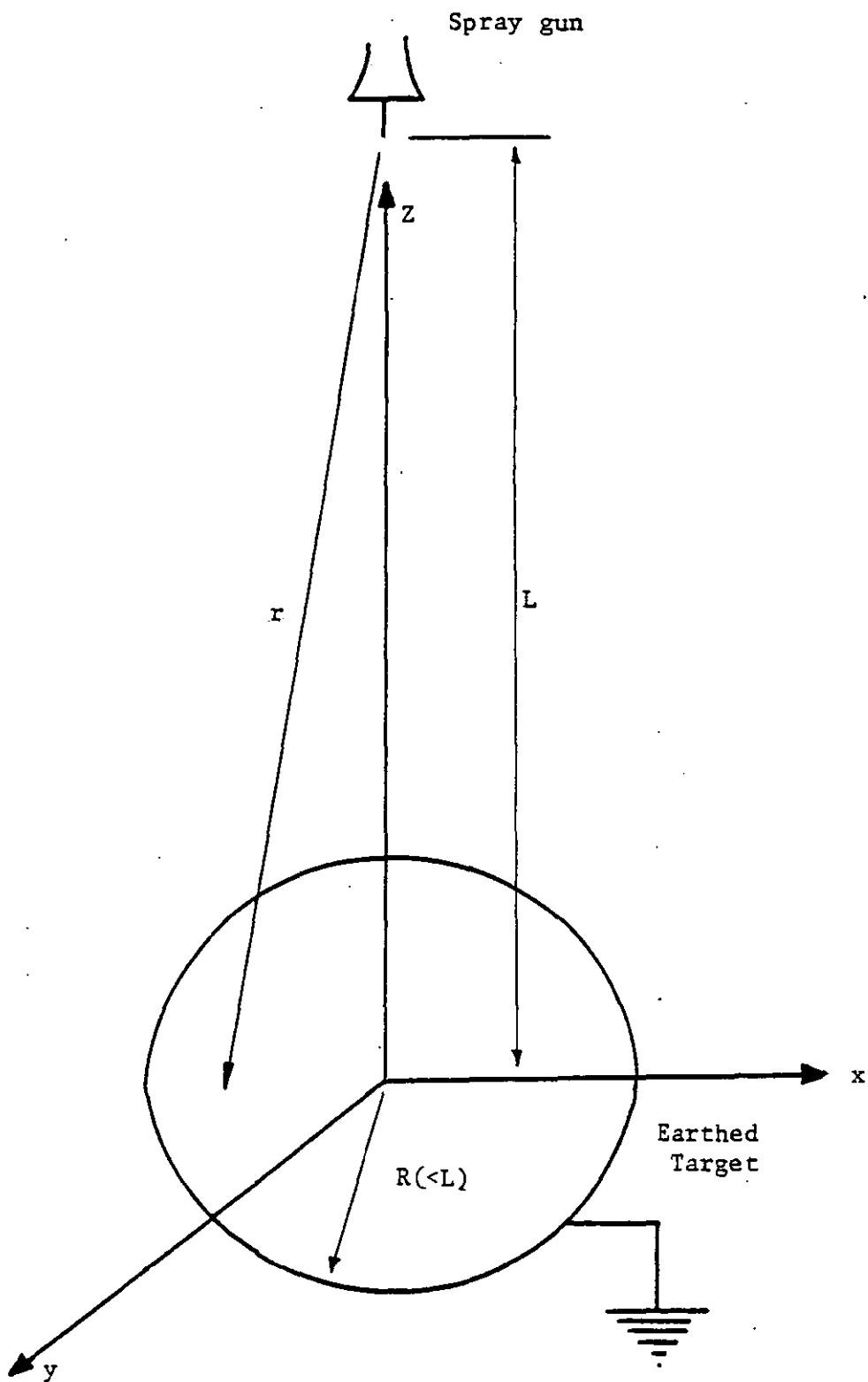
Figure 5.5.   Coordinate System for Analysing Field Between
Gun and Target

Integration gives

$$V = -\frac{\rho}{4\varepsilon_o} r^2 + C_1 \ln r + C_2$$

Since the effect due to a layer of charged particles on the field is greater than that due to space charge the system is considered to have no space charge i.e. ($\rho_s = 0$).

Therefore the boundary conditions are $V(L) = Vp$

$$V(0) = Vo$$

where Vp = voltage of powder layer

Vo = voltage on electrode of radius b

Hence $V = \dfrac{V_o \ln (r/L) - V_p \ln (r/b)}{\ln (b/L)}$

and since $E = \dfrac{-\partial V}{\partial r}$

$$E = \frac{V_o - V_p}{r \ln (L/b)}$$

The field at the electrode is obtained by letting r = b giving

$$E_O = \frac{V_o - V_p}{b \ln (L/b)}$$

and thus $E = \dfrac{bEo}{r}$

The variation of electric field, given by this expression, is shown in Figure 5.6 (S. Wu, 1976).

5.5 The Forces

5.5.1 Drag Force

The force acting on a particle due to the difference in velocities between itself and the fluid around it is dependent on the Reynolds number of the particle:-

Figure 5.6. Variation of Electric Field with Distance from Spray Gun

Using WU Expression

Spray distance = 0.2m

Applied voltage = -60 kV

Electrode radius = 0.005m
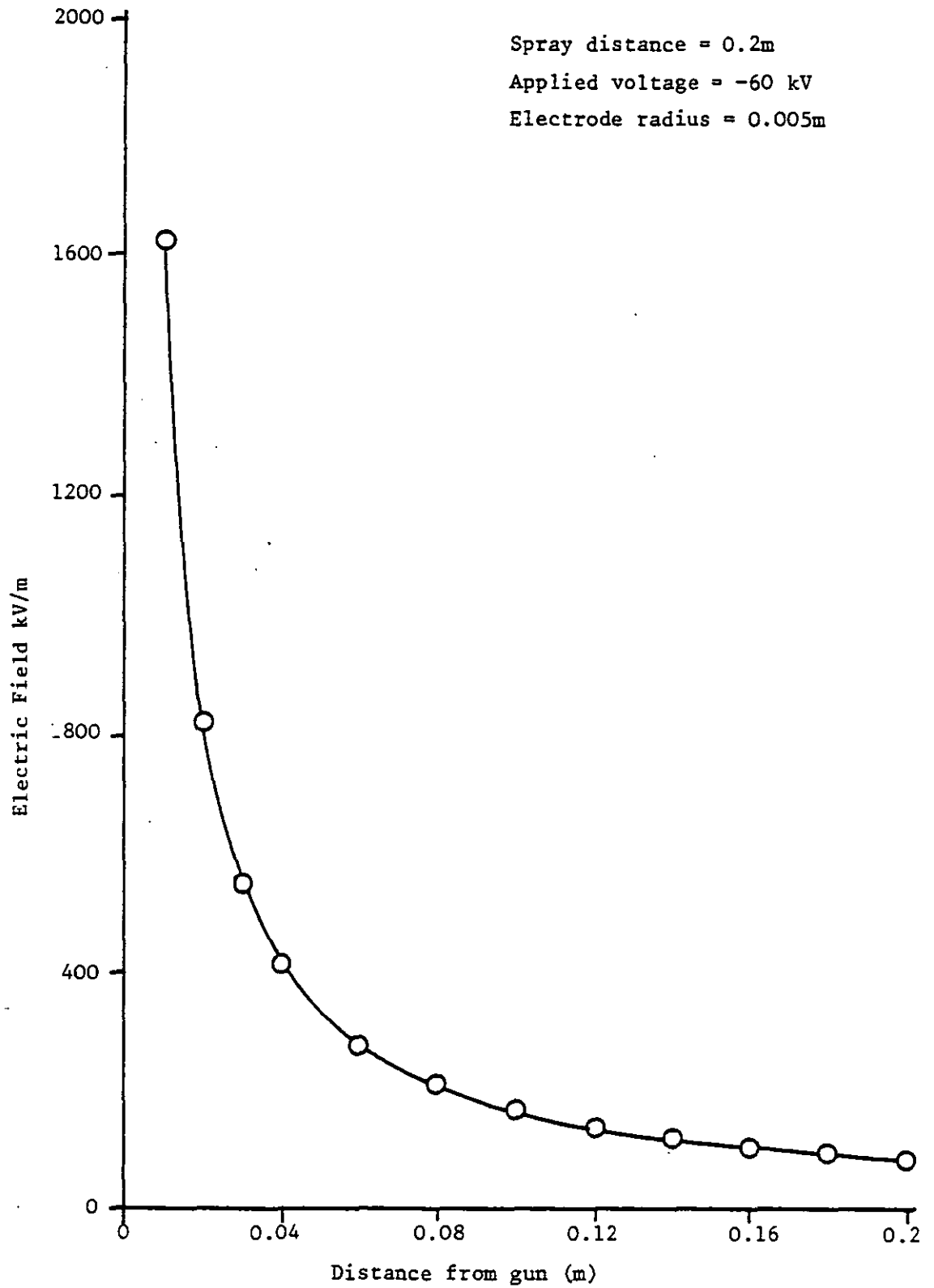
$$Re_p = \frac{\rho_f \, |\vec{V}_{rel}| \, dp}{\mu}$$

where $|\vec{V}_{rel}|$ is the magnitude of the relative velocity between the fluid and particle. The force on the particle can be obtained from Newtons law:-

$$\vec{F}_D = C_D \pi dp^2 \, \frac{\rho_f}{4} \, |\vec{V}_{rel}| \vec{V}_{rel}$$

where C_D is the drag coefficient

If C_D is plotted against the particle Reynolds number a graph as in Figure 5.7 is obtained (J.M. Coulson et al., 1968). It can be seen that for Reynolds numbers of less than 1 the graph is a straight line. This region is described by Stokes Law where

$$C_D = \frac{24}{Re}$$

and from the equation for the force on a particle we have

$$F_D = \frac{24}{Re_p} \, \frac{\pi dp^2}{4} \, \frac{\rho_f}{2} \, |\vec{V}_{rel}| \vec{V}_{rel}$$

which becomes (substituting for Re_p)

$$F_D = 3\pi\mu dp \, V_{rel}$$

For Reynolds numbers between 1 and 1000 the drag coefficient has been described by Schiller and Naumann by the following equation (L. Schiller et al., 1933).

$$C_D = \frac{24}{Re_p} \, (1 + 0.15 \, Re_p^{0.687})$$

whence the equation for the drag force becomes

$$\vec{F}_D = 3\pi\mu dp \, \vec{V}_{rel} \, (1 + 0.15 \, Re_p^{0.687})$$

Figure 5.7. Relationship Between C_D and Re_p for a Sphere

Region A
$$C_D = \frac{24}{Re_p}$$

Region B
$$C_D = \frac{24}{Re_p} (1+0.15Re_p^{0.687})$$

Region C
$$C_D = 0.44$$

Region D
$$C_D = 0.1$$

$\log (C_D/2)$

$C_D/2 = 0.22$

$C_D/2 = 0.05$

$Re_p = 0.2$

$Re_p = 500$

$Re_p = 2 \times 10^5$

$\log Re_p$
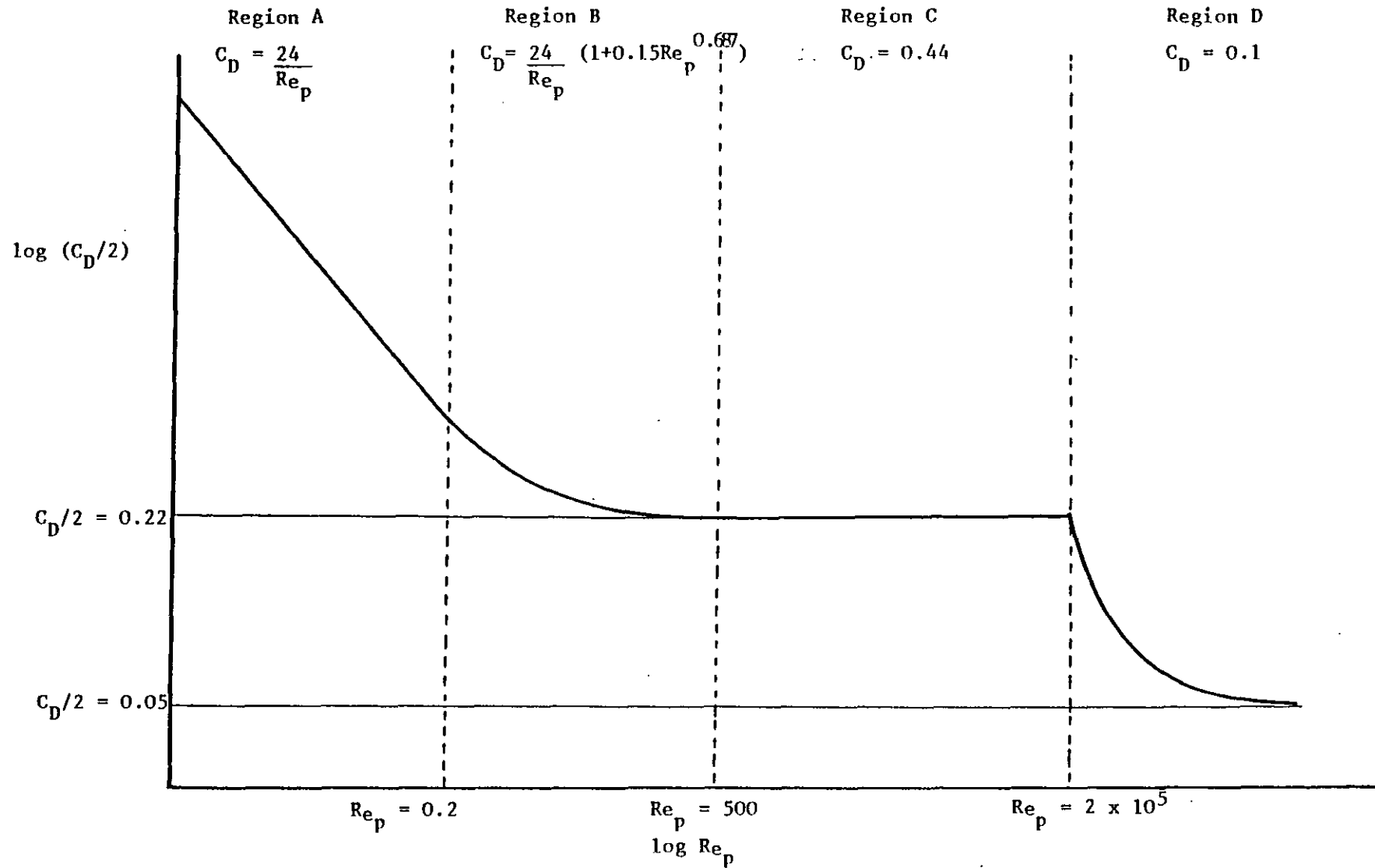
These are the two areas of interest since it is likely that the particles in flight in the EPC process will have Reynolds numbers in one of these two regions.

From experiments with the computer program, as described in Chapter 6, the Reynolds number was typically found to be less than 1.

Hence Stokes Law can be applied and so the components of drag force in the x and y direction are:-

$$F_{D_x} = 3\pi\mu dp \left(u - \frac{dx}{dt}\right)$$

and

$$F_{D_y} = 3\pi\mu dp \left(v - \frac{dy}{dt}\right)$$

The velocity components of the fluid (in this case air) will be dependent on the position relative to the gun and substrate. Therefore a model must be used that describes the variation of these components with radial distance from the gun.

Initially the x component of the air velocity (perpendicular to the substrate) was taken to be a constant and the y component equal to zero. Therefore the air velocity component did not change with position, and in effect the air flowed straight through the substrate. This model was found unsatisfactory since it gave particle velocities near the substrate far in excess of those expected in reality.

Therefore the model representing flow around a flat plate has been used. It is assumed that, after the jet of air has left the gun, at some point between the gun and substrate the air flows perpendicular to the target for a short period (i.e. parallel flow). The air is then perpendicular to a flat plate and the flow is modelled

accordingly. This assumption is of course dependent on the size of the substrate and the magnitude of the errors will be discussed later.

5.5.2 Flow Model

To obtain the equations of the model for flow past a flat plate there is a succession of basic transformations that have to be carried out. The initial model is described by the w and z planes. The transformations are shown in Figure 5.8.

Consider the flow past a circle of radius a of a parallel air stream and transform this by a rotating transformation so that the circle becomes a straight line and the flow is no longer uniform and parallel to it. (H.R. Valentine, 1967).

The flow past a cylinder is given by $w = z_1 + \dfrac{a^2}{z_1}$ and this is then rotated by 90° by the transformation $z_2 = -iz_1$. The final transformation $z = z_2 + \dfrac{a^2}{z_2}$ gives the flow past a flat plate where the length of the plate is 4a. The z plane is then rotated again through 90° by the transformation $z^r = iz$.

The combination of these transformations gives:-

$$z_1 = \frac{-z_2}{i} = iz_2 \qquad \text{(elimination of } z_1)$$

$$w = iz_2 + \frac{a^2}{iz_2} = i\left(z_2 - \frac{a^2}{z_2}\right) \qquad \text{(flow past a circle)}$$

$$w^2 = -\left[z_2 - \frac{a^2}{z_2}\right]^2$$

also

$$z^2 = \left[z_2 + \frac{a^2}{z_2}\right]^2$$

therefore

$$w^2 + z^2 = 4a^2$$

hence

$$w = i\sqrt{z^2 - 4a^2}$$

w-plane

ψ

ϕ

Z_1-plane

y_1

x_1

a

$$w = Z_1 + \frac{a^2}{Z_1}$$

Z_2-plane

y_2

x_2

a

$$Z_2 = -iZ_1$$

y

x

4a

$$Z = Z_2 + \frac{a^2}{Z_2}$$

Overall, $w = i\sqrt{(Z^2 - 4a^2)}$
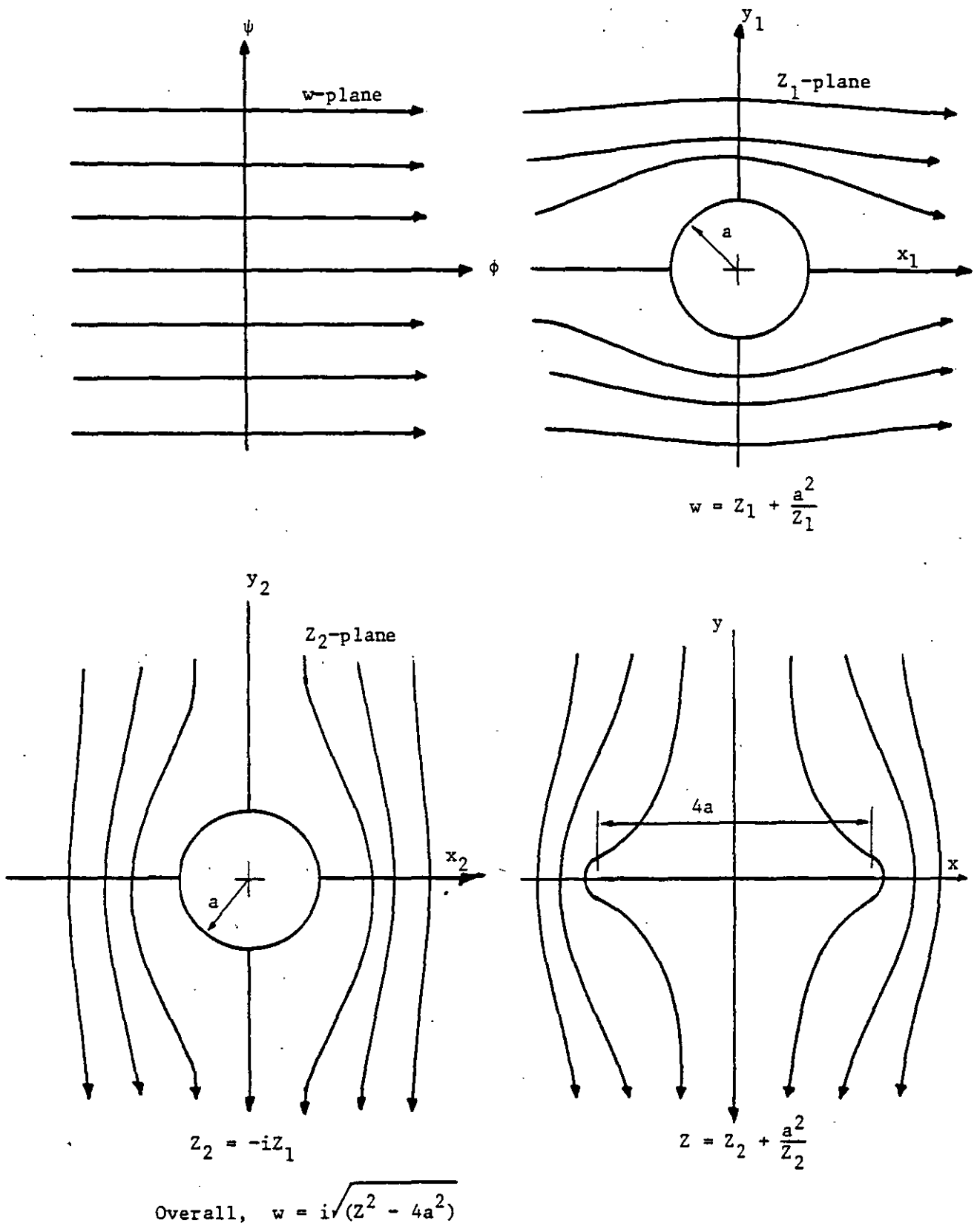
Figure 5.8.   Transformations used for Flow Model

If the half width, 1, is equal to 2a

Then

$$w = i\sqrt{z^2 - 1^2}$$

The final rotation back to the horizontal gives ($z' = iz$)

$$\dot{w} = \sqrt{z'^2 + 1^2}$$

When the original uniform velocity (at infinite) of the fluid is U

then the transformation is

$$\dot{w} = U\sqrt{z^2 + 1^2}$$

From streamline and potential theory we have that

$$w = \phi + i\psi$$

where ψ = stream function ($\psi = f(x,y)$)

with $\quad u = \dfrac{d\psi}{dy}$, $\quad \ddot{v} = \dfrac{-d\psi}{dx}$

and $\quad \phi$ = potential function

with $\quad u = \dfrac{d\phi}{dx}$, $\quad \ddot{v} = \dfrac{d\phi}{dy}$

Since $z = x + iy$

$$\frac{d\ddot{w}}{dz} = \frac{d\ddot{w}}{dx}$$

and so $\quad \dfrac{d\ddot{w}}{dz} = \dfrac{\partial}{\partial x}(\phi + i\psi) = \dfrac{\partial\phi}{\partial x} + \dfrac{i\partial\psi}{\partial x} = u - i\ddot{v}$

$$\frac{d\ddot{w}}{dz} = u - i\ddot{v}$$

By manipulation of this equation and the real and imaginary parts

the conversion can take place as follows:-

$$\frac{d\ddot{w}}{dz} = \frac{Uz}{(z^2 + 1^2)^{\frac{1}{2}}}$$

substituting $z = x + iy$

$$\frac{dw}{dz} = \frac{U(x + iy)}{((x+iy)^2 + 1^2)^{\frac{1}{2}}}$$

$$= \frac{U(x+iy)(x^2-y^2 + 1^2 - 2iyx)^{\frac{1}{2}}}{((x^2-y^2 + 1^2)^2 + 4x^2y^2)^{\frac{1}{2}}}$$

Putting in the form of $Re^{i\theta}$

$$\frac{dw}{dz} = \frac{U(x + iy)(Re^{i\theta})^{\frac{1}{2}}}{((x^2-y^2+1^2)^2 + 4x^2y^2)^{\frac{1}{2}}}$$

where $R = \left[(x^2 - y^2 + 1^2)^2 + (4x^2y^2)\right]^{\frac{1}{2}}$

and $\theta = \tan^{-1}\left[\frac{-2yx}{x^2 + 1^2 - y^2}\right]$

Hence $\frac{dw}{dz} = \frac{U}{R^{\frac{1}{2}}}(x + iy)e^{i\theta/2}$

Substituting for $e^{i\theta/2} = (\cos\theta/2 + i\sin\theta/2)$

$$\frac{dw}{dz} = \frac{U}{R^{\frac{1}{2}}}(x + iy)(\cos\theta/2 + i\sin\theta/2)$$

hence $\frac{dw}{dz} = \frac{U}{R^{\frac{1}{2}}}\left[x\cos\theta/2 - y\sin\theta/2 + i\left(x\sin\theta/2 + y\cos\theta/2\right)\right]$

Since $\frac{dw}{dz} = u - iV$

the velocity components can be seen to be

$$u = \frac{U}{R^{\frac{1}{2}}}\left[x\cos\theta/2 - y\sin\theta/2\right]$$

and

$$v = \frac{-U}{R^{\frac{1}{2}}}\left[x\sin\theta/2 + y\cos\theta/2\right]$$

where θ and R are as described earlier and U is the uniform velocity.

u and v can now be substituted into the drag term equation.

Typical values of the x and y velocity components (u and v) are shown at different distances away from the plate in Figures 5.9 and 5.10. It can be seen that a distance of 0.1m away from the plate the x component of the velocity is 45% of the uniform velocity. It should be noted that this solution gives the air velocity as infinite at the edge of the plate. However in these investigations the edge of the plate can be considered as being at infinite since the area of the plate considered is near the origin and is very small. It should also be mentioned that in these calculations the origin is at the plate but in the main trajectory calculations the origin is at the gun.

5.5.3 Field Force

The field force acting on a particle is dependent on the position of the particle in the field and the charge on the particle i.e.

$$\overrightarrow{F_E} = q\overrightarrow{E}$$

The strength of the field, without space charge, at a radial distance r has been seen to be

$$E_x = \frac{V_o - V_p}{r \ln(L/b)} \cos \theta$$

in the x direction.

Since $\cos \theta = \frac{x}{r}$ and $r = (x_o^2 + y_o^2)^{\frac{1}{2}}$

$$F_{E_x} = q \cdot \frac{V_o}{\ln(L/b)} \cdot \frac{x_o}{(x_o^2 + y_o^2)^{3/2}} \quad ,$$

since V_p is assumed to be zero

and q is given by a previous equation.

The equation is similar for the field force in the y direction.

Figure 5.9. Air Velocity Model for Flow Past a Flat Plate

Uniform Velocity = 1 m/s

Y = 0.09

Y = 0.00

Air Velocity in X Direction (m/s)

Distance from Plate-X (m)
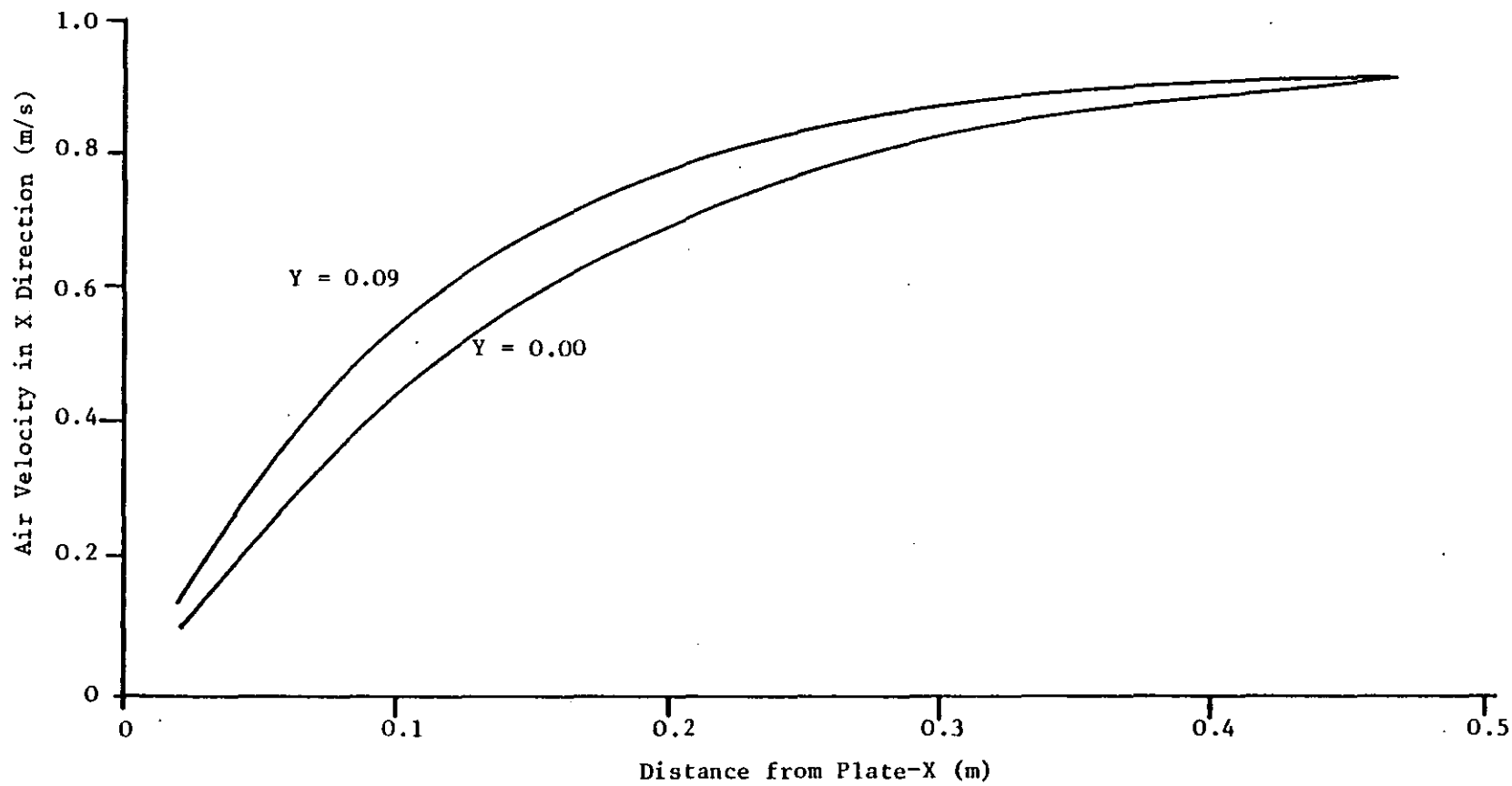
Figure 5.10. Air Velocity Model of Flow Past a Flat Plate

Uniform Velocity = 1 m/s
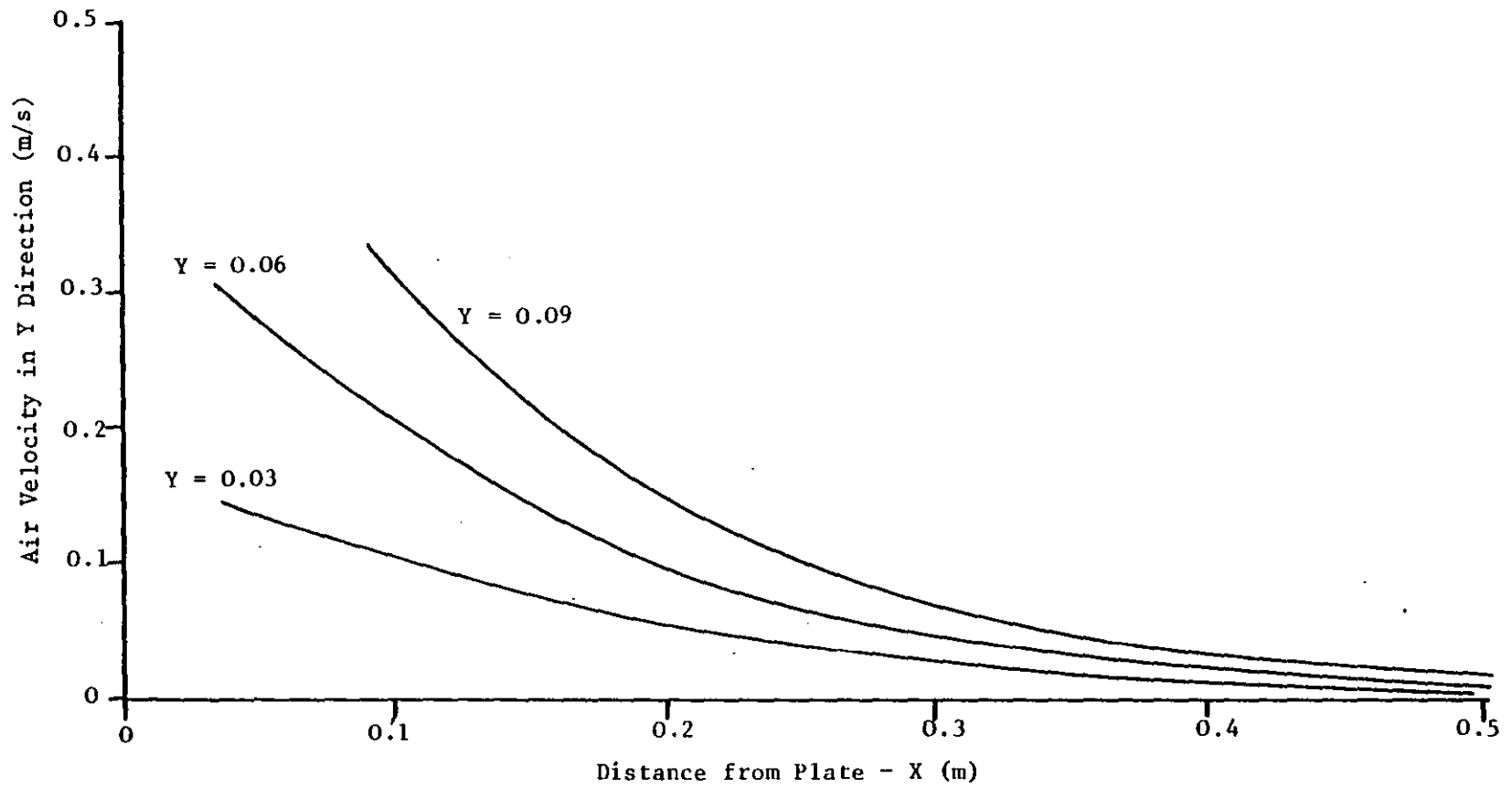
5.5.4 Interparticulate Forces

There are three types of forces that have to be considered here:-

(i)   The image force of the oncoming particle which only has a component in the x direction. The image is due to the induced dipole charge formed in the substrate.

(ii) The repulsive forces due to the packed particles on the substrate − x and y components. The repulsive force is due to the field exerted by the particles of the same charge sign and the force is dependent on the distance between the particles and the charge on each of them.

(iii) The attractive forces due to the attraction of the oncoming particle and the images of the packed particles on the substrate, again induced.

The convention used for the summation of these forces is shown in Figure 5.11. The equations formed are based on the cartesian coordinate system in 2-dimensions using x as the direction from the gun to the substrate and y being the direction that the target lies in. The origin of the two axes is the needle point of the electrode. (Note: different coordinate system to flow model).

An oncoming particle, p_o is considered approaching the substrate on which there is a packing of particles already present. The particles on the substrate, p_i, the images, p_j, and the image of the oncoming particle, p_k, must all be considered.

The force between two particles is given by the equation

$$\vec{F} = \frac{-q_1 \, q_2}{4\pi\varepsilon_o R_{12}^2}$$

Figure 5.11.   Convention used for Calculation of Inter-particulate Forces
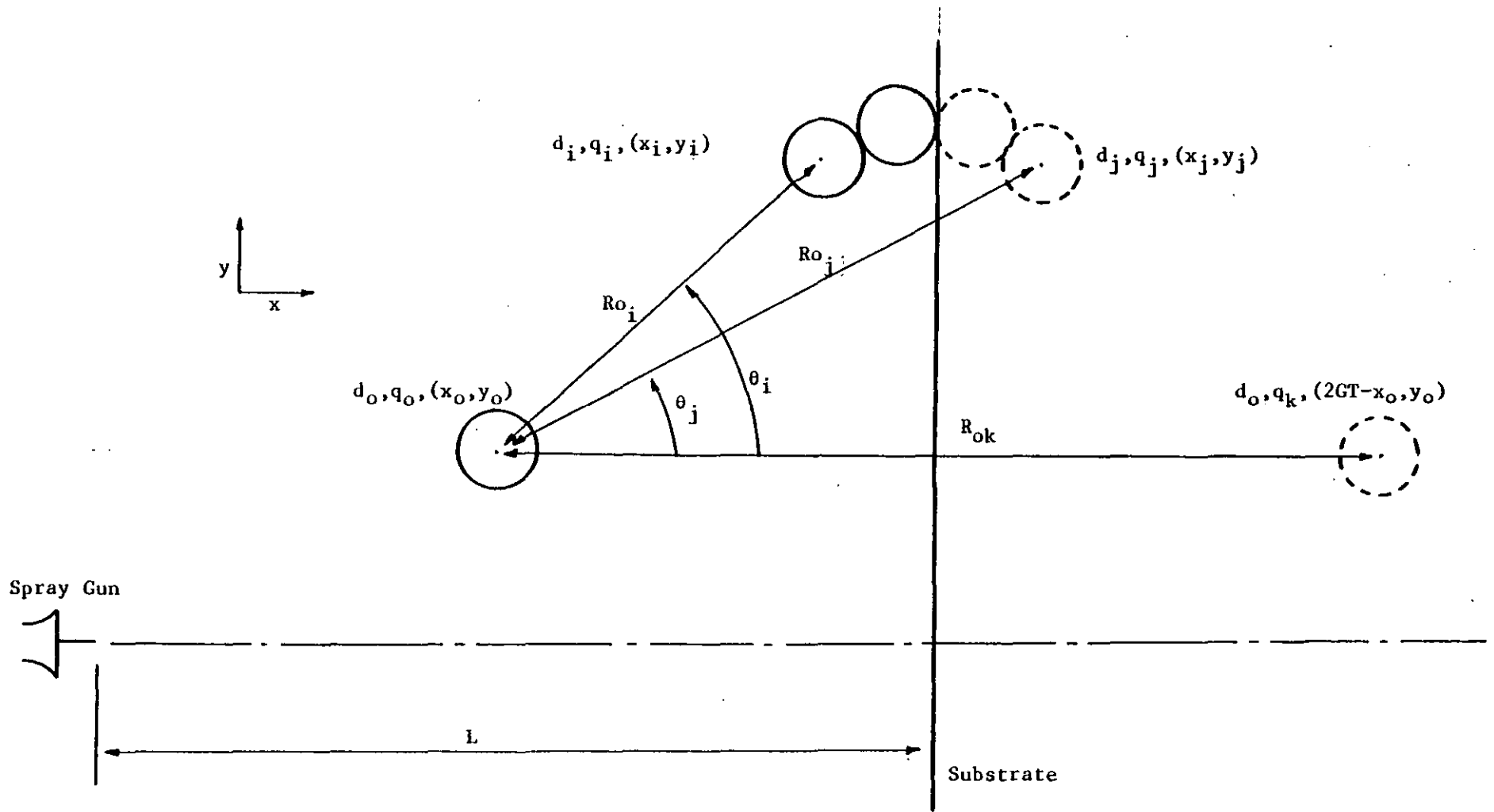
and therefore the component in the x direction is given by

$$F_x = \frac{-q_1 \, q_2}{4\pi\varepsilon_o R_{12}^2} \cos \theta_{12}$$

(S. Oglesby, 1978)

For a monosized distribution it would be assumed that the charge on all particles was the same. Therefore for the force due to a particle in the packed layer (where $q_1 = q_2$)

$$\overrightarrow{F_R} = \frac{-q_o^2}{4\pi\varepsilon_o R_{oi}^2}$$

but for the force due to an induced image (where $q_1 = -q_2$)

$$\overrightarrow{F_A} = \frac{q_o^2}{4\pi\varepsilon_o R_{oj}^2}$$

5.5.6 Image Force

The image force due to the induced image of the oncoming particle is given by

$$F_I = \frac{-q_o q_k}{4\pi\varepsilon_o R_{ok}^2}$$

(no y component)

where $R_{ok} = 2(L - x_o)$ where $(L - x_o)$ is the distance between the particle and the substrate

Therefore

$$F_I = \frac{-q_o q_k}{16\pi\varepsilon_o (L - x_o)^2}$$

and it is assumed that $q_o = -q_k$

5.5.7 Repulsive Force

The repulsive force due to the packed particles is given in a similar way. It is assumed that the charge on the packed particles does not leak away to any appreciable extent. In all these calculations it is assumed that the charge is concentrated at the centre of the particle. The charge is therefore, in the case of

monosized particles, exactly equal to that of the oncoming particle.
Hence

$$\vec{F_i} = \frac{-q_o q_i}{4\pi\epsilon_o R_{oi}}$$

and in the x direction

$$F_{i_x} = \frac{-q_o q_i \cos\theta_i}{4\pi\epsilon_o R_{oi}}$$

From Figure 5.11 it can be seen that

$$\cos\theta_i = \frac{(x_i - x_o)}{R_{oi}} = \left[\frac{x_i - x_o}{(x_i - x_o)^2 + (y_i - y_o)^2} \right]^{\frac{1}{2}}$$

Therefore

$$F_{i_x} = \frac{-q_o q_i}{4\pi\epsilon_o} \left[\frac{(x_i - x_o)}{(x_i - x_o)^2 + (y_i - y_o)^2} \right]^{3/2}$$

The total force acting on the particle in flight will therefore be the
sum of all such individual forces

$$F_{Rx} = \sum_1^i \frac{-q_o q_i}{4\pi\epsilon_o} \left[\frac{(x_i - x_o)}{(x_i - x_o)^2 + (y_i - y_o)^2} \right]^{3/2}$$

and similarly for the y direction.

5.5.8 Attractive Forces

The attractive forces due to the induced images of the
packed particles on the oncoming particle is given by a similar
expression.

In the x direction

$$F_{A_x} = \sum_1^j \frac{-q_o q_j}{4\pi\epsilon_o (R_{oj})^2} \cos\theta$$

which simplifies to

$$F_{A_x} = \sum_{1}^{j} \frac{-q_o q_j}{4\pi\varepsilon_o} \frac{(x_j - x_o)}{(R_{oj})^{3/2}}$$

Combining all these forces gives the final differential equations describing the trajectory of the particle in flight. These are summarised in Table 5.1.

5.6 Other Representations of Forces

The calculation of the repulsive and attractive forces due to the charged particle packing and the equations used have been described. It is found that the calculation of all such individual forces associated with a packing is very time consuming for packings in excess of 50 particles. An upper limit of 300 particles considered is imposed due to the available computing time. These calculations are necessary so that a representation of the packing can be obtained and an insight into the effects of particle size, packing thickness etc on the overall packing can be gained.

However similar investigations can be made by considering particles heading towards a uniform and even packing. A theoretical layer of charge, with a given charge density, can be considered to exist on the substrate.

By calculating the charge on a particle of a certain size and assuming a porosity of packing the charge per unit length and unit thickness (2 dimensional case) can be calculated. In effect this acts as a layer of particles of a given thickness but with a width of one particle diameter (in the 3rd dimension). The charge density in this case has units of coulomb/square metre. The convention used for these theoretical considerations is shown in Figure 5.12.

Table 5.1. Summary of Forces on Particle

Force	x-direction	y-direction
Field	$F_{E_x} = q_o \dfrac{V_o}{\ln(L/b)} \cdot \dfrac{x_o}{R_o^{3/2}}$	$F_{E_y} = q_o \dfrac{V_o}{\ln(L/b)} \cdot \dfrac{y_o}{R_o^{3/2}}$
Drag	$Re < 1$ $F_{D_x} = 3\pi\mu d_o\left(u - \dfrac{dx}{dt}\right)$ $Re > 1$ $F_{D_x} = 3\pi\mu d_o\left(u - \dfrac{dx}{dt}\right)\left[1 + 0.15 Re_p^{0.687}\right]$ where $u = \dfrac{U}{R^{\frac{1}{2}}}(x_o\cos\theta/2 - y_o\sin\theta/2)$ where R and θ are given in the text	$F_{D_y} = 3\pi\mu d_o\left(v - \dfrac{dy}{dt}\right)$ $F_{D_y} = 3\pi\mu d_o\left(v - \dfrac{dy}{dt}\right)\left[1 + 0.15 Re_p^{0.687}\right]$ $v = \dfrac{U}{R^{\frac{1}{2}}}(x_o\sin\theta/2 + y_o\cos\theta/2)$
Image	$F_I = \dfrac{q_o^2}{16\,\varepsilon_o(L-x_o)^2}$	0
Repulsive	$F_{R_x} = \overset{i}{\underset{1}{\Sigma}} \dfrac{-q_o q_i}{4\pi\varepsilon_o} \cdot \dfrac{\lvert x_i - x_o\rvert}{R_{oi}^{3/2}}$	$F_{R_y} = \overset{i}{\underset{1}{\Sigma}} \dfrac{-q_o q_i}{4\pi\varepsilon_o} \cdot \dfrac{\lvert y_i - y_o\rvert}{R_{oi}^{3/2}}$
Attractive	$F_{A_x} = \overset{j}{\underset{1}{\Sigma}} \dfrac{-q_o q_j}{4\pi\varepsilon_o} \cdot \dfrac{\lvert x_j - x_o\rvert}{R_{oj}^{3/2}}$	$F_{A_y} = \overset{j}{\underset{1}{\Sigma}} \dfrac{-q_o q_j}{4\pi\varepsilon_o} \cdot \dfrac{\lvert y_j - y_o\rvert}{R_{oj}^{3/2}}$

Figure 5.12. Convention used for Theoretical Charged Layer Calculations

The force between two charged particles (of the same sign) is

$$\overrightarrow{F_R} = \frac{-q_1 \, q_2}{4\pi\epsilon_o R_{12}^2}$$

and in the x direction the force component is given by

$$F_{R_x} = \frac{-q_1 \, q_2 \, (x_1 - x_2)}{4\pi\epsilon_o \, R_{12}^{3/2}}$$

In considering a uniform charged layer the total force on the oncoming particle is the sum of the forces due to all points in the charged layer. If the layer is on a plate of thickness t and width 2 ℓ. the overall force is

$$F_{R_x} = \frac{-q_o Q_a}{4\pi\epsilon_o} \int_{-\ell}^{\ell} \int_{GT-t}^{GT} \left[\frac{(x-x_o)}{((x-x_o)^2 + (y-y_o)^2)^{3/2}} \right] dxdy$$

where GT is the distance between gun and target, and Q_a is the charge density in terms of coulombs per unit area.

Putting

$$C = \frac{q_o Q_a}{4\pi\epsilon_o}$$

and substituting

$$x' = x - x_o$$

$$y' = y - y_o$$

and

$$x_1 = GT-t-x_o$$

$$x_2 = GT-x_o$$

$$y_1 = -(\ell+y_o)$$

$$y_2 = \ell-y_o$$

the equation becomes

$$F_{R_x} = -C \int_{y_1}^{y_2} \int_{x_1}^{x_2} \left[\frac{x'}{(x'^2 + y'^2)^{3/2}} \right] dx' dy'$$

Hence

$$F_{R_x} = -C \int_{y_1}^{y_2} dy' \left[\frac{-1}{(x'^2 + y'^2)^{\frac{1}{2}}} \right]_{x_1}^{x_2}$$

$$= -C \int_{y_1}^{y_2} dy' \left[\frac{-1}{(x_2^2 + y'^2)^{\frac{1}{2}}} + \frac{1}{(x_1^2 + y'^2)^{\frac{1}{2}}} \right]$$

$$F_{R_x} = -C \left[-\log(y' + \sqrt{x_2^2 + y'^2}) + \log(y' + \sqrt{x_1^2 + y'^2}) \right]_{y_1}^{y_2}$$

$$= -C \log \left[\frac{(y' + \sqrt{x_1^2 + y'^2})}{(y' + \sqrt{x_2^2 + y'^2})} \right]_{y_1}^{y_2}$$

which gives

$$F_{R_x} = -C \log \left[\frac{(y_2 + \sqrt{x_1^2 + y_2^2})}{(y_2 + \sqrt{x_2^2 + y_2^2})} \cdot \frac{(y_1 + \sqrt{x_2^2 + y_1^2})}{(y_1 + \sqrt{x_1^2 + y_1^2})} \right]$$

substituting back

$$F_{R_x} = -C \log \left[\frac{(-y_o) + \sqrt{(GT-t-x_o)^2 + (\ell+y_o)^2}}{(\ell-y_o) + \sqrt{(GT-x_o)^2 + (\ell+y_o)^2}} \cdot \frac{-\ell-y_o + \sqrt{(GT-x_o)^2 + (\ell+y_o)^2}}{-\ell-y_o + \sqrt{(GT-x_o-t)^2 + (\ell-y_o)^2}} \right]$$

If $x_o = GT - 0.5t$, $F_{R_x} = 0$

Similarly in the y direction

$$F_{R_y} = \int_{-\ell}^{\ell} \int_{GT-t}^{GT} \left[\frac{(y-y_o)}{(x-x_o)^2 + (y-y_o)^{2\,3/2}} \right] dx dy$$

Thus

$$F_{R_y} = -C \int_{y_1}^{y_2} \int_{x_1}^{x_2} \left[\frac{y'}{(x'^2 + y'^2)^{3/2}} \right] dx'dy'$$

using the same substitutions, and this becomes

$$F_{R_y} = -C\log \left[\frac{(x_1 + \sqrt{y_2^2 + x_1^2})}{x_2 + \sqrt{y_2^2 + x_2^2}} \cdot \frac{(x_2 + \sqrt{y_1^2 + x_2^2})}{(x_1 + \sqrt{y_1^2 + x_1^2})} \right]$$

Substituting back again the equation for the force on a particle in the y direction due to a charged layer is:-

$$F_{R_y} = -C\log \left[\frac{(GT-t-x_o)+\sqrt{(\ell-y_o)^2+(GT-t-x_o)^2}}{(GT-x_o)+\sqrt{(\ell-y_o)^2+(GT-x_o)^2}} \cdot \frac{(GT-x_o)+\sqrt{(\ell+y_o)^2+(GT-x_o)^2}}{(GT-x_o-t)+\sqrt{(\ell+y_o)^2+(GT-x_o-t)^2}} \right]$$

Hence if $y_o = 0$, i.e. the particle is travelling along the x axis, $F_{R_y} = 0$.

The force on the particle in the x and y directions due to the induced image layer is obtained by exactly the same derivation except that

$$x_1 = GT-x_o$$

and $$x_2 = GT-x_o+t$$

and therefore similar equations are obtained.

Also, for the image force the sign of the constant is reversed due to the image charge layer being of opposite sign

hence $$C = \frac{-q_o Q_a}{4\pi\varepsilon_o}$$

These equations therefore allow the simple calculation of the force on a particle in any position due to a charged layer of chosen thickness, charge density and size. This can then replace the section

of the computer program that calculates interparticle forces and can

show the effects of different thicknesses of layers on the flight

and packing of particles. Other effects, such as that due to changes

in transport air velocity and particle charge can also be observed.

5.7 Comparison with the 3 Dimensional Case

The equations described to represent forces acting on a particle

in flight consider the 2 dimensional case only. This simulation

could be considered as particles being sprayed from a gun in one

plane only and landing on a very narrow substrate, extending in the

same plane. This in itself does not seem an unreasonable qualification

but even if the particles were sprayed in a thin plane the electro-

static forces would give rise to a 3 dimensional effect in the case

of different sized particles. This is due to their centres being in

slightly different positions. In the computer program the charge on

the particles is considered to be concentrated at the centre of each

particle. In reality, of course, they are spread over the surface of

the particle, hence the dependence of saturation charge on surface

area.

If the corresponding equations previously derived for the

repulsive and attractive forces due to a charge layer are extended

for a plate of infinite width a relationship is obtained for 2

dimensions. For 3 dimensions the total force on a particle can be

shown to be zero if an infinite charge layer, and related image layer

are considered.

Although the forces due to drag and the electric field can be

symmetric (in 3 dimensions) about the x axis, the electrostatic forces

cannot. The random landing of particles and subsequent effect on

trajectories due to packed particles leaves no symmetry about the x axis. Therefore any particle trajectory is dependent on all the particles around it and will therefore be forced in one direction or another because of the resultant of all the individual forces.

In this respect the 2-dimensional case must be considered as a large simplification of the true situation. However it is hoped that the simulations gained by this technique do show some of the effects in packing that can occur, albeit only qualitatively.

5.8   Summary

The equations of motion have been developed (in 2 dimensions) for the calculation of the trajectories of individual particles in flight. These equations take into account the electrostatic forces due to all the particles packed on the substrate. Although the summation of these forces requires a vast amount of calculation when more than 50 particles have landed, it is necessary so that effects close to the substrate can be observed.

Various assumptions have been made to arrive at the form of these equations and although they greatly simplify the problem it is thought that this treatment will still provide valuable information.

In the next chapter the computer program, the way in which it works and the experiments carried out will be described.

CHAPTER 6

COMPUTER SIMULATION

6.1 Introduction

6.2 Nag Routines

6.3 Program Description

    6.3.1 Problems encountered

    6.3.2 Main subroutine

    6.3.3 Function subroutine

6.4 Testing of Program

    6.4.1 Drag coefficient

    6.4.2 Starting velocities

    6.4.3 Error testing

    6.4.4 Particle splaying

    6.4.5 Further effects

6.5 Experimental Results and Discussion

    6.5.1 No field force

    6.5.2 Monosized powder

    6.5.3 Size distributed powders

    6.5.4 Theoretical charged layer

    6.5.5 Effect of gravity

6.6 Conclusions

6.7 Summary

6.1 Introduction

In the previous chapter the derivation of the trajectory equations via the force balance on a particle was discussed. The complex nature of the equations is such that straightforward integration by analytical methods is not possible. Numerical methods have therefore to be used. A computer program has been written and employed to enable the calculation of solutions quickly and efficiently.

For this purpose a computer library routine which solves ordinary differential equations has been included in the program that allows control of the integration procedure and will minimise errors to desired levels. There are various routines available from the NAG library which integrate differential equations in various ways. Three such routines have been used, the final one being most suitable for this problem. Restrictions of computing time, accuracy, and type of equations involved led to this choice of routine.

During the development of the program four different computers, of varying size and location, were employed, all of them using the Fortran language. The basis of the program was built around a set of simplifying assumptions, separate to those used in the formation of trajectory equations. These assumptions were:-

(1) The particles are spherical

(2) Only one particle is in flight at any instant in time

(3) Each particle, for a given run, starts at a random point at the same distance from the substrate with identical velocity components.

(4)   No effect due to gravity is considered

(5)   When a particle touches another particle or the substrate it
       remains stationary.

(6)   Each particle carries its equilibrium charge (according to
       its size).

(7)   The particles do not lose any of their charge on contact with
       the packing.

6.2   NAG Routines

One of the simplest NAG routines available for numerical
integration of ordinary differential equations (Type DØ2ABF) was
first used to solve the trajectory equations (Nottingham Algorithms'
Group, 1973). This is based on Merson's form of the Runge-Kutta
method of numerical integration. It was discovered that no solution
could be obtained using this routine since to work within prescribed
error limits an infinitely small step length was required. This is
characteristic of a stiff system of equations. Stiff systems of
equations are those which have rapidly decaying transient solutions
(or whose Jacobian matrices have eigenvalues with large negative
real parts). The degree of stiffness (given as the ratio of the
largest to smallest real parts, in magnitude) may vary across the
range of integration.

Gear's method of integration is more efficient for stiff systems
and therefore the NAG routine DØ2AJF was employed (NAGFLIB, 1976).
Although solutions were achieved with this routine, it was found that
the program became very time consuming (in terms of c.p.u. time) when
dealing with large numbers of particles. A newer, more efficient
routine, DØ2QBF, was therefore used and it was found that this worked

much quicker than its predecessor. This routine integrates a stiff system of ordinary differential equations also using Gear's method but has a greater variety of facilities for interrupting the calculation. The routine, and its use, is fairly complex (NAGFLIB, 1978).

D$\emptyset$2QBF advances the solution of equations

$$Z_i' = F_i(T, Z_1, Z_2 \ldots Z_N)$$

where $i = 1, 2 \ldots N$

over an integration range using a number of steps of a variable-order variable-step Gear method. The stepsize and order are chosen so that the local error estimate is kept within a prescribed error bound. The way in which the size of the error bound was chosen is described later.

The equations are contained in a subroutine which is called by the NAG routine after initial values for the variables have been set. Interrupt procedures allow for the access of information during the course of the integration.

The integration can also be stopped at any point in time by such interruptions, a facility which was not available in earlier routines.

The information obtained also provides enough data for accurate interpolation between integration points using other suitable NAG routines. Since the routine only solves first order differential equations it is necessary to describe the trajectory by four equations. The subjects of the equations are given as follows:

$$\frac{dZ_1}{dt} = \frac{d^2x}{dt^2} = f_1(t,Z_1,Z_2,Z_3,Z_4)$$

$$\frac{dZ_2}{dt} = \frac{dx}{dt} = f_1(t,Z_1,Z_2,Z_3,Z_4)$$

$$\frac{dZ_3}{dt} = \frac{d^2y}{dt^2} = f_1(t,Z_1,Z_2,Z_3,Z_4)$$

$$\frac{dZ_4}{dt} = \frac{dy}{dt} = f_1(t,Z_1,Z_2,Z_3,Z_4)$$

hence $Z_2 = x$, $Z_4 = y$ and Z_1 and Z_3 represent the velocity of the particle in the x and y directions respectively.

The program is initially supplied with:-

(1)   initial values of t and Z_i

(2)   the length of the integration range

(3)   the number of differential equations

(4)   a set of control variables

(5)   the Error bound

(6)   interrupt conditions

(7)   a failure parameter and type of error test parameter

and (8)   working space (dimensioned spare variables)

The routine chooses a step size which just keeps within the error bound and then evaluates the derivatives in terms of T, Z_1, Z_2, Z_3 and Z_4. The trajectory is calculated and continues until the particle is close to the substrate. The routine is then interrupted after each integration step to compare the particle position relative to other stationary packed particles and the substrate.

The NAG routine has not been internally reprogrammed in any way and its working will not be described here. Literature is available on the program and the method of integration (NAGFLIB, 1978; G. Hall et al, 1976; A.C. Hindmarsh, 1974; C.W. Gear, 1971).

If the program fails due to an error in the NAG routine (IFAIL > 0 on exit) a set of information variables are printed which describe the current status of the routine. This includes the type of error encountered. Common errors found were:-

(1)   integration range finished before particle was found to have landed.

(2)   start parameters set wrongly

(3)   stepsize too small for solution to be obtained.

The number of successful/unsuccessful integration steps, maximum/ minimum stepsize used, last integration point calculated and the maximum values of the differentials are just some of the outputs available. Although the routine is complex and considerable time is required to understand it, it is very versatile when handled efficiently.

The mode of operation of the program will now be described.

6.3   Program Description

Apart from the NAG routine (which is called from the Library) the program is split into two main sections:-

(1)   Main subroutine which handles the setting of variables, initial conditions and determination of when the flight of particle is over (i.e. it has hit another particle or the substrate).

(2)   Function subroutine which calculates the individual force components which are combined to form the differential equations.

The overall scheme of the program is shown in Figure 6.1 which gives a simplified flow chart.

6.3.1 Problems Encountered

The computation time for calculating the sum of all individual interparticulate forces (electrostatic, including images) is not in itself too large, but when this procedure is carried out many thousands of times the restraints on computer time becomes important. This requires that the program is written in such a way that there is no wasteful computation. Careful use of variables and arrays and avoidance of repeated operations are just some of the considerations.

In one of its earliest forms using DØ2AJF the program took just under one hour of c.p.u. time on the Loughborough University ICL 1904S computer to calculate the trajectories of 50 particles. For the next fifty particles the c.p.u. time was nearly four times as long and since this was nearing the available computer users time. alternative methods were sought.

Using a computer link from Loughborough via Nottingham a program file was created and used to run programs on the CDC 7600 at the Manchester computer centre. This very large main frame machine allowed a much larger number of trajectories to be considered. However, due to the unavoidable low priority status being used development was extremely slow. The computer plots took approximately two weeks from the day of program execution to return to Loughborough.

The latest version of the NAG routine, DØ2QBF, was written into a program initially developed on the DEC 10 at ICI plc, Runcorn with the cooperation of the Process Technology Group. The program was streamlined with particular attention being paid to the assignment of

Figure 6.1. Simplified Flow Chart of Program Procedure

```
                    MAIN subroutine
                          │
                          ▼
                  Dimension Variables
                          │
                          ▼
                     Input Data
                          │
                          ▼
           Call plotter, draw axes and label
                          │
                          ▼
                    Set Constants
                          │
                          ▼
                  Print initial data
                          │
                          ▼
           Calculate random start point ──────────┐
                          │                        ▼
                          │   ◄──────────── Call NAG GØ5CAF
                          ▼
           Calculate particle diameter ───────────┐
                          │                        ▼
                          │   ◄──────────── Call NAG GØ5CAF
                          ▼
               Set boundary conditions
                          │
                          ▼
                 Calculate constants
                          │
                          ▼
              Set flags for NAG routine
                          │
                          ▼
                 Call NAG routine ──────────────────┐
                    DØ2QBF                           ▼
   plot & print trajectory  ◄──────────    │    NAG routine  ◄──────┐
                          │                         │                │
                          ▼                         ▼                │
                Check particle position     Call FUNCTION subroutine │
                relevant to other                   │                │
                particles ────────┐                 ▼                │
                          │        │         Calculate all forces    │
                          ▼        │                 │                │
              Compare to substrate │                 ▼                │
                          │        │         Set up differential ────┘
                          ▼        │             equations
                 Calculate final ◄─┘
                   position
                          │
                          ▼
               Plot final position
                          │
                          ▼
                        STOP
```

variables for calculation constants where parts of equations were continually repeated. The combination of this routine and programming allowed 150 trajectories to be calculated in 1 hour and 350 in approximately three and a half hours.

Moving the program onto ICI's VAX 11/780 computer (manufactured by DEC) also enabled the use of the BENSON electrostatic plotter which reduced plotting time to one quarter and gave 'on the spot' print-outs. VAX stands for Virtual Address eXtension and is an extension of the PDP-11 computers (D.R. Mason et al, 1978). It is a very powerful minicomputer which is suited to having a small number of users with large programs.

In terms of software, the determination of the final position of particles caused many problems. As a particle approaches the substrate it is possible that it can collide with any other stationary particle or the substrate. Each time a check is made on its position relative to all others many operations have to be carried out. Careful programming was necessary in order to keep this to a minimum and a variety of methods were considered. Finally, the most simple method was chosen. Once a particle in flight reaches the start of the powder layer the distance between the centres of particles are compared to the addition of the two radii. This is carried out after each integration step. More precise details are given later.

Error testing is also important. Not only must the accuracy of the results be checked but invisible errors (i.e. typing and input errors) must be detected by the user. Hand computations are therefore carried out to check the magnitude of forces, velocities, correct signs etc. such that the trends observed agree to an extent with those expected.

6.3.2 Main Subroutine

From Figure 6.1 it can be seen that the main subroutine
is responsible for all of the operations apart from calculating the
differential equations and the integration procedure.

The input of data comes from a data file unique to each run
condition. Basically the initial velocity, type of powder and start
positions are read in via this file. This command file also controls
output and assigns the name of the data file for the plotter.

The plotter file is opened and data is sent for the drawing
of axes, labelling and printing of conditions. The GINO-F language
is used for drawing (GINOF, 1976). Following input of the data on
file, all of the initial conditions, constants and printouts are
completed before setting the NAG routine control variables. A random
number generator, NAG G∅5CA5/G∅5CBF, is used to give random numbers
for the calculation of start position and particle size (if not
monosize distribution) (NAGFLIB, 1977a; NAGFLIB, 1977b). If a size
distribution is being considered the random number is used in connection
with a number size distribution to obtain a particle diameter which,
together with all other particle sizes, is representative of the
distribution.

The mass, charge and other calculation constants can then be
obtained.

The NAG controls are set such that initially the integration
will run without interruption until a specified value in the x
direction is reached.

Interruption then occurs at a suitable distance away from the
substrate where the plotting of the trajectory commences. Once this
point has been reached the integration is interrupted after each

integration step. Control variables are therefore readjusted accordingly.

Each time the integration is interrupted control is given back to the main subroutine from NAG. If the particle has not reached a distance equal to that of the highest particle in the packing the particles position is simply recorded, plotted and the program returns to NAG. The trajectory progress is printed if desired. Individual component forces printout is also available if required.

If the particle is within the layer then it follows a program seqeunce as summarised in Figure 6.2.

If a failure is detected by the NAG routine then a controlled stop is carried out. This means that with an IFAIL > 0 on exit from the NAG routine the program prints the control variables which gives valuable information for the assessment of the cause of the error.

6.3.3 Function Subroutine

This routine formulates the differential equations and therefore calculates the forces acting on a particle in the x and y directions. All of the statements in this routine have been simplified as far as possible so that the c.p.u. time is reduced. For each trajectory approximately 250 integration steps are used and for each call of this subroutine approximately 600 operations are carried out for each comparison with a 100 particle packing. Therefore for 350 particles at least 10^9 operations are performed in this subroutine alone. Wherever calculation constants can be used for each new particle, calculation is done in the main subroutine. A summary of the routine is given in Figure 6.3.

Figure 6.2. Simplified Flow Chart for MAIN Subroutine (Stopping Section)

New coordinates from NAG routine

Check for failure in NAG

Check time of integration and y position

Print trajectory or forces

Compare particle position with that
of uppermost particle

Compare position with other stationary
particles in reverse order

if out of
bounds

compare
and record
highest   if collision

Yes

check rest to see
if another one
has been hit

Check with
substrate

Record
dummy
position

if not
reached
layer

No

if collision

record as old position

plot trajectory

calculate position
by interpolation

recall NAG routine

calculate position
on substrate

interpolate other variables

plot final position and finish trajectory

check to see if last particle is highest

Print position and if hit, particle number

RESTART LOOP

Figure 6.3. Simplified Flow Chart of FUNCTION Subroutine

From NAG routine

↓

Calculate x and y air velocities
using model

↓

Calculate Particle Reynolds number

↓

Calculate x and y components of drag force

↓

Calculate image force

↓

Calculate x and y components of field force

↓

Calculate distance between oncoming and stationary
particle and its image

↓

Calculate angles between image and particle

↓

Calculate attractive and repulsive forces

↓

Sum with those already calculated

↓

Develop 4 differential equations

↓

Return to NAG routine

if
1st
particle   next
particle

The use of arrays is purposely limited. On entry to this subroutine the x and y coordinates and velocities are transferred to single variables since they are used many times and this reduces computing time. The air velocities at the new coordinates are calculated using the flow model and the calculation of forces follows. Eventually the differential equations are produced:-

In x direction

F(1) = (Drag force + field force + Image force + Particulate forces)/

mass of particle $= \dfrac{d^2x}{dt^2}$

F(2) = Velocity of particle $= \dfrac{dx}{dt}$

In y direction

F(3) = (Drag force + field force + particulate forces)/Mass of

particle $= \dfrac{d^2y}{dt^2}$

F(4) = Velocity of particle $= \dfrac{dy}{dt}$

The program is shown in Figures D1 (a-p) with explanations of each variable used in the program given in Appendix D. For calculations considering a layer of charge the appropriate equations are substituted into the FUNCTION subroutine for the particle summation loop. The relevant section of program is shown in Figures D2(a-b). A typical printout from a run of 10 particles, all 25μm diameter, is given in Figures D3(a-e) with suitable explanations.

6.4   Testing of Program

In order to check that some of the assumptions and method of programming gives meaningful results the program has to be tested in several ways.

6.4.1   Drag Coefficient

The drag coefficient used in the determination of the drag force is dependent on the size of the particle Reynold's number. If Re_p < 1 then Stokes Law applies but if it is greater than 1 modification to the drag coefficient is required. Therefore, in the trajectory printout, the particle Reynolds number is given after each integration step. Typically the Reynolds number for a 10μm particle is less than 0.3, but it does depend on the size of the particle and the relative velocity. However, as the particle approaches the plate the Reynolds number is often less than 0.001. Hence the assumption that

$$C_D = \frac{24}{Re} \qquad \text{appears reasonable.}$$

Typical values of Re_p obtained from trajectories of particles during which no field is applied are shown in Table 6.1.

The maximum Reynolds numbers occur at the start of the trajectory when the velocities of the particle are set. Therefore the relative velocity is maximum at this time. The minimum values are usually obtained when the particle is close to the substrate. These figures show that, although the initial starting conditions are an approximation, in the area of interest (close to the substrate) Stokes Law will apply.

Table 6.1. <u>Reynolds Numbers of Particles During Flight Without</u>
<u>Applied Field</u>

Particle Velocity m/s	Particle Diameter = 10μm Re_p[†]	Particle Diameter = 25μm Re_p[†]	Particle Diameter = 50μm Re_p[†]
1	<0.0001	0.0007	0.0061
3	0.0004	0.0068	0.0668
5	0.0012	0.0205	0.2636
7	0.0022	0.0395	1.377[*]
10	0.0047	0.0930	6.441[o]

[†]Re_p taken for particle at a distance of 1 cm from substrate.

No particles landed on substrate except

[*]where 8 landed

[o]where all 10 landed

6.4.2 Starting Velocities

Due to the very complex nature of the air flow exit the
spray gun between the electrode and target, whose representation
is out of the scope of this work, a simplified model is used. In
the last chapter formulae were developed for representing the air
flow around a flat plate. For the calculation of trajectories
leading up to the packing of particles on a plate it is necessary
to use some initial starting conditions.

On assuming a uniform gas velocity heading towards the plate
it is possible using the equations of Chapter 5 to calculate the
component air velocities at any position. It has been assumed that
the trajectories start mid-way between gun and target. The initial
velocities of the particles are assumed to be equal to the uniform
gas velocity, as used in the flow model, in the x direction and zero
in the y direction. For a uniform velocity of 1 m/s this would mean
a discrepancy in the x direction air and particle velocities of
approximately 0.5 m/s.

In order that these starting conditions did not cause severe
errors in the trajectory calculation a computer program was formed
in which only the drag and inertia forces on the particles were
considered. A run using varying sized particles then showed how the
particle velocity settled after the initial start.

This experiment can also be considered in a theoretical
manner. Considering the forces acting on the particle in the x
direction (neglecting gravity) and assuming that the air velocity
is not dependent on x:-

$$M \frac{dV_{rel}}{dt} = -3\pi\mu d_p V_{rel} \quad \text{(assuming Stokes' Law applies)}$$

Integration gives $\quad \dfrac{V_{rel}}{V_{rel_0}} = e^{-t/\tau}$

where $\quad \tau = \dfrac{M}{3\pi\mu dp}$

The time taken for the relative velocity to be halved is given by $t = \tau \ln 2$.

For a 10µm diameter particle in air this time would be 2.3×10^{-5} secs. To reduce the relative velocity to within 1% of the initial relative velocity would therefore take approximately seven of these times (i.e. 0.2 msecs). The distance travelled in this time (assuming average $V_{rel} = 0.75$ m/s) would be 120µm.

This agrees well with results from the computer program. For ten different particles, from slightly different y starting positions, the distance taken for the particle to settle to within 1% of the air velocity was between 200µm and 2900µm (16µm diam). The times taken were between 0.4 msecs and 3.5 msecs. The results are shown in Table 6.2.

It therefore appears that these starting conditions are not unreasonable since the particles reach a steady state generally within 0.5 - 3% of their total flight distance. It does depend though on the velocity and size of particles as can be seen from the table. Since the area of interest is close to the substrate these results suggest that any approximate starting velocity conditions could be used whilst still maintaining accuracy in the observation area.

Table 6.2. Effect of Initial Starting Conditions on Particle Trajectory Without Field

Diameter of Particle (µm)	Flight time to particle velocity within 1% of air velocity (milliseconds)	Distance Travelled (µm)
6.7	0.675	379
6.7	0.674	378
5.4	0.363	211
8.2	0.860	500
9.3	1.14	757
9.7	1.21	697
10.4	1.36	892
16.1	3.43	2629
8.7	0.96	657
5.8	0.42	246

TOL = 10^{-7}

Uniform Air Velocity = 1 m/s

6.4.3 Error Testing - Setting of Tolerance Bound

The NAG routine works in such a way that it chooses the largest integration step possible which just keeps the estimated errors within a tolerance bound provided by the user. The larger the tolerance the larger the integration steps since less accuracy is required. Although this means faster computation the results may not represent the true system. In severe cases the particles can 'jump' across the whole of the particle layer and the substrate by a considerable amount. This effect is caused by the very large integration steps being used in the initial, smoother running part of the integration range. The influence on the particles of the charged layer, in this situation, is not observed due to the very slow response of the system to its presence. The stopping section of the program is also reliant on the fact that the step size is small enough that particles cannot be 'jumped over' within the packing.

A series of computer experiments were carried out in which the effects of changing tolerance error were observed. For each run the start conditions remained the same but the final positions were recorded for each of 10 particles. The tolerance error chosen for further experiments was that employed when the final positions of particles had not altered significantly compared to the next largest tolerance error.

The convergence of solutions to a constant value with changes in tolerance bound can be clearly seen in Figures 6.4 to 6.6. The tolerance error chosen on this basis was 10^{-7}. The figures show how a consistent solution is produced as the tolerance bound is decreased. In general it appears that larger particles do not need as small tolerance errors as small ones. Figure 6.7 compares the plotted

Figure 6.4.   Calculated Y Position vs. Tolerance Bound

Figure 6.5. Calculated Y Position vs. Tolerance Bound

Figure 6.6.   Calculated Y Position vs. Tolerance Bound

Uniform Velocity = 10 m/s
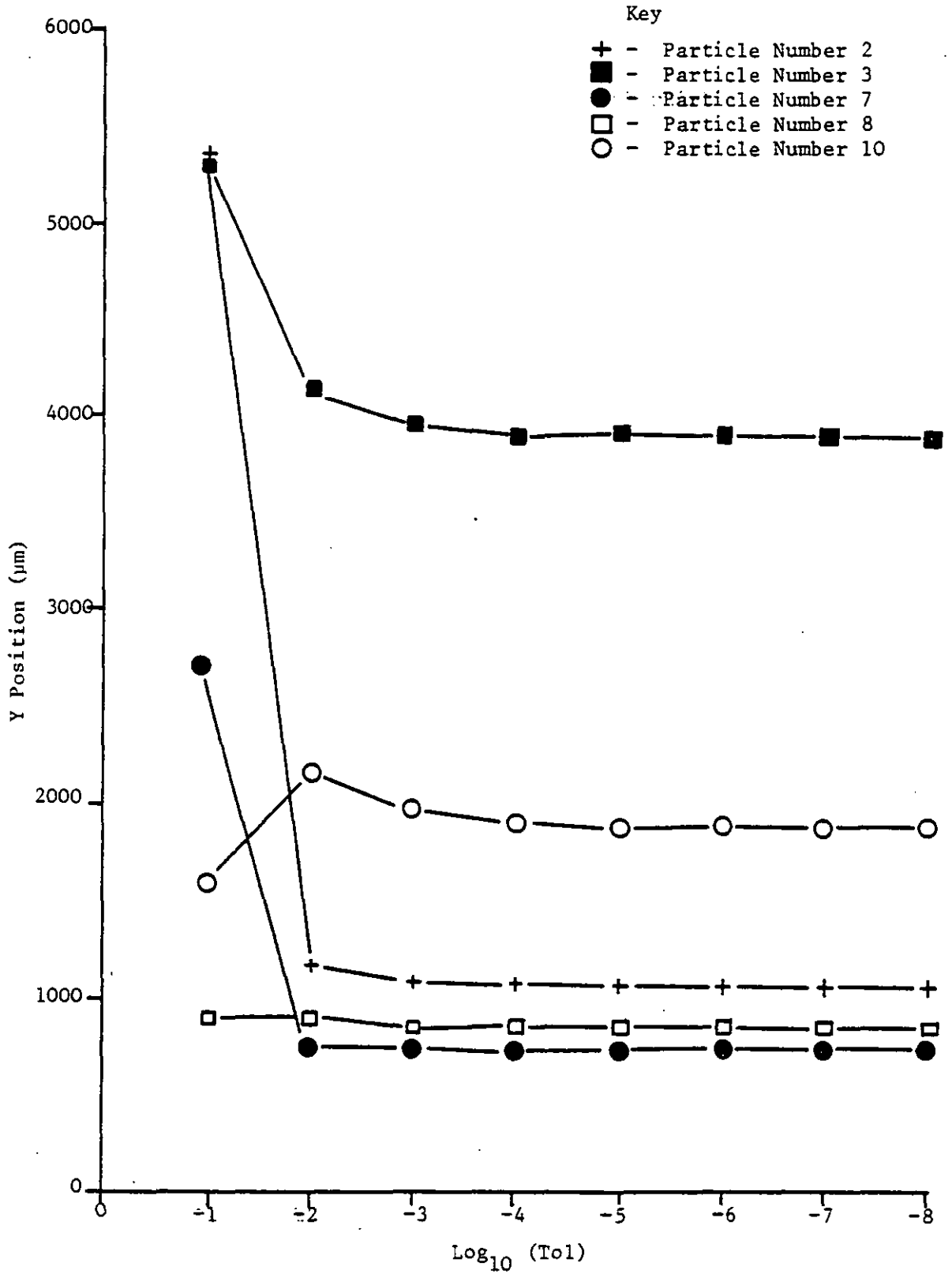
Key

+ − Particle Number 2
■ − Particle Number 3
● − Particle Number 7
□ − Particle Number 8
○ − Particle Number 10

Tolerance
Bound = 0.1

Tolerance
Bound = 0.01

Tolerance
Bound = 1×10^{-8}
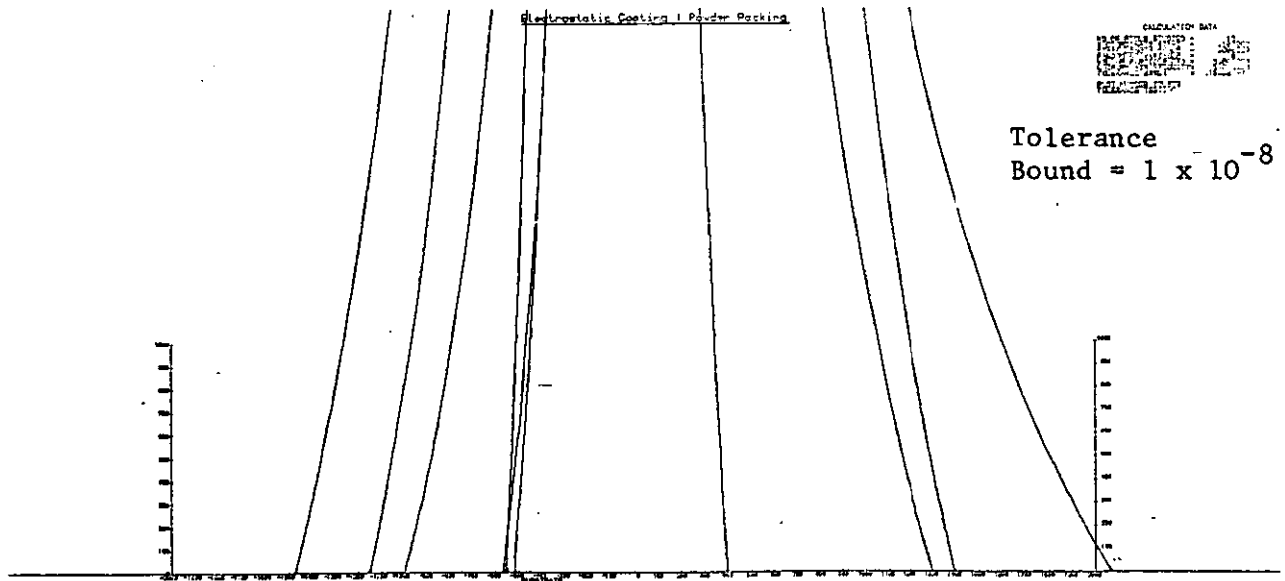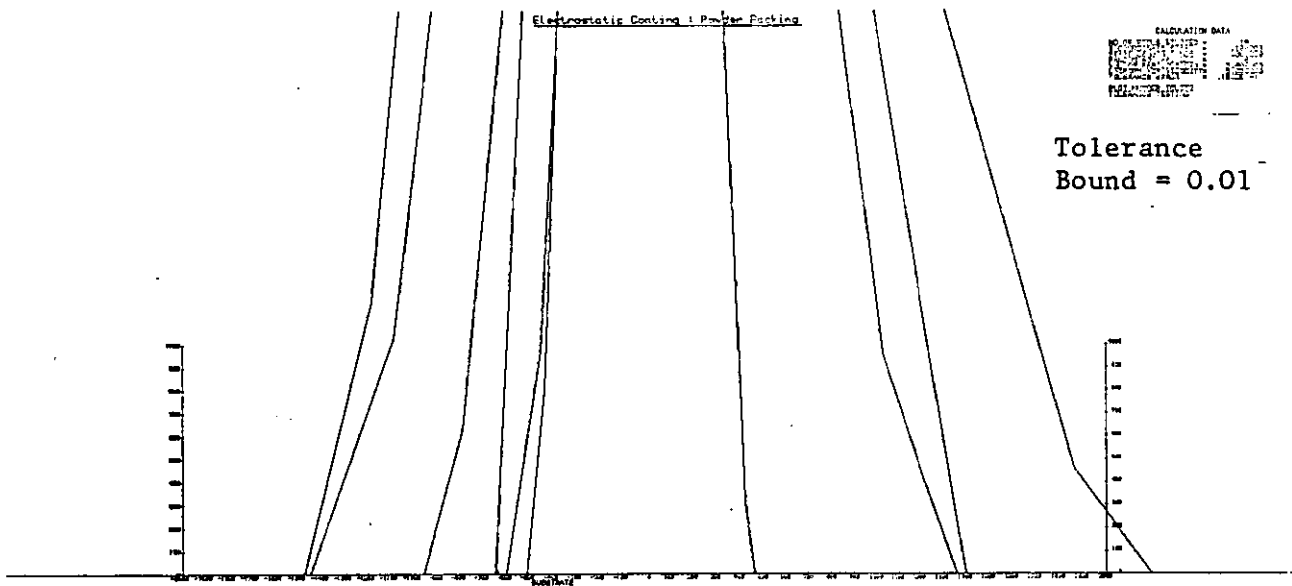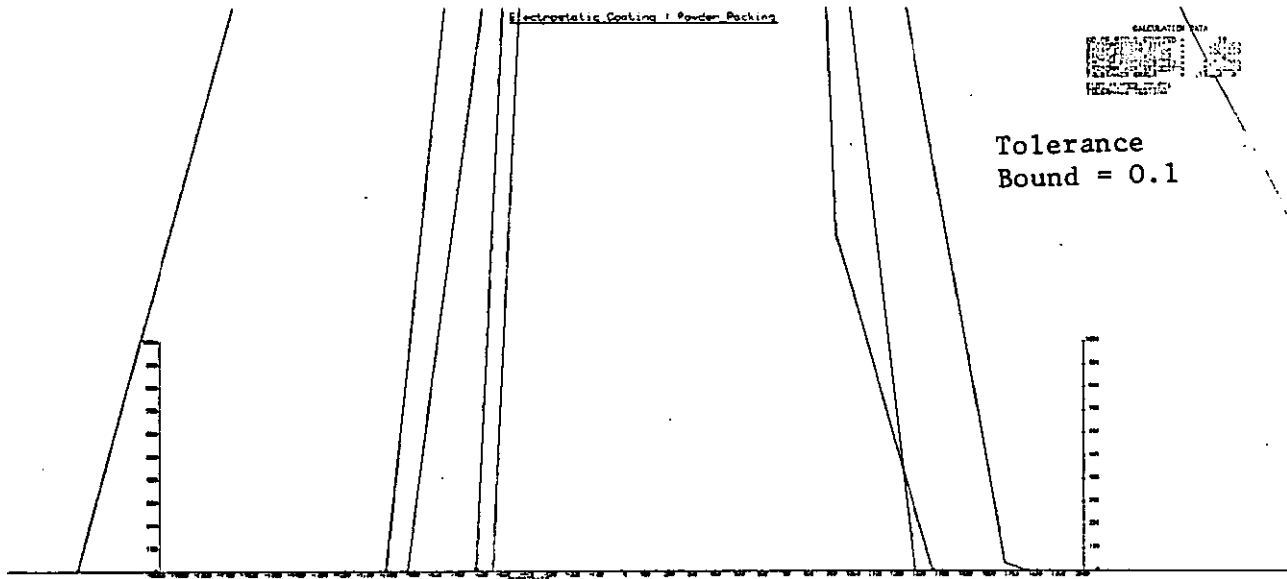
trajectories for three of the tolerances. For large bounds the trajectory consists of long straight line steps due to the limited accuracy of integration. For a bound of 10^{-8} the trajectories are extremely smooth and integration steps are in the order of 10^{-5} seconds, which typically represents a movement of <10µm. (This is dependent on the size of particle and velocities but it is found that the distance between steps decreases on nearing the substrate or packing).

6.4.4 Particle 'Splaying'

From a series of test runs it was found that changes in air transport velocity caused large changes in the area covered. This meant that comparison of packings was difficult since a different number/unit area of particles were being sprayed for each situation. The widths of the spray close to the substrate were therefore measured and compared (as shown in Table 6.3) for various conditions. It was observed that the width increased as velocity increased. However, for very large particles (50µm) at high velocities their inertia caused the particles not to follow the streamlines and hence in this case the width of spray actually decreased.

The start lengths were rescaled so that the width of spray was approximately the same in each experiment. The predicted start widths, shown in Table 6.4, were therefore used to obtain equal areas of spraying so that better comparisons could be made.

6.4.5 Further Effects

When the packing on the substrate is built up it is sometimes found that particles, particularly small ones, can either (i) be repelled a long distance away from the spray zone or (ii) reach an equilibrium position in space above the packing and hence have very long flight times (in excess of 0.5 s). Since in both these

Table 6.3. Effect of Air Velocity on Splaying of Particles of Different Sizes Starting at Identical Positions

Particle size, μm Start length* μm	10 300	17.5 400	25 500	25 1000	50 1000	Dist 700
Velocity m/s	Width of band[†], μms					
1.0	1350	1350	1480	2960	2210	4420
3.0	2610	2280	2120	4240	2270	<6000
5.0	3580	2970	2600	5200	2090	>6000
7.0	4364	3450	2820	–	1760	>6000
10.0	5450	4090	3060	–	1520	>6000

[†] measured at a distance of 1500μm from substrate

* width of start band 0.1m from substrate

Table 6.4. Predicted Start Widths for Equal Areas of Coverage with Variation in Operating Conditions

Velocity m/s	Start length[†], µm				
1.0	430	580	680	890	310
3.0	230	350	460	870	200
5.0	170	270	380	940	130
7.0	140	230	350	1100	100[*]
10.0	110	190	320	130	100[*]
Particle Size, µm	10	17.5	25	50	Dist.

[†] calcaulated on basis of results from Table 6 to cover area of 2000µm wide

[*] approximated values

cases any further computation for the given particle gives no
additional information the integration is controllably stopped.

For case (i), when the particle is beyond a distance of
0.009m from the area of interest the integration is stopped and the
particle position is logged at (-999, -999). In this way the particle
is then too far away to contribute to the interparticulate forces but
the coordinates indicate in the printout what has occurred. In
case (ii) once the particle has been in flight for longer than 0.45s
its final position is logged as the last current position. In the
printout it is shown to have hit particle number 999 which again
indicates what has happened. Both these precautions avoid wasting
computer time.

6.5 Experimental Results and Discussion

The computer simulation program has been used to primarily
observe the effects of particle size, air velocity, charged layers on
the packing of particles on a substrate. A comparison is also made
between monosized and size distributed powders.

Computer plots are used to pictorially represent the packing,
with each particle trajectory also being plotted. The forces acting
on a particle at any stage in its flight can be known from the print-
out and a few examples are given in the text.

Nearly 100 experimental runs have been carried out. It is
impossible to describe in detail each one and so several runs which
are considered representative are discussed in fuller detail.
However, the plots for all runs, if not given in the main text, can
be found in Appendix E.

6.5.1 No Field Force

In determining the flow regime that must be described for the calculation of drag force (drag coefficient equation) experiments were carried out in which no field forces and no particle charges were considered. Figures 6.8 to 6.14 show some of the results of these runs. In each figure an inset shows the same experimental conditions but with field and electrostatic forces acting on the particles. The scale of the inset is exactly the same as the main figure. In general, without an applied field, the particles do not reach the substrate but follow the air streamlines around the plate. Hence deposition does not occur.

As particle size increases the spread of the spray becomes narrower and, in fact, for 50μm particles starting with a velocity of 5 m/s contact with the substrate is made. However, since there is no electrostatic forces, the particles would be unlikely to remain on the substrate.

Figures 6.11 to 6.14 show the effect of uniform velocity on the spread of particles. As velocity increases inertia causes the particles to deviate from the flow of air. At a velocity of 10 m/s the particle trajectories appear very similar to those where field forces are acting.

These experiments clearly show the importance of the electro-static forces for the deposition of particles on the substrate. This appears particularly true for small particles which tend to follow the air flow.

Figure 6.8. Trajectories of Particles With and Without Electrostatic Forces – Particle diameter = 10μm, Uniform Velocity = 5 m/s
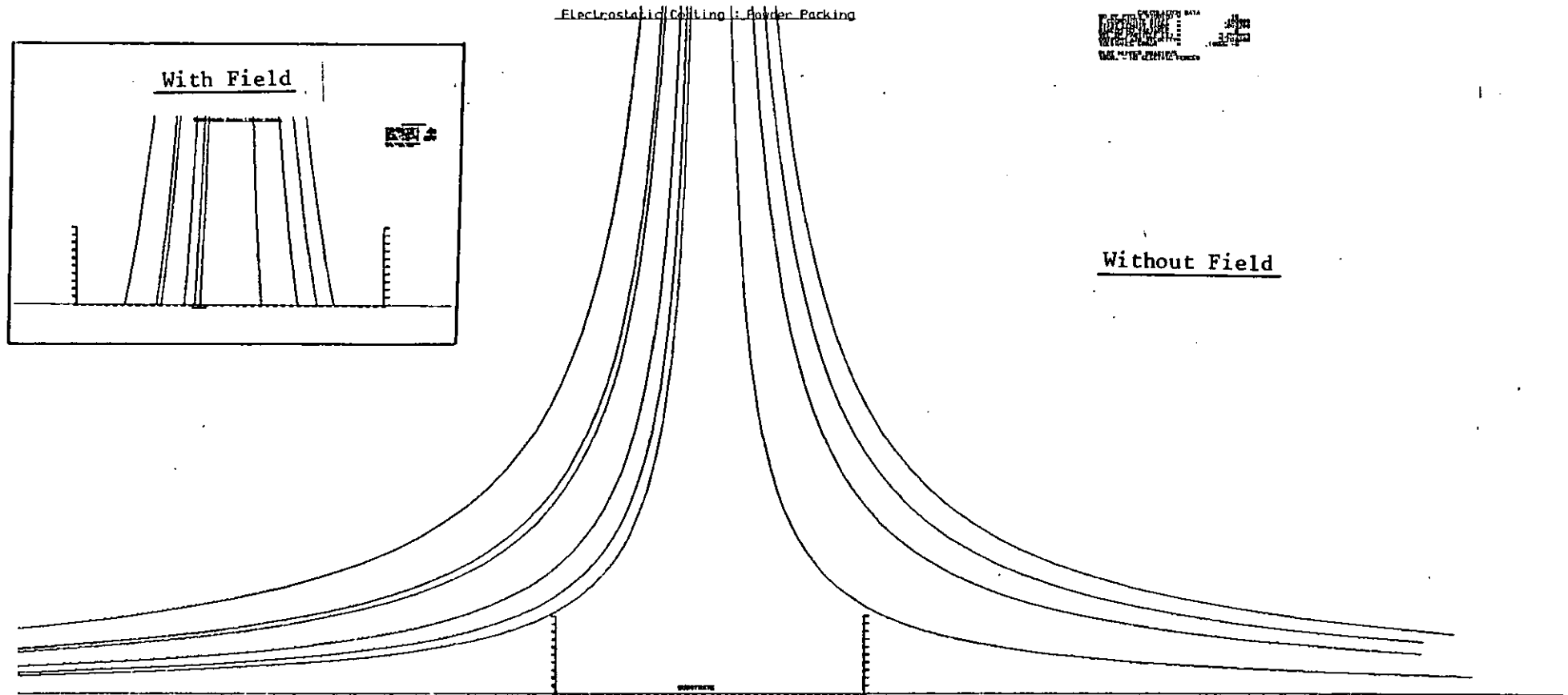
Figure 6.9. Trajectories of Particles With and Without Electrostatic Forces — Particle diameter = 25μm, Uniform Velocity = 5 m/s
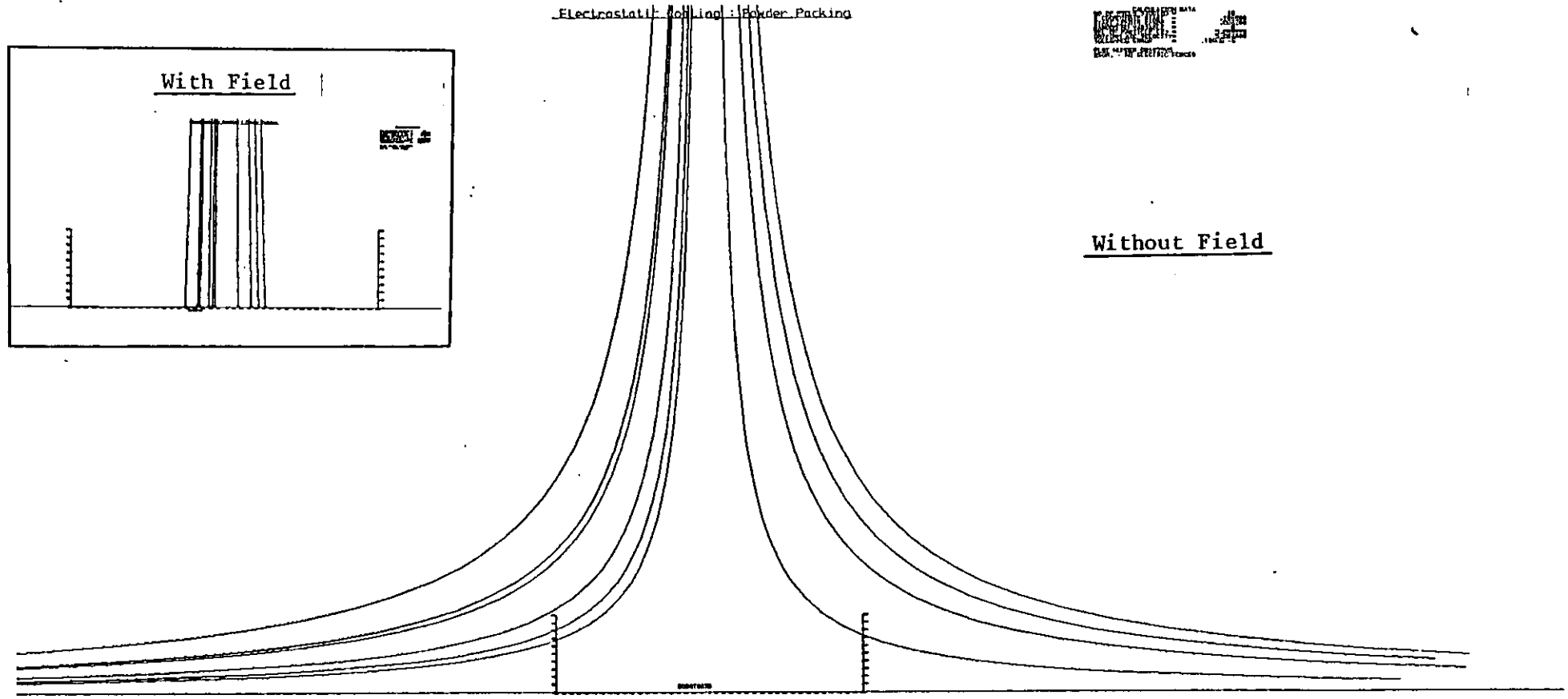
Figure 6.10. Trajectories of Particles With and Without Electrostatic Forces – Particle diameter = 50µm, Uniform Velocity = 5 m/s

With Field

Electrostatic Column: Powder Packing

Without Field
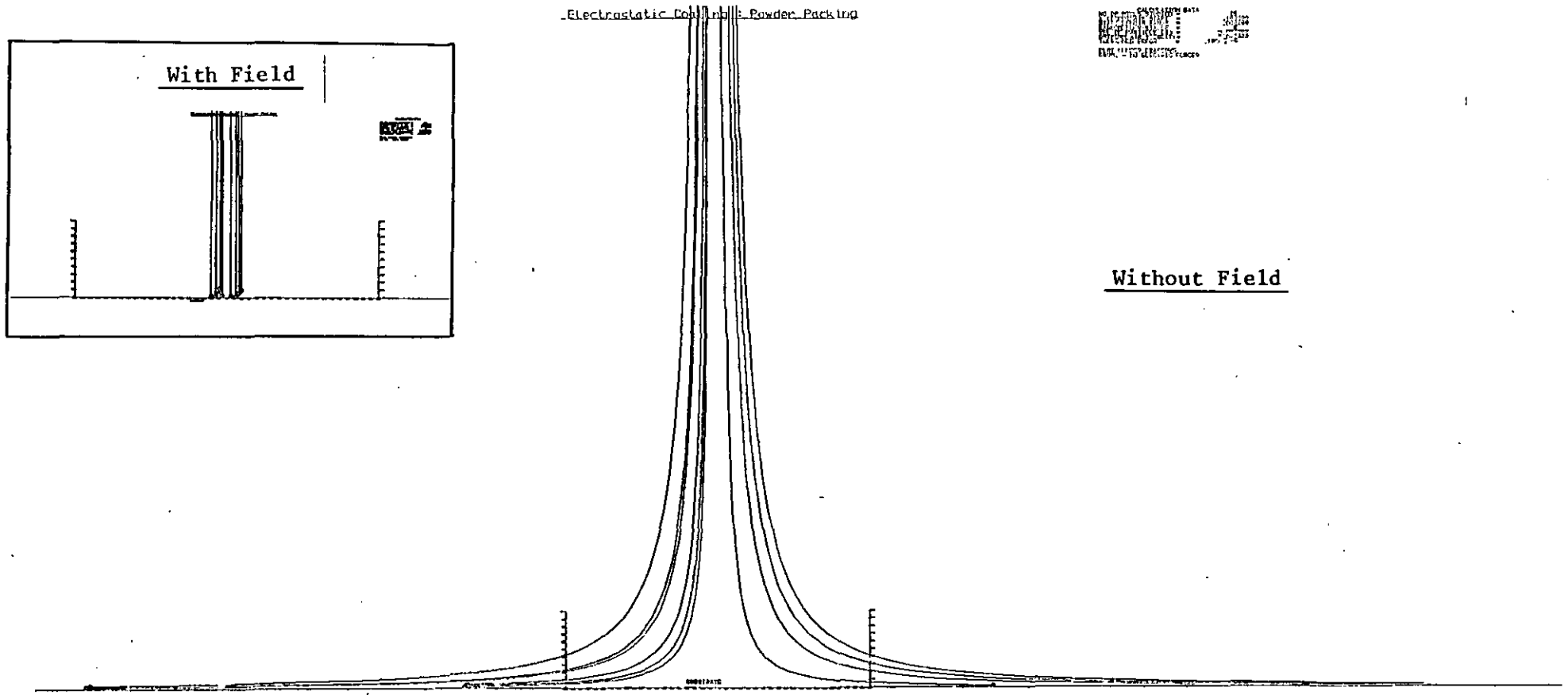
Figure 6.11.   Trajectories of Particles With and Without Electrostatic Forces – Particle diameter = 50µm, Uniform Velocity = 1 m/s
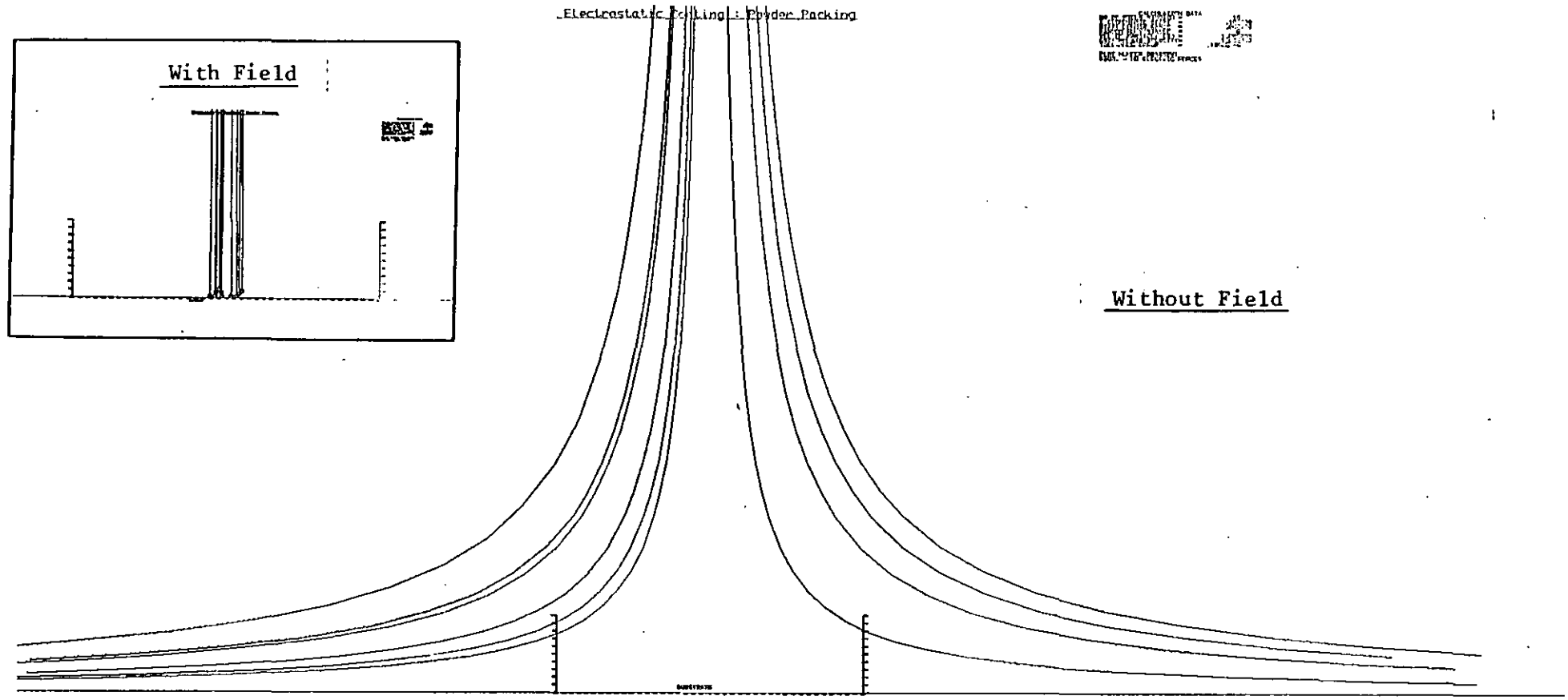
Figure 6.12. **Trajectories of Particles With and Without Electrostatic Forces – Particle diameter = 50μm, Uniform Velocity = 3 m/s**
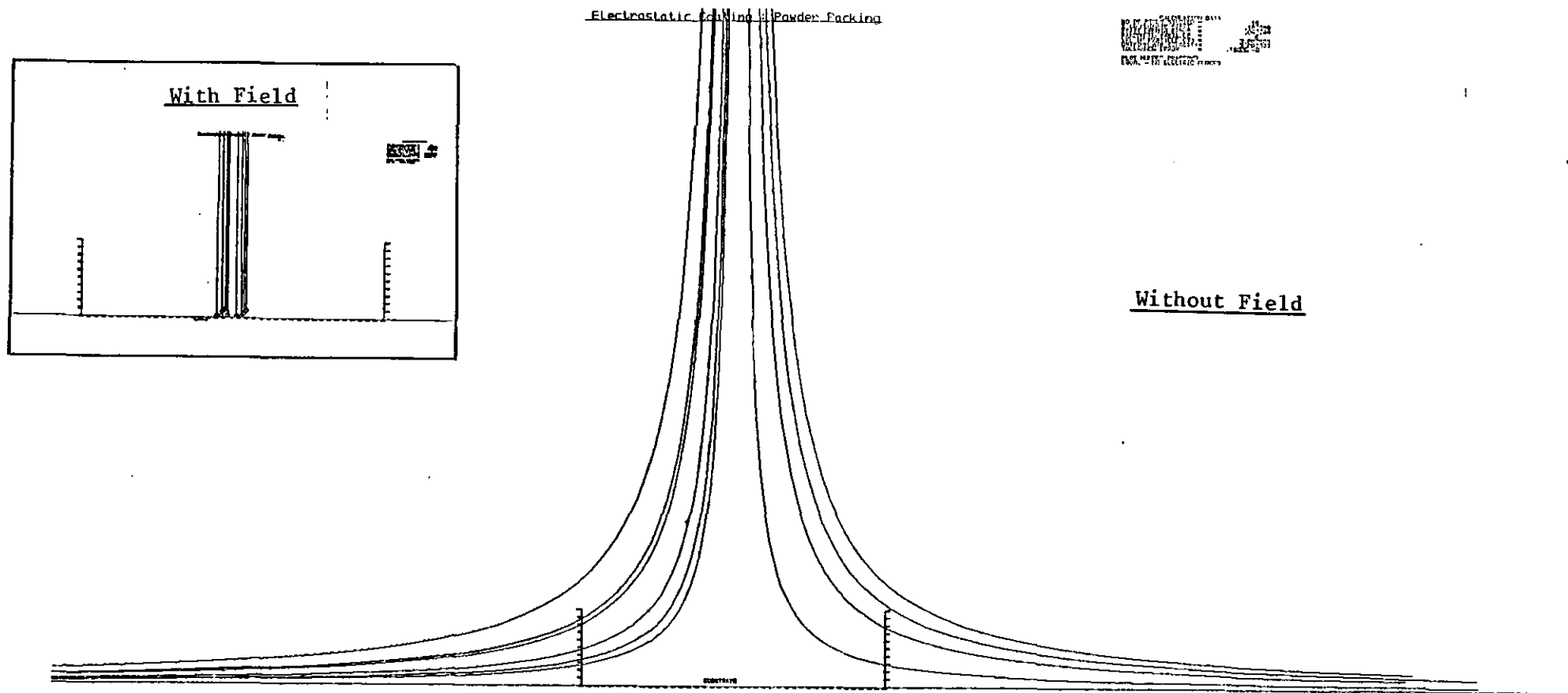
Figure 6.13.　Trajectories of Particles With and Without Electrostatic Forces - Particle diameter = 50μm,
Uniform Velocity = 7 m/s

Electrostatic Coalled : Powder Packing

With Field

Without Field
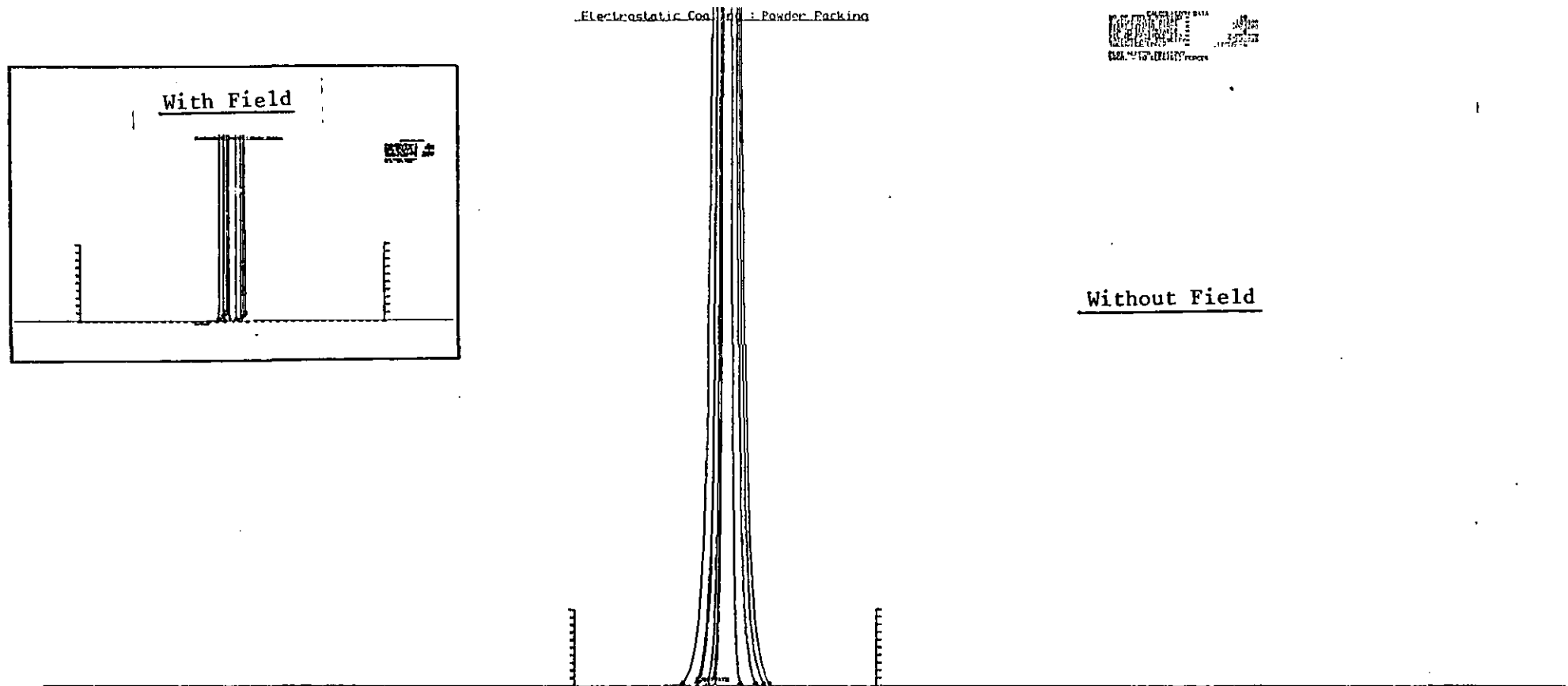
Figure 6.14: Trajectories of Particles With and Without Electrostatic Forces - Particle diameter = 50μm, Uniform Velocity = 10 m/s
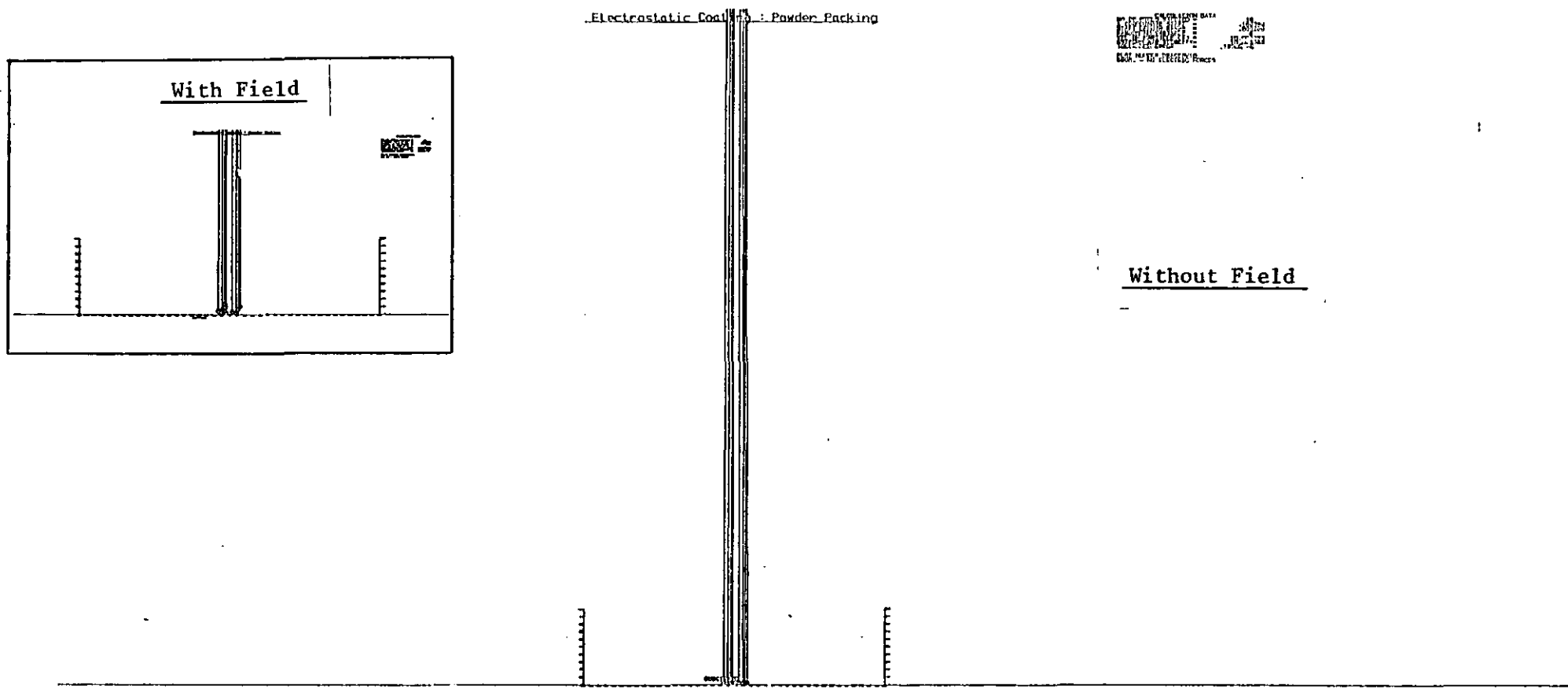
6.5.2 <u>Monosized Powders</u>

Earlier it was discussed how changes in particle size and velocity caused varying amounts of 'splaying' of particles and hence gave different amounts of coverage on the substrate. Experiments were therefore split into two sections:-

(i) those in which various start widths were employed to achieve equal areas of coverage over the range of conditions

(ii) those in which the start widths were kept constant.

In order to compare the effects of size and velocity on particle packing it is primarily the first section that will be discussed in detail. Due to the large extent of splaying in the second case for the smaller particles comparison of the effects of packing on particle trajectories is difficult since the coating is very thin.

Experiments were conducted for four different particle sizes (10μm, 17μm, 25μm and 50μm diameters) and five uniform air velocities (1,3,5,7 and 10 m/s).

The variation in conditions was used so that effects of these parameters could be observed to give indications of the dominant forces acting on the particles. In general those experiments using a uniform air velocity of 5 m/s will be discussed to a fuller extent since this relates more to the real system (M.L. Ang, 1981). However the other results are valuable in showing the changes in observed effects. Also it can be seen from Figure 6.15 that in a typical commercial powder 90% by number of the particles are less than 17μm diameter. Therefore the experiments involving 10μm particles are more relevant than others.

Figure 6.15. Number Size Distribution of Epoxy Powder
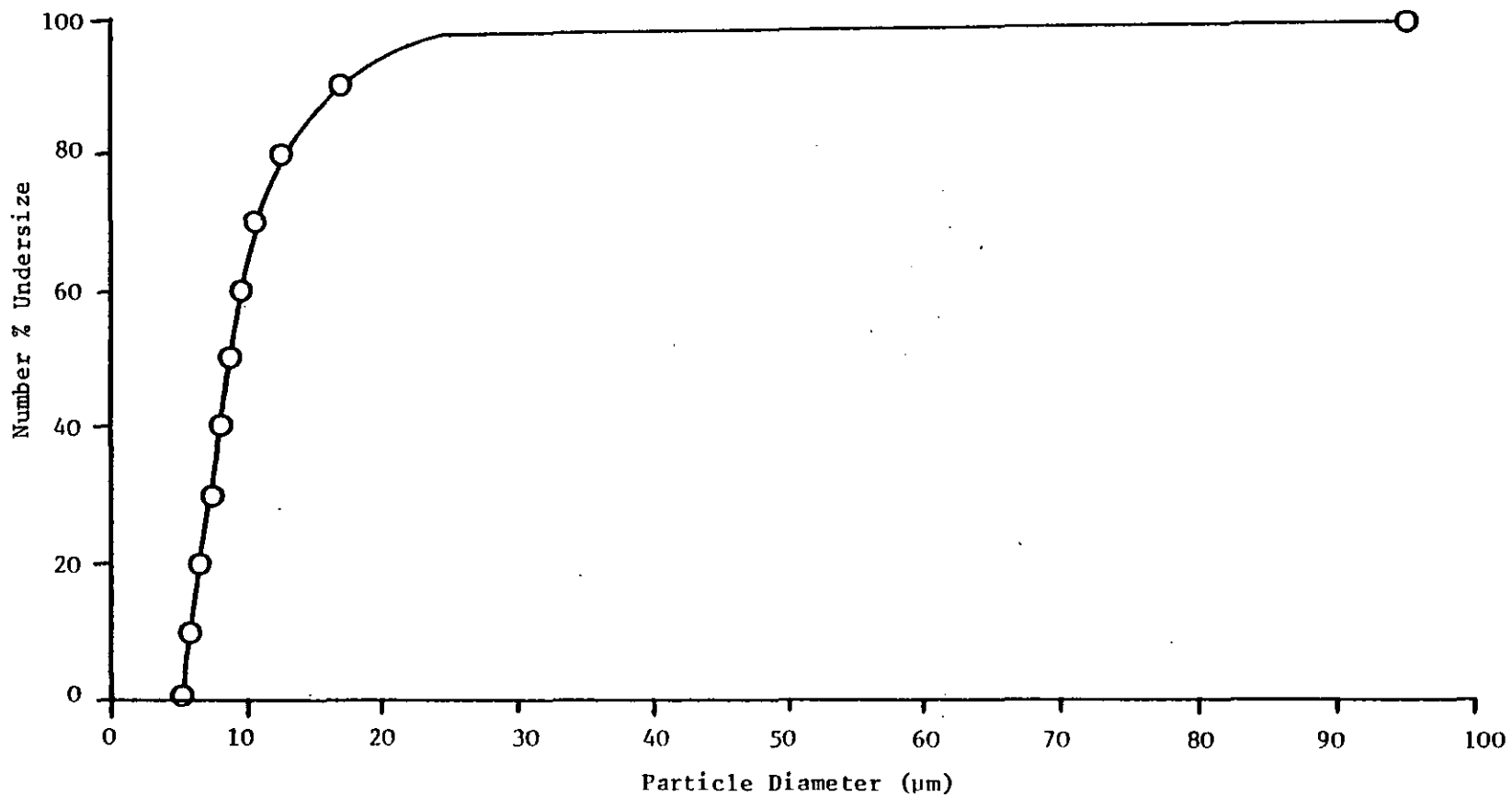
Figures 6.16 to 6.19 show packings of 300 particles of the four
different sizes at a uniform gas velocity of 5 m/s. Figures E1 to
E16 show results at other velocities. From general observations of
these plots the following remarks can be made:-

(i)   Small particles deviate from streamline trajectories more than
        large particles. Their movements are much more 'jerky' than
        larger particles.

(ii)   When particles of larger sizes are repelled from a section of
        coating, the particles take longer before they start returning
        to the substrate. There is more evidence of 25μm particles being
        'shot' away from the coating and landing in uncovered regions.

(iii)   With small particles it can be observed that some reach an
        equilibrium position from which they do not subsequently move.
        However, once this position has been calculated it is assumed
        that the particle remains stationary and therefore is not
        affected by any other particle entering the near vicinity. In
        practice this would not occur and the presence of other
        particles coming close to the one in equilibrium would cause
        this situation to be disturbed.

(iv)   Dendrite type formations are formed which for large particles
        can be very tall (>10 particle diameters). The upper layers of
        the packings appear more open and this phenomena agrees with
        microscopic observations.

        Deep crevasses between the dendrite structures are observed in
        the plots. It must be stated, however, that the computer
        simulation assumes that on touching particles remain stationary.
        No bounce-off or collapse of such formations occurs. However,
        the simulated effect does appear very similar to that observed
        in spray coatings.

Figure 6.16. Trajectories of Particles of a Monosized Powder – Particle diameter = 10μm, Uniform Velocity = 5 m/s, Start Width = 0.00017 m.
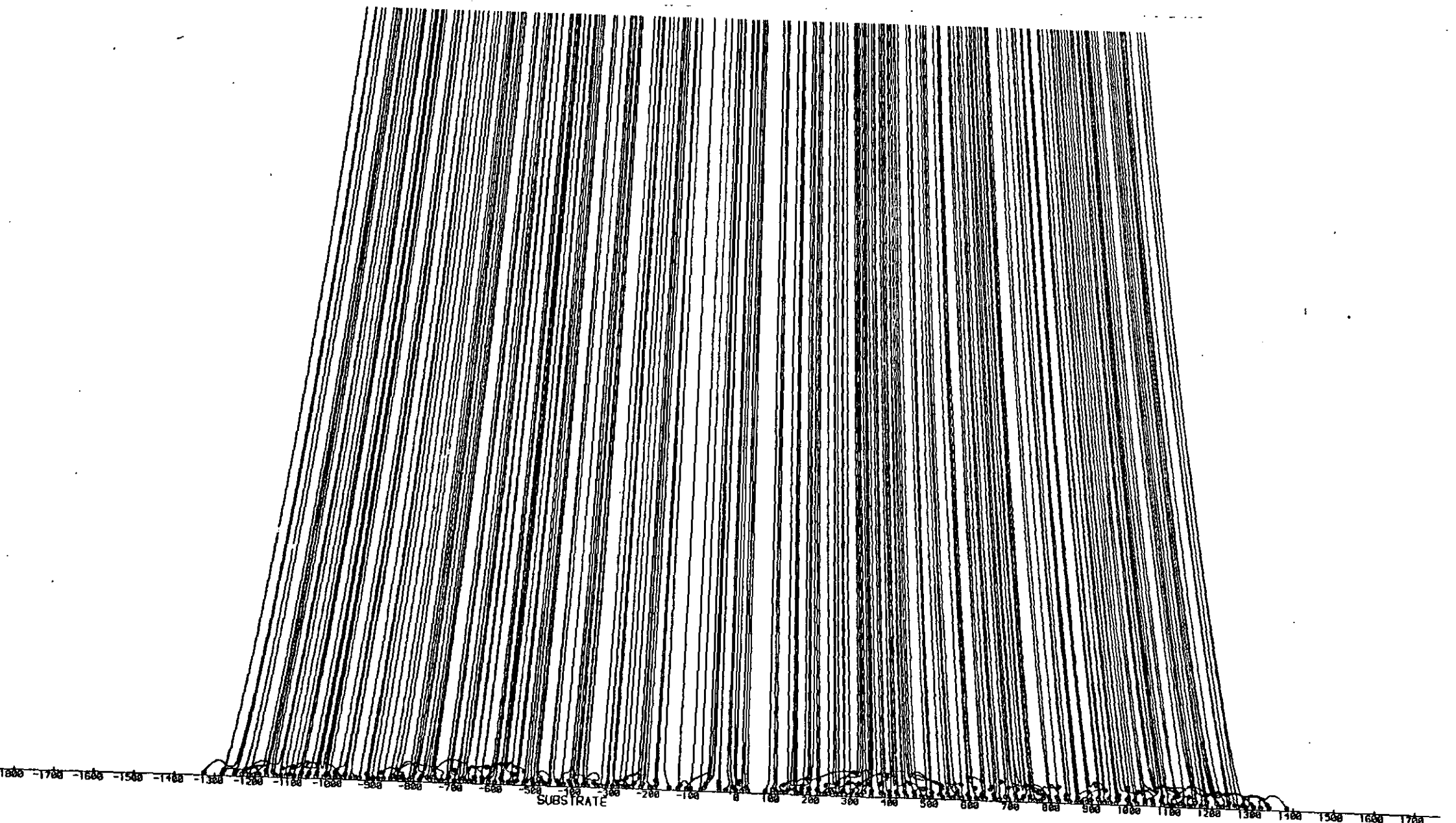
Figure 6.17. Trajectories of Particles of a Monosized Powder – Particle diameter = 17μm, Uniform Velocity = 5 m/s, Start Width = 0.00027 m
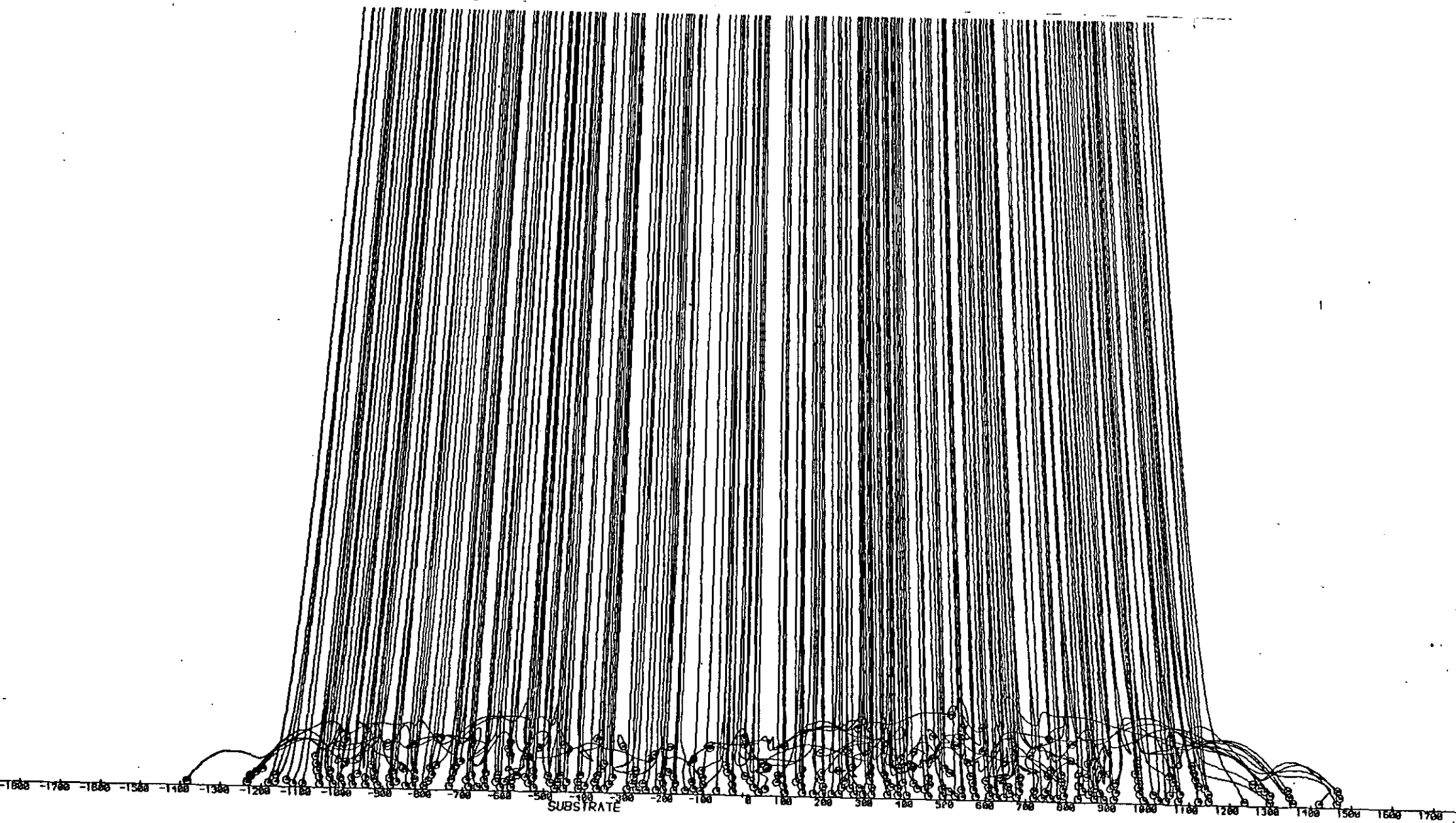
Figure 6.18.   Trajectories of Particles of a Monosized Powder – Particle diameter = 25µm, Uniform Velocity = 5 m/s, Start Width = 0.00038 m
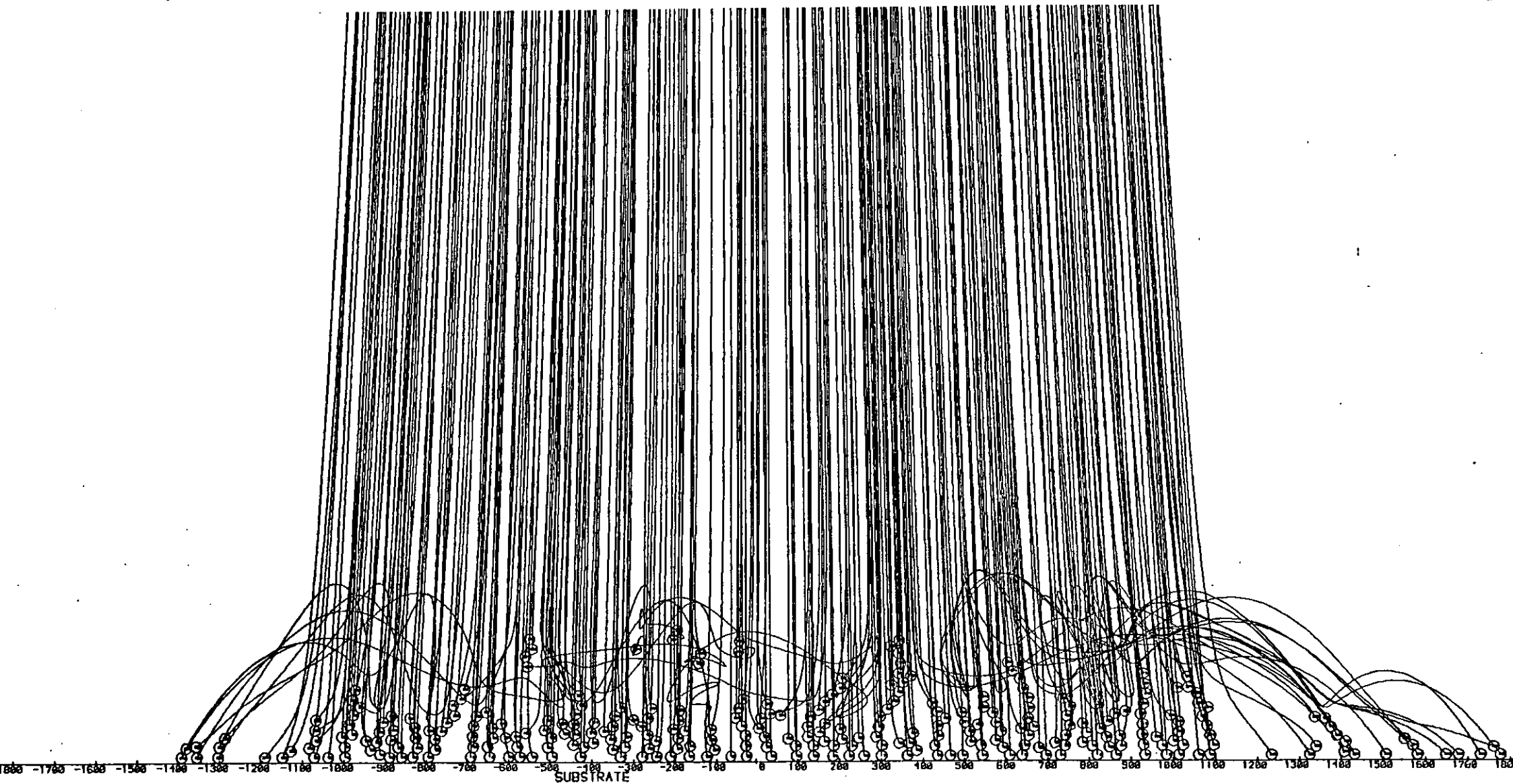
Figure 6.19. Trajectories of Particles of a Monosized Powder - Particle diameter = 50μm, Uniform Velocity = 5 m/s, Start Width = 0.00094 m
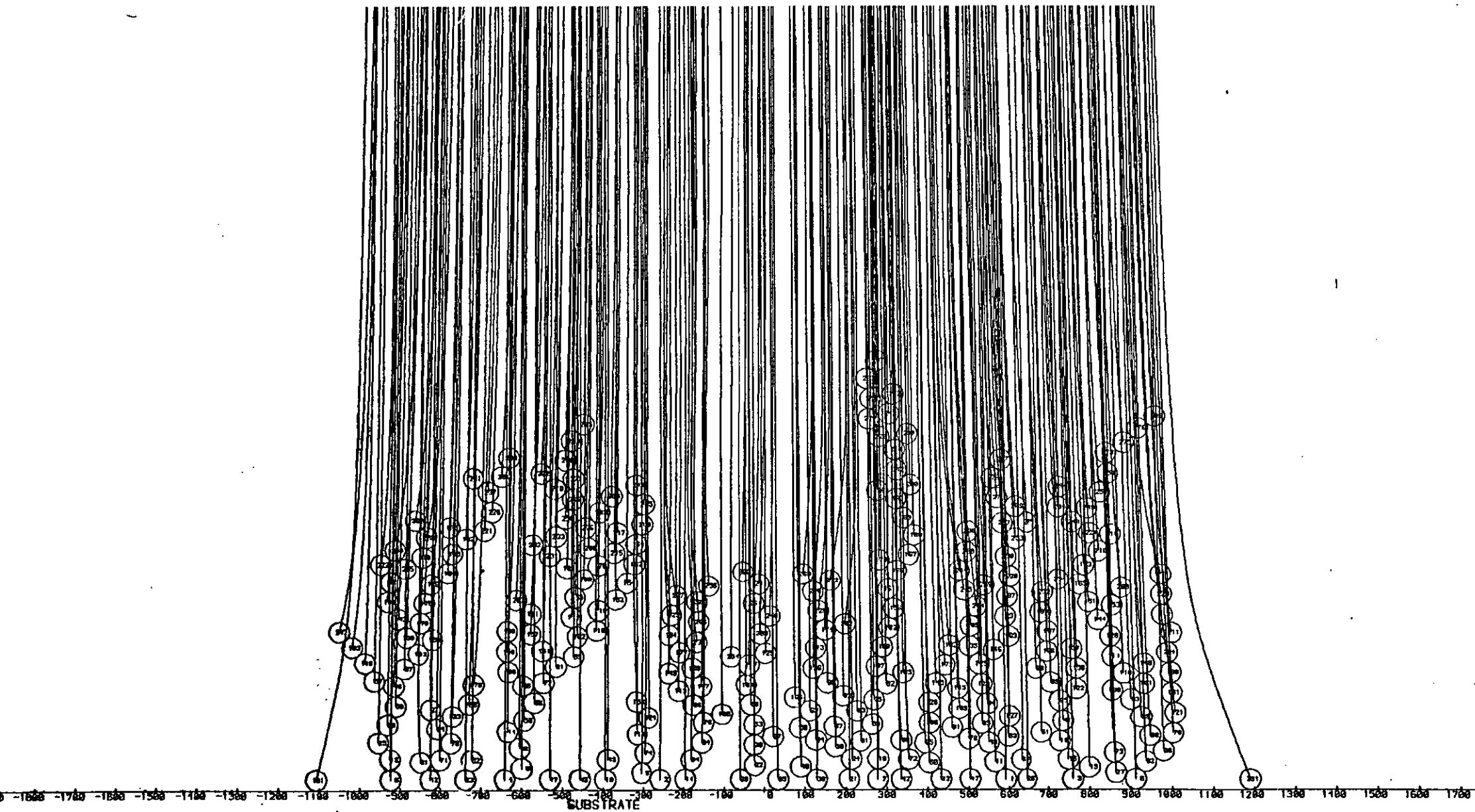
(v)   50µm particles appear relatively unaffected by packings of
        particles up to 1000µm in height. Their trajectories deviate
        by only small amounts, and this is more typical at the edge of
        the area considered.

        The individual component forces have been recorded at points
along a particle trajectory for three different particle sizes.
This allows comparison of the magnitude of each of the forces acting
on the particle and gives an indication of which is the dominant
force or forces. Tables 6.5 to 6.10 show the results of this analysis
for particle sizes of 10µm, 25µm and 50µm using a uniform air
velocity of 5 m/s. Tables 6.5 to 6.7 consider the tenth particle
of each packing whilst the other three tables consider the 200th
particle. The figures in these tables were obtained from the force
and trajectory printouts for each run.

        In considering the tenth particle of each packing and comparing
for the three different sizes the following effects are observed:-

(i)   For small particles the drag and field forces during the initial
        stages of the trajectory are very similar in magnitude (but
        opposite in direction).

(ii)   Since only a few particles have already landed, the image force
        is the largest force just before the particle lands. For larger
        particles the packing is much closer and so the interparticulate
        forces are correspondingly larger. The 50µm particle has
        actually landed on top of two others and so the interparticulate
        force in the x direction is large and negative.

(iii)   For large particles the drag term is dominant but the field
        force increases relative to it as the particle approaches the
        substrate. This is due to the relative velocity between the

Table 6.5. Individual Forces Acting on the 10th Particle in Flight

			Particle Velocities		Air Velocities		
$X^{\dagger}$ (m)	Y (µm)	Time in flight (secs)	U_p (m/s)	V_p (m/s)	U_{air} (m/s)	V_{air} (m/s)	Re_p
0.100	-39	-	5.00	0.00	-	-	-
0.110	-42	0.004	2.37	0.00	2.06	0.00	0.174
0.150	-68	0.025	1.46	0.00	1.23	0.00	0.128
0.190	-235	0.074	0.41	-0.01	0.24	-0.01	0.096
0.199	-492	0.103	0.20	-0.01	0.03	-0.01	0.096
*	-588	0.110	0.20	-0.02	0.00	-0.01	0.112

	DRAG		FIELD		IMAGE	PARTICULATE	
$X^{\dagger}$ (m)	F_{D_x} (N)	F_{D_y} (N)	F_{E_x} (N)	F_{E_y} (N)	F_I (N)	$\Sigma(F_{R_x}+F_{A_x})$ (N)	$\Sigma(F_{R_y}+F_{A_y})$ (N)
0.100	-	-	-	-	-	-	-
0.110	-5.2E-10	1.8E-13	4.9E-10	-1.9E-13	3.1E-18	-2.5E-20	-4.8E-24
0.150	-3.8E-10	1.4E-13	3.6E-10	-1.7E-13	9.7E-18	-1.4E-19	-1.5E-22
0.190	-2.9E-10	2.6E-13	2.9E-10	-3.4E-13	2.2E-16	-1.5E-17	-3.7E-19
0.199	-2.8E-10	5.1E-10	2.7E-10	-6.8E-13	1.6E-14	-4.0E-15	8.9E-17
*	-3.4E-10	9.1E-13	2.7E-10	-8.0E-13	9.6E-10	6.0E-13	-5.5E-14

Particle size = 10µm, Uniform Velocity, U = 5 m/s, Particle Number 10

Start Width = 0.0002m

* last but one caluclated x position, distance from substrate = 5µm

$\dagger$ approximate x position from spray gun

Table 6.6. Individual Forces Acting on the 10th Particle in Flight

			Particle Velocities		Air Velocities		
$X^\dagger$ (m)	Y (μm)	Time in Flight (secs)	U_p (m/s)	V_p (m/s)	U_{air} (m/s)	V_{air} (m/s)	Re_p
0.100	-39	-	5.00	0.00	-	-	-
0.110	-40	0.002	3.52	0.00	2.06	0.00	2.049
0.150	-59	0.018	1.88	0.00	1.23	0.00	0.913
0.190	-140	0.052	0.73	0.00	0.26	0.00	0.660
0.199	-211	0.068	0.46	-0.01	0.03	-0.01	0.604
*	-225	0.070	0.45	-0.02	0.00	-0.01	0.632

	DRAG		FIELD		IMAGE	PARTICULATE	
$X^\dagger$ (m)	F_{D_x} (N)	F_{D_y} (N)	F_{E_x} (N)	F_{E_y} (N)	F_I (N)	$\Sigma(F_{R_x}+F_{A_x})$ (N)	$\Sigma(F_{R_y}+F_{A_y})$ (N)
0.100	-	-	-	-	-	-	-
0.110	-6.1E-9	-1.9E-13	3.1E-9	-1.1E-12	1.2E-16	-2.4E-18	-1.1E-21
0.150	-2.7E-9	5.7E-13	2.3E-9	-9.1E-13	3.8E-16	-1.3E-17	-1.9E-20
0.190	-2.0E-9	5.6E-13	1.8E-9	-1.3E-12	9.1E-15	-1.6E-14	-2.9E-17
0.199	-1.8E-9	7.3E-13	1.7E-9	-1.8E-12	8.9E-13	-1.1E-12	-1.7E-13
*	-1.9E-9	4.4E-11	1.7E-9	-1.9E-12	5.9E-9	8.1E-10	-4.9E-10

Particle size = 25μm, Uniform Velocity, U = 5 m/s, Particle Number 10

Start Width = 0.0002m

* last but one calculated x position, distance from substrate = 12.5μm

† approximate x position from spray gun

Table 6.7. Individual Forces Acting on the 10th Particle in Flight

$X^{\dagger}$ (m)	Y (µm)	Time in Flight (secs)	Particle Velocities		Air Velocities		Re_p
			U_p (m/s)	V_p (m/s)	U_{air} (m/s)	V_{air} (m/s)	
0.100	-39	-	5.00	0.00	-	-	-
0.110	-39	0.002	4.72	0.00	2.07	0.00	7.45
0.150	-47	0.012	3.28	0.00	1.22	0.00	5.79
0.190	-70	0.028	1.70	0.00	0.28	0.00	3.99
0.199	-82	0.035	1.26	0.00	0.03	0.00	3.46
*	-84	0.036	1.20	0.00	0.00	0.00	3.37

$X^{\dagger}$ (m)	DRAG		FIELD		IMAGE	PARTICULATE	
	F_{D_x} (N)	F_{D_y} (N)	F_{E_x} (N)	F_{E_y} (N)	F_I (N)	$\Sigma(F_{B_x}+F_{A_x})$ (N)	$\Sigma(F_{R_y}+F_{A_y})$ (N)
0.100	-	-	-	-	-	-	-
0.110	-2.2E-8	-3.9E-12	1.2E-8	-4.5E-12	1.9E-15	-1.4E-16	-1.5E-19
0.150	-1.7E-8	-2.4E-13	9.1E-9	-2.8E-12	6.2E-15	-8.5E-16	-1.8E-18
0.190	-1.2E-8	-1.3E-13	7.2E-9	-2.6E-12	1.3E-13	-7.7E-14	-9.4E-16
0.199	-1.0E-8	1.2E-13	6.8E-9	-2.8E-12	1.4E-11	-8.7E-11	-1.2E-11
*	-1.0E-8	9.0E-12	6.8E-9	-2.9E-12	1.1E-9	-3.5E-8	6.3E-10

Particle size = 50µm, Uniform Velocity, U = 5 m/s, Particle Number 10

Start width = 0.0002m

* last but one calculated x position, distance from substrate = 120µm

$\dagger$ approximate x position from spray gun

particle and air decreasing. The interparticle electrostatic forces, although increasing, cannot slow down the particle enough to stop it from landing.

(iv)   In the y direction, the forces are generally much smaller than those in the x direction, but the field force is generally the largest until the particles are close to the packing when electrostatic forces increase and cause the particle to move laterally, whence the drag force increases.

(v)   In general it is observed that the field and drag forces do not change by any appreciable extent over the range of the trajectory. The electrostatic forces however can increase by 10 orders of magnitude between the start point (0.1m from substrate) and the substrate.

(vi)   The particle Reynolds number (Re_p) for 10μm particles is less than one throughout the trajectory and it is only for 50μm that Re_p is greater than one for any length of time.

When the 200th particle is considered it is observed that the magnitude of some of the forces has changed, especially near to the substrate. From Tables 6.8 to 6.10 the following observations are made:-

(i)   Small particles are heavily influenced by the electrostatic forces near the substrate. The repulsive forces are 2-4 times larger than the drag or field forces. The drag and field forces are of similar size throughout the trajectory and hence the balance of forces is controlled by the electrostatic forces. It is noticeable that in the example of the 10μm particle the particulate electrostatic force in the x direction was positive on landing. This was because it found a path between the packing to the substrate and therefore had many similar charged

Table 6.8. Forces Acting on the 200th Particle in Flight

X † (m)	Y (μm)	Time in Flight (secs)	Particle Velocities		Air Velocities		Re_p
			U_p (m/s)	V_p (m/s)	U_{air} (m/s)	V_{air} (m/s)	
0.100	30	-	5.0	-	-	-	-
0.110	33	0.004	2.37	0.00	2.06	0.0	0.17
0.150	53	0.025	1.46	0.00	1.23	0.00	0.13
0.190	171	0.072	0.44	0.00	0.27	0.00	0.10
0.199	390	0.104	0.19	0.01	0.03	0.01	0.09
*	558	0.112	0.18	-0.04	0.00	0.01	0.10

X † (m)	DRAG		FIELD		IMAGE	PARTICULATE	
	F_{D_x} (N)	F_{D_y} (N)	F_{E_x} (N)	F_{E_y} (N)	F_I (N)	$\Sigma(F_{R_x}+F_{R_y})$ (N)	$\Sigma(F_{R_y}+F_{A_y})$ (N)
0.100	-	-	-	-	-	-	-
0.110	-5.2E-10	-1.4E-13	4.9E-10	1.4E-13	3.1E-18	-9.6E-10	-6.7E-22
0.150	-3.8E-10	-1.1E-13	3.6E-10	1.3E-13	9.7E-18	-5.4E-18	-3.4E-21
0.190	-2.9E-10	-2.0E-13	2.9E-10	2.6E-13	2.2E-16	-5.8E-16	7.6E-18
0.199	-2.8E-10	-4.1E-13	2.7E-10	5.3E-13	2.1E-14	-2.8E-13	1.1E-14
*	-3.0E-10	8.9E-11	2.7E-10	7.6E-13	1.0E-9	1.1E-9	1.6E-10

Particle size = 10μm, Uniform Velocity, U = 5 m/s, Particle Number 200

* last but one calculated x position, distance from substrate = 5μm

† approximate x position from spray gun

Table 6.9. Forces Acting on the 200th Particle in Flight

			Particle Velocities		Air Velocities		
$X^\dagger$ (m)	Y (μm)	Time in Flight (secs)	U_p (m/s)	V_p (m/s)	U_{air} (m/s)	V_{air} (m/s)	Re_p
0.100	68	–	5.0	0.00	–	–	–
0.110	70	0.002	3.52	0.00	2.06	0.00	2.04
0.150	103	0.018	1.88	0.00	1.23	0.00	0.91
0.190	242	0.052	0.73	0.01	0.26	0.01	0.66
0.199	367	0.068	0.45	0.01	0.03	0.01	0.59
*	1325	0.075	0.29	0.17	0.00	0.03	0.45

	DRAG		FIELD		IMAGE	PARTICULATE	
$X^\dagger$ (m)	F_{D_x} (N)	F_{D_y} (N)	F_{E_x} (N)	F_{E_y} (N)	F_I (N)	$\Sigma(F_{R_x}+F_{R_y})$ (N)	$\Sigma(F_{R_y}+F_{A_y})$ (N)
0.100	–	–	–	–	–	–	–
0.110	-6.1E-9	3.3E-13	3.1E-9	2.0E-12	1.2E-16	-2.4E-16	-5.6E-20
0.150	-2.7E-9	-9.9E-13	2.3E-9	1.6E-12	3.8E-16	-1.3E-15	7.5E-19
0.190	-2.0E-9	-9.6E-13	1.8E-9	2.3E-12	9.2E-15	-1.6E-13	3.6E-15
0.199	-1.8E-9	-4.1E-12	1.7E-9	3.1E-12	8.8E-13	-8.6E-11	5.9E-12
*	-1.2E-9	-5.8E-10	1.7E-9	1.1E-11	6.1E-9	3.5E-10	3.6E-11

Particle size = 25μm, Uniform Velocity, U = 5 m/s, Particle Number 200

* last but one calculated x position, distance from substrate = 13μm

$\dagger$ approximate x position from spray gun

<u>Table 6.10.</u> <u>Forces Acting on the 200th Particle in Flight</u>

$X^{\dagger}$ (m)	Y (μm)	Time in Flight (secs)	Particle Velocities		Air Velocities		Re_p
			U_p (m/s)	V_p (m/s)	U_{air} (m/s)	V_{air} (m/s)	
0.100	169	0.000	5.00	0.00	–	–	–
0.110	170	0.002	4.72	0.00	2.07	0.00	7.45
0.150	202	0.012	3.28	0.00	1.22	0.00	5.79
0.190	300	0.029	1.67	0.01	0.26	0.01	3.96
0.199	357	0.035	1.21	0.02	0.03	0.01	3.32
*	362	0.035	1.13	0.03	0.02	0.01	3.18

$X^{\dagger}$ (m)	DRAG		FIELD		IMAGE	PARTICULATE	
	F_{D_x} (N)	F_{D_y} (N)	F_{E_x} (N)	F_{E_y} (N)	F_I (N)	$\Sigma(F_{R_x}+F_{R_y})$ (N)	$\Sigma(F_{R_y}+F_{A_y})$ (N)
0.100	–	–	–	–	–	–	–
0.110	-2.2E-8	1.8E-11	1.2E-8	1.9E-11	1.9E-15	-1.7E-14	4.5E-17
0.150	-1.7E-8	1.0E-12	9.1E-9	1.2E-11	6.2E-15	-9.9E-14	5.8E-16
0.190	-1.2E-8	5.2E-13	7.2E-9	1.1E-11	1.4E-13	-1.1E-11	4.5E-13
0.199	-9.9E-9	-6.2E-11	6.8E-9	1.2E-11	1.5E-11	-8.9E-9	1.0E-9
*	-9.3E-9	-2.0E-10	6.8E-9	1.2E-11	2.8E-11	-4.7E-8	2.8E-8

Particle size = 50μm, Uniform Velocity, U = 5 m/s, Particle Number 200

* last but one calculated x position, distance from substrate = 753μm

† approximate x position from spray gun

particles above it (see Figure 6.21). The resultant force, in the x direction, was therefore towards the substrate.

(ii) Large particles have consistently high drag forces throughout the flight showing that the particle has very high inertia. Although the electrostatic forces become much larger as the particle approaches the packing the inertia cannot be overcome and the 50µm hits the packing at a velocity of over 1 m/s. At this time the electrostatic force in the x direction is five times the size of the drag force.

(iii) On comparing electrostatic forces of the 200th and 10th particles it can be clearly seen that the forces are an order of magnitude larger at 1 cm away from the substrate for the 200th particle, due to the charged layer that has been built.

Since effects due to inertia were noticed for the 50µm particles when no field is applied, the forces acting on a 50µm particle at different velocities have been tabulated in Tables 6.11 to 6.13.

From these tables it can be seen that:-

(i) At low velocities (1 m/s) the field forces acting on the charged particle cause an increase in particle velocity. Initially the field force is larger than the drag force and so the particle actually accelerates. This is one of the few occasions that, at the start of the trajectory, the field force is larger than the drag force.

As the field force decreases with increasing distance from the gun the drag force again dominates. At higher velocities the drag force is always greater than the field force (in the x direction).

Table 6.11. Forces Acting on a 50μm Particle in Flight

$X^\dagger$ (m)	Y (μm)	Time in Flight (secs)	Particle Velocities		Air Velocities		Re_p
			U_p (m/s)	V_p (m/s)	U_{air} (m/s)	V_{air} (m/s)	
0.100	-92	-	1.00	0.00	-	-	-
0.110	-96	0.007	1.59	0.00	0.41	0.00	3.330
0.150	-130	0.031	1.47	0.00	0.25	0.00	3.428
0.190	-182	0.064	1.00	0.00	0.06	0.00	2.641
0.199	-201	0.075	0.89	0.00	0.00	0.00	2.501
*	-205	0.076	0.89	-0.02	0.00	0.00	2.507

$X^\dagger$ (m)	DRAG		FIELD		IMAGE	PARTICULATE	
	F_{D_x} (N)	F_{D_y} (N)	F_{E_x} (N)	F_{E_y} (N)	F_I (N)	$\Sigma(F_{R_x}+F_{R_y})$ (N)	$\Sigma(F_{R_y}+F_{A_y})$ (N)
0.100	-	-	-	-	-	-	-
0.110	-1.0E-8	6.0E-12	1.2E-8	-1.1E-10	2.0E-15	-4.7E-17	-1.2E-18
0.150	-1.0E-8	7.8E-12	9.1E-9	-8.0E-12	6.0E-15	-2.5E-16	-1.4E-18
0.190	-7.9E-9	6.5E-12	7.2E-9	-7.0E-12	1.1E-12	-2.1E-14	-6.5E-16
0.199	-7.4E-9	6.8E-12	6.8E-9	-6.9E-12	1.5E-11	-2.5E-11	-9.2E-12
*	-7.4E-9	1.3E-10	6.8E-9	-6.9E-12	2.4E-8	6.9E-9	-8.9E-9

Particle size = 50μm, Uniform Velocity, U = 1.0 m/s, Particle Number 5

* last but one calculated x position, distance from substrate = 25μm

$\dagger$ approximate x position from spray gun

Table 6.12. Forces Acting on a 50μm Particle in Flight

| X† (m) | Y (m) | Time in Flight (secs) | Particle Velocities | | Air Velocities | | Re_p |
			U_p (m/s)	V_p (m/s)	U_{air} (m/s)	V_{air} (m/s)	
0.100	-92	-	5.00	0.00	-	-	-
0.110	-93	0.002	4.72	0.00	2.07	0.00	7.447
0.150	-110	0.012	3.28	0.00	1.22	0.00	5.789
0.190	-162	0.028	1.70	0.00	0.28	0.00	3.990
0.199	-192	0.035	1.26	0.00	0.025	0.00	3.470
*	-197	0.036	1.22	-0.02	0.00	0.00	3.456

| X† (m) | DRAG | | FIELD | | IMAGE | PARTICULATE | |
	F_{D_x} (N)	F_{D_y} (N)	F_{E_x} (N)	F_{E_y} (N)	F_I (N)	$\Sigma(F_{R_x}+F_{R_y})$ (N)	$\Sigma(F_{R_y}+F_{A_y})$ (N)
0.100	-	-	-	-	-	-	-
0.110	-2.2E-8	-9.1E-12	1.2E-8	-1.1E-11	1.9E-15	-4.5E-17	-1.1E-19
0.150	-1.7E-8	-5.5E-13	9.1E-9	6.7E-12	6.2E-15	-2.7E-16	-1.4E-18
0.190	-1.2E-8	-3.1E-13	7.2E-9	-6.2E-12	1.3E-13	-2.4E-14	-7.2E-16
0.199	-1.0E-8	-3.6E-13	6.8E-9	-6.6E-12	1.5E-11	-2.6E-11	-9.6E-12
*	-1.0E-8	9.2E-11	6.8E-9	-6.7E-12	2.4E-8	7.5E-9	-1.0E-8

Particle size = 50μm, Uniform Velocity, U = 5 m/s, Particle Number 5

* last but one calculated x position, distance from substrate = 25μm

† approximate x position from spray gun

Table 6.13. **Forces Acting on a 50μm Particle in Flight**

$X^{\dagger}$ (m)	Y (μm)	Time in Flight (secs)	Particle Velocities		Air Velocities		Re_p
			U_p (m/s)	V_p (m/s)	U_{air} (m/s)	V_{air} (m/s)	
0.100	-91	-	10.00	0.00	-	-	-
0.110	-92	0.001	9.51	0.00	4.12	0.00	15.146
0.150	-100	0.006	7.23	0.00	2.49	0.00	13.319
0.190	-126	0.013	4.25	0.00	0.55	0.00	10.397
0.199	-139	0.015	3.34	-0.01	0.05	-0.01	9.245
*	-141	0.016	3.25	-0.01	0.00	-0.01	9.133

$X^{\dagger}$ (m)	DRAG		FIELD		IMAGE	PARTICULATE	
	F_{D_x} (N)	F_{D_y} (N)	F_{E_x} (N)	F_{E_y} (N)	F_I (N)	$\Sigma(F_{R_x}+F_{R_y})$ (N)	$\Sigma(F_{R_y}+F_{A_y})$ (N)
0.100	-	-	-	-	-	-	-
0.110	-4.5E-8	-2.5E-10	1.2E-8	-1.0E-11	1.9E-15	-4.8E-17	-1.1E-19
0.150	-4.0E-8	-1.7E-10	9.1E-9	-6.1E-12	5.9E-15	-2.6E-16	-1.1E-18
0.190	-3.1E-8	-1.3E-11	7.2E-9	-4.8E-12	1.3E-13	-2.6E-14	-6.1E-16
0.199	-2.8E-8	-1.3E-11	6.8E-9	-4.7E-12	1.5E-11	-3.0E-11	-8.2E-12
*	-2.7E-8	2.2E-11	6.8E-9	-4.8E-12	5.9E-9	-4.2E-9	-2.0E-8

Particle size = 50μm, Uniform Velocity, U = 10 m/s, Particle Number 5

* last but one calculated x position, distance from substrate = 50μm

$\dagger$ approximate x position from spray gun

(ii)   At 10 m/s uniform velocity the drag force is dominant for the
whole of the trajectory and the particle lands at a velocity of
over 3 m/s.

(iii) Although the electrostatic forces increase by several orders
of magnitude they are still 3 orders of magnitude less than the
drag force at a distance of only 1000μm from the substrate.
Hence for normal thicknesses of coatings repulsion of these
particles will not occur (except perhaps after having landed).

From the computer plots it is shown that small particles (10μm)
are strongly influenced by the electrostatic forces due to packed
particles on the substrate. These particles are subject to a great
deal of movement close to the packing before they eventually land.
In Tables 6.5 and 6.8 it is shown how, close to the substrate, all
forces acting on the particle are of similar size. Since small
particles approach the packing at very low velocities (0.2 m/s) they
can respond to any sudden increase in force acting on the particle.
This is usually due to it approaching some packed particles on the
substrate.

Figures 6.20 to 6.22 show the final stages of the 200th 10μm
particle for velocities of 1 m/s, 5 m/s and 10 m/s. These correspond
to small sections of packings shown in Figures 6.16, E1 and E4.
The trajectories are subject to 180° turns in the direction of travel and
are obviously related to the packing that is present in the close
vicinity to them.

Also, (i) as velocity increases it is observed that the
particles generally travel closer to the packing than at lower velocities.

Figure 6.20.   Trajectory of Particle Number 200 Close to the Substrate

Particle diameter   =   10μm

Uniform velocity   =   1 m/s
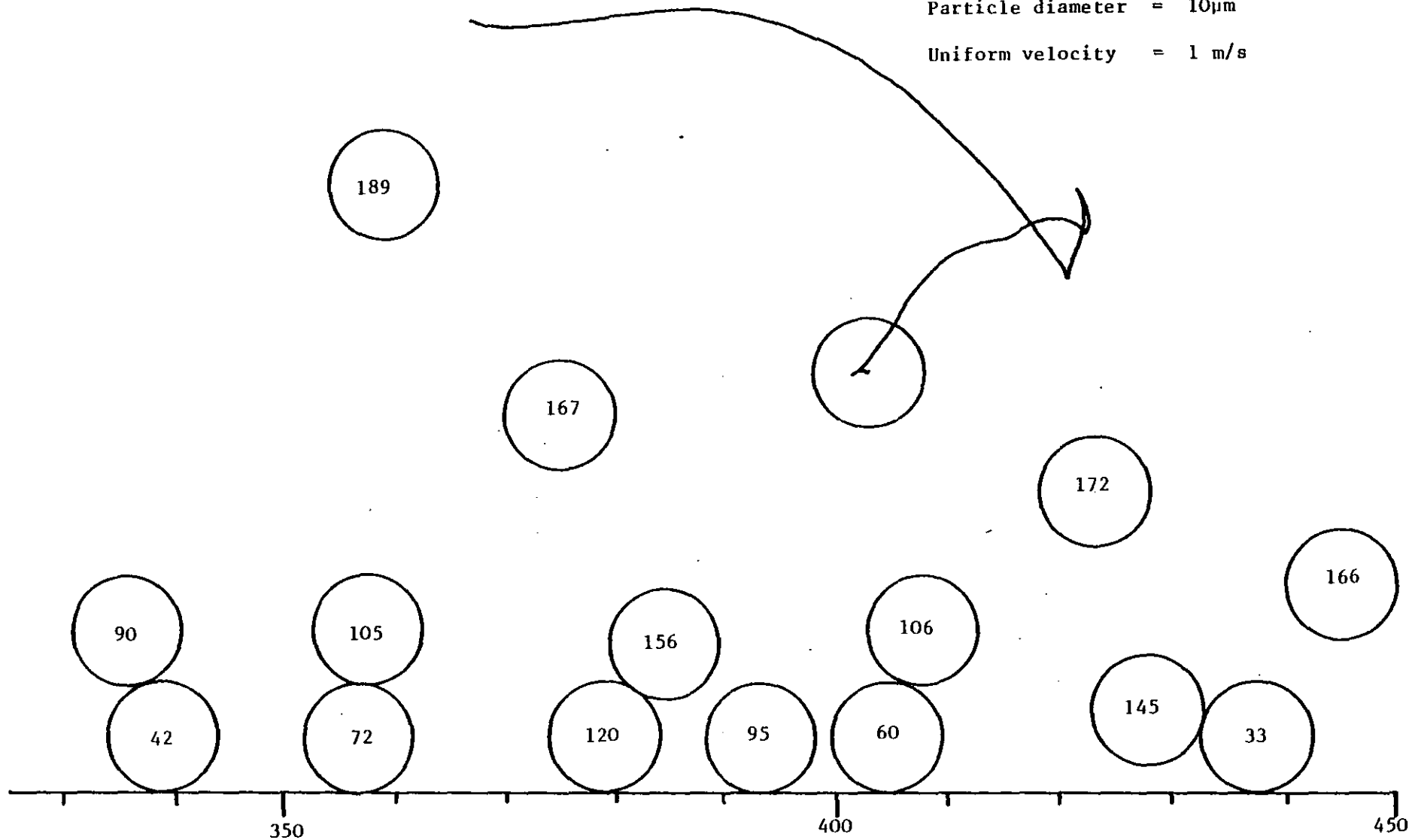
Figure 6.21. Trajectory of Particle Number 200 Close to the Substrate
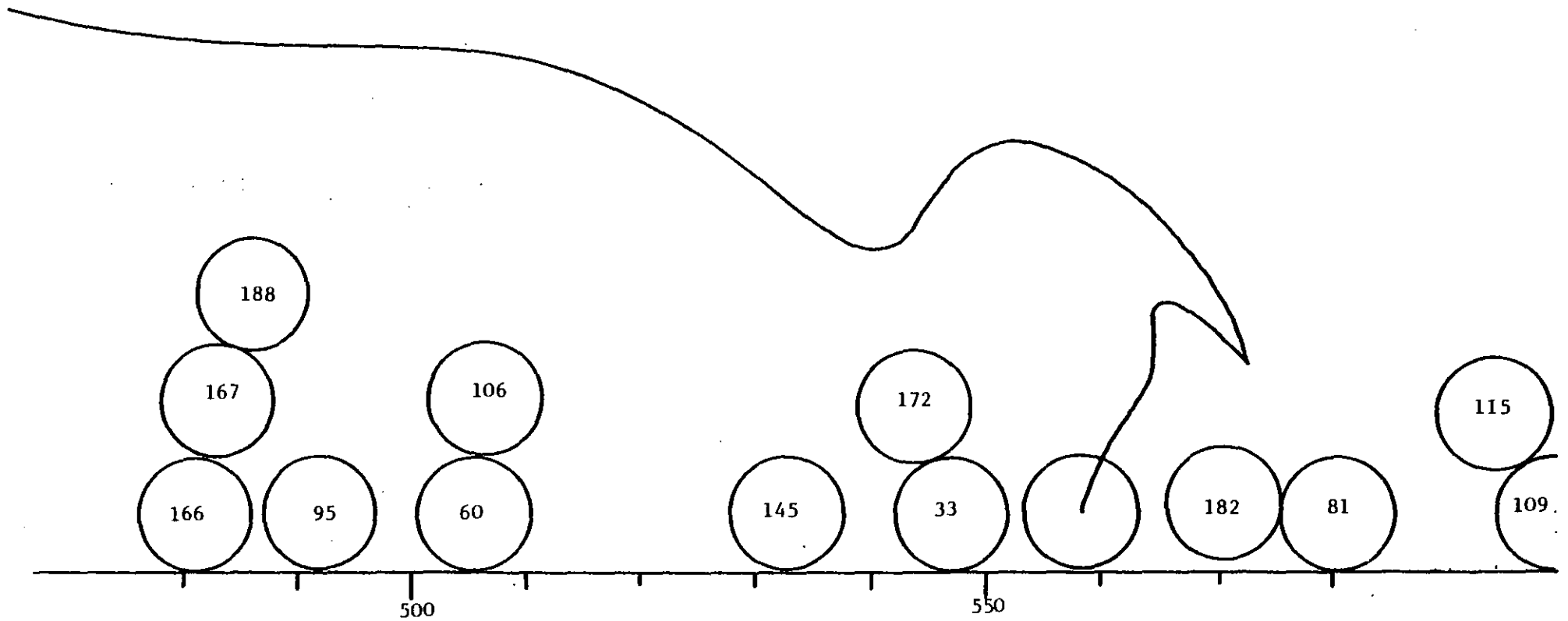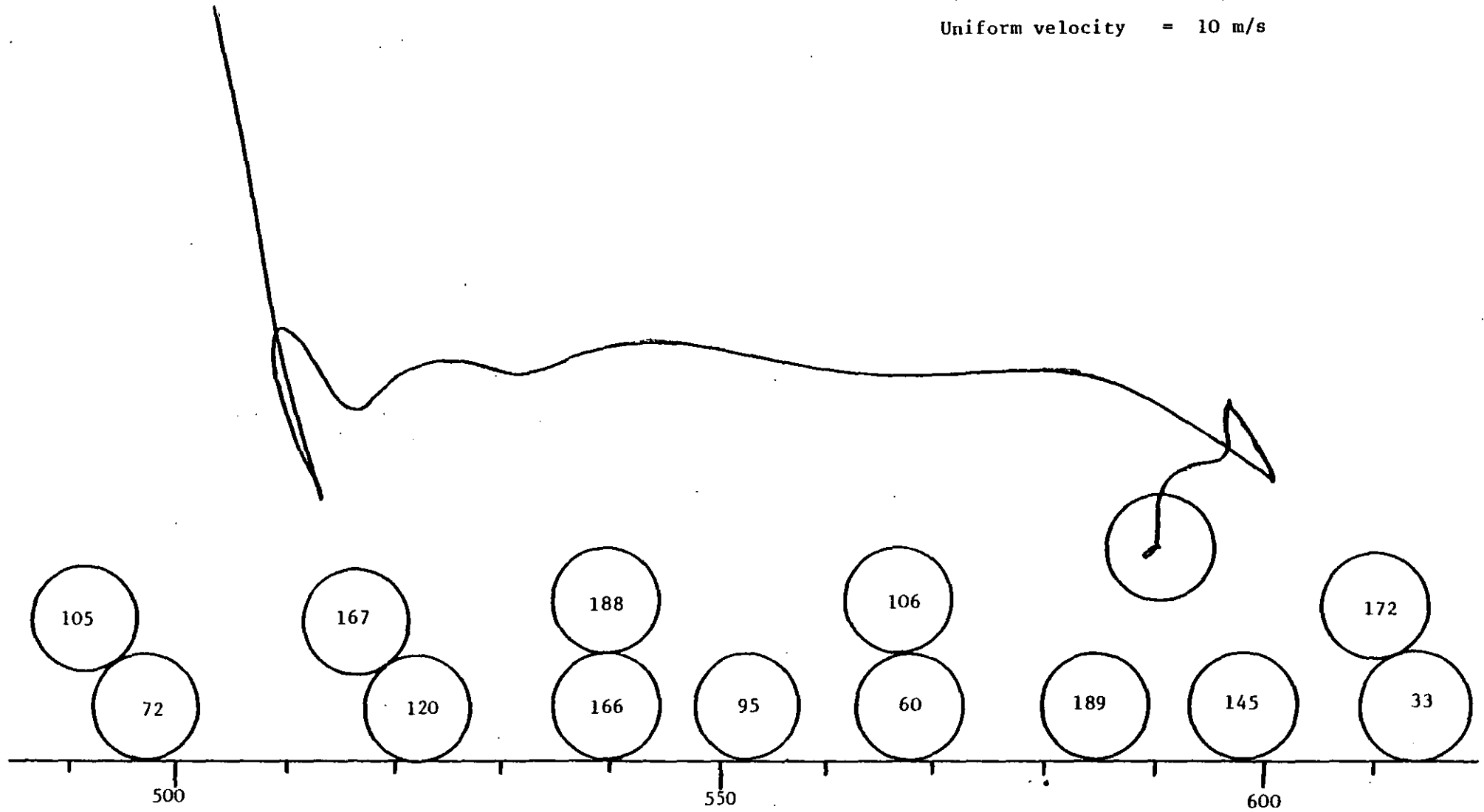
Particle diameter = 10μm

Uniform velocity = 5 m/s

Figure 6.22. Trajectory of Particle Number 200 Close to the Substrate

Particle diameter = 10μm

Uniform velocity = 10 m/s

(ii) it is less likely that the particle finds an equilibrium

position at higher velocities since the electrostatic forces

do not have such a marked effect as at low velocities.

(iii) Thicker packings are obtained when using higher uniform air

velocities.

In Figures 6.20 and 6.22 the final particle position is in

'mid-air' since its time of flight is already greater than 0.45

seconds. The computer printout shows that for each case the x and y

velocities of the particle at these positions are zero and hence all

the forces are balanced. In Figure 6.20 (1 m/s) there are other

particles which are also stationary above the packing. Unfortunately

due to limitations of the program the particles are not moved once

their trajectory has finished. In reality the presence of particle

200 would probably cause all of them to move to new positions, some

possibly landing on the substrate or packing.

Typically, these figures show that small particles will 'search'

for areas of low population (less repulsive force) and then try to

land. In Figure 6.21 this was achieved but although the particle

turned back in Figure 6.22 particles 189 and 145 were on the substrate

which stopped it from landing. Particle 200 had therefore committed

itself to entering in a 'valley' (bounded by Nos 106, 60, 172, 33)

where eventually it reached a balanced position.

By observing these examples in greater detail it can be

understood how small particles are able to cover the substrate to a

larger extent than can larger ones. Although in the property testing

experiments no difference in adhesion qualities was noticed it is

possible, for poorer flowing powders, that small particles are needed

to ensure full contact and wetting of the substrate.

Similar results are observed for experiments in which the start width was constant (Figures E17 to E36). In these plots the splaying of particles is clearly shown and comparisons show how particle size and air velocity affect this. The very small areas of coverage of 50μm particles enhance the dendrite effect and show how very thick packings could be obtained if these formations did not collapse.

In general these plots show similar effects to the first set of plots and therefore the conclusions based on these results are not affected by the splaying effect.

6.5.3 Size Distributed Powders

It was found that simulating a mixture of particle sizes was much more difficult than monosized powders. Therefore, results have to be unfortunately limited in their scope. The splaying of particles of different sizes caused problems since the majority of large particles landed in a small area in the centre of the plate. However, as mentioned in Chapter 3, this is a real effect and segregation of a powder does occur with a static gun.

Nevertheless, interesting effects are observed by considering a distribution. The splaying effect is enhanced because such a small number of particles are considered and the start width at $x = 0.1$ is the same for all sizes. This procedure was adopted since any alteration of start width with size would suggest preferential deposition of particles (especially large ones) and the number distribution representing a powder would not be kept constant. The plots are shown in Figures 6.23 to 6.27 for five different operating velocities.

Figure 6.23. Trajectories of Particles of a Size Distributed Powder – Uniform Velocity = 1 m/s, Start Width = 0.00031 m

Figure 6.24. Trajectories of Particles of a Size Distributed Powder – Uniform Velocity = 3 m/s, Start Width = 0.00020 m
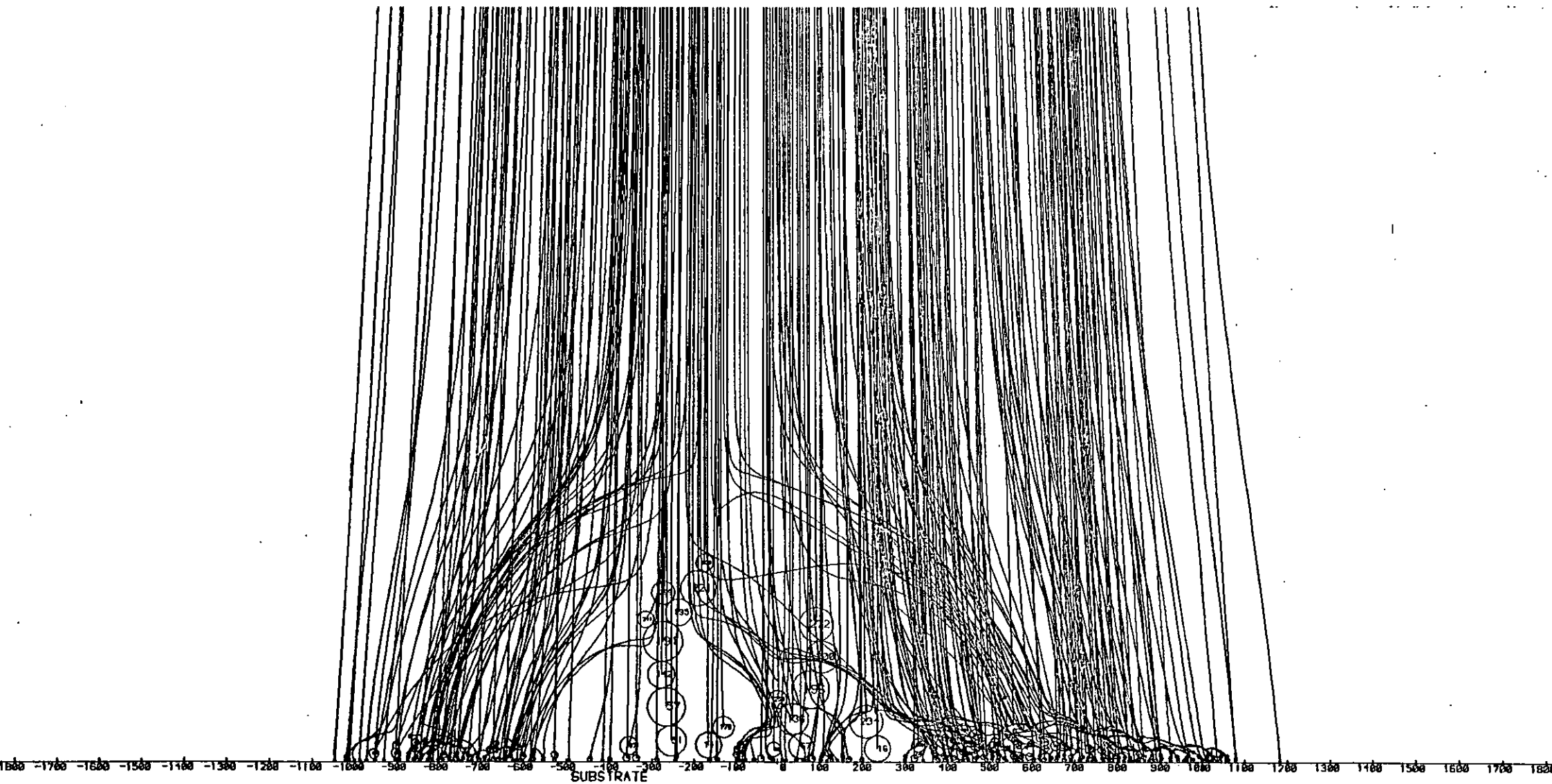
Figure 6.25. Trajectories of Particles of a Size Distributed Powder – Uniform Velocity = 5 m/s, Start Width = 0.00013 m
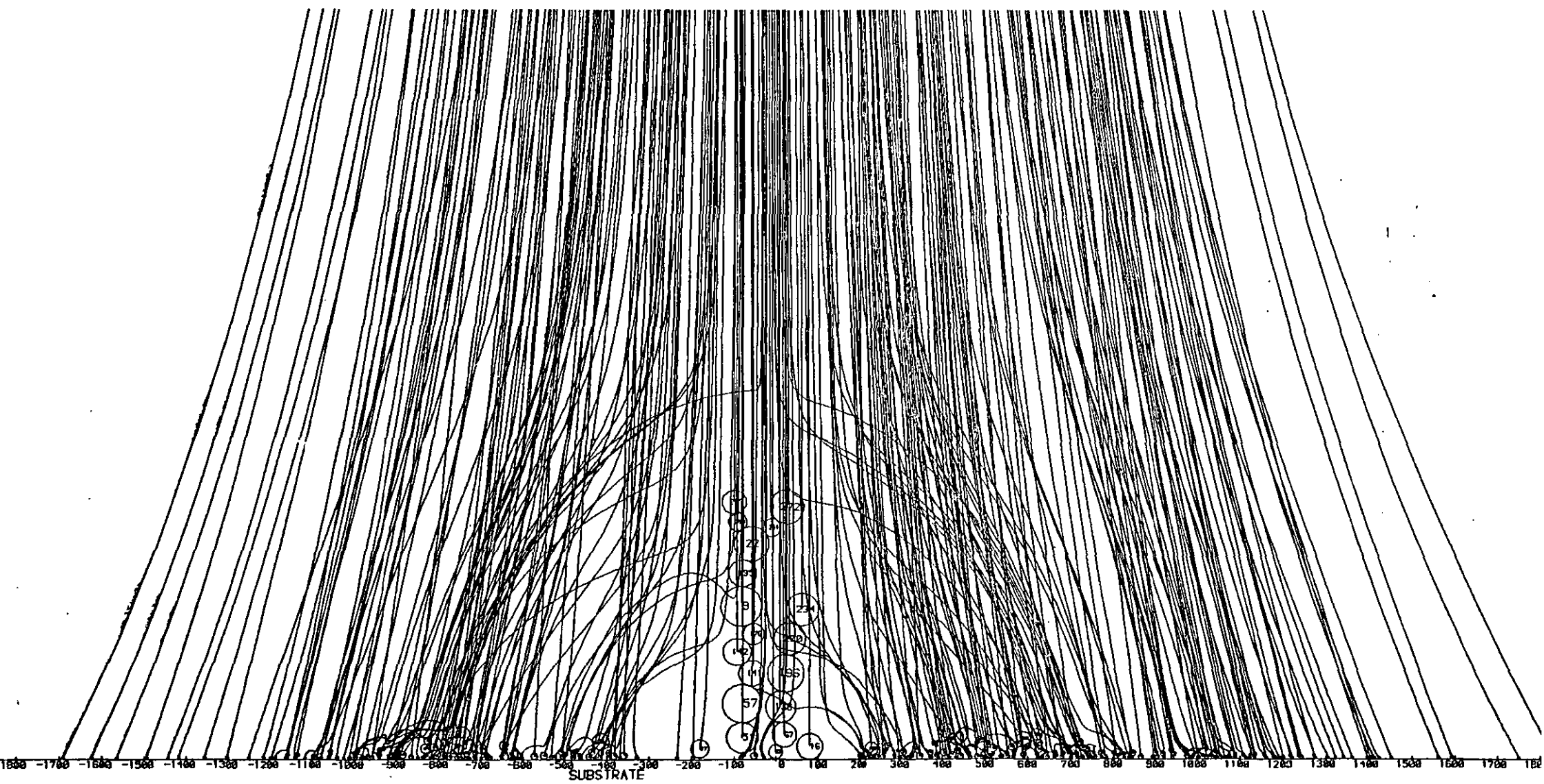
Figure 6.26.   Trajectories of Particles of a Size Distributed Powder - Uniform Velocity = 7 m/s, Start Width = 0.00010
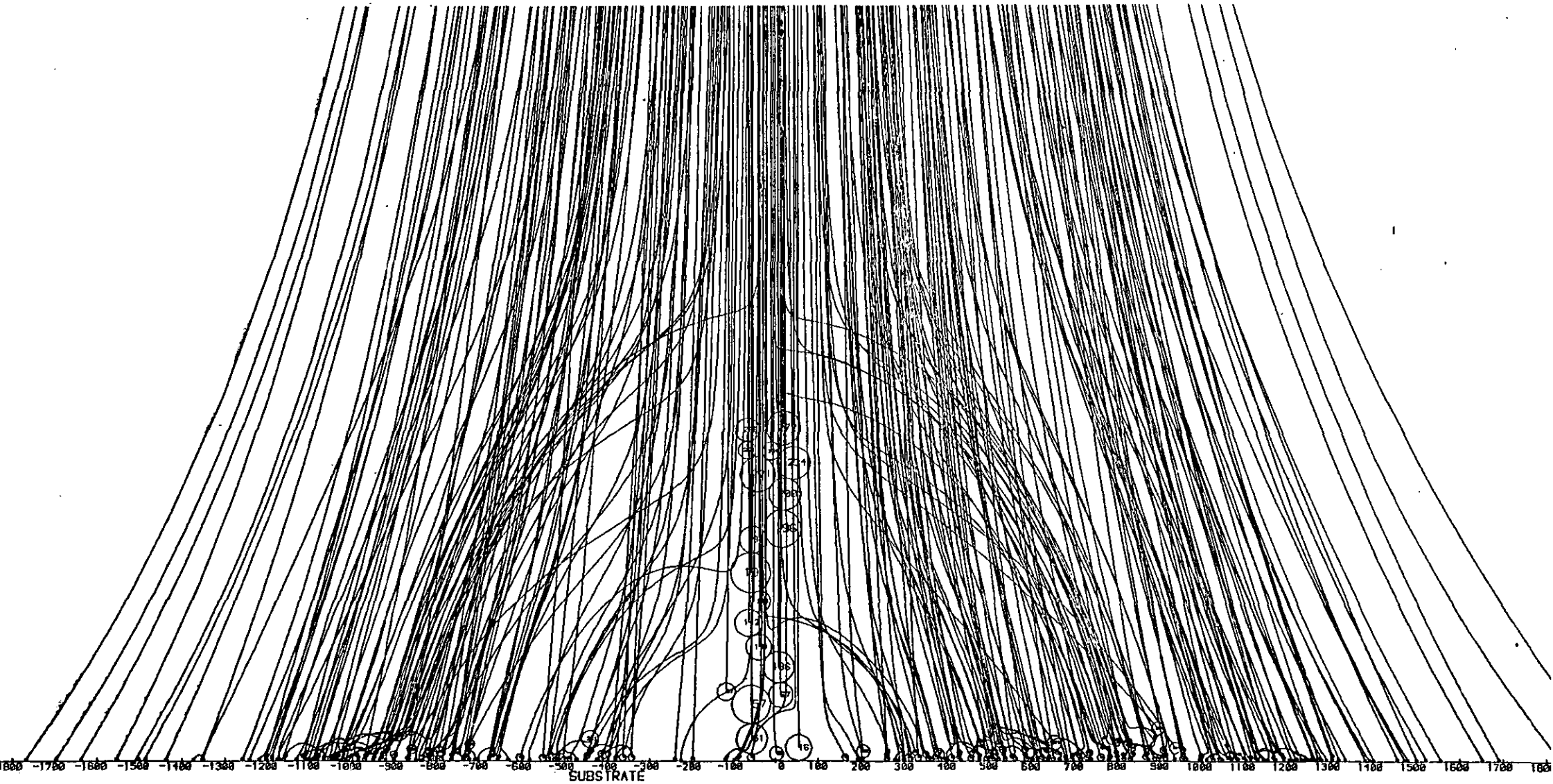
Figure 6.27. Trajectories of Particles of a Size Distributed Powder – Uniform Velocity = 10 m/s, Start Width = 0.00010
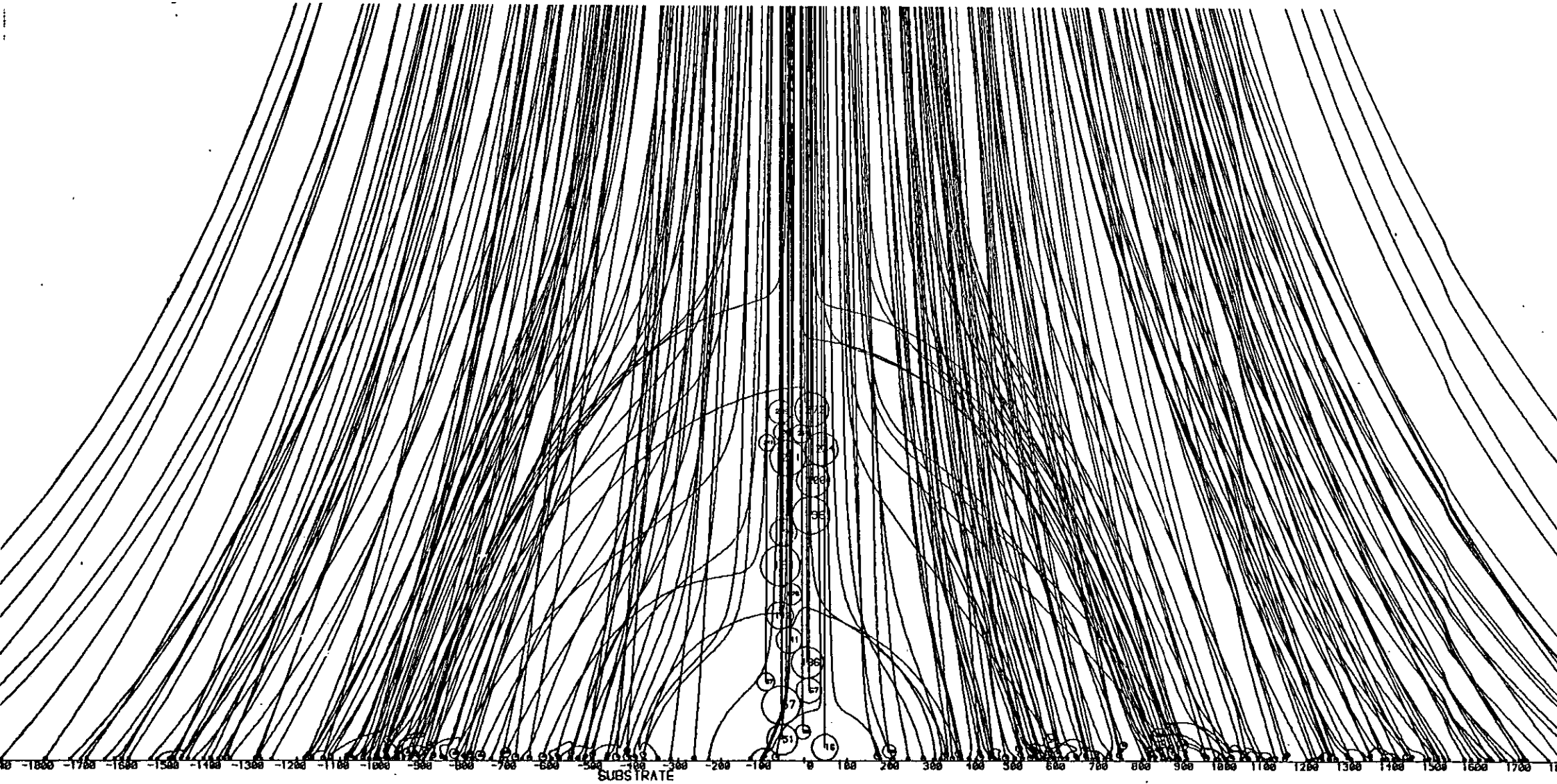
The following effects are observed:-

(i) As velocity increases the severity of the segregation of particle sizes across the substrate increases.

(ii) There is less meandering of the particles with increase in uniform velocity.

(iii) At higher velocities the large dendrite formation of particles in the centre of the substrate causes a shadowing effect since small particles are repelled away from it. The tall dendrite therefore has a larger overall effect compared to small dendrites formed at low velocities and alters the trajectories of small particles at an earlier stage (compare Figure 6.24 - 3 m/s with Figure 6.27 - 10 m/s).

(iv) Similarly to the monosized results, small particles are responsible for covering more of the substrate whilst large particles tend to form tree formations.

Although these results can only represent a fraction of the packing that is usually produced, they show that small particles will not land in areas where there is a thickness of coating due to large particles. This agrees with the experimental findings in that fines are lost when a commercial size distribution is sprayed.

Small particles are therefore repelled from the dendrite structures to thinner layers of coating. As a surface becomes completely covered and layers are built the fine particles will not be able to land and so will be oversprayed. From these results and those of the monosized experiments it is suggested that only a fixed amount of fines can be coated onto a substrate over and above a given thickness of coating. Therefore, if thick films are required, small

particles are wasted once the first few layers have been completed.

Similar effects are found when the start width is constant for various transport air velocities (see Figures E37 to E41).

6.5.4 Theoretical Charged Layer

In the last Chapter equations were derived for the calculation of force on a particle due to a charged layer of a given thickness across the width of the plate. Experiments, using these equations, have been carried out for three particle sizes, three velocities and three layer thicknesses (50μm, 100μm, 250μm thick).

In each situation the charge density (charge/unit area) has been taken as 2.22×10^{-5} coulomb/m^2. Some of the results obtained are shown in Figures 6.28 to 6.33 and the remaining plots to complete the series are shown in Figures E42 to E62.

The results can be summarised as follows:-

(i)   For velocities of 1 to 10 m/s no 10μm particles landed on a layer of charge of any thickness employed here.

(ii)   25μm particles landed on 50μm and 100μm thick layers at any velocity but none landed on the 250μm thick layer.

(iii) All 50μm particles landed under all conditions.

(iv)   For conditions in which the particles did not land an equilibrium distance from the charged layer was reached and the particles travelled away from the centre of the plate. All particles had the same trajectory after having reached this equilibrium distance.

(v)   As the thickness of charge layer was increased so the equilibrium distance increased.

Figure 6.28. Trajectories of Particles Approaching a Charged Layer 250µm thick – Particle diameter = 10µm, Uniform Velocity = 5 m/s

CHARGED LAYER

SUBSTRATE
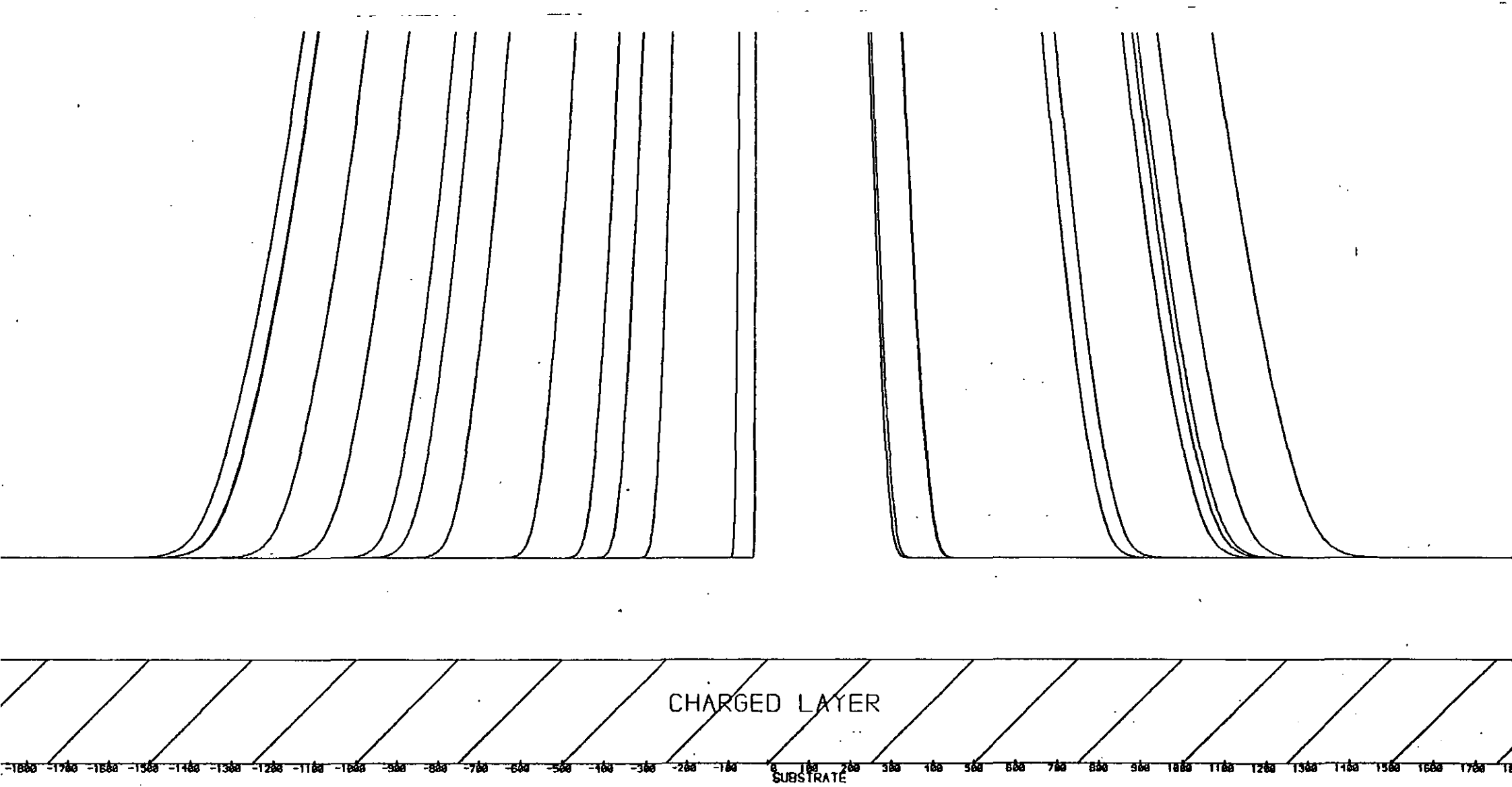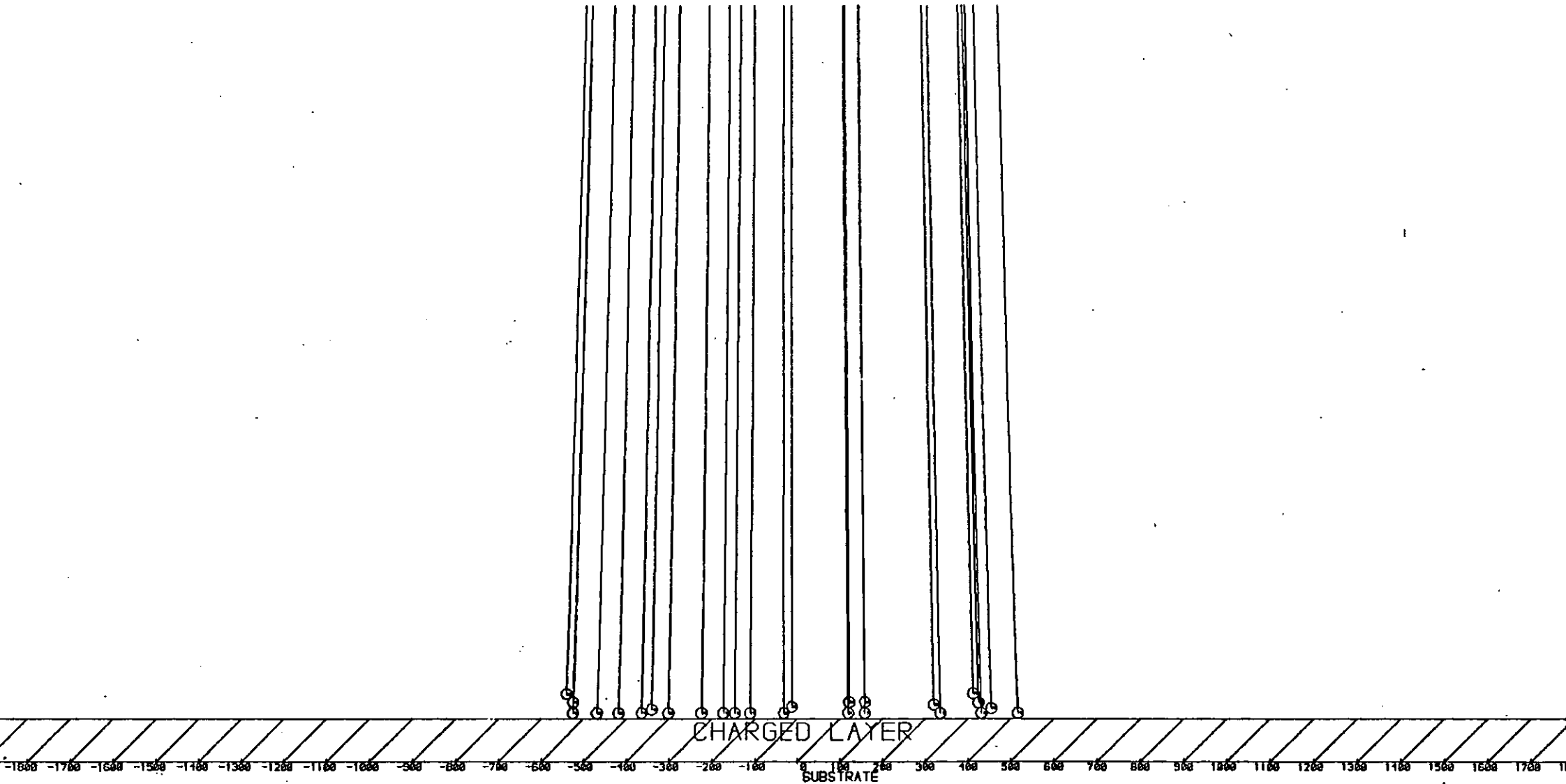
Figure 6.30. Trajectories of Particles Approaching a Charged Layer 250μm thick – Particle diameter = 25μm, Uniform Velocity = 1 m/s
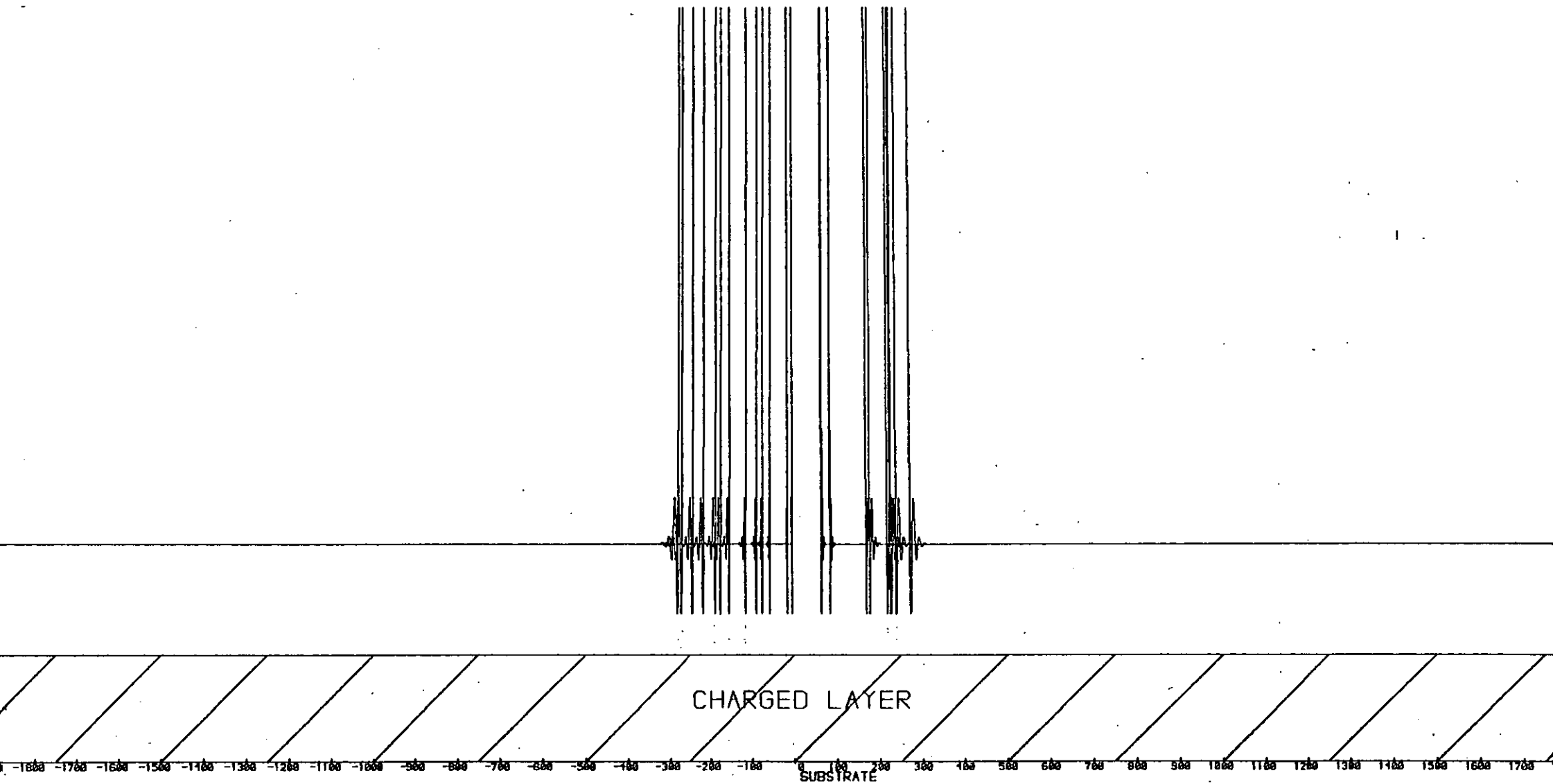
Figure 6.31. Trajectories of Particles Approaching a Charged Layer 250µm thick – Particle diameter = 25µm, Uniform Velocity = 5 m/s
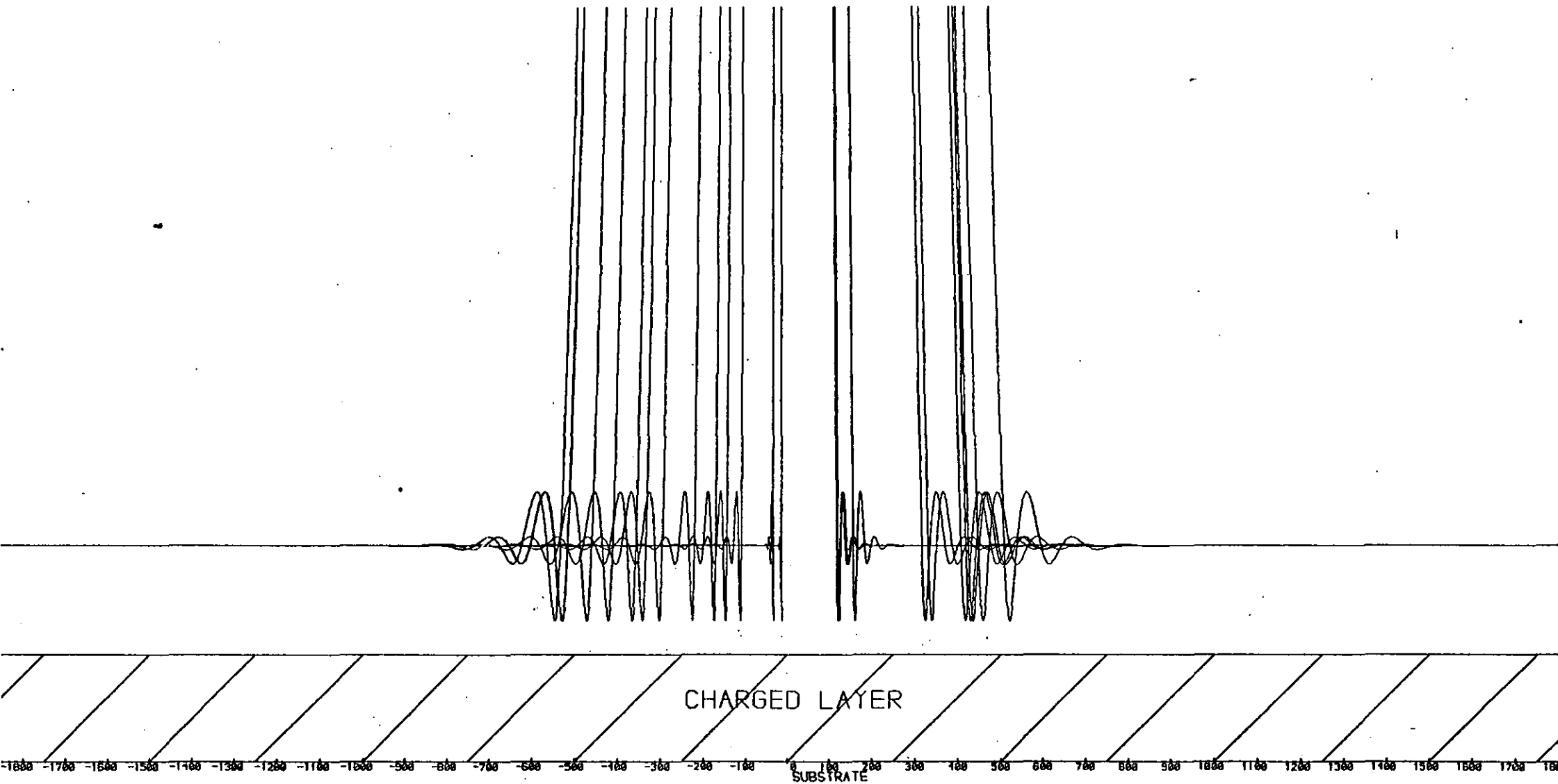
Figure 6.32. Trajectories of Particles Approaching a Charged Layer 250µm thick – Particle diameter = 25µm, Uniform Velocity = 10 m/s
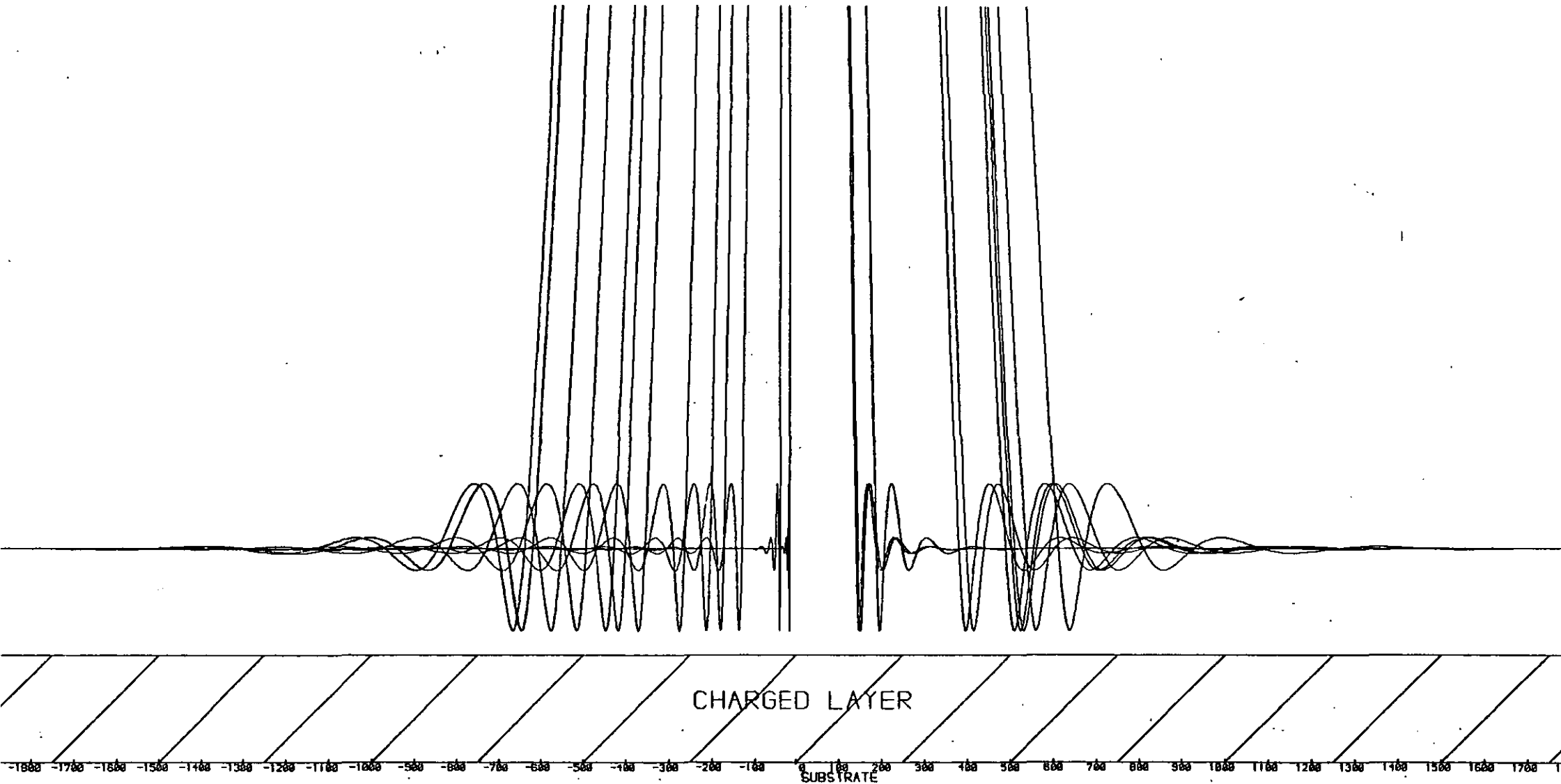
Figure 6.33. Trajectories of Particles Approaching a Charged Layer 250μm thick - Particle diameter = 50μm, Uniform Velocity = 5 m/s

CHARGED LAYER

SUBSTRATE
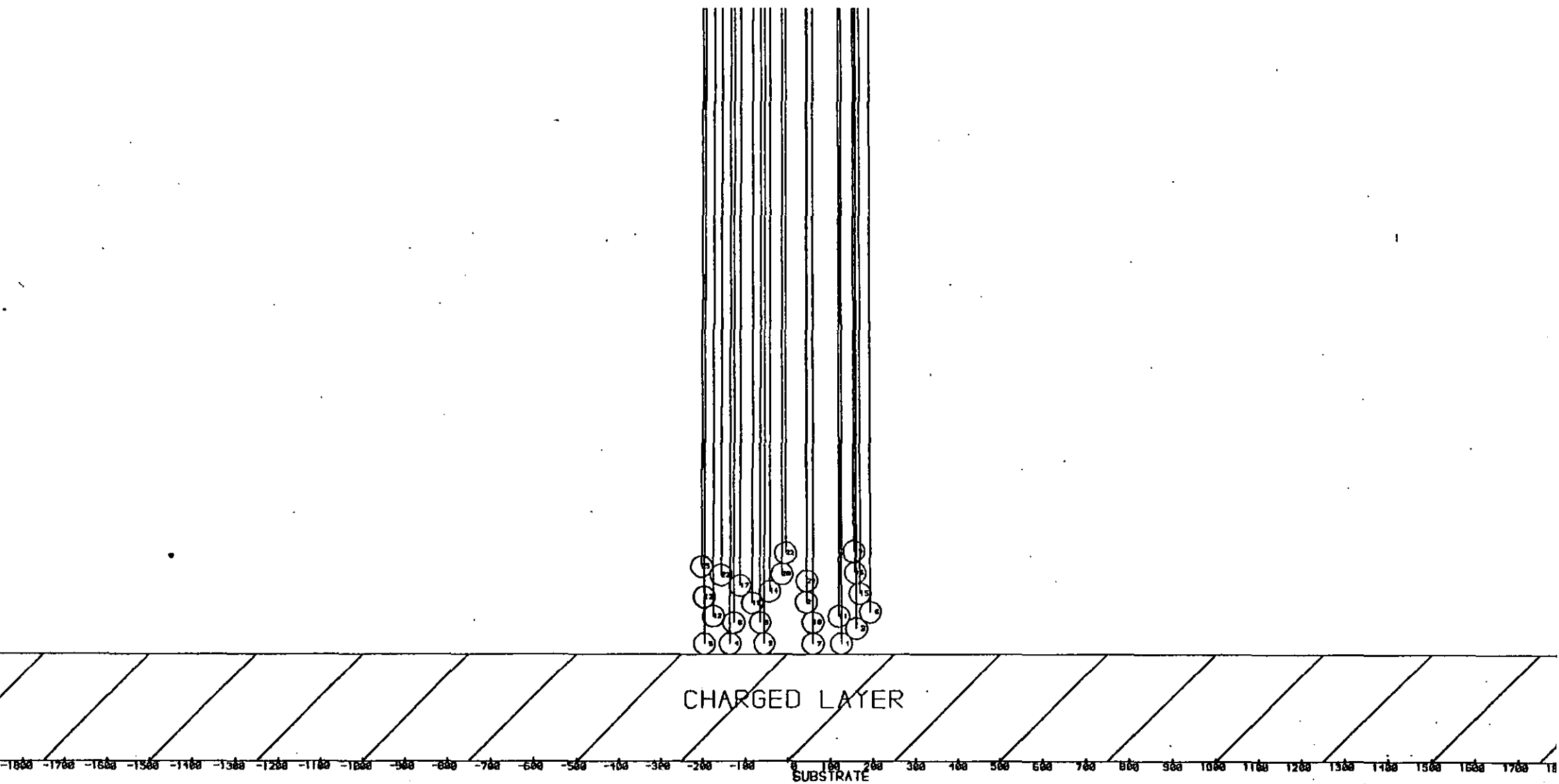
(vi) Uniform air velocity was found to have little effect on the equilibrium distance compared to the effect of layer thickness.

Table 6.14 shows the distance of the equilibrium trajectory from the charge layer for each of the conditions considered and shows the effects of remarks (v) and (vi). It is also observed that, as velocity increases, the closest distance of the trajectory to the charge layer is smaller.

Since the 25μm particles are deposited at low velocities (1 and 5 m/s) but not at 10 m/s, the forces acting on a 25μm particle have been recorded in Tables 6.15 and 6.16 for various positions during the trajectory.

Table 6.15 shows the forces from the start point until the particle reaches its closest position to the charge layer.

In the early stages of flight the drag force is dominant. As the particle approaches the substrate the electrostatic forces increase and $\overrightarrow{V_{rel}}$ drops and so therefore the drag force correspondingly decreases. Eventually the repulsive forces cause the particle to turn around and at this point the repulsive forces are greater than the addition of the drag and field forces. Table 6.16 shows results of the trajectory after this point and Figure 6.34 is a pictorial representation of this situation.

As the particle turns and heads back towards the gun (Point A) the repulsive force drops proportional to $1/d^2$, where d is the distance between particle and layer. The field force, however, changes negligibly over this distance and so then becomes the dominant force. The relative velocity of the particle slowly approaches zero and then

Table 6.14. Variation of Distance of Equilibrium Trajectories from Charge Layer with Velocity and Thickness of Layer

Particle Diameter (μm)	Uniform Velocity m/s	Distance from Layer of Equilibrium Trajectory μm		
10	1	52(43)	105(101)	259(258)
	5	51(43)	102(98)	247(246)
	10	51(42)	100(96)	233(233)
25	1	landed	landed	261(223)
	5	landed	landed	257(180)
	10	landed	landed	249(57)
50	1	landed	landed	landed
	5	landed	landed	landed
	10	landed	landed	landed
		50	100	250
		Thickness of charge layer (μm)		

* Figures in brackets represent closest position of trajectory from charge layer.

Table 6.15. **Forces Acting on a Particle in the Vicinity of a Layer of Charge**

			Particle Velocities		Air Velocities		
$X^{\dagger}$ (m)	Y (μm)	Time in Flight (secs)	U_p (m/s)	V_p (m/s)	U_{air} (m/s)	V_{air} (m/s)	Re_p
0.100	-95	0.000	5.00	0.00	-	-	-
0.110	-98	0.003	3.45	0.00	2.04	0.00	1.98
0.150	-143	0.018	1.88	0.00	1.23	0.00	0.91
0.190	-337	0.052	0.73	-0.01	0.26	-0.01	0.66
0.199	-513	0.068	0.42	-0.01	0.03	-0.01	0.55
*	-545	0.070	0.00	-0.01	0.01	-0.01	0.01

	DRAG		FIELD		IMAGE	PARTICULATE	
$X^{\dagger}$ (m)	F_{D_x} (N)	F_{D_y} (N)	F_{E_x} (N)	F_{E_y} (N)	F_I (N)	$\Sigma(F_{R_x}+F_{R_y})$ (N)	$\Sigma(F_{R_y}+F_{A_y})$ (N)
0.100	-	-	-	-	-	-	-
0.110	-5.8E-9	-2.0E-13	3.1E-9	-2.7E-12	1.2E-16	-5.2E-14	-2.4E-17
0.150	-2.7E-9	1.4E-12	2.3E-9	-2.2E-12	3.8E-16	-1.6E-13	-4.8E-17
0.190	-2.0E-9	1.3E-12	1.8E-9	-3.2E-12	9.0E-15	-3.6E-12	-4.0E-17
0.199	-1.6E-9	1.6E-12	1.7E-9	-4.4E-12	9.0E-13	-3.7E-10	-6.3E-18
*	4.6E-11	1.7E-12	1.7E-9	-4.6E-12	9.0E-12	-5.4E-9	-2.1E-18

Particle size = 25μm, Uniform Velocity, U = 5 m/s, Particle Number 25

* closest calculated x position to layer, distance from substrate = 330μm

$\dagger$ approximate x position from spray gun

Table 6.16. Forces Acting on a Particle Approaching a Layer of Charge

$X^\dagger$ (μm)	Y (μm)	Time in Flight (secs)	Particle Velocities		Air Velocities		Re_p
			U_p (m/s)	V_p (m/s)	U_{air} (m/s)	V_{air} (m/s)	
630	−587	0.073	0.00	−0.02	0.02	−0.01	0.03
462(A)	−643	0.077	0.00	−0.02	0.01	−0.02	0.01
523(B)	−699	0.080	0.00	−0.02	0.01	−0.02	0.01
498(C)	−758	0.083	0.00	−0.02	0.01	−0.02	0.01
509(D)	−828	0.087	0.00	−0.02	0.01	−0.02	0.01
506(E)	−9708	0.182	0.00	−0.25	0.01	−0.24	0.03

$X^\dagger$ (μm)	DRAG		FIELD		IMAGE	PARTICULATE	
	F_{D_x} (N)	F_{D_y} (N)	F_{E_x} (N)	F_{E_y} (N)	F_I (N)	$\Sigma(F_{R_x}+F_{R_y})$ (N)	$\Sigma(F_{R_y}+F_{A_y})$ (N)
630	5.9E-11	1.8E-12	1.7E-9	−5.0E-12	2.5E-12	−1.1E-9	−4.3E-18
462(A)	4.1E-11	2.0E-12	1.7E-9	−5.5E-12	4.6E-12	−2.2E-9	−3.5E-18
523(B)	5.3E-11	2.2E-12	1.7E-9	−6.0E-12	3.5E-12	−1.6E-9	−4.3E-18
498(C)	4.9E-11	2.4E-12	1.7E-9	−6.5E-12	4.0E-12	−1.8E-9	−4.4E-18
509(D)	5.2E-11	2.6E-12	1.7E-9	−7.0E-12	3.8E-12	−1.7E-9	−4.9E-18
506(E)	5.3E-11	3.0E-11	1.7E-9	−8.3E-11	3.8E-12	−1.8E-9	−6.9E-17

$\dagger$ approximate x position from substrate

Particle size = 25μm, Uniform Velocity, U = 5 m/s, Particle Number 25

Figure 6.34.   Trajectory of Particle Number 25 Close to the Charged Layer
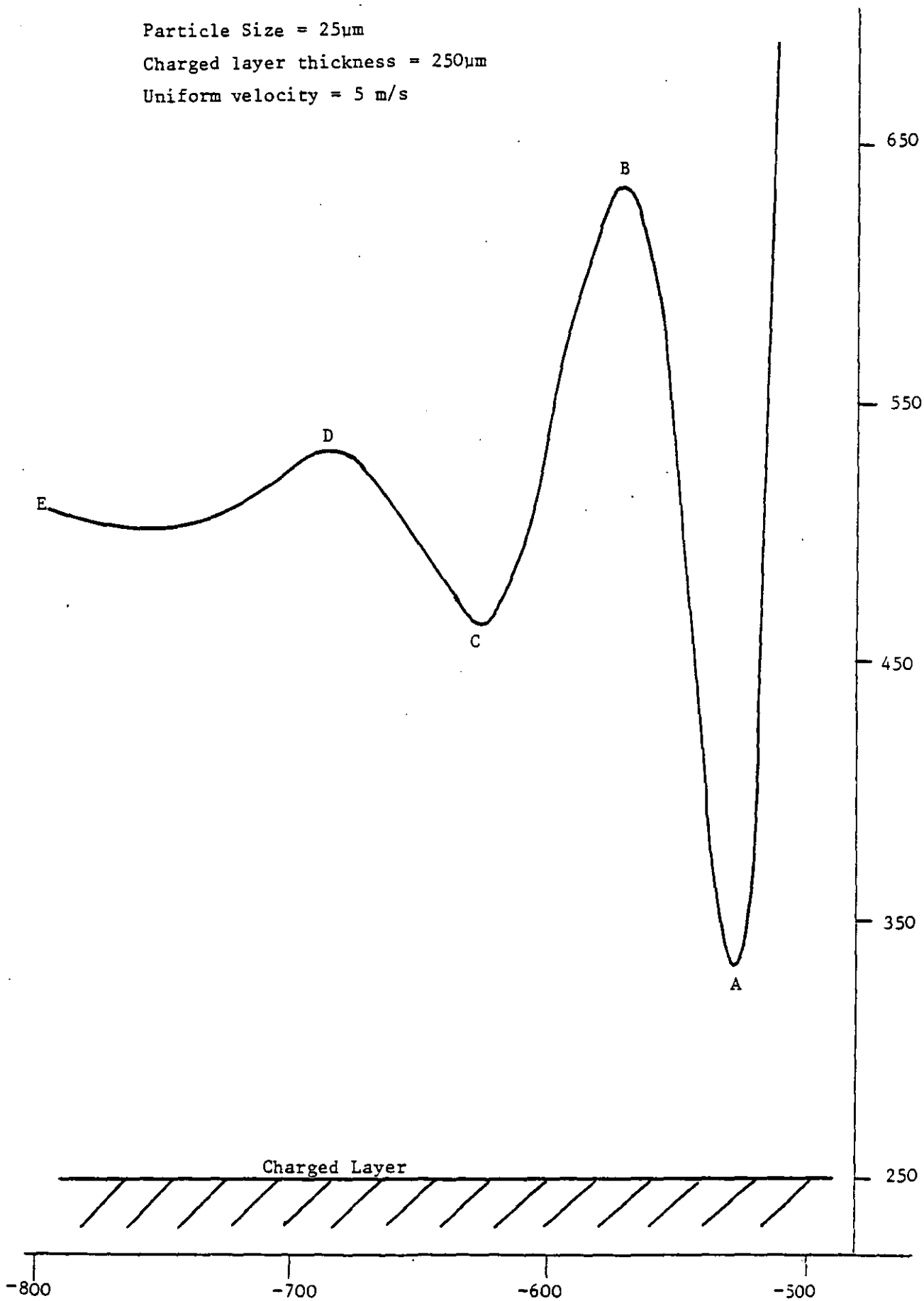
the field pushes it back towards the substrate (Point B). Whilst

this occurs, the y components of the field and electrostatic forces

slowly push the particle in the y direction (in this case negatively)

such that it is moving away from the centre of the plate.

The particle oscillates several times being pushed in either x

direction by the field and electrostatic forces (Points C & D).

Eventually a situation very close to an equilibrium balance of forces

in the x direction is reached (Point E). As the particle travels

away in the y direction the field (x) will decrease slightly, compared

to the electrostatic force, and hence the x position of the particle

slowly increases away from the substrate. Since all particles, for

a given set of conditions, are the same size they follow the same

trajectory, irrespective of their initial y positions.

The trajectories of 10μm particles approaching the substrate

are not as oscillatory since they approach the equilibrium distance

at much lower velocities and their stopping distances are much shorter.

The inertia of the 25μm particles allows them to come closer to

the substrate before they are turned away.

Overall these experiments have been extremely valuable. They

have shown that, for identical coating thicknesses and air velocities,

the landing of particles is dependent on particle size. Also, these

results agree with the quantitative analysis of size distributions

before and after spraying. For a given set of operating conditions,

at some juncture small particles will be repelled whilst larger

particles will continue to be deposited. Therefore a change in size

distribution will occur through the particle packing, with small

particles closest to the substrate.

6.5.5 Effect of Gravity

The force due to gravity acting on the particles has not been included in these experiments since its effects are dependent on the plane in which the target is positioned. Obviously the gravity force is greater for larger particles since it is proportional to mass.

For comparison of the magnitude of forces acting on a particle, the size of the forces due to gravity are

$$10\mu m \text{ particle} - 5.14 \times 10^{-10} N$$
$$25\mu m \text{ particle} - 8.03 \times 10^{-9} N$$
$$50\mu m \text{ particle} - 6.43 \times 10^{-8} N$$

For particles of the order of $10\mu m$ in size the force is approximately equal to the drag and field forces acting on the particle throughout its trajectory. When packings are present, the inter-particulate electrostatic forces will be greater than the force due to gravity close to the substrate and hence similar effects would be expected as have been already observed. However, gravity would cause any overall displacement of landing position compared to those obtained here. Again its effects close to the substrate are reduced compared to other sized particles because of the short stopping distances of very small particles.

For large particles the effect due to gravity will be more dependent on the location of the substrate. If vertical, the large particles would land at lower positions on the substrate, or possibly miss completely. Higher operating air velocities would help overcome this as the particles leave the gun with more inertia.

For horizontal surfaces, depending on their position relative to the gun, gravity would give the particles more inertia towards the plate and hence thicker coatings would be expected.

6.6 Conclusions

The writing of a computer program to simulate the trajectories of particles sprayed towards a substrate has given an insight into the mechanism of packing of particles by this process in a qualitative manner.

The method and working of the computer program has been described together with the necessary tests that are required to ensure correct computation and calculation. Many stated assumptions have been used in order to simplify the system such that a reasonably large number of particles can be considered. Preliminary experiments showed that

(a)   the tolerance bound required to give representative results was 10^{-7}

(b)   that Re_p is generally less than 1 close to the substrate and hence Stokes Law can be applied

and

(c)   that the particle velocities, although initially approximated, reach a tangible solution in the first few centimetres of the trajectory.

The monosized experiments have shown that each powder size range will tend to have a maximum thickness that can be coated onto the substrate. Small particles are strongly influenced by electro-static forces close to the substrate and due to their mobility are able to find uncoated areas of substrate. Large particles are dominated by their own inertia and in general the forces due to the powder packing are not strong enough to cause any appreciable deviation in their trajectories. These particles form dendrite type formations which agrees with experimental evidence.

In these computer experiments particles were found to reach an equilibrium position where the resultant of all forces acting on the particle was zero. Close up studies of the movement of 10μm particles have shown how this can occur and also how particles follow the contours of the particle packing.

Throughout the computer experiments it has been noticeable that both particle size and air velocity affect the splaying of the particles. Decreasing particle size and increasing velocity enhances this effect. The size distributed powder results confirmed the observations of size segregation across a coating. Large particles were prolific in the centre whilst small particles landed towards the outside of the plate. Large particles tend to cause a shadowing effect in that small particles are deflected far away from them and hence parts of the substrate are left less populated close to a large particle dendrite tree.

Since three hundred particles took approximately 3 hours to compute, a wide, thick coating could not be simulated by this method. The experiments involving a charged layer allowed an advanced coating (i.e. thicker) to be considered but required less computing time. The plots showed that for a coating of 50μm or thicker no 10μm particles would be deposited for velocities between 1 and 10 m/s. 25μm particles were repelled from a 250μm thick layer but 50μm particles always landed. Hence for identical coatings and conditions the plots have shown that deposition is related to particle size. Large particles will continue to be deposited as the packing increases in thickness and small particles are repelled.

6.7 <u>Summary</u>

By using a computer program to simulate the packing of particles on a substrate, a valuable insight has been gained into understanding which forces act dominantly on particles in different circumstances.

Results of computer analysis have shown good agreement with experimental results and have given indications of the reasons behind observed effects. By considering the effects of a charged layer and different air velocities on monosized powder distributions the size segregation effect that was quantified in Chapter 4 has been confirmed. Although such simulations can only be considered qualitative they have endorsed experimental trends.

CHAPTER 7

FINAL DISCUSSION AND SUMMARY

7.1 Aims of the Investigations

7.2 Summary of Results of Investigations

    7.2.1 Testing of Properties

    7.2.2 Packing and Stoving

    7.2.3 Trajectory Equation

    7.2.4 Computer Simulation

7.3 Limitations of this Work

    7.3.1 Experimental

    7.3.2 Theoretical

7.4 Future Work

7.5 Final Concluding Remarks

7.1 Aims of the Investigation

The electrostatic powder coating industry has many advantages over other industries in the finishing markets. However its growth has been curtailed to approximately 10% of the world market due to the limitations of use by major coating producers. Problems associated with colour change and control of film thickness have been paramount in causing this curtailment.

The aim of these investigations has been to observe the effects produced by changing the particle size distribution of the powder used to produce spray coatings. In particular, changes in physical properties of the coatings have been monitored for a variety of different sized powders. This has been combined with studies of particles packing onto substrates so that improved operating procedures (e.g. optimisation of size distribution etc) can be suggested based on the results of such investigations. It is important that if the size distribution of a powder is altered to gain (i) higher deposition efficiency, (ii) control of film thickness, or (iii) reduction of problems associated with colour change, that there is no undue deterioration in physical properties of the film.

Although several workers have carried out fundamental investigations into the role of operational parameters on deposition efficiency surprisingly little attention has been given to the effect of physical characteristics of the powder on the properties of coatings. Previous research has been summarised in the text and clearly shows that a great deal of information is available with regards to obtaining high deposition efficiencies by controlling operational variables, such as charging voltage, substrate width

etc etc. However individual forces acting on each particle (due to the influence of such parameters) has not been considered and it has been one of the aims of this work to obtain a clearer understanding of which forces are most important in the electrostatic spraying process.

Other researchers, who have dealt with the levelling of powder coatings, acknowledge that the irregularities in the powder layer can affect the final film produced i.e. extent of orange peel. Similarly, although the fusing and flowing of the powder layer and the effect of formulation has been investigated, little insight into the way in which a packing is actually formed has been obtained.

A literature survey revealed numerous methods which are frequently used in industry for analysing powder coatings. The primary difficulty associated with such testing techniques is that no single property can be measured without encompassing another. This is especially true for mechanical type tests where a variety of inter-related properties are measured. The analysis of data from quality testing techniques also presents problems. Comparisons to standards are often required and even then the significance of differences obtained must be questioned.

A series of tests were adopted and used in conjunction with a developed experimental procedure for providing reproducible test samples for the different powders used. Coatings were prepared, tested and collated with thickness, powder type and physical property measured. By considering only one powder in these experiments the effects of powder formulation could be neglected. Similarly effects due to stoving were neglected since identical conditions were used throughout the production period.

The results from these tests were indicative of the fact that a commercial powder had been chosen. The coatings, as expected, had generally excellent physical properties and hence identification of any significant differences in their physical properties was made all the more difficult.

The mechanisms and effects associated with the packing of particles on a substrate were investigated both experimentally and theoretically.

Although practical investigations were very simple in nature they permitted observations of how different sized particles are distributed in a packing. Results of these exploratory experiments led to quantitative analysis in which the powder size distributions were determined before and after spraying.

Theoretical investigations were carried out in order to understand some of the observed phenomena. A fundamental approach was taken to investigate the role of forces acting on particles of different size in flight. Although such approach has to be necessarily qualitative, the aim was to gain an overall insight into the forces that primarily act on particles in flight, and especially when particles come close to the substrate. It was then the intention to try and apply the results, with reservations on applicability, to the general system.

Information obtained from computer experiments enabled the forces acting on a particle at any point in its trajectory to be considered and compared to other positions, different sized particles and various operating conditions. Although the simulations were restricted to 2 dimensions several interesting effects were observed.

Therefore the overall scheme of research was:-

(i) Development of a reproducible coating technique.

(ii) Production of test samples using narrow size fractions of a commercial powder.

(iii) Assessment of the physical properties of coatings by a suitable test procedure.

(iv) Observations of particles packing and stoving.

(v) Development of trajectory equations to describe the flight of particles.

(vi) Simulations of particles packing under different operating conditions, including studying

    (a)   monosized powders

    (b)   size distributed powder

    (c)   layer of charge on substrate

for changes in particle size (a,c), transport air velocity (a,b,c) and thickness of charge layer (c).

7.2   Summary of Results of Investigations

7.2.1   Testing of Properties

The results of tests on these coatings for properties of gloss, roughness, adhesion etc showed that there is no significant difference for changes in particle size sprayed or thickness of coating. Narrow size fractioned powders showed no trends, with the results being scattered about an average value. The commercial powder did show more marked trends for roughness and gloss with changes in thickness. When comparing the spread of results from these tests with low and high quality finishes it could be concluded that the variations were very small.

This work suggested that any change made to the size distribution of the powder sprayed, in order to increase or control deposition, would not appreciably effect the surface finish. This is an important conclusion.

7.2.2 Packing and Stoving

Simple stoving experiments suggested that the excellent flow characteristics of the epoxy resin powder were responsible for the small variations in testing results.

From microscopic observations of packings (unfused) a variation of size distribution was observed through the packing depth and an overall change in distribution between the powder sprayed and deposited was quantified. A loss of fines was determined and it appeared from observations that this was primarily from the upper layers of the coatings.

7.2.3 Trajectory Equation

Using a force balance, a set of trajectory equations were developed to describe the flight of particles to the substrate. Several simplifying assumptions were used to allow easier handling of these equations. Although straightforward models were used for the air flow, electric field and calculation of drag coefficient, individual interparticulate electrostatic forces were incorporated. The approach was kept 2 dimensional to permit pictorial representation of the results, where 3-dimensional analysis would have given many problems.

7.2.4 Computer Simulation

The trajectory equations were found to be of a stiff nature. A suitable NAG library routine was employed to effect numerical integration over the flight range. Many problems were encountered in handling the 'physical' situation of particles landing on a substrate and in minimising computing time. Summation of all interparticulate electrostatic forces at each step of the integration limited the number of particles that could be considered due to the restraints on computer time.

Although several assumptions in the program have been used the overall representations appear very reasonable. The flow model appeared adequate and when no electrostatic forces were applied it was shown that deposition would not occur in the majority of cases. Starting the trajectories mid-way between gun and target with approximated initial velocities was also shown to be reasonable.

The results obtained show clearly similar effects to those observed in the practical experiments. Particle size and transport air velocity were both found to be very important in determining the type of packings produced.

From simulations of the spraying of monosized particles it has been shown that smaller particles tend to produce thin packings covering a higher percentage of area of the substrate. These particles are seen to be strongly influenced by electrostatic forces in the vicinity of the packing and substrate. Their movements are jerky, frequently change direction, whilst large particles trajectories are more streamline being less influenced by the charged packing structures. Transport air has been observed to

influence the thickness of packings. This is due to the splaying
effect and also the change in the balance between aerodynamic and
electrostatic forces.

Results from studies with size distributed powders indicate
that large particles produce 'shadow' areas in which there is an
absence of fines. As the packing becomes thicker so more fines are
repelled and large particles become abundant in central and upper
regions of the coating. Both these effects show good agreement with
experimental findings.

Large particles formed tall dendrite type structures which did
not occur for small particles. These large particle tree formations
gave rise to the formation of large crevasses and valleys in the
upper layers of the packing which is not so noticeable close to the
substrate due to the presence of the small particles.

Consideration of a theoretical charged layer showed how particles
of different size behave in different ways. This set of experiments
allowed particles approaching much thicker coatings to be studied.
Results indicated that particle size was more important than air velocity in
determining whether particles landed on a coating. It was clearly
shown that as the thickness of a coating increases deposition is
subject to size restrictions. Small particles are not deposited with
thick coatings and in such cases the balance of forces close to the
substrate is of paramount importance.

Although the flow pattern, surroundings and plate size in a
coating system will undoubtedly be different for each industrial
application, these results have outlined the important factors in
particle deposition. In the production of thick coatings a wide size

distributed powder will produce a fines rich overspray and will

drastically reduce deposition efficiency as coating thickness

increases. For thinner films better control would be obtained if

less large particles were used. Increased movement of spray guns

will cause less size segregation and hence produce more uniform

films.

7.3   Limitations of this Work

In carrying out any piece of research limitations of time and

resources means that certain areas are not as fully investigated as

they could be and that simplifying assumptions have to be applied.

This work is no exception and it is important to recognise not only

the achievements but the limitations of the work.

7.3.1   Experimental

Narrow size distributed powders and a commercial powder

were chosen for tests on film properties with the intended exclusion

of effects due to formulation. It appears from the results of these

tests and stoving observations that the results could be strongly

related to the powder formulation used, whereas more definite trends

might be observed for other types of powders.

7.3.2   Theoretical

There are many assumptions that have been incorporated

into the computer program to allow for a relatively easy method of

solution to be followed.

Also excluded are some effects that would be readily observed

in the real situation but are very difficult to simulate. Together

these are summarised below:-

(1)   2 dimensional only

(2)   Simple air model

(3)   No gravity force

(4)   No bounce-off or movement of particles after landing

(5)   Small area considered

(6)   One particle in flight at a time

(7)   Spherical particles

(8)   No space charge

(9)   No leakage of charge from packing

However, the aim has been to gain an insight into the important parameters that effect the process and this has been achieved to a considerable extent.

Development could be continued so that the above list is shortened as far as is reasonably possible. This would serve to make the simulation closer to reality than at present.

In its present form, therefore, the computer simulation technique can only be considered as a qualitative method of observing the effects of forces acting on particles, even though the trends that have been already observed do agree qualitatively with those obtained experimentally.

7.4   Future Work

The investigations reported here have provided important conclusions with regards to the electrostatic coating process. Both experimental and theoretical work has shown how particles behave in different ways according to their size and the operating conditions employed.

It has been shown that for the commercial type powder little change in physical properties of the coating occurs with change in

particle size or film thickness. However, stoving experiments suggest that this could be due to the powder's excellent flow properties. Hence further experimental work could be performed to investigate whether these observations are true for other powder formulations. This work has purposely avoided changes in formulation since the experimental program was already very extensive. Future work could therefore be restricted to the testing of fewer properties i.e. just adhesion and gloss. Comparisons could be made between poorer flowing powders and excellent flowing powders. The effect of size ranges could also be investigated in this way with regards the levelling of the powder and in turn related to the porosity of the packing.

Investigations into particle packing have shown how various sizes behave differently with regards deposition. This area could be more fully investigated by

(i)   Measurement of size distributions of powder on a plate at different coating times.

(ii) Collection and size analysis of overspray.

(iii) High speed colour cine filming of a spray of particles landing on a substrate using a powder with coloured size fractions.

The computer program has enabled effects of changing air velocity and particle size to be studied. Trends showing the way in which the magnitude of forces acting on the particles change have been described and this itself has proved very valuable for understanding the coating system. However the program is subject to many simplifying assumptions and therefore there is plenty of scope for changes to be made in an attempt to simulate the real system more closely:-

(i)   Air flow. The model for air flow is currently based on flow

        past a flat plate and the trajectory is started half way

        between the gun and target. Development of equations to

        describe the air flow from the gun (including taking into

        account the type of deflector, nozzle etc) would help to optimise

        the system with regards deposition efficiency, gun design etc.

(ii)   At present only 2-dimensional analysis is made. Although this

        does give indications of trends, the effect of a packing on

        a particle in flight would be different for the three dimensional

        case. The setting up of the equations is not in itself

        difficult but representation of 3-D results would require

        considerable thought.

(iii)   During computer experiments it was found that for large numbers

        of particles (∿300) solving the trajectory equations came close

        to the user time limit. The time for computation increases

        rapidly as the number of particles landed increases since each

        particle in the packing is used for the calculation of electrostatic

        forces and is checked for collision. The use of a theoretical

        model to simulate a layer of uniform charge aided this situation,

        but reduces the amount of information that can be gained e.g.

        packing orientation, porosity, size segregation etc. If a

        packing model could be developed to describe the force acting

        on the particle due to the packing this could reduce computation

        substantially.

(iv)   No attention is given in respect of space charge and only one

        particle is considered in flight at any instant. The program

        could be adjusted so that, say, 300 particles were in flight at

once and so the effect of each particle in flight on the others would be taken into account. It would then be less likely that a particle would reach an equilibrium condition as shown in the plots here. This technique would require more computation time since 300 particles have to be compared and accounted for through each of the 300 particle trajectories.

(v)   In trying to accomplish (iv) particle bounce would need to be considered since it would be very probable that particles would collide in flight.

(vi)   As gravity is ignored in the experiments reported in this work, the positional direction of the substrate is of little consequence. The packing of particles onto a 3-dimensional object (i.e. a cube) would possibly produce very interesting information on how particles are deposited on surfaces facing different directions. The air flow model would require adjustment, but if accomplished the wrap around effect could be investigated.

(vii)   The problems due to splaying were very marked due to the program being based on a static type gun. The comparison of packings obtained by using a gun which traverses across the object could show the type of coatings produced by robot guns in an industrial plant, and also reduce the problems due to the effects of splaying.

7.5   Final Concluding Remarks

The intention of the investigations reported here was to ascertain whether changes in the particle size distribution of electro-statically sprayed powders effect the final finish of the coatings produced. A positive conclusion formed on the basis of data obtained

from the testing of several hundred sample plates was that particle size or film thickness did not affect the physical properties of coatings for the epoxy powder employed. This suggests that any change in the size distribution of the powder can be made to increase deposition efficiency or to control film thickness without fear of losing the excellent physical properties associated with powder coating.

The use of a computer simulation technique has given an understanding of real effects observed in the laboratory, and although simplified, has been extremely useful in indicating the important operating parameters of the electrostatic powder coating process. It has enabled the process to be studied from a novel fundamental standpoint rather than in the more usual experimental manner. Further development of this technique should therefore be instigated to widen the range of applicability.

REFERENCES

Listed in alphabetical order of first named authors

REFERENCES

I.D. Aitken, 1968, Proc. Int. Sym. Powder Coatings, Paper No V/18, 13-15 Feb.

R. Allen, 1973, Ind. Fin. Surf. Coatings, 25 (301), 20-27.

M.L. Ang, 1981, Ph.D. Trajectories of Charged Particles in Electrostatic Powder Coating Systems, Loughborough University.

Anon, 1974, Prod. Fin., 39 (3), 24-25.

Anon, 1976, Ind. Fin. Surf. Coatings, 28 (332), 17-23.

Anon, 1976, Ind. Fin. Surf. Coatings, 28 (331), 10-16.

Anon, 1974, Prod. Fin., 39 (2), 20-21.

R.A. Ashdown, 1974, Prod. Fin., 39 (2), 33-36.

ASTM Recommended Practices for Testing Polymeric Powders and Powder Coatings, 1973, D3451-75.

ASTM Handbook of ASTM Standards, 1975, Part 27.

J.D. Bassett, R.P. Corbett, J. Cross, 1975, Inst. Phys. Conf. Ser., No 27.

D.R. Birchenough, M.J. Marshall, 1972, Ind. Fin. Surface Coatings, 24 (288), 4-7.

R.R. Blakely, 1977, Ind. Fin. Surf. Coatings, 29 (344), 28-36.

J. Boxall, J.A. Fraunhofer, 1974, J. Paint Manufacture, 44 (5), 26-29.

A.W. Bright, 1977, J.O.C.C.A., 60(1), 23-27.

British Standard Methods of Tests for Paints, 1974, B.S. 3900, Part E7.

British Standard Method of Tests for Paints, 1974, B.S. 3900, Part E6.

British Standards Method of Tests for Paints, 1967, B.S. 3900, Part D2.

W. Brushwell, 1973, Ind. Fin. Surface Coating, 25 (297), 24-30.

G.D. Cheever, 1975, J. Appl. Polym. Sci., 19, 147-163.

A.E. Claxton, 1975, Preprints Oil & Colour Chemists Assoc. Biennial

Confs., Scarborough, June, 28-34.

J.H. Colling, W.E. Craker, J. Dunderdale, 1968, J.O.C.C.A., 51,

514-546.

M. Cowley, 1974, Ind. Fin. Surf. Coatings, 25 (308), 20-21.

W. Crisp, 1973, Ind. Fin. Surf. Coatings, 24, 299.

J. Cross, 1975, Static Electrification, Inst. Phys. Conf. Ser.,

No 27, 202-213.

J.A. Cross, S. Singh, A.B. Ahmed, 1980, J.O.C.C.A., 63, 326-329.

V.K. Croutch, 1976, 4th American Conf. on Powder Coating, Toronto,

Canada.

E.W. Drew, 1977, Prod. Fin., 41(11), 8-10.

M.J. Drury, 1974, Prod. Fin, 39(2), 37-38.

J.A. Fraunhofer (Part 1), 1971, Prod. Fin., 35(8), 22-25.

J.A. Fraunhofer (Part 6), 1972a, Prod. Fin., 36(9), 47-52.

J.A. Fraunhofer (Part 7), 1972b, Prod. Fin., 36(11), 12-18.

J.A. Fraunhofer (Part 8), 1972c, Prod. Fin. 37(1), 20-25.

S. Gabriel, 1975, J.O.C.C.A., 58, 52-61.

N.I. Gaynes, 1977, Testing of Organic Coatings, Noyes Data Corp.

GINOF User Manual, 1976, Issue 2, Computer Aided Design Centre,

Cambridge.

A. Golovoy, 1973a, J. Paint Tech., 45(580), 42-48.

A. Golovoy, 1973b, J. Paint Tech., 45(585), 74-79.

A. Golovoy, 1973c, J. Paint Tech., 45(585), 68-73.

A. Golovoy, A.D. Colvin, 1975, J. Paint Tech., 47(604), 65-70.

R. Goudie, 1974, Prod. Fin., 39(3), 14-17.

H.K. Hammond III, 1974, Official Digest, April, 360-365.

Handbook of Chemistry and Physics, 1977, 58th Ed., CRC Press.

M.J. Hannon, D. Rhum, K.F. Wissburn, 1976, J. Coatings Tech., $\underline{48}$ (621), 42-54.

G.F. Hardy, 1974, J. Paint Tech., $\underline{46}$(599), 73-82.

S.T. Harris, 1976, The Technology of Powder Coatings, Portcullis Press.

S. Huey, 1964, Symp. Gloss Measurement, Official Digest, April.

D. Jarvis, 1974, Prod. Fin., $\underline{39}$(3), 12-13.

M.B. Kilcullin, 1975, Preprints Oil Col. Chem. Assoc. Biennal Conf., Scarborough, 50-61.

C.H.J. Klaren, 1977, J.O.C.C.A., $\underline{60}$, 205-213.

K. Koffmann, T. Kosbahn, 1966, Farbe. U. Lacke, $\underline{72}$(2), 119-127.

C. Korf, 1976, Powder Coating, R.A. Chandler Ltd.

T. Kosbahn, 1964, Farbe. U. Lacke, $\underline{70}$(9), 693-702.

S. Kut, 1972, Prod. Fin., $\underline{36}$(4), 21-29.

S. Kut, 1971a, Prod. Fin., $\underline{36}$(3), 32-38.

S. Kut, 1971b, Prod. Fin., $\underline{36}$(2), 28-30.

S. Kut, 1971c, Prod. Fin., $\underline{36}$(1), 31-37.

S. Kut, 1974, Prod. Fin., $\underline{39}$(2), 25-31.

P.G. DeLange, 1978, Fin. Ind., $\underline{2}$(3), 35-38.

T.D.T. Latter, 1976, Prod. Fin., $\underline{40}$(8), 46-47.

R. Lever, 1978, Fin. Ind., $\underline{2}$(2), 41-44.

B. Lindberg, 1975, Preprints Oil Col. Chem. Assoc., Biennial Conf., Scarborough, 105-119.

M.J. Marshall, D.R. Birchenough, 1972, Prod. Fin., $\underline{37}$(2), 40-41.

D.R. Mason, J.L. Stevens, 1978, Introductory Course to VAX 11/780, ICI Corporate Laboratory.

S.L. Mason, 1974, Prod. Fin., 39(2), 22-24.

W.J. McGill, 1977, J.O.C.C.A., 60, 121-126.

E. Miller, 1974, Fundamentals of Powder Coating, S.M.E.

C.A. Mitton, 1968, Accelerated Environmental Testing, Paper No V/17, Proc. Int., Symp., Powder Coatings.

A.D. Moore, 1973, Electrostatics and its Applications, Wiley Interscience.

Myers and Long (Ed.), 1968, Characterisation of Coatings, Physical Techniques Part 1, Marcel Dekker.

NAGFLIB, 1976, NAG library routine DØ2AJF, Integration of a system of first order ordinary differential equations over a range using a divided difference formulation of Gear's method for stiff systems of equations 1387/0 : Mk 5.

NAGFLIB, 1977a, NAG library routine GO5CAF, Generation of a pseudo-random real number, uniformly distributed between 0 and 1, 1443/0 : Mk 6.

NAGFLIB, 1977b, NAG library routine GØ5CBF, Setting the state of the generation storage to a repeatable value, 1440/0 : Mk 6.

NAGFLIB, 1978, NAG library routine DØ2QBF - Integration of a stiff system of first order differential equations using a variable-order, variable-step Gear method, 1640/0 : Mk 7.

K.C. O'Neill, 1977, Aust. O.C.C.A. Proc. News, 14, 6-12.

V.G. Nix, J.S. Dodge, 1973, J. Paint Tech., 45(586), 59-63.

Nottingham Algoriths Group, 1973, NAG Library routine DØ2ABF, Integration of a system of ordinary differential equations over a range using Merson's Method.   Doc. No. 564.

S. Oglesby, Jnr, G.B. Nichols, 1978, Electrostatic precipitation, Marcel Dekker Inc, New York.

P.H. Ong et al., 1975, Static Electrification, Inst. Physics Conf. Ser., No 27.

S.E. Orchard, 1962, J. Appl. Sci. Research, $\underline{11}$(A), 451-465.

D. Payne, 1973, Ind. Fin. Surf. Coatings, $\underline{24}$, 299.

M.M. Pauthenier, M. Moreau-Hanot, 1932, J. Phys. Radium, $\underline{3}$(7), 590-615.

F.W. Peek, 1929, Dielectric Phenomena in High Voltage Engineering, 3rd Ed. McGraw-Hill.

P.P.I. Company, 1963, Brice Phoenix Light Scattering Photometer Instruction Manual Operation Manual OM-2000, Philadelphia, USA.

A. Quach, 1973, Ind. Eng. Chem. Prod. Res. Dev., $\underline{12}$(2), 110-116.

P.S. Quinney, N.J. Tighe, 1971, Br. Polym. J., $\underline{3}$(10), 274-278.

L. Schiller, A. Naumann, 1933, Z. Ver. deut. Ing. $\underline{77}$, 318.

S. Singh, 1979, Coordinated Powder Research Programme. Southampton University, Progress Report, June.

S. Singh, 1980a, C.P.R.P. Southampton University Progress Report, Jan.

S. Singh, 1980b, C.P.R.P. Southampton University Progress Report, March.

J. Smarsh, 1972, J. Paint Tech., $\underline{44}$ (565), 30-37.

S. Spindel, 1973, Am. Paint. Tech., $\underline{26}$, 33-38.

G.T. Spitz, 1973, ACS Div. Org. Coatings Plastics Chem. Papers, $\underline{33}$(2) 502-507.

R.C. Spragg, D.J. Whitehouse, 1972, Measurement and Control, $\underline{5}$, 95-101.

H. Stein, 1972, Ind. Fin. Surf. Coatings, $\underline{24}$(294), 32-33.

B. Svoboda, O. Kolar, 1962, Chem. Prumysl, $\underline{12}$(7), 281-384.

M. Tahan, 1974, J. Paint Tech., $\underline{46}$(59)), 35-47.

M. Tahan, B.J. Tighe, 1974, J. Paint Tech., $\underline{46}$(590), 48-57.

J.D. Tiernay, 1975, Prod. Fin., $\underline{39}$(11), 14-15.

Y.C. Ting, 1978, M.Sc. Thesis, Back Ionisation in Electrostatically deposited layers, Southampton University Elec. Eng. Dept.

J.D. Toff, 1979, Prod. Fin., $\underline{43}$(11), 10-12.

H.R. Valentine, 1967, Applied Hydrodynamics, 2nd Ed. Butterworths.

K. Venlet, 1973, Ind. Fin. Surf. Coatings, $\underline{25}$(299), 30-41.

B. Whiting, J.K. Dennis, 1977, Report, Dept. Metallurgy and Materials, University Aston in Birmingham.

W.G. Willows, 1968, Powder Coatings Int. Symp., 13-15 Feb, London.

S.M. Wolpert, 1973, ACS Div. Org. Coatings, Plast. Chem. Papers, $\underline{33}$(2), 485-492.

S. Wolpert, J.J. Wojtkowiak, 1972, ACS Div. Org. Coatings, Plast. Chem. Papers, $\underline{32}$(2), 456-461.

S. Wu, 1976, Polym. Plast. Tech. Eng., $\underline{7}$(2), 119-220.

U. Zorll, 1972, Progr. Org. Coatings, $\underline{1}$, 113-154.

U. Zorll, 1963, Deutsche Farben-Zeitschrift, $\underline{17}$(1), 6-12.

NOMENCLATURE

a   radius of wire of electrode; radius of particle; half width of plate

b   ionic mobility, radius of electrode

C   calculation constant in interparticulate electrostatic force

C_D drag coefficient

d   diameter

d_p diameter of particle

E   field strength, resultant field

E_o Uniform field

E_c critical electrical breakdown strength

F   Force

F_{A_x} force between particles of opposite charge in x direction

F_{D_x} drag force in x direction

F_{E_x} field force acting on particle in x direction

F_{I_x} image force in x direction

F_{R_x} force between particles of like charge in x direction

GT   distance between gun and target

l   half width of plate

L   distance between gun and target

m   roughness factor

q   charge on particle

q_s saturation charge

Q_a charge density of theoretical layer of charge

r   radial distance from electrode

r_c radius of curvature of corona glow region

R   calculation variable (define in Section 5.5.2); distance between two particles

Re_p particle Reynold's Number

t   time; thickness of theoretical layer of charge

u   velocity of air in x direction

U   uniform air velocity

v   velocity of air in y direction

V_{rel} relative velocity between air and particle

V   voltage potential

V_o voltage potential at electrode

x   displacement in X-direction

y   displacement in Y-direction

z   displacement in Z-direction

θ Angle to horizontal; calculation variable as defined in section

ε dielectric constant of powder

ε_o permittivity of free space

μ viscosity of fluid

ρ density of fluid

ρ_f density of fluid

ρ_i ionic charge density

τ time constant

ϕ potential function

ψ steam function

Subscripts for use with x, y, q, d and R

i   refers to a packed particle

j   refers to the image of a packed particle

k   refers to the image of the oncoming particle

o   refers to the oncoming particle

APPENDIX A

GLOSS TEST RESULTS

Table A1. **Gloss Test Results at Various Film Thicknesses for Commercial Powder**

		Film Thickness (μm)												
		22	27	33	37	42	47	52	56	62	67	74	85	100
Gloss Factor	Average	20.68	22.04	26.30	27.19	26.43	28.07	28.04	29.95	27.49	30.45	29.34	30.91	30.99
	Standard Deviation	1.36	0.92	1.79	1.11	4.44	0.80	1.60	1.84	1.64	1.25	1.71	2.23	1.26
	Probable Error	0.608	0.411	0.801	0.496	1.986	0.358	0.716	0.823	0.733	0.559	0.765	0.997	0.563
Peak Height (mV)	Average	99.4	101.2	102.6	103.8	102.8	105.6	104.6	106.0	105.2	108.8	103.2	108.2	105.8
	Standard Deviation	2.94	2.14	1.96	1.72	6.55	2.42	3.14	3.16	3.25	3.66	2.79	3.92	3.31
	Probable Error	1.315	0.957	0.877	0.769	2.929	1.082	1.404	1.413	1.453	1.637	1.248	1.753	1.480
Width at Half Peak Height (DEG)	Average	4.82	4.60	3.92	3.82	3.89	3.76	3.74	3.55	3.83	3.57	3.53	3.51	3.42
	Standard Deviation	0.24	0.14	0.21	0.10	0.32	0.06	0.13	0.16	0.14	0.09	0.24	0.17	0.07
	Probable Error	0.107	0.063	0.094	0.045	0.143	0.027	0.058	0.072	0.063	0.040	0.107	0.076	0.031

Table A2.   Gloss Test Results at Various Film Thicknesses for <10µm Size Range Powder

		Film Thickness (µm)											
		16	22	28	32	37	44	56	62	67	74	84	95
Gloss Factor	Average	21.48	17.36	18.25	17.71	22.35	18.56	25.31	18.38	25.28	22.91	25.10	24.46
	Standard Deviation	3.24	0.46	3.20	3.30	1.93	2.68	4.49	2.71	3.36	2.23	2.54	2.82
	Probable Error	1.449	0.206	1.431	1.476	0.863	1.199	2.008	1.212	1.503	0.997	1.136	1.261
Peak Height (mV)	Average	99.8	90.2	92.8	90.8	94.4	90.8	97.2	88.0	97.2	96.2	95.2	96.4
	Standard Deviation	5.78	2.32	4.78	4.12	3.14	2.93	5.19	3.52	5.74	3.71	3.54	4.03
	Probable Error	2.584	1.038	2.138	1.843	1.404	1.310	2.321	1.574	2.567	1.659	1.583	1.802
Width at Half Peak Height (DEG)	Average	4.73	5.20	5.20	5.29	4.25	4.96	3.94	4.86	3.89	4.23	3.82	3.98
	Standard Deviation	0.56	0.12	0.64	0.86	0.29	0.51	0.58	0.47	0.34	0.32	0.24	0.33
	Probable Error	0.250	0.0537	0.286	0.385	0.130	0.228	0.259	0.210	0.152	0.143	0.107	0.148

Table A3. Gloss Test Results at Various Film Thicknesses for 10-20μm Size Range Powder

		Film Thickness (μm)								
		18	22	27	32	37	42	46	56	62
Gloss Factor	Average	29.88	28.57	29.75	31.59	31.21	32.24	29.25	30.55	31.99
	Standard Deviation	2.92	0.87	1.53	1.96	0.79	1.04	2.43	1.71	0.73
	Probable Error	1.306	0.389	0.684	0.877	0.353	0.465	1.087	0.765	0.326
Peak Height (mV)	Average	110.4	105.4	108.6	111.2	109.0	110.0	106.8	107.2	108.6
	Standard Deviation	2.42	2.33	2.58	2.04	1.79	2.76	2.14	4.79	1.85
	Probable Error	1.082	1.042	1.154	0.912	0.801	1.234	0.957	2.142	0.827
Width at Half Peak Height (DEG)	Average	3.73	3.69	3.66	3.53	3.49	3.41	3.67	3.51	3.40
	Standard Deviation	0.34	0.09	0.12	0.17	0.07	0.08	0.27	0.09	0.09
	Probable Error	0.152	0.040	0.055	0.076	0.031	0.036	0.121	0.040	0.040

Table A4. **Gloss Test Results at Various Film Thicknesses for 20-30μm Size Range Powder**

		Film Thickness (μm)											
		27	32	37	42	48	52	57	62	67	71	77	84	100
Gloss Factor	Average	28.83	29.59	30.18	30.42	31.08	30.35	31.02	29.64	29.24	31.43	31.30	29.34	29.37
	Standard Deviation	1.60	0.74	0.91	1.70	1.58	1.34	1.65	0.86	1.86	1.87	3.29	4.22	4.75
	Probable Error	0.716	0.331	0.407	0.760	0.707	0.599	0.738	0.385	0.832	0.836	1.471	1.887	2.124
Peak Height (mV)	Average	104.2	106.8	107.0	107.2	107.8	107.8	106.0	103.0	104.8	107.6	105.0	103.8	103.6
	Standard Deviation	2.93	0.98	1.10	3.66	1.17	1.83	2.19	3.74	2.79	3.44	4.52	5.31	3.50
	Probable Error	1.310	0.438	0.492	1.637	0.523	0.818	0.979	1.673	1.248	1.538	2.021	2.375	1.565
Width at Half Peak Height (DEG)	Average	3.62	3.61	3.55	3.53	3.48	3.56	3.42	3.48	3.59	3.43	3.38	3.75	3.59
	Standard Deviation	0.11	0.08	0.09	0.13	0.16	0.13	0.12	0.14	0.15	0.16	0.23	0.48	0.42
	Probable Error	0.049	0.036	0.040	0.058	0.072	0.058	0.0537	0.062	0.067	0.072	0.103	0.215	0.189

Table A5. Gloss Test Results at Various Film Thicknesses for 30-40μm Size Range Powder

		Film Thickness (μm)														
		29	33	37	42	48	52	57	62	67	72	77	82	87	93	104
Gloss Factor	Average	27.09	28.23	27.38	29.63	28.51	28.25	30.59	28.58	28.00	26.73	26.91	26.21	27.30	27.06	28.60
	Standard Deviation	1.32	1.49	0.99	2.29	1.98	2.30	1.36	0.87	1.37	0.69	1.55	1.48	1.01	2.49	2.18
	Probable Error	0.59	0.67	0.44	1.02	0.89	1.03	0.61	0.39	0.61	0.31	0.69	0.66	0.45	1.11	0.93
Peak Height (mV)	Average	106.4	107.8	106.4	107.6	105.4	105.2	110.25	106.2	106.6	105.8	104.6	102.4	104.8	104.8	108.0
	Standard Deviation	2.33	2.48	3.56	2.06	2.15	4.79	3.34	1.94	1.36	0.98	1.62	2.87	1.33	3.82	1.9
	Probable Error	0.91	1.11	1.59	0.92	0.96	2.14	1.49	0.87	0.61	0.44	0.72	1.28	0.60	1.71	0.85
Width at Half Peak Height (DEG)	Average	3.93	3.83	3.89	3.65	3.71	3.74	3.61	3.73	3.82	3.96	3.90	3.92	3.84	3.90	3.80
	Standard Deviation	0.12	0.14	0.16	0.21	0.20	0.16	0.07	0.12	0.20	0.10	0.18	0.16	0.15	0.30	0.31
	Probable Error	0.05	0.06	0.07	0.09	0.09	0.07	0.03	0.05	0.09	0.05	0.08	0.07	0.07	0.13	0.14

Table A6. Gloss Test Results at Various Film Thicknesses for 40–50μm Size Range Powder

		Film Thickness (μm)												
		33	37	42	47	52	57	63	75	84	92	97	106	135
Gloss Factor	Average	25.97	25.85	28.58	28.38	27.46	26.95	26.92	28.86	30.37	27.97	28.00	27.42	28.61
	Standard Deviation	0.83	3.72	2.19	1.58	0.97	1.73	1.63	3.05	0.94	2.68	1.43	2.36	2.59
	Probable Error	0.371	1.664	0.979	0.707	0.434	0.774	0.729	1.364	0.420	1.199	0.640	1.055	1.158
Peak Height (mV)	Average	104.4	104.4	105.0	106.8	103.0	104.6	103.0	106.0	108.2	104.6	105.4	105.6	107.0
	Standard Deviation	1.96	2.28	2.10	2.79	1.10	4.36	2.37	4.15	1.60	3.72	1.96	3.01	2.76
	Probable Error	0.88	1.02	0.94	1.25	0.49	1.95	1.06	1.86	0.72	1.66	0.88	0.35	1.23
Width at Half Peak Height (DEG)	Average	4.02	4.10	3.69	3.77	3.75	3.89	3.83	3.70	3.57	3.76	3.77	3.87	3.76
	Standard Deviation	0.10	0.56	0.24	0.18	0.09	0.14	0.17	0.27	0.10	0.25	0.15	0.23	0.26
	Probable Error	0.05	0.25	0.11	0.08	0.04	0.06	0.08	0.12	0.05	0.12	0.07	0.10	0.12

Table A7. Gloss Test Results at Various Film Thicknesses for +50μm Size Range Powder

		Film Thickness (μm)														
		38	43	47	52	57	62	67	71	76	81	87	92	97	104	122
Gloss Factor	Average	27.10	28.15	28.71	30.99	28.92	29.32	30.00	30.89	29.72	29.09	28.99	29.37	29.00	29.59	30.70
	Standard Deviation	2.46	2.33	0.83	1.22	1.37	1.10	1.46	3.01	2.27	3.26	1.22	1.16	1.59	2.04	1.91
	Probable Error	1.10	1.04	0.37	0.55	0.61	0.49	0.65	1.35	1.02	1.46	0.55	0.52	0.71	0.91	0.85
Peak Height (mV)	Average	103.8	106.2	105.2	108.2	105.6	105.8	105.4	106.8	105.0	101.8	104.8	106.2	104.8	107.00	107.20
	Standard Deviation	3.19	2.04	2.48	2.04	2.73	3.71	1.02	1.94	2.45	8.35	1.72	2.14	3.19	2.68	1.47
	Probable Error	1.43	0.91	1.11	0.91	1.22	1.66	0.46	0.87	1.10	3.73	0.77	0.96	1.43	1.20	0.66
Width at Half Peak Height (DEG)	Average	3.85	3.80	3.66	3.49	3.66	3.61	3.52	3.49	3.55	3.51	3.62	3.62	3.62	3.63	3.50
	Standard Deviation	0.25	0.33	0.04	0.09	0.10	0.11	0.16	0.29	0.21	0.17	0.10	0.11	0.13	0.20	0.18
	Probable Error	0.11	0.15	0.02	0.04	0.05	0.05	0.07	0.13	0.09	0.08	0.05	0.05	0.06	0.09	0.08

Table A8. **Results of Linear Regression Fit to Experimental Data from Gloss Test**

Powder Type	Measured Quantity	Slope	Y Intercept	Correlation Coefficient	t = 15	t = 100
Commercial	Gloss Factor	0.117	21.17	0.850	22.92	32.87
	Peak Height	0.0829	99.91	0.726	101.2	108.2
	Width	-0.0145	4.63	0.802	4.41	3.18
<10μm	Gloss Factor	0.084	17.13	0.669	18.4	25.5
	Peak Height	0.0292	92.58	0.210	93.0	95.5
	Width	-0.0167	5.39	0.750	5.14	3.72
10-20μm	Gloss Factor	0.043	28.93	0.505	29.6	33.2
	Peak Height	-0.0193	109.31	0.157	109.0	107.4
	Width	-0.006	3.79	0.723	3.70	3.19
20-30μm	Gloss Factor	0.0027	29.98	0.065	30.0	30.3
	Peak Height	-0.038	107.97	0.473	107.4	104.2
	Width	0.00	3.54	0.017	3.54	3.54
30-40μm	Gloss Factor	-0.014	28.81	0.274	38.6	27.4
	Peak Height	-0.0268	107.8	0.330	107.4	105.1
	Width	0.0041	3.75	0.234	3.81	4.16
40-50μm	Gloss Factor	0.018	26.53	0.450	26.8	28.3
	Peak Height	0.024	103.5	0.480	103.9	105.9
	Width	-0.0018	3.93	0.395	3.90	3.75
+50μm	Gloss Factor	0.019	27.98	0.448	28.3	29.9
	Peak Height	0.0083	104.98	0.131	105.1	105.8
	Width	-0.0022	3.77	0.495	3.74	3.55

Table A9. **Linear Regression Results for Gloss Test at**
Various Film Thicknesses

Using data from Table 3.2

Film Thickness		30μm	50μm	70μm	100μm
Gloss Factor	Slope	−0.066	−0.069	−0.077	−0.086
	Intercept	31.15	31.56	32.16	32.87
	d = 15μm	30.16	30.52	30.96	31.58
	d = 55μm	27.52	27.76	27.88	28.14
Peak Height	Slope	−0.097	−0.077	−0.053	−0.012
	Intercept	109.8	108.9	107.8	106.1
	d = 15μm	108.3	107.7	107.0	105.9
	d = 55μm	104.5	104.7	104.9	105.5
Peak Width	Slope	0.0052	0.0065	0.0079	0.0073
	Intercept	3.52	3.44	3.36	3.34
	d = 15μm	3.60	3.54	3.48	3.45
	d = 55μm	3.81	3.80	3.79	3.74

Calculations do not include <10μm size range

FIGURE A1   GLOSS FACTOR VS. FILM THICKNESS
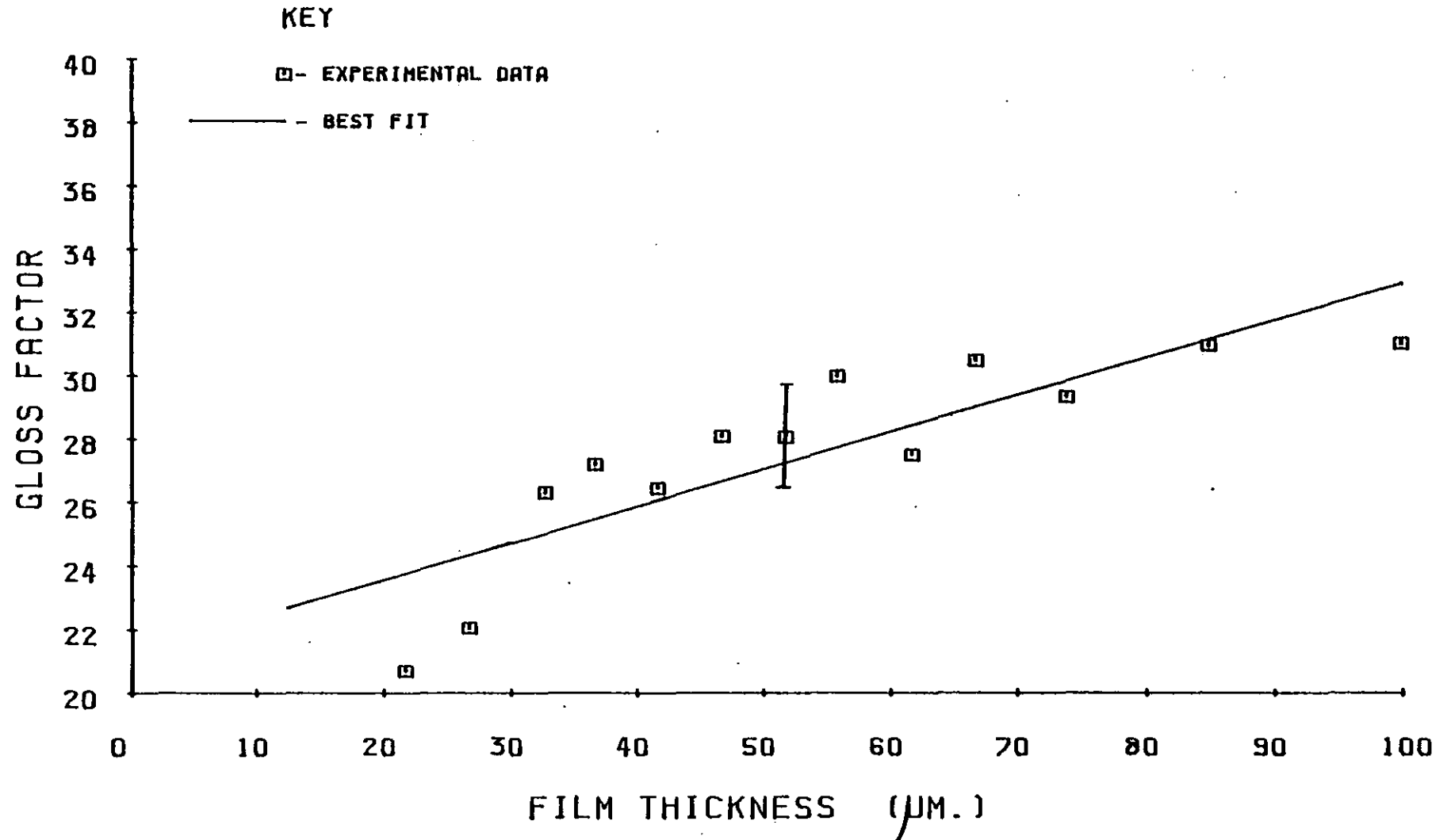
FIGURE A2   GLOSS FACTOR VS. FILM THICKNESS
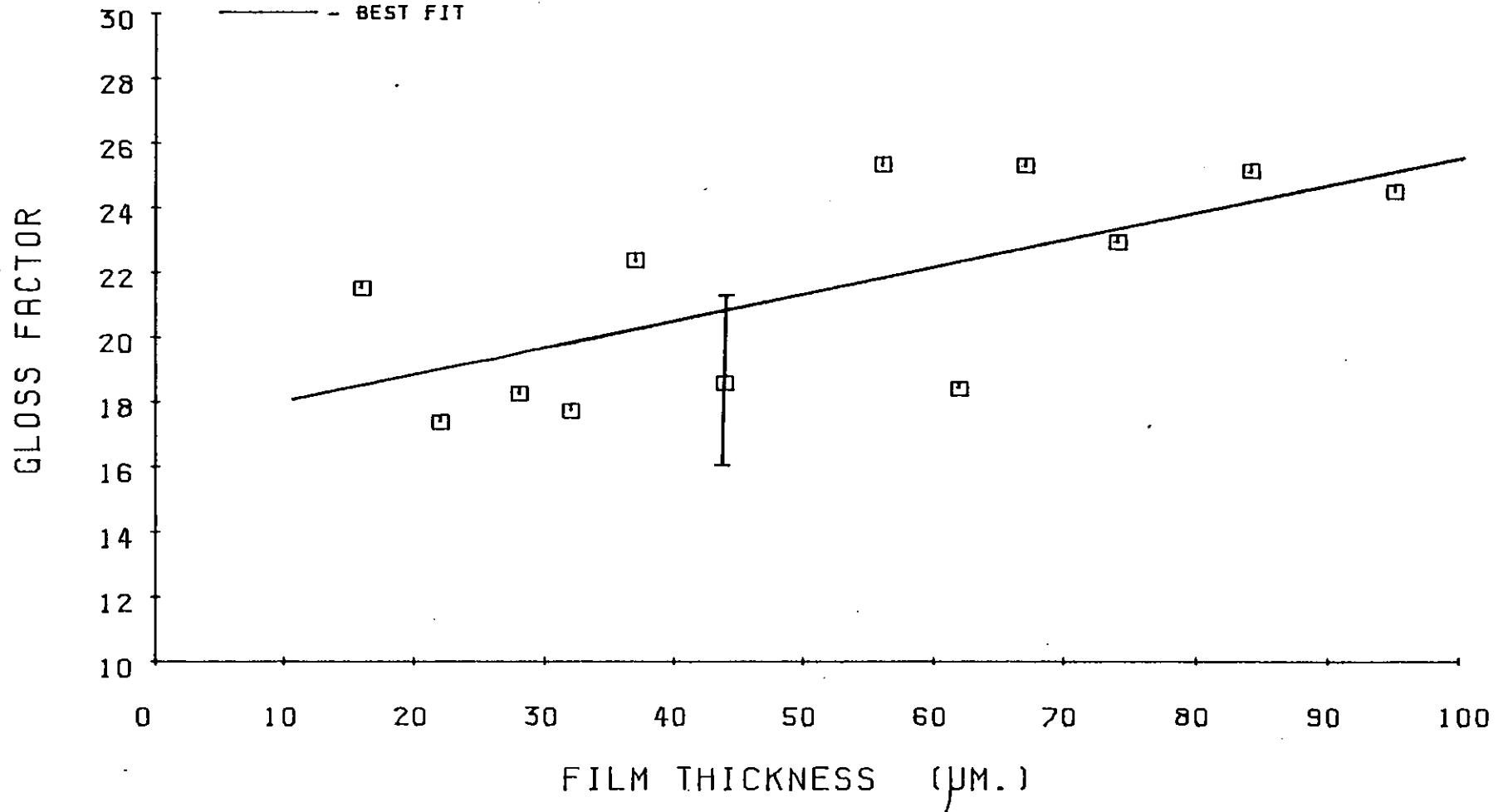
FIGURE A3   GLOSS FACTOR VS. FILM THICKNESS
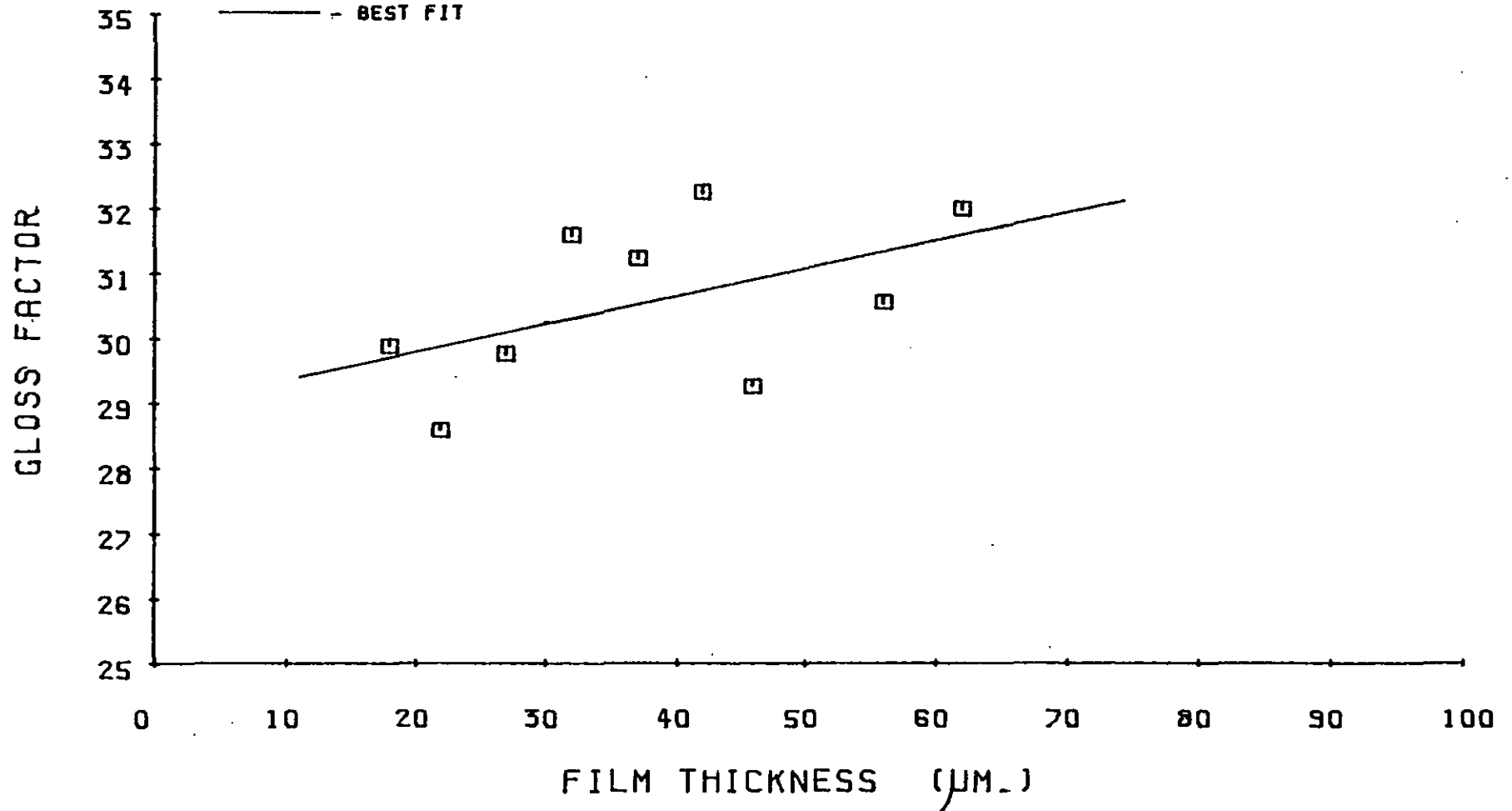
FIGURE A4   GLOSS FACTOR VS. FILM THICKNESS
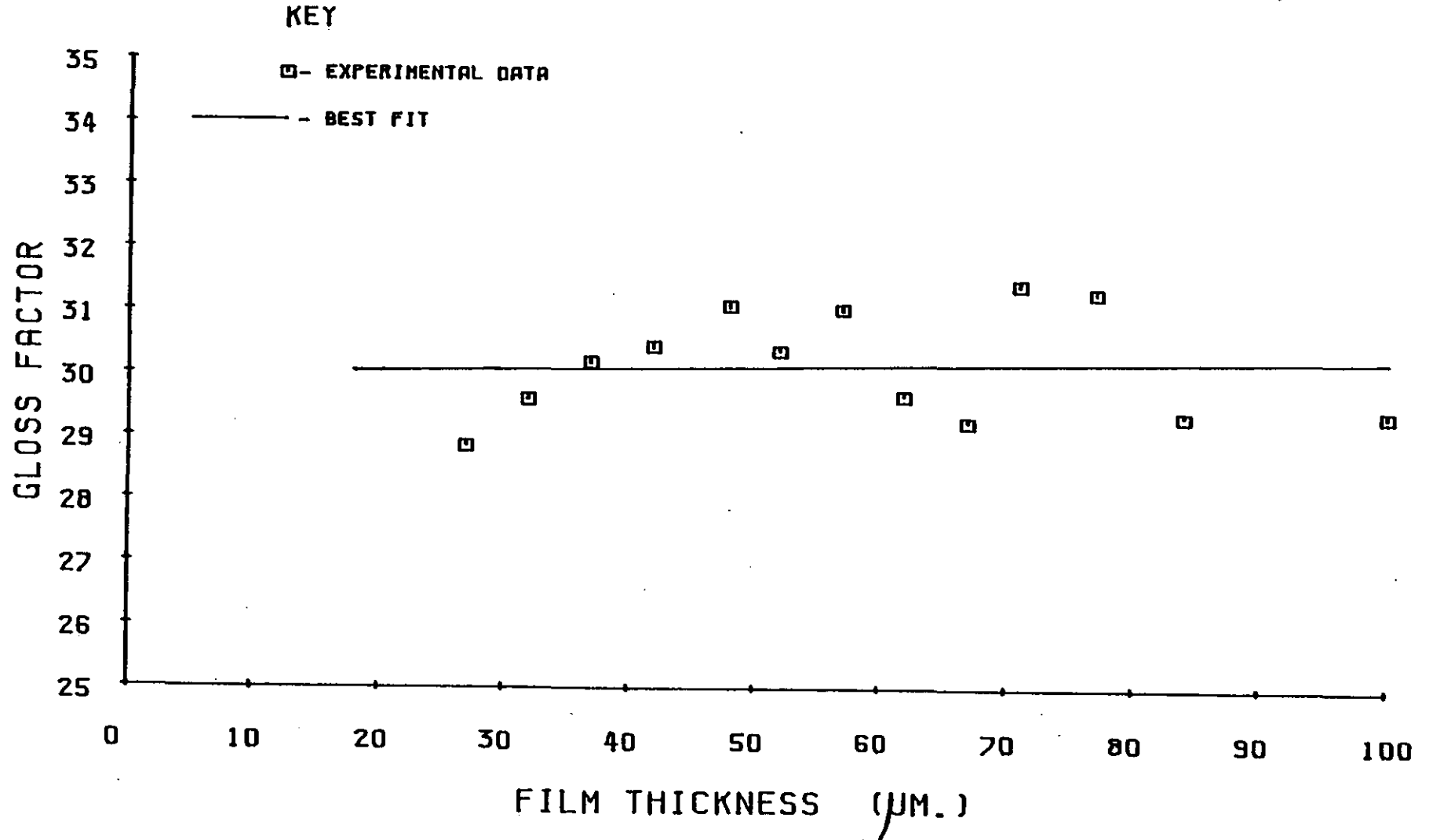
FIGURE A5   GLOSS FACTOR VS. FILM THICKNESS

POWDER SIZE RANGE : 30-40µM.

KEY

□- EXPERIMENTAL DATA
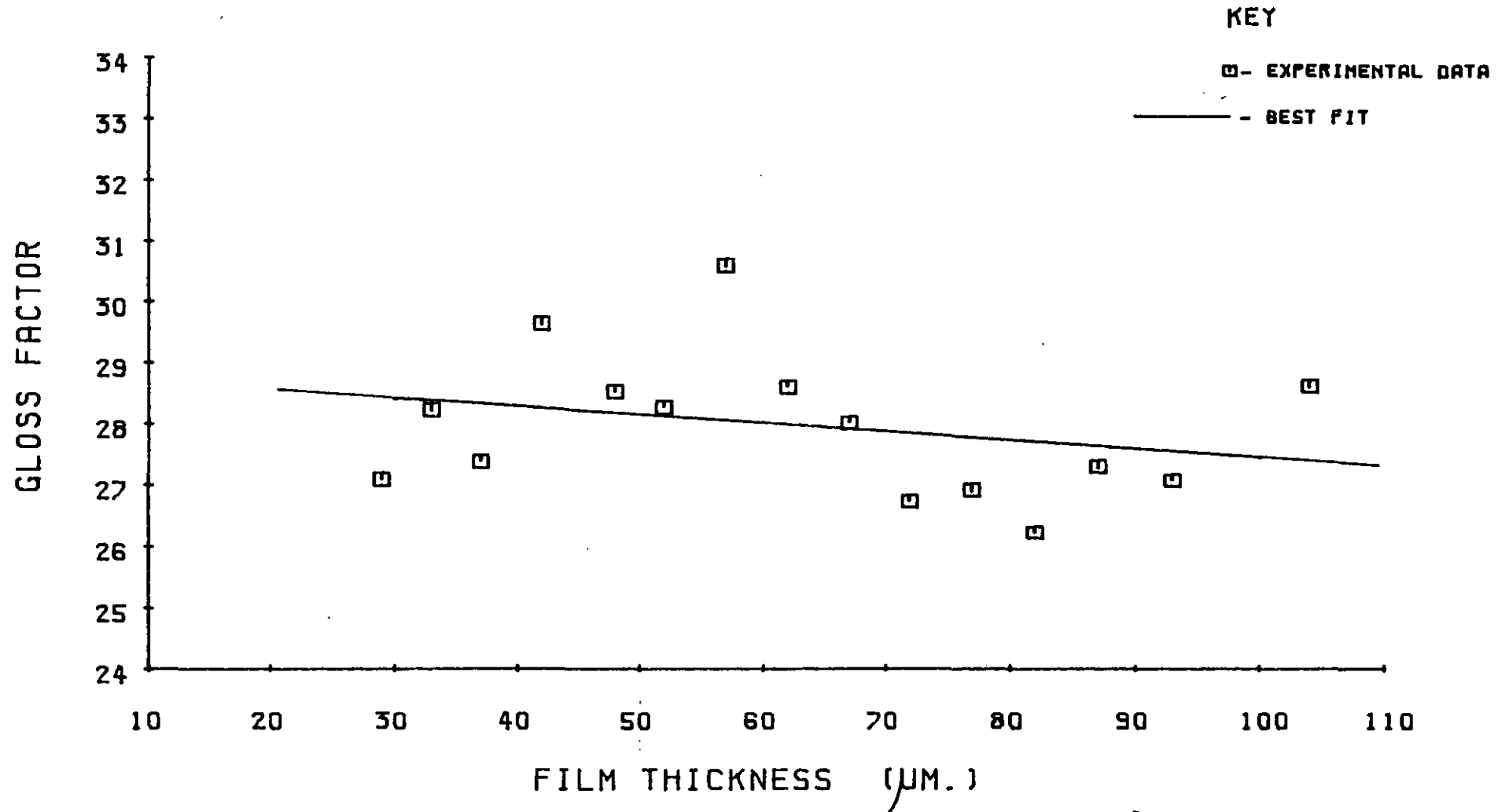
───── - BEST FIT

FIGURE A6   GLOSS FACTOR VS. FILM THICKNESS
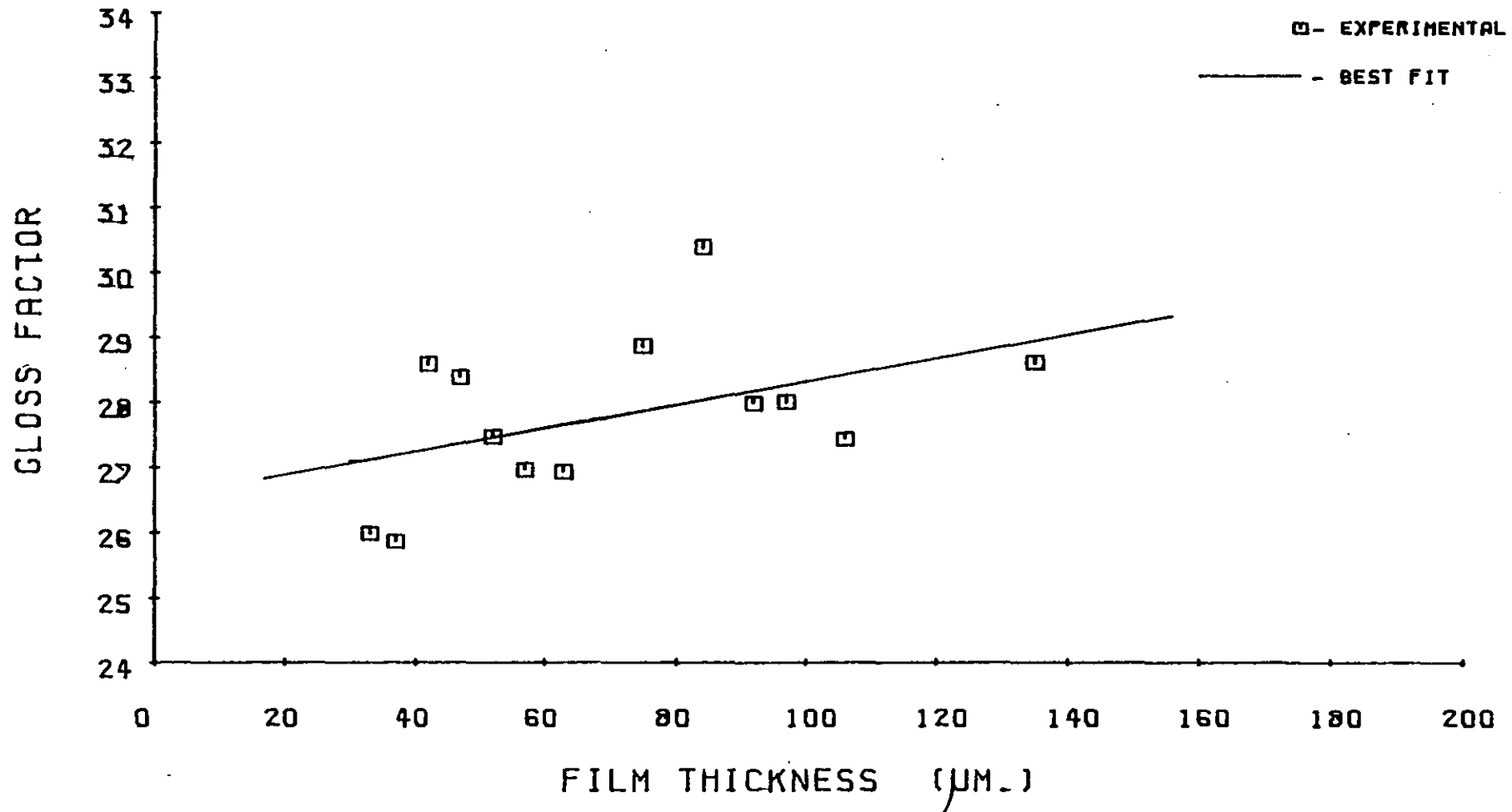
FIGURE A7   GLOSS FACTOR VS. FILM THICKNESS

POWDER SIZE RANGE : >50µM.

KEY

▣ – EXPERIMENTAL DATA
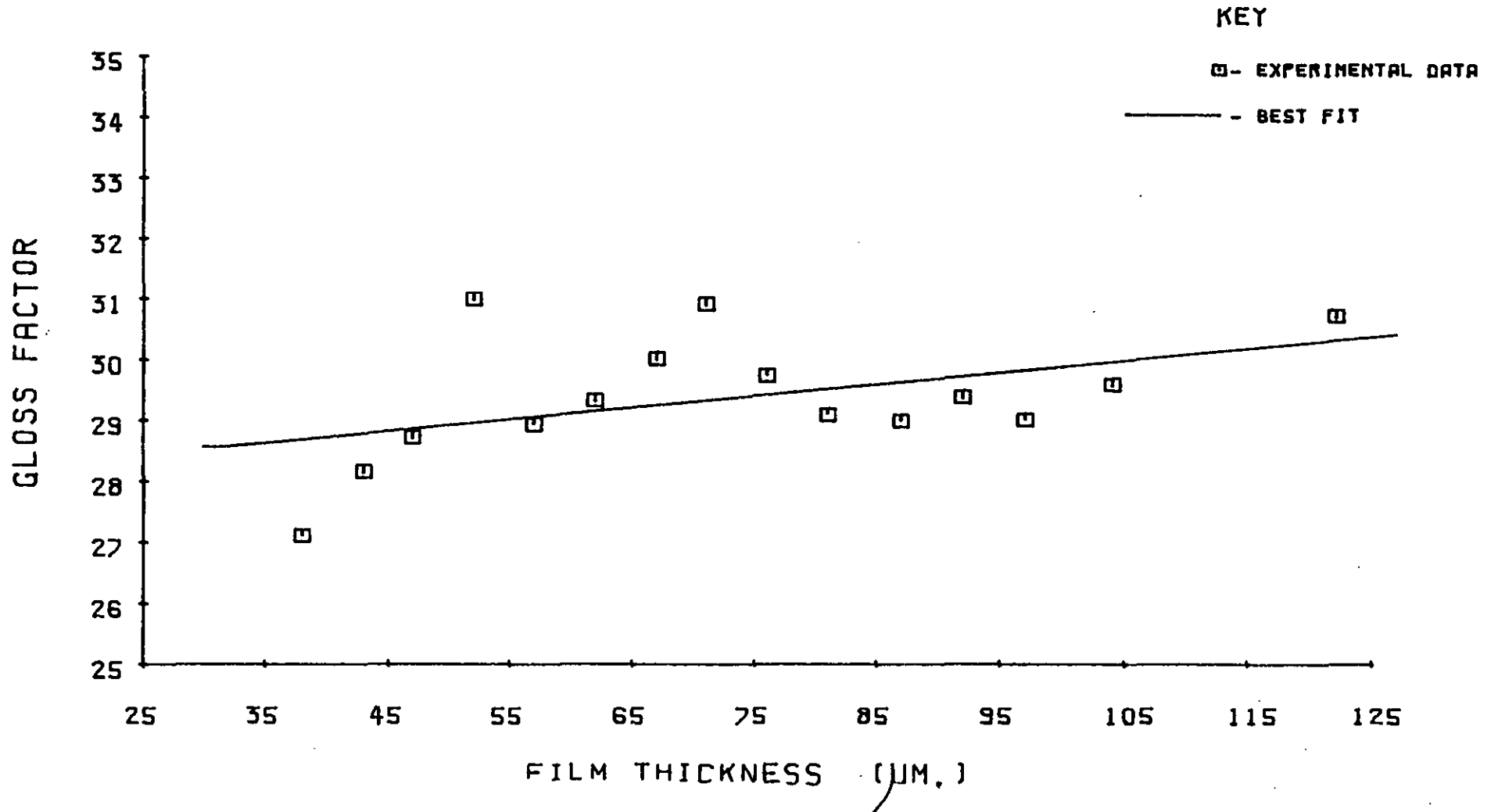
———— – BEST FIT

FIGURE A8   PEAK HEIGHT VS. FILM THICKNESS
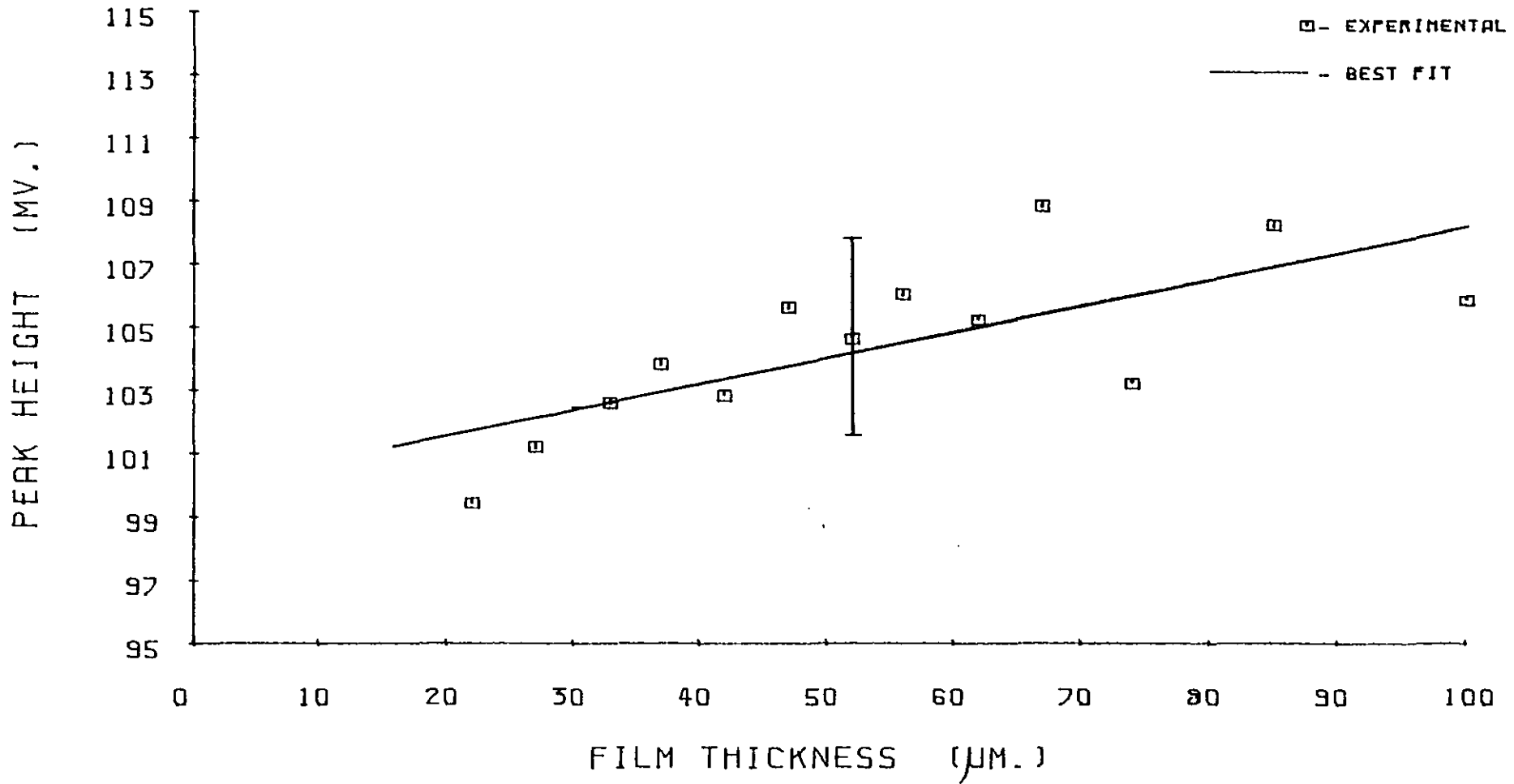
FIGURE A9 PEAK HEIGHT VS. FILM THICKNESS

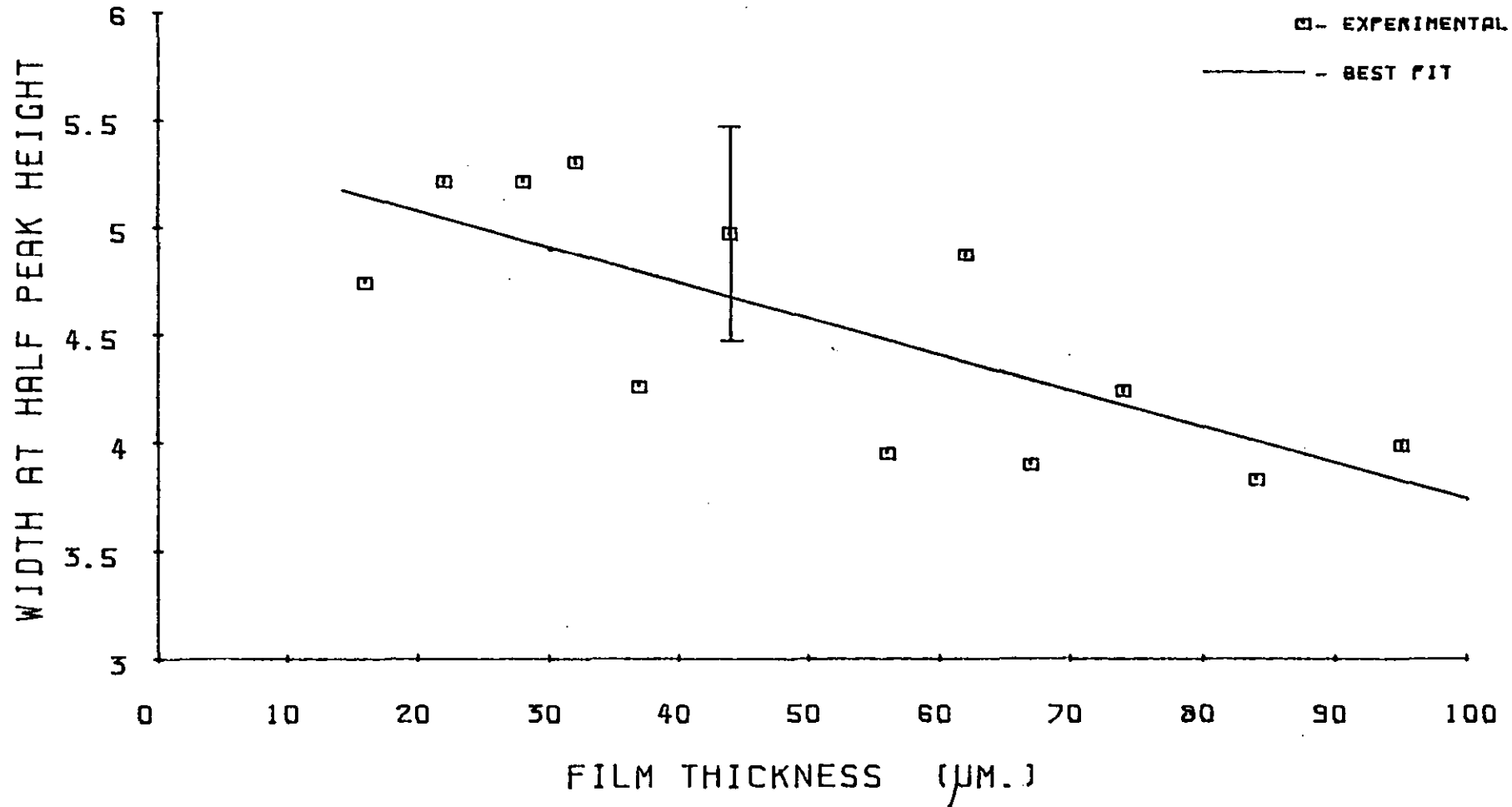POWDER SIZE RANGE : <10µM.

KEY

▣ – EXPERIMENTAL DATA

—— – BEST FIT
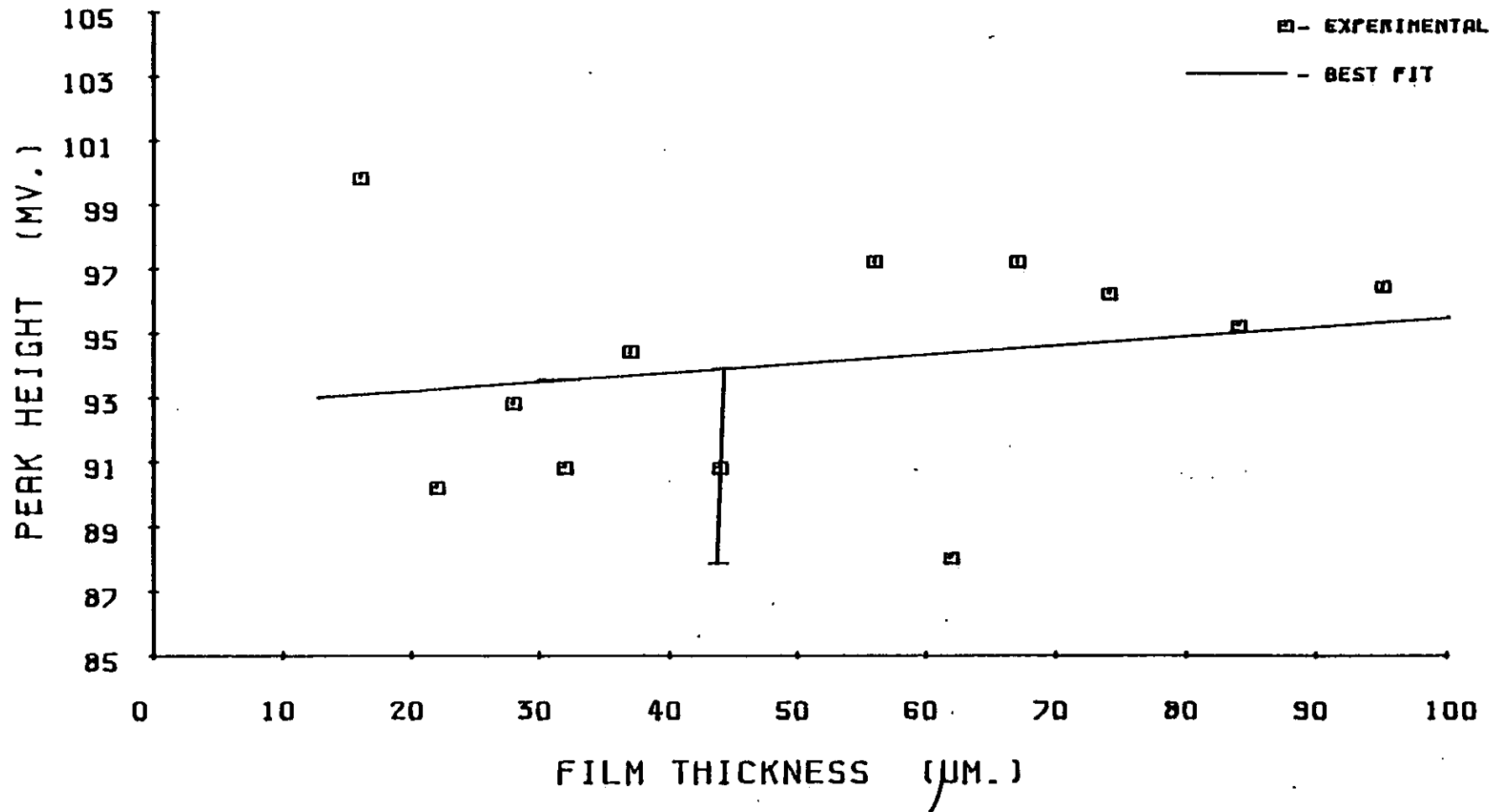
FIGURE A10   PEAK HEIGHT VS. FILM THICKNESS
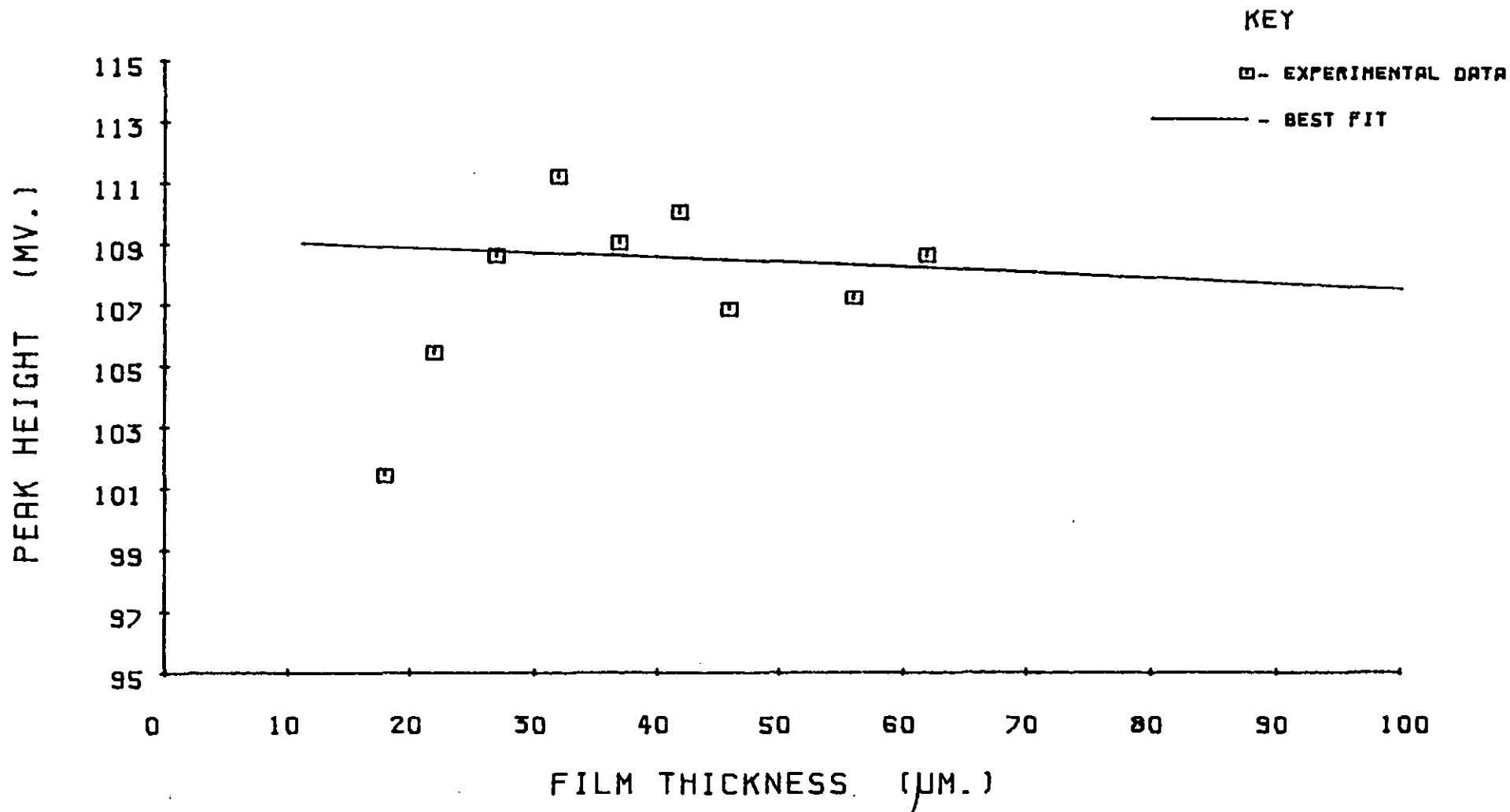
FIGURE A11   PEAK HEIGHT VS. FILM THICKNESS
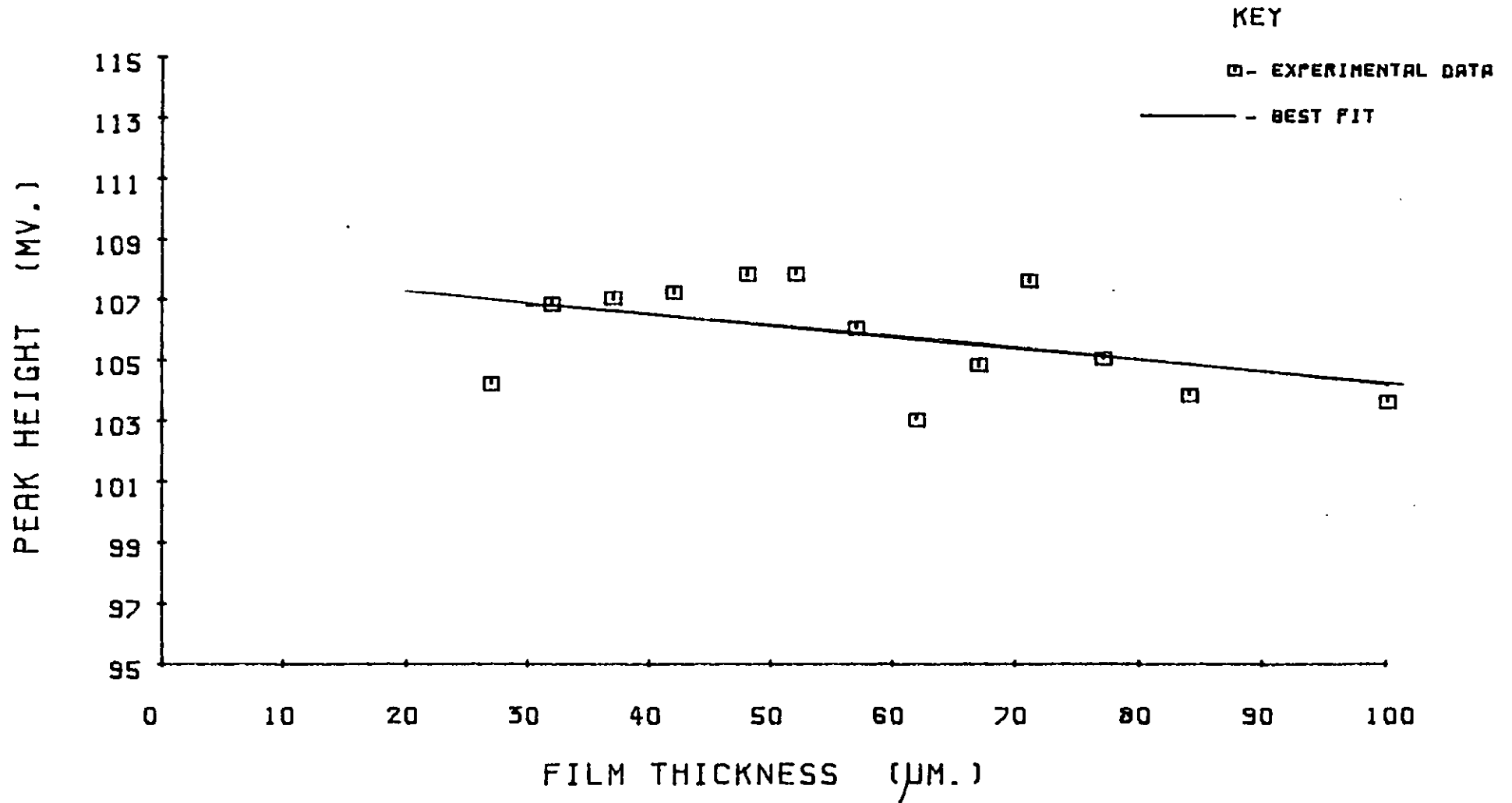
FIGURE A12   PEAK HEIGHT VS. FILM THICKNESS

POWDER SIZE RANGE : 30-40μM.
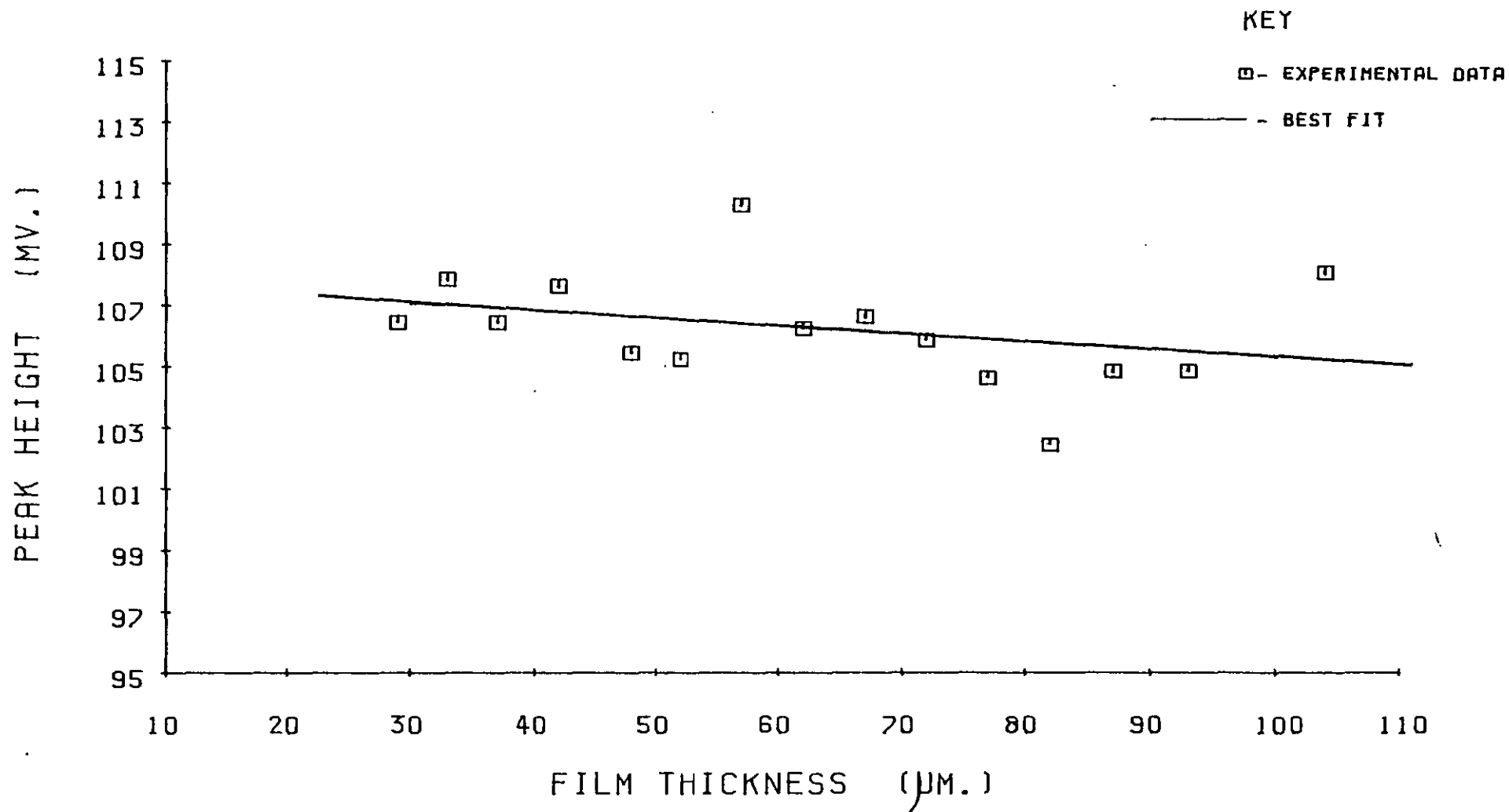
FIGURE A13   PEAK HEIGHT VS. FILM THICKNESS

POWDER SIZE RANGE : 40-50μM.

KEY

▣– EXPERIMENTAL DATA
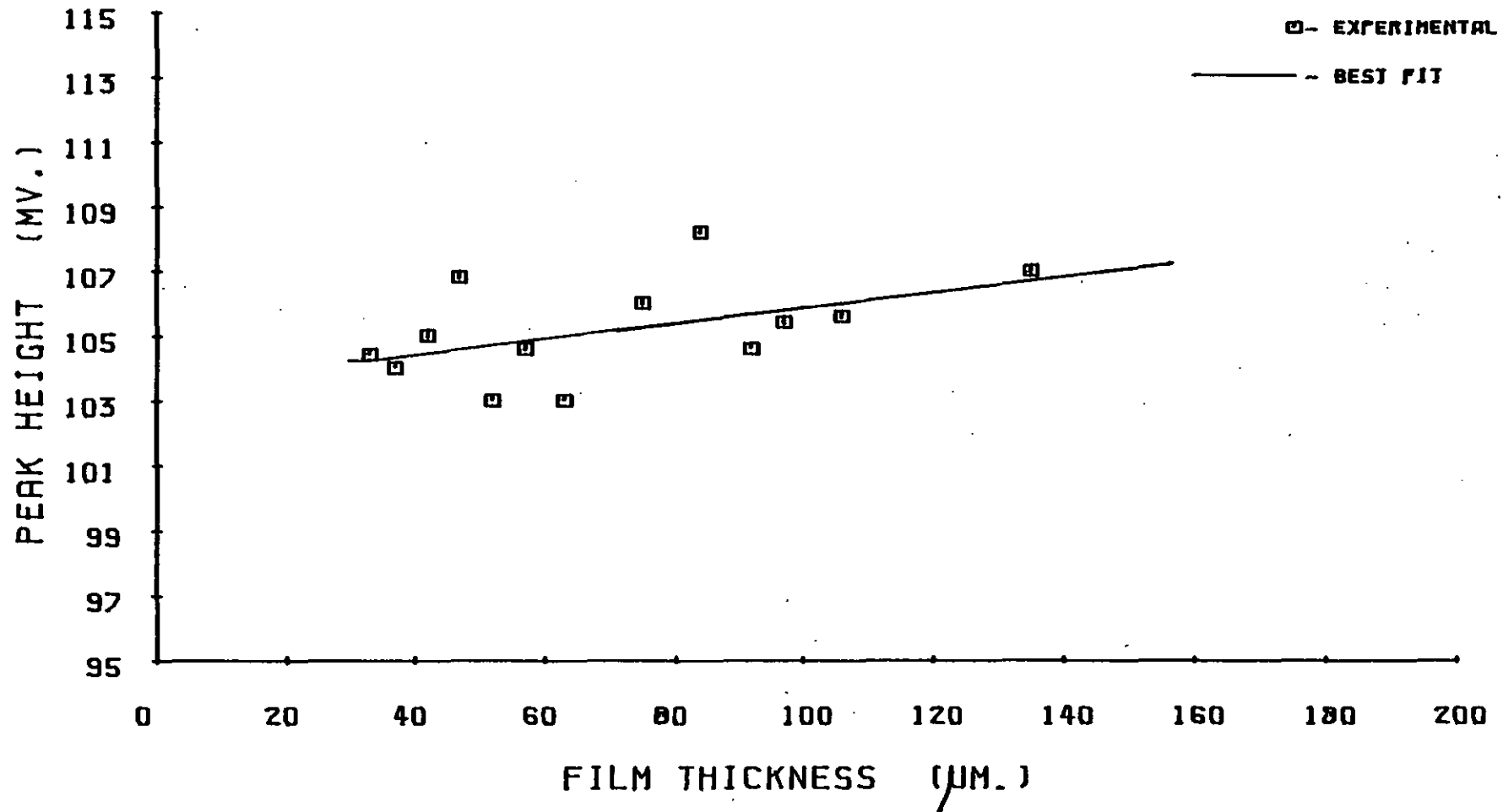
──── ~ BEST FIT

FIGURE A14   PEAK HEIGHT VS. FILM THICKNESS
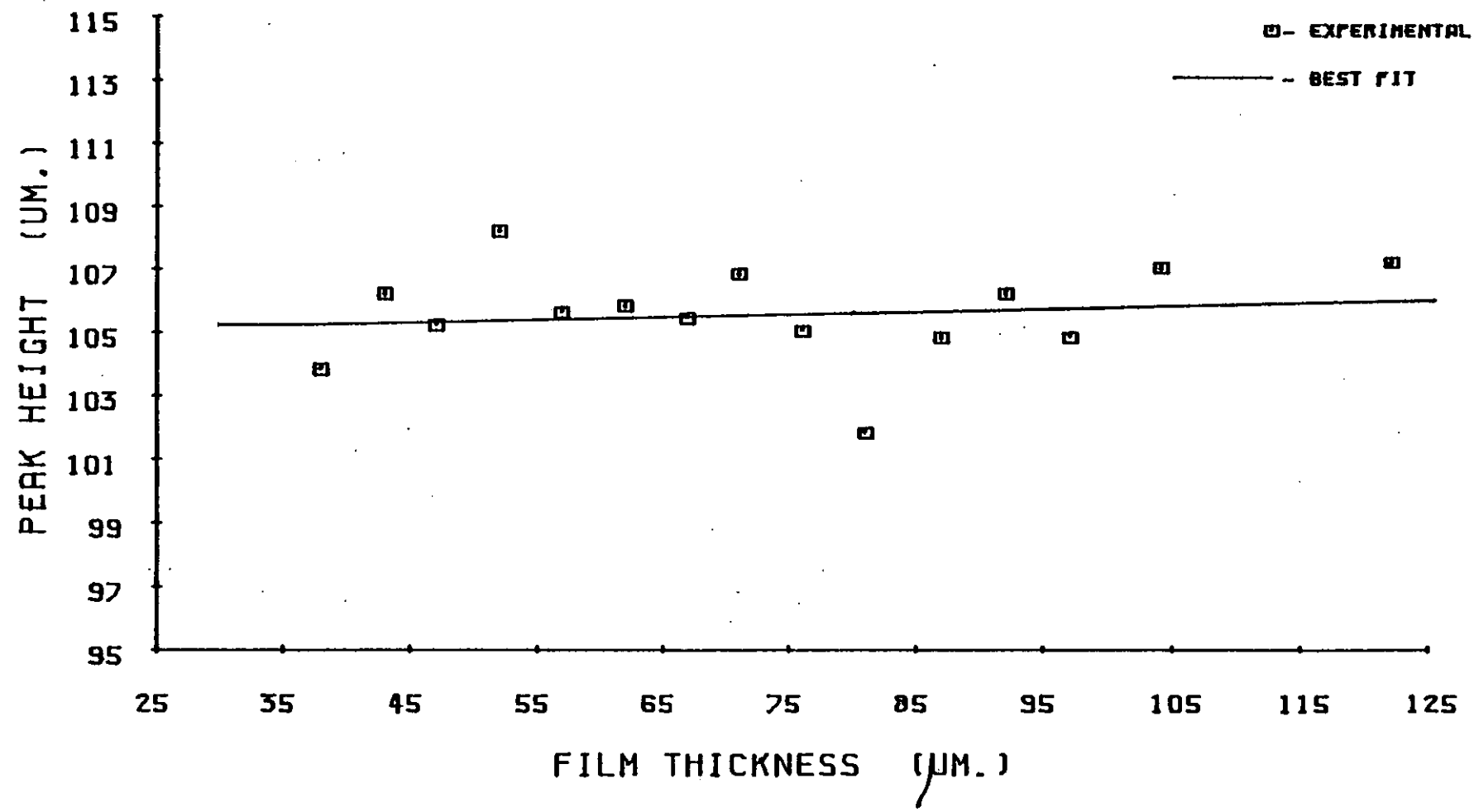
FIGURE A15   WIDTH AT HALF PEAK HEIGHT VS. FILM THICKNESS
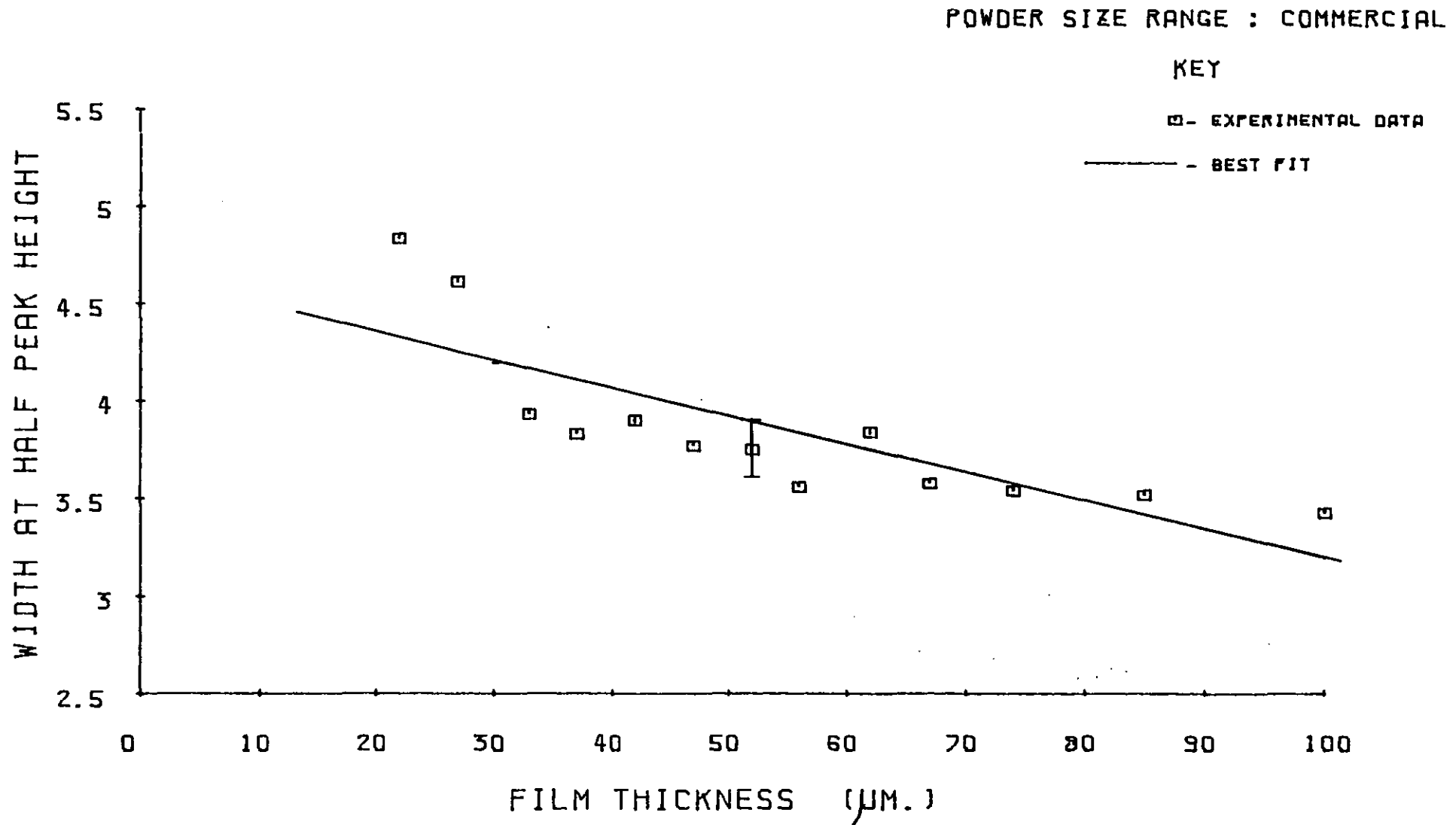
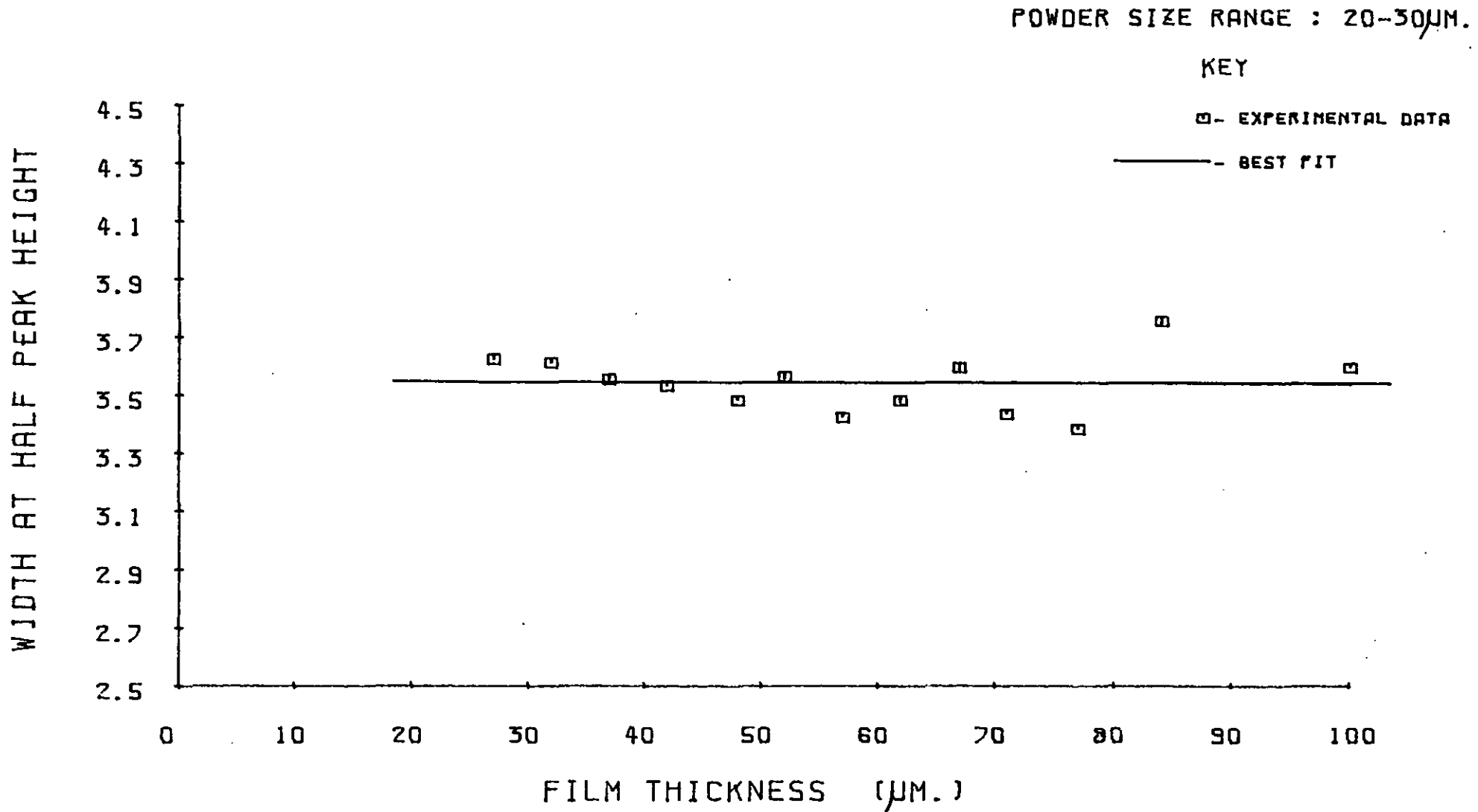FIGURE A16   WIDTH AT HALF PEAK HEIGHT VS. FILM THICKNESS

FIGURE A17   WIDTH AT HALF PEAK HEIGHT VS. FILM THICKNESS
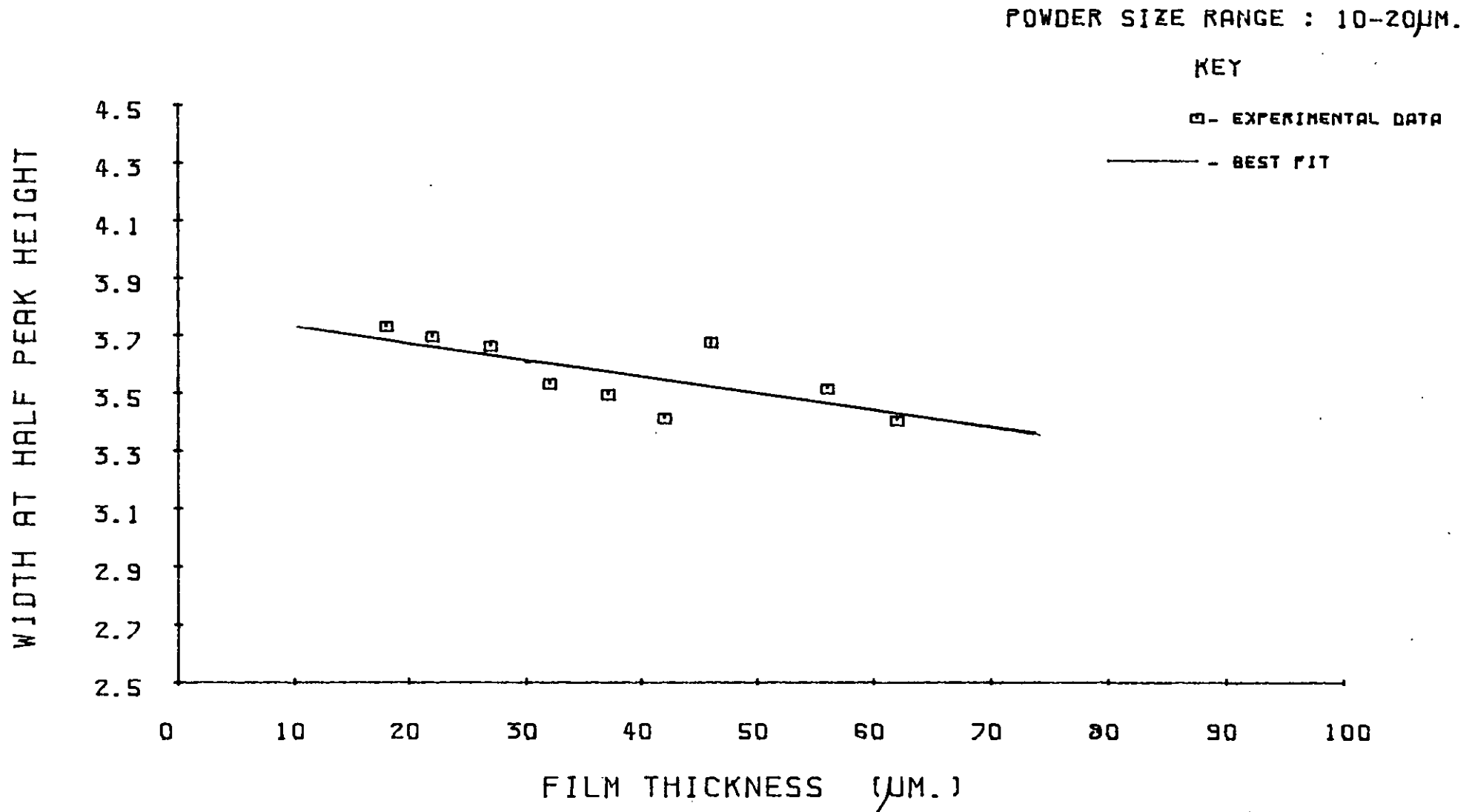
FIGURE A18   WIDTH AT HALF PEAK HEIGHT VS. FILM THICKNESS

FIGURE A19   WIDTH AT HALF PEAK HEIGHT VS. FILM THICKNESS

POWDER SIZE RANGE : 30-40μM.
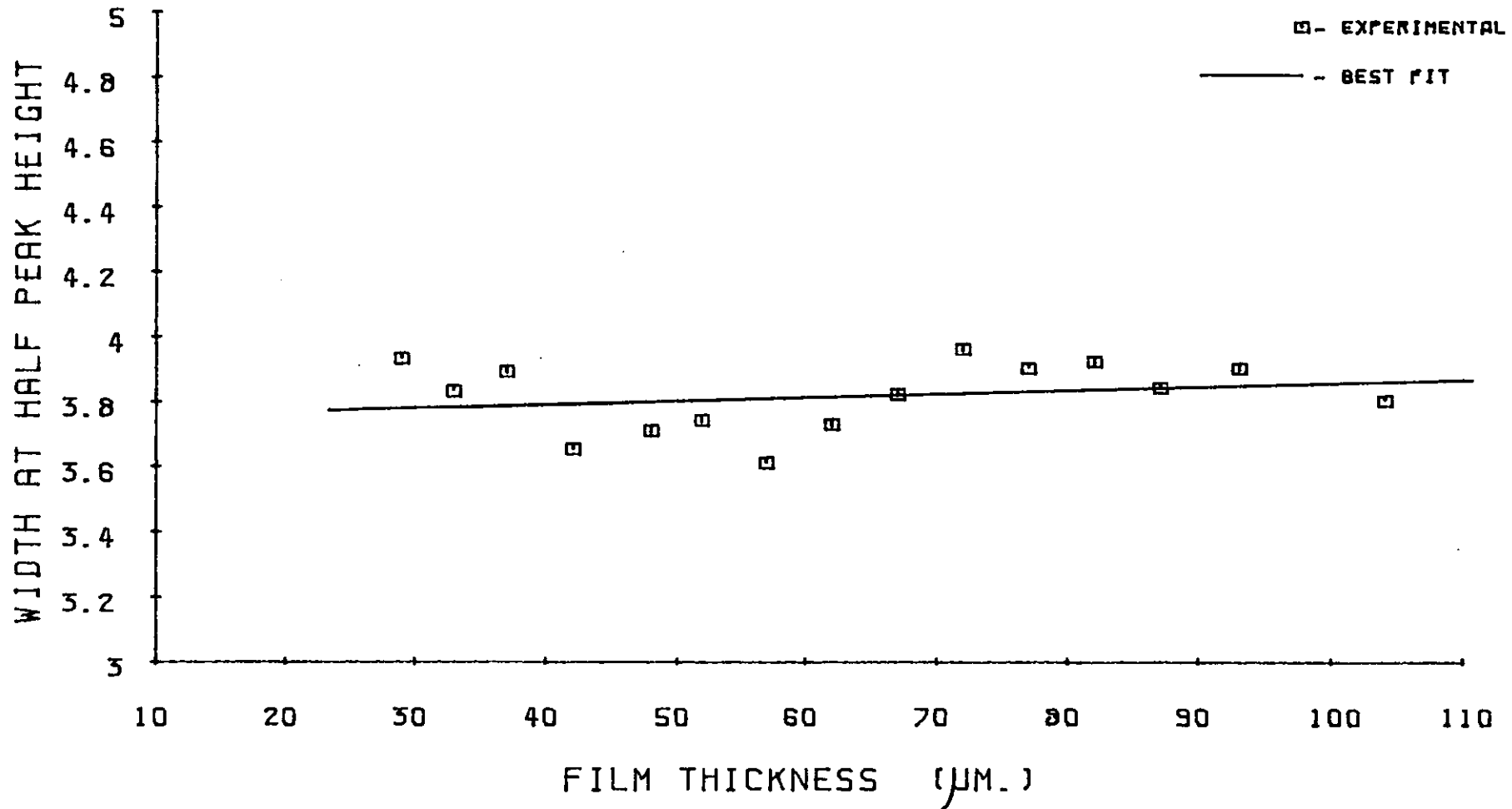
KEY

□ - EXPERIMENTAL DATA

——— - BEST FIT

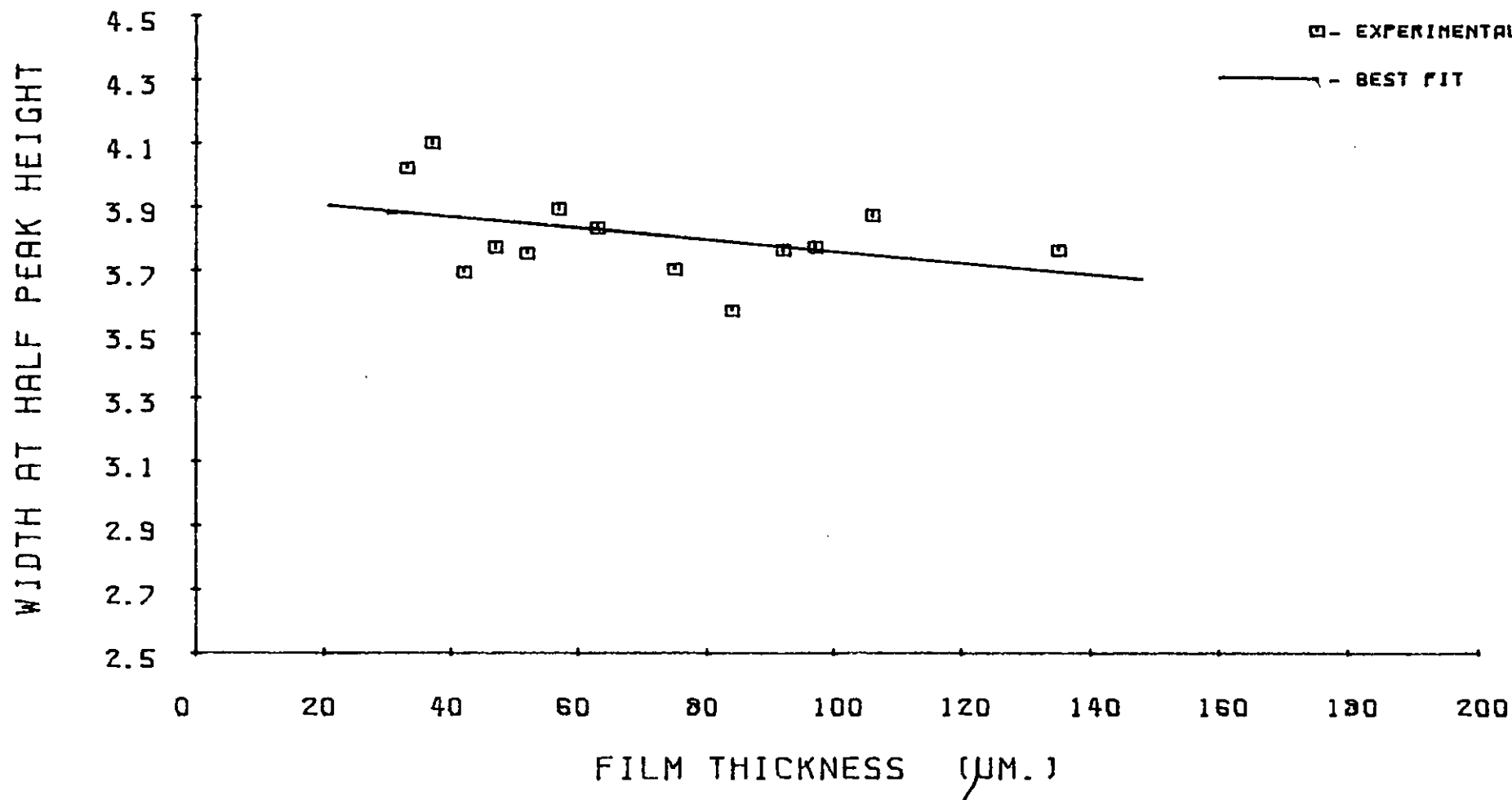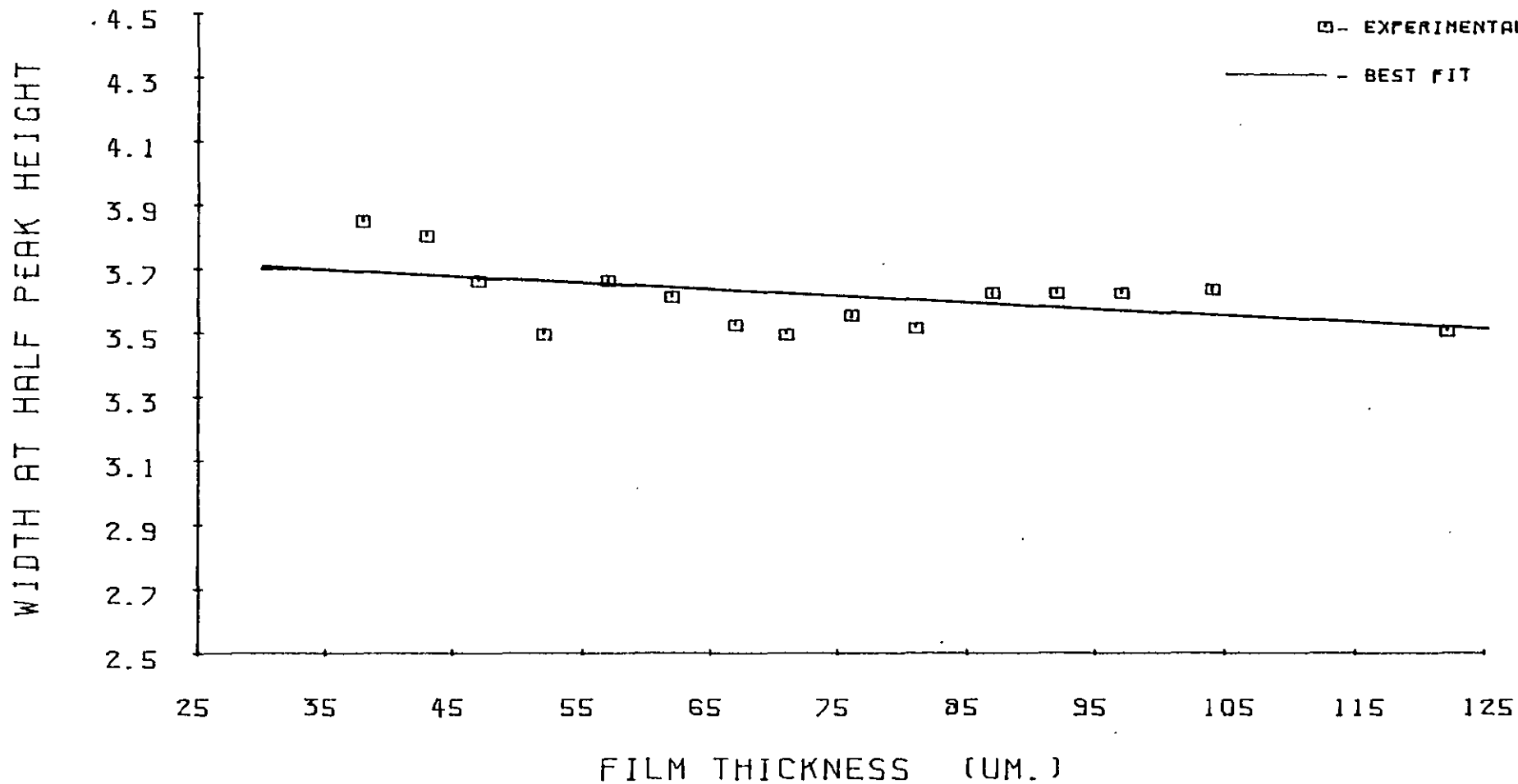FIGURE A20   WIDTH AT HALF PEAK HEIGHT VS. FILM THICKNESS

FIGURE A21   WIDTH AT HALF PEAK HEIGHT VS. FILM THICKNESS

APPENDIX B

ROUGHNESS TEST RESULTS

Table B1. **Surface Roughness Results at Various Film Thicknesses for Commercial Powder**

		Film Thickness (µm)												
		22	27	33	37	42	47	52	56	62	67	74	85	100
Roughness Average (µm)	Average	1.03	0.99	0.73	0.76	0.70	0.53	0.56	0.50	0.54	0.51	0.40	0.42	0.45
	Standard Deviation	0.21	0.29	0.25	0.22	0.16	0.21	0.09	0.08	0.11	0.14	0.11	0.08	0.12
	Probable Error	0.05	0.06	0.06	0.05	0.04	0.03	0.02	0.02	0.03	0.03	0.03	0.02	0.03
Roughness Wavelength (mm)	Average	0.56	0.53	0.46	0.50	0.15	0.34	0.37	0.36	0.38	0.33	0.36	0.35	0.28
	Standard Deviation	0.09	0.10	0.09	0.15	0.06	0.08	0.10	0.08	0.07	0.08	0.16	0.17	0.09
	Probable Error	0.02	0.02	0.02	0.03	0.01	0.02	0.02	0.02	0.02	0.02	0.04	0.05	0.03

Table B2. Surface Roughness Results at Various Film Thicknesses for <10µm Size Range Powder

		Film Thickness (µm)											
		16	22	28	32	37	44	56	62	67	74	84	95
Roughness Average (µm)	Average	0.86	1.09	1.33	1.29	1.21	1.44	1.01	1.34	1.00	1.12	0.97	0.78
	Standard Deviation	0.20	0.29	0.35	0.39	0.39	0.28	0.42	0.27	0.36	0.40	0.33	0.23
	Probable Error		0.06	0.08	0.09	0.09	0.07	0.15	0.09	0.10	0.11	0.08	0.06
Roughness Wavelength (mm)	Average	0.47	0.67	0.77	0.79	0.78	0.92	0.72	0.91	0.74	0.83	0.71	0.59
	Standard Deviation	0.07	0.15	0.16	0.19	0.19	0.16	0.25	0.16	0.22	0.27	0.17	0.14
	Probable Error		0.03	0.04	0.04	0.04	0.04	0.09	0.05	0.06	0.07	0.04	0.04

Table B3. **Surface Roughness Results at Various Film Thicknesses for 10-20μm Size Range Powder**

		Film Thickness (μm)								
		18	22	27	32	37	42	46	56	62
Roughness Average (μm)	Average	0.33	0.35	0.40	0.37	0.38	0.35	0.40	0.24	0.24
	Standard Deviation	0.42	0.11	0.12	0.06	0.09	0.10	0.21	0.05	0.05
	Probable Error	0.01	0.02	0.03	0.01	0.02	0.02	0.06	0.01	0.01
Roughness Wavelength (mm)	Average	0.23	0.25	0.22	0.26	0.23	0.21	0.23	0.14	0.15
	Standard Deviation	0.04	0.06	0.06	0.14	0.05	0.06	0.09	0.05	0.05
	Probable Error	0.01	0.01	0.01	0.03	0.01	0.01	0.03	0.01	0.01

Table B4. **Surface Roughness Results at Various Film Thicknesses for 20-30μm Size Range Powder**

		Film Thickness (μm)												
		27	32	37	42	48	52	57	62	67	71	77	84	100
Roughness Average (μm)	Average	0.45	0.44	0.39	0.41	0.38	0.37	0.31	0.35	0.38	0.38	0.40	0.45	0.53
	Standard Deviation	0.11	0.11	0.12	0.06	0.07	0.07	0.05	0.09	0.13	0.12	0.10	0.17	0.29
	Probable Error	0.02	0.02	0.03	0.01	0.02	0.02	0.01	0.02	0.03	0.03	0.03	0.04	0.08
Roughness Wavelength (mm)	Average	0.30	0.29	0.28	0.29	0.26	0.28	0.21	0.24	0.27	0.29	0.32	0.34	0.56
	Standard Deviation	0.05	0.08	0.07	0.08	0.04	0.08	0.04	0.06	0.09	0.08	0.14	0.12	0.42
	Probable Error	0.01	0.12	0.12	0.02	0.01	0.02	0.01	0.01	0.02	0.02	0.04	0.03	0.12

Table B5. **Surface Roughness Results at Various Film Thicknesses for 30-40μm Size Range Powder**

		Film Thickness (μm)														
		29	33	37	.42	48	52	57	62	67	72	77	82	87	93	102
Roughness Average (μm)	Average	0.46	0.54	0.56	0.50	0.43	0.43	0.37	0.46	0.39	0.33	0.38	0.37	0.40	0.33	0.31
	Standard Deviation	0.62	0.16	0.09	0.13	0.10	0.12	0.11	0.08	0.10	0.09	0.08	0.09	0.11	0.09	0.06
	Probable Error	0.03	0.04	0.02	0.03	0.02	0.03	0.03	0.03	0.02	0.03	0.03	0.02	0.03	0.02	0.02
Roughness Wavelength (mm)	Average	0.25	0.31	0.32	0.32	0.26	0.26	0.27	0.29	0.24	0.22	0.23	0.22	0.25	0.28	0.22
	Standard Deviation	0.04	0.07	0.06	0.07	0.04	0.06	0.10	0.06	0.06	0.06	0.06	0.05	0.06	0.13	0.08
	Probable Error	0.02	0.02	0.01	0.02	0.01	0.01	0.02	0.03	0.01	0.02	0.02	0.01	0.01	0.04	0.03

Table B6. Surface Roughness Results at Various Film Thicknesses for 40–50μm Size Range Powder

		Film Thickness (μm)												
		33	37	42	47	52	57	63	75	84	92	97	106	135
Roughness Average (μm)	Average	0.96	0.83	0.68	0.65	0.48	0.50	0.55	0.55	0.44	0.41	0.39	0.37	0.28
	Standard Deviation	0.30	0.25	0.22	0.22	0.16	0.16	0.18	0.08	0.10	0.08	0.11	0.06	0.04
	Probable Error	0.07	0.06	0.05	0.05	0.04	0.04	0.04	0.03	0.03	0.02	0.03	0.02	0.01
Roughness Wavelength (mm)	Average	0.61	0.54	0.49	0.51	0.34	0.41	0.39	0.37	0.36	0.33	0.30	0.34	0.23
	Standard Deviation	0.16	0.13	0.12	0.22	0.08	0.10	0.15	0.06	0.09	0.10	0.07	0.19	0.12
	Probable Error	0.04	0.03	0.03	0.05	0.02	0.02	0.03	0.02	0.03	0.03	0.02	0.06	0.03

Table B7. **Surface Roughness Results at Various Film Thicknesses for +50μm Size Range Powder**

		Film Thickness (μm)														
		38	43	47	52	57	62	67	71	76	81	87	92	97	104	122
Roughness Average (μm)	Average	0.80	0.75	0.74	0.62	0.57	0.62	0.53	0.55	0.46	0.48	0.45	0.53	0.45	0.46	0.39
	Standard Deviation	0.14	0.12	0.13	0.17	0.15	0.19	0.14	0.18	0.13	0.13	0.13	0.10	0.18	0.15	0.13
	Probable Error	0.04	0.03	0.03	0.04	0.04	0.04	0.03	0.04	0.04	0.04	0.03	0.02	0.06	0.04	0.04
Roughness Wavelength (mm)	Average	0.45	0.46	0.49	0.45	0.37	0.41	0.37	0.41	0.33	0.33	0.33	0.38	0.40	0.33	0.34
	Standard Deviation	0.07	0.08	0.18	0.11	0.08	0.11	0.08	0.11	0.09	0.07	0.06	0.12	0.08	0.13	0.10
	Probable Error	0.02	0.02	0.04	0.03	0.02	0.02	0.02	0.03	0.02	0.02	0.02	0.03	0.03	0.03	0.03

Table B8. Linear Regression fits of Roughness Average and Wavelength Results

Powder Type	Measured Quantity	Slope	Y Intercept	Correlation Coefficient	t = 15	t = 100
Commercial	Roughness Average	-0.0076	1.037	0.860	0.923	0.277
	Roughness Wavelength	-0.0032	0.576	0.868	0.528	0.256
<10μm	Roughness Average	-0.0003	1.272	0.367	1.268	1.271
	Roughness Wavelength	0.0006	0.711	0.118	0.72	0.771
10-20μm	Roughness Average	-0.0025	0.434	0.613	0.397	0.184
	Roughness Wavelength	-0.0023	0.299	0.808	0.265	0.069
20-30μm	Roughness Average	0.0027	0.221	0.595	0.262	0.491
	Roughness Wavelength	0.0024	0.164	0.609	0.2	0.404
30-40μm	Roughness Average	-0.0028	0.593	0.842	0.551	0.313
	Roughness Wavelength	-0.0009	0.317	0.601	0.304	0.227
40-50μm	Roughness Average	-0.0054	0.929	0.867	0.848	0.389
	Roughness Wavelength	-0.0031	0.618	0.880	0.572	0.308
+50μm	Roughness Average	-0.0045	0.889	0.889	0.822	0.439
	Roughness Wavelength	-0.0017	0.513	0.755	0.488	0.343

Table B9. **Linear Regression Results for Roughness Average and Roughness Wavelength at Various Film Thicknesses**

Using data from Table 3.3

Film Thickness		30μm	50μm	70μm	100μm
Roughness Average	Slope	0.0125	0.0102	0.0056	0.0043
	Intercept	0.11	0.13	0.20	0.21
	d = 15μm	0.29	0.29	0.28	0.27
	d = 55μm	0.79	0.69	0.51	0.45
Roughness Wavelength	Slope	0.0076	0.0068	0.0061	0.0046
	Intercept	0.082	0.086	0.09	0.11
	d = 15μm	0.20	0.19	0.18	0.18
	d = 55μm	0.50	0.46	0.43	0.37

Calculations do not include <10μm size range

FIGURE B1   ROUGHNESS AVERAGE VS. FILM THICKNESS

FIGURE 82   ROUGHNESS AVERAGE VS. FILM THICKNESS
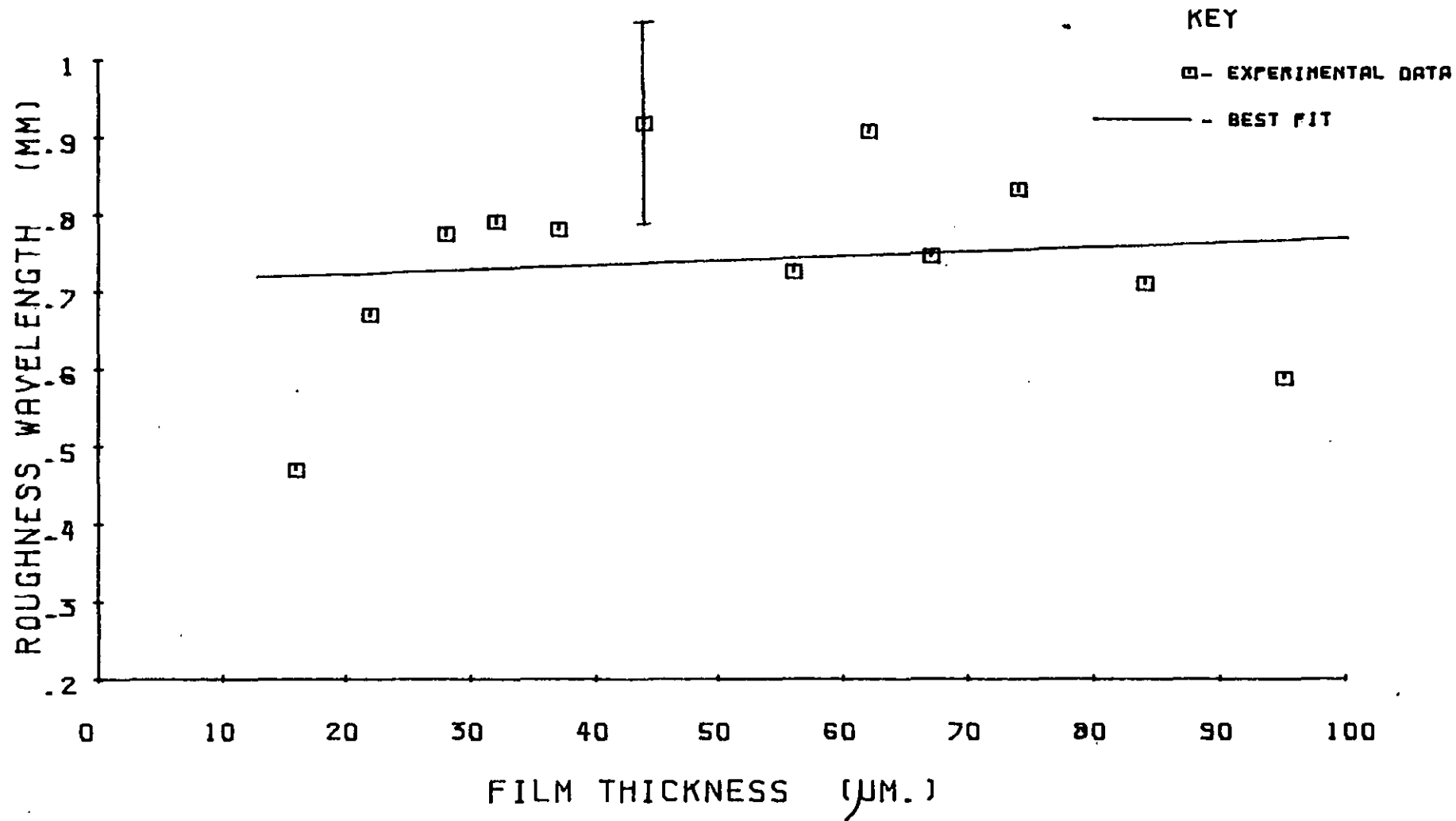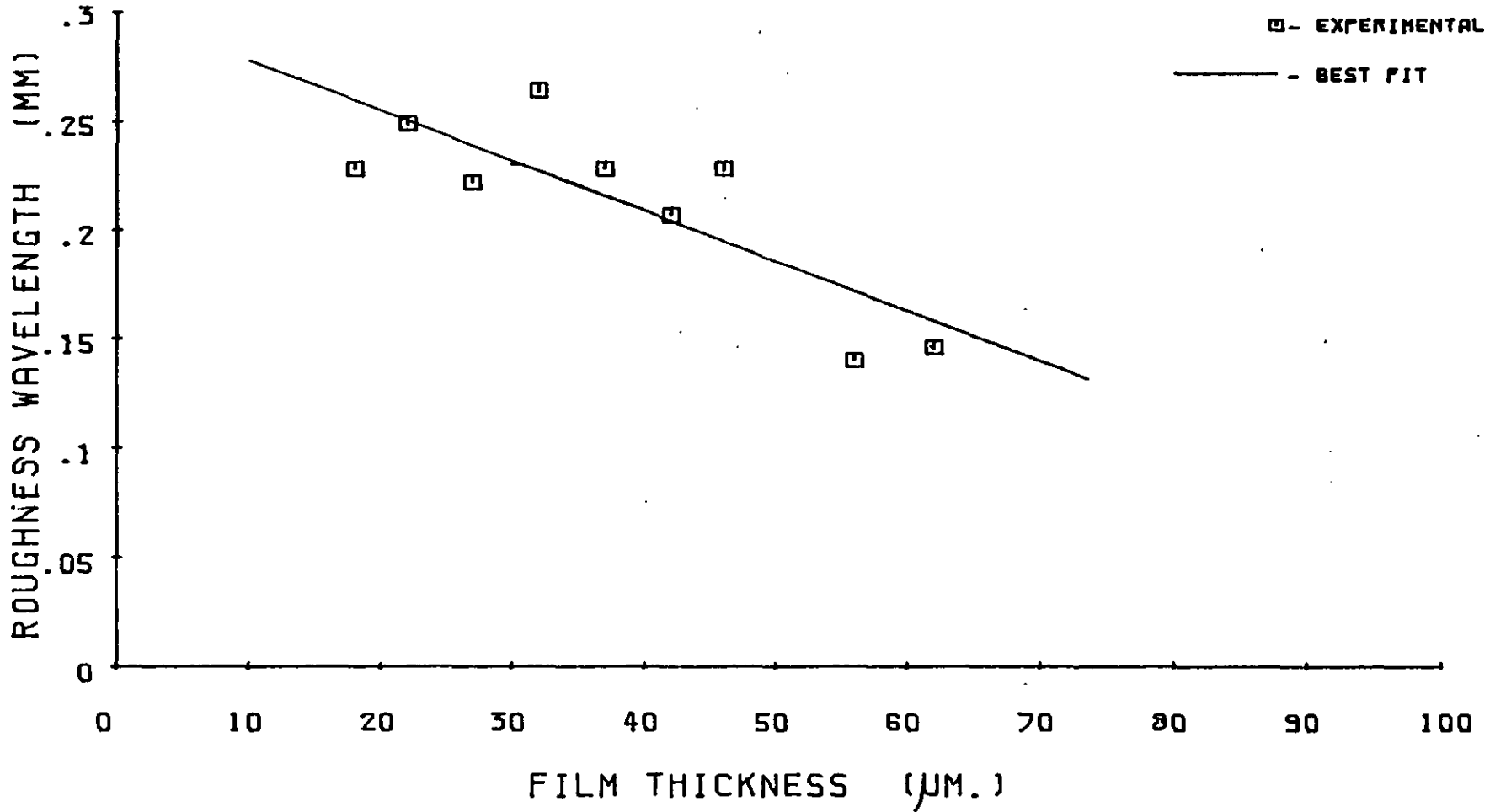
FIGURE B3   ROUGHNESS AVERAGE VS. FILM THICKNESS

POWDER SIZE RANGE : 10-20µM.

KEY

□- EXPERIMENTAL DATA
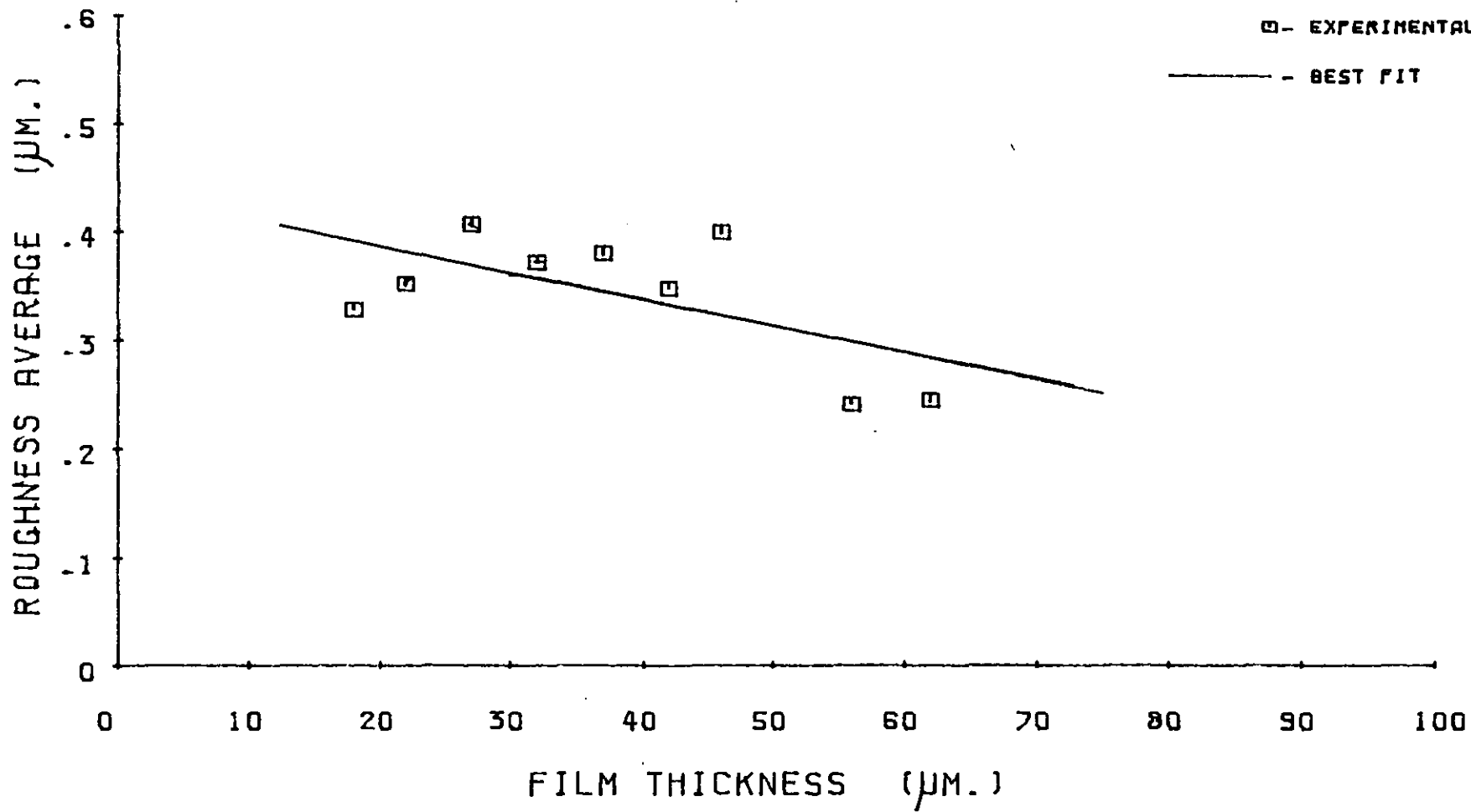
———— - BEST FIT

FIGURE B4 ROUGHNESS AVERAGE VS. FILM THICKNESS
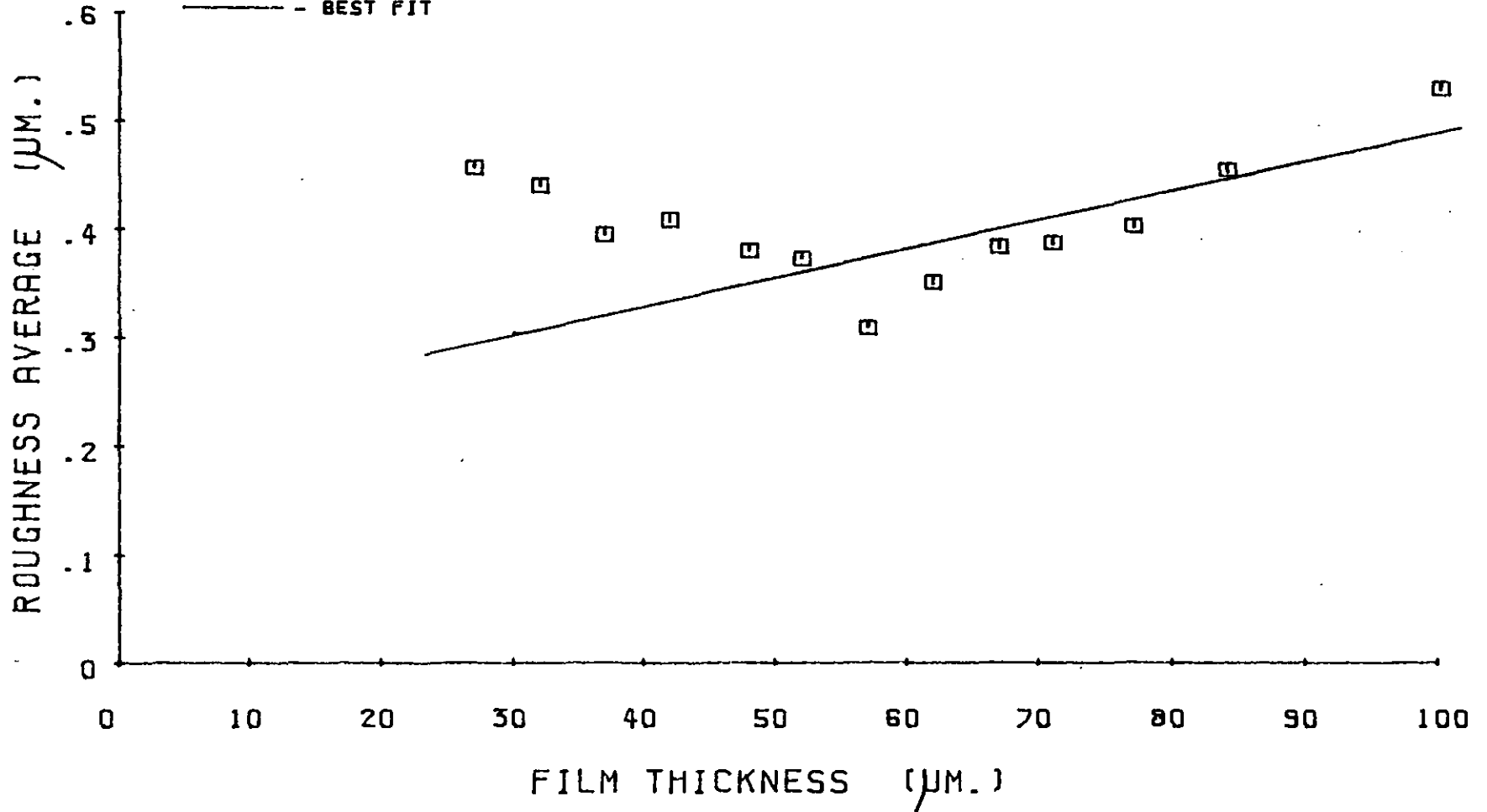
FIGURE B5   ROUGHNESS AVERAGE VS. FILM THICKNESS
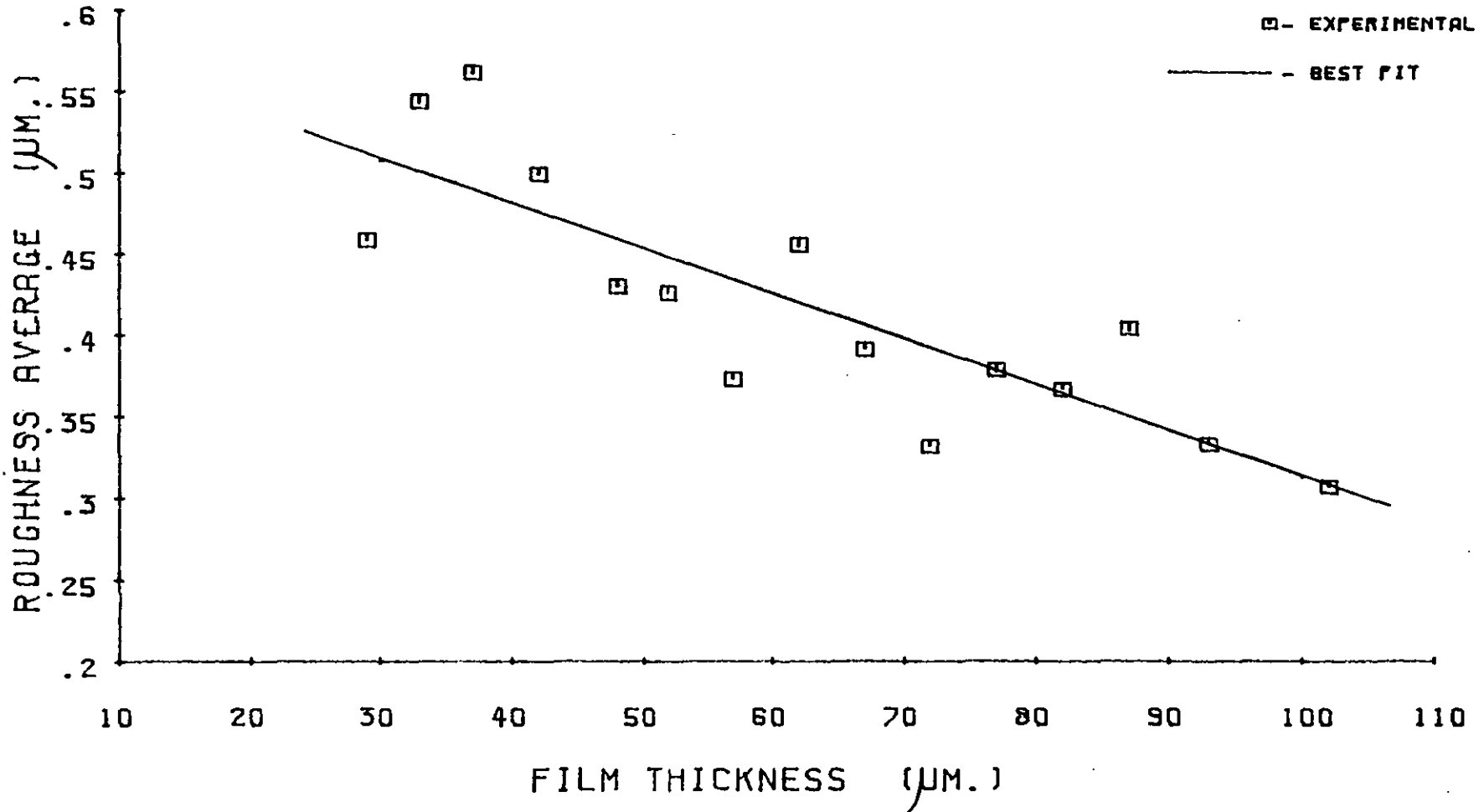
FIGURE B6   ROUGHNESS AVERAGE VS. FILM THICKNESS
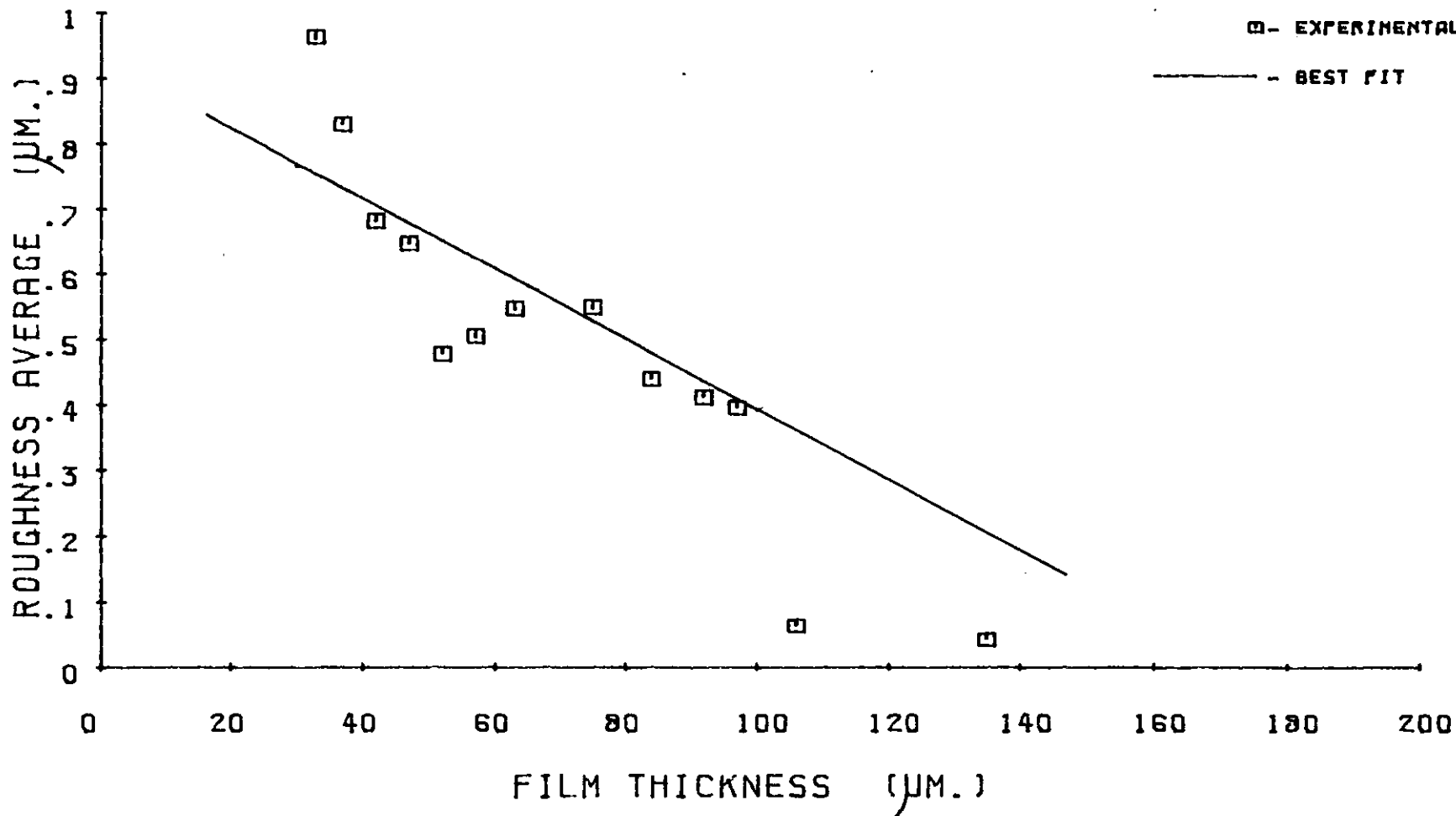
FIGURE B7   ROUGHNESS AVERAGE VS. FILM THICKNESS
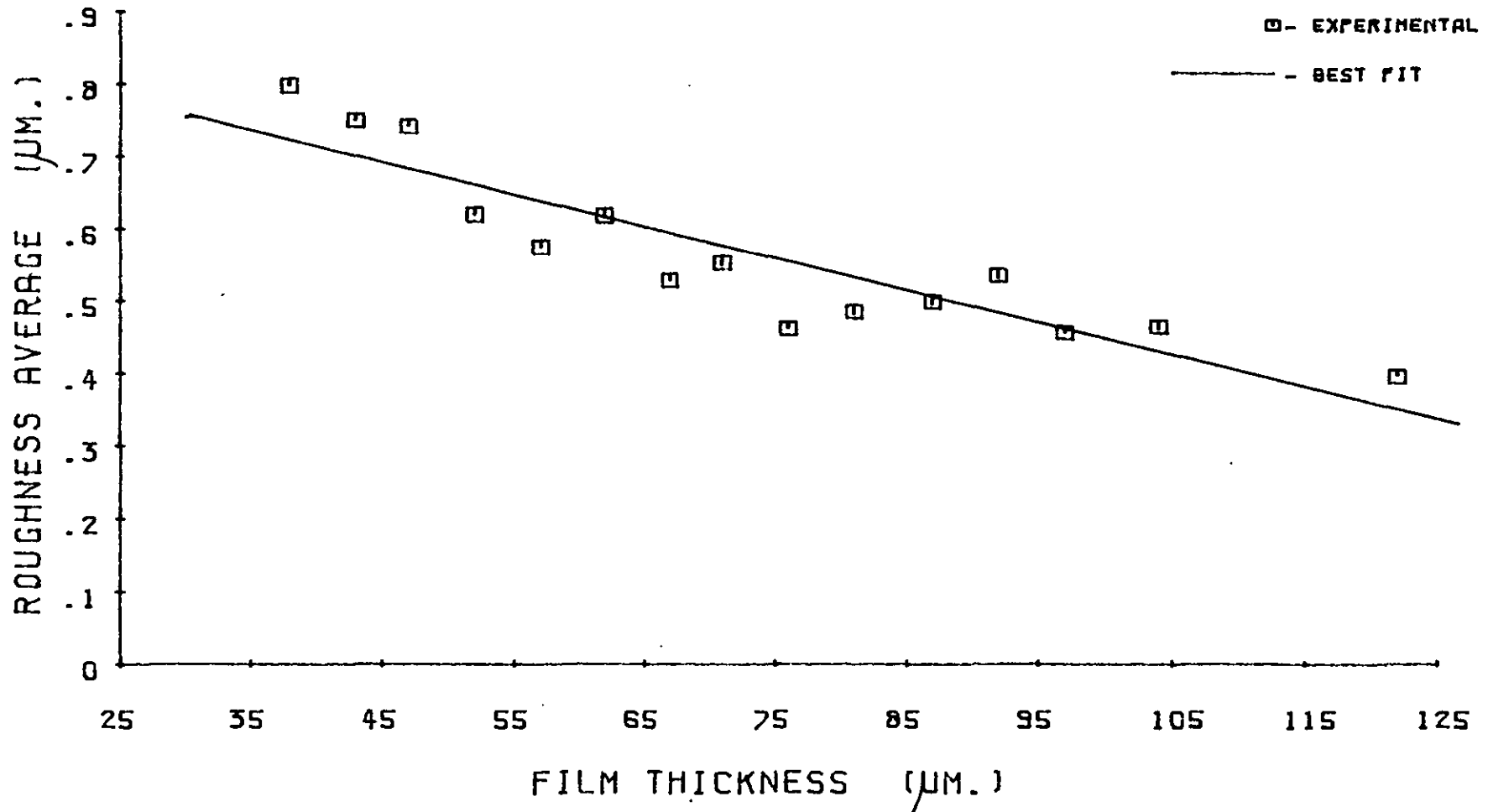
FIGURE 88   ROUGHNESS WAVELENGTH VS. FILM THICKNESS

POWDER SIZE RANGE :   COMMERCIAL
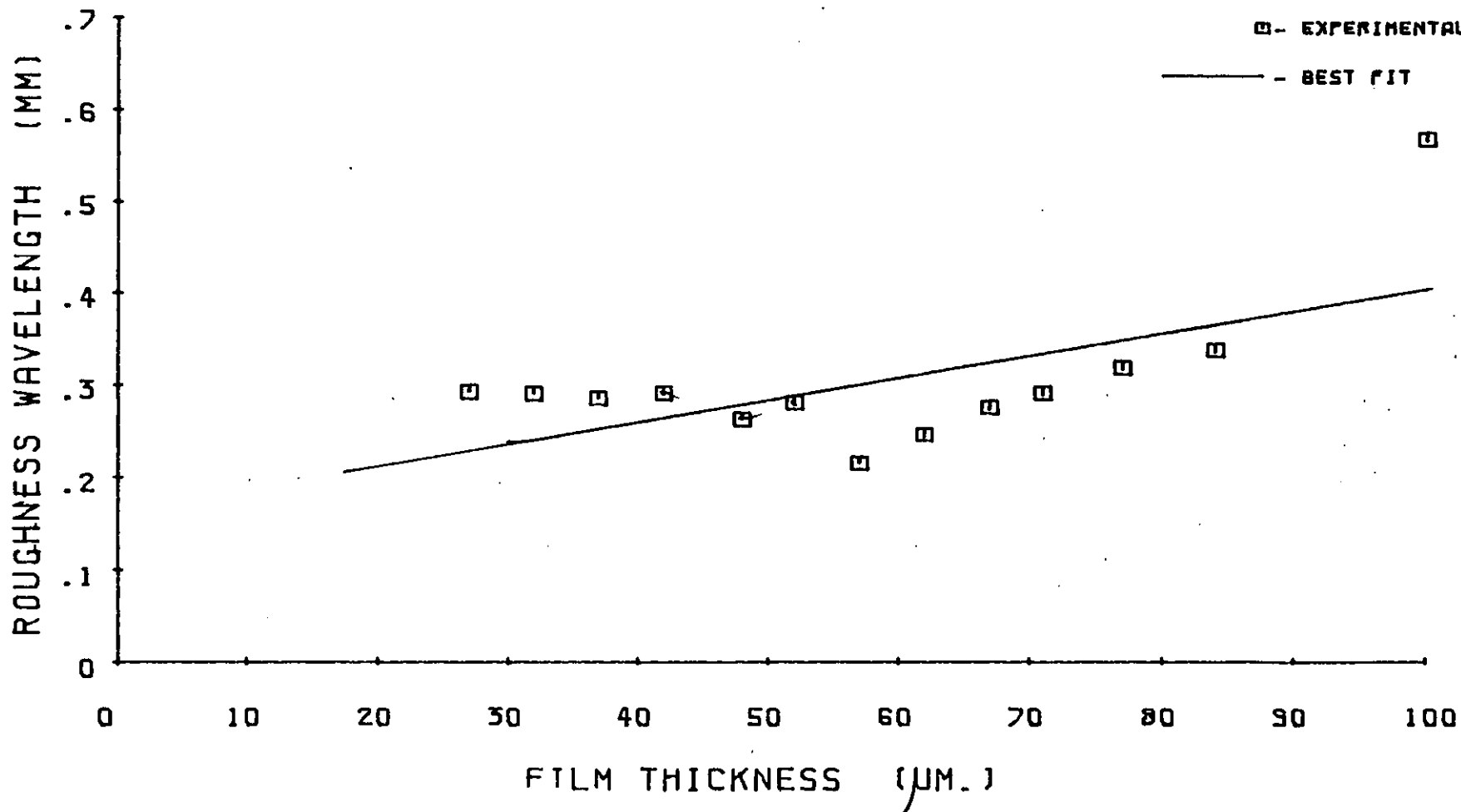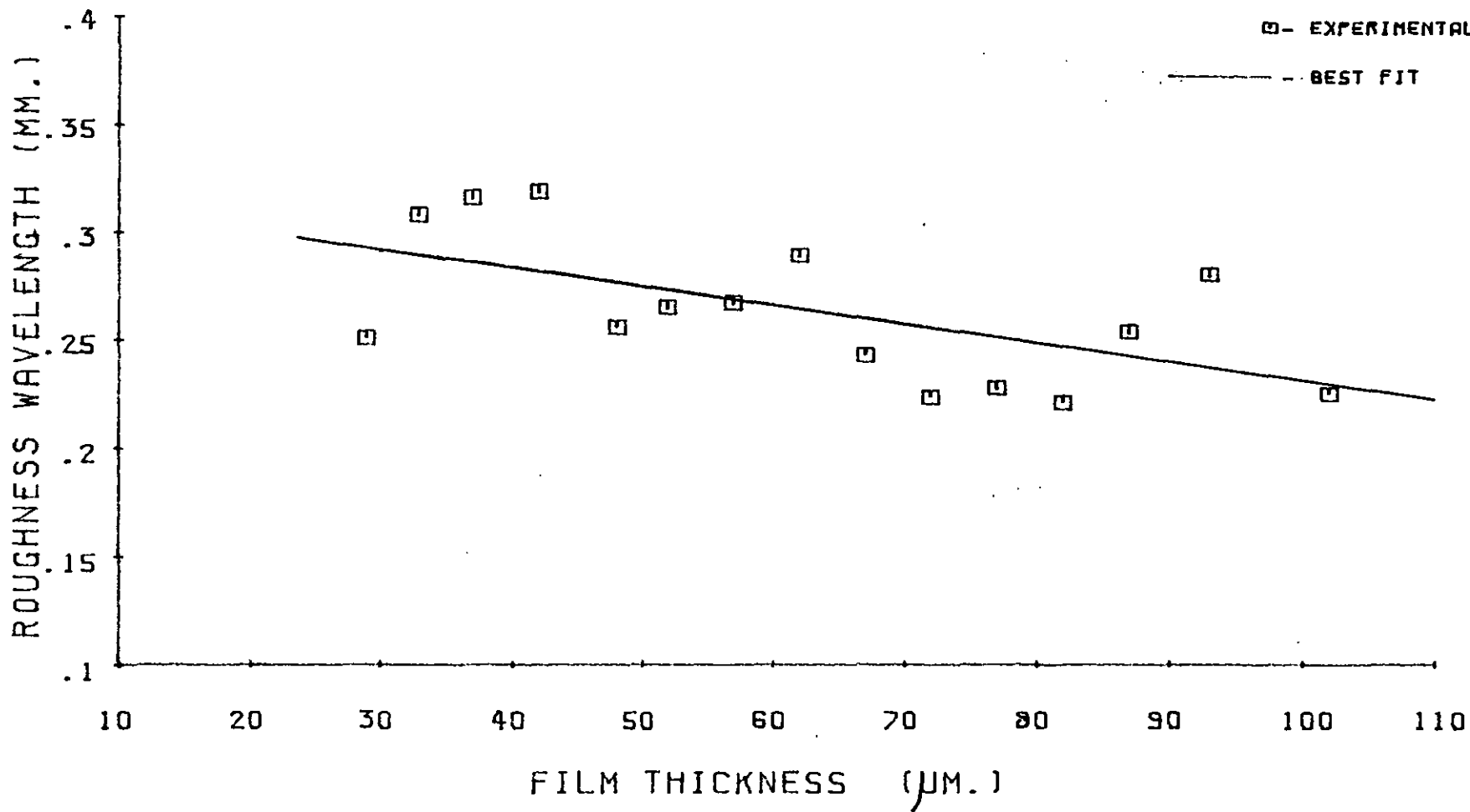
KEY

▣– EXPERIMENTAL DATA
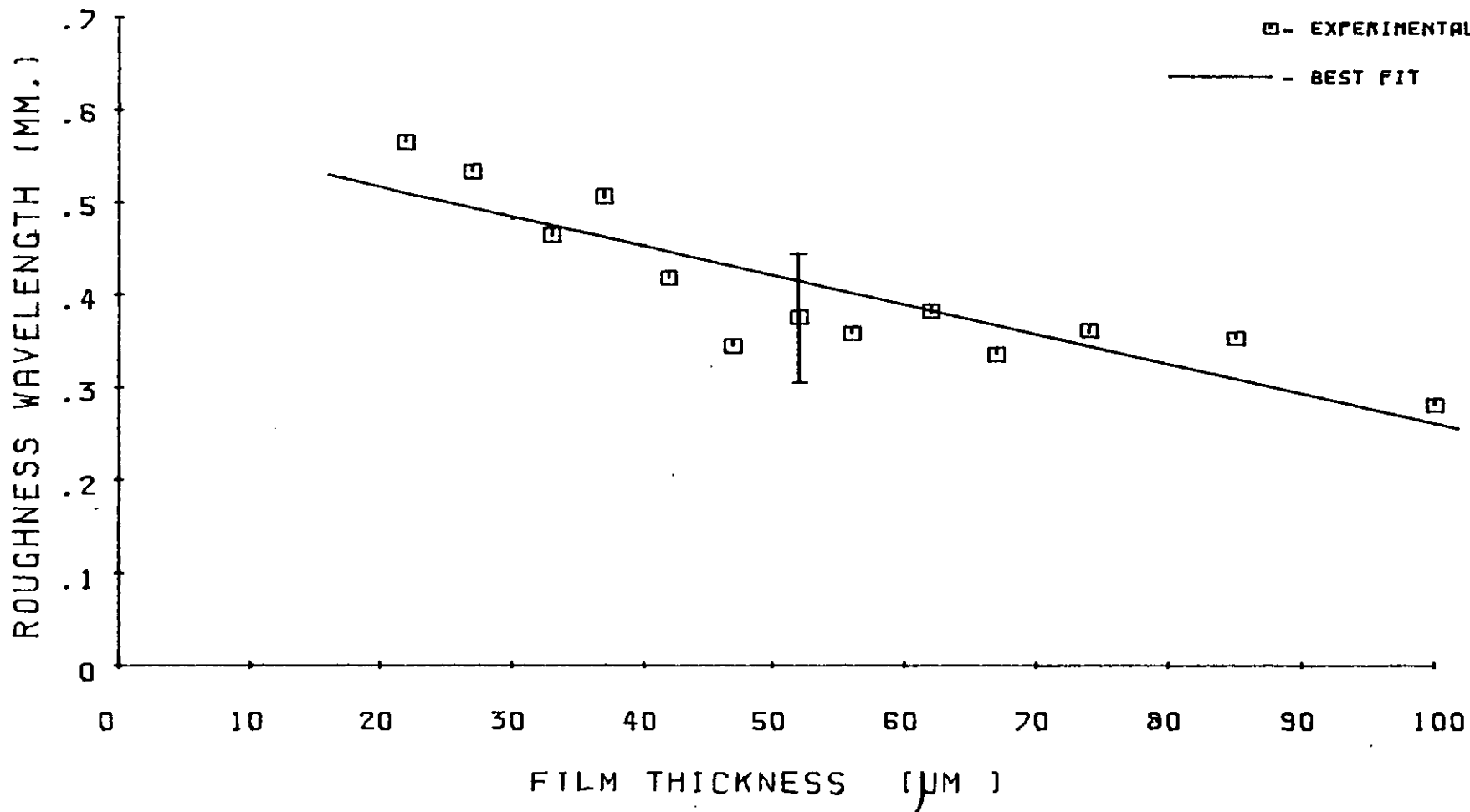
———— – BEST FIT

FIGURE B9   ROUGHNESS WAVELENGTH VS. FILM THICKNESS

POWDER SIZE RANGE : <10µM.

KEY

□- EXPERIMENTAL DATA

——— - BEST FIT

FIGURE B10   ROUGHNESS WAVELENGTH VS. FILM THICKNESS

FIGURE B11   ROUGHNESS WAVELENGTH VS. FILM THICKNESS

FIGURE B12   ROUGHNESS WAVELENGTH VS. FILM THICKNESS

FIGURE B13   ROUGHNESS WAVELENGTH VS. FILM THICKNESS
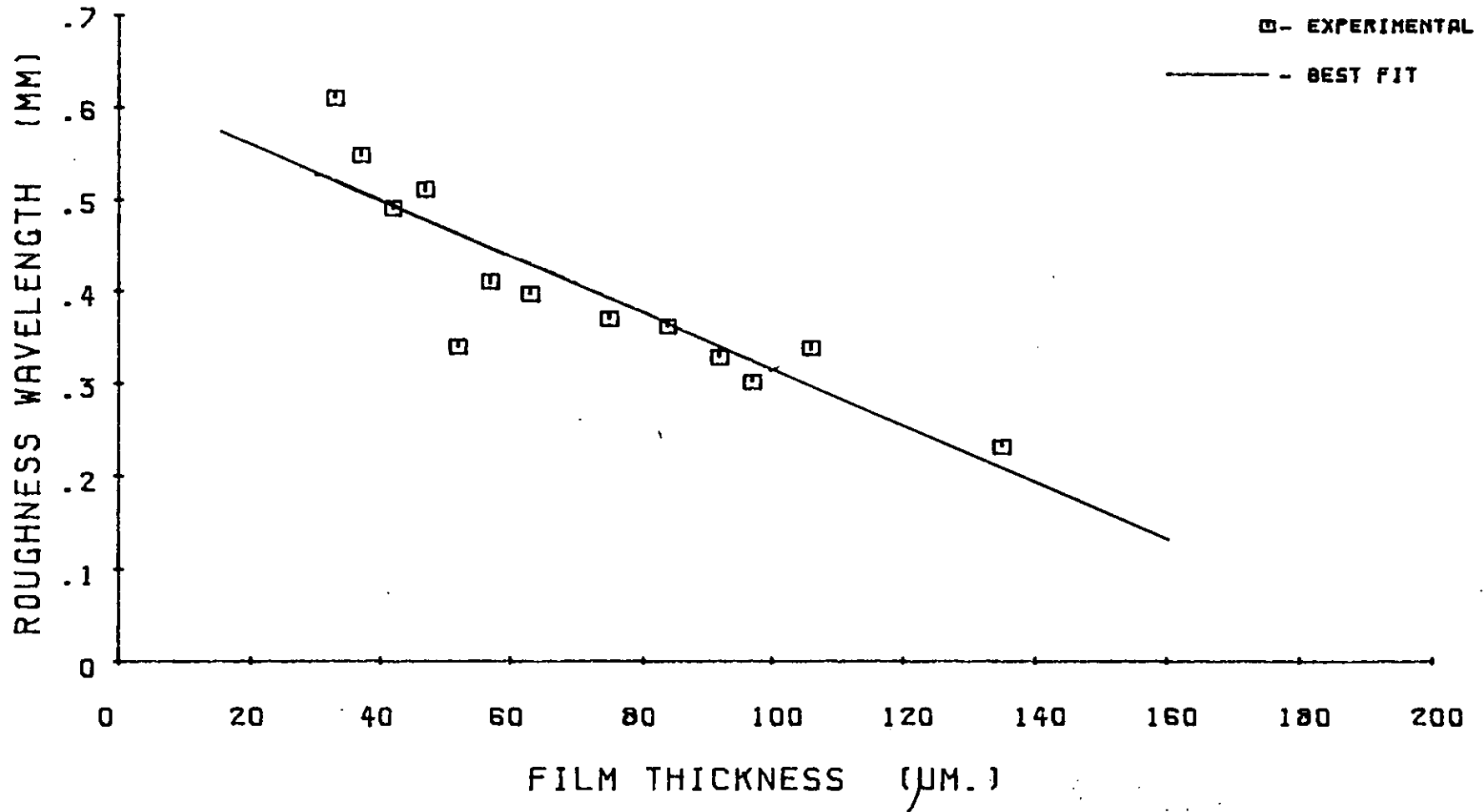
FIGURE B14   ROUGHNESS WAVELENGTH VS. FILM THICKNESS
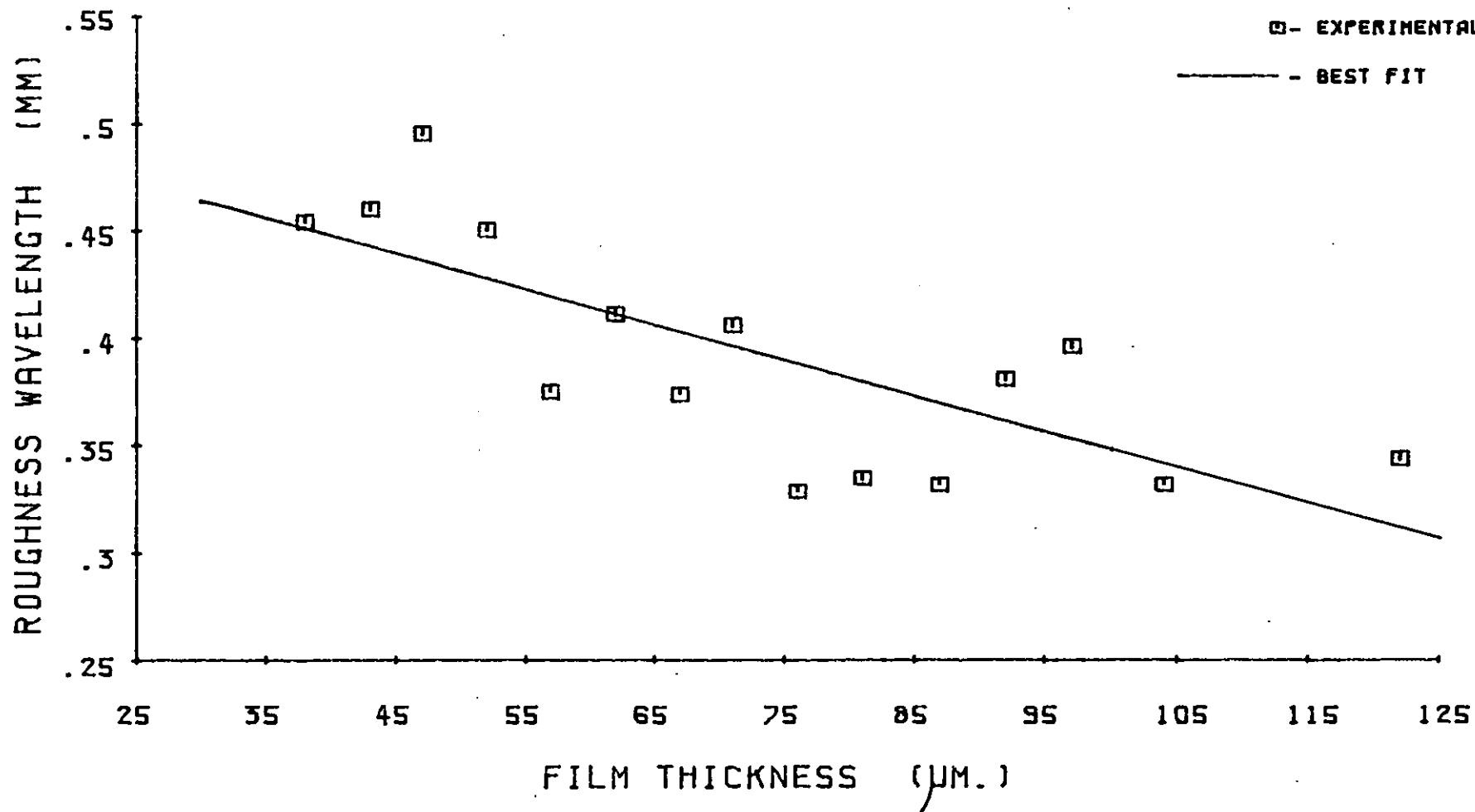
APPENDIX C

MICROSCAL SIZE DISTRIBUTION ANALYSIS RESULTS

Table C1.   Microscal Photosedimentometer Analysis of Powder 1.   Before Spraying

Optical Density	Sample 1 Ht. of Scan (cms) : 16.4 Time to Scan(mins): 24.2			Sample 2 Ht. of Scan (cms) : 17.1 Time to Scan(mins): 17.8			Sample 3 Ht. of Scan (cms) : 17.2 Time to Scan(mins): 18.0			Averages †	
	Time (mins)	Size (µm)	cum. wt% undersize	Time (mins)	Size (µm)	cum. wt% undersize	Time (mins)	Size (µm)	cum. wt% undersize	Size (µm)	cum. wt% undersize
–	–	–	–	–	–	–	–	–	–	10	5.7
–	–	–	–	–	–	–	(0.96) 3.4	55.5	100.0	15	7.3
0.8	–	–	–	3.0	55.7	100.0	5.3	46.2	69.7	20	10.9
0.7	(0.68) 1.2	78.4	100.0	6.2	41.5	71.6	7.0	40.1	53.9	25	19.1
0.6	4.3	48.8	72.1	9.3	34.2	50.4	9.3	34.7	40.2	30	29.5
0.50	6.7	41.4	50.5	13.3	29.5	32.9	12.5	30.9	28.4	35	42.0
0.45	8.2	37.2	41.3	16.8	26.0	25.4	14.8	28.0	23.1	40	57.1
0.40	10.2	33.1	33.0	22.0	22.8	18.7	18.6	25.0	18.3	45	70.2
0.35	13.1	29.2	25.7	26.0	20.1	12.9	23.0	23.2	14.1	50	82.1
0.30	17.0	25.3	19.2	28.4	17.6	7.8	25.2	21.7	10.1	60	
0.25	20.5	21.5	13.6	31.0	9.1	3.3	27.2	15.8	6.4		
0.20	23.2	9.9	8.8	42.0	0.9	1.0	37.0	5.5	3.7		
0.15	–	–	–	–	–	–	–	–	–		

† values obtained from size distribution curves

Table C2. Microscal Photosedimentometer Analysis of Powder 1. After Spraying

| | Sample 1 | | | Sample 2 | | | Sample 3 | | | | Averages † | |
| | Ht. of Scan (cms) : 16.4 Time to Scan(mins): 24.2 | | | Ht. of Scan (cms) : 17.1 Time to Scan(mins): 17.8 | | | Ht. of Scan (cms) : 17.2 Time to Scan(mins): 18.0 | | | | | |
Optical Density	Time (mins)	Size (μm)	cum. wt% undersize	Time (mins)	Size (μm)	cum. wt% undersize	Time (mins)	Size (μm)	cum. wt% undersize		Size (μm)	cum. wt% undersize
–											10	4.9
–											15	5.6
0.8	1.0	89.6	100.0	(0.75) 3.4	58.8	100.0	(0.75) 1.3	90.1	100.0		20	7.3
0.7	2.5	61.5	72.6	3.9	54.2	89.2	1.9	69.6	85.3		25	10.9
0.6	4.2	49.2	53.8	4.7	48.9	69.3	3.8	52.4	62.6		30	16.8
0.50	6.0	43.0	38.8	5.9	44.7	51.4	5.7	45.3	45.6		35	24.5
0.45	7.1	39.5	32.2	6.7	41.9	43.2	6.7	42.1	38.2		40	34.7
0.40	8.4	36.0	26.1	7.7	39.0	35.5	7.6	39.1	31.3		45	47.3
0.35	10.4	31.9	20.6	8.9	36.2	28.3	9.0	36.0	25.0		50	62.3
0.30	13.6	27.9	15.8	10.4	32.9	21.7	10.6	32.4	19.1		60	82.3
0.25	17.9	24.4	11.5	13.1	28.8	15.7	13.8	28.1	13.8			
0.20	22.9	21.3	7.8	17.8	24.1	10.4	18.4	23.9	9.2			
0.15	26.6	9.8	4.5	21.3	10.8	6.0	21.3	11.0	5.4			

† values obtained from size distribution curves

Table C3. Microscal Photosedimentometer Analysis of Powder 2. Before Spraying

Optical Density	Sample 1			Sample 2			Sample 3			Averages	
	Ht. of Scan (cms) : 17.5 Time to Scan(mins): 17.0			Ht. of Scan (cms) : 17.5 Time to Scan(mins): 21.8			Ht. of Scan (cms) : 17.5 Time to Scan(mins): 19.2				
	Time (mins)	Size (µm)	cum. wt% undersize	Time (mins)	Size (µm)	cum. wt% undersize	Time (mins)	Size (µm)	cum. wt% undersize	Size (µm)	cum. wt% undersize
–	–	–	–	(1.0) 4.3	50.1	100.0	(0.94) 1.3	89.8	100.0	10	5.8
–	–	–	–	(0.9) 6.2	42.0	80.3	(0.9) 2.0	68.5	88.1	15	7.5
0.8	(0.73) 0.9	104.6	100.0	8.7	35.8	63.7	4.0	50.8	65.3	20	10.0
0.7	1.6	71.6	87.6	11.7	31.0	49.6	6.4	40.8	48.5	25	15.5
0.6	4.5	46.7	59.3	15.4	27.1	37.4	9.5	33.8	34.9	30	24.5
0.50	8.1	37.7	40.9	20.0	24.6	26.7	13.5	29.5	23.7	35	35.5
0.45	10.2	33.8	33.5	22.1	23.4	21.9	16.2	27.0	18.8	40	45.8
0.40	12.5	30.7	26.8	22.9	22.4	17.3	19.2	24.5	14.3	45	55.5
0.35	15.0	27.8	20.7	23.8	21.1	12.9	21.2	22.1	10.3	50	
0.30	17.7	25.4	15.2	25.2	15.8	8.7	23.0	15.3	6.6	60	
0.25	19.1	20.1	10.2	33.4	5.7	5.6	32.5	4.9	4.0		
0.20	25.7	7.9	6.3	–	–	–	–	–	–		
0.15	–	–	–	–	–	–	–	–	–		

† values obtained from size distribution curves

Table C4. **Microscal Photosedimentometer Analysis of Powder 2. After Spraying**

Optical Density	Sample 1 Time (mins)	Size (μm)	cum. wt% undersize	Sample 2 Time (mins)	Size (μm)	cum. wt% undersize	Sample 3 Time (mins)	Size (μm)	cum. wt% undersize	Averages † Size (μm)	cum. wt% undersize
	Ht. of Scan (cms) : 17.5 Time to Scan(mins): 15.0			Ht. of Scan (cms) : 17.2 Time to Scan(mins): 12.8			Ht. of Scan (cms) : 17.6 Time to Scan(mins): 14.6				
–										10	6.8
–				(0.95) 1.5	77.8	100.0	(0.93) 1.8	74.2	100.0	15	6.9
0.8	1.6	77.0	100.0	3.1	57.9	68.9	3.2	58.3	73.5	20	7.6
0.7	3.1	57.6	74.8	4.7	48.0	53.5	4.6	49.0	57.5	25	10.5
0.6	5.0	46.5	55.9	6.5	40.9	40.7	6.4	41.9	44.0	30	18.0
0.50	7.2	40.6	40.7	8.9	36.4	29.8	8.6	37.5	32.5	35	28.3
0.45	8.5	37.4	34.1	10.2	34.0	24.9	9.9	35.0	27.4	40	39.3
0.40	10.0	34.5	28.0	11.8	31.3	20.4	11.3	32.3	22.6	45	50.0
0.35	11.7	31.7	22.3	13.6	28.6	16.2	13.6	29.6	18.2	50	60.0
0.30	14.1	28.7	17.1	14.8	26.6	12.4	15.4	27.5	14.1	60	
0.25	16.2	26.1	12.4	15.8	23.6	8.9	16.3	25.7	10.3		
0.20	17.6	12.5	8.2	18.4	10.8	5.7	17.6	12.3	6.8		
0.15	–	–	–	–	–	–	–	–	–		

† values obtained from size distribution curves

Table C5. Microscal Photosedimentometer Analysis of Powder 3. Before Spraying

Optical Density	Sample 1 Ht. of Scan (cms) : 17.5 Time to Scan(mins): 22.0			Sample 2 Ht. of Scan (cms) : 17.5 Time to Scan(mins): 15.7			Sample 3 Ht. of Scan (cms) : 17.5 Time to Scan(mins): 27.2			Averages †	
	Time (mins)	Size (µm)	cum. wt% undersize	Time (mins)	Size (µm)	cum. wt% undersize	Time (mins)	Size (µm)	cum. wt% undersize	Size (µm)	cum. wt% undersize
-	-	-	-	-	-	-	(1.0) 5.8	43.7	100.0	10	5.4
0.9	(0.83) 1.0	104.6	100.0	-	-	-	7.9	37.7	80.0	15	6.5
0.8	1.4	79.1	89.2	-	-	-	10.5	32.9	62.7	20	9.3
0.7	3.3	54.4	62.0	1.2	79.4	100.0	13.6	28.9	47.7	25	14.9
0.6	6.0	41.3	43.3	4.2	47.4	62.7	17.6	25.4	34.4	30	23.0
0.50	9.8	34.5	29.1	8.3	37.1	40.5	22.7	23.0	22.8	35	32.8
0.45	12.0	31.2	23.2	10.6	32.9	31.8	26.2	20.5	17.5	40	43.4
0.40	14.7	28.0	17.8	13.4	29.4	24.1	30.2	16.6	12.8	45	54.2
0.35	18.3	24.5	13.0	16.2	26.2	17.2	34.8	11.8	9.0	50	
0.30	23.4	17.9	8.8	18.2	22.4	11.1	40.1	4.6	6.3	60	
0.25	31.8	6.7	5.7	21.3	13.1	5.8	-	-	-		
0.20	-	-	-	31.7	2.9	2.8	-	-	-		
0.15	-	-	-	-	-	-	-	-	-		

† values obtained from size distribution curves

Table C6. Microscal Photosedimentometer Analysis of Powder 3. After Spraying

Optical Density	Sample 1			Sample 2			Sample 3			Averages †	
	Ht. of Scan (cms) : 17.5 Time to Scan(mins): 21.5			Ht. of Scan (cms) : 17.5 Time to Scan(mins): 18.5			Ht. of Scan (cms) : 17.5 Time to Scan(mins): 11.2				
	Time (mins)	Size (µm)	cum. wt% undersize	Time (mins)	Size (µm)	cum. wt% undersize	Time (mins)	Size (µm)	cum. wt% undersize	Size (µm)	cum. wt% undersize
-	(1.0) 1.7	76.7	100.0	(1.0) 1.7	80.1	100.0	(0.1) 18.8	9.8	4.0	10	3.5
0.9	2.6	65.1	69.8	2.4	67.8	80.5	-	-	-	15	4.0
0.8	3.6	56.0	55.1	3.3	58.2	64.0	-	-	-	20	6.7
0.7	4.7	48.4	42.4	4.4	50.4	49.9	-	-	-	25	11.0
0.6	6.5	40.7	31.5	5.9	43.1	37.6	(0.56) 1.1	95.2	100.0	30	16.5
0.50	9.4	34.9	22.3	8.2	38.0	27.2	1.9	75.0	76.9	35	22.5
0.45	12.0	31.2	18.3	9.7	34.7	22.5	2.8	62.6	61.7	40	29.5
0.40	14.6	28.4	14.8	11.8	31.5	18.3	3.9	53.8	49.1	45	36.5
0.35	17.4	25.9	11.6	14.3	28.4	14.5	5.1	46.7	38.2	50	44.0
0.30	21.1	23.1	8.6	17.8	25.1	11.0	6.9	39.8	28.7	60	
0.25	23.9	19.7	6.0	20.8	21.7	8.0	9.7	33.5	20.7		
0.20	27.2	15.1	3.8	23.3	18.6	5.4	12.6	27.3	13.9		
0.15	32.3	6.2	2.1	25.9	8.5	3.1	16.1	21.8	8.4		

† values obtained from size distribution curves

Table C7. Microscal Photosedimentometer Analysis of Powder 4. Before Spraying

	Sample 1			Sample 2			Sample 3			Averages †	
	Ht. of Scan (cms) : 17.5 Time to Scan(mins): 18.5			Ht. of Scan (cms) : 17.5 Time to Scan(mins): 21.7			Ht. of Scan (cms) : 17.5 Time to Scan(mins): 19.2				
Optical Density	Time (mins)	Size (µm)	cum. wt% undersize	Time (mins)	Size (µm)	cum. wt% undersize	Time (mins)	Size (µm)	cum. wt% undersize	Size (µm)	cum. wt% undersize
–				(1.2) 1.6	65.3	100.0				10	6.5
–				7.7	37.8	46.8				15	9.1
0.8				10.7	32.2	36.6				20	14.1
0.7				14.5	27.9	27.8				25	20.9
0.6	0.7	91.5	100.0	19.0	23.5	20.3	(0.56) 0.8	97.9	100.0	30	29.0
0.50	5.7	43.2	53.7	24.5	19.8	13.9	2.7	65.0	70.3	35	37.9
0.45	8.5	36.0	42.8	26.7	17.4	11.2	4.6	48.9	54.9	40	46.7
0.40	11.8	31.0	33.7	28.9	15.2	8.8	6.4	41.6	42.5	45	56.5
0.35	15.4	26.2	25.8	30.8	13.2	6.8	8.7	35.9	32.0	50	
0.30	20.6	21.5	19.2	32.6	11.2	5.0	11.6	30.5	22.9	60	
0.25	23.7	18.7	13.8	34.3	5.1	3.5	16.8	24.7	15.2		
0.20	25.1	8.9	9.0				22.4	16.9	8.9		
0.15							30.5	6.1	4.6		

† values obtained from size distribution curves

Table C8. Microscal Photosedimentometer Analysis of Powder 4. After Spraying

Optical Density	Sample 1 Ht. of Scan (cms) : 17.5 Time to Scan(mins): 15.4			Sample 2 Ht. of Scan (cms) : 17.5 Time to Scan(mins): 13.8			Sample 3 Ht. of Scan (cms) : 17.5 Time to Scan(mins): 15.0			Averages †	
	Time (mins)	Size (µm)	cum. wt% undersize	Time (mins)	Size (µm)	cum. wt% undersize	Time (mins)	Size (µm)	cum. wt% undersize	Size (µm)	cum. wt% undersize
–	(0.98) 1.1	98.9	100.0							10	3.8
–	(0.9) 1.6	80.0	80.5				(0.82) 1.2	99.7	100.0	15	5.1
0.8	2.6	63.2	60.7	(0.73) 1.0	103.0	100.0	1.4	83.1	94.1	20	6.6
0.7	4.1	51.2	45.1	1.5	78.5	89.5	2.6	63.2	69.6	25	9.7
0.6	6.0	42.7	32.5	3.1	57.1	62.9	4.1	51.0	50.9	30	14.5
0.50	8.4	37.4	21.9	5.2	47.1	43.6	6.1	43.9	35.9	35	21.3
0.45	10.1	33.9	17.3	6.5	42.4	35.6	7.3	40.2	29.4	40	29.2
0.40	12.5	30.1	13.1	7.9	30.4	28.4	8.7	36.6	23.5	45	37.2
0.35	15.9	26.2	9.4	9.7	34.2	21.9	10.7	32.2	18.1	50	47.4
0.30	18.2	22.9	6.2	12.5	29.8	16.1	14.6	27.4	13.3	60	
0.25	20.3	13.9	3.3	15.4	25.3	11.1	17.5	22.6	9.3		
0.20	31.1	3.3	1.6	18.2	18.6	6.8	20.9	10.1	6.0		
0.15				24.5	7.1	3.6					

† values obtained from size distribution curves

APPENDIX D

COMPUTER PROGRAM LISTING AND PRINTOUT

ccccccccccccccccccccccccccccccccccccccccccccccccccccccccccccccccccccccccc

C   ELECTROSTATIC POWDER COATING - PARTICLE PACKING

ccccccccccccccccccccccccccccccccccccccccccccccccccccccccccccccccccccccccc

C   THIS PROGRAM IS AN ATTEMPT TO SIMULATE PACKING OF ELECTROSTATICALLY
C   SPRAYED PARTICLES ONTO AN EARTHED SUBSTRATE TAKING INTO ACCOUNT
C   ALL THE FORCES ACTING ON THE PARTICLES I.E. DRAG,INERTIA,GRAVITY,
C   IMAGE, AND INTER-PARTICULATE ATTRACTION AND REPULSION FORCES.
C   THE DIFFERENTIAL EQUATIONS WHICH DESCRIBE THE PARTICLE TRAJECT-
C   ORIES ARE INTEGRATED USING A NAG LIBRARY ROUTINE TO CALCULATE THE
C   PATH OF A PARTICLE AND FINDITS FINAL PACKED POSITION.
C   THE X-COORDINATE START POSITION IS ARBITARILY CHOSEN SOMEWHERE
C   BETWEEN THE GUN AND TARGET AND A RANDOM NUMBER ROUTINE IS USED
C   FOR THE STARTING POSITION IN THE Y-DIRECTION. IT IS ASSUMED THAT
C   THE PARTICLES ARE SPHERICAL AND THAT WHEN THEY TOUCH THEY REMAIN
C   IN THAT POSITION.
C   SOLVING THE O.D.E.'S IS ACHIEVED BY NUMERICAL INTEGRATION OVER
C   A RANGE USING GEAR'S METHOD FOR STIFF EQUATIONS. THE OUTPUT IS
C   CONTROLLED BY CONTROL PARAMETERS AND THE INTEGRATION BY A TOLER-
C   ANCE ERROR, BUT THE OPTIMUM STEP LENGTH IS DETERMINED BY THE
C   ROUTINE. THE FINAL POSITION OF THE PARTICLE IS CALCULATED BY
C   INTERPOLATION OF THE LAST WO COMPUTED COORDINATES OF THE ONCOMING
C   PARTICLE, THE LAST STEP BEING THE ONE THAT PASSES INTO A PACKED
C   PARTICLE OR THE SUBSTRATE.

C   THE COMPUTER PROGRAM IS SPLIT INTO THE FOLLOWING SECTIONS :-

C   (1)   READING OF DATA INTO PROGRAM

C   (2)   SETTING SCALES AND AXES FOR PLOT

C   (3)   INITIAL CONDITIONS AND SIZE DISTRIBUTION

C   (4)   STARTING OF TRAJECTORY CALCULATIONS & CALLING NAG ROUTINE

C   (5)   CHECKING PARTICLE POSITION & PRINTING TRAJECTORY

C   (6)   COMPARISON WITH STATIONARY PARTICLES & TRAJECTORY PLOTTING

C   (7)   FINDING COLLISION PARTICLE & CALCULATING FINAL POSITION

C   (8)   POSITION ON SUBSTRATE

C   (9)   INTERPOLATION OF OTHER VARIABLES

C   (10)   OUTPUT OF FINAL POSITION

C   (11)   CALCULATION OF FORCES - IN SUBROUTINE

C   (12)   CALCULATION OF INTERPARTICULATE FORCES

```
CCCCCCCCCCCCCCCCCCCCCCCCCCCCCCCCCCCCCCCCCCCCCCCCCCCCCCCCCCCCCCCCCCCCCC

C       SECTION 1 .

CCCCCCCCCCCCCCCCCCCCCCCCCCCCCCCCCCCCCCCCCCCCCCCCCCCCCCCCCCCCCCCCCCCCCC

        INTEGER RANDO,XSTEPS,YSTEPS,NEGSTP,CHECK,JK,FORCEP
        INTEGER IND,NUMBER,N,IW,IW1,MPED,COMENT,PLOTNO,IFAIL,K,JJ,JW
        INTEGER ID1,ID2,I,J,KK,M

        REAL*8 CHXJJ,CHYJJ,CHDSQ,AIRVX,AIRVY,CHRAD,CHRSQ
        REAL*8 FP1,FP2,FP3,FP4,INTX1,INTX2,CSQ,P,R1,R2,TYPE
        REAL*8 STARTL,PTST,XLST,UNF,HEIGHT,UP,VP,TRAJPR,CHARGE
        REAL*8 UNITSP,XPAPER,YPAPER,AXISST,XLTH,YLTH,A,B
        REAL*8 Q,DTRIB(11),RFRONT,PI,CAXIS,VISC,ELSTR,DIECST,PERM
        REAL*8 GUNTAR,FRONT,TIPRAD,PHI,DENS,CELEC,SQH
        REAL*8 CGUN,CIMGUN,CCRGE,CMASS,C1DRAG,TEND,TOL,R,CEFLEC
        REAL*8 FRAC,FRAC10,DIAM,D(500),RADIUS,X1(500),Y1(500)
        REAL*8 PC(500),REYCON,REY,FLIGHT(500),START1(500)
        REAL*8 START,MASS,CFORCE,CDRAG,IE6,RAD,NUX,NUY,SIZE,T,Z(4)
        REAL*8 CIN(7),COMM(5),CON(5),COUT(16),PW(4,4),W(4,22)
        REAL*8 PRINTX,PRINTY,PRINTH,OLDX,OLDY,OVELX,OVELY,OY,OX
        REAL*8 VELX,VELY,X,Y,XJJ,YJJ,DTPSQ,RADJJ,RADSQ,CX,CY
        REAL*8 GRAD,INCEPT,C,A1,B1,INTX,INTY,LEVER,INTU,INTV,OLDT,PRINTD
        REAL*8 PRINTS,INTT,TRAJST,XAXIS,E,DTRIB0,GRAV

        REAL*8 DRAGX,DRAGY,IMAGE,FIELDX,FIELDY,FTOTX,FTOTY
        DIMENSION PLOTNO(7),COMENT(7)


        COMMON/BL3/DRAGX,DRAGY,IMAGE,FIELDX,FIELDY,FTOTX,FTOTY,AIRVX,AIRVY
        COMMON/BL1/UNF,HEIGHT,GUNTAR,CELEC,SQH,CGUN,CEFLEC,NUMBER
        COMMON/BL2/CIMGUN,D,PC,CHARGE,MASS,CFORCE,CDRAG,X1,Y1,GRAV,I,CSQ
        COMMON/BL4/REYCON,REY




        EXTERNAL FCN,D02QBF
        EXTERNAL SETCPU



C
C --- SET UP CALL TO  MAILBOX . USED TO KILL JOB AFTER
C --- DAY SHIFT HAS BEEN SET BY THE OPERATOR
C
        CALL MAILBX(SETCPU)
C         INITIAL CONDITIONS
C         _____

C         NUMBER OF PARTICLES
          CALL X04AAF(1,5)
          CALL X04ABF(1,5)
          READ(5,3096)NUMBER
C         GUN TO TARGET DTANCE
          GUNTAR=0.2D0
C         RANDOM NUMBER GENERATOR START NUMBER
          RANDO=0
C         START LENGTH FOR PARTICLES IN Y DIRECTION
        CALL INPUT(5)
        CALL INPF(STARTL)
```

```
        JW=6
C       START DTANCE OF START LENGTH FROM Y AXIS
        PTST=STARTL/-2.0D0
C       TOLERANCE ERROR
      CALL INPUT(5)
      CALL INPF(TOL)
C       START LENGTH IN X DIRECTION
        XLST=0.1D0
C       AIR GAS VELOCITY WHEN IN NORMAL FLOW
      CALL INPUT(5)
      CALL INPF(UNF)
      CALL INPUT(5)
      CALL INPF(TYPE)
      CALL INPUT(5)
      CALL INPF(DTRIB0)
        IF(DTRIB0.EQ.0)GO TO 1
        DO 1 I=1,11
              DTRIB(I)=DTRIB0
1       CONTINUE
        READ(5,55)FORCEP
55      FORMAT(I3)
        READ(5,122)(PLOTNO(I),I=1,7)
        READ(5,122)(COMENT(I),I=1,7)
C       HEIGHT OF TARGET PLATE
        HEIGHT=0.2D0
C       INITIAL PARTICLE VELOCITY IN X DIRECTION
        UP=UNF
C       INITIAL PARTICLE VELOCITY IN Y DIRECTION
        VP=0.0D0
C       START OF TRAJECTORY PRINT
        TRAJPR=GUNTAR-0.0999999D0


CCCCCCCCCCCCCCCCCCCCCCCCCCCCCCCCCCCCCCCCCCCCCCCCCCCCCCCCCCCCCCCCCCCCCCCCCCCCCC

C       SECTION 2

CCCCCCCCCCCCCCCCCCCCCCCCCCCCCCCCCCCCCCCCCCCCCCCCCCCCCCCCCCCCCCCCCCCCCCCCCCCCCC

C       PLOT CONDITIONS
C       _____

        CALL SAVDRA
C       UNIT SCALE FOR PLOTTING
        UNITSP=0.0800D0
C       LENGTH OF PAPER IN X DIRECTION
        XPAPER=10000.0D0
C       LENGTH OF PAPER IN Y DIRECTION
        YPAPER=2500.0D0
C       START OF AXIS AWAY FROM ORIGIN IN X DIRECTION
        AXISST=0.0
C       NUMBER OF STEP LENGTHS IN X DIRECTION
        XSTEPS=40
C       NUMBER OF STEP LENGTHS IN Y DIRECTION
        YSTEPS=10
C       LENGTH OF EACH STEP IN X
        XLTH=100
C       LENGTH OF EACH STEP IN Y
        YLTH=100
C       NUMBER OF NEGATIVE STEPS IN X
        NEGSTP=20
        CALL UNITS(UNITSP)
        CALL DEVPAP(XPAPER,YPAPER,1)
        CALL WINDOW(2)
        CALL CHASIZ(30.0,30.0)
        CALL MOVTO2((XSTEPS*XLTH+2000.0)/2-500.0,YPAPER-50.0)
```

```
          CALL CHAHOL(55H E*LLECTROSTATIC *UC*LOATING : *UP*LOWD
         1ER *UP*LACKING*.)
          CALL MOVTO2((XSTEPS*XLTH+2000.0)/2-470.0,YPAPER-60.0)
          CALL LINTO2((XSTEPS*XLTH+2000.0)/2-500.0+1180,YPAPER-60.0)
          CALL CHASIZ(20.0,20.0)
          A=(XSTEPS*XLTH)+1000.0
          CALL MOVTO2(A,YPAPER-100.0)
          CALL CHAHOL(30H            CALCULATION DATA *.)
          B=YPAPER-150.0
          CALL MOVTO2(A,B)
          CALL CHAHOL(25H NO OF PTCLS STUDIED = *.)
          CALL MOVTO2(A,B-25.0)
          CALL CHAHOL(25H X COORDINATE START  = *.)
          CALL MOVTO2(A,B-50.0)
          CALL CHAHOL(25H START LENGTH RANGE   = *.)
          CALL MOVTO2(A,B-75.0)
          CALL CHAHOL(25H RANDOM NO VARIABLE   = *.)
          CALL MOVTO2(A,B-100.0)
          CALL CHAHOL(25H VEL OF PARTICLE (X) = *.)
          CALL MOVTO2(A,B-125.0)
          CALL CHAHOL(25H UNIFORM AIR VELOCITY= *.)
          CALL MOVTO2(A,B-150.0)
          CALL CHAHOL(25H TOLERANCE ERROR      = *.)
          CALL MOVTO2(A,B-200.0)
          CALL CHAARR(PLOTNO,7,4)
          CALL MOVTO2(A,B-225.0)
          CALL CHAARR(COMENT,7,4)
          A=A+400.0
          CALL MOVTO2(A,B)
          CALL CHAINT(NUMBER,11)
          CALL MOVTO2(A,B-25.0)
          CALL CHAFIX(XLST,14,6)
          CALL MOVTO2(A,B-50.0)
          CALL CHAFIX(STARTL,14,6)
          CALL MOVTO2(A,B-75.0)
          CALL CHAINT(RANDO,11)
          CALL MOVTO2(A,B-100.0)
          CALL CHAFIX(UP,14,6)
          CALL MOVTO2(A,B-125.0)
          CALL CHAFIX(UNF,14,6)
          CALL MOVTO2(A+60.0,B-150.0)
          CALL CHAFLO(TOL,10)
          CALL MOVTO2(A-400.0,B-200.0)
C        LABELLING OF AXES

C        X AXIS

          XAXIS=1000.0+(XLTH*NEGSTP)
          CALL MOVTO2(1000.0,50.0)
          CALL LINTO2((1000.0+XSTEPS*XLTH),50.0)
          CALL LINTO2((1000.0+XSTEPS*XLTH),(YSTEPS*YLTH)+50.0)
          CALL MOVTO2(1000.0,50.0)
          CALL LINTO2(1000.0,(YSTEPS*YLTH)+50.0)
          CALL MOVTO2((1000.0+XSTEPS*XLTH)/2-5.0,5.0)
          CALL CHAHOL(12H SUBSTRATE*.)
          CALL CHASIZ(15.0,15.0)
          ID1=XSTEPS+1
          DO 10 I=1,ID1
                M=(I-(NEGSTP+1))*XLTH+AXISST
                Q=(I-1)*XLTH+1000.0
                CALL MOVTO2(Q,55.0)
                CALL LINTO2(Q,45.0)
                CALL MOVTO2(Q-50.0,30.0)
                CALL CHAINT(M,5)
10        CONTINUE
```

```
C .
 ·C        Y AXIS
 ·C

          ID2=YSTEPS+1
          DO 11 I=1,ID2
                  M=(I-1)*YLTH
                  Q=(I-1)*YLTH+50.0
                  CALL MOVTO2(1005.0,Q)
                  CALL LINTO2(995.0,Q)
                  CALL MOVTO2(930.0,Q-5.0)
                  CALL CHAINT(M,4)
                  C=1000.0+(XSTEPS*XLTH)
                  CALL MOVTO2(C-5.0,Q)
                  CALL LINTO2(C+5.0,Q)
                  CALL MOVTO2(C+10.0,Q)
                  CALL CHAINT(M,4)
11        CONTINUE


          CALL MOVTO2(0.0,50.0)
          CALL LINTO2(XPAPER,50.0)


CCCCCCCCCCCCCCCCCCCCCCCCCCCCCCCCCCCCCCCCCCCCCCCCCCCCCCCCCCCCCCCCCCCCCC

C         SECTION 3

CCCCCCCCCCCCCCCCCCCCCCCCCCCCCCCCCCCCCCCCCCCCCCCCCCCCCCCCCCCCCCCCCCCCCC

C         SETTING CONDITIONS
C
C         _____
C
C         SIZE DTRIBUTION OF PARTICLES
C
          IF(DTRIB0.NE.0)GO TO 11222
          DTRIB(1)=0.000005D0
          DTRIB(2)=0.00000575D0
          DTRIB(3)=0.0000065D0
          DTRIB(4)=0.00000725D0
          DTRIB(5)=0.000008D0
          DTRIB(6)=0.00000875
          DTRIB(7)=0.0000095D0
          DTRIB(8)=0.0000105D0
          DTRIB(9)=0.0000125D0
          DTRIB(10)=0.0000170D0
          DTRIB(11)=0.000095D0
11222     CONTINUE
          RFRONT=0.0D0
          PI=4*DATAN(1.0D0)
          CAXIS=XAXIS-AXISST
C         VISCOSITY OF AIR
          VISC=0.0000178D0
C         ELECTRODE STRENGTH
          ELSTR=6D05
C         DIELECTRIC CONSTANT
          DIECST=4.0D0
C         PERMITTIVITY OF FREE SPACE
          PERM=8.85D-12
C         ELECTRODE NEEDLE RADIUS
          TIPRAD=0.005D0
C         FIELD POTENTIAL
          PHI=60000.0D0
C         DENSITY OF POWDER
          DENS=1000
          FRONT=GUNTAR
```

```
C        CALCULATION CONSTANTS
C
C        _____
         CELEC=4*PI*PERM
         SQH=HEIGHT**2
         CGUN=PHI/(DLOG(GUNTAR/TIPRAD))
         CIMGUN=2*GUNTAR.
         CCRGE=3*PI*(DIECST/(DIECST+2.0))*PERM*ELSTR
         CMASS=PI*DENS/6
         C1DRAG=3*PI*VISC
C
C        TIME OF INTEGRATION FOR EACH PARTICLE (MAX)
         TEND=5.0D0
         WRITE(JW,1000)
         WRITE(JW,1020)
         WRITE(JW,1021)
         WRITE(JW,123)(PLOTNO(I),I=1,7)
         WRITE(JW,122)(COMENT(I),I=1,7)
         WRITE(JW,1023)NUMBER
         WRITE(JW,1024)RANDO.
         WRITE(JW,1025)XLST
         WRITE(JW,1026)STARTL
         WRITE(JW,1027)UNF
         WRITE(JW,1028)HEIGHT
         WRITE(JW,1029)UP
         WRITE(JW,1030)VP
         WRITE(JW,1031)TOL
         WRITE(JW,1032)TEND
         WRITE(JW,1033)TRAJST
122      FORMAT(7A4)
123      FORMAT('  PLOT FILE NAME IS  ',7A4)
1020     FORMAT(2(1X/),30H            BOUNDARY CONDITIONS)
1021     FORMAT(30H            ---------------------)
1023     FORMAT(20H NO OF PARTICLES   = ,I10)
1024     FORMAT(20H RANDOM NUMBER GEN= ,I10)
1025     FORMAT(20H X START FROM GUN = ,E20.10)
1026     FORMAT(20H START WIDTH IN Y = ,E20.10)
1027     FORMAT(20H UNIFORM AIR VEL  = ,E20.10)

1028     FORMAT(20H HEIGHT OF TARGET = ,E20.10)
1029     FORMAT(20H INITIAL X VEL.   = ,E20.10)
1030     FORMAT(20H INITIAL Y-VEL.   = ,E20.10)
1031     FORMAT(20H TOLERANCE ERROR  = ,E20.10)
1032     FORMAT(20H INTEGRATION TIME = ,E20.10)
1033     FORMAT(20H TRAJECTORY START = ,E20.10)
         WRITE(JW,1000)


CCCCCCCCCCCCCCCCCCCCCCCCCCCCCCCCCCCCCCCCCCCCCCCCCCCCCCCCCCCCCCCCCCCCCCCCCC

C        SECTION 4

CCCCCCCCCCCCCCCCCCCCCCCCCCCCCCCCCCCCCCCCCCCCCCCCCCCCCCCCCCCCCCCCCCCCCCCCCC

C        CALCULATION OF SIZE AND START POSITION
         CALL G05CBF(RANDO)
         DO 14 I=1,NUMBER
               R=G05CAF(R)
               FRAC=G05CAF(FRAC)
               FRAC10=FRAC*10
               IND=0
               DO 16 J=1,10
                     E=J
                     IF(FRAC10.LT.E)GO TO 11115
16             CONTINUE
```

```
11115          DIAM=DTRIB(J+1)-((J-FRAC10)*(DTRIB(J+1)-DTRIB(J)))
               D(I)=DIAM
               RADIUS=DIAM/2
               START=STARTL*R+PTST
               START1(I)=START

C        CALCULATION CONSTANTS

               CHARGE=CCRGE*(DIAM**2)
               CSQ=CHARGE**2
               PC(I)=CHARGE
               MASS=(DIAM**3)*CMASS
               REYCON=DIAM*1.0/VISC
               GRAV=0
               CEFLEC=CHARGE*CGUN
               CFORCE=CHARGE/CELEC
               CDRAG=C1DRAG*DIAM
               IE6=1D06
               RAD=RADIUS*IE6
               NUX=RAD/3
               NUY=RAD/6
               SIZE=RAD/2.5
               CALL CHASIZ(SIZE,SIZE)
C        BOUNDARY CONDITIONS FOR EACH PARTICLE
               T=0.0D0
               Z(1)=UP
               Z(2)=XLST
               Z(3)=VP
               Z(4)=START
               N=4

C        SETTING OF NAG CONTROL PARAMETERS

               CIN(1)=1.0D0
               CIN(2)=0.0D0
               CIN(3)=0.0D0
               CIN(4)=0.0D0
               CIN(5)=0.0D0
               CIN(6)=0.0D0
               COMM(1)=0.0D0
               COMM(2)=0.0D0
               COMM(3)=1.0D0
               W(1,21)=-999
               W(2,21)=TRAJPR
               W(3,21)=-999
               W(4,21)=-999
               COMM(4)=0.0D0
               COMM(5)=0.0D0
               X=0.0D0
               Y=0.0D0
               VELX=0.0D0
               VELY=0.0D0
               OLDX=0.0D0
               OLDY=0.0D0
               OVELX=0.0D0
               OVELY=0.0D0
               OLDT=0.0D0
               MPED=0
               IFAIL=1
               IW=4
               IW1=22
C        PRINT HEADING FOR TRAJECTORY TABLE

               PRINTX=(GUNTAR-Z(2))*IE6
```

```
                    PRINTY=Z(4)*IE6
                    PRINTH=CIN(5)

            IF(I.NE.FORCEP)GO TO 11333
            WRITE(JW,3008)
            WRITE(JW,3031)I
            WRITE(JW,3008)                              .
            WRITE(JW,3030)
            WRITE(JW,3008)
11333       CONTINUE
            IF (TYPE.EQ.0)GO TO 10000
                    WRITE(JW,3008)
                    WRITE(JW,3043)I
                    WRITE(JW,3044)
                    WRITE(JW,3008)
                    WRITE(JW,3060)DIAM
                    WRITE(JW,3061)START
                    WRITE(JW,3062)PTST
                    WRITE(JW,3063)CHARGE
                    WRITE(JW,3064)MASS
            WRITE(JW,3008)
                    WRITE(JW,3045)
                    WRITE(JW,312)T,PRINTX,PRINTY,Z(1),Z(3),AIRVX,AIRVY,PRINTH


C       CALL TO NAG ROUTINE

10000   CALL D02QBF(T,TEND,N,Z,CIN,TOL,FCN,COMM,CON,COUT,MPED,
        1PEDERV,PW,W,IW,IW1,IFAIL)

CCCCCCCCCCCCCCCCCCCCCCCCCCCCCCCCCCCCCCCCCCCCCCCCCCCCCCCCCCCCCCCCCCCCCCCC

C       SECTION 5

CCCCCCCCCCCCCCCCCCCCCCCCCCCCCCCCCCCCCCCCCCCCCCCCCCCCCCCCCCCCCCCCCCCCCCCC



C       COMES OUT OF D02QBF WHEN REACHING FRONT OR EVERY STEP AFTERWARDS

                    IF(IFAIL.GT.0)GO TO 99999
                    IF(IND.EQ.1)GO TO 10005
                    W(2,21)=-999
                    COMM(4)=1.
                    IND=1
                    OY=(GUNTAR-Z(2))*IE6+50.0
                    OX=(Z(4)*IE6)+CAXIS
                    CALL MOVTO2(OX,OY)
                    GO TO 10006
10005               VELX=Z(1)
                    VELY=Z(3)
                    X=Z(2)
                    Y=Z(4)

C       CHECK IF PARTICLE IS OUT OF BOUNDS OR IN LAYER REGION

                    IF(T.GT.TEND-0.5)GO TO 22333
                    IF(Y.LT.-0.01D0)GO TO 22333
                    IF(Y.GT.0.01D0)GO TO 22333
                    PRINTX=(GUNTAR-X)*IE6
                    PRINTY=Y*IE6

C       STEPLENGTH

                    IF(I.NE.FORCEP)GO TO 11334
```

```
                    WRITE(JW,313)T,PRINTX,PRINTY,DRAGX,DRAGY,FIELDX
          1         ,FIELDY,IMAGE,FTOTX,FTOTY
11334               CONTINUE
                    IF(TYPE.EQ.0)GO TO 11111
                    PRINTH=COUT(4)-COUT(5)
                    WRITE(JW,312)T,PRINTX,PRINTY,VELX,VELY,AIRVX,AIRVY,PRINTH,REY
```

CCCCCCCCCCCCCCCCCCCCCCCCCCCCCCCCCCCCCCCCCCCCCCCCCCCCCCCCCCCCCCCCCCCC

```
C       SECTION 6
```

CCCCCCCCCCCCCCCCCCCCCCCCCCCCCCCCCCCCCCCCCCCCCCCCCCCCCCCCCCCCCCCCCCCC

```
C       CHECK ON POSITION RELATIVE TO SUBSTRATE & OTHER PARTICLES

11111               CONTINUE
                    IF(X+RADIUS+RFRONT.LT.FRONT)GO TO 10001
                    IF(I.EQ.1)GO TO 10001
                    K=I-1
                    DO 31 J=1,K
                            JJ=I-J
                            XJJ=X1(JJ)
                            YJJ=Y1(JJ)
                            DTPSQ=(X-XJJ)**2+(Y-YJJ)**2
                            RADJJ=D(JJ)/2
                            RADSQ=(RADIUS+RADJJ)**2
                            IF(DTPSQ.LT.RADSQ)GO TO 10222
31                  CONTINUE
10001               IF(X+RADIUS.GT.GUNTAR)GO TO 10003


C       PARTICLE HAS PASSED THROUGH ALL CHECKS BUT MUST BE IN
C       TRAJECTORY PRINT REGION AND SO THEREFORE PLOT STEP
C       X AND Y ARE REVERSED FOR PLOTTING

                    CX=(Y*IE6)+CAXIS
                    CY=(GUNTAR-X)*IE6+50.0
                    CALL LINTO2(CX,CY)
                    OX=CX
                    OY=CY
10006               OLDX=X
                    OLDY=Y
                    OLDT=T
                    OVELX=VELX
                    OVELY=VELY
                    IFAIL=1
                    GO TO10000
C       PARTICLE IS FOUND TO HIT ANOTHER PARTICLE
C       CALCULATE INTERSECTION OF LINE BETWEEN TWO TRAJECTORY POINTS
C       AND CIRCLE OF RADIUS (RADIUS+RADJJ)

C       CHECK IS NOW CARRIED OUT TO SEE IF ANY OTHER PARTICLE
C       IS HIT. SEARCH CARRIES ON THROUGH REST OF STATIONARY PARTICLES
```

CCCCCCCCCCCCCCCCCCCCCCCCCCCCCCCCCCCCCCCCCCCCCCCCCCCCCCCCCCCCCCCCCCCC

```
C       SECTION 7
```

CCCCCCCCCCCCCCCCCCCCCCCCCCCCCCCCCCCCCCCCCCCCCCCCCCCCCCCCCCCCCCCCCCCC

```
10222               IF(JJ.EQ.1)GO TO 10002
                    CHECK=JJ-1
                    DO 32 JK=1,CHECK
```

```
                        JJ=CHECK+1-JK
                        CHXJJ=X1(JJ)
                        CHYJJ=Y1(JJ)
                        CHDSQ=(X-CHXJJ)**2+(Y-CHYJJ)**2
                        CHRAD=D(JJ)/2
                        CHRSQ=(RADIUS+CHRAD)**2
                        IF(CHDSQ.LT.CHRSQ)GO TO 10022
32                  CONTINUE
                    JJ=CHECK+1
                    GO TO 10002

C       ANOTHER PARTICLE HAS BEEN FOUND - NOW FIND OUT WHICH ONE
C       HAS THE LEAST OVERSHOOT - BIGGER THE DIFFERENCE THE MORE IT
C       HAS OVER SHOT

10022               IF((CHRSQ-CHDSQ).LT.(RADSQ-DTPSQ))GO TO 32
                    RADSQ=CHRSQ
                    DTPSQ=CHDSQ
                    XJJ=CHXJJ
                    YJJ=CHYJJ
                    GO TO 10222

C       THE NEAREST PARTICLE TO THE LAST POINT ON THE TRAJECTORY
C       IS NOW RECORDED AND SO INTERPOLATION ROUTINE COMMENCES

10002               GRAD=(Y-OLDY)/(X-OLDX)
                    INCEPT=Y-GRAD*X

C       NOW USING X**2+Y**2=R**2 CALCULATE INTERCEPT

                    P=GRAD*XJJ+INCEPT-YJJ
                    A=1+GRAD**2
                    B=2*GRAD*P
                    C=P**2-RADSQ
                    IF(B.LT.0)GO TO 888
                    R1=(-B-DSQRT(B**2-4*A*C))/(2*A)
                    GO TO 8888
888                 R1=(-B+DSQRT(B**2-4*A*C))/(2*A)
8888                CONTINUE
                    R2=C/(A*R1)
                    INTX1=XJJ+R1
                    INTX2=XJJ+R2
                    IF(INTX1.GT.INTX2)GO TO 10010
                    INTX=INTX1
                    GO TO 10011
10010               INTX=INTX2
10011               INTY=GRAD*INTX+INCEPT

C       NOW GO AND CALCULATE 'LEVER' ,OTHER VARIABLES AND
C       PLOT FINAL POINT

                    GO TO 10007

CCCCCCCCCCCCCCCCCCCCCCCCCCCCCCCCCCCCCCCCCCCCCCCCCCCCCCCCCCCCCCCCCC

C       SECTION 8

CCCCCCCCCCCCCCCCCCCCCCCCCCCCCCCCCCCCCCCCCCCCCCCCCCCCCCCCCCCCCCCCCC

C       CALCULATION OF FINAL POSITION ON SUBSTRATE USING EQUATION
C       OF LINE BETWEEN OLD & NEW POSITION
```

```
C       WE KNOW THAT X MUST EQUQAL 'GUNTAR-RADIUS'


10003   JJ=0
             GRAD=(Y-OLDY)/(X-OLDX)
             INCEPT=Y-GRAD*X
             INTX=GUNTAR-RADIUS
             INTY=GRAD*INTX+INCEPT


CCCCCCCCCCCCCCCCCCCCCCCCCCCCCCCCCCCCCCCCCCCCCCCCCCCCCCCCCCCCCCCCCC

C       SECTION 9

CCCCCCCCCCCCCCCCCCCCCCCCCCCCCCCCCCCCCCCCCCCCCCCCCCCCCCCCCCCCCCCCCC


C       NOW GO AND CALCULATE 'LEVER' AND OTHER VARIABLES

10007        LEVER=(X-INTX)/(X-OLDX)
             X1(I)=INTX
             Y1(I)=INTY
             INTV=VELY-LEVER*(VELY-OVELY)
             INTU=VELX-LEVER*(VELX-OVELX)
             INTT=T-LEVER*(T-OLDT)
             FLIGHT(I)=INTT



C       PLOT POSITION OF PARTICLE AND TRAJECTORY
C
             CX=(INTY*IE6)+CAXIS
             CY=(GUNTAR-INTX)*IE6+50.0
             CALL MOVTO2(CX,CY-RAD)
             CALL ARCBY2(0.0,RAD,0.0,0.0,0)
             CALLMOVTO2(CX-NUX,CY-NUY)
             CALL CHAINT(I,3)
             CALL MOVTO2(CX,CY)
             CALL LINTO2(OX,OY)

C       THEN PRINT FINAL POSITION
C       COMPARE POSITION OF PARTICLE TO FRONT ONE

             IF(INTX.GT.FRONT)GO TO 10008
             FRONT=INTX
             RFRONT=RADIUS
10008        CONTINUE
             IF(TYPE.EQ.0)GO TO 21111

CCCCCCCCCCCCCCCCCCCCCCCCCCCCCCCCCCCCCCCCCCCCCCCCCCCCCCCCCCCCCCCCCC

C       SECTION 10

CCCCCCCCCCCCCCCCCCCCCCCCCCCCCCCCCCCCCCCCCCCCCCCCCCCCCCCCCCCCCCCCCC


             WRITE(JW,3045)
             WRITE(JW,3000)
             WRITE(JW,3006)I
             WRITE(JW,3007)
             WRITE(JW,3001)T,OLDT,INTT
             WRITE(JW,3002)VELX,OVELX,INTU
             WRITE(JW,3003)X,OLDX,INTX
             WRITE(JW,3004)VELY,OVELY,INTV
             WRITE(JW,3005)Y,OLDY,INTY
```

```
              WRITE(JW,3008)
              WRITE(JW,3000)

C      CONTINUING FINAL PRINTOUT

              WRITE(JW,3008)
              PRINTD=RADIUS*IE6
              PRINTX=(GUNTAR-INTX)*IE6
              PRINTY=INTY*IE6
              PRINTS=START*IE6
              WRITE(JW,3009)PRINTD
              WRITE(JW,3010)PRINTX
              WRITE(JW,3011)PRINTY
              WRITE(JW,3012)INTT
              WRITE(JW,3013)PRINTS
              WRITE(JW,3008)
              WRITE(JW,3000)
              WRITE(JW,3008)


              GO TO 21111

22333         INTY=999.99
              JJ=0
              INTX=999.999

C      PRINT FINAL PARTICLE POSITION & HIT NUMBER

21111  CONTINUE
       IF(I.NE.FORCEP)GO TO 11335
       WRITE(JW,3008)
       WRITE(JW,3030)
11335  CONTINUE
       WRITE(JW,3075)I,INTX,INTY,JJ,DIAM
14     CONTINUE


       WRITE(JW,1001)
       WRITE(JW,1002)
       WRITE(JW,1003)
       DO 18 J=1,NUMBER
              FP1=(GUNTAR-X1(J))*IE6
              FP2=START1(J)*IE6
              FP3=Y1(J)*IE6
              FP4=D(J)*IE6
              WRITE(JW,1004)J,FLIGHT(J),FP1,FP2,FP3,FP4
18     CONTINUE
       WRITE(JW,1005)
       WRITE(JW,1000)



       WRITE(JW,3071)FRONT,RFRONT
       WRITE(JW,3008)
       WRITE(JW,3072)AIRVX
       WRITE(JW,3073)AIRVY
       WRITE(JW,3080)DRAGX
       WRITE(JW,3081)DRAGY
       WRITE(JW,3082)IMAGE
       WRITE(JW,3083)FIELDX
       WRITE(JW,3084)FIELDY
       WRITE(JW,3085)FTOTX
       WRITE(JW,3086)FTOTY
1000   FORMAT(///'#############################################
      1#############################################')
```

```
1001    FORMAT(//,´
       1                    FINAL PARTICLE POSITION´)
1002    FORMAT(´
       1             ─────────────────────────´)
1003    FORMAT(/////,´                    ·                    FLIGHT TIME          HEIGHT FRO
       1M PLATE       Y START       Y COORDINATE        PARTICLE D
       2IAMETER´)
1004    FORMAT(2(1X/),13H PARTICLE NO ,I3,3H    ,5F20.10)
1005    FORMAT(4(1X/))
3000    FORMAT(//´ *******************************************************
       1*******************************************************´)
3001    FORMAT(20H          NEW TIME = ,E20.10,20H            OL
       1D TIME = ,E20.10,20H      INTPL´D TIME = ,E20.10)
3002    FORMAT(20H         NEW X VEL = ,E20.10,20H          OLD X VE
       1L = ,E20.10,20H     INTPL´D X VEL = ,E20.10)
3003    FORMAT(20H        NEW X COORD = ,E20.10,20H        OLD X COO
       1RD = ,E20.10,20H  INTPL´D X COORD = ,E20.10)
3004    FORMAT(20H          NEW Y VEL = ,E20.10,20H          OLD Y VE
       1L = ,E20.10,20H     INTPL´D Y VEL = ,E20.10)
3005    FORMAT(20H         NEW Y COORD = ,E20.10,20H        OLD Y COOR
       1D = ,E20.10,20H  INTPL´D Y COORD = ,E20.10)
3006    FORMAT(2(1X/),33H FINAL PARTICLE POSITION - NUMBER,I3)
3007    FORMAT(38H ──────────────────────────────────)
3008    FORMAT(3(1X/))
3009    FORMAT(20H     PARTICLE SIZE = ,F20.10)
3010    FORMAT(20H      X COORDINATE = ,F20.10)
3011    FORMAT(20H      Y COORDINATE = ,F20.10)
3012    FORMAT(20H     TIME IN FLIGHT = ,F20.10)
3013    FORMAT(20H      START Y COORD = ,F20.10)
3043    FORMAT(´ ELECTROSTATIC POWDER COATING TRAJECTORY - PARTI
       1CLE NUMBER ´,I3)

3044    FORMAT(´ ──────────────────────────────────────────── ───
       1─────────────´)
3031    FORMAT(´                 PARTICLE TRAJECTORY - FORCES ON PARTICLE NO.
       1 ´,I3)
3030    FORMAT(´    TIME ·X COORDINATE Y COORD    DRAG X        DRAG Y
       1        FIELD X     FIELD Y      IMAGE     TOT INTER X  TOT INTER Y´)
3045    FORMAT(´     TIME       X COORDINATE
       1 Y COORDINATE    X VELOCITY     Y VEL
       2OCITY    AIR VEL X    AIR VEL Y    STEP LENGTH   REYNOLDS NO         ´,/)
313     FORMAT(F8.5,F12.4,F10.4,7E12.4)
312     FORMAT(F12.6,2F12.4,4F12.6,E14.4,F12.4)
3071    FORMAT(//,´ X COORDINATE OF HIGHEST PARTICLE = ´,E20.10,
       1/,´ RADIUS OF THIS PARTICLE = ´,E20.10,//)
3072    FORMAT(´ AIR VELX= ´,E20.10)
3073    FORMAT(´ AIR VELY= ´,E20.10)
3075    FORMAT(/´ PARTICLE ´,I3,´ LANDED , X = ´,F14.7,´ , Y =
       1´,F14.7,´ HIT PARTICLE NO. ´,I3,´ PARTICLE DIAMETER = ´,F14.7)
3080    FORMAT(´ DRAGX   = ´,E20.10)
3081    FORMAT(´ DRAGY   = ´,E20.10)
3082    FORMAT(´ IMAGE   = ´,E20.10)
3083    FORMAT(´ FIELDX  = ´,E20.10)
3084    FORMAT(´ FIELDY  = ´,E20.10)
3085    FORMAT(´ FTOTX   = ´,E20.10)
3086    FORMAT(´ FTOTY   = ´,E20.10,///)
3096    FORMAT(I3)



C       ERROR STATUS CONTROL - OUTPUT OF NAG PARAMETERS


99999   DO 91 KK=1,4
```

```
                    WRITE(JW,3015)KK,COUT(KK),KK,CIN(KK),KK,CON(KK),
          1         KK,COMM(KK)
91        CONTINUE
          KK=5
          WRITE(JW,3016)KK,COUT(KK),KK,CIN(KK),KK,CON(KK)
          DO 92 KK=6,7
                    WRITE(JW,3017)KK,COUT(KK),KK,CIN(KK)
92        CONTINUE
          DO 93 KK=8,16
                    WRITE(JW,3018)KK,COUT(KK)
93        CONTINUE
          WRITE(JW,3333)IFAIL
          CALL DEVEND
3333      FORMAT('   IFAIL= ',I3)
3060      FORMAT(' DIAMETER OF PARTICLE = ',E20.10)
3061      FORMAT(' START POSITION IN Y  = ',E20.10)
3062      FORMAT(' DISTANCE FROM ORIGIN = ',E20.10)
3063      FORMAT(' CHARGE ON PARTICLE   = ',E20.10)
3064      FORMAT(' MASS OF PARTICLE     = ',E20.10)
3015      FORMAT('  COUT NO.',I2,2X,E13.6,'     CIN NO.',I2
          1,2X,E13.6,'    CON NO.',I2,2X,E13.6,'      COMM NO.',I2
          1,2X,E13.6)
3016      FORMAT('  COUT NO.',I2,2X,E13.6,'     CIN NO.',I2,2X
          1,E13.6,'    CON NO.',I2,2X,E13.6)
3017      FORMAT('  COUT NO.',I3,2X,E13.6,'     CIN NO.',I2,2X,E
          113.6)
3018      FORMAT('  COUT NO.',I2,2X,E13.6)


          STOP
          END




          SUBROUTINE FCN(T,Z,F)

CCCCCCCCCCCCCCCCCCCCCCCCCCCCCCCCCCCCCCCCCCCCCCCCCCCCCCCCCCCCCCCCCCCCCC

C         SECTION 11

CCCCCCCCCCCCCCCCCCCCCCCCCCCCCCCCCCCCCCCCCCCCCCCCCCCCCCCCCCCCCCCCCCCCCC



          REAL*8 X,Y,X1(500),Y1(500),T,Z(4),F(4),VELX,VELY,CSQ
          REAL*8 SQX,SQY,NEWX,GUNTAR,SQNX,RCONS,CELEC,HEIGHT
          REAL*8 SQH,SQRRC,THETA,SINT,COST,AIRVX,AIRVY,UNF,DRAGX
          REAL*8 DRAGY,CDRAG,IMAGE,CHARGE,ELEC,CGUN,FIELDX,FIELDY
          REAL*8 FTOTX,FTOTY,XI,YI,IMX,IMY,CIMGUN,CEFLEC
          REAL*8 DIFIMX,DIFIMY,DIFXI,DIFYI,DTSQJ,DTSQI,SQRDI
          REAL*8 SQRDJ,COSI,COSJ,SINI,SINJ,ATTFX,ATTFY,REPFX,REPFY,CONST
          REAL*8 CFORCE,PC(500),PARTFX,PARTFY,MASS,GRAV,D(500)
          REAL*8 DIFVX,DIFVY,VREL,REY,REYCON


          INTEGER I,IND3,II


          COMMON/BL1/UNF,HEIGHT,GUNTAR,CELEC,SQH,CGUN,CEFLEC,NUMBER
          COMMON/BL2/CIMGUN,D,PC,CHARGE,MASS,CFORCE,CDRAG,X1,Y1,GRAV,I,CSQ
          COMMON/BL3/DRAGX,DRAGY,IMAGE,FIELDX,FIELDY,FTOTX,FTOTY,AIRVX,AIRVY
```

```
        COMMON/BL4/REYCON,REY


        X=Z(2)
        Y=Z(4)
        VELX=Z(1)
        VELY=Z(3)
        SQX=X**2
        SQY=Y**2

C       VELOCITY PROFILE CALCULATIONS

        NEWX=X-GUNTAR
        SQNX=NEWX**2
        RCONS=DSQRT((SQNX-SQY+SQH)**2+(2*NEWX*Y)**2)
        SQRRC=DSQRT(RCONS)
        THETA=DATAN((-2*NEWX*Y)/(SQNX-SQY+SQH))
        SINT=DSIN(THETA/2)
        COST=DCOS(THETA/2)
        AIRVX=-UNF*(NEWX*COST-Y*SINT)/SQRRC
        AIRVY=UNF*(NEWX*SINT+Y*COST)/SQRRC
        DIFVX=AIRVX-VELX
        DIFVY=AIRVY-VELY
        VREL=DSQRT(DIFVX**2+DIFVY**2)
        REY=REYCON*VREL

C       DRAG FORCE

        DRAGX=CDRAG*(AIRVX-VELX)
        DRAGY=CDRAG*(AIRVY-VELY)

C       IMAGE FORCE

        IMAGE=CSQ/(CELEC*(2*(GUNTAR-X)))**2)

C       FIELD FORCES

        ELEC=CEFLEC/(SQX+SQY)
        FIELDX=ELEC*X
        FIELDY=ELEC*Y


CCCCCCCCCCCCCCCCCCCCCCCCCCCCCCCCCCCCCCCCCCCCCCCCCCCCCCCCCCCCCCCCCCCCCC

C       SECTION 12

CCCCCCCCCCCCCCCCCCCCCCCCCCCCCCCCCCCCCCCCCCCCCCCCCCCCCCCCCCCCCCCCCCCCCC

C       INTER PARTICUIATE FORCES

        FTOTX=0.0D0
        FTOTY=0.0D0
        IF(I.EQ.1)GO TO 22222
        IND3=I-1
        DO 21 II=1,IND3
                XI=X1(II)
                YI=Y1(II)
                IMX=CIMGUN-XI
                IMY=YI
                DIFIMX=IMX-X
                DIFIMY=IMY-Y
                DIFXI=XI-X
                DIFYI=YI-Y
                DTSQJ=DIFIMX**2+DIFIMY**2
                DTSQI=DIFXI**2+DIFYI**2
```

```
                    SQRDI=DSQRT(DTSQI)
                    SQRDJ=DSQRT(DTSQJ)
                    COSI=DIFXI/SQRDI
                    COSJ=DIFIMX/SQRDJ
                    SINI=DIFYI/SQRDI
                    SINJ=DIFIMY/SQRDJ

                    ATTFX=COSJ/DTSQJ
                    ATTFY=SINJ/DTSQJ
                    REPFX=COSI/DTSQI
                    REPFY=SINI/DTSQI

                    CONST=CFORCE*PC(II)
                    PARTFX=(ATTFX-REPFX)*CONST
                    PARTFY=(ATTFY-REPFY)*CONST

                    FTOTX=FTOTX+PARTFX
                    FTOTY=FTOTY+PARTFY

21      CONTINUE

22222   F(1)=(DRAGX+FIELDX+IMAGE+FTOTX)/MASS
        F(2)=VELX
        F(3)=(DRAGY+FIELDY+GRAV+FTOTY)/MASS
        F(4)=VELY
        RETURN
        END

$
```

```
C       SEGMENT OF PROGRAM 'LAYER.FOR'

C       USED FOR THE CALCULATION OF TRAJECTORY OF PARTICLES TOWARDS A
C       SUBSTRATE COVERED WITH A THEORETICAL LAYER OF CHARGE.




CCCCCCCCCCCCCCCCCCCCCCCCCCCCCCCCCCCCCCCCCCCCCCCCCCCCCCCCCCCCCCCCCCCCCCCC

C       SECTION 11

CCCCCCCCCCCCCCCCCCCCCCCCCCCCCCCCCCCCCCCCCCCCCCCCCCCCCCCCCCCCCCCCCCCCCCCC


C       CALCULATION OF INTERPARTICULATE FORCES ACTING ON ONCOMING PARTICLE.
C       A THEORETICAL LAYER OF CHARGE OF THICKNESS 'THICK' IS ASSUMED TO
C       EXIST ACROSS THE WHOLE WIDTH OF THE PLATE. AN OVERALL CHARGE DENSITY
C       IS CALCULATED (PER UNIT AREA) ON THE BASIS OF THE SIZE OF PARTICLES
C       AND A POROSITY OF PACKING FACTOR.
C       THIS APPROACH SAVES ALL THE SUMMATIONS OF INDIVIDUAL PARTICLE FORCES.
C       A MODEL IS USED FOR BOTH THE REAL & IMAGE LAYERS

C       INTER PARTICULATE FORCES

        FTOTX=0.0D0
        FTOTY=0.0D0
        WID=HEIGHT/2.0D0
        WIDN=WID-Y
        AGUNTH=GUNTAR-X+THICK
        GUNTH=GUNTAR-THICK-X
        GUNN=GUNTAR-X
        WIDP=WID+Y
        NWIDN=-WID-Y


        T1=WIDN+DSQRT(GUNTH**2+WIDN**2)
        T2=NWIDN+DSQRT(GUNN**2+WIDP**2)
        B1=WIDN+DSQRT(GUNN**2+WIDN**2)
        B2=NWIDN+DSQRT(GUNTH**2+WIDP**2)

        REPFX=-CFORCE*CAREA*DLOG(T1*T2/(B1*B2))

        T1=GUNTH+DSQRT(WIDN**2+GUNTH**2)
        T2=GUNN+DSQRT(WIDP**2+GUNN**2)
        B1=GUNN+DSQRT(WIDN**2+GUNN**2)
        B2=GUNTH+DSQRT(WIDP**2+GUNTH**2)

        REPFY=-CFORCE*CAREA*DLOG(T1*T2/(B1*B2))

        T1=WIDN+DSQRT(GUNN**2+WIDN**2)
        T2=NWIDN+DSQRT(AGUNTH**2+WIDP**2)
        B1=WIDN+DSQRT(AGUNTH**2+WIDN**2)
        B2=NWIDN+DSQRT(GUNN**2+WIDP**2)

        ATTFX=CFORCE*CAREA*DLOG(T1*T2/(B1*B2))

        T1=GUNN+DSQRT(WIDN**2+GUNN**2)
        T2=AGUNTH+DSQRT(WIDP**2+AGUNTH**2)
        B1=AGUNTH+DSQRT(WIDN**2+AGUNTH**2)
```

```
B2=GUNN+DSQRT(WIDP**2+GUNN**2)

ATIFY=CFORCE*CAREA*DLOG(T1*T2/(B1*B2))


FTOTX=REPFX+ATIFX
FTOTY=REPFY+ATIFY


F(1)=(DRAGX+FIELDX+IMAGE+FTOTX)/MASS
F(2)=VELX
F(3)=(DRAGY+FIELDY+GRAV+FTOTY)/MASS
F(4)=VELY
RETURN
END


$
```

Explanation of Computer Program Variables

##

BOUNDARY CONDITIONS

PLOT FILE NAME IS   PLOT NUMBER FIELD25V5
25 UM - WITH FIELD
NO OF PARTICLES   =   10
RANDOM NUMBER GEN=   0
X START FROM GUN =   0.1000000000E+00
START WIDTH IN Y =   0.2000000000E-03
UNIFORM AIR VEL   =   0.5000000000E+01
HEIGHT OF TARGET =   0.2000000000E+00
INITIAL X VEL.   =   0.5000000000E+01
INITIAL Y-VEL.   =   0.0000000000E+00
TOLERANCE ERROR   =   0.1000000000E-06
INTEGRATION TIME =   0.5000000000E+01
TRAJECTORY START =   0.0000000000E+00

FIELD25V.LOG;1   28-JUN-1982 11:49:04.10   Page 2

##

PARTICLE   1 LANDED , X =   0.1999875 , Y =   0.0003362 HIT PARTICLE NO.   0 PARTICLE DIAMETER =   0.000025

PARTICLE   2 LANDED , X =   0.1999875 , Y =   -0.0001467 HIT PARTICLE NO.   0 PARTICLE DIAMETER =   0.000025

PARTICLE   3 LANDED , X =   0.1999875 , Y =   0.0004320 HIT PARTICLE NO.   0 PARTICLE DIAMETER =   0.000025

PARTICLE   4 LANDED , X =   0.1999875 , Y =   -0.0003642 HIT PARTICLE NO.   0 PARTICLE DIAMETER =   0.000025

PARTICLE   5 LANDED , X =   0.1999875 , Y =   -0.0005252 HIT PARTICLE NO.   0 PARTICLE DIAMETER =   0.000025

PARTICLE   6 LANDED , X =   0.1999875 , Y =   0.0005188 HIT PARTICLE NO.   0 PARTICLE DIAMETER =   0.000025

PARTICLE   7 LANDED , X =   0.1999875 , Y =   0.0001581 HIT PARTICLE NO.   0 PARTICLE DIAMETER =   0.00002!

PARTICLE   8 LANDED , X =   0.1999875 , Y =   -0.0003390 HIT PARTICLE NO.   0 PARTICLE DIAMETER =   0.00002!

PARTICLE   9 LANDED , X =   0.1999875 , Y =   -0.0001746 HIT PARTICLE NO.   0 PARTICLE DIAMETER =   0.00002!

PARTICLE TRAJECTORY - FORCES ON PARTICLE NO.   10

TIME	X COORDINATE	Y COORD	DRAG X	DRAG Y	FIELD X	FIELD Y	IMAGE	TOT INTER X	TOT INTER Y
			dx/dt	dy/dt	u	v	Re_p		

```
0.00000  99999.6415  -39.4061 -0.1159E-07 -0.2956E-11  0.3392E-08 -0.1337E-11  0.9775E-16 -0.1759E-17 -0.7331E-21
 0.000000 99999.6415    -39.4061    4.999928    0.000000    2.236062   -0.000705    0.3585E-07
0.00000  99999.4623  -39.4061 -0.1159E-07 -0.2956E-11  0.3392E-08 -0.1337E-11  0.9775E-16 -0.1759E-17 -0.7331E-21
 0.000000 99999.4623    -39.4061    4.999892    0.000000    2.236058   -0.000705    0.3585E-07
0.00001  99931.3334  -39.4061 -0.1154E-07 -0.2927E-11  0.3389E-08 -0.1334E-11  0.9788E-16 -0.1763E-17 -0.7347E-21
 0.000014  99931.3334    -39.4061    4.986258   -0.000007    2.234839   -0.000705    0.3585E-07
0.00003  99863.3899  -39.4063 -0.1149E-07 -0.2899E-11  0.3387E-08 -0.1333E-11  0.9801E-16 -0.1767E-17 -0.7371E-21
 0.000027  99863.3899    -39.4063    4.972706   -0.000014    2.233623   -0.000705    0.1364E-04
0.00004  99795.6307  -39.4065 -0.1144E-07 -0.2871E-11  0.3385E-08 -0.1331E-11  0.9815E-16 -0.1770E-17 -0.7391E-21
 0.000041  99795.6307    -39.4065    4.959236   -0.000021    2.232410   -0.000706    0.1364E-04
0.00005  99728.0548  -39.4069 -0.1139E-07 -0.2843E-11  0.3382E-08 -0.1329E-11  0.9828E-16 -0.1774E-17 -0.7411E-21
 0.000055  99728.0548    -39.4069    4.945848   -0.000028    2.231199   -0.000706    0.1364E-04
0.00008  99582.7292  -39.4079 -0.1128E-07 -0.2783E-11  0.3378E-08 -0.1325E-11  0.9857E-16 -0.1782E-17 -0.7455E-21
 0.000084  99582.7292    -39.4079    4.917210   -0.000043    2.228594   -0.000707    0.1364E-04
0.00011  99438.2425  -39.4094 -0.1117E-07 -0.2724E-11  0.3373E-08 -0.1322E-11  0.9885E-16 -0.1789E-17 -0.7498E-21
 0.000114  99438.2425    -39.4094    4.888945   -0.000058    2.226002   -0.000707    0.2917E-04
```

```
PARTICLE NO   7        0.0702027584      12.5000000000       27.8136610985      158.1201105699      25.00000000

PARTICLE NO   8        0.0702073011      12.5000000000      -59.7520649433     -339.0430918210      25.00000000

PARTICLE NO   9        0.0702074308      12.5000000000      -30.4767370224     -174.6374118500      25.00000000

PARTICLE NO  10        0.0702074229      12.5000000000      -39.4060909748     -225.3507913551      25.00000000
```

##

X COORDINATE OF HIGHEST PARTICLE =   0.1999875000E+00
RADIUS OF THIS PARTICLE =   0.1250000000E-04

```
AIR VELX=      0.3051863770E-03   ┐
AIR VELY=     -0.5634038404E-02   │
DRAGX   =     -0.1876140255E-08   │
DRAGY   =      0.4448313203E-10   ├─────────── Forces at last calculated position in trajectory
IMAGE   =      0.6559142565E-08   │
FIELDX  =      0.1695927004E-08   │
FIELDY  =     -0.1911099020E-11   │
FTOTX   =      0.8247810659E-09   │
FTOTY   =     -0.4687975680E-09   ┘
```

Figure D3(e). Output Parameters for Error Analysis and for Checking Efficiency of Routine

```
COUT NO. 1   0.358489E-07    CIN NO. 1   0.500000E+01    CON NO. 1   0.100000E+02    COMM NO. 1   0.000000E+00
COUT NO. 2   0.261985E-02    CIN NO. 2   0.000000E+00    CON NO. 2   0.100000E+03    COMM NO. 2   0.000000E+00
```

FIELD25V.LOG;1   28-JUN-1982 11:49:04.10   Page 10

```
COUT NO. 3.   0.000000E+00    CIN NO. 3   0.000000E+00    CON NO. 3   0.120000E+01    COMM NO. 3   0.000000E+00
COUT NO. 4    0.702065E-01    CIN NO. 4   0.000000E+00    CON NO. 4   0.130000E+01    COMM NO. 4   0.100000E+01
COUT NO. 5    0.702049E-01    CIN NO. 5   0.358489E-07    CON NO. 5   0.140000E+01
COUT NO.  6   0.500000E+01    CIN NO. 6   0.157788E-05
COUT NO.  7   0.428217E+00    CIN NO. 7   0.400000E+01 ──── the last integration point (time)
COUT NO. 8    0.196000E+03 ──── last but one integration point (COUT 4-5) = stepsize)
COUT NO. 9    0.900000E+01
COUT NO.10    0.000000E+00 ──── the number of successful integration steps used for the last particle
COUT NO.11    0.277556E-16
COUT NO.12    0.293874E-38 ──── the number of unsuccessful integration steps
COUT NO.13    0.194862E-17
COUT NO.14    0.500000E+01
COUT NO.15    0.400000E+01
COUT NO.16    0.320000E+02
IFAIL=    0 ──── Failure condition
FORTRAN STOP
  QUASIMODO    job terminated at 28-JUN-1982 11:49:03.91

  Accounting information:
  Buffered I/O count:          66      Peak working set size:   172
  Direct I/O count:           145      Peak virtual size:       286
  Page faults:               1536      Mounted volumes:           0
  Elapsed CPU time:   0 00:00:48.37    Elapsed time:     0 00:02:27.09
```

Appendix E

Computer Plots of Particle Trajectories

For each plot (i) the tolerance bound employed was 10^{-7}

        (ii) the start point was 0.1m from the substrate

        (iii) Gun to target distance was 0.2m

        (iv) The random number variable was 0

        (v) The number of particles studies was 300 (E1-E41)

For Figures E17 to E62 the start width was 0.0002 m

Figure E1. Particle Trajectories for Monosized Powder – Particle diameter = 10μm, Uniform Velocity = 1 m/s, Start Width = 0.00043 m
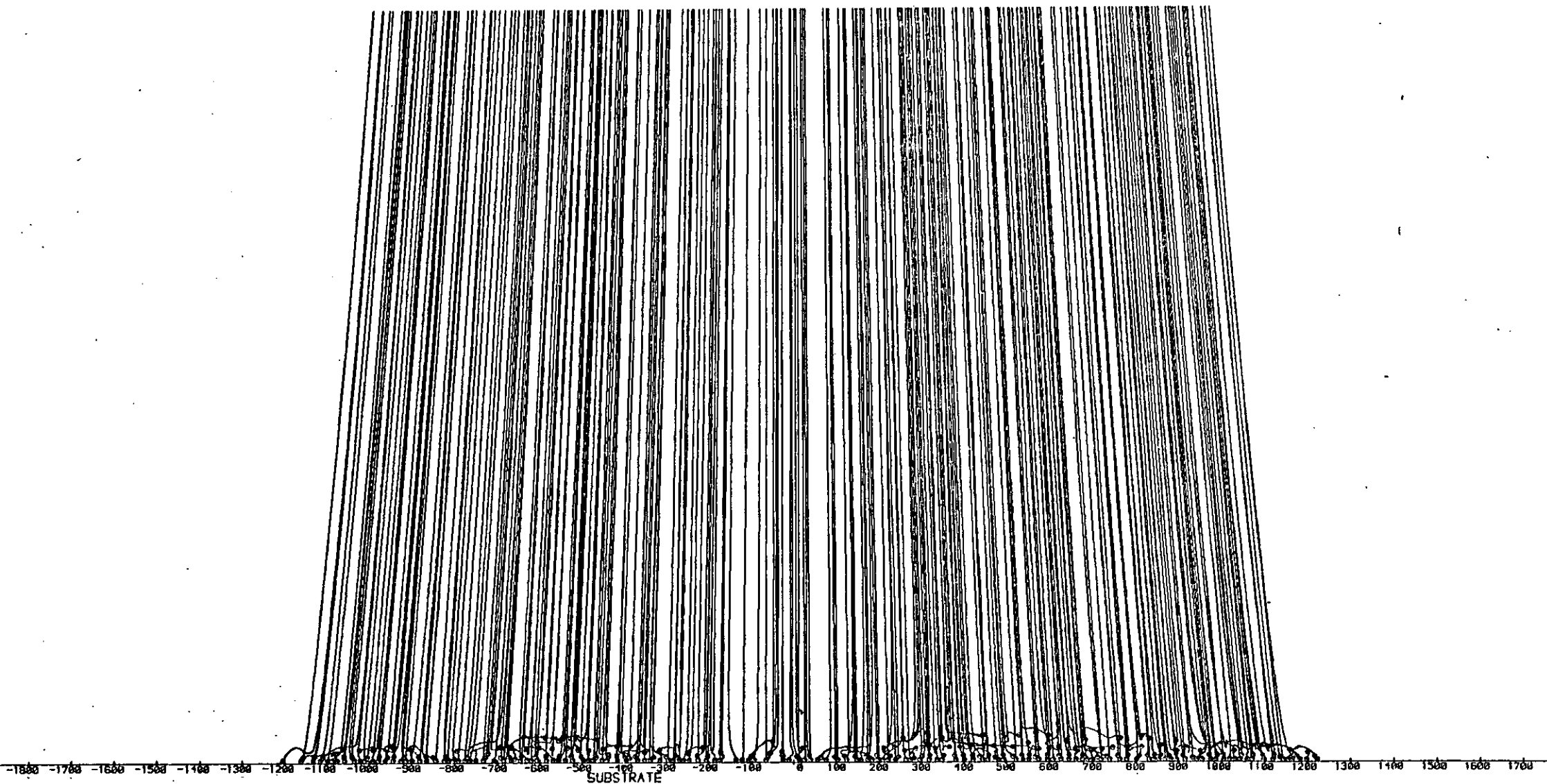
Figure E3. Particle Trajectories for Monosized Powder – Particle diameter = 10μm, Uniform Velocity = 7 m/s, Start Width = 0.00014 m
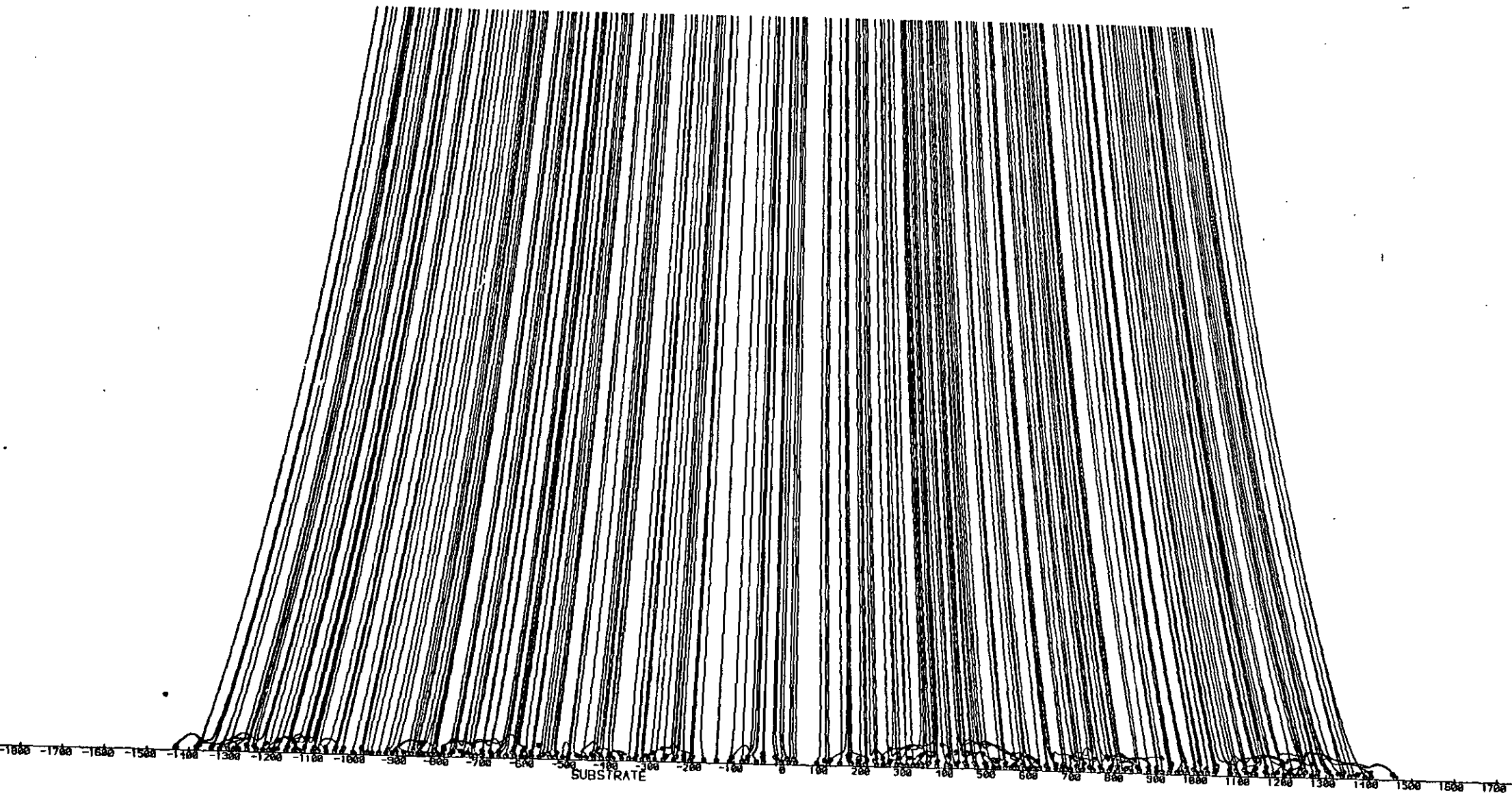
Figure E4. Particle Trajectories for Monosized Powder – Particle diameter = 10µm, Uniform Velocity = 10 m/s, Start Width = 0.00011 m
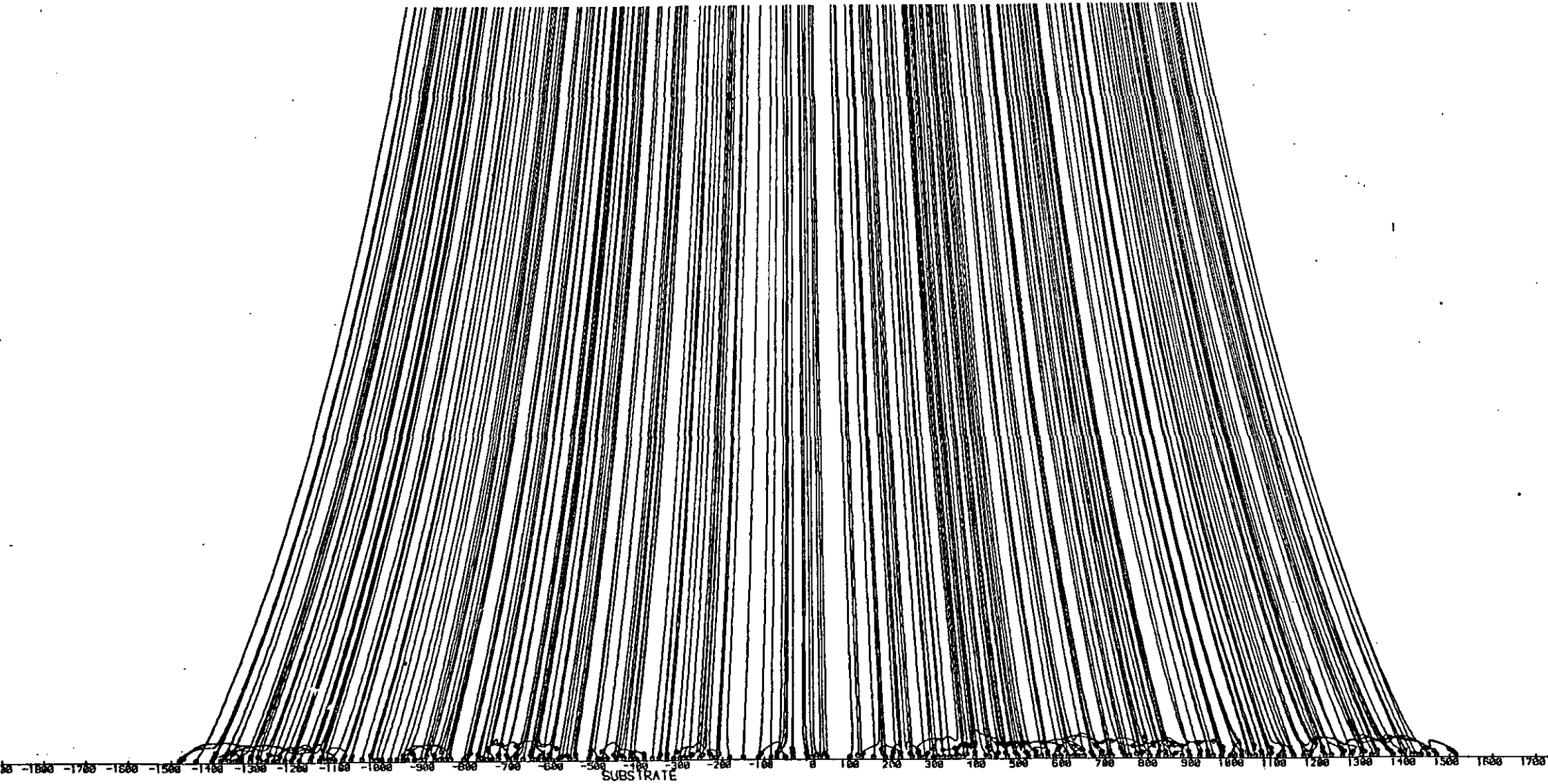
Figure E5. Particle Trajectories for Monosized Powder − Particle diameter = 17μm, Uniform Velocity = 1 m/s, Start Width = 0.00058 m
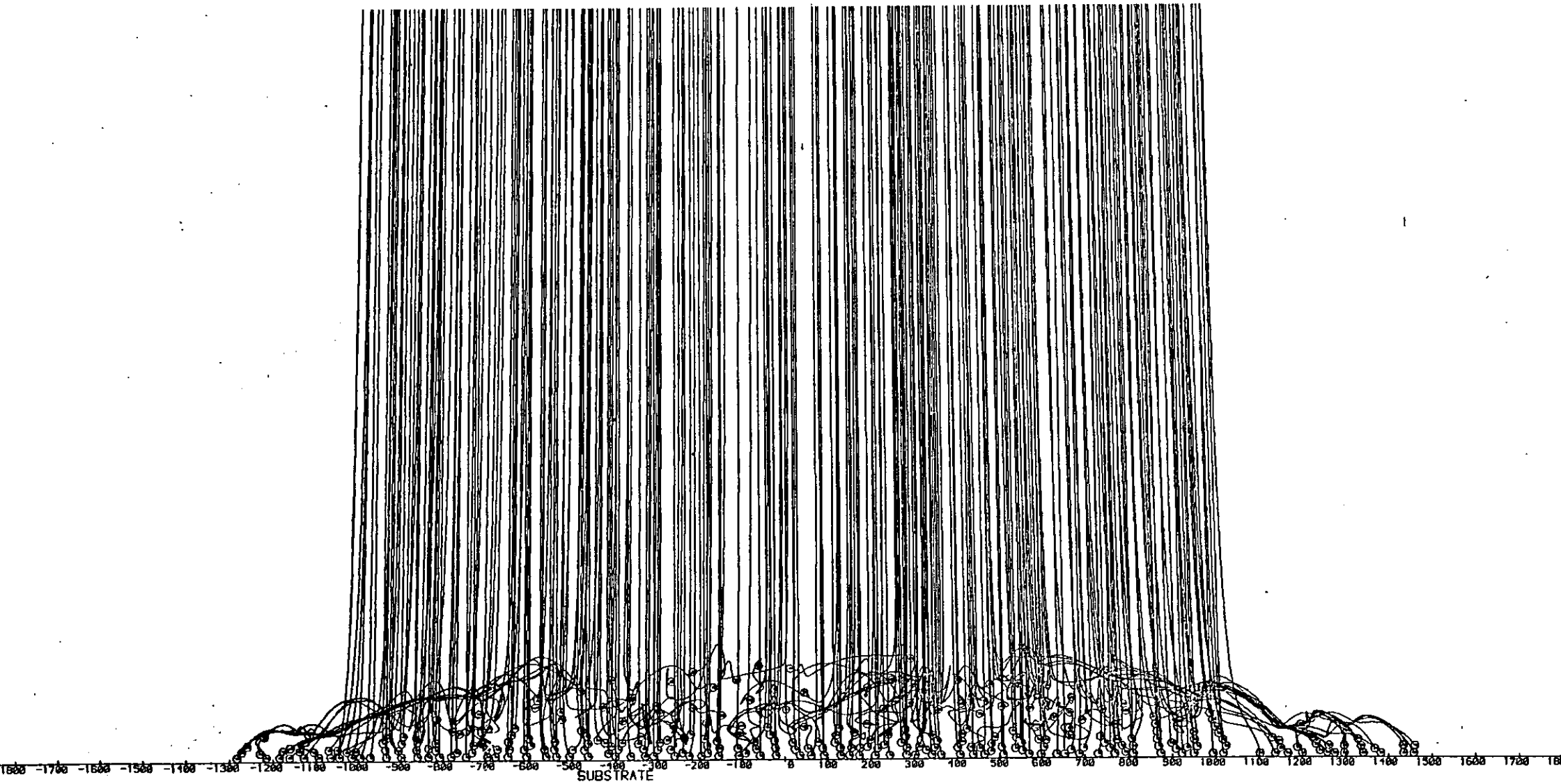
Figure E6. Particle Trajectories for Monosized Powder – Particle diameter = 17μm, Uniform Velocity = 3 m/s, Start Width = 0.00035 m
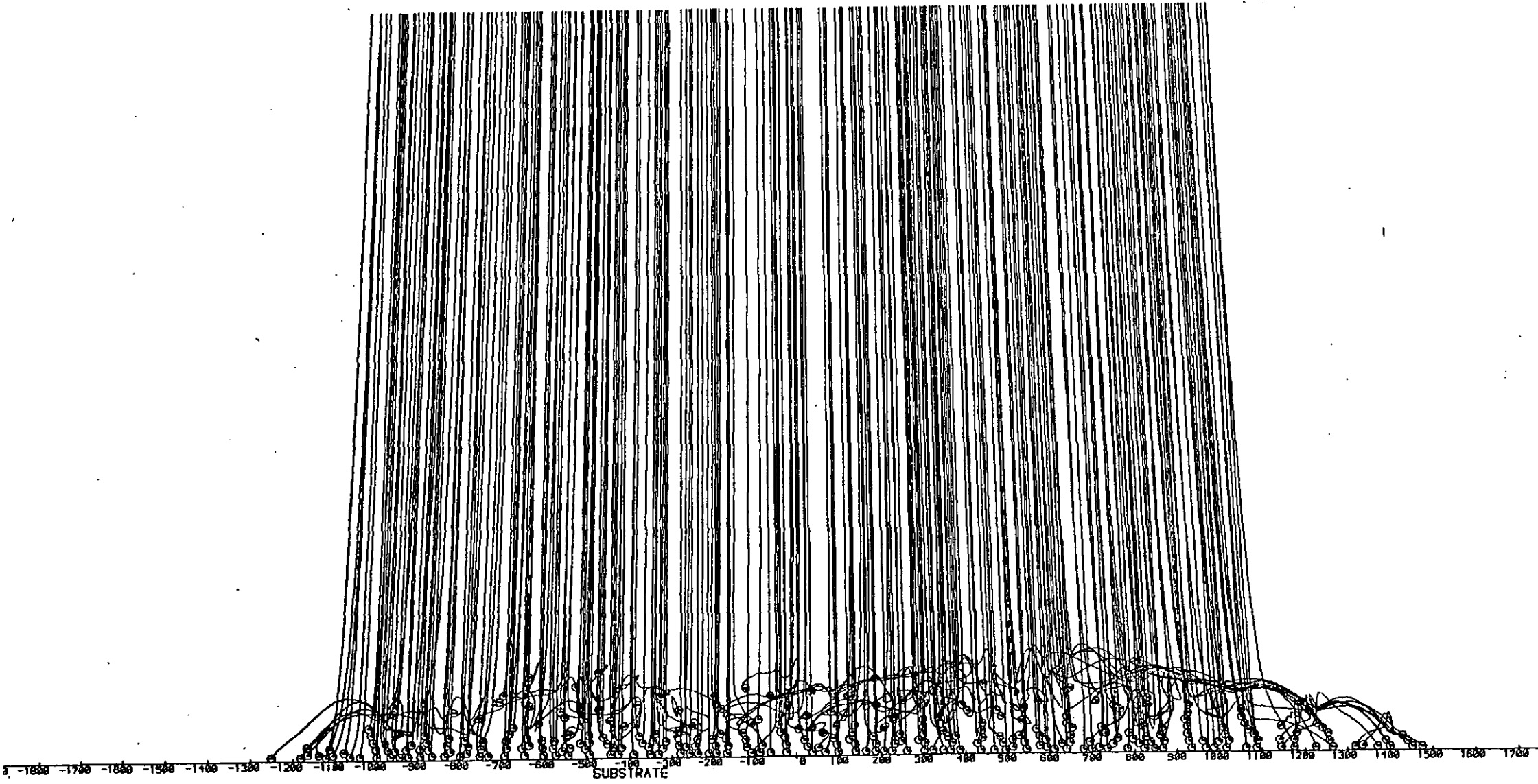
Figure E7. Particle Trajectories for Monosized Powder – Particle diameter = 17μm, Uniform Velocity = 7 m/s, Start Width = 0.00023 m
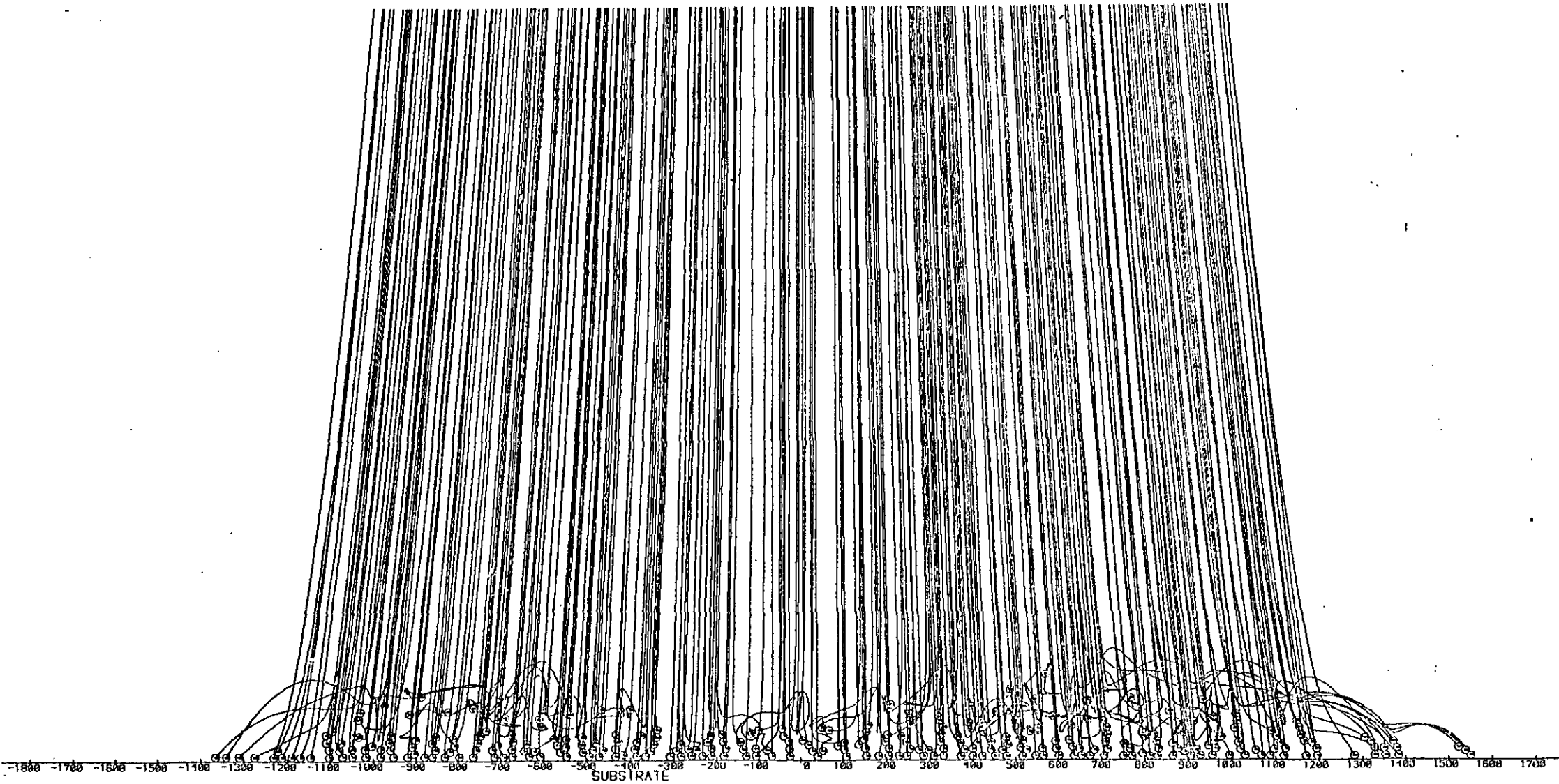
Figure E8. Particle Trajectories for Monosized Powder - Particle diameter = 17μm, Uniform Velocity = 10 m/s, Start Width = 0.00019 m
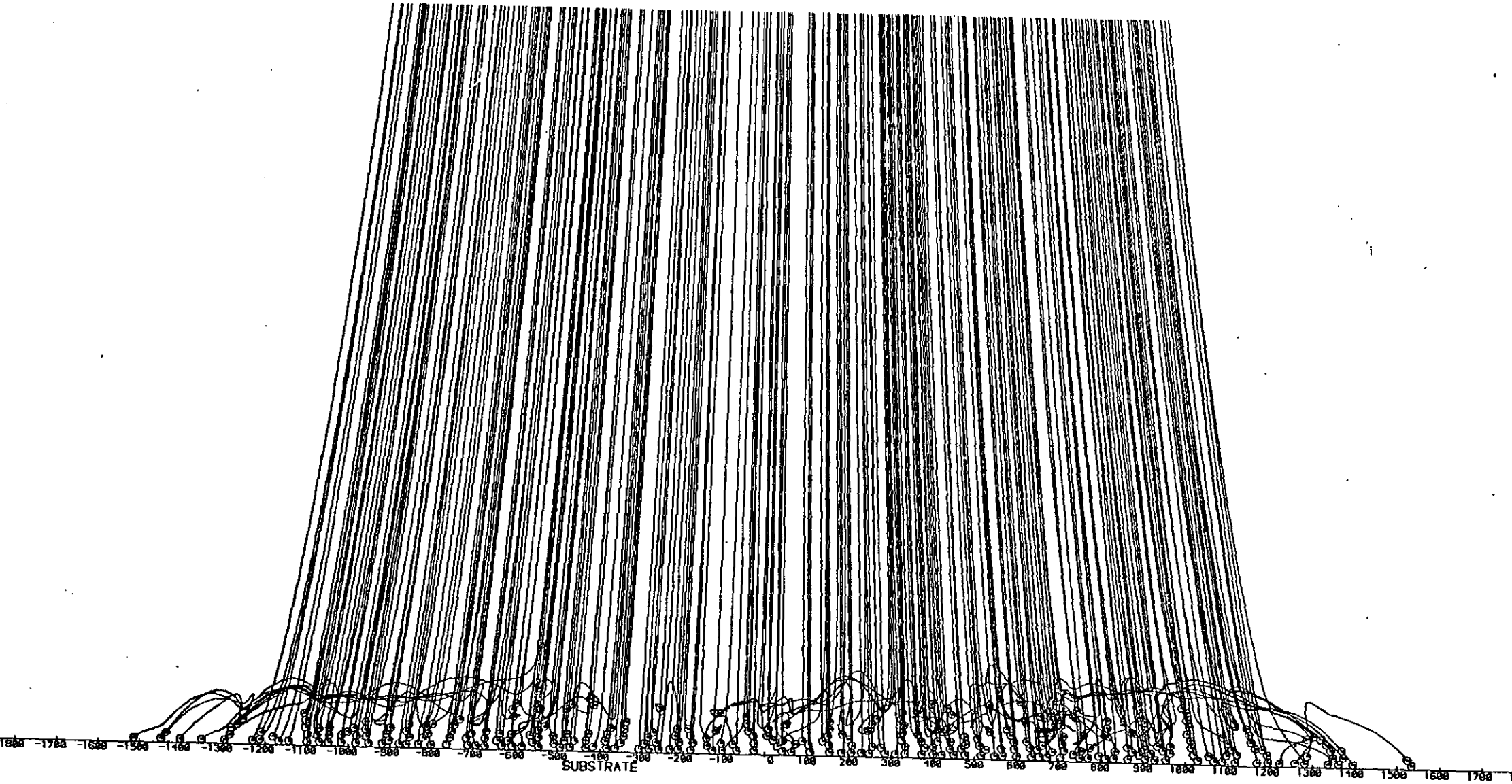
Figure E9. Particle Trajectories for Monosized Powder – Particle diameter = 25μm, Uniform Velocity = 1 m/s, Start Width = 0.00068 m
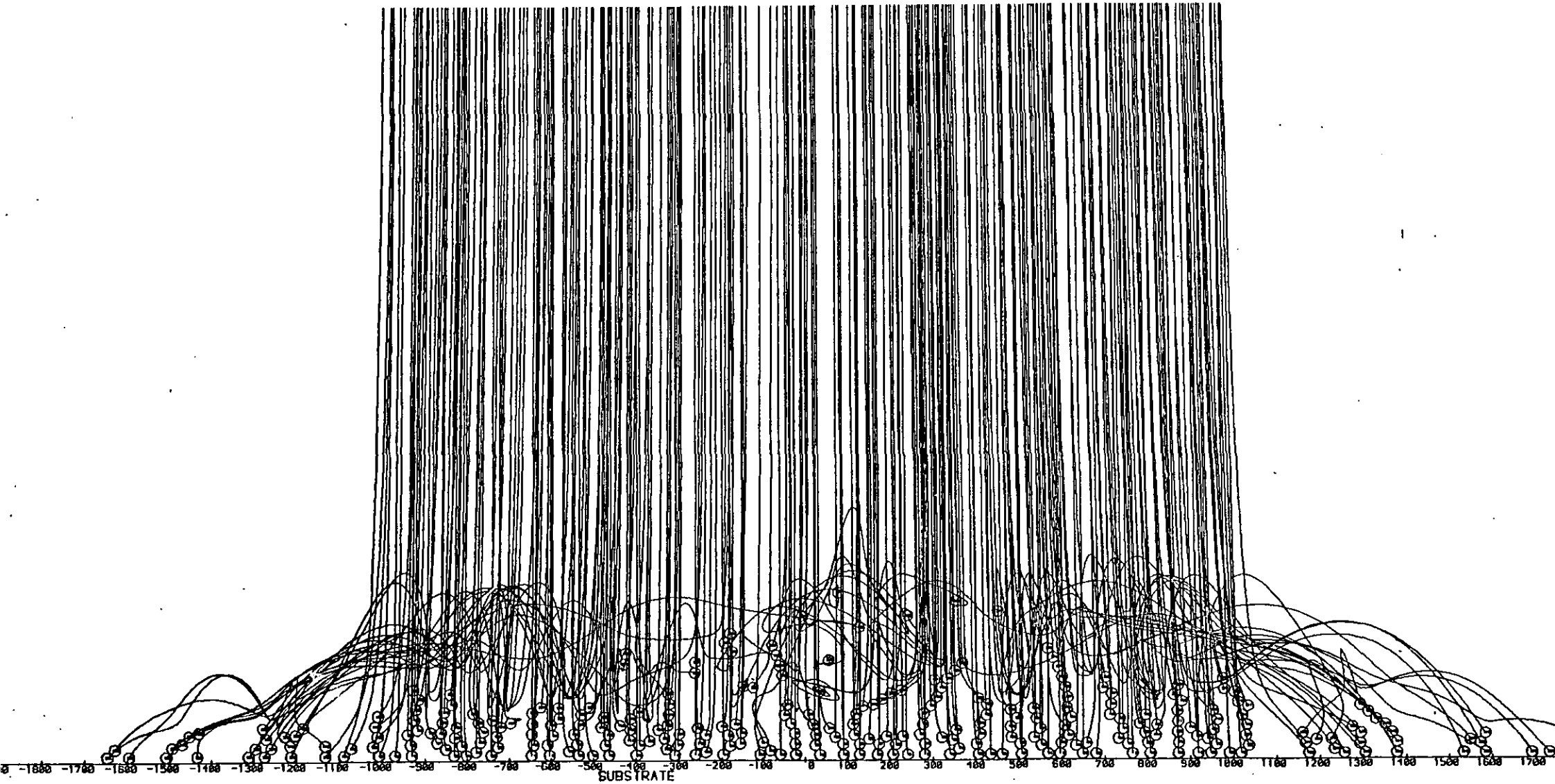
Figure E10: Particle Trajectories for Monosized Powder – Particle diameter = 25µm, Uniform Velocity = 3 m/s, Start Width = 0.00046 m
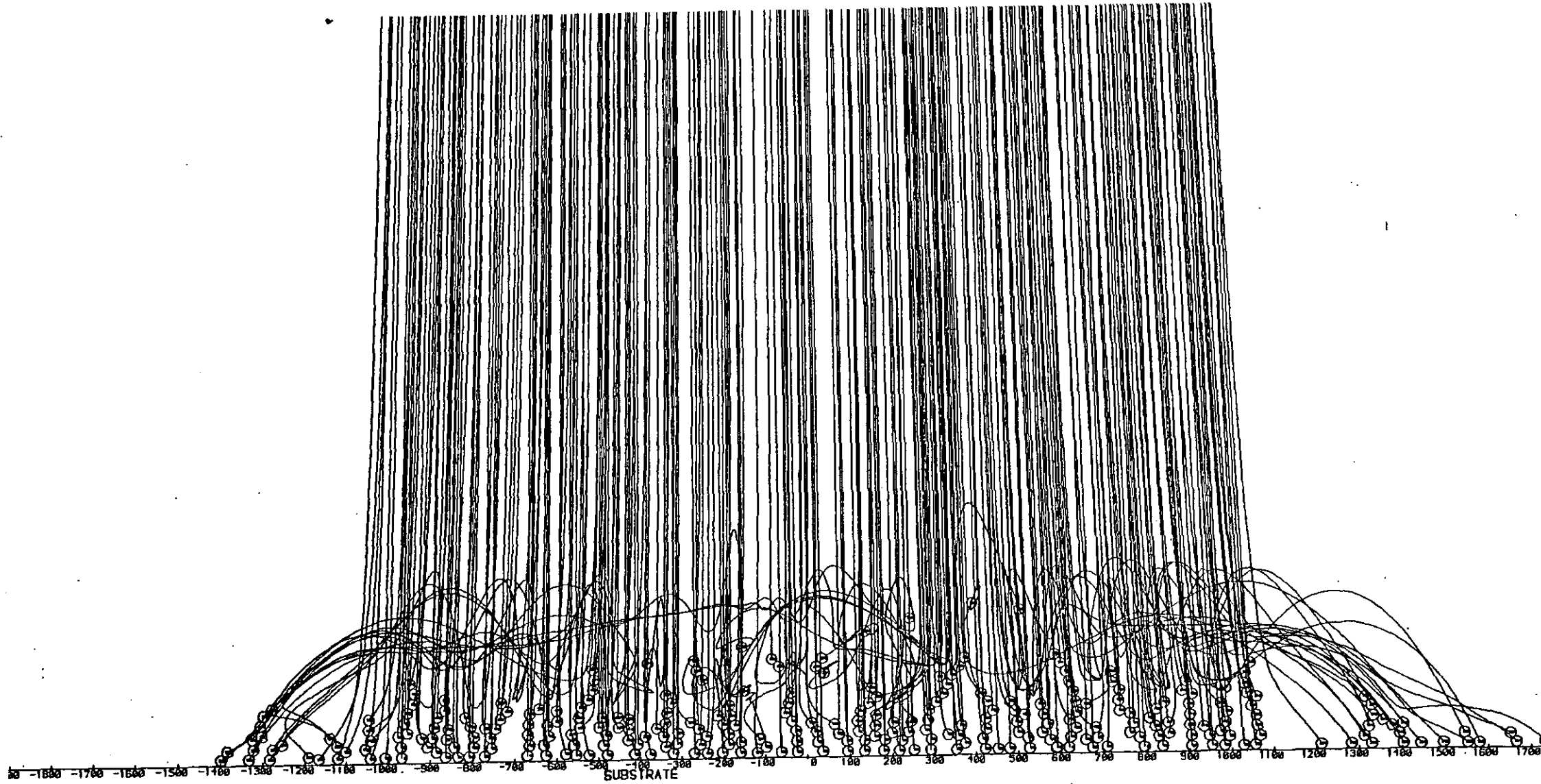
Figure E11. Particle Trajectories for Monosized Powder – Particle diameter = 25μm, Uniform Velocity = 7 m/s, Start Width = 0.00046 m
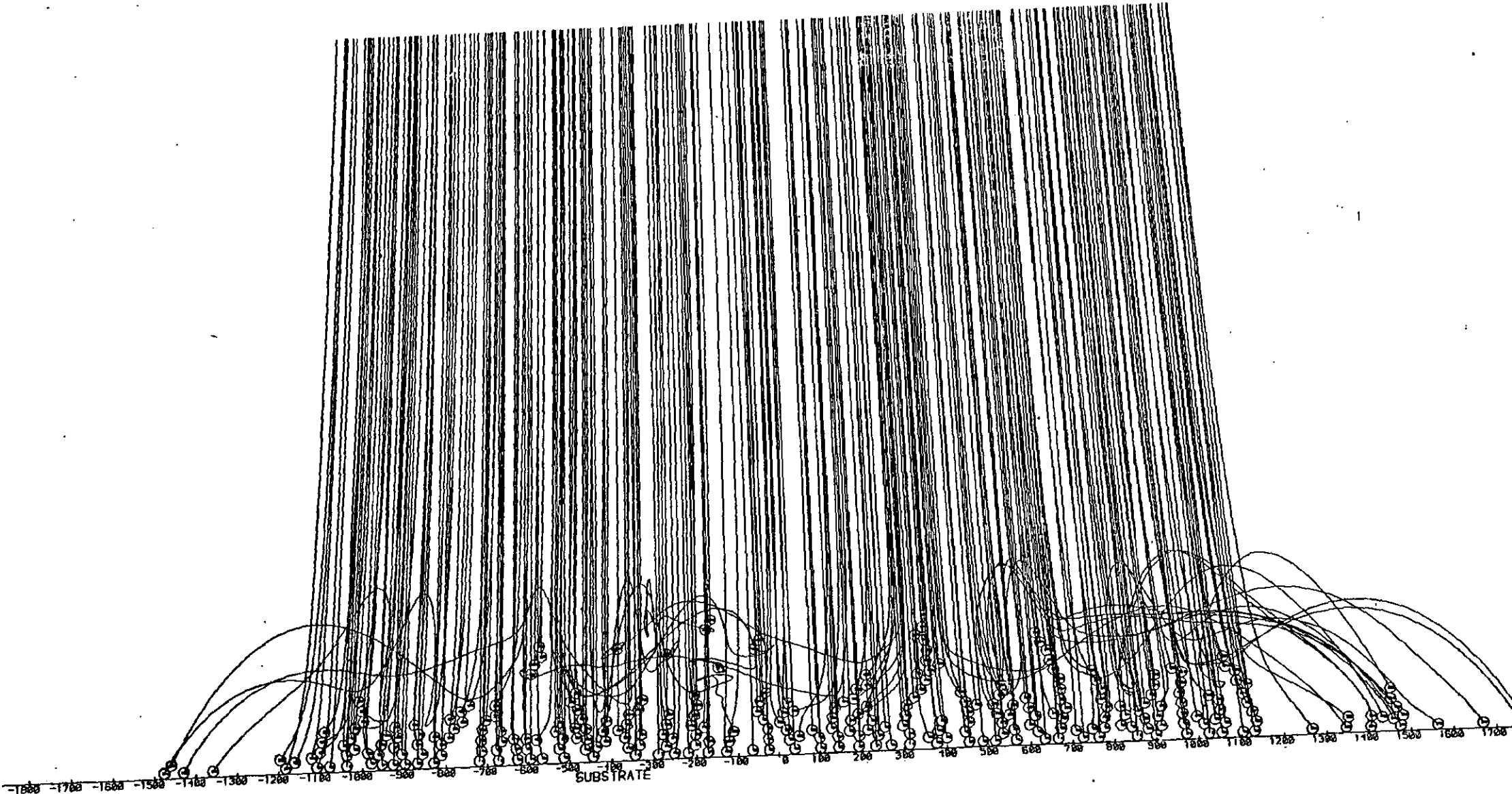
Figure E12. Particle Trajectories for Monosized Powder — Particle diameter = 25μm, Uniform Velocity = 10 m/s, Start Width = 0.00032 m
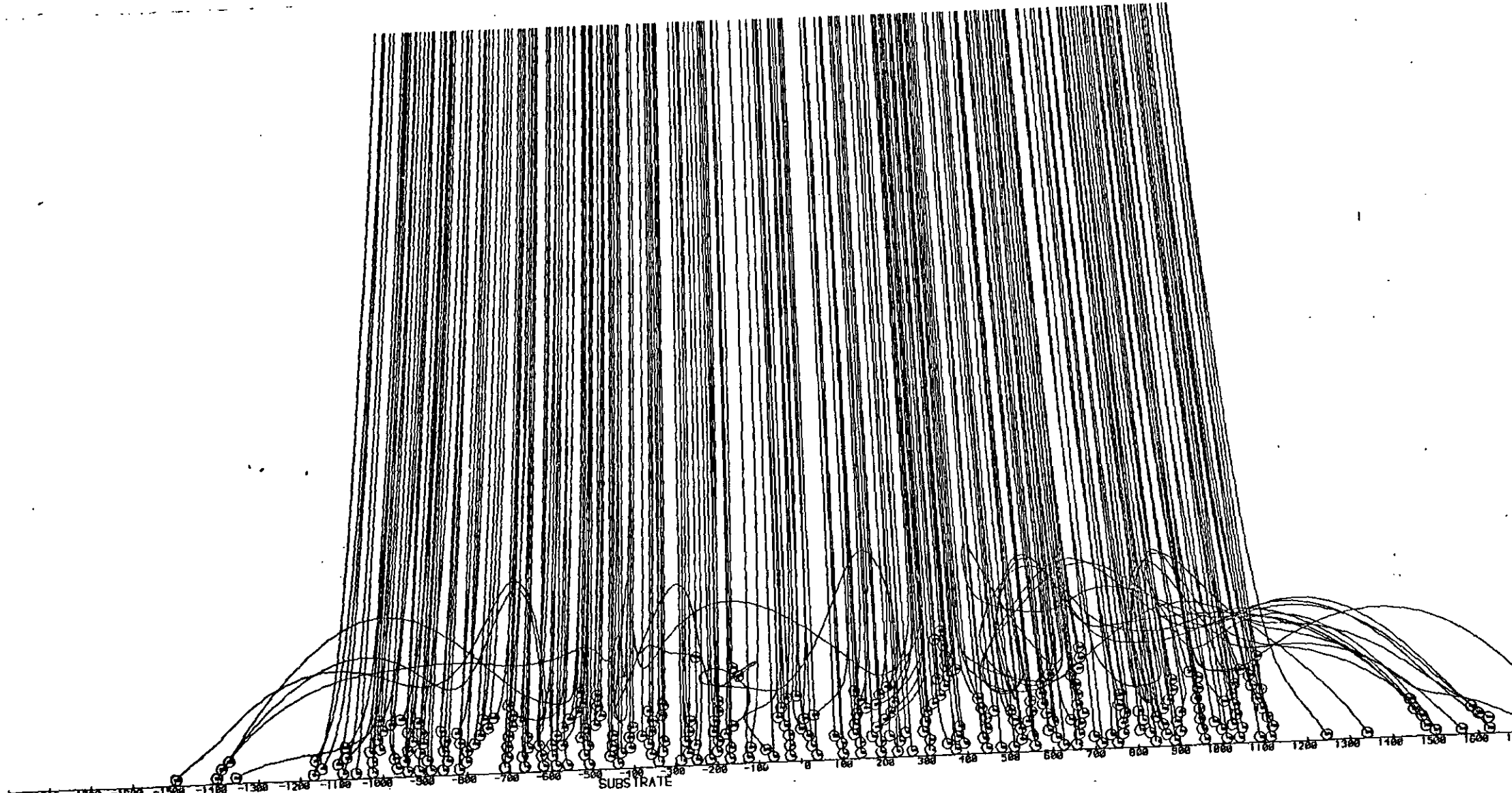
Figure E13. Particle Trajectories for Monosized Powder – Particle diameter = 50µm, Uniform Velocity = 1 m/s, Start Width = 0.00089 m
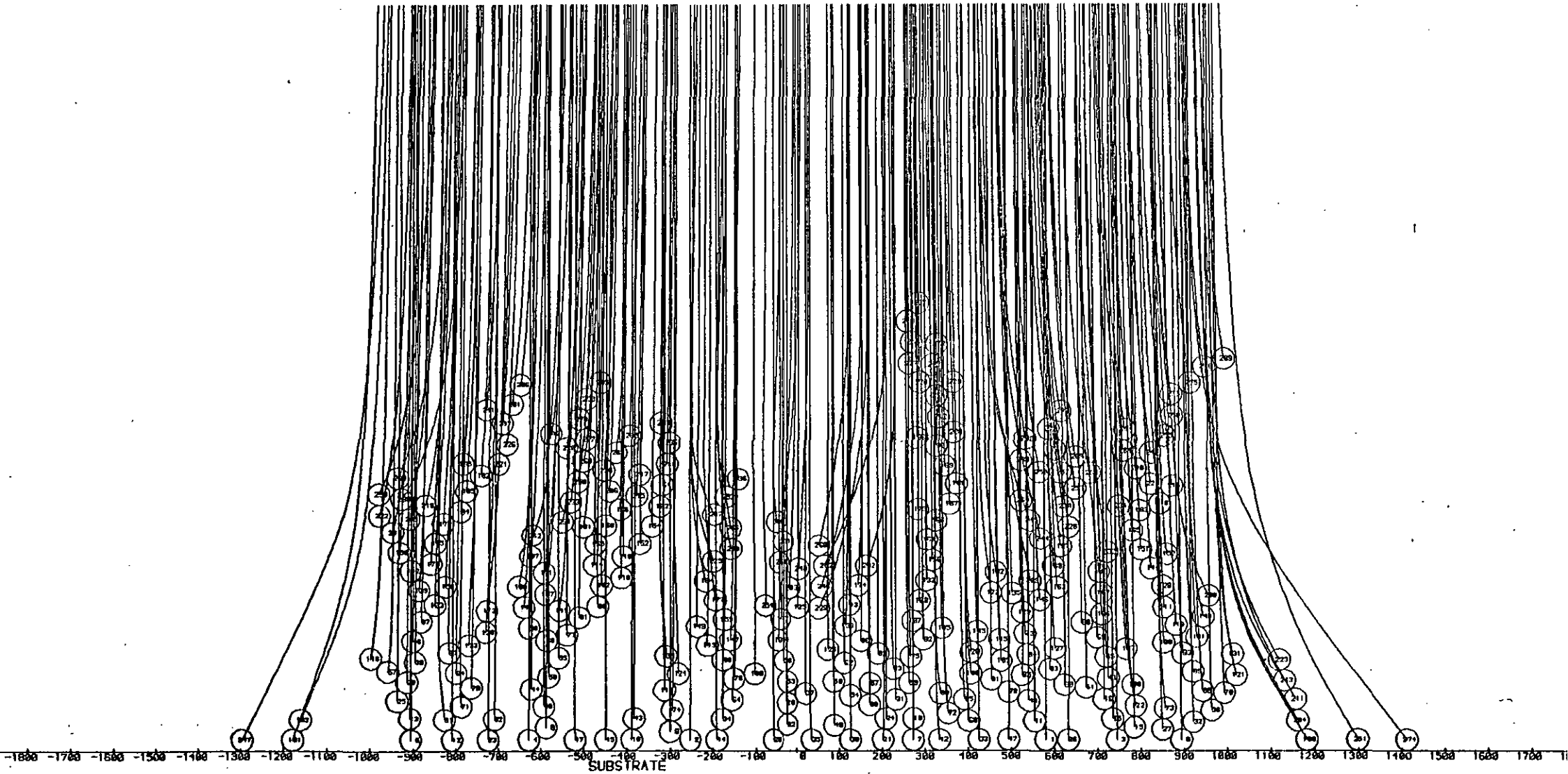
Figure E14. Particle Trajectories for Monosized Powder – Particle diameter = 50μm, Uniform Velocity 3 m/s, Start Width = 0.00087 m
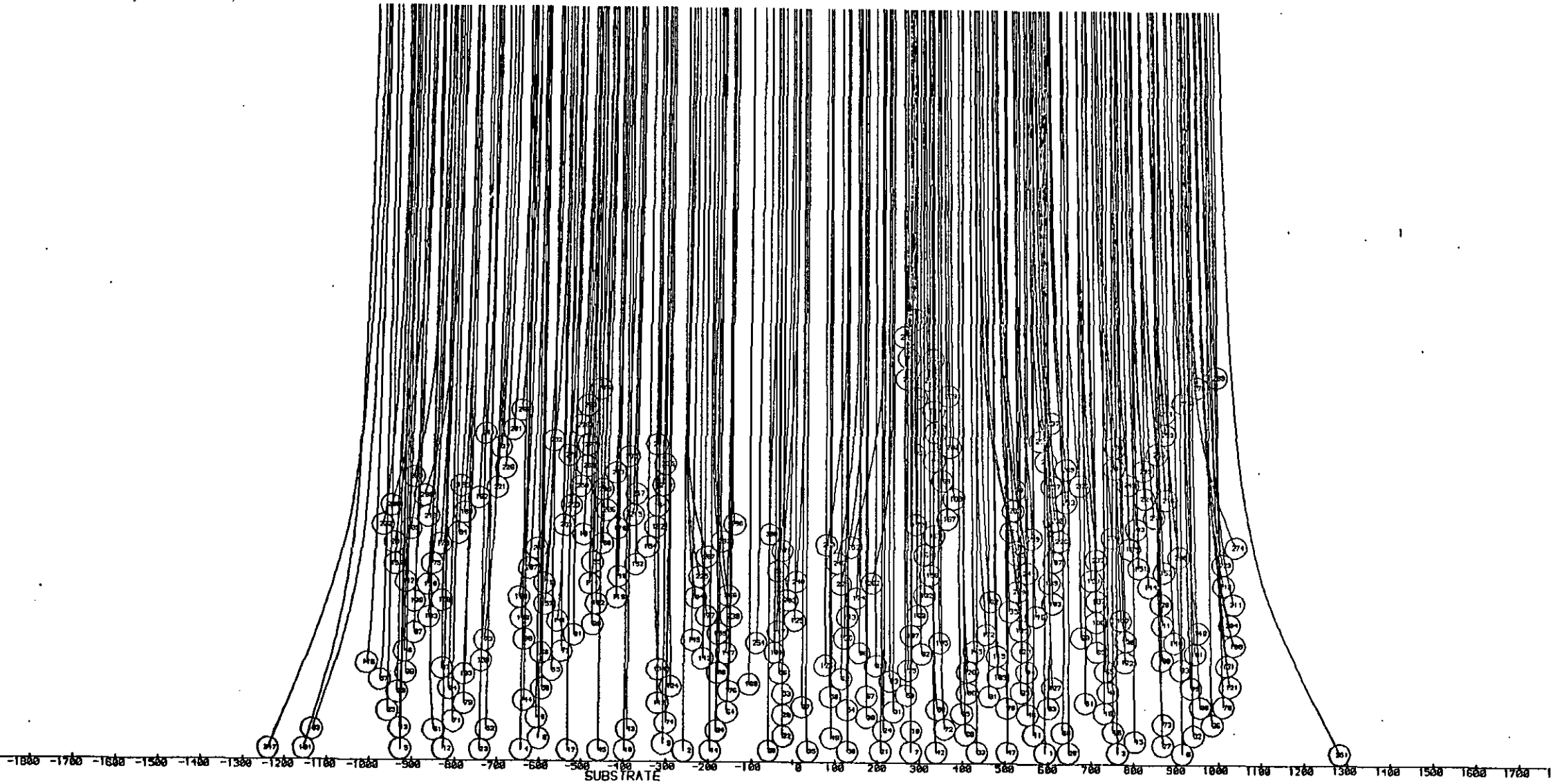
Figure E15: Particle Trajectories for Monosized Powder — Particle diameter = 50μm, Uniform Velocity = 7 m/s, Start Width = 0.00110 m
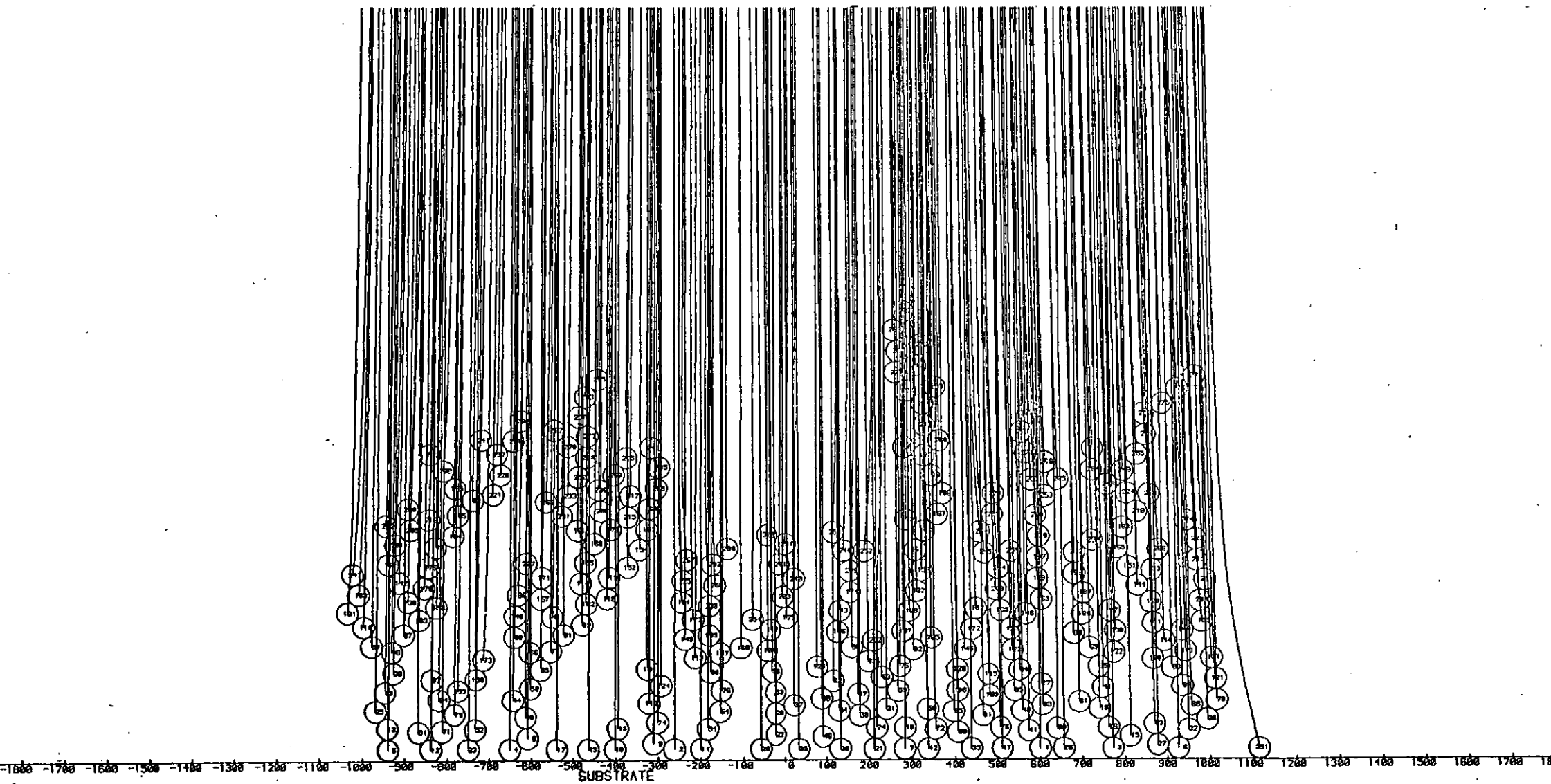
Figure E16. Particle Trajectories for Monosized Powder - Particle diameter = 50µm, Uniform Velocity = 10 m/s, Start Width = 0.00130 m
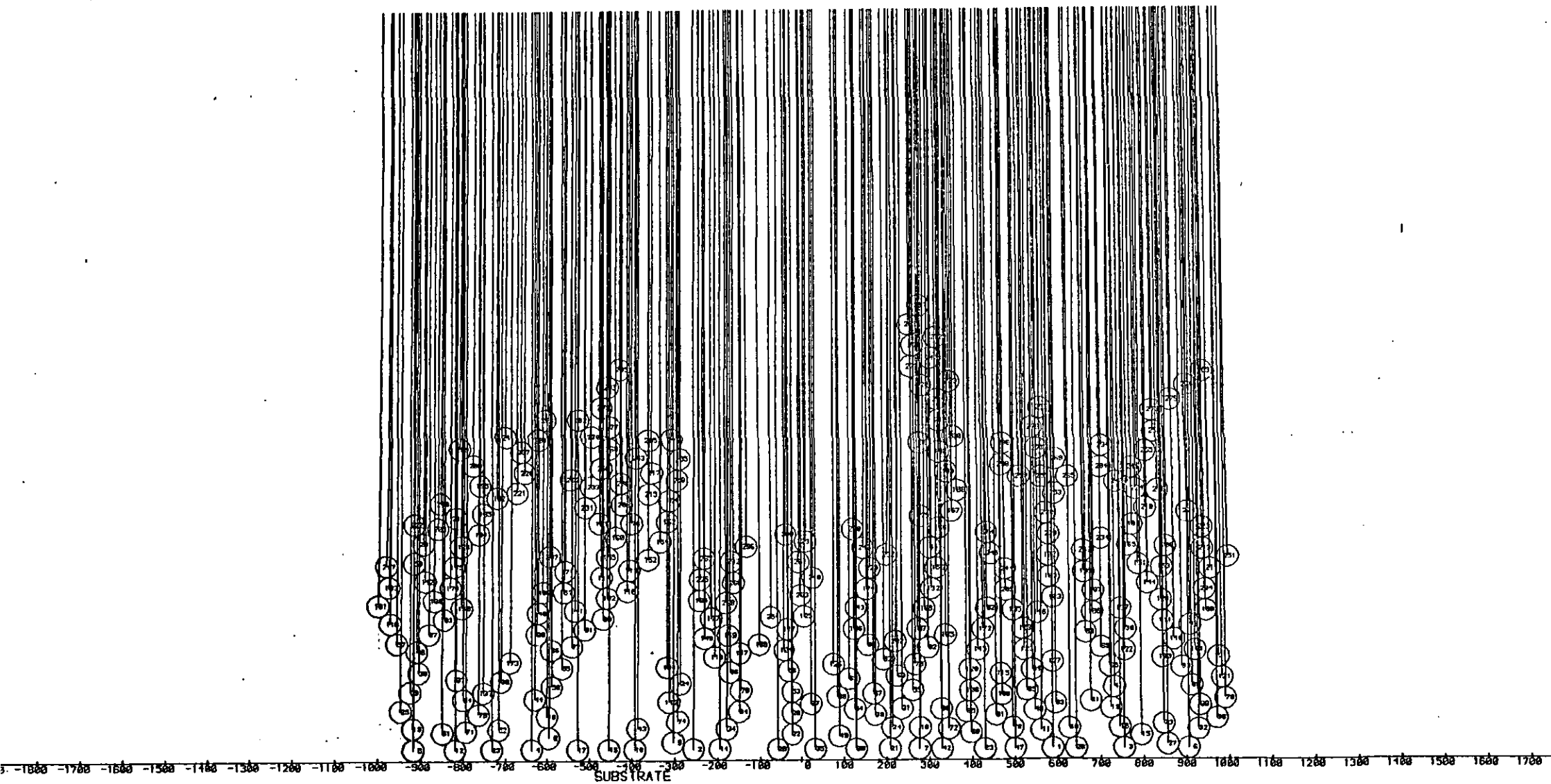
Figure E17. Trajectories of Particles for Monosized Powder – Particle diameter = 10μm, Uniform Velocity = 1 m/s
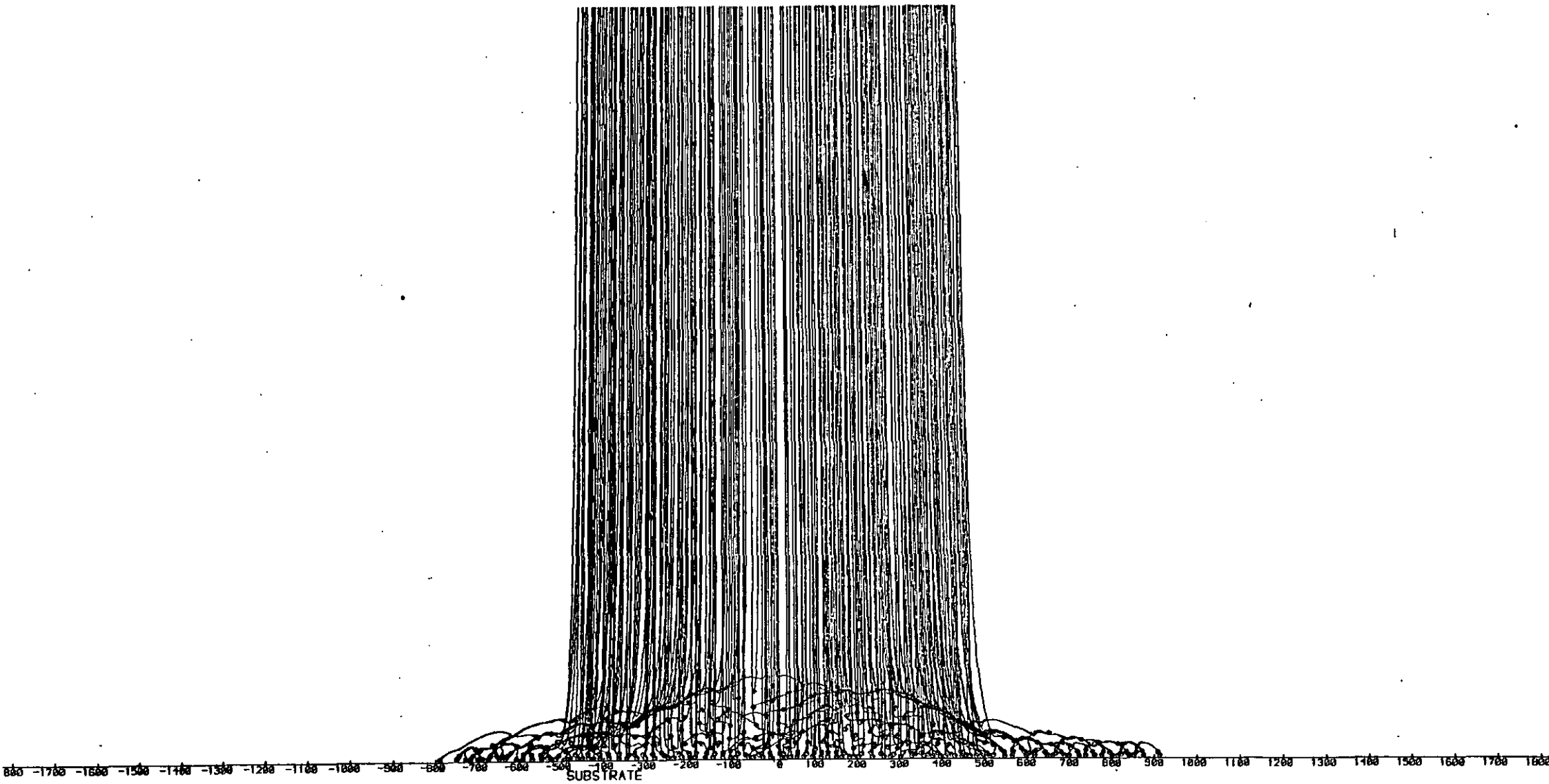
Figure E18. Trajectories of Particles for Monosized Powder - Particle diameter = 10μm, Uniform Velocity = 3 m/s
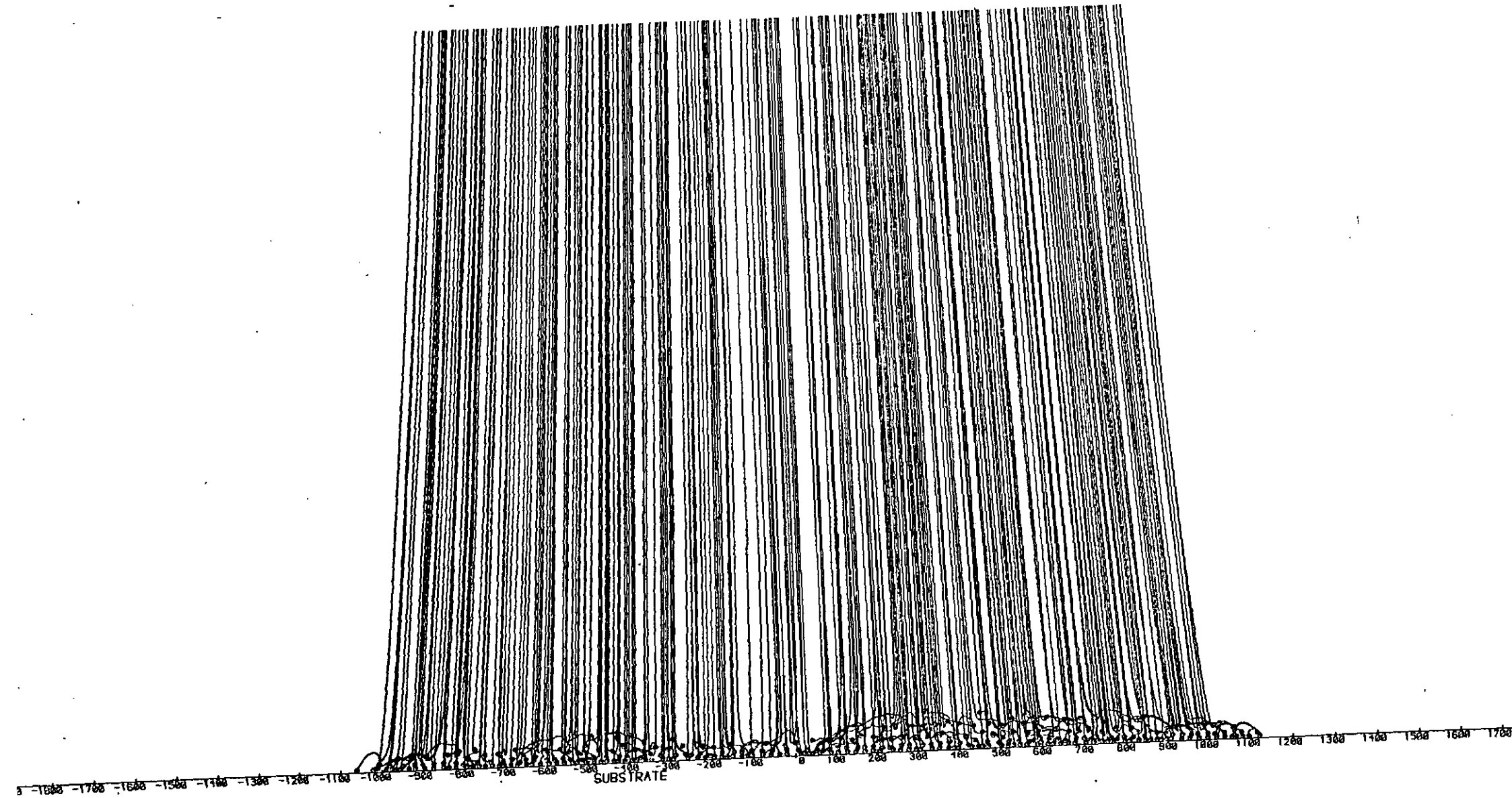
Figure E19. Trajectories of Particles for Monosized Powder – Particle diameter = 10µm, Uniform Velocity = 5 m/s
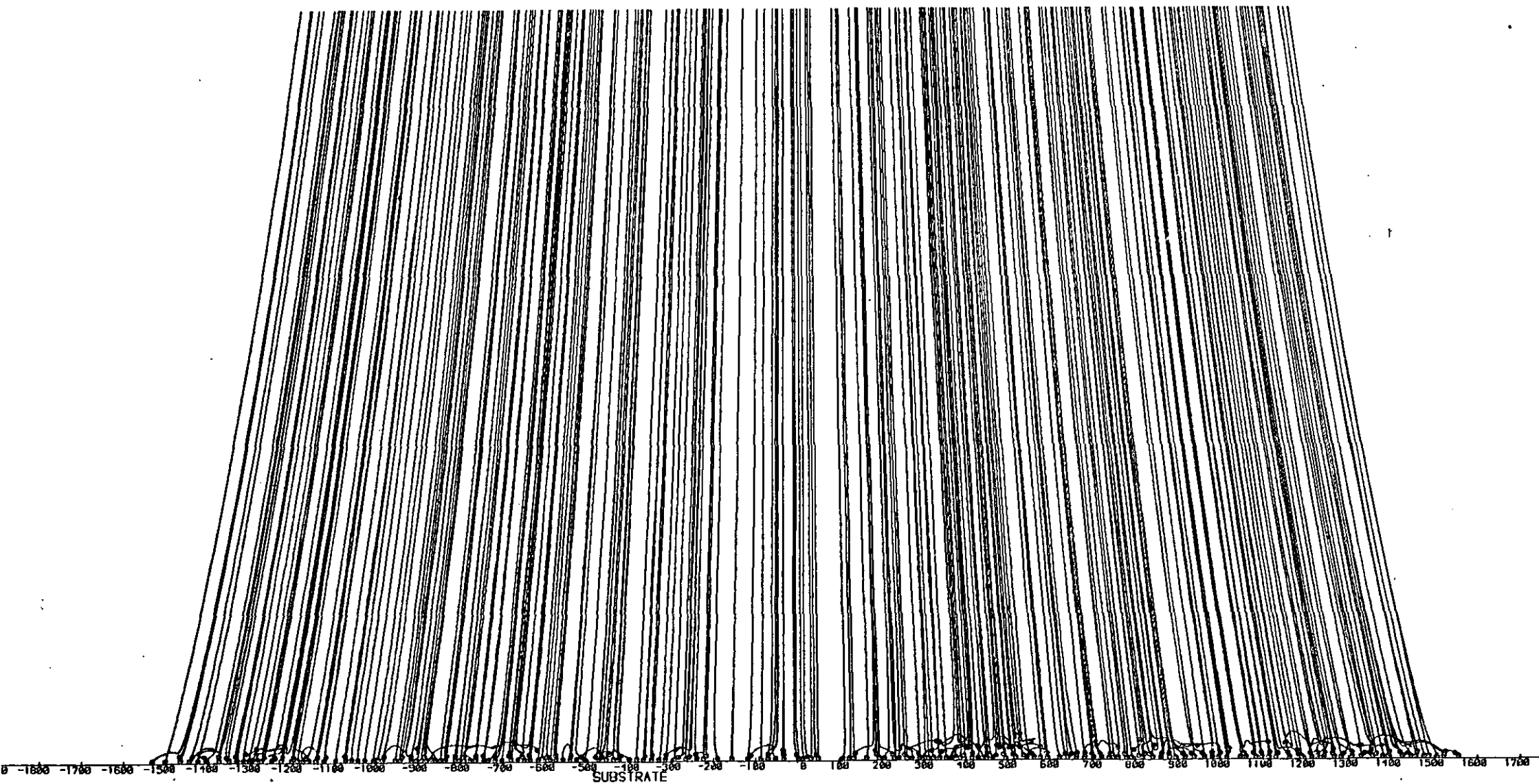
Figure E20. Trajectories of Particles for Monosized Powder – Particle diameter = 10μm, Uniform Velocity = 7 m/s

SUBSTRATE
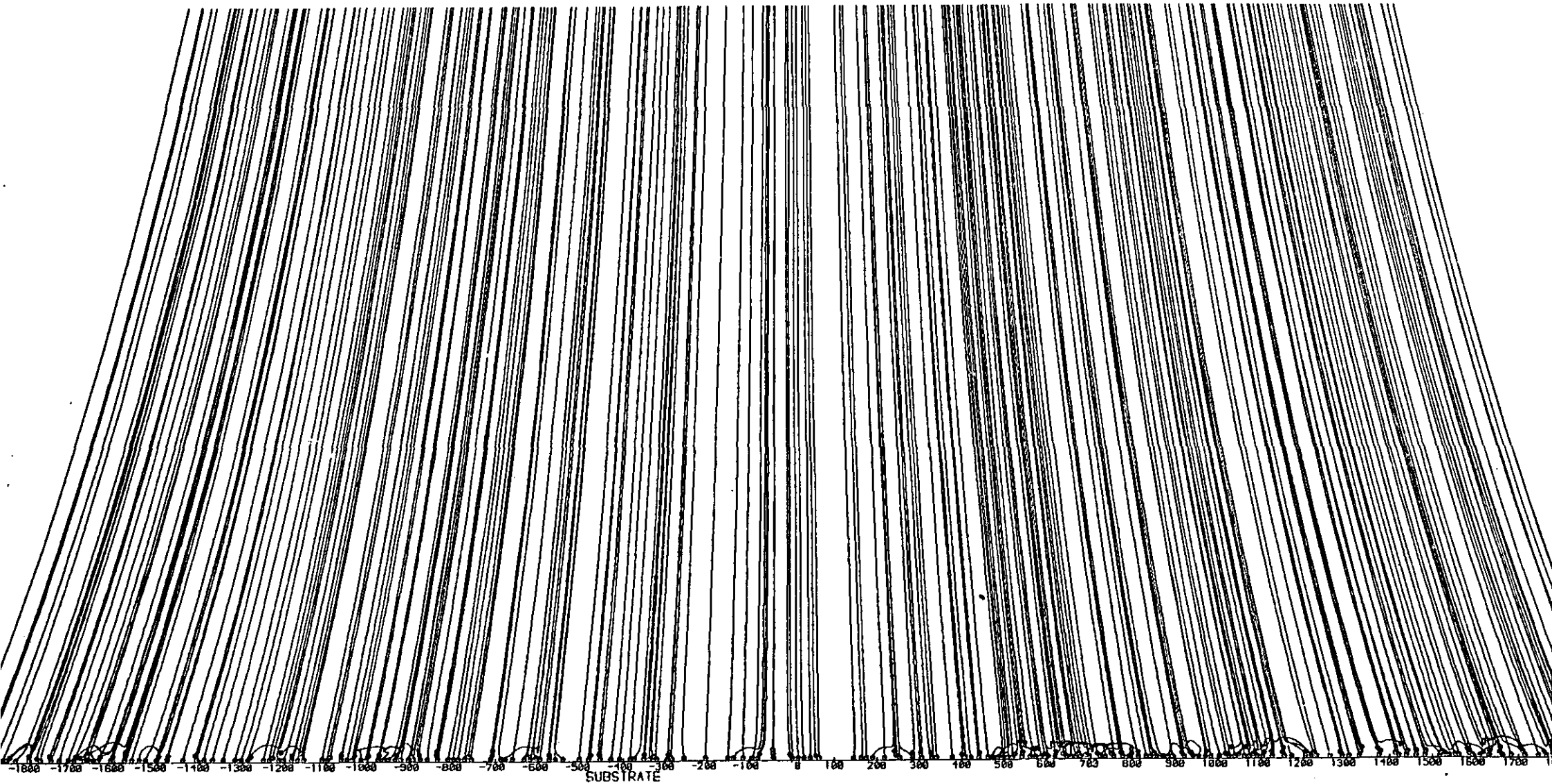
Figure E21. Trajectories of Particles for Monosized Powder – Particle diameter = 10μm, Uniform Velocity = 10 m/s
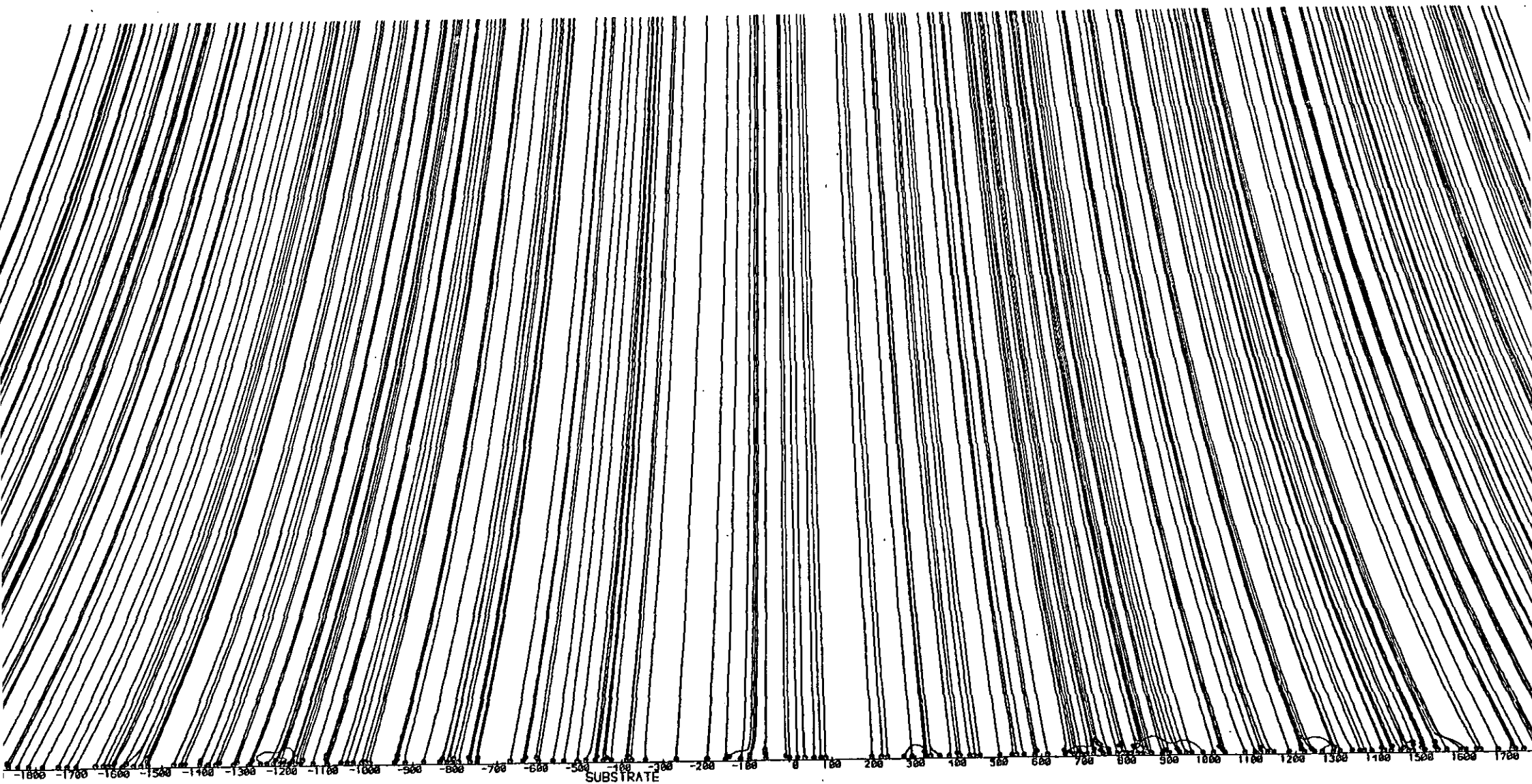
Figure E22. Trajectories of Particles for Monosized Powder – Particle diameter = 17μm, Uniform Velocity = 1 m/s
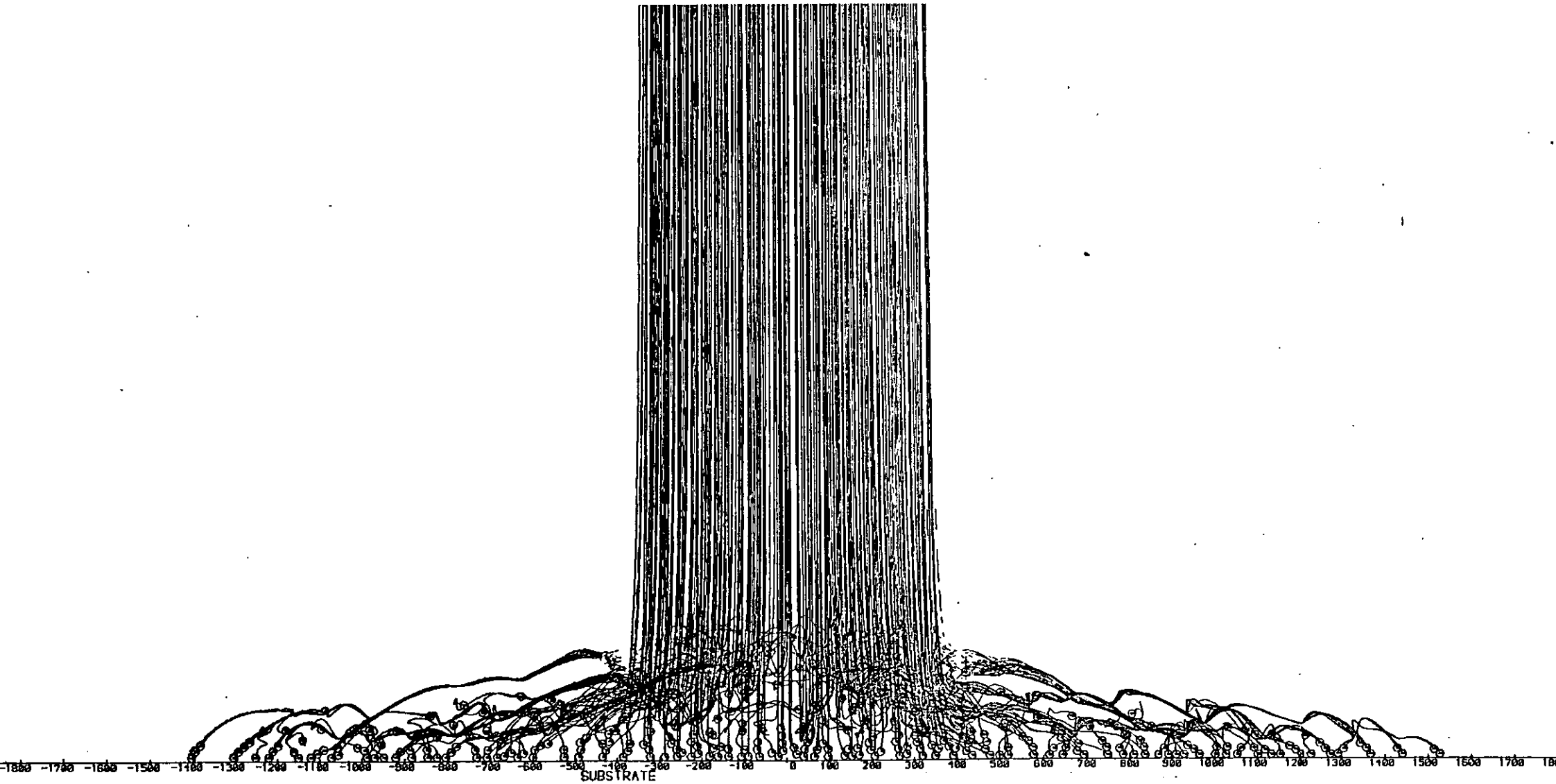
Figure E23.   Trajectories of Particles for Monosized Powder – Particle diameter = 17μm, Uniform Velocity = 3 m/s
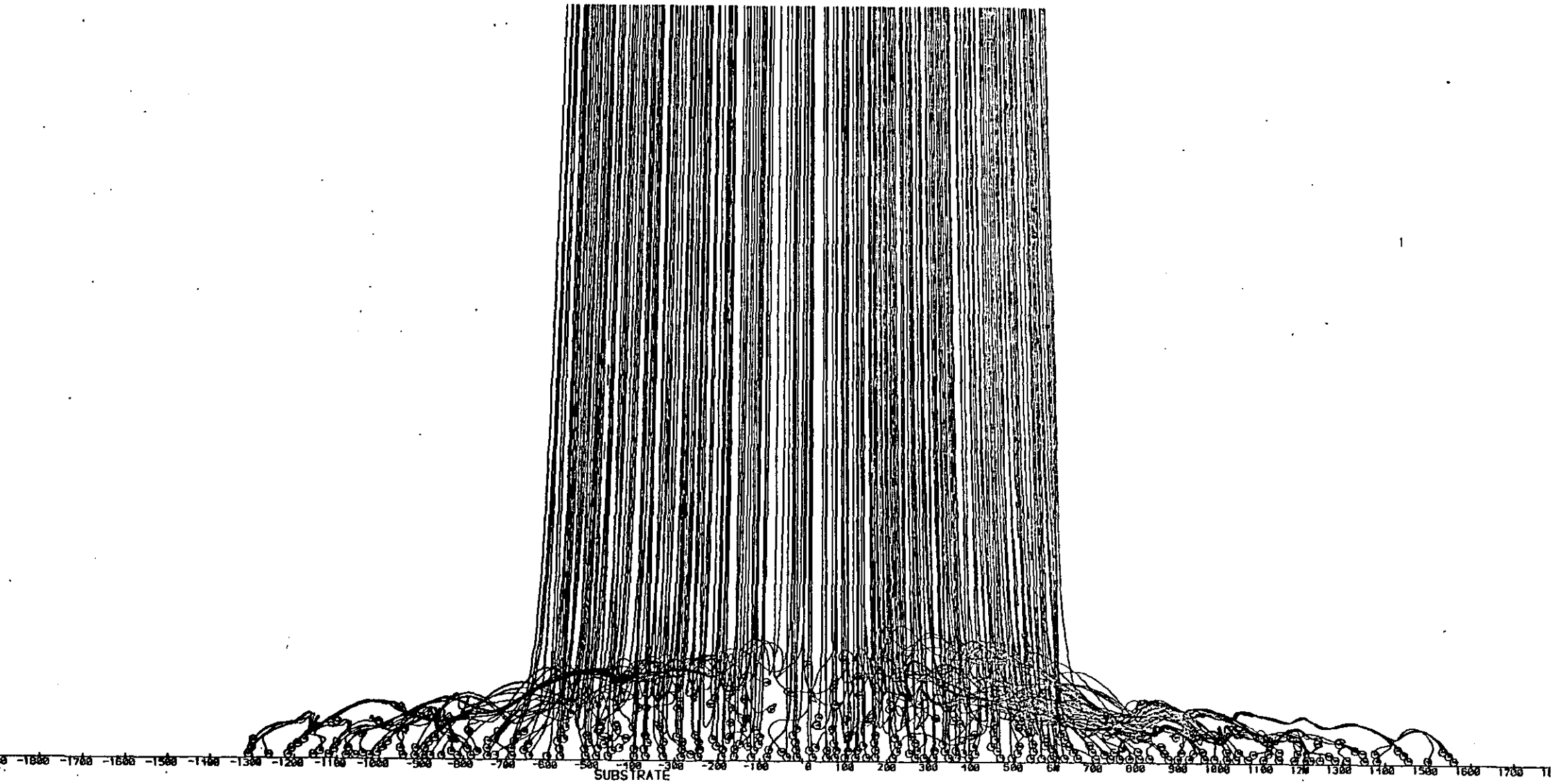
Figure E24.   Trajectories of Particles for Monosized Powder – Particle diameter = 17µm, Uniform Velocity = 5 m/s

SUBSTRATE
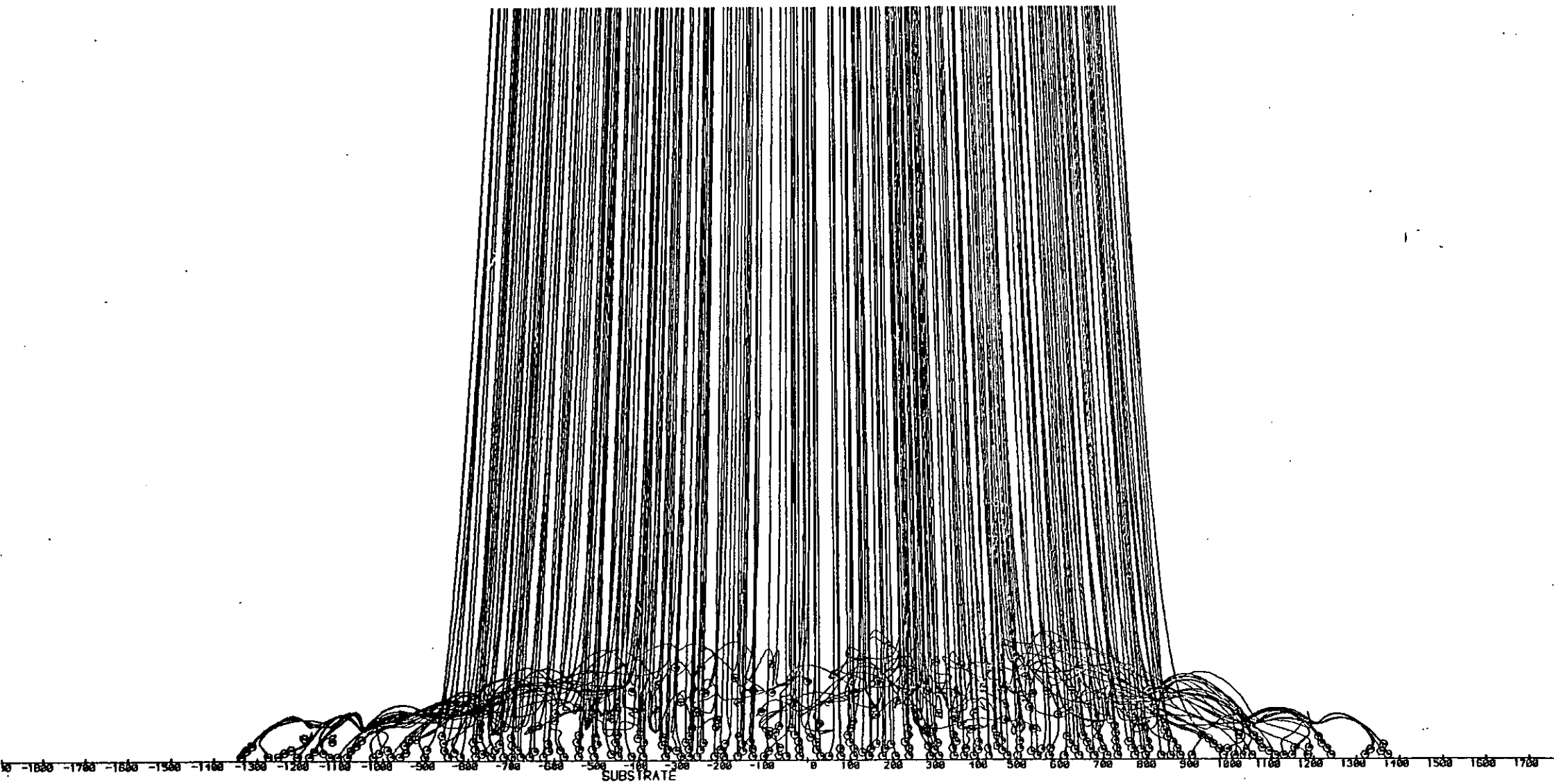
Figure E25. Trajectories of Particles for Monosized Powder – Particle diameter = 17μm, Uniform Velocity = 7 m/s
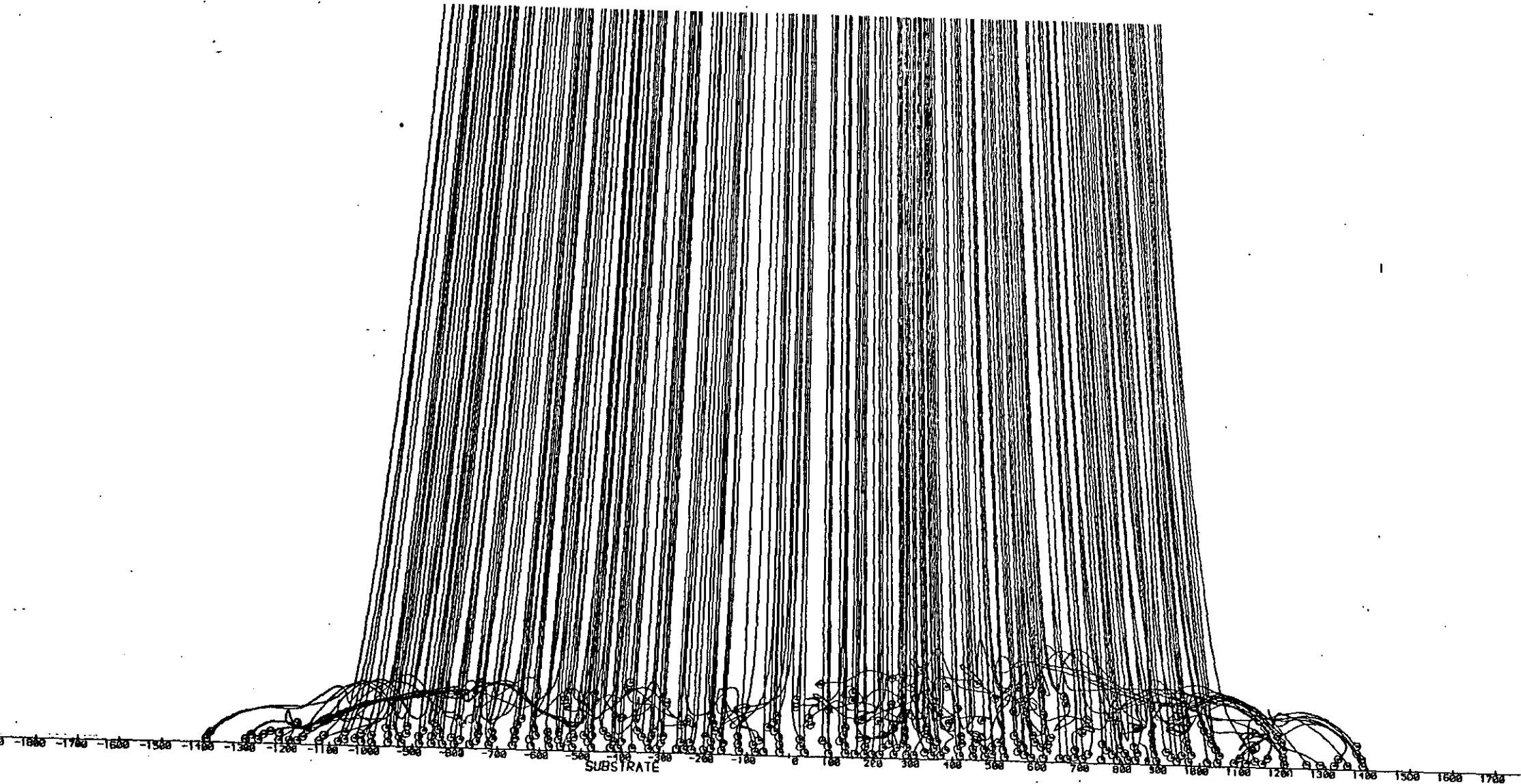
Figure E26. Trajectories of Particles for Monosized Powder – Particle diameter = 17μm, Uniform Velocity = 10 m/s
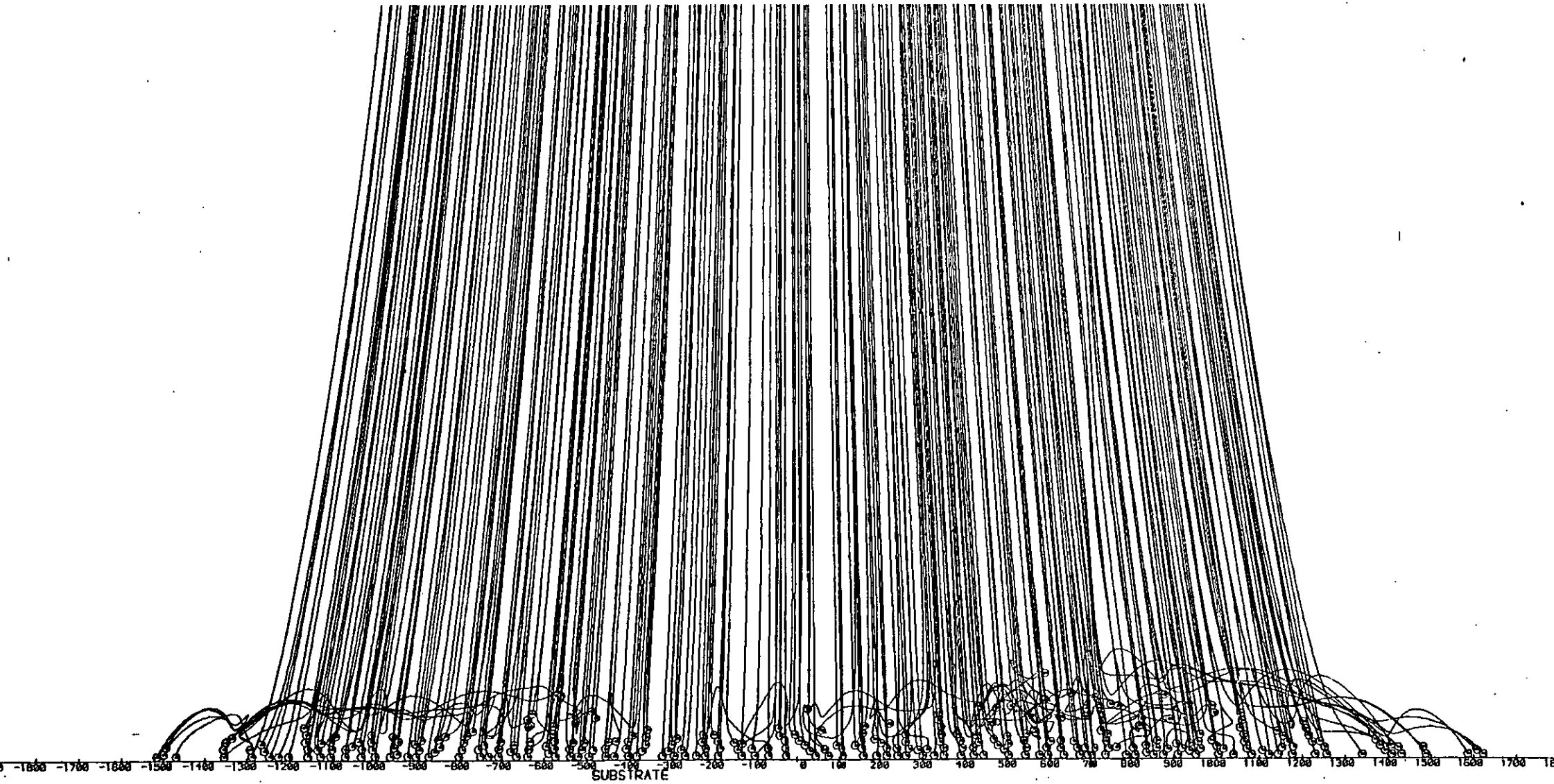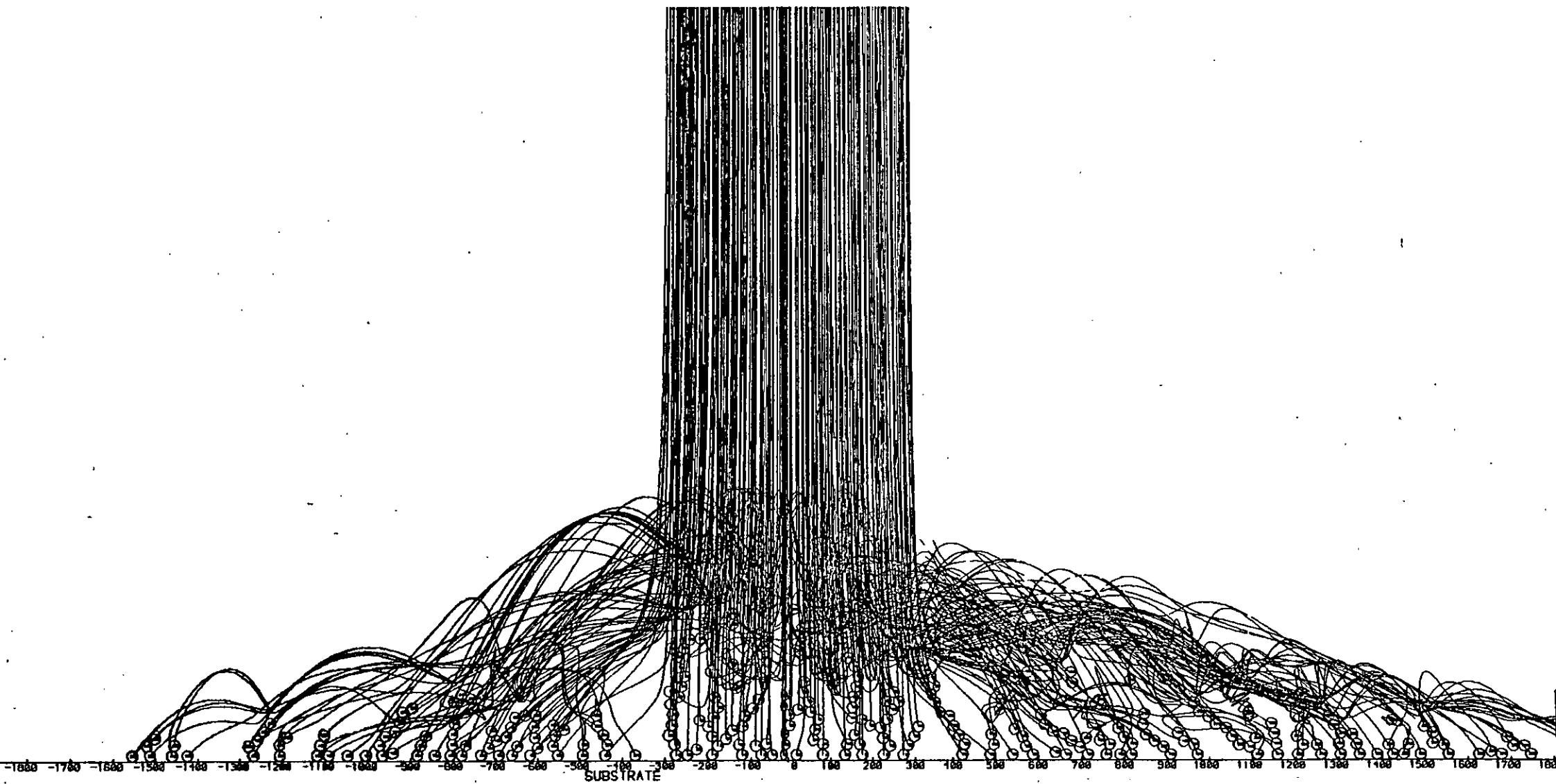
Figure E28. Trajectories of Particles for Monosized Powder – Particle diameter = 25μm, Uniform Velocity = 3 m/s
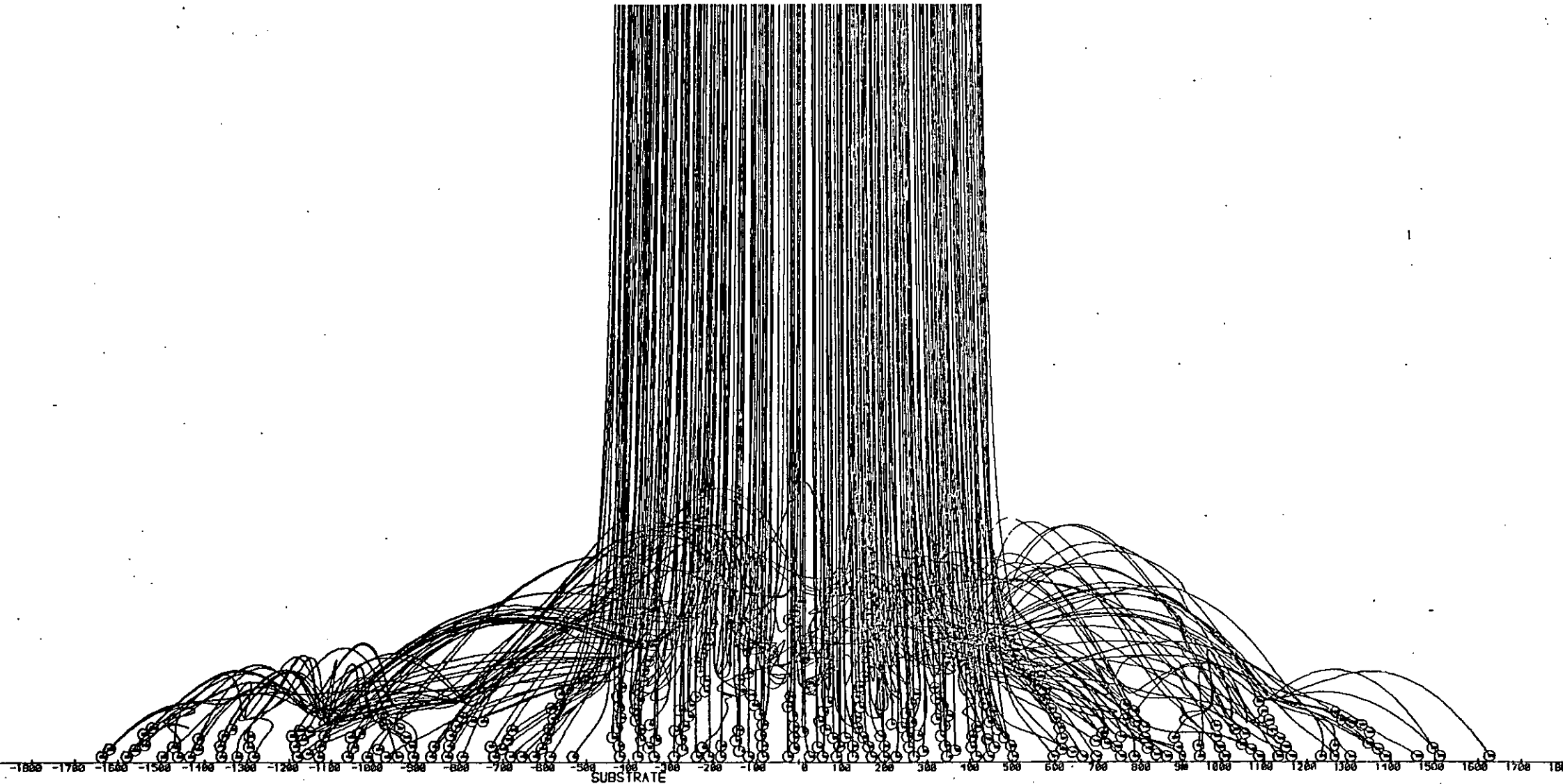
Figure E29. Trajectories of Particles for Monosized Powder — Particle diameter = 25μm, Uniform Velocity = 5 m/s
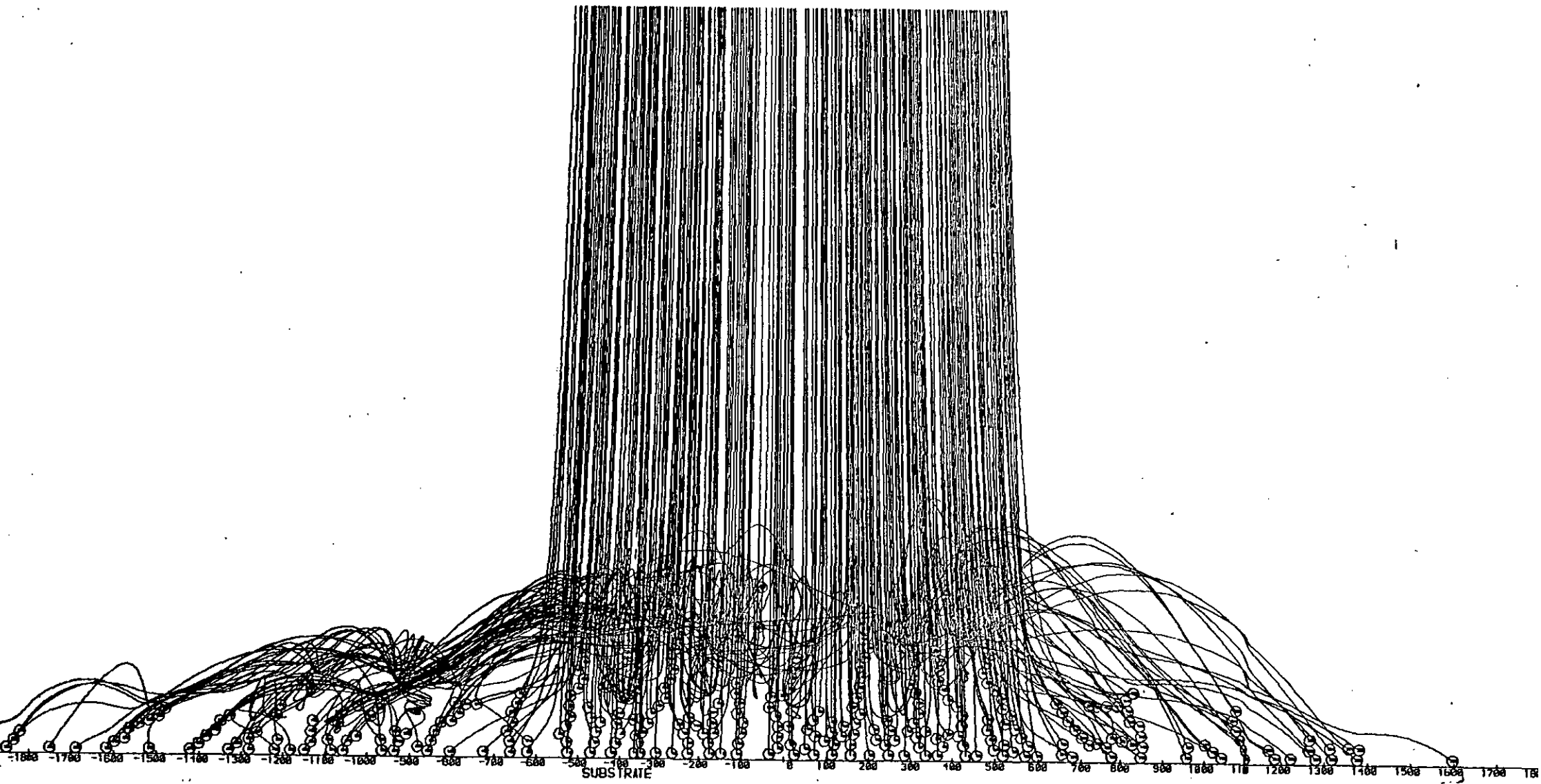
Figure E30. Trajectories of Particles for Monosized Powder – Particle diameter = 25μm, Uniform Velocity = 7 m/s
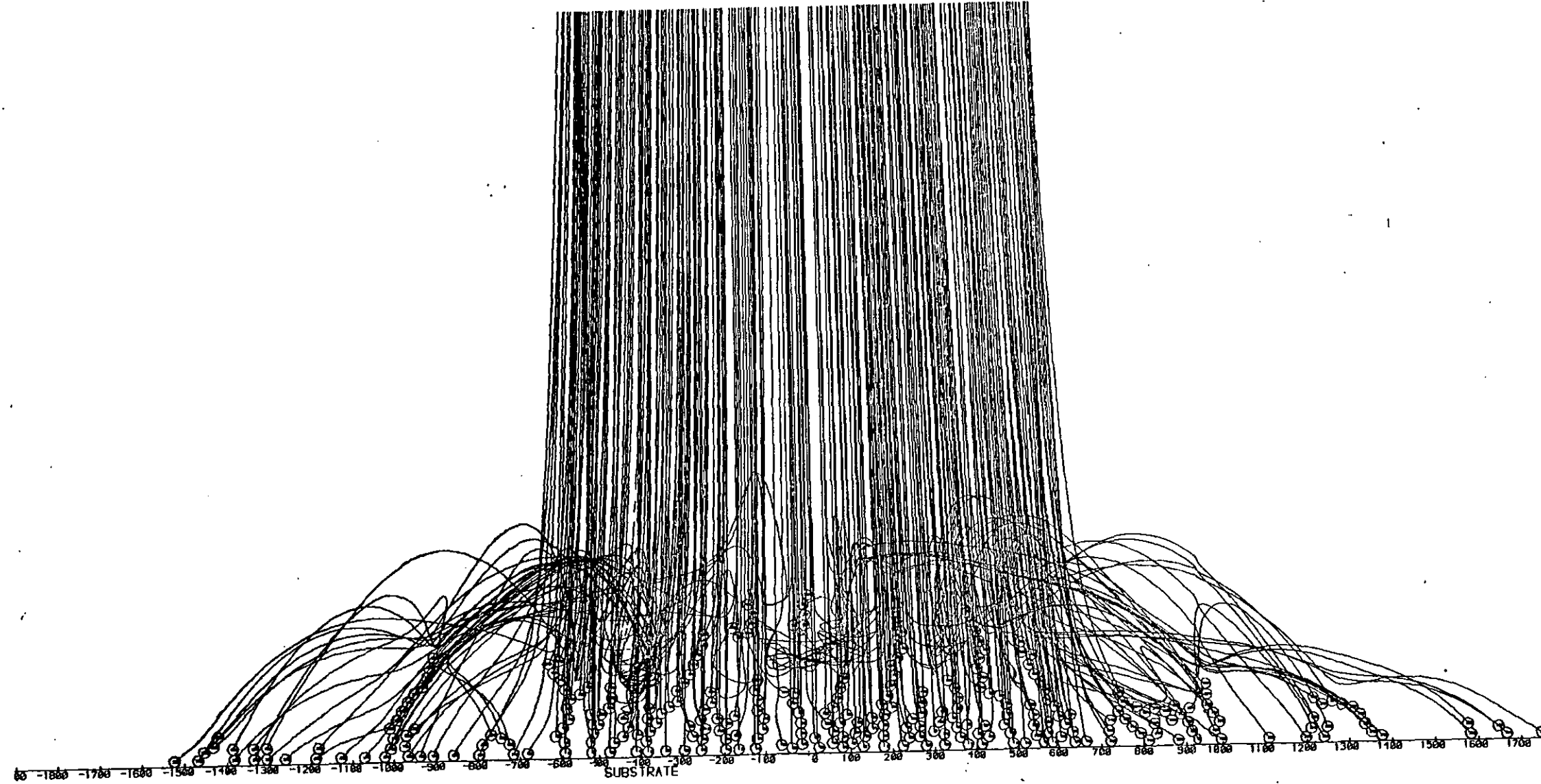
Figure E31. Trajectories of Particles for Monosized Powder – Particle diameter = 25μm, Uniform Velocity = 10 m/s
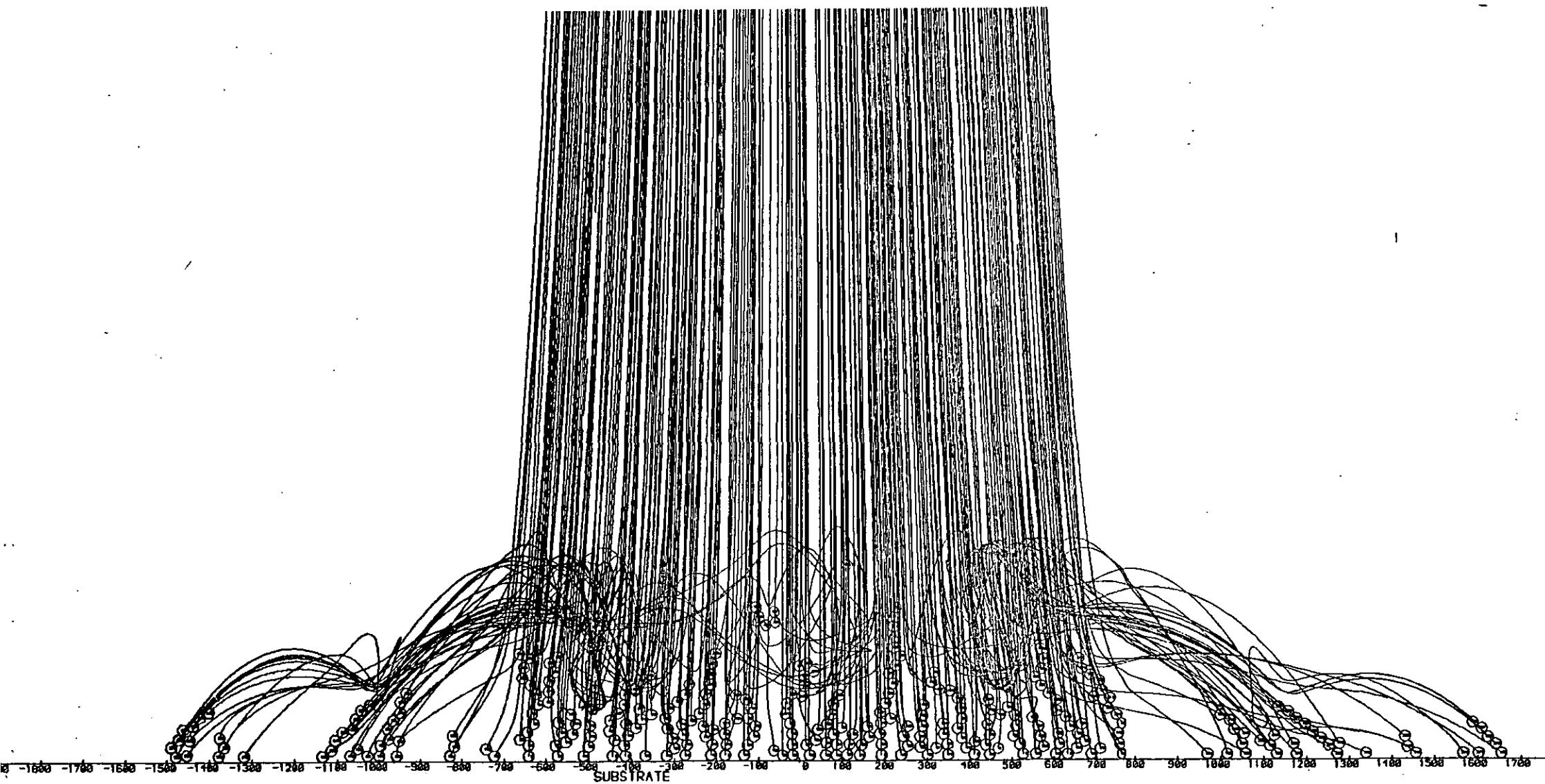
Figure E32. Trajectories of Particles for Monosized Powder – Particle diameter = 50μm, Uniform Velocity = 1 m/s
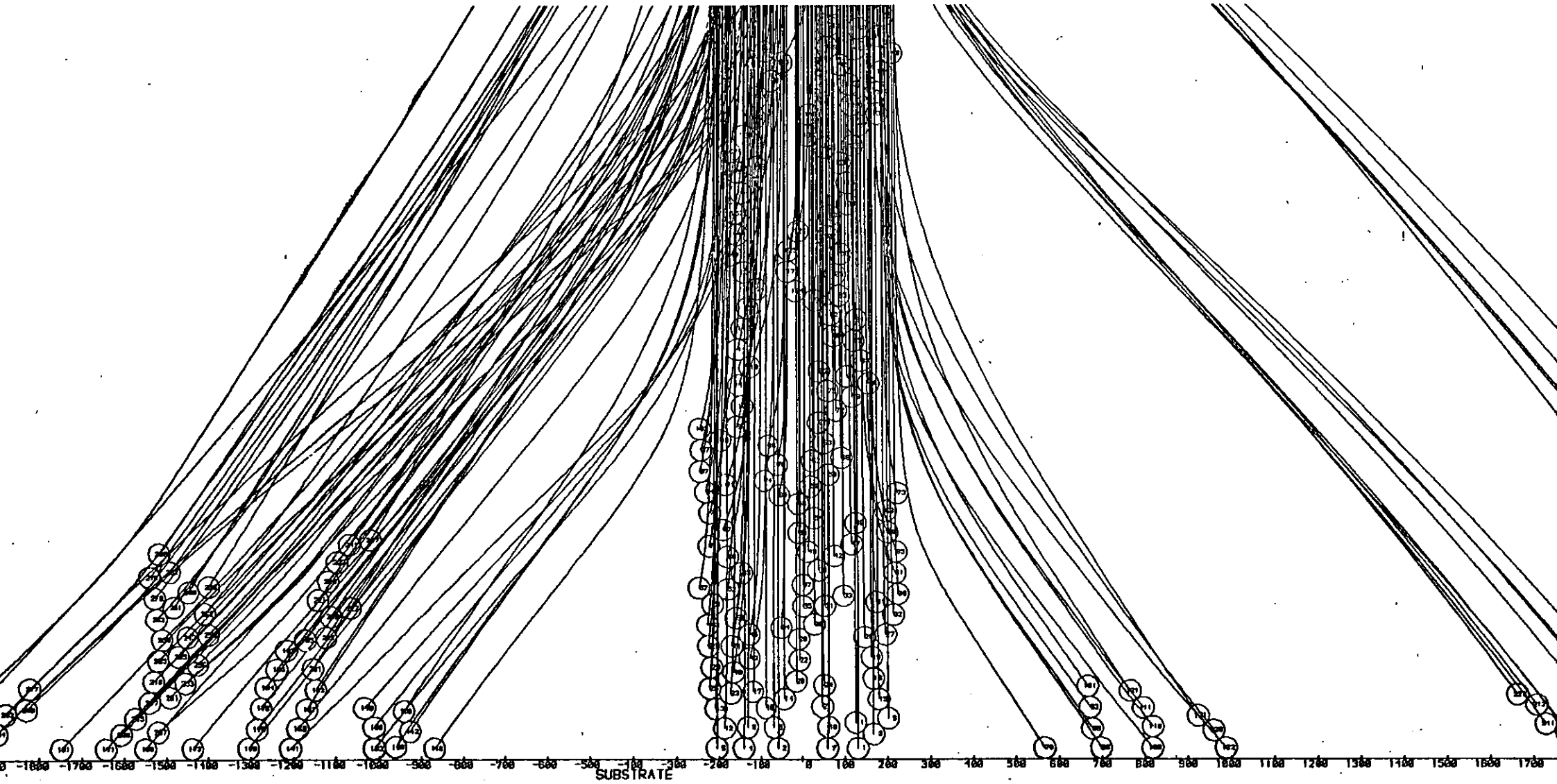
Figure E33.   Trajectories of Particles for Monosized Powder – Particle diameter = 50μm, Uniform Velocity = 3 m/s
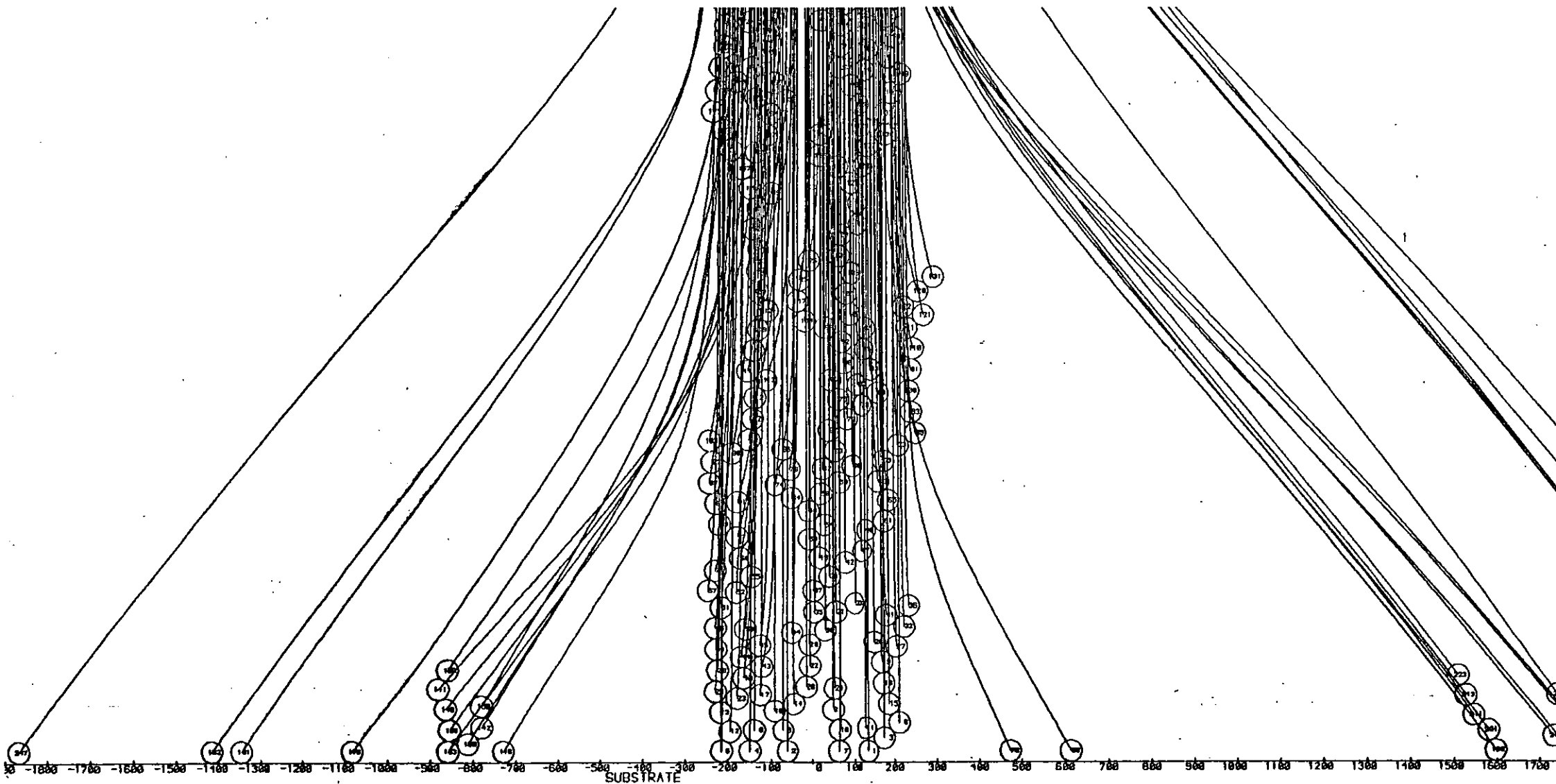
Figure E34. Trajectories of Particles for Monosized Powder - Particle diameter = 50µm, Uniform Velocity = 5 m/s
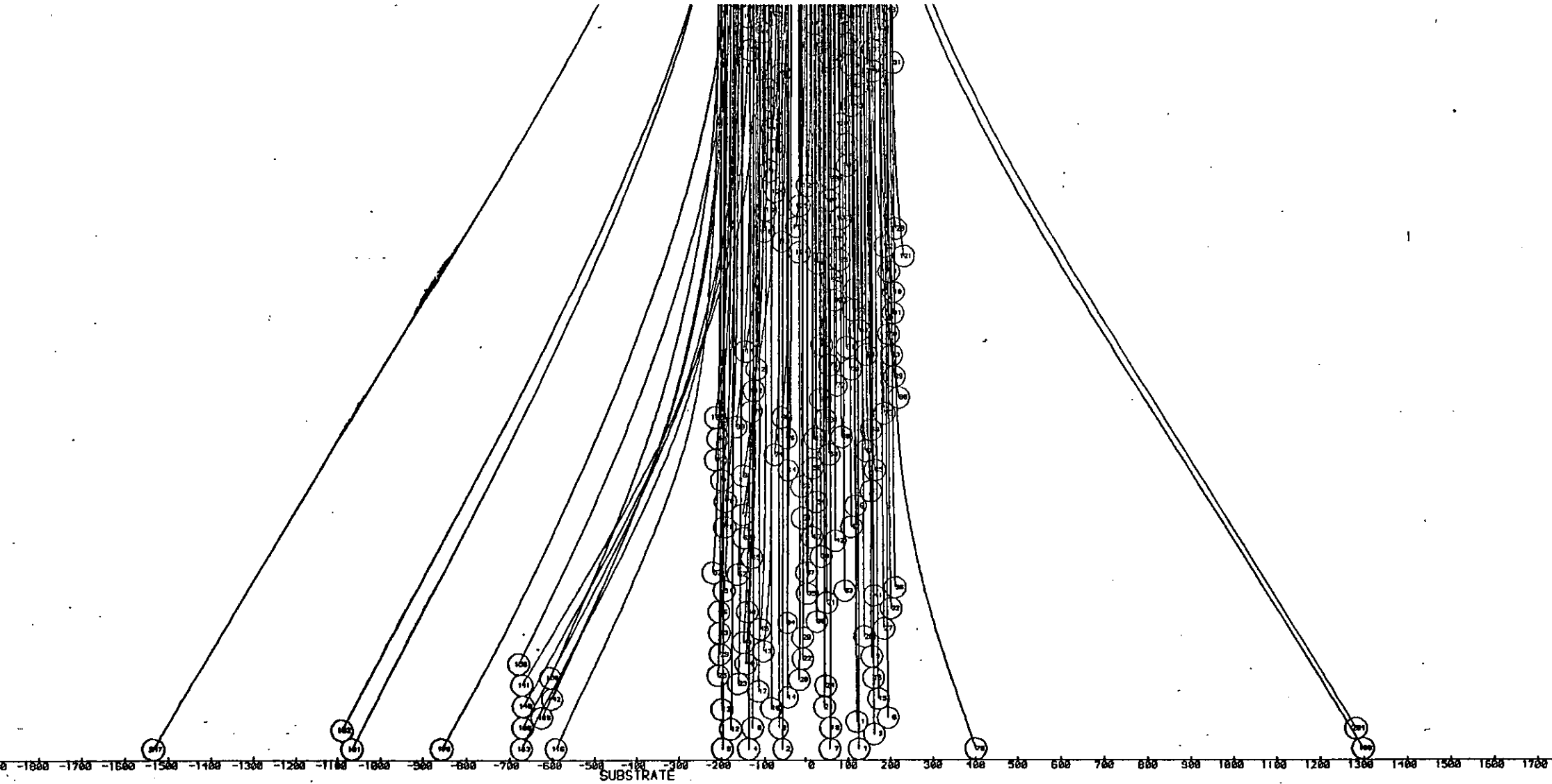
Figure E35. Trajectories of Particles for Monosized Powder – Particle diameter = 50µm, Uniform Velocity = 7 m/s
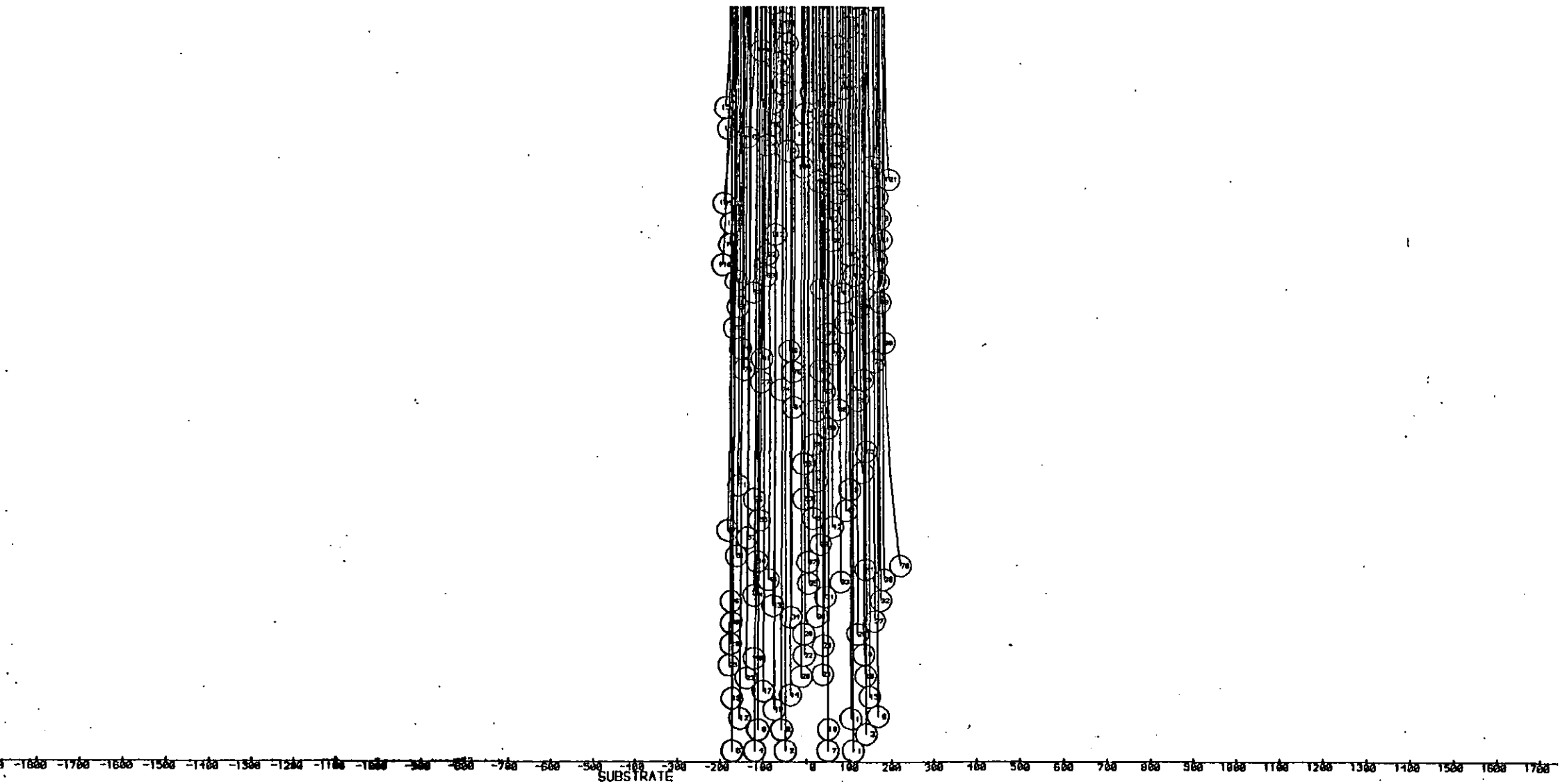
Figure E36. Trajectories of Particles for Monosized Powder – Particle diameter = 50μm, Uniform Velocity = 10 m/s

Figure E37. Particle Trajectories for a Size Distributed Powder - Uniform Velocity = 1 m/s

Figure E38. Particle Trajectories for a Size Distributed Powder - Uniform Velocity = 3 m/s
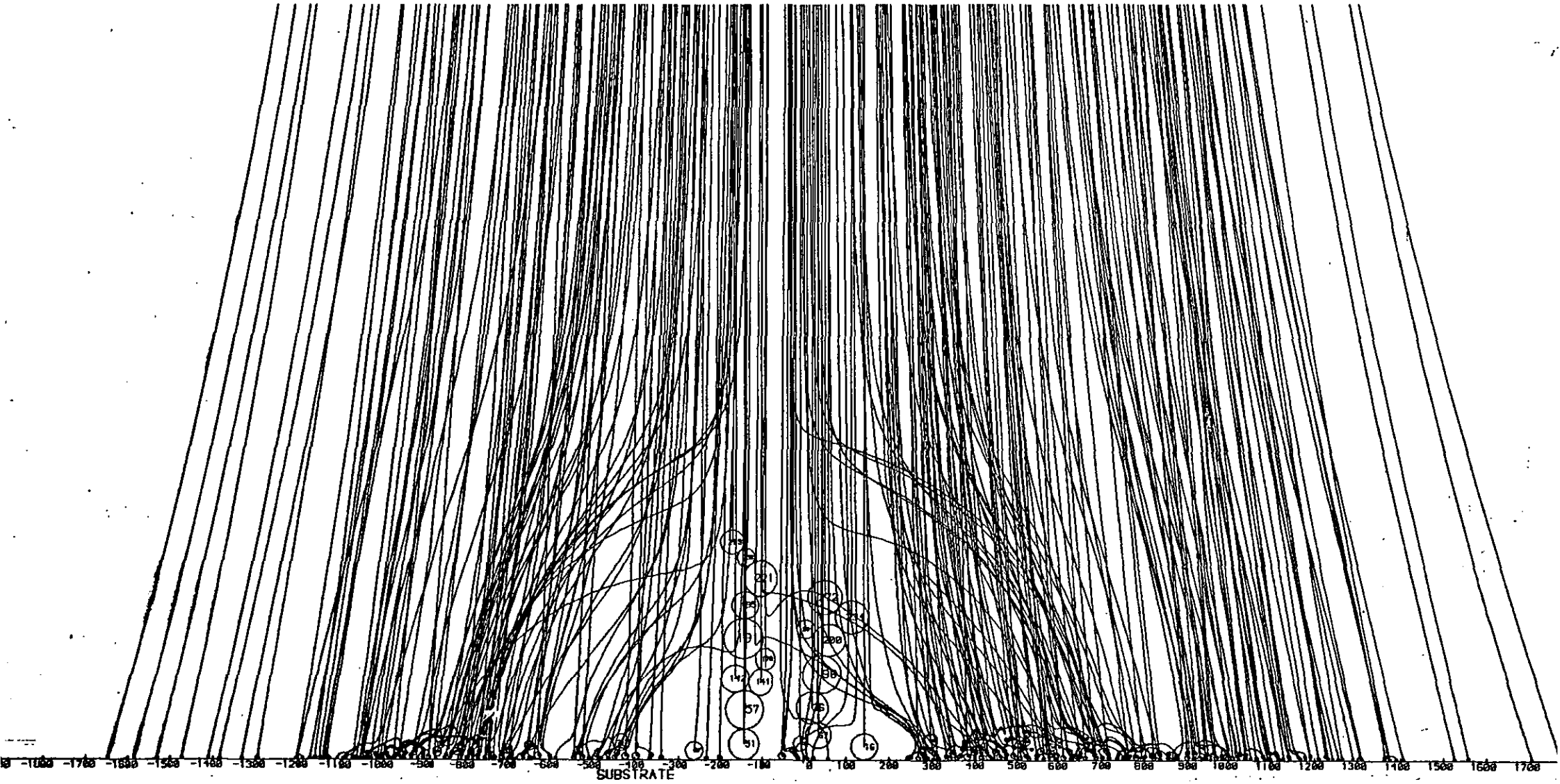
Figure E39. Particle Trajectories for a Size Distributed Powder - Uniform Velocity = 5 m/s
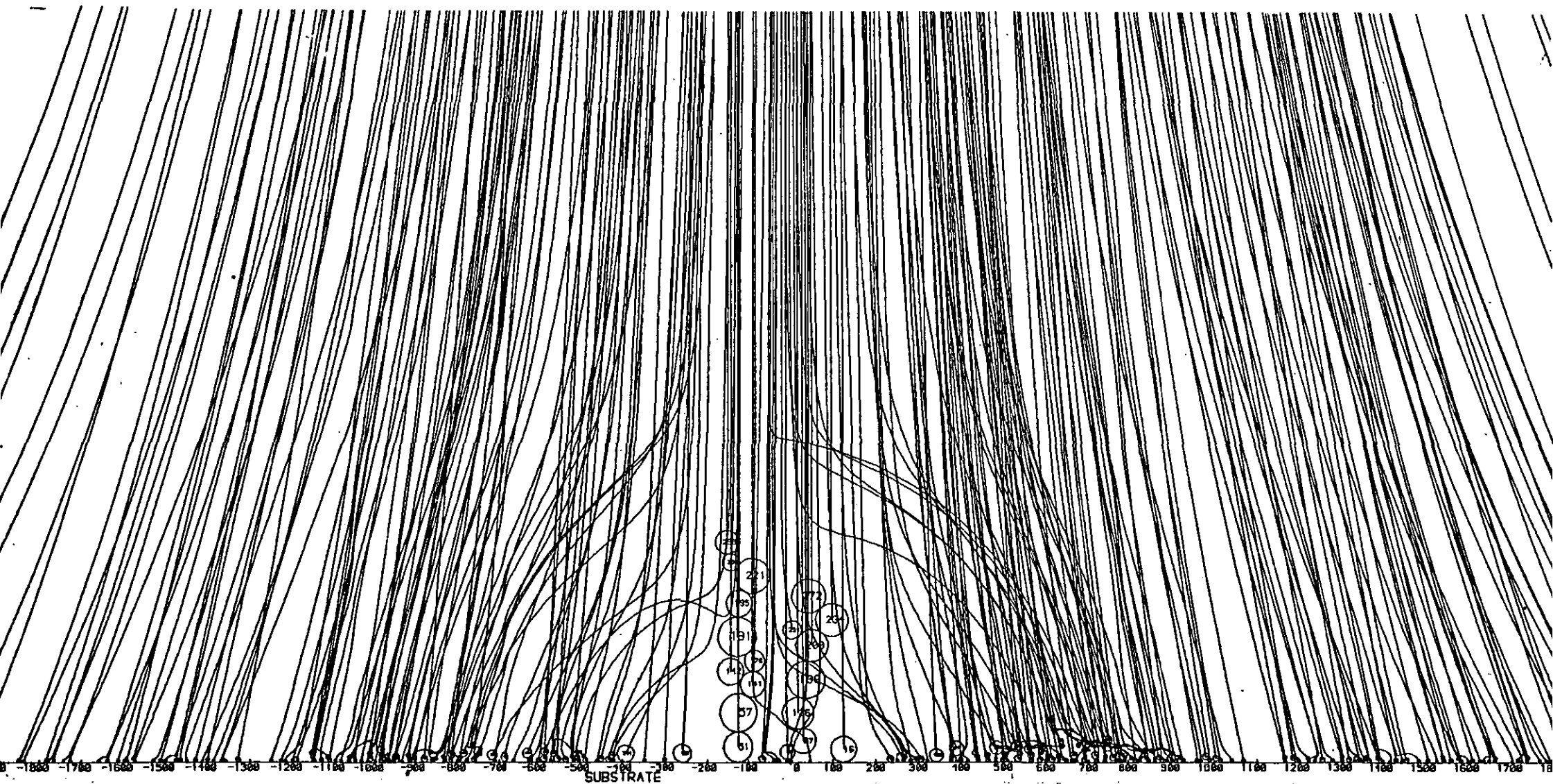
Figure E40. Particle Trajectories for a Size Distributed Powder - Uniform Velocity = 7 m/s
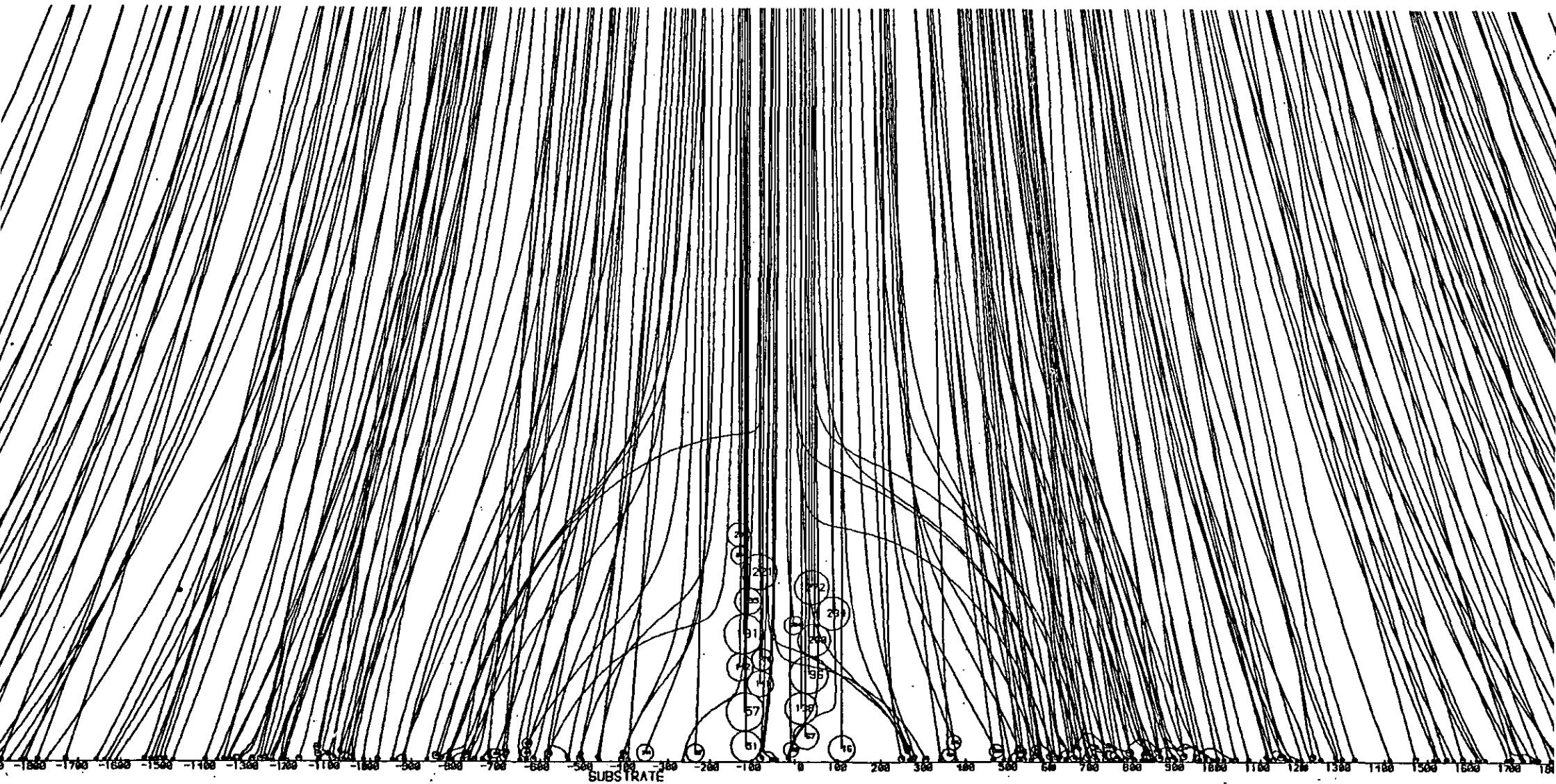
Figure E41.   Particle Trajectories for a Size Distributed Powder - Uniform Velocity = 10 m/s
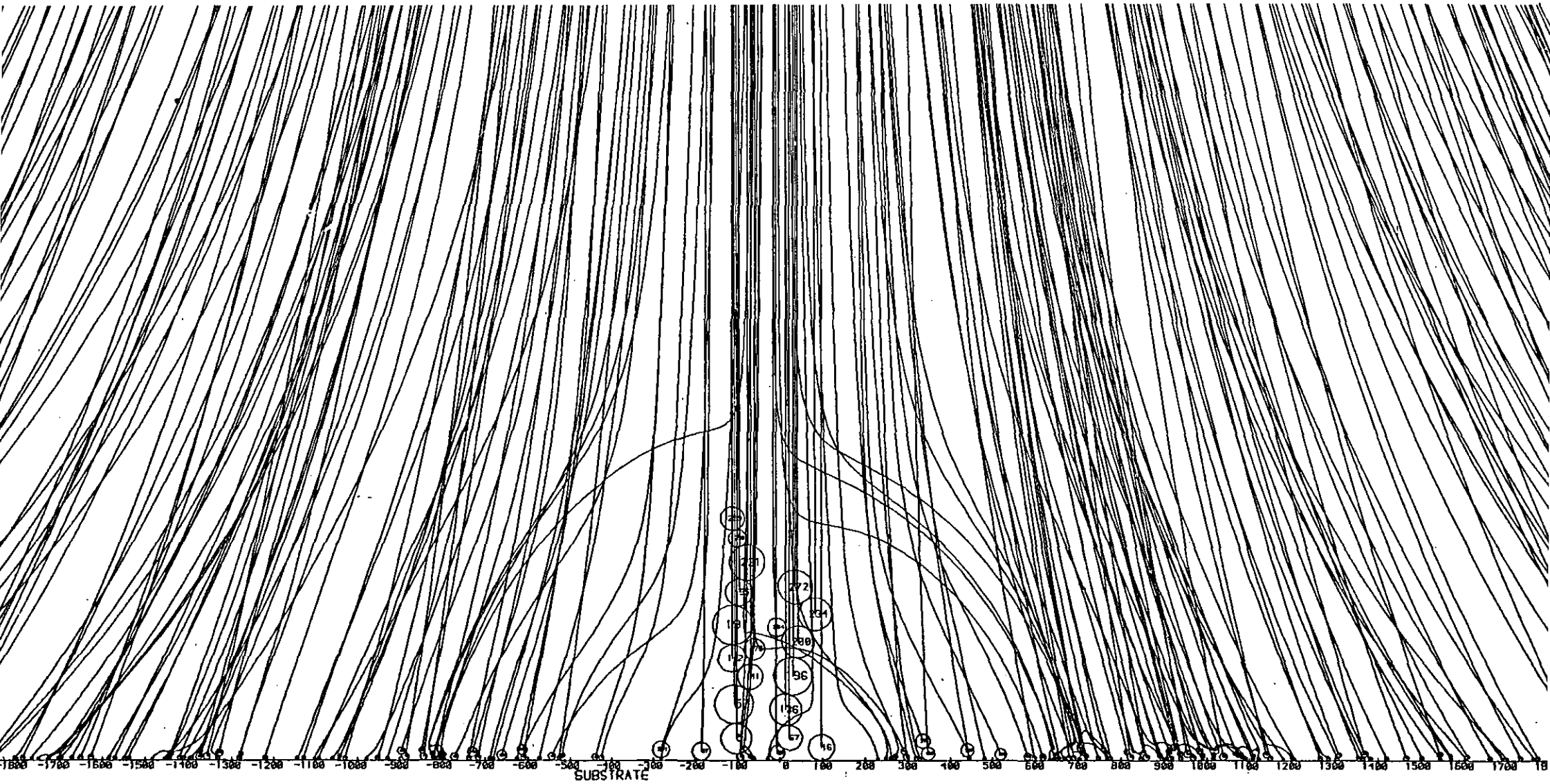
Trajectories of Particles Approaching a Charged Layer 50μm thick - Particle diameter = 10μm, Uniform Velocity = 1 m/s
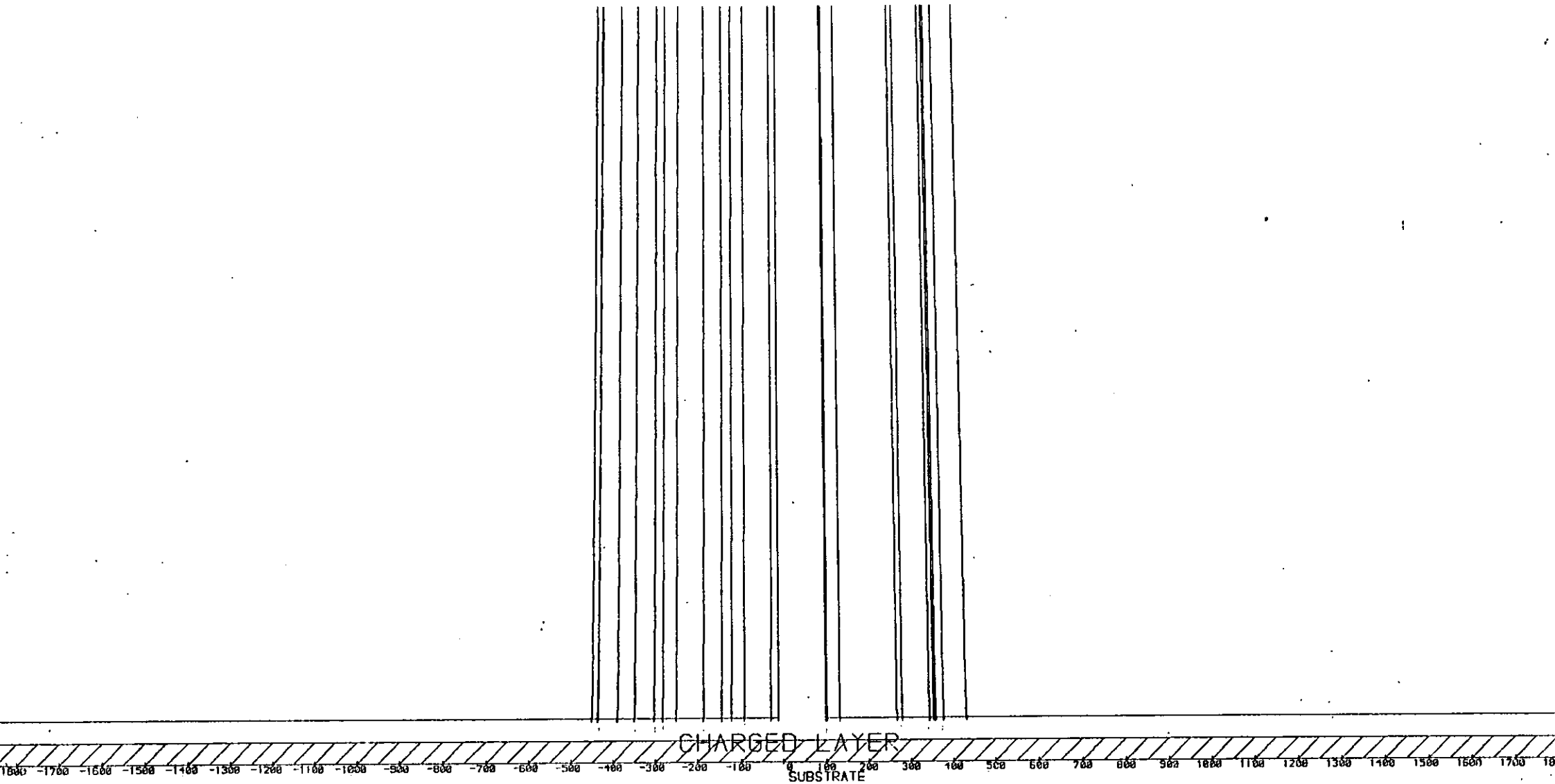
Figure E43. Trajectories of Particles Approaching a Charged Layer 100μm thick – Particle diameter = 10μm, Uniform Velocity = 1 m/s
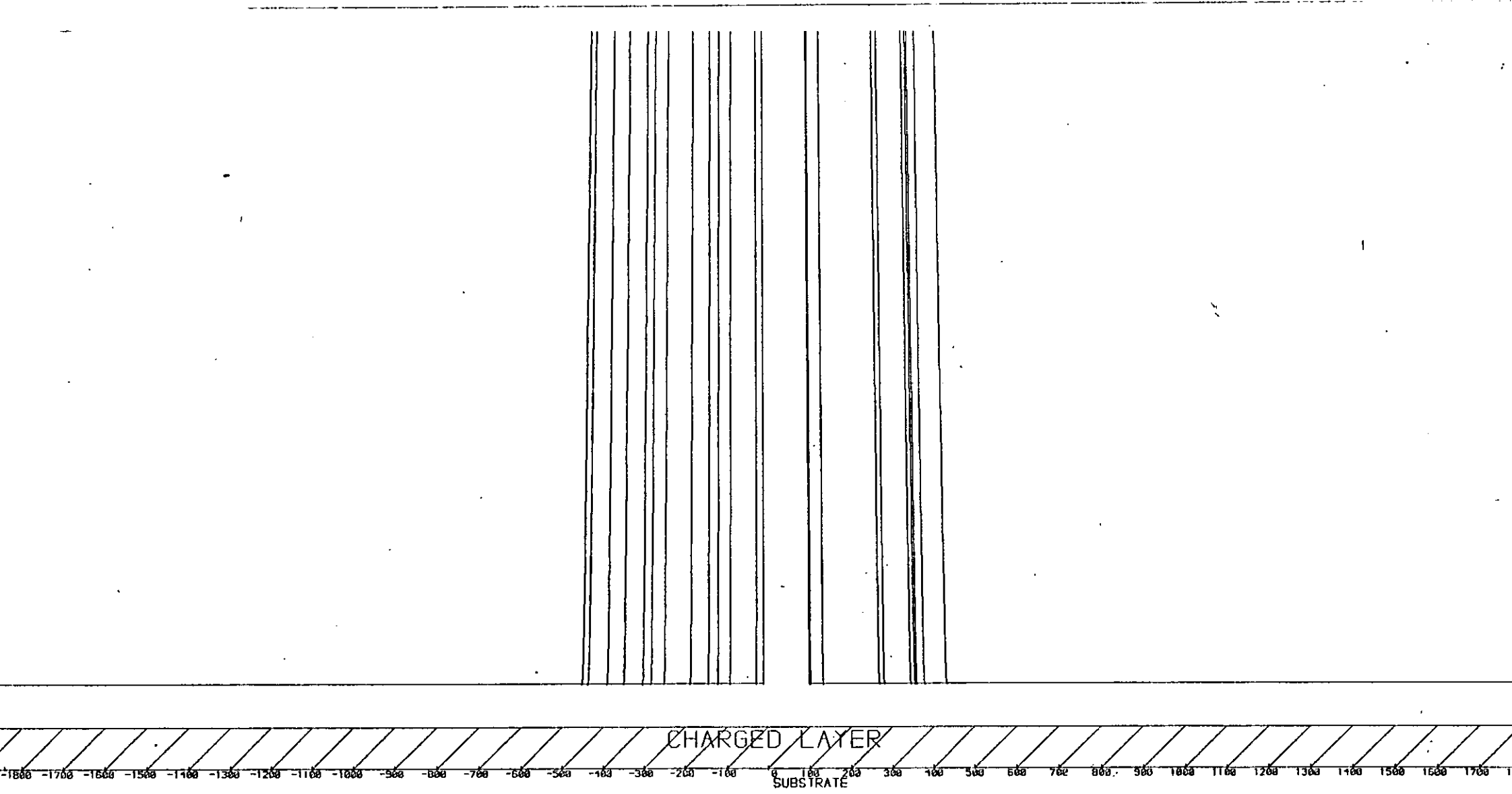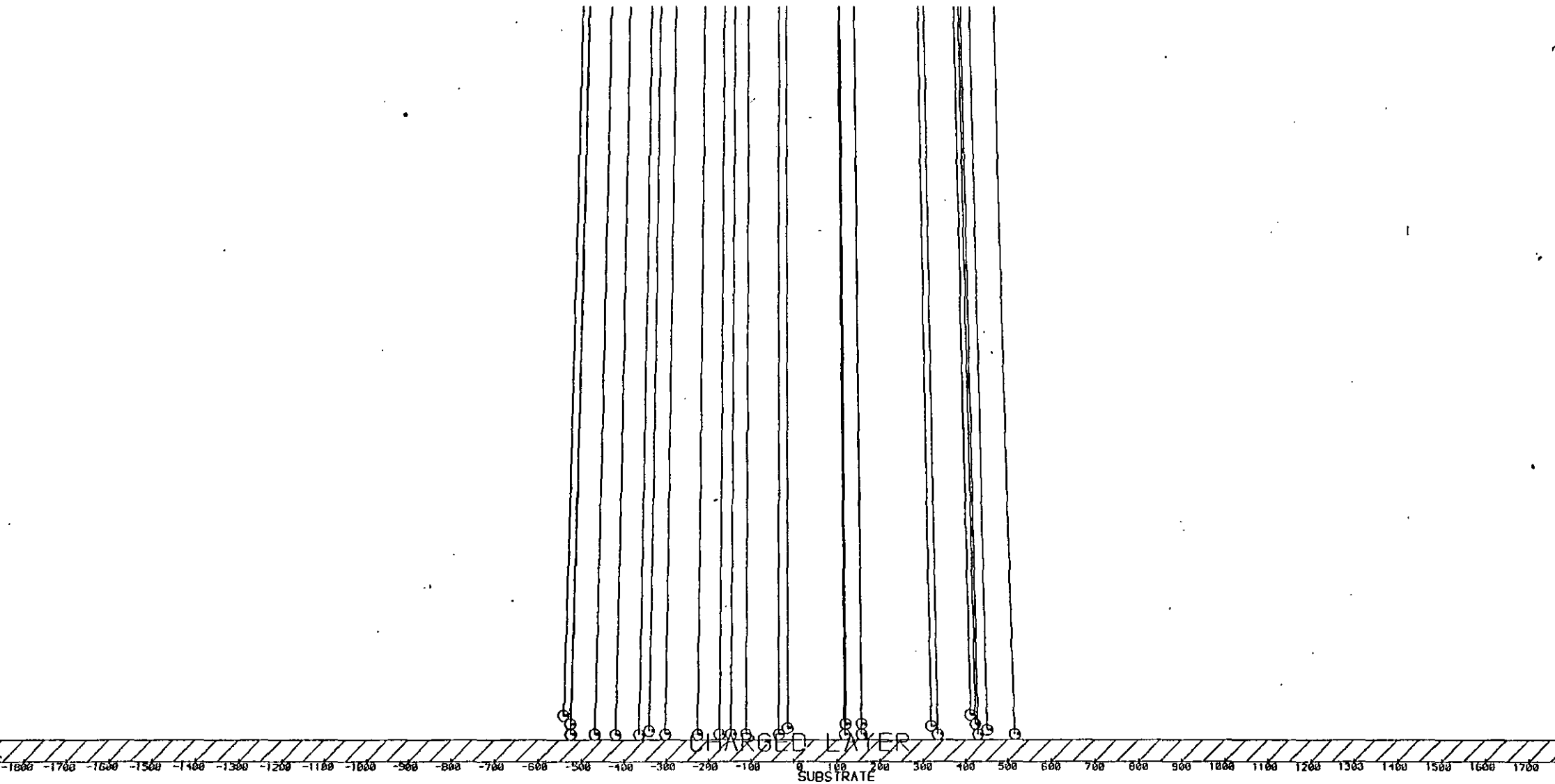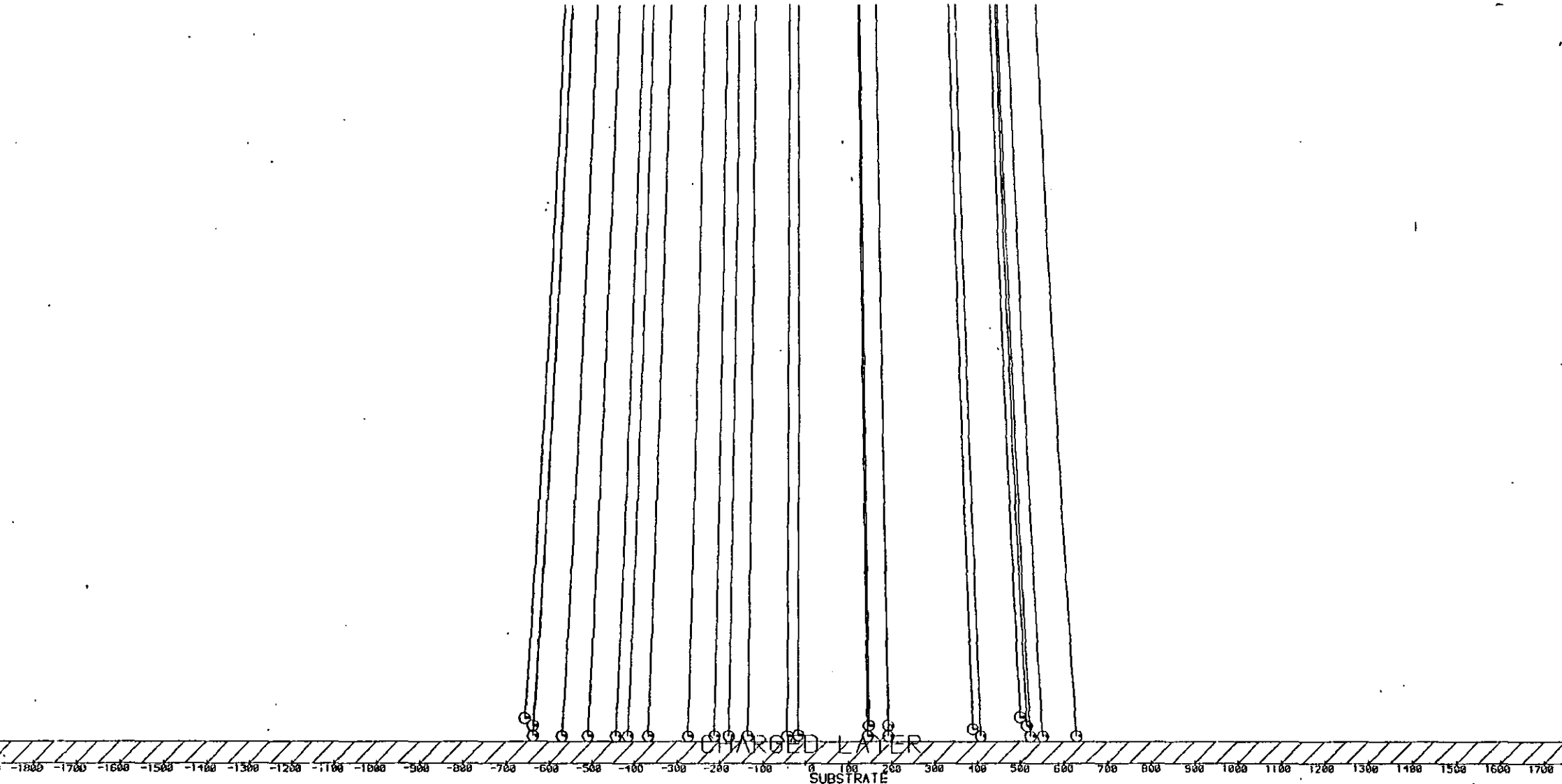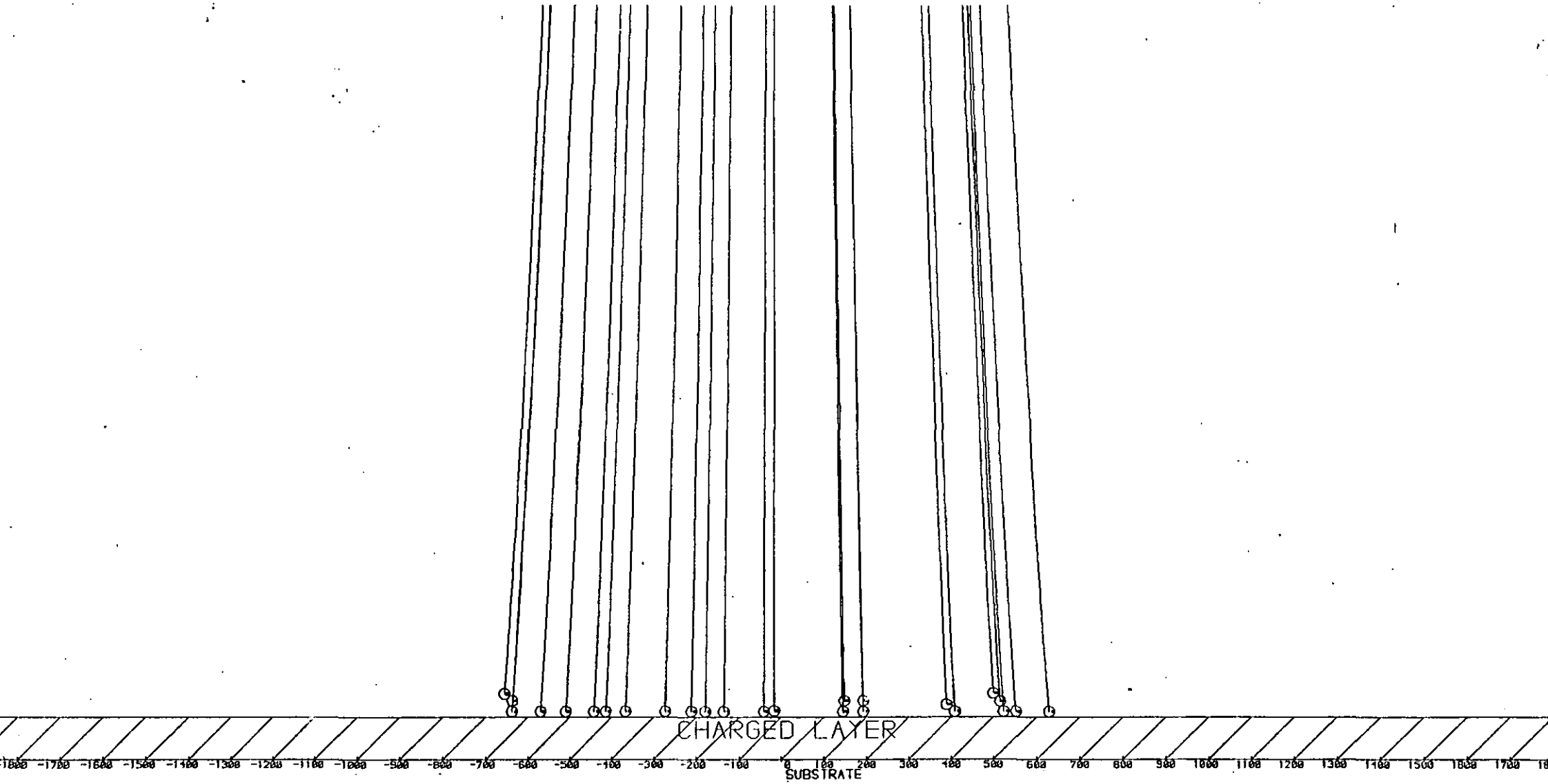
Figure E44. <u>Trajectories of Particles Approaching a Charged Layer 250µm thick – Particle diameter = 10µm, Uniform Velocity = 1 m/s</u>

CHARGED LAYER

SUBSTRATE

-1800 -1700 -1600 -1500 -1400 -1300 -1200 -1100 -1000 -900 -800 -700 -600 -500 -400 -300 -200 -100 0 100 200 300 400 500 600 700 800 900 1000 1100 1200 1300 1400 1500 1600 1700
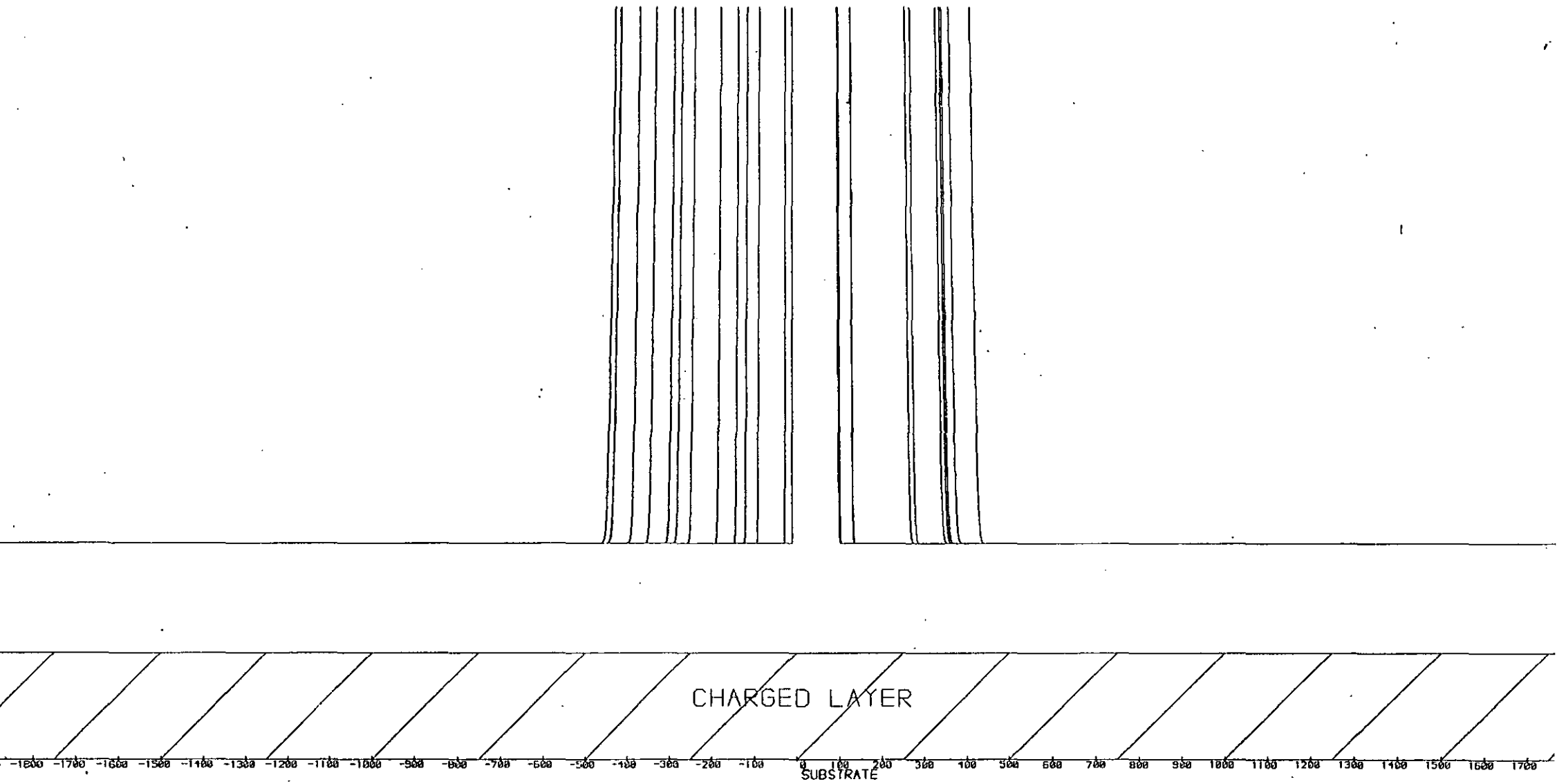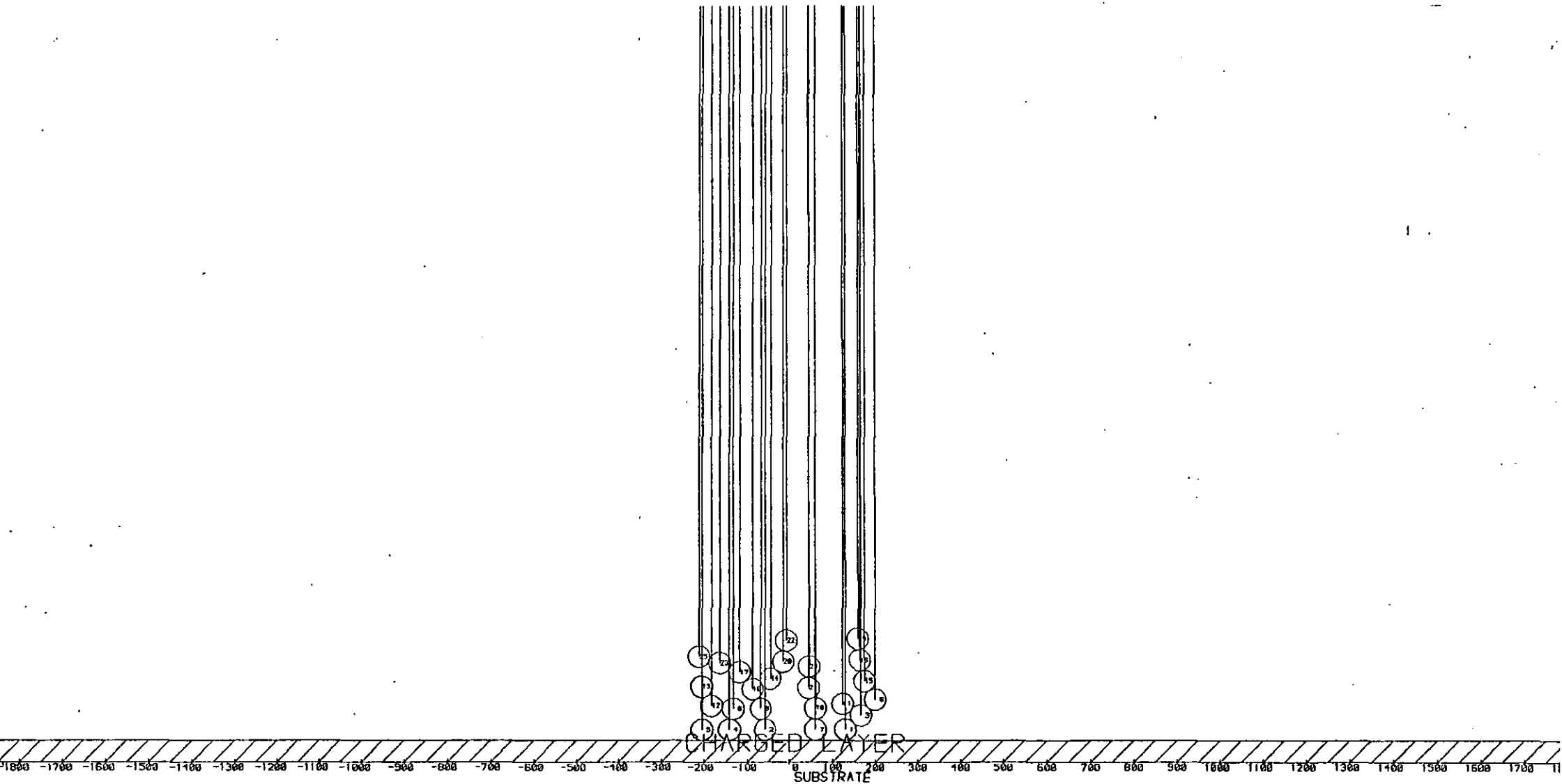
Figure E45.   Trajectories of Particles Approaching a Charged Layer 50μm thick – Particle diameter = 10μm,
Uniform Velocity = 5 m/s
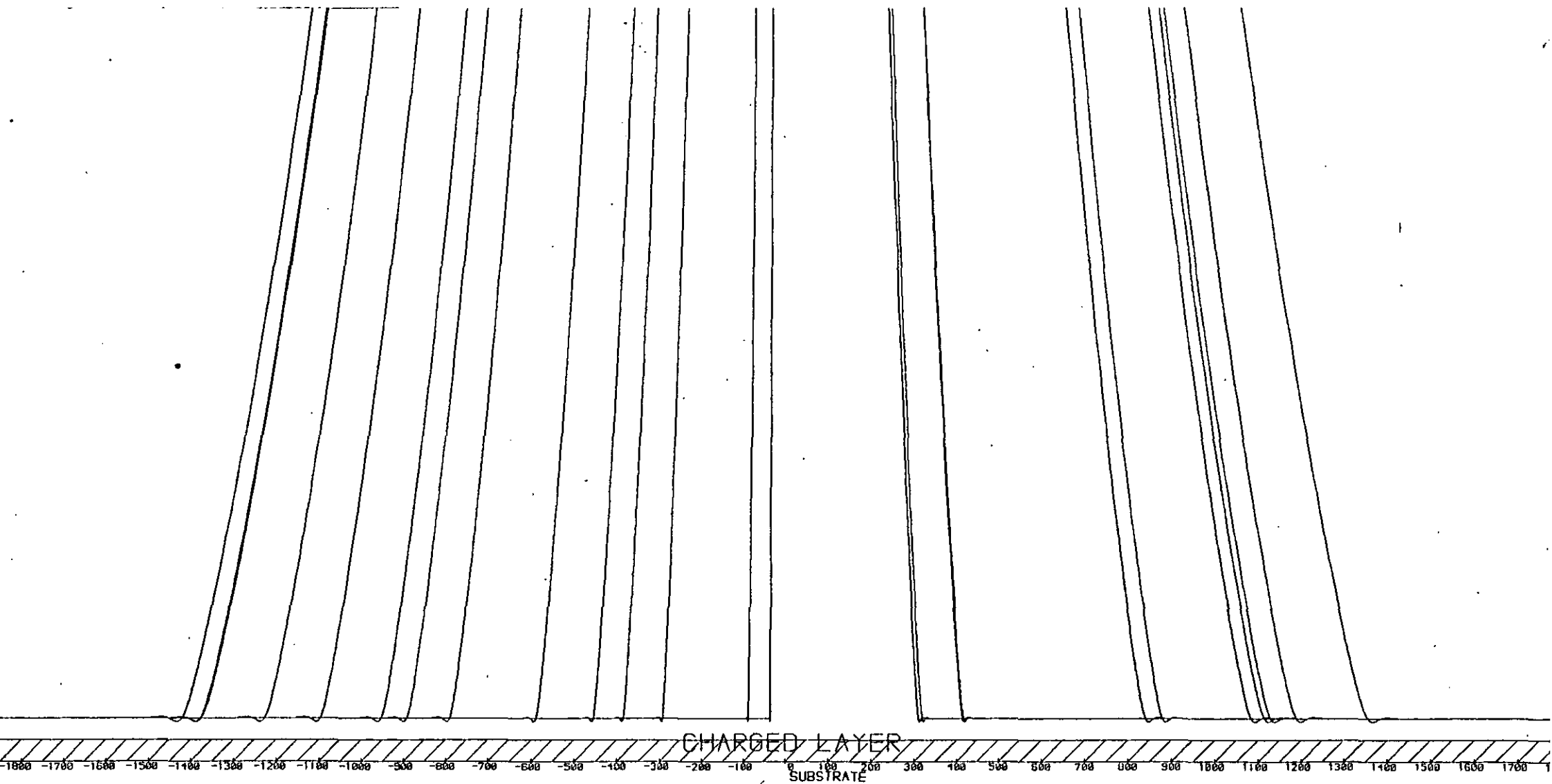
Figure E46. Trajectories of Particles Approaching a Charged Layer 100μm thick – Particle diameter = 10μm, Uniform Velocity = 5 m/s

CHARGED LAYER

SUBSTRATE
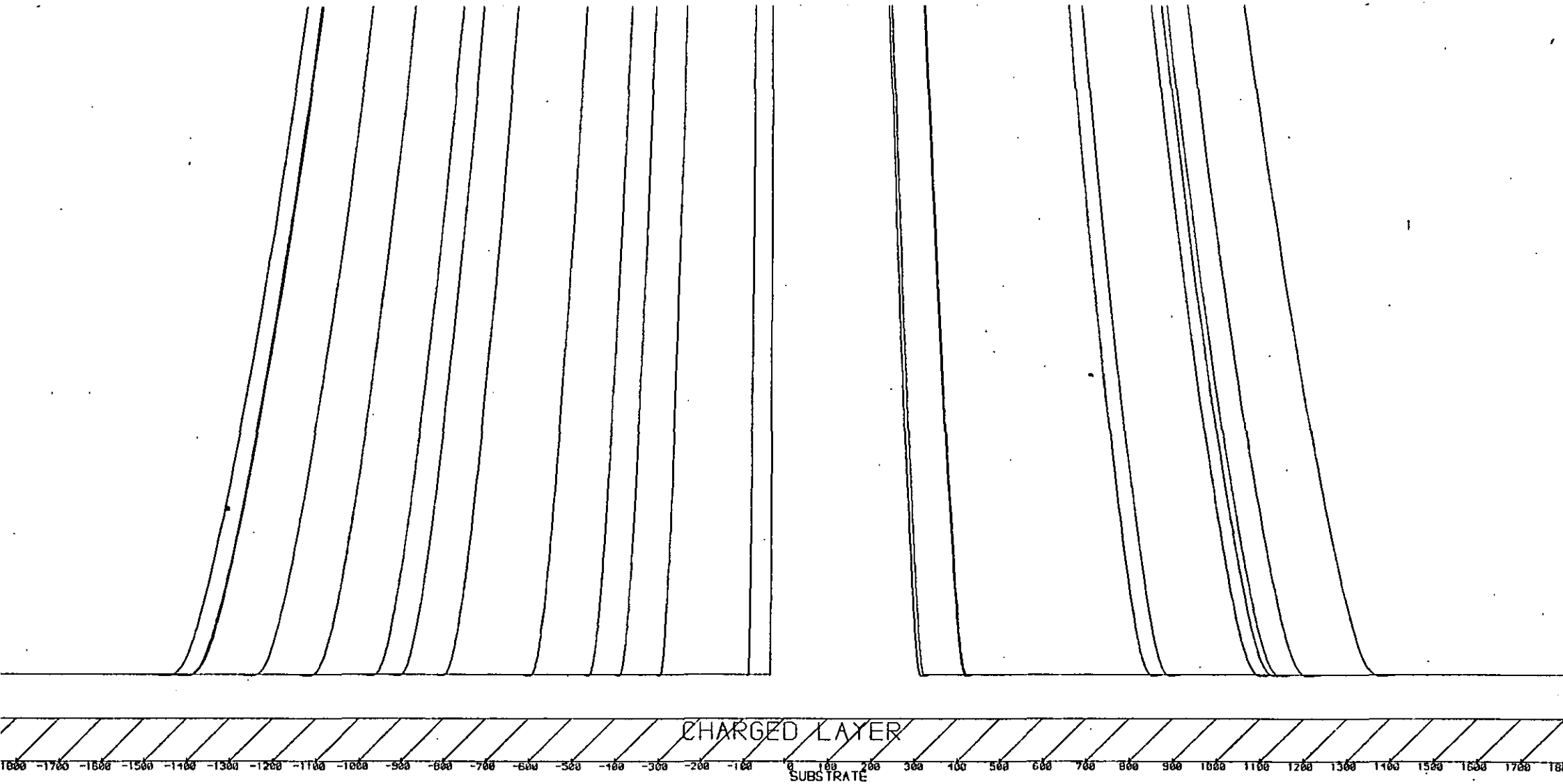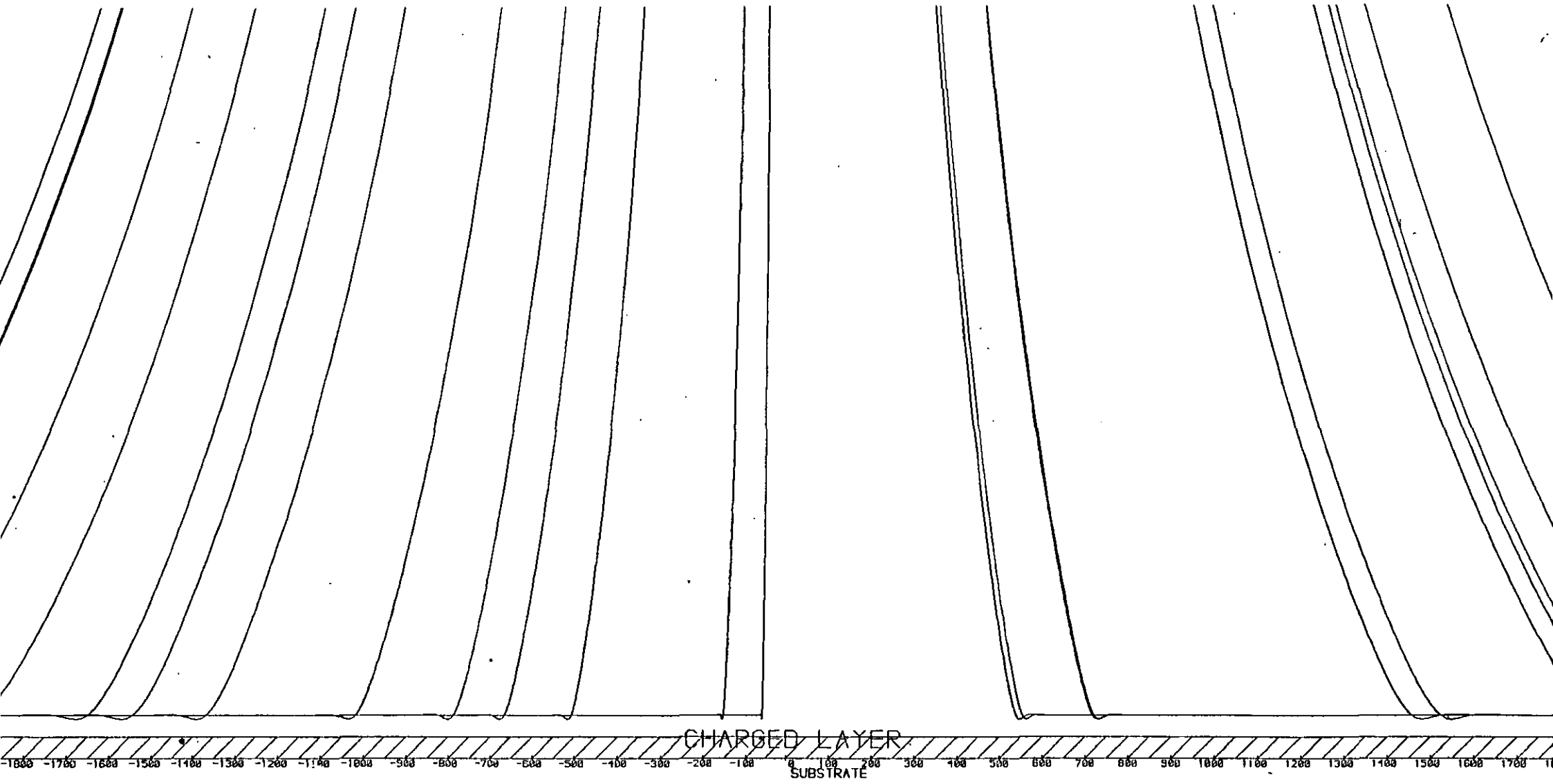
Figure E48: Trajectories of Particles Approaching a Charged Layer 100μm thick – Particle diameter = 10μm, Uniform Velocity = 10 m/s
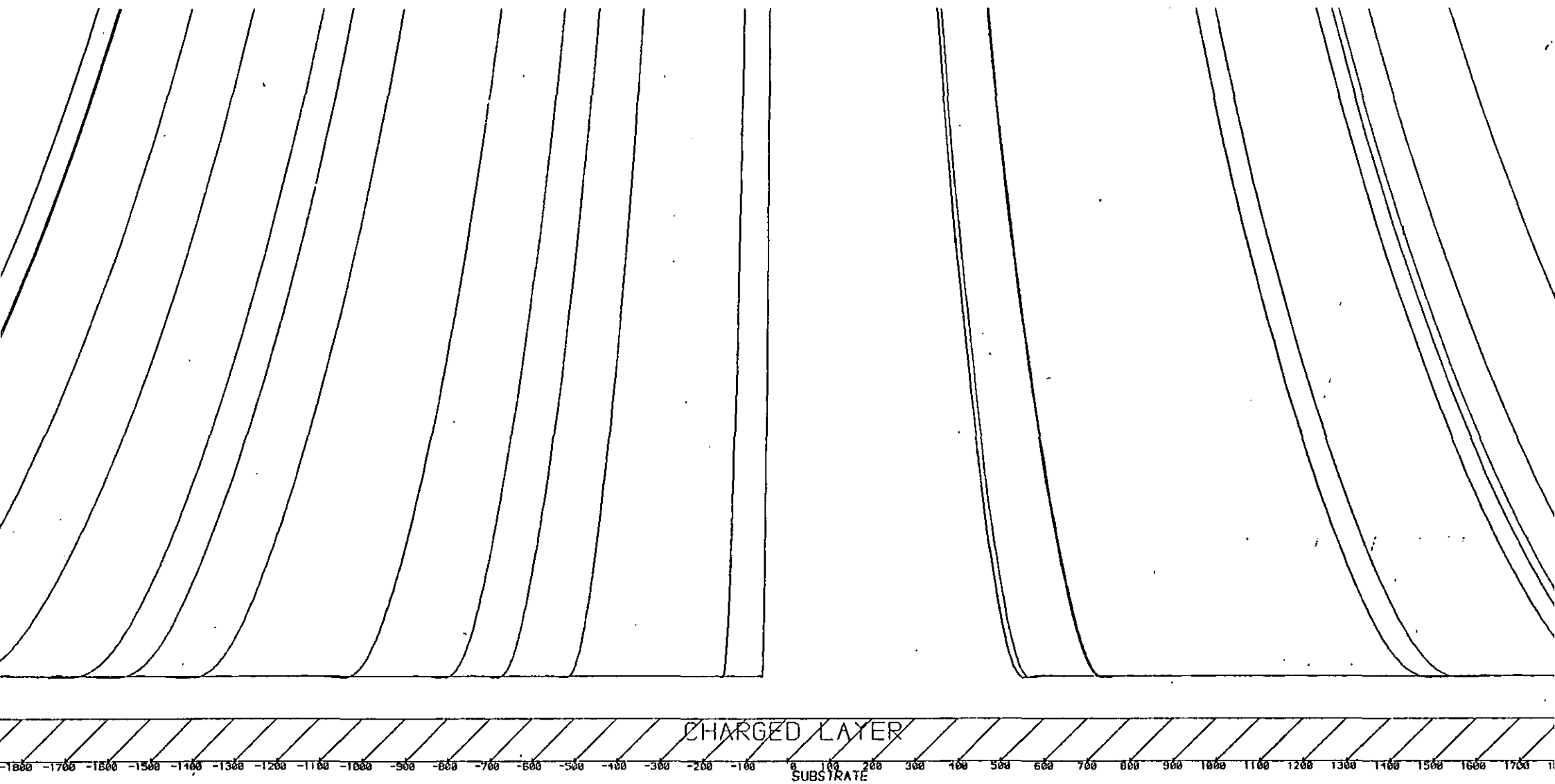
Figure E49: Trajectories of Particles Approaching a Charged Layer 250μm thick – Particle diameter = 10μm, Uniform Velocity = 10 m/s
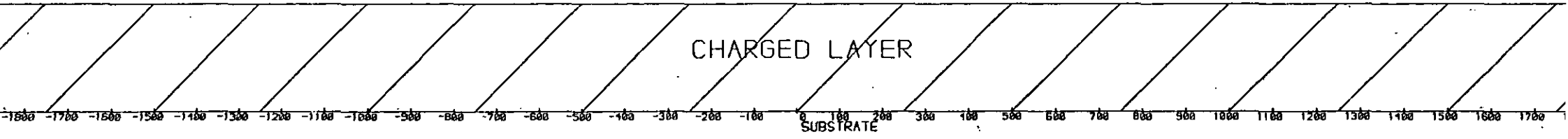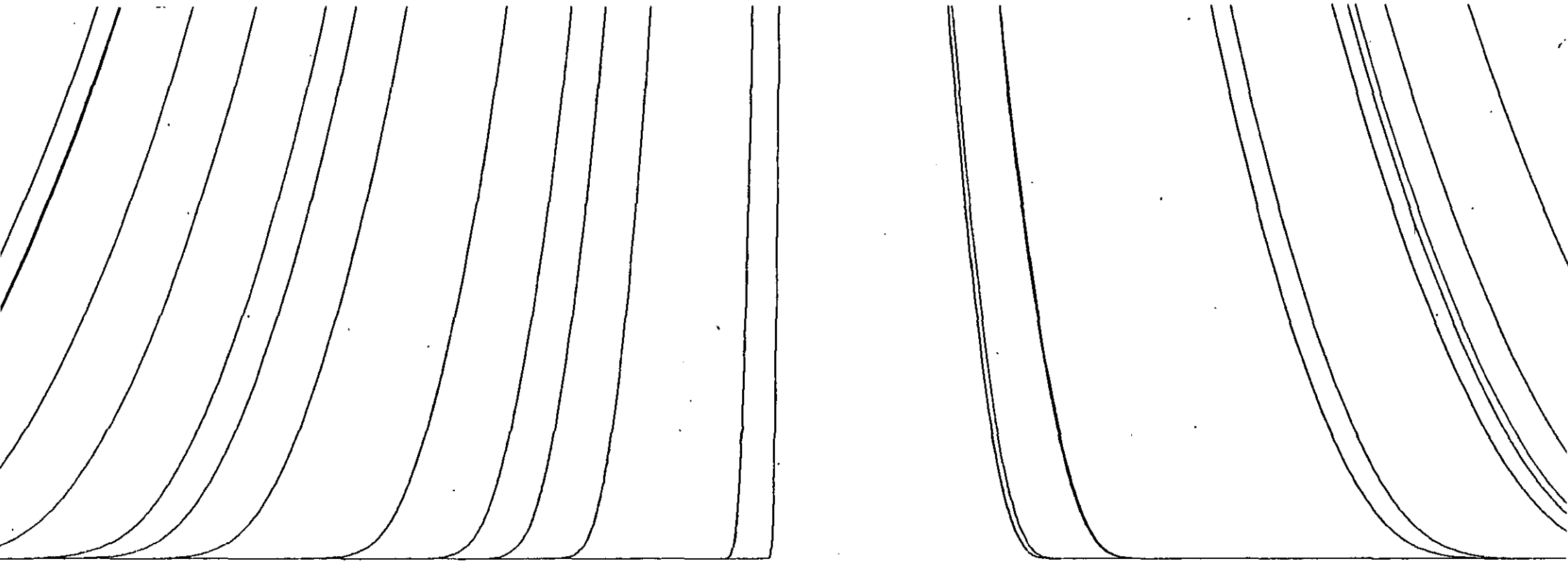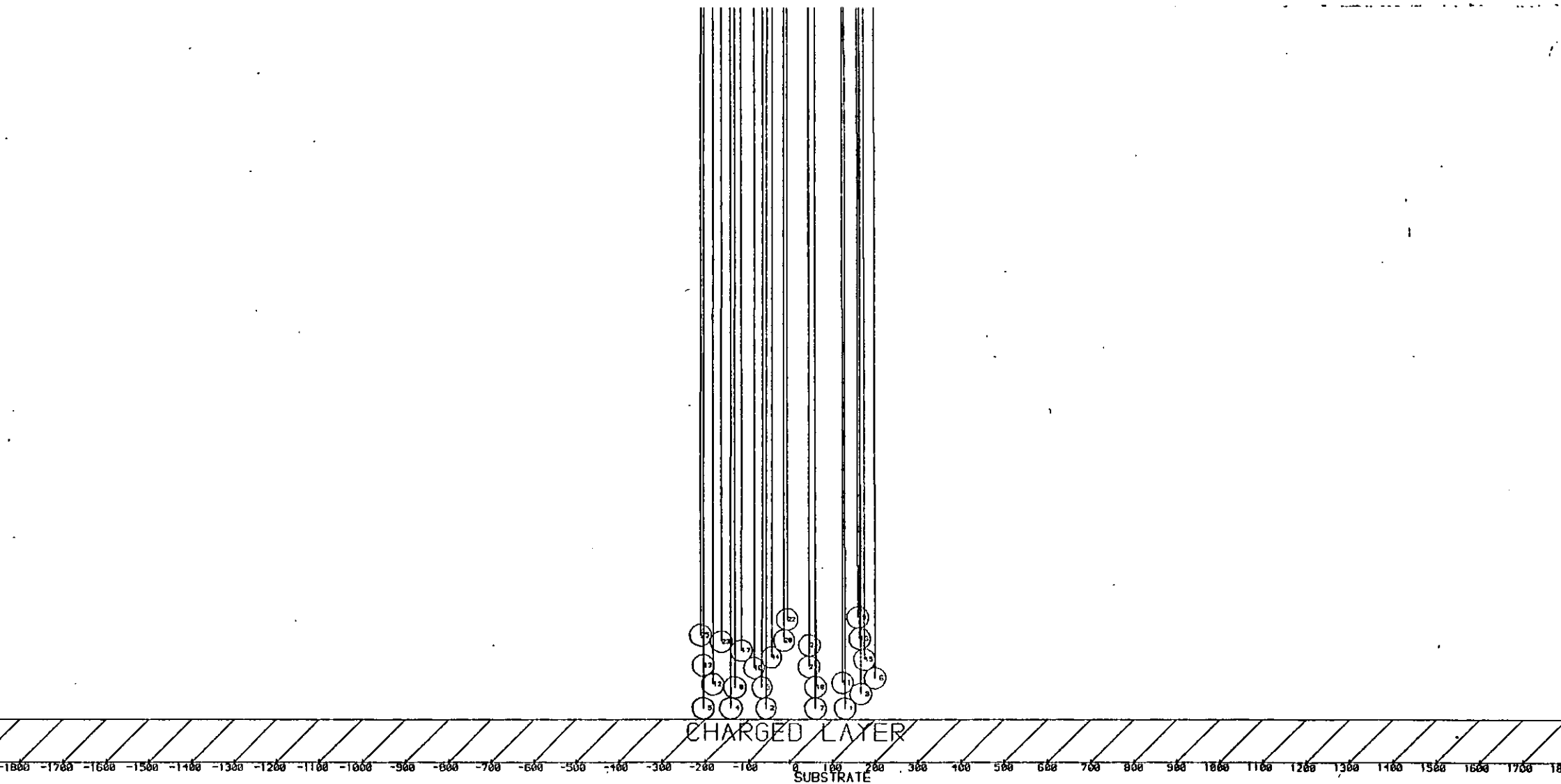
Figure E50. Trajectories of Particles Approaching a Charged Layer 50μm thick – Particle diameter = 25μm, Uniform Velocity = 1 m/s
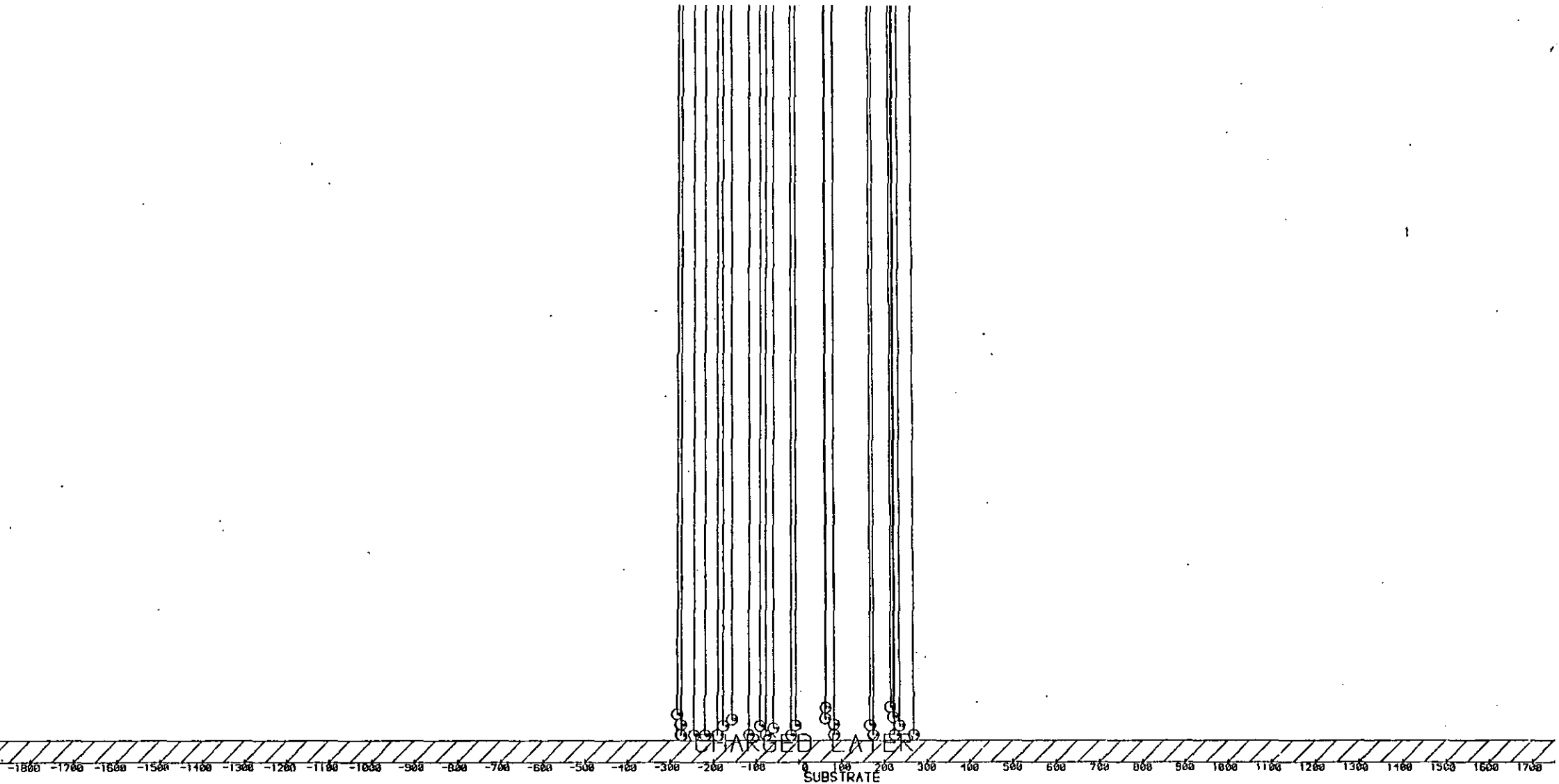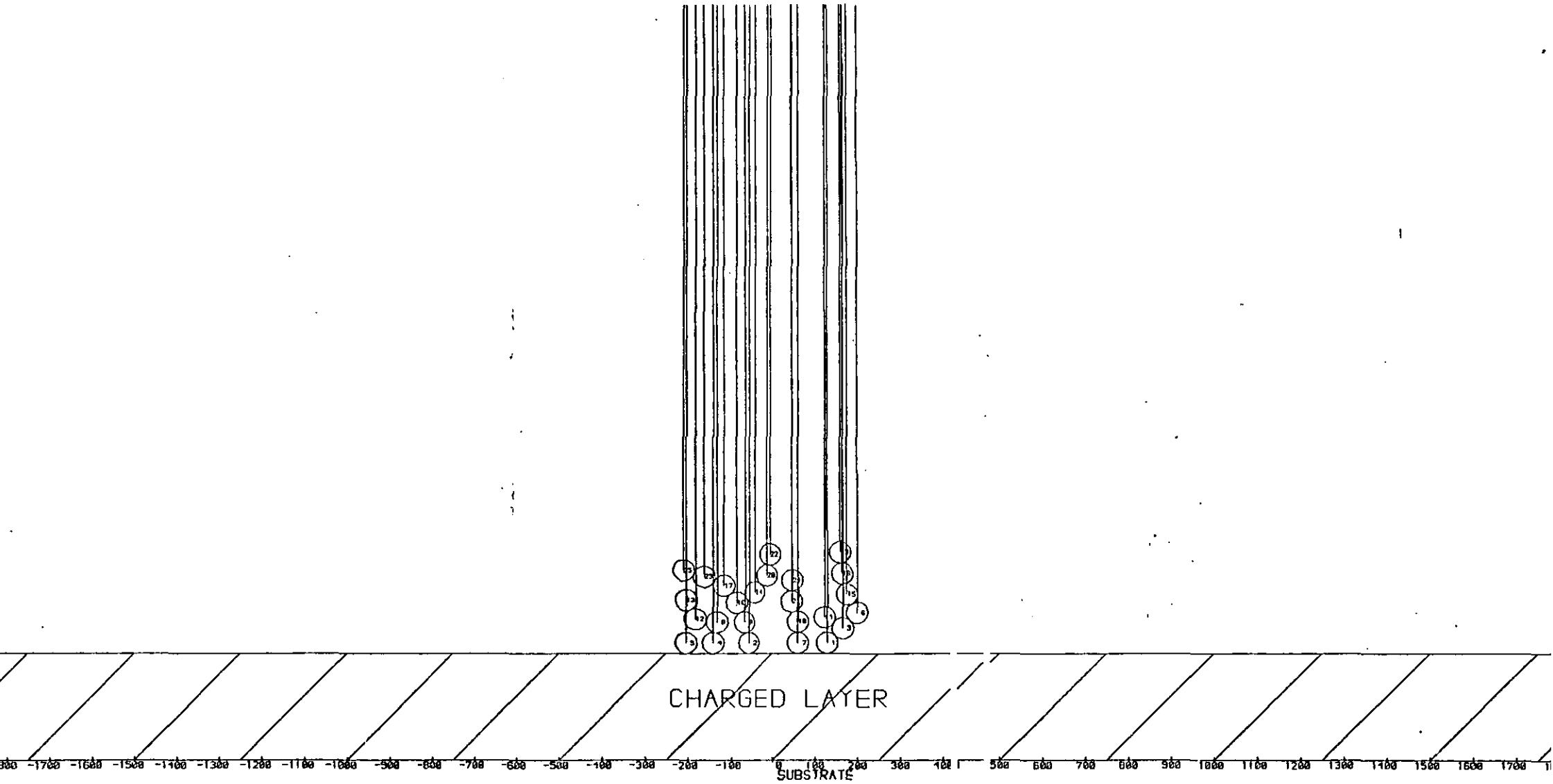
Figure E51. Trajectories of Particles Approaching a Charged Layer 100µm thick – Particle diameter = 25µm, Uniform Velocity = 1 m/s
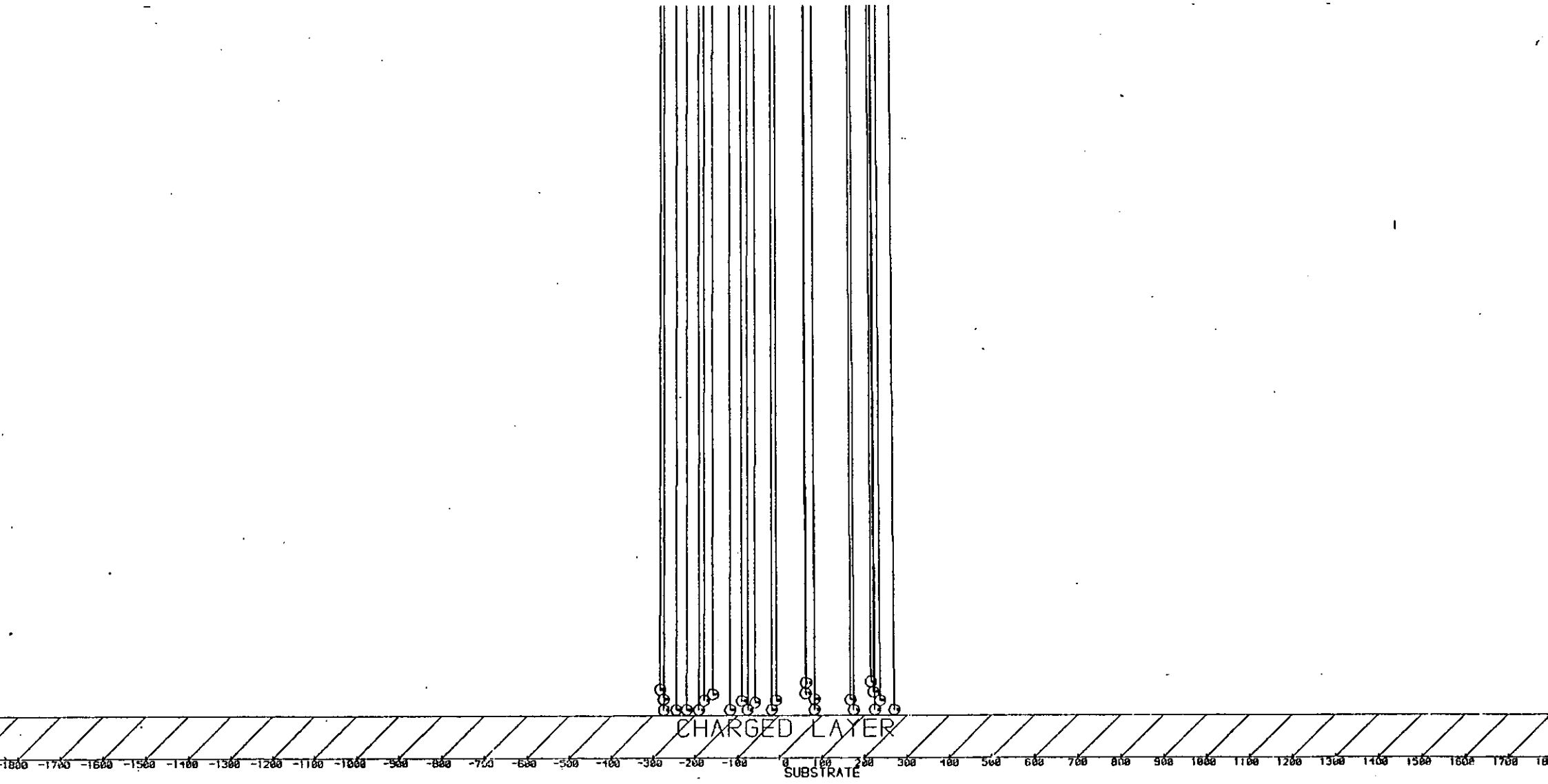
Figure E52. Trajectories of Particles Approaching a Charged Layer 50μm thick – Particle diameter = 25μm, Uniform Velocity = 5 m/s
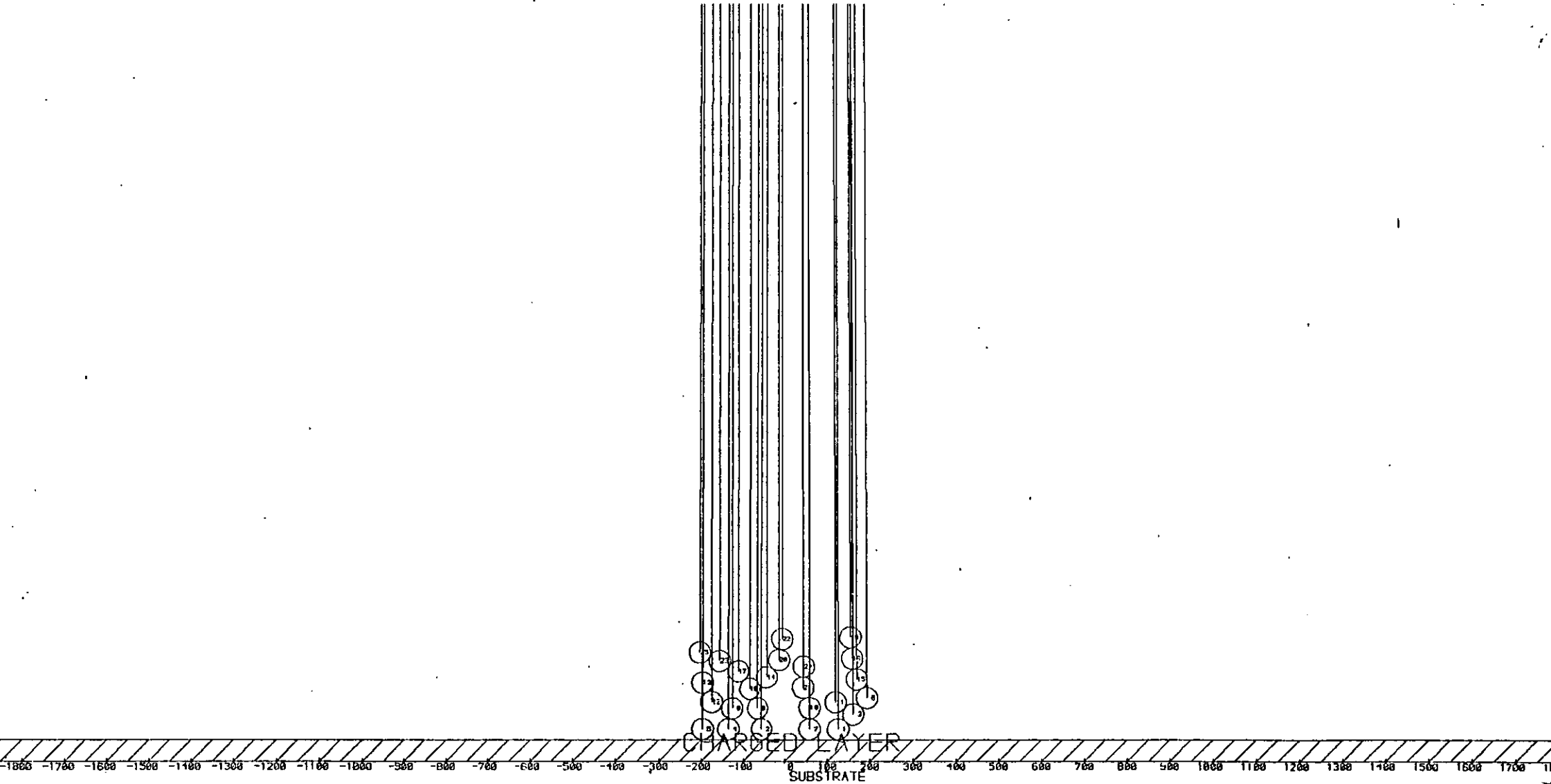
Figure E53. Trajectories of Particles Approaching a Charged Layer 50μm thick – Particle diameter = 25μm, Uniform Velocity = 10 m/s

Figure E54. Trajectories of Particles Approaching a Charged Layer 100µm thick – Particle diameter = 25µm, Uniform Velocity = 10 m/s

Figure E56. Trajectories of Particles Approaching a Charged Layer 100μm thick - Particle diameter = 50μm, Uniform Velocity = 1 m/s
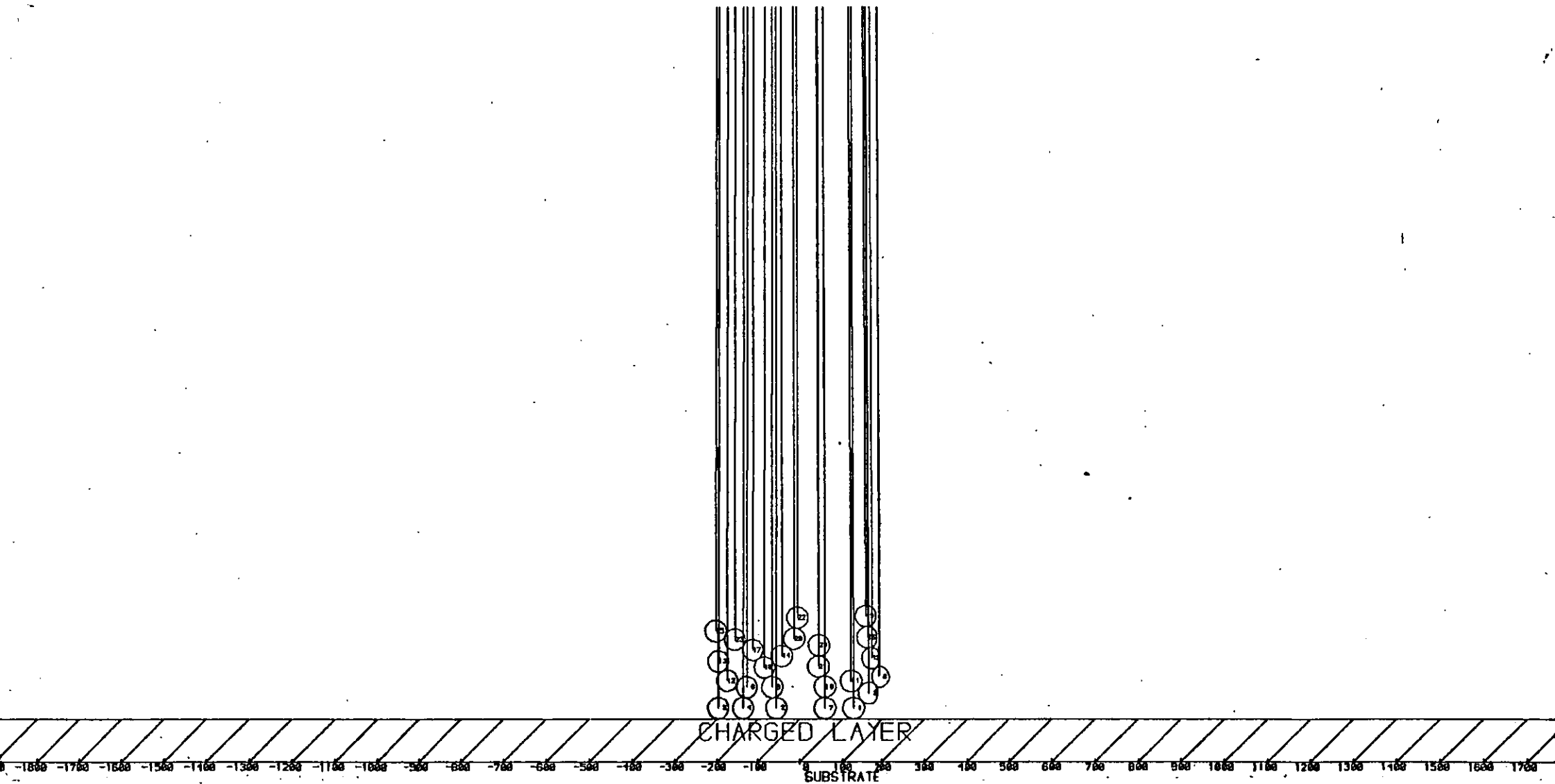
Figure E57. Trajectories of Particles Approaching a Charged Layer 250μm thick – Particle diameter = 50μm, Uniform Velocity = 1 m/s

Figure E58. Trajectories of Particles Approaching a Charged Layer 50μm thick – Particle diameter = 50μm, Uniform Velocity = 5 m/s

Figure E59. Trajectories of Particles Approaching a Charged Layer 100μm thick – Particle diameter = 50μm, Uniform Velocity = 5 m/s

Figure E60. Trajectories of Particles Approaching a Charged Layer 50μm thick – Particle diameter = 50μm, Uniform Velocity = 10 m/s
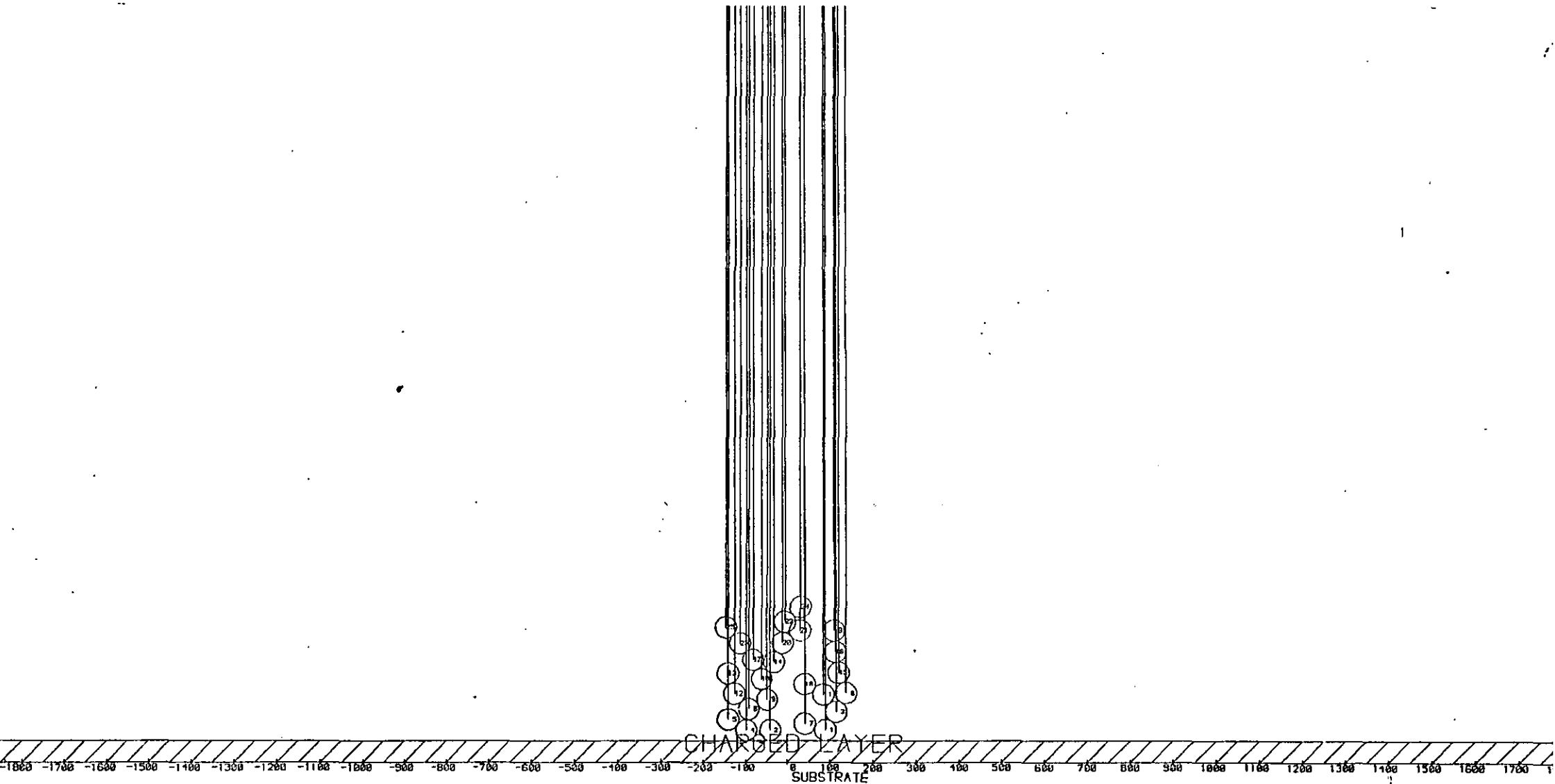
Figure E61. Trajectories of Particles Approaching a Charged Layer 100μm thick - Particle diameter = 50μm, Uniform Velocity = 10 m/s
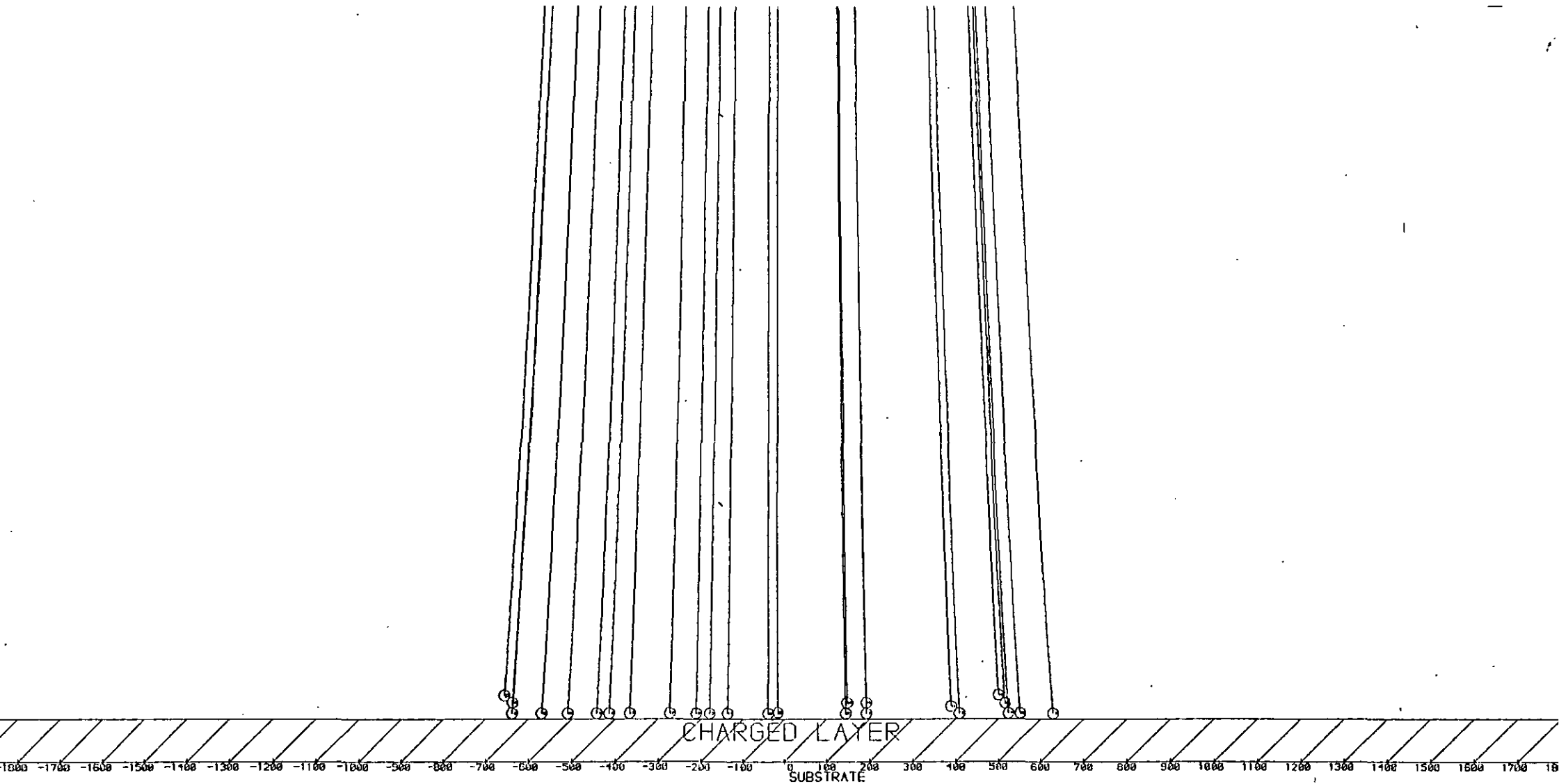
Figure E62. Trajectories of Particles Approaching a Charged Layer 250μm thick — Particle diameter = 50μm, Uniform Velocity = 10 m/s